UNIVERSITY OF STELLENBOSCH

DEPARTMENT OF MECHANICAL ENGINEERING

Report to the

WATER RESEARCH COMMISSION

on

COOLING TOWER PERFORMANCE EVALUATION

by

D G Kröger

WRC Report No. 478/1/96
ISBN 1 86845 230 1

PRETORIA
April 1996

EXECUTIVE SUMMARY

COOLING TOWER PERFORMANCE EVALUATION

Saving of water with air-cooled heat exchangers

COOLING TOWER PERFORMANCE EVALUATION

(i) In view of South Africa's limited water resources it is obvious that the use of this valuable asset should be as meaningful as possible. Large quantities of water are presently required for cooling in the power, chemical, petro-chemical, process and other industries. Typically approximately 2ℓ of water are evaporated to generate 1 kWh of electrical energy i.e. to allow 10 bulbs of 100 W each to burn for one hour. By employing dry-cooling systems in new power plants no cooling water is required. Although the capital cost of a dry-cooling system is often higher than of a wet system this is not always the case. While wet-cooling systems are rapidly becoming more costly due to the increasing cost of water and its treatment, recent developments in dry-systems have resulted in reductions in capital cost of more than 15 percent.

It is projected that the demand for dry-cooling will increases quite significantly in the foreseeable future in all industries requiring cooling. An example of the increased demand in dry-cooling in the power industry in the U.S.A. is shown in figure 1.

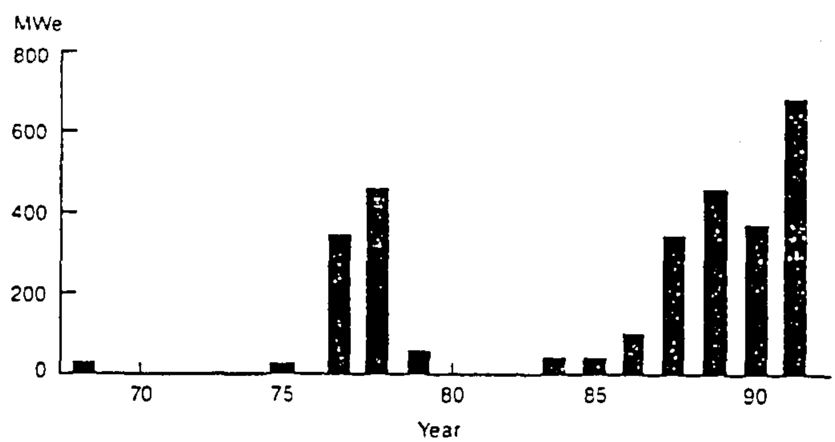

Figure 1: Growth of annually installed dry-cooled generation capacity in the U.S.A.

Although many industries require cooling to relatively low temperature which cannot always be attained with dry-cooling alone, this problem can in part be overcome by combinations of dry and wet or hybrid cooling systems that will still result in dramatic savings in water.

In view of environmental considerations, dirty wet-cooling tower water (blowdown) is posing an additional problem in areas where zero-discharge conditions are specified i.e. this water must be treated on site, thereby introducing additional costs.

In many areas of South Africa cooling water is simply not available any more. The siting of a large new steel plant is presently receiving much attention in view of its potential environmental impact and in particular the need for large quantities of cooling water. In part the problem may be overcome by installing dry-cooling systems.

(ii) *The selection and design of the optimum cooling system for any large plant* requires expertise and careful evaluation. The main objective of this study is to supply information that is required to make an informed decision as to the most effective cooling system that should be selected for a certain plant, taking into consideration technical, environmental and cost factors. Furthermore, computer programs are presented for the performance evaluation of three different types of cooling systems (direct dry-cooling, indirect dry-cooling and wet-cooling). With the available information it is however possible for an engineer to prepare similar programs for the many different types or combinations of industrial air-cooled systems as found in practice.

(iii) The final contract report DGK 5/95/1 entitled "Cooling Tower Performance Evaluation" elaborates on the following topics:

<u>Chapter 1</u>: Air-cooled heat exchangers and cooling towers.

In this chapter the reader is introduced to the many different types of wet and dry cooling systems that are found in practice.

Mechanical draft wet-cooling towers can be either of the induced or forced draft type. Although technical considerations usually dictate the choice of a particular cooing system, historic and other local factors have often in the past played a major role in the selection of the type of cooling system.

Mechanical draft cooling towers can be quite small (both induced draft and forced draft) but very large induced draft single cell units (fans of up to 15 m in diameter) or multi-cell units of different geometries have been constructed. The fill may be arranged for cross-flow or counter-flow. While counter-flow units may require more cooling water pumping power, cross-flow units tend to be more sensitive to winds.

Generally induced draft wet-cooling systems have found most application in the USA in all types of industries. By contrast very few large systems of this type have been constructed in South Africa where due to cost structures etc. concrete natural draft cooling towers are preferred.

Where very large cooling plants are required, hyperbolic concrete natural draft cooling towers become an attractive alternative. Although they may initially be more expensive than mechanical draft systems, no fan power is required. In very windy areas counterflow arrangement of the fill is preferred as is the case in most large cooling towers in South Africa. Although many large cross-flow cooling towers are in operation throughout the world, there does appear to be a trend towards the counterflow arrangement.

In areas where very high towers are not desirable, the height may be reduced by installing fans along the inlet periphery of the tower in order to improve the draft.

In Europe an increasing number of gas desulfurization plants have been installed inside natural draft cooling towers to ensure better dispersion of flue gases.

In areas where cooling water is expensive or not available, air-cooled heat exchangers become cost effective. Although air-cooled heat exchangers have found application in the petro-chemical and process industries for many years, they have only during the last few years become more common at power plants. This is particularly so in the case of combined cycle plants and to a lesser extent at very large base load plants.

Dry-cooling plants may be of the direct or indirect type. In the case of the former steam is ducted directly from the turbine exhaust to the mechanical draft air-cooled condenser. This configuration is attractive in areas where fuel costs are low or the power plant is relatively small. The more costly indirect cooling plant is preferred at very large power plants or where fuel costs are higher. The largest of these types of cooling systems are found at respectively the Matimba and Kendal power plants in South Africa.

In areas where a limited amount of cooling water is available, dry/wet cooling systems have been constructed. The most successful of these systems are the Heller type cooling towers incorporation spray or jet condensers and auxiliary evaporative coolers for more effective power plant operation during exceptionally hot periods. These systems also include mechanical draft evaporative preheater/peak coolers which make operation possible during sub-zero ambient conditions and assist in enhancing performance when ambient temperatures are high.

Wet/dry cooling towers have in recent years become more common at power plants located in more densely populated areas where plumes and excessive noise levels are unacceptable. By mixing the moist plume air with a predetermined quantity of heated dry air the plume can be made essentially invisible during the day, while operation in the more effective entirely wet mode is possible at night. The wet/dry or hybrid cooling systems usually also include passive noise control devices.

These systems are generally very expensive and are not likely to find application in South Africa.

The fundamental conservation equations of mass, momentum and energy form the basis for solving fluid flow and heat transfer problems. The characteristics of these equations are discussed and they are presented in a form that makes them applicable directly to the performance evaluation or thermal-flow design of cooling systems.

Chapter 2: Fluid mechanics.

This chapter introduces certain fundamental fluid dynamic concepts and relations that are essential for the flow dynamic design of cooling systems. The basics relevant to viscous flow are presented primarily to define much of the terminology used in later chapters. Details are given for flows in differently shaped ducts (round, elliptical, flattened) as they occur in practical heat exchangers.

Equations relevant to both laminar and turbulent flows are presented. The dependence of these equations on thermo-physical properties, especially when operating under non-adiabatic conditions is elaborated on.

The complexities of flows in duct systems having appurtenances that cause flow fields to interact, thereby complicating analysis are highlighted. Numerous analytical and empirical equations are presented for determining flow losses in different types of appurtenances.

Reference is also made to different studies concerning the flow characteristics in heat exchanger manifolds. Drag coefficients are listed for different geometries and loss coefficients are given for screens and gauzes (protective screens in fan systems or for protection against hail).

Chapter 3: Heat transfer.

The fundamentals of heat transfer that are relevant to the performance evaluation or design of cooling systems are presented.

Details of conduction in cartesian and cylindrical coordinate systems are given. The concepts of convective and overall heat transfer coefficients are defined.

Analytical and empirical equations for determining the convective heat transfer coefficient under laminar, transitional and turbulent flow conditions in different geometries are presented.

The influences of secondary flow patterns due to buoyancy effects on these transfer coefficients are described.

With the information available on conduction and convection heat transfer, it is possible to evaluate the performance of different extended surfaces or fins. Simplified equations are also presented for design purposes.

The fundamentals of condensation heat transfer are treated in considerable detail since they are of relevance in the design of air-cooled steam condensers. A number of useful equations that quantify the transfer coefficient and the pressure drop inside ducts are presented. Many of these equations are new and were developed during this research project. Some of these results will undoubtedly result in the improved design of air-cooled steam condensers in future.

The transfer equations are incorporated in the definition of the logarithmic mean temperature and the effectiveness - NTU methods as applicable in the design of heat transfer equipment.

Chapter 4: Mass transfer and evaporative cooling.

In this chapter psychrometric principles are applied in the performance evaluation of cooling towers, evaporative coolers and systems incorporating adiabatic pre-cooling. Since there is usually both a heat and mass transfer process between air and some wetted surface, information on mass transfer is presented. Because of the analogy that exists between momentum, heat and mass transfer, there is a similarity in the equations employed.

A series of empirical equations describing the mass transfer coefficient in different geometries is presented. The origin of the psychrometric chart and its different characteristic curves are described.

The transfer processes in a wet-cooling tower or evaporative cooler are deduced from first principles resulting in Merkels equation. The merits and limitations of this theoretical model are discussed and other more sophisticated approaches are referred to.

Geometries and performance characteristics of many different types of fills or packs for cooling towers are listed. These include splash, trickle film and extended film fills. The fill material properties are compared and evaluated.

A detailed deduction of the fundamental equations that are relevant to the design of evaporative coolers is presented. The analysis is applicable to both cross-flow and counterflow coolers. Various empirical equations for the relevant transfer coefficient and pressure loss coefficients are given.

A significant amount of cooling occurs in the rain zone of a wet cooling tower. A detailed analysis is presented which ultimately results in an expression for the transfer coefficient as a function of among other parameters, the mean droplet diameter in the rain zone.

This new equation as well as more sophisticated equations with which the transfer coefficients can be predicted in circular and rectangular rain zones were developed as part of this research project.

To reduce losses of cooling water to the environment, droplet or drift eliminators are installed above or after the fill in a wet cooling system. The performance characteristic of different eliminators were determined experimentally and correlations are presented for use in the design of cooling towers.

To enhance the performance of dry cooling systems during periods of high ambient temperature, spray or adiabatic pre-cooling of the air may be considered. Details of how adiabatic pre-cooling will affect the performance of a cooling system are given.

Chapter 5: Heat transfer surfaces.

The most expensive and most critical component of any air-cooled heat exchanger is the heat transfer surface area. Owing to the relatively low heat transfer coefficient on the air-side, extended surfaces or fins are required to increase the surface area density, thereby improving the overall conductance, resulting in a lighter and more compact heat exchanger.

Finned tubes may be round, elliptical, flattened or otherwise streamlined to reduce the flow resistance on the air-side. Different types and shapes of fins are either an integral part of the tube or attached to the tube by mechanical means only, or by soldering, brazing, galvanizing or welding. To improve the heat transfer characteristics, the fin surface may be roughened, cut, corrugated or perforated. In certain applications, sections of the surface are stamped out to create spaces separating the adjacent fins.

The performance characteristics of extended surfaces are normally determined under idealized conditions in windtunnels designed specifically for this purpose. Details of how such surfaces should be tested as well as different procedures for interpreting the results are presented. A novel new method for presenting the results is proposed. This method has in general been well received by individuals involved in evaluating the performance of heat exchanger test bundles. A detailed numerical example is presented to show how the method is to be applied.

Further empirical equations are presented with which the air-side heat transfer coefficient as well as the pressure drop for different fin geometries and tube layouts can be evaluated. Tube row correction factors are also given.

Since most air-cooled steam condensers have their heat exchanger bundles arranged in the form of A-frames, the air flow and its corresponding losses through such a configuration was studied in considerable detail and equations are presented for application in a practical design.

Corrosion, erosion and fouling have especially in certain areas of the world contributed to the ineffective operation of air-cooled heat exchangers. While traces of chlorine in the atmosphere tend to attack aluminum surfaces, galvanized steel surfaces are more susceptible to sulphur in the atmosphere. Other examples of fouling and erosion of the finned surfaces are listed.

To ensure good performance of finned tubes it is important that the thermal contact between the fin and the outer tube surface is sound. Poorly wrapped-on or extruded fins have been found to be quite unacceptable for application in large cooling systems. Even in the care of galvanized finned tubes great care must be taken during the galvanizing process to ensure a cavity free region between the fin and the tube.

A detailed study was conducted to determine the influence of free stream turbulence on the performance of finned tube heat exchanger bundles. It was clearly shown that high turbulence in the upstream air can considerably increase the effective heat transfer coefficient.

In the design of any heat exchanger it is important that attention be given to the design of manifolds on the process fluid side to ensure a good flow distribution. It is shown that a poor flow distribution will considerably reduce the heat transfer capability of the heat exchanger.

Chapter 6: Fans

Different types of fans find application in air-cooled heat exchangers and evaporative coolers including axial -, centrifugal -, mixed - and cross-flow types. Since the fan is a critical component of the air-cooled heat exchanger its selection and incorporation in the design of the total cooling system is very important. When selecting a fan for a particular application, factors such as cost, performance (stability of operation, ease of control, power consumption, flow range), mechanical arrangement (convenience of installation), self cleaning blade properties and noise emission must be taken into consideration.

The performance characteristics of fans are determined in test facilities that must comply with specifications as set out in one of many codes or standards. An example of a particular test facility is described in detail and particulars are presented whereby test data obtained in such a facility can be evaluated to give the performance characteristics of a particular fan.

A detailed study was conducted to determine the influence of the fan tip clearance on performance. Results show that a large tip clearance can have a very negative effect and that every effort should be made to minimize tip clearance.

When installing a fan in a practical installation the interaction of the structure with the fan (fan system effect) usually reduces fan performance. Results are presented with which this effect can be quantified. Details of plenum losses and shroud effects are also presented.

Chapter 7: Natural draft cooling towers.

Natural draft cooling towers are found in power plants throughout the world. Different shapes and types of structures exist, but their fundamental function is the same, i.e. to create, by means of buoyancy effects, the flow of air through the fill or bundles of finned tube heat exchangers.

An analysis is presented for the evaluation of dry cooling towers having the heat exchanger bundles located horizontally in the base of the tower or vertically along its periphery. The analysis presented in this chapter is by far the most detailed of any work to date and incorporates much new design information that was generated during this investigation and was not previously available.

Among the new information is an extensive experimental investigation into the inlet losses and flow distribution in cooling towers. Outlet conditions were also investigated numerically.

The problem of cold air inflow into the top of the cooling tower is also addressed. Different models are presented with which the onset of cold inflow can be determined. With this information it is thus possible to design a cooling tower such that cold inflow does not occur.

The design method proposed in this chapter has been applied in evaluating the performance of dry-cooling towers in South Africa and overseas. In the case of the local towers the theoretical predictions were found to be in excellent agreement with measurements conducted at the towers.

With this information it will thus be possible to design or evaluate the performance of future dry-cooling towers to be erected in the power or chemical industries in South Africa.

Chapter 8: Air-cooled heat exchangers.

In this chapter the reader is introduced to different types of air-cooled heat exchangers as found in various industries.

The geometric characteristics of typical air-cooled heat exchangers as found in the petro-chemical industry are described and performance analyses for forced and induced draft units are presented. This section is followed by an analysis of an air-cooled condenser as found in direct dry-cooled power plants. These analyses are the most sophisticated methods presently available and incorporate all the newest research results obtained during this study.

A section is given to the description of the problem of the presence of non-condensables in steam condensers. Various types of dephlegmator or de-aerator concepts are described and their merits are evaluated.

In any successful design of an industrial air-cooled heat exchanger details must be available whereby inlet losses to the heat exchanger can be quantified. Extensive tests were conducted during the project in order to quantify these losses. New empirical equations are presented for this purpose. These equations take into consideration fan platform height, walkway width, inlet roundings, fan unit width, etc.

In addition to inlet flow losses recirculation of hot plume air tends to reduce the performance especially in the case of forced draft heat exchangers. The problem is analysed numerically and the results are compared to experimental data. Practical empirical equations are presented for application in design.

Chapter 9: System selection and optimization.

In the design of a base load power plant, the selection and matching of various components is of the utmost importance in order to achieve effective operation and power output. Details are presented in this chapter, showing how the cooling system can be optimized in a particular power plant. A similar approach is followed in the case of a large petro-chemical or process plant.

Chapter 10: Environmental effects.

The performance of all air-cooled heat exchangers and cooling towers are affected by changes in ambient conditions. Changes in temperature generally exert the biggest influence while winds, inversions, rain, snow, hail and solar radiation have a lesser effect.

In this chapter the dynamics of the atmosphere are expressed in terms of equations that are employed in the design of cooling systems. The lapse rate is deduced for dry air as well as for air containing a considerable amount of water vapor.

Characteristics of the planetary boundary layer and the formation of inversions are discussed.

All cooling systems are influenced by winds to a greater or lesser extent. Experimental results showing changes in approach temperature difference at different wind speeds for dry- and wet-cooling towers are shown. In general cooling towers having the heat exchanger or fill located horizontally in the base of the tower tend to be less sensitive to winds than towers having vertical arrangements around the periphery.

During windy periods the velocity distribution through heat exchangers located horizontally in the base of a natural draft cooling tower is highly distorted resulting in a reduction in performance. This problem can be considerably reduced by installing appropriate windwalls and having relatively deep (in the direction of inlet air flow) tower supports.

Atmospheric inversions reduce the performance of a cooling tower. Various approximate but adequate approaches with which this effect can be quantified, are presented. Since temperature inversions usually occur at night when the demand for power is relatively low, inversions do not pose a serious problem.

iv) In view of the very extensive theoretical and experimental work that has been done, it is now possible to evaluate the performance characteristics of large industrial cooling systems to a high degree of accuracy. Furthermore three computer programs have been prepared with which the performance of dry and wet cooling systems can be evaluated under different operating conditions. The objectives of the contract have thus been reached.

In addition to having achieved the specified objectives of the contract, it should also be stressed that more than 30 graduate students have been involved in this program. I believe that this is an important contribution to the high level manpower needs of South African industry.

Although existing relevant information of other researchers is employed in the proposed performance evaluation, most of the really important and valuable new developments in the field were made at the University of Stellenbosch, making it the undisputed leader in this field.

With this information it is possible to design cooling systems, or to evaluate critically, systems to be purchased by South African industries. Improved new designs catering for the particular needs of a plant in a particular area can lead to enhanced performance, e.g. less or no cooling water is required for generating power, producing steel or chemicals. The cooling systems of existing plants can be modified and improved to increase electrical output and other products at lower costs. New plants can be located in areas where no water is available or which is ecologically sensitive and where pollutants cannot be discharged. The programs have already been used by ESKOM to evaluate cooling system performance locally and internationally where no such facilities were available in the past. If correctly applied the degree of accuracy possible in predicting cooling system performance is exceptional. The present program for natural draught dry cooling towers was employed to predict the performance of a dry-cooling tower at the Kendal power plant. It was found that the prediction of the heat rejection rate was within 1.5% of the measured value!

(v) Although methods and computer programs have been developed to evaluate the performance or to design large industrial cooling systems, refinements and extensions are possible. As new needs arise and cost structures change, new developments and research will be required. Since a center of expertise exists in this field at the University of Stellenbosch it is imperative that the newest developments in the field should be monitored and that the existing data bank should be expanded as new information becomes available. This center will make available information or act on a consultancy basis to the benefit of South African industries. Continuing limited financial support for this purpose should be maintained.

I would like to thank the Water Research Commission for its financial support, and trust that this study will benefit South Africa's people, its industry and its environment and in particular lead to the preservation and more effective use of our valuable and limited water resources.

Prof D.G. Kröger

Stellenbosch, 1 August 1995

c:\dep\1996\dgk\jan\wnk2.doc

CONTENTS

PREFACE

This report is the result of an extensive theoretical and experimental study initiated with a view to making available methods and information with which the performance of different types of industrial cooling towers can be reliably evaluated. To demonstrate the application of the information included in this report, computer programs for the performance evaluation of a wet-cooling tower as well as an indirect and a direct dry-cooling tower are presented in separate reports [DGK 5/95/2, DGK 5/95/3, DGK 5/95/4].

The financial support for this research effort, provided by the Water Research Commission, is gratefully acknowledged, as is the valuable inputs of the Steering Committee members, viz :

Dr T C Erasmus
Prof P J Erens
Mr A J Ham
Mr A D Kimpton
Mr Z Olsha
Dr D v/d S Roos
Mr D J de V Swanepoel
Mr M Zunckel

LIST OF SYMBOLS

A	Area, m^2
a	Coefficient, or constant, or length, m, or surface area per unit volume, m^{-1}
b	Exponent, or constant, or length, m
C	Coefficient, or heat capacity rate mc_p, W/kg, or C_{min}/C_{max}, or cost, \$
c_p	Specific heat at constant pressure, J/kgK
c_v	Specific heat at constant volume, J/kgK
D	Diffusion coefficient, m^2/s
d	Diameter, m
d_e	Equivalent or hydraulic diameter, m
E	Elastic modulus, N/m^2
Ey	Characteristic pressure drop parameter, m^{-2}
e	Effectiveness
F	Force, N
F_T	Temperature correction factor
f	Friction factor
G	Mass velocity, kg/sm^2
g	Gravitational acceleration, m/s^2, or gap, m
H	Height, m
h	Heat transfer coefficient, W/m^2K
h_D	Mass transfer coefficient, m/s
h_d	Mass transfer coefficient, kg/m^2s
i	Enthalpy, J/kg
i_{fg}	Latent heat, J/kg
J	Bessel function
K	Loss coefficient or incremental pressure drop number
k	Thermal conductivity, W/mK
L	Length, m
L_{hy}	Hydraulic entry length, $x/(d_e Re)$
M	Molecular weight, kg/mole, or torque, Nm
N	Revolutions per second, s^{-1}
m	Mass flow rate, kg/s
NTU	Number of transfer units, UA/C_{min}

Ny	Characteristic heat transfer parameter, m^{-1}
n	Number
P	Pitch, m, or power, W
P_e	Perimeter, m
p	Pressure, N/m^2
p_{cr}	Critical pressure, N/m^2
Q	Heat transfer rate, W
q	Heat flux, W/m^2
R	Gas constant, J/kgK, or thermal resistance, m^2K/W
Ry	Characteristic flow parameter, m^{-1}
r	Radius, m
s_t	Yield or ultimate stress, N/m^2
T	Temperature, °C or K
Tu	Turbulence intensity
t	Thickness, m
U	Overall heat transfer coefficient, W/m^2K
u	Internal energy, J/kg
V	Volume flow rate m^3/s
v	Velocity, m/s
W	Work, J, or width, m
w	Humidity ratio
X	Mole fraction
x	Co-ordinate, or elevation, m, or distance, m, or quality
Y	Defined by equation (4.2.4)
y	Co-ordinate or P/d
z	Co-ordinate or elevation, m
α	Thermal diffusivity, $k/\rho c_p$, or thermal expansion coefficient, or void fraction
α_e	Energy coefficient defined by equation (1.4.4)
β	Volume coefficient of expansion, K^{-1}, or porosity
γ	c_p/c_v
Δ	Differential
δ	Boundary layer thickness, m, or condensate film thickness, m
ϵ	Surface roughness, m
η	Efficiency

θ Angle, °, or temperature differential, °C

λ Eigenvalue

μ Dynamic viscosity, kg/ms

ν Kinematic viscosity, m^2/s, or Poisson's ratio

ρ Density, kg/m^3

σ Area ratio, or surface tension, N/m

τ Shear stress, N/m^2, or time, s

ϕ Potential function, or angle, °, or defined by equation (3.2.21), equation (3.3.13) or equation (4.2.3)

Dimensionless Groups

Eu Euler number, $\Delta p/(\rho v^2)$

Fr Froude number, $v^2/(Lg)$

Fr_D Desimetric Froude number, $\rho v^2/(\Delta \rho L g)$

Gr Grashof number, $g\rho^2 L^3 \beta \Delta T/\mu^2$ or $g\rho^2 d^3 \beta \Delta T/\mu^2$ for a tube

Gz Graetz number $RePrd/L$ for a tube

Ku Kutateladze number $i_{fg}/(c_p \Delta T)$

Le_f Lewis factor, $h/(c_p h_d)$

Nu Nusselt number, hL/k or hd/k for a tube

Pe Péclet number, RePr

Pr Prandtl number, $\mu c_p/k$

Re Reynolds number, $\rho vL/\mu$ or $\rho vd/\mu$ for a tube

Sc Schmidt number, $\mu/(\rho D)$

Sh Sherwood number, hDd/D

St Stanton number, $h/(\rho v c_p)$ or $Nu/(RePr)$

Subscripts

a Air, or based on air side area

acc Acceleration

av Mixture of dry air and water vapor

abs Absolute

app Apparant

b	Base, or bundle, or bend
c	Contraction, or cold, or contact, or condensate, or critical, or constant
cp	Constant properties
ct	Cooling tower
ctc	Cooling tower contraction
cte	Cooling tower expansion
cv	Control volume
D	D'Arcy, or drag, or drop, or diffusion
d	Diameter, or diagonal, or downstream, or drop, or dynamic
db	Drybulb
de	Drift eliminator
dr	Droplet
dif	Diffuser
e	Energy, or expansion, or effective, or equivalent
f	Fin, or friction
F	Fan
fi	Fill
fr	Frontal
ft	Fin tip
fs	Fill support
g	Gas or ground
H	Height
h	Hot
he	Heat exchanger
i	Inlet, or inside
id	Ideal
il	Inlet louver
iso	Isothermal
j	Colburn j-factor, St $Pr^{0.67}$, or jet, or junction
l	Laminar or longitudinal
ℓm	Logarithmic mean
m	Mean, or momentum, or model, or mass transfer, or mixture
max	Maximum
min	Minimum

n	Nozzle
o	Outlet, or outside, or initial, or oil
ob	Obstacle
p	Constant pressure, or production, or plate
pl	Plenum
q	Constant heat flux
r	Root, or row, or radial co-ordinate
re	Effective root
red	Reducer
rz	Rain zone
s	Screen, or steam, or static, or saturation, or process stream
sp	Spray
T	Constant temperature, or temperature, or T-junction, or test
ΔT	Constant temperature difference
t	Total, or tube, or tape, or transversal, or turbulent, or transition
th	Thermal
tp	Two-phase
tr	Tube row
ts	Tube cross-section, or tower support
tus	Windtunnel cross-section
v	Vapor
w	Water or wall or wind
wb	Wetbulb
wd	Water distribution system
x	Co-ordinate, or quality
y	Co-ordinate
z	Co-ordinate
θ	Inclined or yawed
π	At 180°
∞	Infinite, or free stream

CHAPTER 1

AIR-COOLED HEAT EXCHANGERS AND COOLING TOWERS

1.0 INTRODUCTION

In any power generating or refrigeration cycle, heat has to be discharged. This is also true in many chemical and process plant cycles. In a fossil-fired power station with an efficiency of about 40 percent, at least 45 percent of the heat input has to be rejected through the cooling system. In the case of a nuclear plant with an efficiency of only 33 percent, even more heat has to be rejected. The task of choosing the source of cooling is becoming increasingly complex. Dwindling supplies of cooling water and adequate plant sites, rapidly rising water costs usually at well beyond inflation rates in most industrialized countries, noise restrictions [90HI1] and other environmental considerations and proliferating legislation, all contribute to the complexity [75ST1, 75VG1].

The hydrosphere has for decades been the commonly used heat sink. The simplest and cheapest cooling method was to direct water from a river, dam or ocean to a plant heat exchanger and to return it, heated, to its source. In industrialized countries, the permissible rise in temperature of such cooling water is often limited, thus limiting the use of natural water for once-through cooling.

Because of restrictions on thermal discharges to natural bodies of water, most new generating capacity or industries requiring cooling, will have to make use of closed cycle cooling systems. In some areas cooling lakes or spray ponds and canals may be appropriate, although evaporative, or wet, cooling tower systems generally are the most economical choice for closed cycle cooling where an adequate supply of suitable water is available at a reasonable cost to meet the substantial make-up water requirements of these systems. Air-cooled heat exchangers are found in chemical and process plants where fluids at temperatures of 60°C or higher are to be cooled. The use of dry-cooling systems is often justified where cooling water is not available or is very expensive. In certain applications dry/wet or wet/dry cooling systems offer the best option [81BA1, 89MI1].

1.1 WET-COOLING TOWERS

The development, practice and performance of wet-cooling towers have been described in numerous publications [59MC1, 75BE1, 81CH1, 90HI1].

1.1.1 MECHANICAL DRAFT

In a conventional mechanical draft wet-cooling system (also sometimes referred to as a cooling tower) as shown in figure 1.1.1, turbine exhaust steam condenses in a surface condenser giving up heat to the cooling water circulating through the condenser tubes. The warm water leaving the condenser is piped to the cooling system where it flows downward through the fill or packing which serves to break the water up into small droplets or spreads it into a thin film in order to maximize the surface contact between the water and the cooling air which is drawn through the fill by the axial flow fan. The water, after being cooled by a combination of evaporation and convective heat transfer, is again pumped through the condenser in a continuous circuit. One to three percent of the water is lost by evaporation.

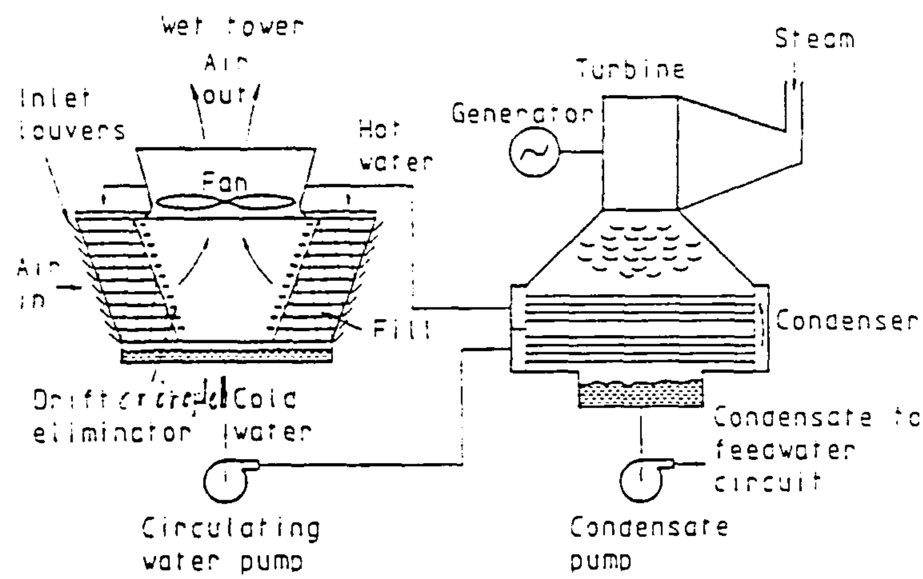

Figure 1.1.1: Mechanical draft wet-cooling system installed in a power plant.

There are a number of different types of evaporative-, or wet-cooling systems, which are distinguished by the method used to move air through the tower (mechanical draft or natural draft) and the arrangement of the fill section (crossflow or counterflow of air and water streams). Furthermore mechanical draft towers may be of forced draft or induced draft design. Forced draft towers have fans or blowers that are located where the ambient air stream enters the tower and forces the air through the tower as shown schematically in figure 1.1.2. These towers are characterized by high air inlet velocities and relatively low exit velocities and are thus susceptible to recirculation of the hot, moist plume air.

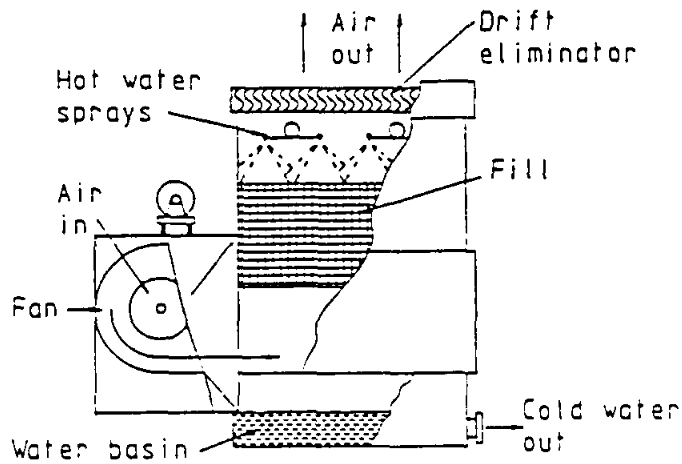

Figure 1.1.2: Forced draft cooling tower.

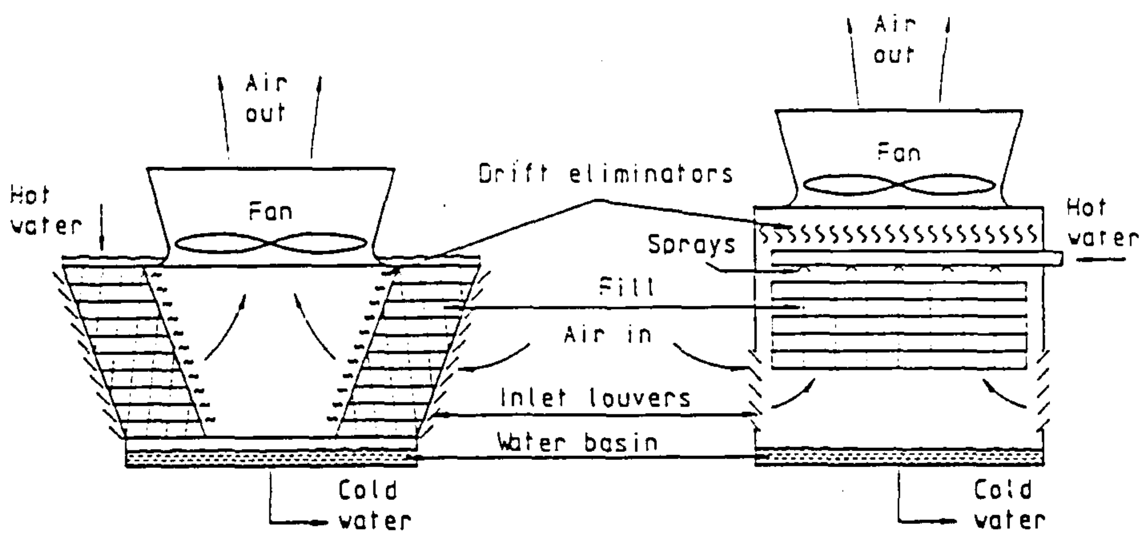

(a) Mechanical draft crossflow (b) Mechanical draft counterflow

Figure 1.1.3: Induced draft cooling towers.

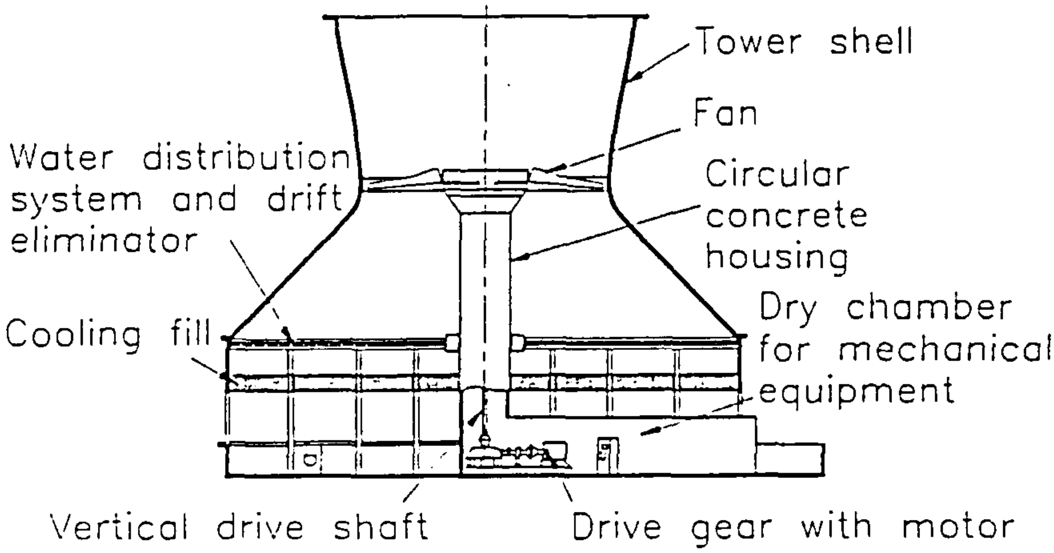

Figure 1.1.4: Single-cell circular induced draft cooling tower.

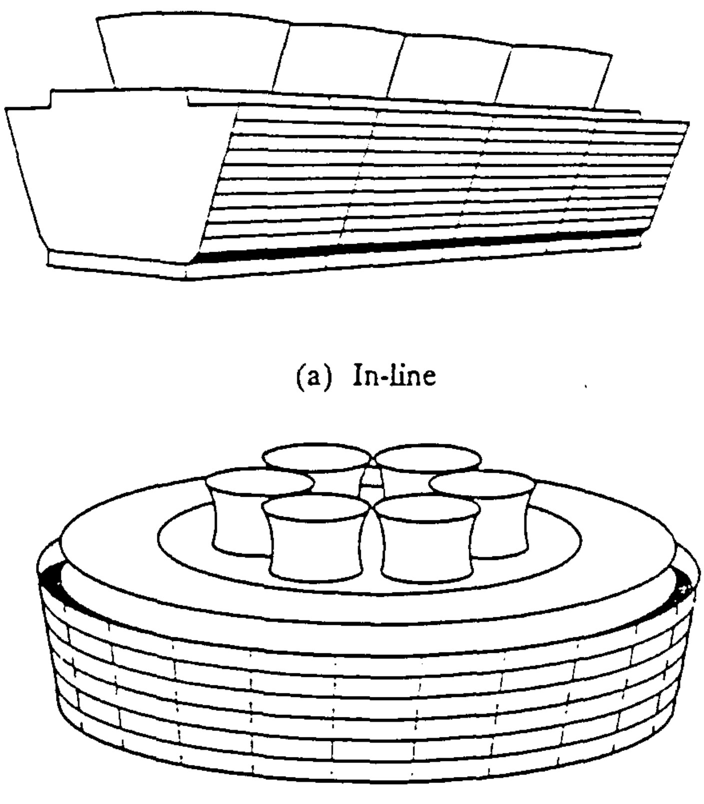

(a) In-line

(b) Round

Figure 1.1.5: Alternative mechanical draft wet-tower arrangements.

Induced draft towers, as shown in figure 1.1.3, have an air discharge velocity that is much higher than the entrance velocity. Plume recirculation is a much smaller problem in induced draft towers than it is in forced draft towers. However, more fan power is usually required to move the same mass of air because the air has a lower density (i.e. it is warmer and contains more water vapor than inlet air).

A section through a large single-cell circular induced draft cooling tower is shown in figure 1.1.4. The fan-drive equipment is located in a chamber isolated from the water system. Fans having diameters of up to 28m are employed in such towers.

Mechanical draft towers have traditionally been used in an in-line arrangement of individual cells to form a rectangular bank as shown in figure 1.1.5(a). A more recent development is the round mechanical draft tower with multiple fans a shown in figure 1.1.5(b).

1.1.2 NATURAL DRAFT

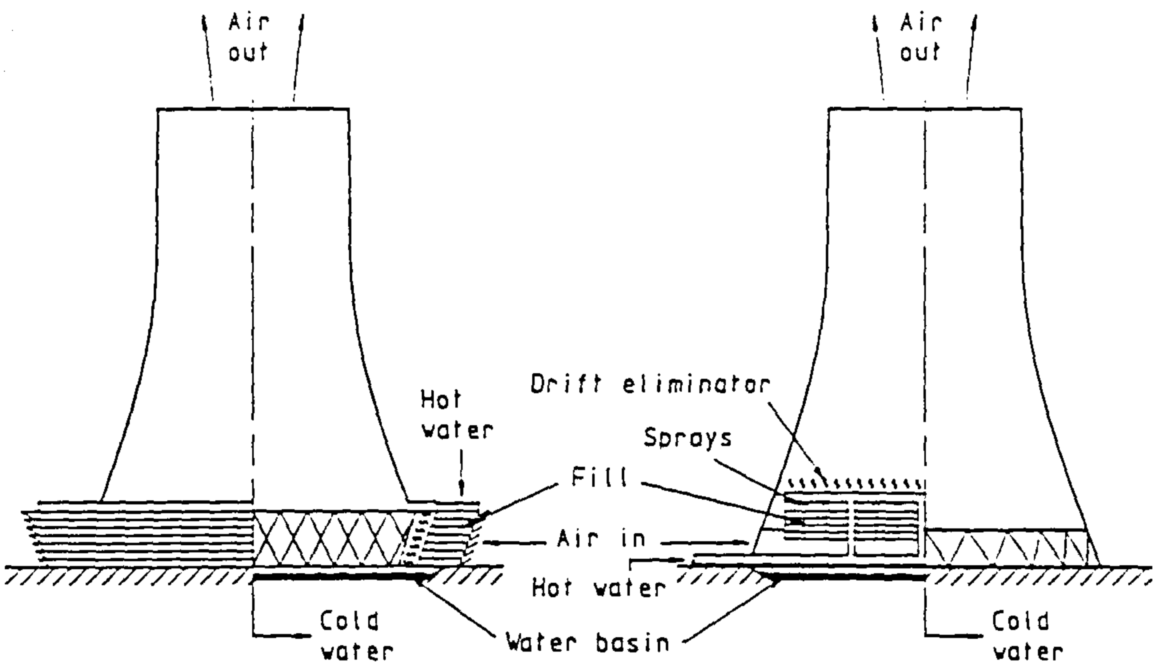

(a) Crossflow (b) Counterflow

Figure 1.1.6: Natural draft cooling towers.

In natural draft wet cooling towers, the required air flow through the fill is created by the difference in density between the heated humidified air inside the tower and the heavier ambient air outside the tower. Crossflow and counterflow fill arrangements as shown in figure 1.1.6 are encountered.

Crossflow towers have a fill configuration in which the air flows essentially perpendicular to the downward falling water. The hot water is delivered through risers to distribution basins above the packing and is distributed by gravity through low pressure nozzles in the floor of the basin.

A modern concrete cooling tower usually has a hyperbolic shaped shell which may be up to 180m in height [89GO1]. It is possible to reduce the size of the tower by installing axial flow fans at its base [76GA1]. Although the cost of the structure is reduced, this is offset by the capital cost of the fan installation and the running costs.

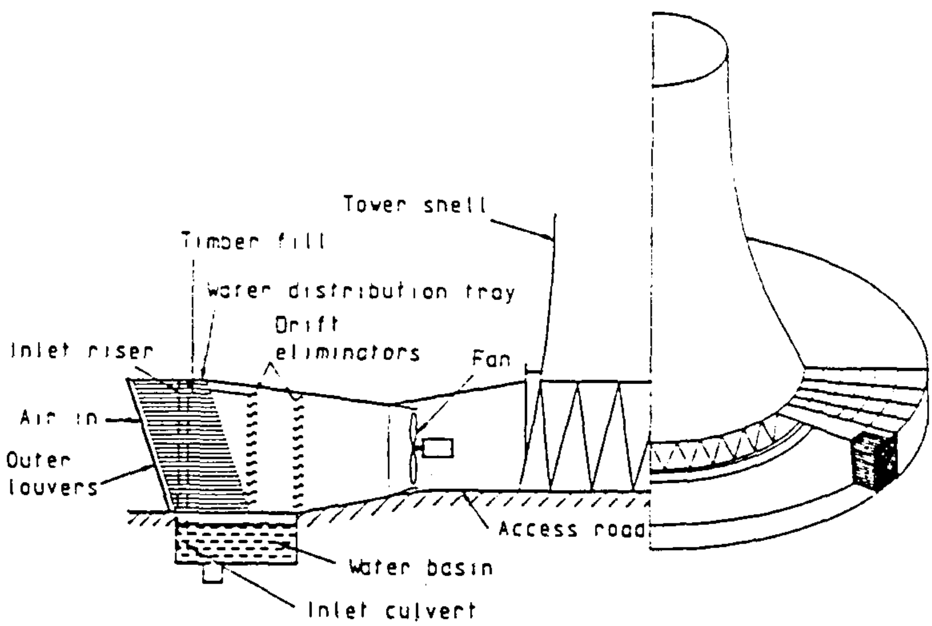

Figure 1.1.7: Fan-assisted crossflow cooling tower.

Fan-assisted natural draft cooling towers may be considered where excessive plume recirculation in alternative multi-bank mechanical draft units make these unacceptable.

Figure 1.1.7 illustrates the design proposal for the Ince B power plant fan assisted draft tower [76GA1, 77JO1]. The tower is 117 m tall and has a shell base diameter of 86 m. The roofed structure that surrounds the base and houses the crossflow fill and 35 fans is 172 m in outside diameter. The fans consume 6 MW(e) at the design point, 0.6 percent of the station output. The fill consists of a prefabricated design of timber-lath splash bars. Two arrays of corrugated louvers are necessary to cope with the high air and water mass fluxes of an assisted draft tower. Compared with the usual design, the trailing edges of the louvers are slightly extended to ensure a close approach to axial flow at the fan entry.

The relative merits of different cooling towers and fill arrangements are outlined by Lefevre [77LE1].

In view of environmental considerations, cooling towers incorporating ducts that introduce desulphurized flue gas into the plume for better dispersion are operational at a number of power plants. An example of such a system is shown in schematically in figure 1.1.8 [88PE1].

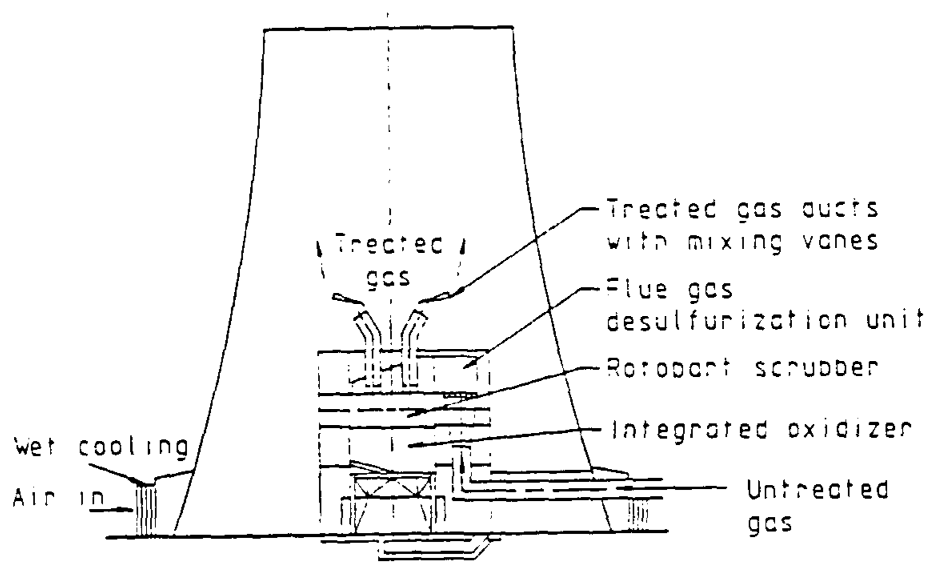

Figure 1.1.8: Crossflow cooling tower with flue gas desulphurization unit.

In a modern fossil-fuelled power plant equipped with a wet-cooling system, an average of between 1.6 and 2.5 liters of cooling water typically will be required for cooling per kWh of net generation. Thus, a 600 MW(e) coal-fired plant operating at 70 percent annual capacity factor typically would require between 5 x 10^6 m^3 and 10 x 10^6 m^3 of make-up water annually to replace cooling tower evaporation losses alone. In addition, a portion of the circulating cooling water must be systematically discharged as blowdown in order to limit the buildup of dissolved solids in the circulating water. A small amount of cooling water also will be lost as drift, i.e., the carryover of entrained water droplets by the air passing through and out of the tower. For conventional wet-cooling towers operating in non-zero discharge plants, blowdown and drift losses combined typically will range from about 20 percent to 50 percent of evaporative losses, corresponding to from 6 cycles to 3 cycles of concentration of dissolved solids in the circulating water. A cycle of concentration is the ratio of dissolved solids in the circulating water to that of the make-up water. Blowdown will account for essentially all of these losses since drift losses should preferably be less than 0.01 percent of the circulating water flow rate in a well-designed tower [87PE1]. On this basis, total wet-cooling system make-up water requirements for the 600 MW(e) coal-fired plant used in this example could exceed 11 x 10^6 m^3 per year with a waste stream averaging nearly 10000 m^3 per day requiring disposal if low quality make up water is used. Figure 1.1.9 shows three natural draft counterflow cooling towers each connected to the condenser of a 600 MW(e) turbine.

Figure 1.1.9: Natural draft counterflow cooling towers.

Nuclear generating units typically reject 45 percent to 50 percent more heat to the condenser cooling water per kWh of net generation than fossil-fuelled units. The heat rejection per kWh of net generation from geothermal power plants typically will be four or more times as great as from fossil-fuelled plants. Wet-cooling system make up water requirements and blowdown, therefore, will be correspondingly greater for nuclear and geothermal power plants, while makeup water requirements and blowdown for combined cycle power plants, in which only about one third of the total electrical output is generated in the steam cycle, generally will be less than one half of those for conventional fossil-fuelled plants of comparable size.

If the water supply used to provide make up is variable, a storage reservoir may be required in order to ensure that an adequate supply is available at all times. Evaporation and seepage losses from such a reservoir can add as much as 20 percent to overall make up water requirements.

In the past, water costs generally have been a very small component of total busbar energy production costs. With municipalities and developers seeking to acquire water rights to meet anticipated growth and future needs, water costs have increased dramatically in some areas. When other increased costs associated with the use of water for power plant cooling such as pumping costs, water treatment costs, blowdown disposal costs, and environmental study and permit acquisition costs are added in, water related costs become more significant. Restrictive legislation which could establish water use priorities unfavorable to utilities or chemical plants, is potentially, of even greater consequence to industry than rising water costs.

The currently available options for reducing or eliminating plant cooling system make up requirements and waste water include the use of wet-cooling systems designed to operate with high cycles of concentrating dissolved solids in the circulating water, the use of various types of dry-cooling systems which make no consumptive use of water, and the use of various types of cooling tower systems which combine dry- and wet-cooling technology.

General studies to determine the comparative economics of alternative heat rejection systems should not fail to consider all of the potential advantages offered by the use of water conserving systems. For example, dry-cooled or dry/wet-cooled plants need not be located at the same site as the base case wet-cooled plant with which they are being compared and should take into account the siting flexibility afforded by the use of the water conserving systems. Fuel cost savings resulting from locating a coal-fired plant at the mine mouth where there may not be enough water available to permit the use of wet-cooling could be substantially greater than the accompanying increase in transmission costs. Further, the use of a water conserving heat rejection system could permit expansion of existing generating facilities at a site without sufficient water to serve additional wet-cooled capacity, thereby taking advantage of existing support and service facilities and rights-of-way. Even with an adequate water supply at a given site, the use of a water conserving system could, in some cases, reduce indirect project costs and lead times by reducing environmental study, public hearing, and permit requirements. Other factors, including the changes in micro climate, corrosion of equipment, piping and structural steel, emission of chemicals, poor visibility and freezing of ground or road surfaces located near cooling towers plumes as well as potential health hazards [86CR1] (legionnaires' disease) in poorly maintained systems, cannot be ignored in practice. The impact of all these factors on the comparative economics of alternative heat rejection systems will depend upon the unique circumstances of each particular application.

For the foreseeable future, wet-cooling towers are expected to remain the economical choice, in most cases, where an adequate supply of suitable make up water is available at a reasonable cost. Decreasing water availability and increasing water costs and more stringent environmental and water use and accessibility regulations will, however, make a water conserving heat rejection system a practical and economical choice for more power plant [77SU1] and other applications, especially if the effectiveness of such systems can be improved [80MC1].

1.2 AIR-COOLED HEAT EXCHANGERS

1.2.1 MECHANICAL DRAFT

Air-cooled finned tube heat exchangers also referred to as air coolers or mechanical draft dry-cooling towers (large air-cooled heat exchangers) are found in chemical plants, process industries and power plants throughout the world. While the performance of wet-cooling systems is primarily dependent on the ambient wetbulb temperature, the performance of air-cooled heat exchangers is determined by the drybulb temperature of the air which is higher than the wetbulb temperature and experiences more dramatic daily and seasonal changes. Although the capital cost of an air-cooled heat exchanger is usually higher than that of a water-cooled alternative (this need not always be the case) the cost of providing suitable cooling water and other running expenses may be such that the former is more cost effective over the projected life of the system. Other considerations are also of importance depending on the process or application [74MA1]. In arid areas where insufficient or no cooling water is available, air-cooled systems are the only effective method of heat rejection.

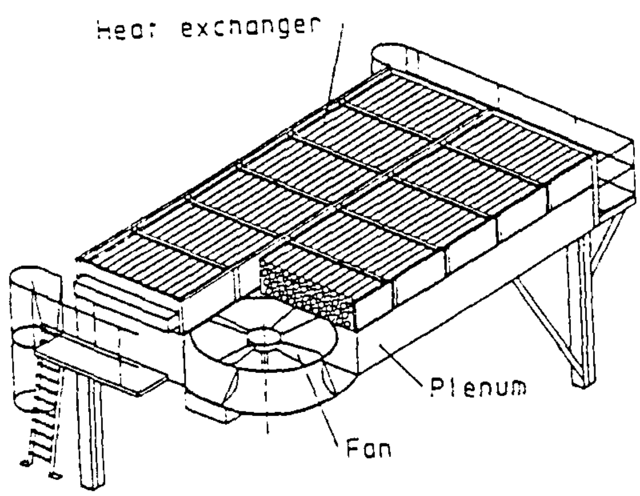

Figure 1.2.1: Forced draft air-cooled heat exchanger.

Various air-cooled heat exchanger configurations are found in practice. In some situations the choice of design is however critical to the proper operation of the plant. Air-cooled heat exchangers may be of the forced or induced draft type. In the case of the former the fans are installed in the cooler inlet air stream below the finned tube heat exchanger bundle as shown for a particular example in figure 1.2.1, with the result that the power consumption for a given air mass flow rate is less than that for the induced draft configuration. The fan drives located in the cooler airflow below the unit are also easier to maintain and the fans are not exposed to high temperatures, which makes the choice of construction material less critical.

Since the escape velocity of the air from the top of the bundle is low (2.5 m/s to 3.5 m/s) the unit is susceptible to hot plume air recirculation. This problem may be accentuated by the proximity of similar heat exchangers or other structures. Anti-recirculation fences or windwalls are often fitted in such cases. Generally the air flow distribution through the heat exchanger is not as uniform as for the induced draft installation. Since the heat exchanger is open to the atmosphere the performance can change measurably due to wind, rain, hail or solar radiation. Hail screens may be required to protect the finned surfaces.

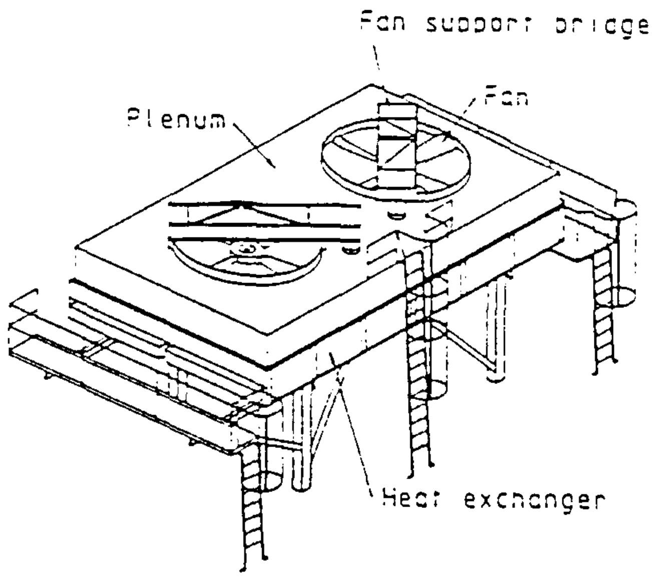

Figure 1.2.2: Induced draft air-cooled heat exchanger.

An induced draft system as shown schematically in figure 1.2.2 is less sensitive to changes in weather conditions. Generally the air flow distribution through the heat exchangers is more uniform than in a forced draft unit and because of the relatively high escape velocity of the air from the fan this type of system is less susceptible to crosswinds and plume recirculation. The usually higher fan power consumption for a given air mass flow rate and the fact that the fan and its drive system are exposed to the warm air stream, are disadvantages of this configuration.

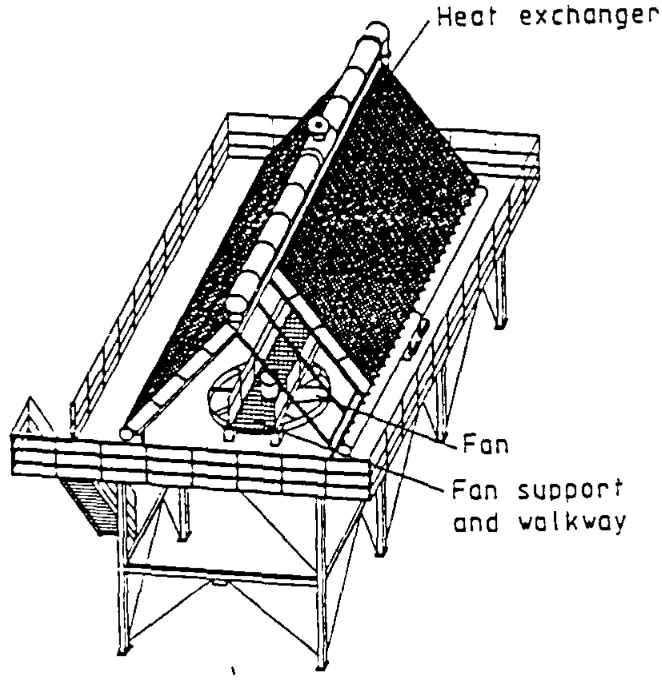

Figure 1.2.3: A-frame air-cooled condenser.

In large air-cooled condensers the finned tube bundles may be sloped at some angle up to 60° with the horizontal (A-frame) as shown in figure 1.2.3, in order to reduce plot area. This arrangement however generally has a higher air-side pressure drop.

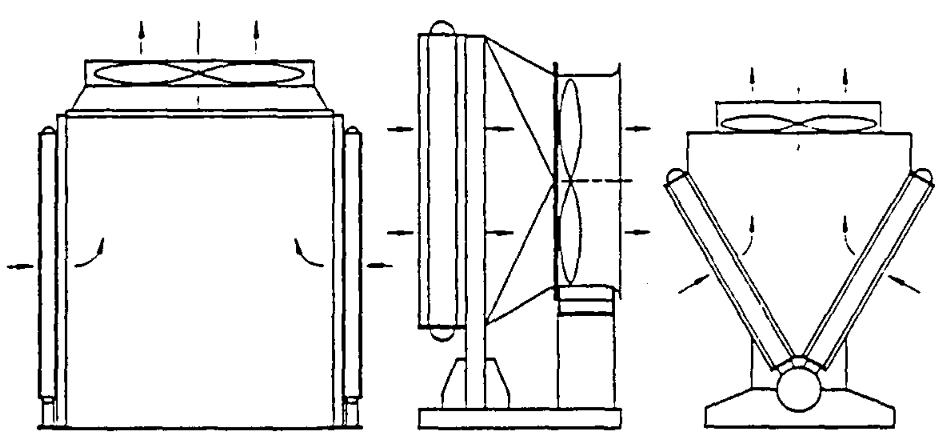

(a) Rectangular (b) Vertical (c) V-configuration

Figure 1.2.4: Air-cooled heat exchangers configurations.

For practical reasons other configurations as shown in figure 1.2.4 may be preferred. The rectangular arrangement (figure 1.2.4(a)) is very compact and finds application in closed circuit cooling plants while the vertical arrangement (figure 1.2.4(b)) is suitable for smaller plants. The V-configuration (figure 1.2.4(c)) is often used with counterflow condensers.

There are basically two types of air-cooled or dry-cooling systems that find application in power plants. In the so-called direct system, also sometimes referred to as the GEA system, the turbine exhaust steam is piped directly to the air-cooled finned tube condenser as shown in figure 1.2.5. The finned tubes are arranged in the form of an A-frame or delta to reduce the required land area. The steam exhaust pipe has a large diameter and is required to be as short as possible to minimize pressure losses. A forced or induced flow of cooling air through the finned tube bundles is created by axial flow fans.

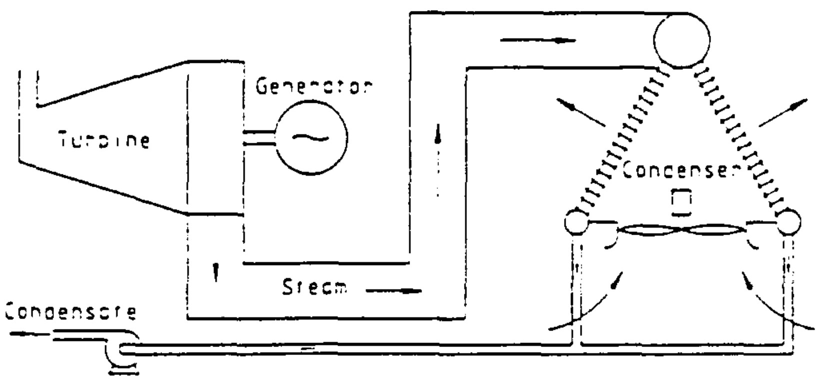

Figure 1.2.5: Direct air-cooled condensing system.

The application of the direct cooling system in small power generating units effectively became a reality in the 1930's, [41HA1, 71HE1].

In 1970 a 160 MW(e), direct dry-cooled power plant was commissioned at Utrillas/Teruel in Spain. This relatively arid area is located 1200 m above sea level. Exhaust steam leaves the turbine through two 3.5 m diameter pipes and is fed to heat exchanger bundles located above the turbine house as shown in figure 1.2.6 [72MA1].

The bundles consist of galvanized elliptical finned tubes arranged in a staggered pattern as shown in figure 1.2.7. Forty 5.6 m diameter axial flow fans with their drive units, are suspended form vibration proof bridges on the condenser platform below the A-frames.

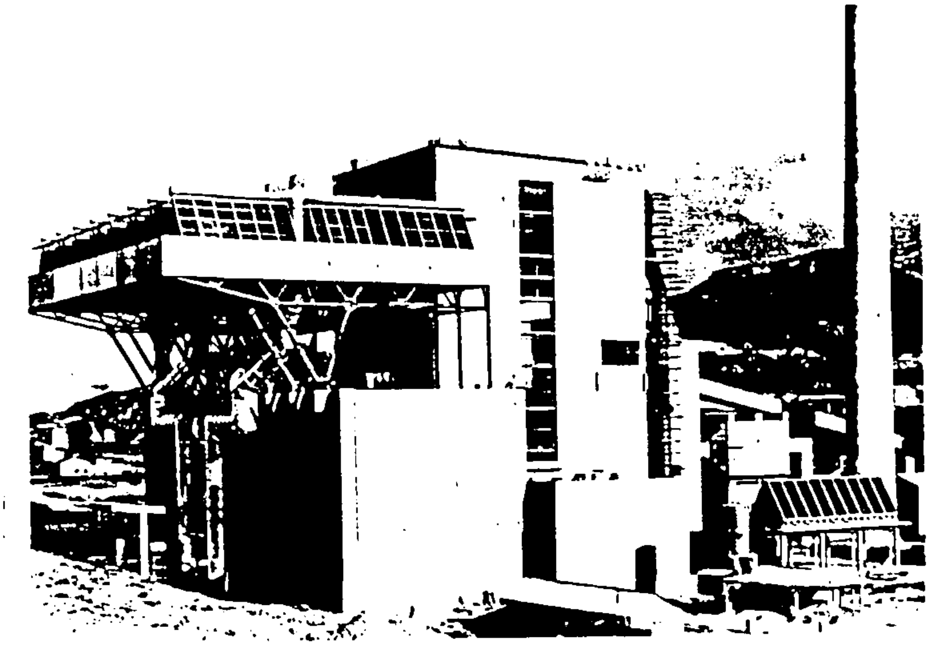

Figure 1.2.6: Utrillas power plant, Spain.

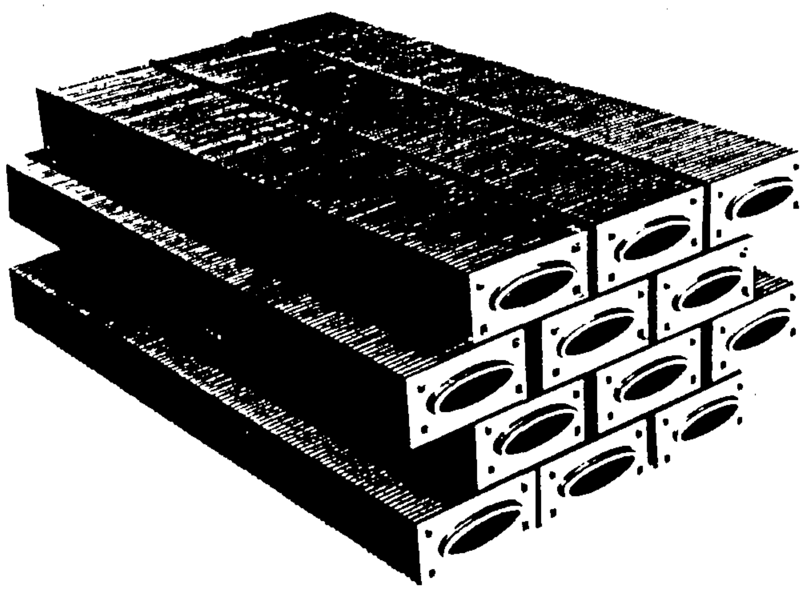

Figure 1.2.7: Galvanized elliptical finned tubes.

The 365 MW(e) Wyodak power plant near Gillette, Wyoming in the USA, was for many years the largest direct air-cooled plant in operation.

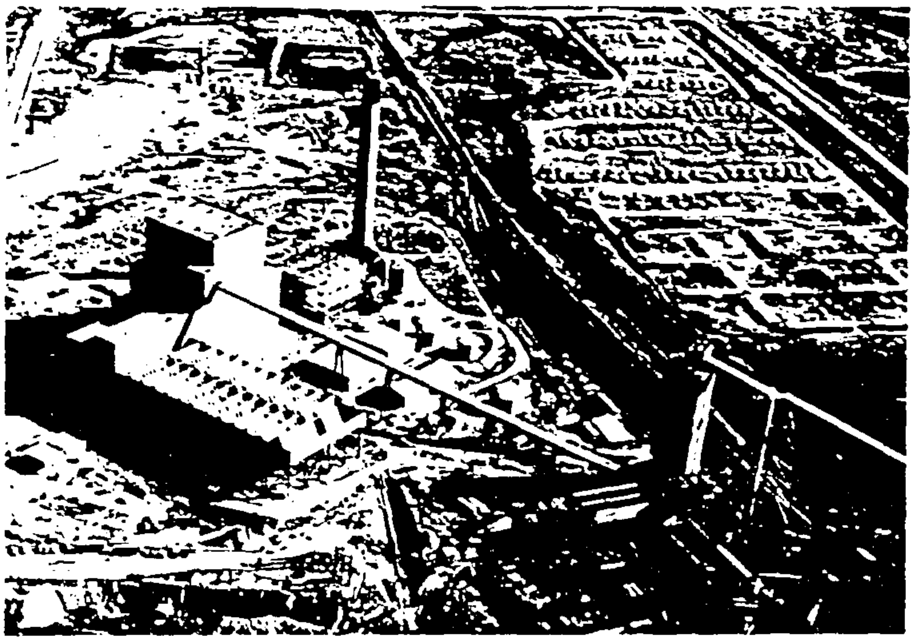

Figure 1.2.8(a): Wyodak power plant, USA.

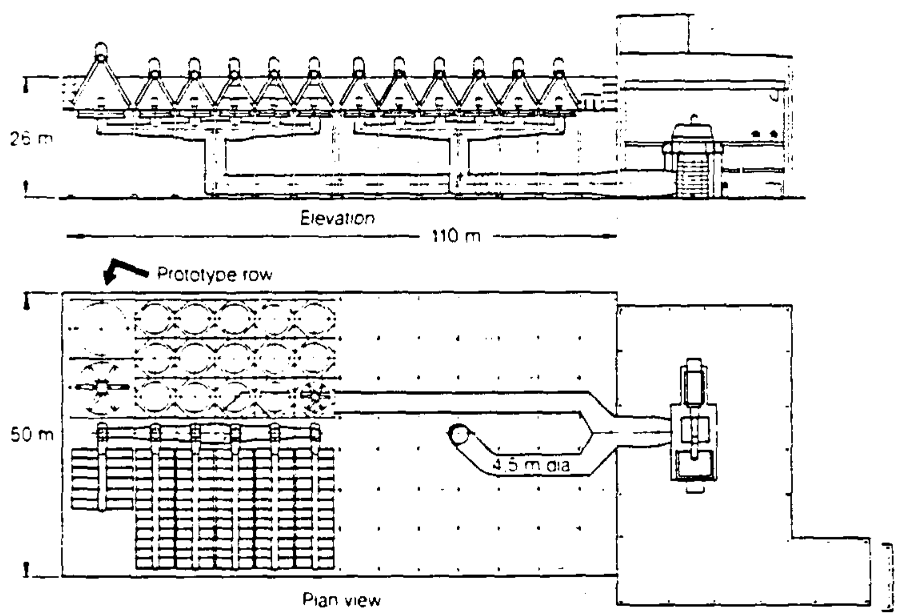

Figure 1.2.8(b): Schematic of Wyodak air-cooled condenser.

The plant is located in an arid coal-rich area 1240 m above sea level where extreme climatic conditions are experienced (–40°C to 43°C). The plant shown in figure 1.2.8 became operational in 1978. Details of its dimensions, operation and performance are reported by Schulenberg [77SC1] and Kosten et al [81KO1].

natural draft wet-cooling towers.

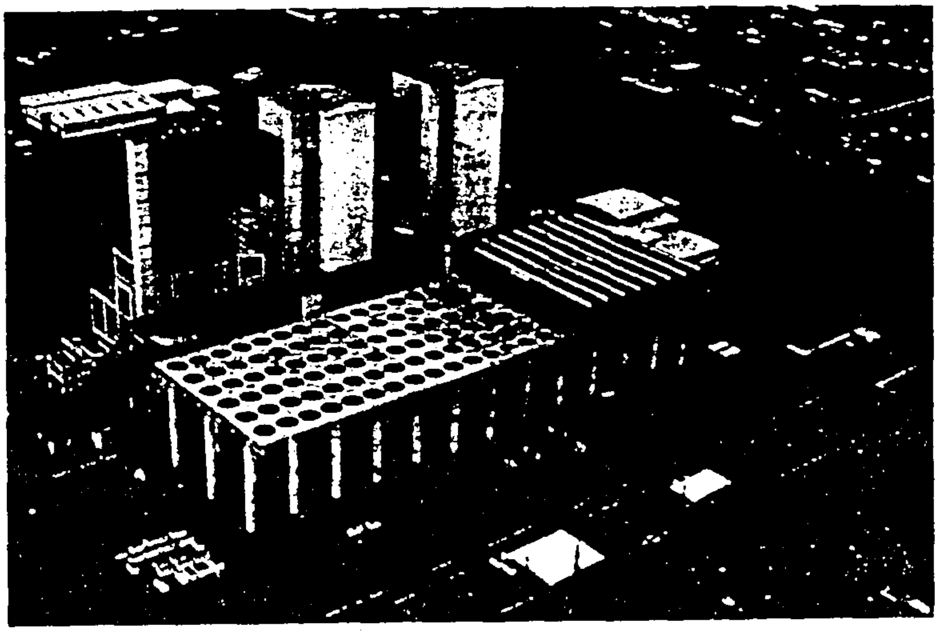

Figure 1.2.10: Majuba power plant, South Africa.

In other modern air-cooled condensers increasing attention is being given to the reduction of noise levels [93ST1, 93SM1].

1.2.2 NATURAL DRAFT

A schematic drawing of an indirect dry-cooling tower incorporating a direct contact spray condenser is shown in figure 1.2.11. Recooled water from the cooling tower is introduced into the condenser via nozzles, such that the turbine exhaust steam condenses directly on the droplets or water jet [74BU1, 91MI1]. A part of the condensate is returned to the boiler but most is pumped, at a positive gauge pressure, to finned tube heat exchangers located at the base of a natural draft cooling tower. The recooled water returns to the condenser via an energy recovery turbine, through which its pressure drops to below ambient conditions. This particular layout is also referred to as the Heller system, after the Hungarian engineer who originally proposed the concept [50HE1, 91SZ1].

The Heller system has found application at numerous power plants throughout the world. In 1962, a 120 MW(e) turbine rejecting 169 MW heat through a hyperbolic concrete natural draft dry-cooling tower, was commissioned at the Rugeley power plant in Great

In 1987 the 4 x 150 MW(e) Touss direct air-cooled plant was commissioned in Iran.

Presently the world's largest direct air-cooled power plant, Matimba, became fully operational in 1991 at Ellisras in the Republic of South Africa [84VO1, 87KN1, 90KN1, 91KN1]. Large reserves of coal justified the erection of a dry-cooled plant in this relatively arid part of the country. A photo of the 6 x 665 MW(e) plant is shown in figure 1.2.9.

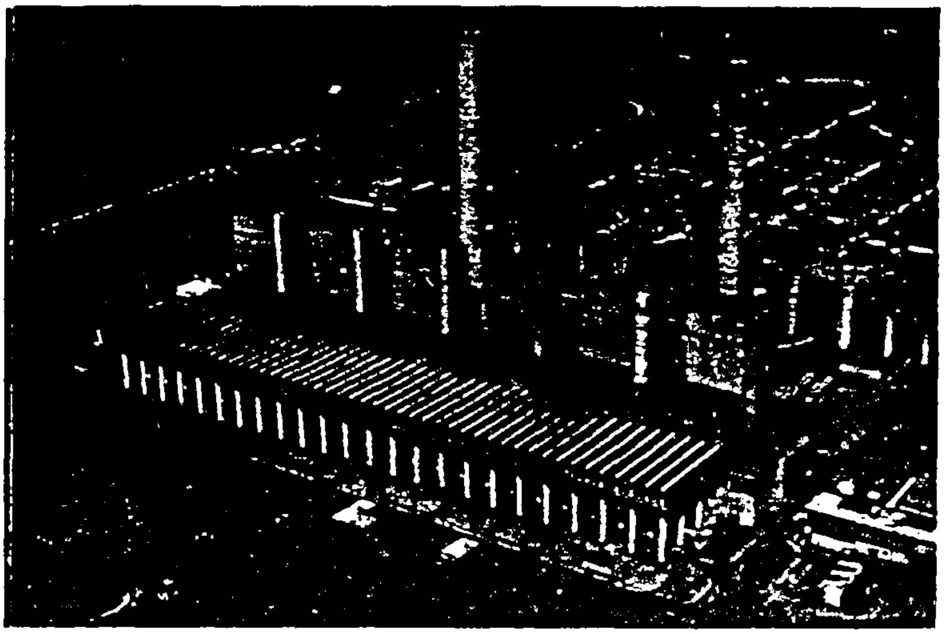

Figure 1.2.9: Matimba power plant, South Africa.

The air-cooled condenser consists of 384 heat exchanger bundles per unit, each 3 m wide and 9.6 m long, made up of two rows of galvanized plate finned elliptical tubes as shown schematically in figure 5.1.1 (4), and arranged in the A-frame configuration with an apex angle of 56°. Air is forced through the bundles by 48 axial flow fans per unit, each 9.1 m in diameter, located underneath the bundles and about 45 m above ground level. Each fan is driven by a 270 KW electric motor through a bevel spur gearbox. Each condenser unit covers a plot area of 72 m x 85 m. A total of 905 MW heat is rejected per condenser unit at a turbine outlet pressure of 17.9 x 10^3 N/m^2 and an ambient air temperature of 18°C and a pressure of 91.33 x 10^3 N/m^2.

A system similar to that of the Matimba air-cooled condenser is also employed in three of the six 665 MW(e) units at the Majuba power plant in the Eastern Transvaal, South Africa. As shown in figure 1.2.10, cooling for the remaining three turbines is provided by

Britain. An aerial view of the tower is shown in figure 1.2.12. Note the size of the tower and the relatively high inlet compared to the wet counterflow cooling towers [69CH1].

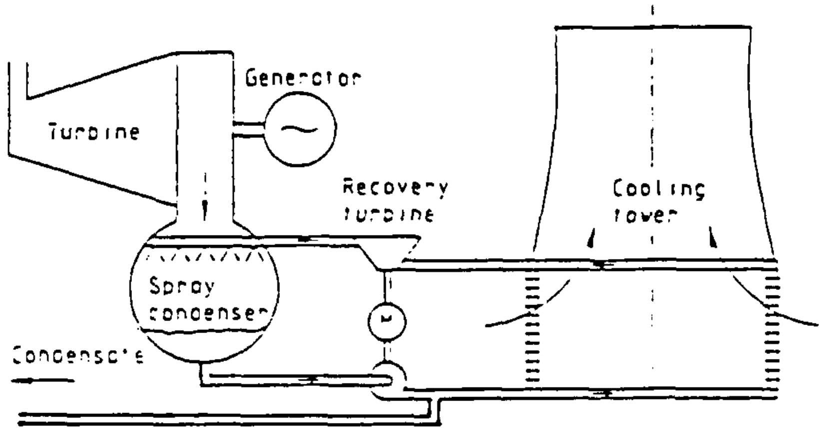

Figure 1.2.11: Indirect dry-cooling system.

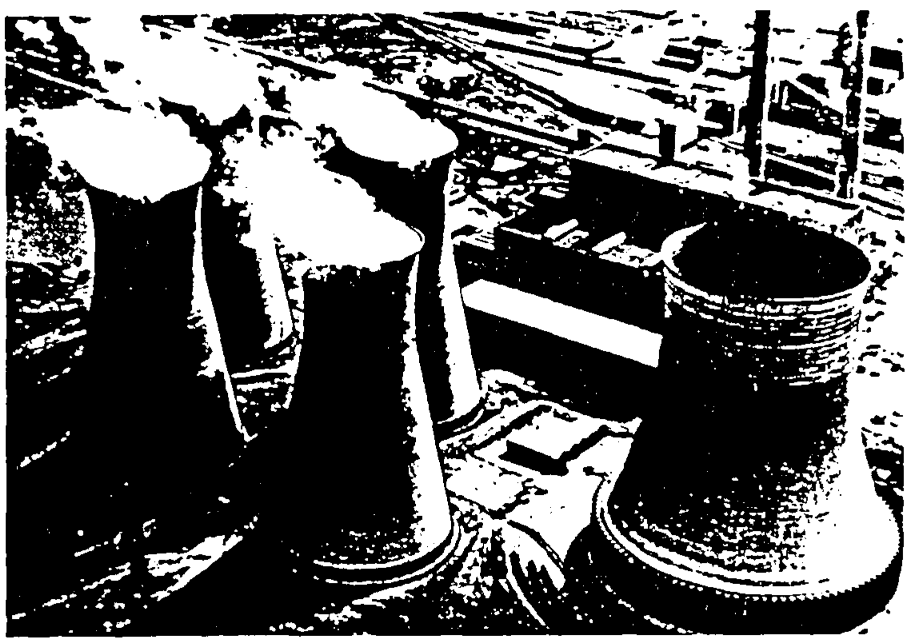

Figure 1.2.12: Rugeley power plant, Great Britain.

A similar design was commissioned in 1967 at the Ibbenbüren power station in the Federal Republic of Germany, where a 150 MW(e) turbine had been installed [69SC1].

During the period 1969 - 1972 a total of 2 x 100 MW(e) and 2 x 220 MW(e) generating capacity was installed at the Gagarin power station at Gyöngyös (Visonta) in Hungary.

In the natural draft towers at this plant, the heat exchanger deltas were in all cases arranged vertically around the base of the tower, to maximize the air-side surface area. Since the bundles are self-supporting, water distribution is relatively simple and installation is straightforward, as shown in figure 1.2.13, resulting in reduced cost when compared with other layouts. Each delta is approximately 15 m in length and consists of slotted aluminum plate finned tubes as shown in figure 1.2.14(a).

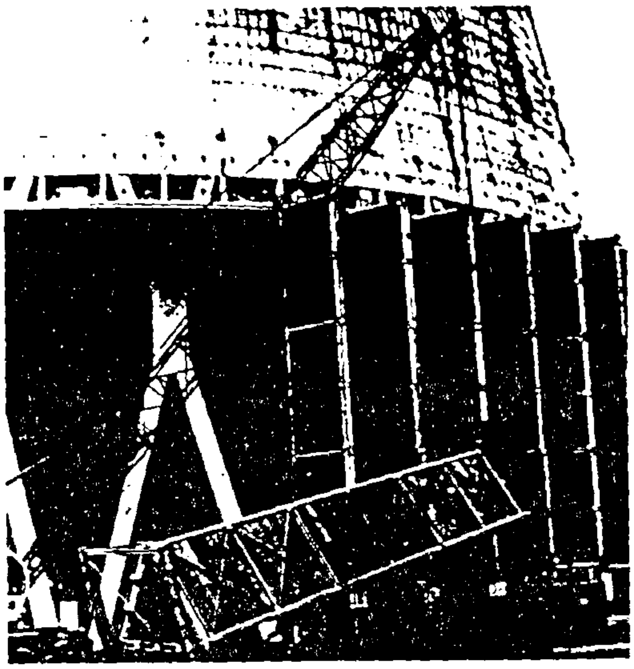

Figure 1.2.13: Installing a heat exchanger

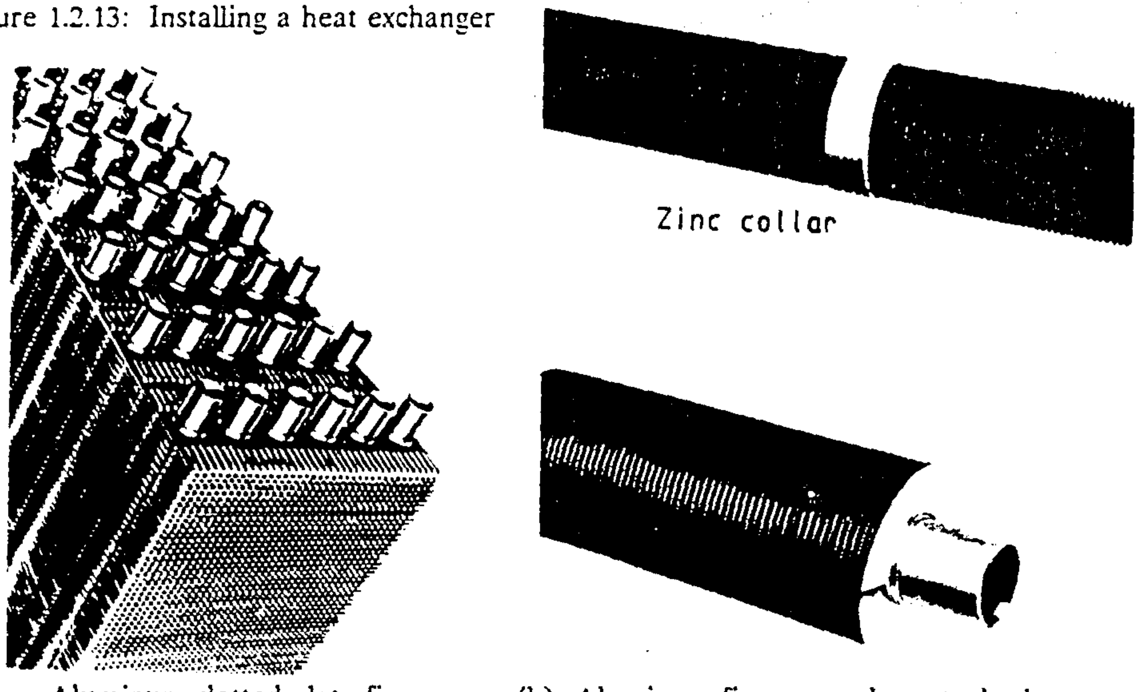

(a) Aluminum slotted plate fin (b) Aluminum fin wrapped on steel tube

Figure 1.2.14: Finned tubes.

Measurements at the Rugeley and at other similar towers, indicate that this bundle arrangement tends to be relatively sensitive to winds, resulting in a reduction in cooling capacity. Alternative arrangements as shown in figure 1.2.15 were subsequently considered with a view to reducing the sensitivity to wind.

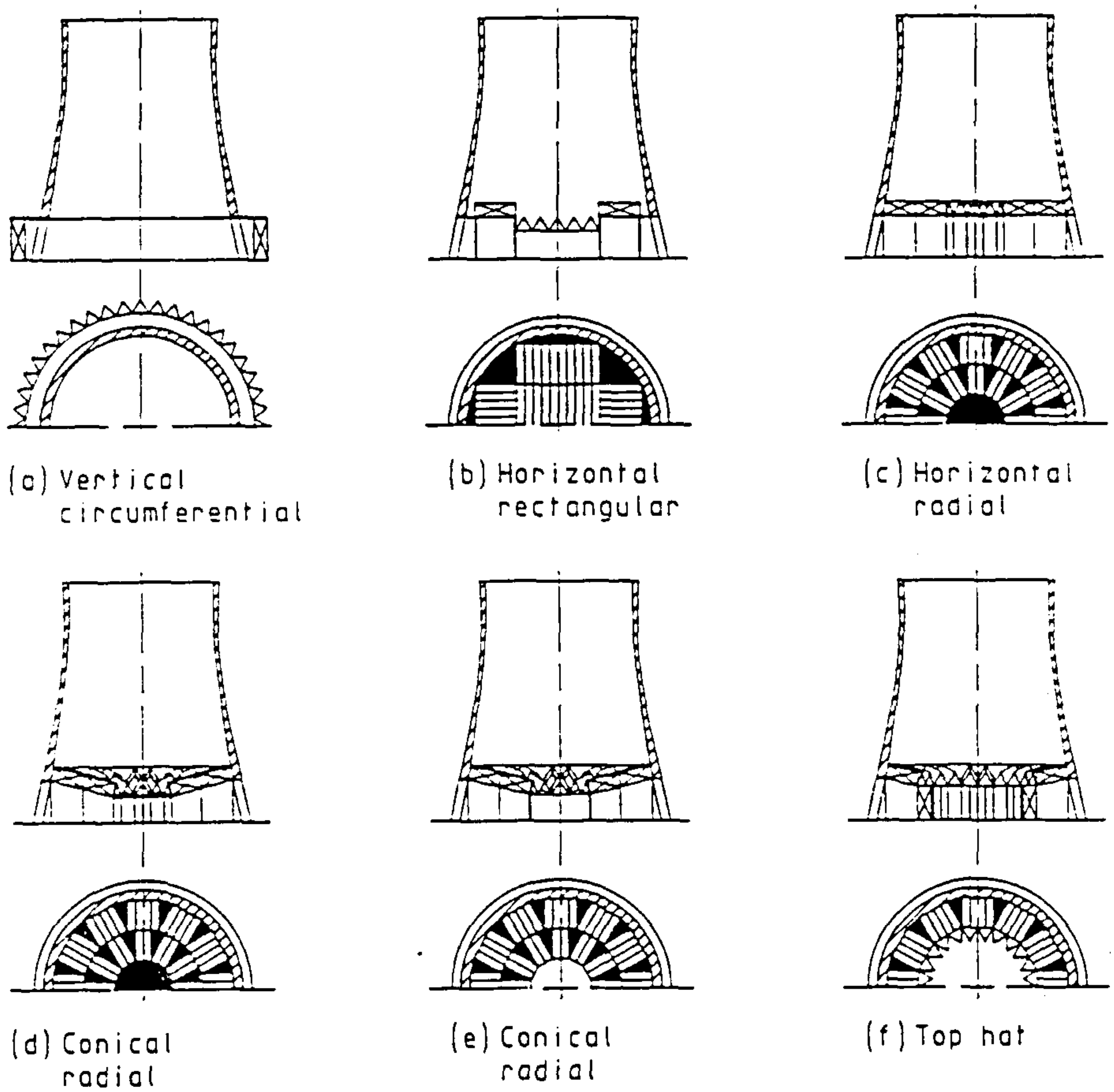

Figure 1.2.15: Heat exchanger bundle arrangements.

The cooling tower which was erected at the Grootvlei power plant in the Republic of South Africa in 1971 has its heat exchanger deltas installed essentially horizontally at two different levels in the inlet cross-section of the tower a shown in figure 1.2.15(b). The heat transfer surface in the Grootvlei tower (Grootvlei 5) consists of galvanized steel tubes onto which an aluminum fin is tension wound as shown in figure 1.2.14(b). Regularly spaced zinc collars prevent fins from unwinding. Details of the system are given by van der Walt et al [74VA1].

During the period 1971 - 1974 four dry-cooling towers, as shown in figure 1.2.16, were constructed at the Razdan power plant in Armenia, to cool 2 x 210 MW(e) and 2 x 200 MW(e) turbines. The towers have welded steel frames covered with corrugated aluminum sheets. This type of construction was utilized due to earthquake hazards in the region. The towers are 120 m high and have an outlet diameter of 60 m. Heller-type finned tube bundles 15 m high are located around the periphery at the base of the towers. Motor operated louvers mounted before the deltas protect the finned surfaces and allow the airflow to be controlled.

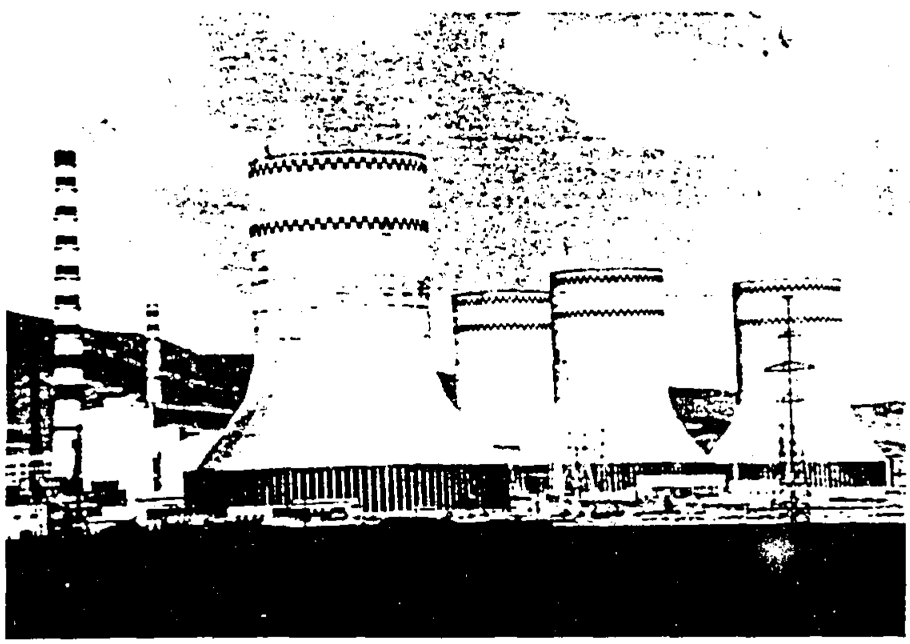

Figure 1.2.16: Dry-cooling towers at the Razdan power plant, Armenia.

Other more recent Heller systems include the 8 x 250 MW(e) Shahid Rajai power plant in Iran, the 2 x 200 MW(e) Datong power plant in China and the 2x200 MW(e) Teschrin plant which commenced operation in 1993 [94SP1].

In some indirect cooling systems, a conventional surface condenser is employed instead of the spray condenser. Due to the additional barrier offered by the surface condenser, thereby reducing radiations hazards, this is the only system that is likely to be considered where dry-cooling of a nuclear plant is required.

An indirect cooling system incorporating a surface condenser to cool a 200 MW(e) turbine was commissioned at the Grootvlei power plant in South-Africa in 1978 (Grootvlei 6). The heat exchanger bundles, consisting of staggered steel tubes with wrapped on aluminum fins similar to those at Grootvlei 5, are arranged essentially horizontally in a radial pattern, as shown in figure 1.2.15(c), in the inlet cross-section of the 120 m high concrete tower.

Another variation in heat exchanger layout is found at the 134 m high Candiota cooling tower in Brazil which has bundles made up of plate finned elliptical tubes arranged as shown in figure 1.2.15(e), with an ineffective cylindrical section in its center.

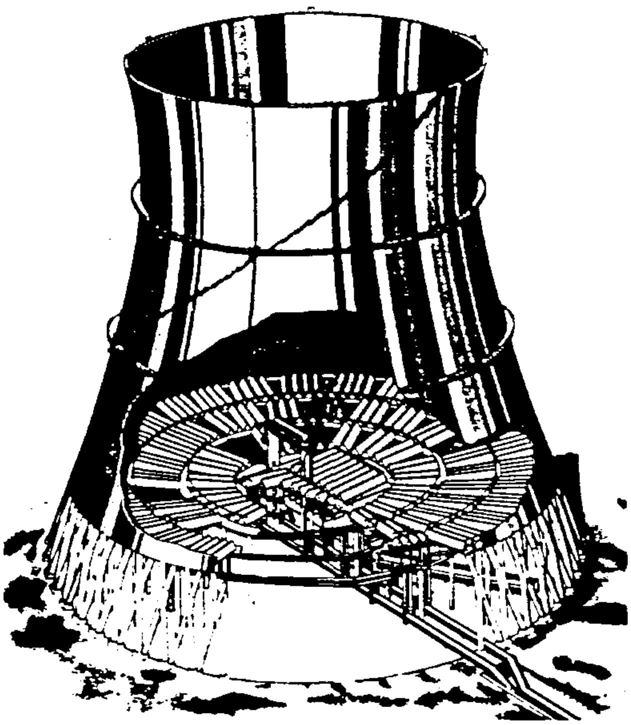

Figure 1.2.17: Kendal cooling tower, South Africa.

The Kendal power plant in the Republic of South Africa is the largest indirect dry-cooled plant in the world and has a total of 6 x 686 MW(e) turbines [87TR1, 89TR1, 90TR1]. The six hyperbolic concrete natural draft cooling towers are each 165m high with a base diameter of 163m and each tower is equipped with 500 heat exchanger bundles arranged in concentric circles at the base of the tower as shown in figure 1.2.17. The helically wound galvanized elliptical finned tubes as shown in figure 4.1.1(3), have a total length of approximately 2000 km per tower. The circuit includes a conventional surface condenser.

Compared to a wet cooling system, approximately 50×10^6 m^3 water is saved annually.

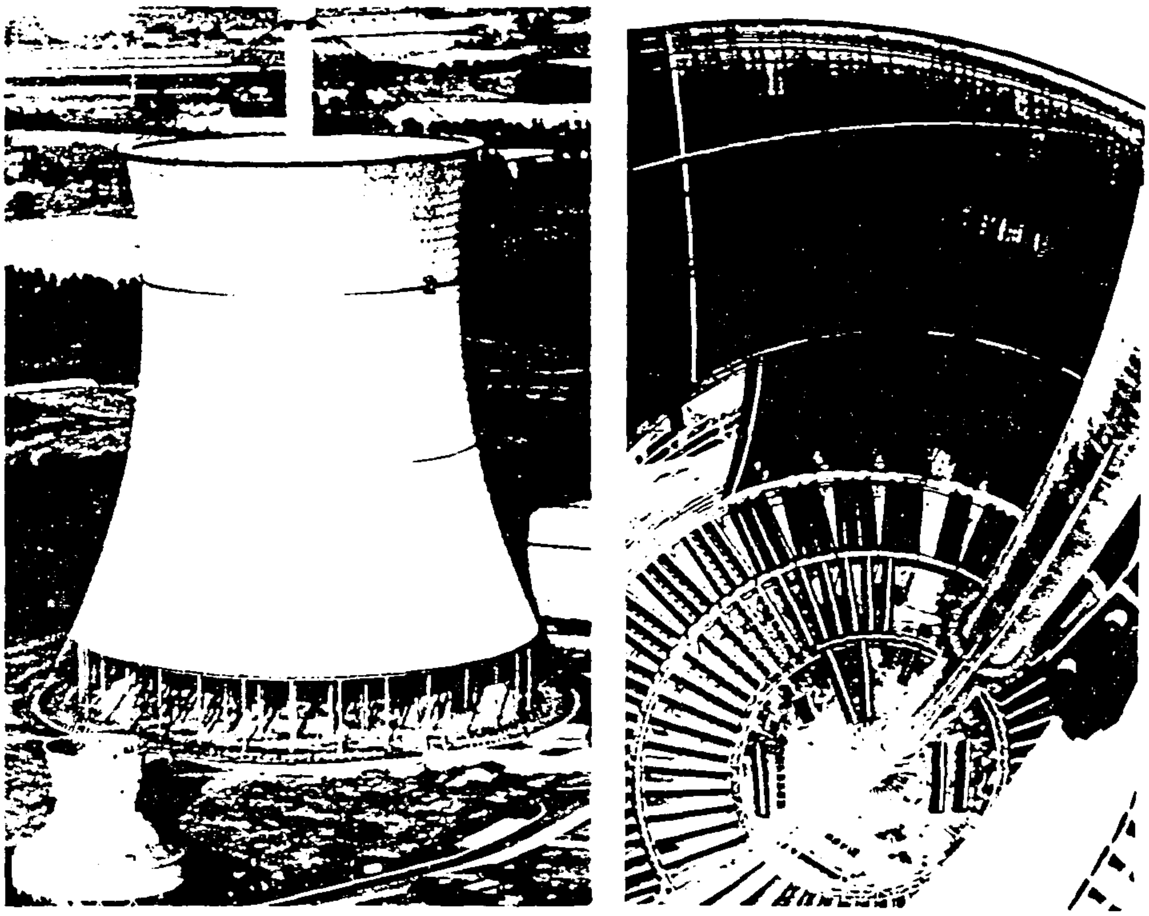

(a) Cable tower (b) Radial heat exchanger layout

Figure 1.2.18: Schmehausen cooling tower, Fed. Rep. Germany.

A novel cable tower was erected to serve the 300 MW(e) turbine at the Schmehausen nuclear plant in Germany. Figure 1.2.18 show the cable cooling tower shell, supported by a reinforced concrete pylon 180 m high. The cable net which is covered by aluminum sheets is held in position by two rings supported by the pylon. The heat exchanger bundles are arranged in a radial pattern on three concentric rings in the inlet cross-sectional area to the tower. Each bundle is 15 m long and consists of galvanized elliptical finned tubes [73HI1, 78VO1].

1.3 DRY/WET AND WET/DRY COOLING SYSTEMS

Dry/wet cooling systems have been developed to save water in arid regions, while avoiding the high cost of fully dry-cooling systems, and to ensure relatively low process fluid temperatures where necessary.

An excessive rise in cooling water temperature during periods of peak ambient temperature and demand, will result in a loss of efficiency of a turbogenerator set. In such a case, the dry section of the system may be sized to reject the total heat load at a low ambient temperature while maintaining the turbine back pressure within specified limits. The heat-rejection capacity of the dry section at the peak ambient temperature is then determined. The difference between the heat dissipation capacity required in order not to exceed the specified turbine back pressure and the dry section capacity at peak ambient temperature is the required capacity of the wet section of the cooling system [78EN1, 78LA1]. Another way of sizing wet sections of a dry/wet cooling system may be by limiting the quantity of make-up water according to the local water availability.

Wet/dry cooling systems designed primarily for plume abatement are essentially wet systems with just enough dry-cooling added to reduce the relative humidity of the combined effluent from the wet and dry section below the point where a visible plume will form under cool, high relative humidity ambient conditions [84ER1, 86AL1]. When a single cooling tower incorporates a wet and a dry section this is also sometimes referred to as a hybrid system. Hybrid systems may however also consist of other combinations e.g. an evaporative condenser that is built into a wet-cooling tower [83FI1].

By combining features of an air-cooled heat exchanger and a wet-cooling tower it is possible to create a hybrid evaporative cooler which may offer reduced operating costs for particular duties.

As illustrated schematically in figure 1.3.1, the evaporative cooler in conventional form may be regarded as a cooling tower in which the packing is replaced by a bank of corrosion resistant smooth or finned tubes carrying the process fluid. Air is drawn through the tubes while water falls over the tubes. Some water is lost by evaporation while the remainder falls into a sump from which it is recirculated. The loss of water by evaporation is about the same as from a cooling tower having the same duty, but of course the secondary circulation loop through a heat exchanger with its additional resistance to heat transfer is eliminated. If a bank of finned tubes is used in an evaporative cooler it may be possible to reduce the annual water consumption by operating the unit dry during winter months when the ambient temperature is low.

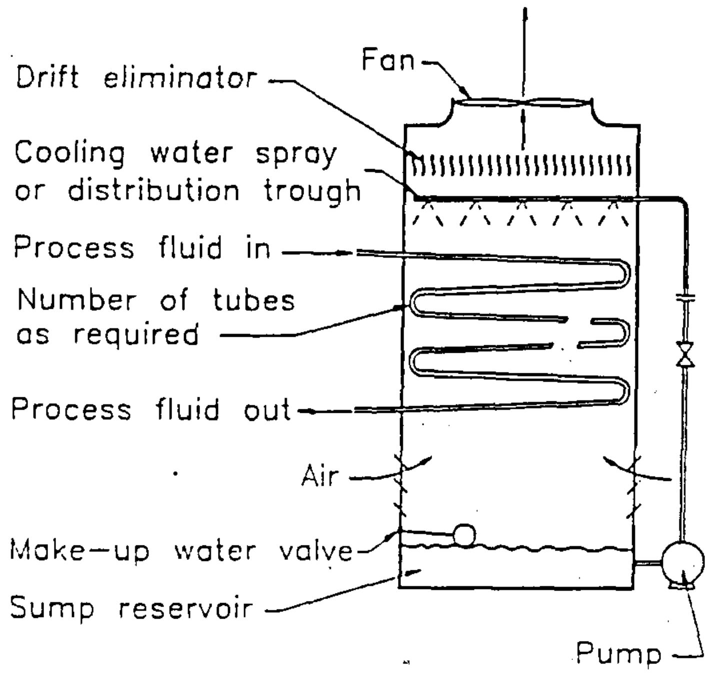

Figure 1.3.1: Evaporative cooler.

There are potentially other ways of combining dry and wet-cooling in a single heat rejection system [76VO1, 88NO1, 89MI1]. These include deluge enhancement, combinations of dry and wet-cooling units and by precooling the entering air by humidification.

In the case of the former, the performance of a dry-cooled system is enhanced during periods of high ambient temperature and/or high cooling demand by deluging the airside of the heat transfer surface with water. The air flowing over the deluged film of water causes evaporation and thus lowers the air/water interface temperature. The resultant increase in temperature difference between the internal hot fluid and the external deluge film substantially increases the rate of heat transfer. It is found that the rate of heat transfer can be increased by a factor of up to five by deluging the air-side surface of the heat exchangers, in comparison with a dry-cooled system at equivalent temperature and air-side pressure drop conditions. A concept which incorporates this form of cooling is the Heller/EGI Advanced Dry/deluged (HEADd) combined cooling system which is basically the indirect dry-cooling system shown schematically in figure 1.2.11, but in addition includes auxiliary and preheater/peak dry/wet cooling units [86BO1, 88BO1].

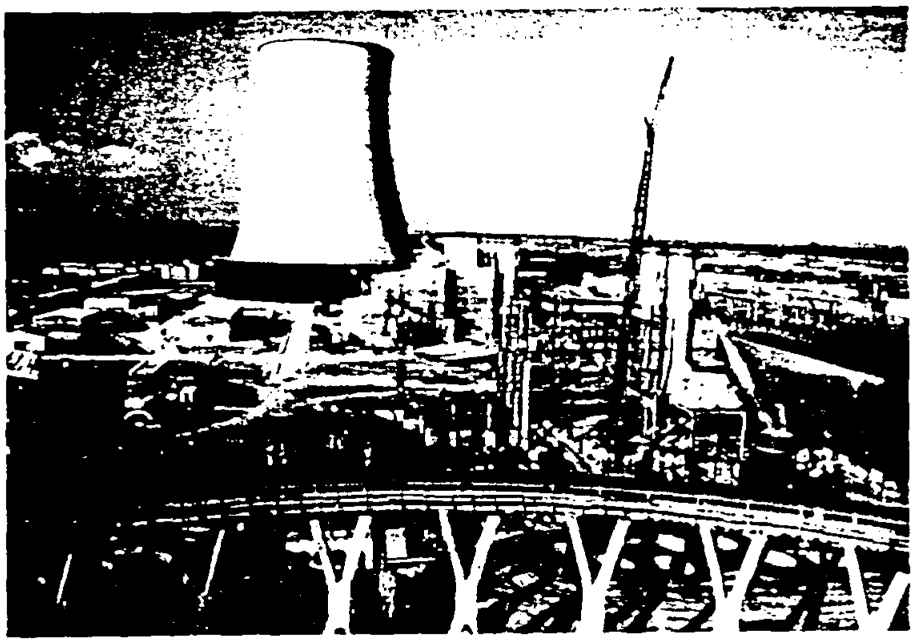

Figure 1.3.2: Trakya cooling towers with power plant on right.

A good example of this type of system is found at the 1200 MW(e) combined cycle, Trakya power station in Turkey, which consists of two 600 MW(e) plants as shown in figure 1.3.2 [91JA1]. Each plant has two identical units consisting of two 2 x 100 MW(e) gas turbine sets connected to separate heat recovery steam generating boilers, each of which is connected to a 100 MW(e) steam turbine. Cooling water from the cooling tower is injected into direct contact spray condensers to condense steam from the double exhaust turbines. The mixed cooling water and condensate is then extracted from the bottom (hot-well) of each condenser by two 50 percent duty circulating water pumps.

About 3 percent of this flow, which corresponds to the amount of steam condensed, is fed to the boiler feed water system by condensate booster pumps, while the remaining water is returned to the natural draft cooling tower. The concrete cooling tower is 135 m high with a diameter at the base of 121.6m. Self-supporting 20m high aluminum heat exchanger bundles are arranged in a delta configuration with an apex angle of 50° around the tower base circumference. The air flow through the louvers can be controlled by electrically adjustable louvers.

In addition to the vertical cooling deltas consisting of a modified version of Forgo-type perforated plate-fin MBV treated aluminum surfaces as shown in figure 5.1.9, the cooling system incorporates mechanical draft dry/wet preheater/peak coolers located inside the tower and auxiliary dry/wet coolers outside the tower.

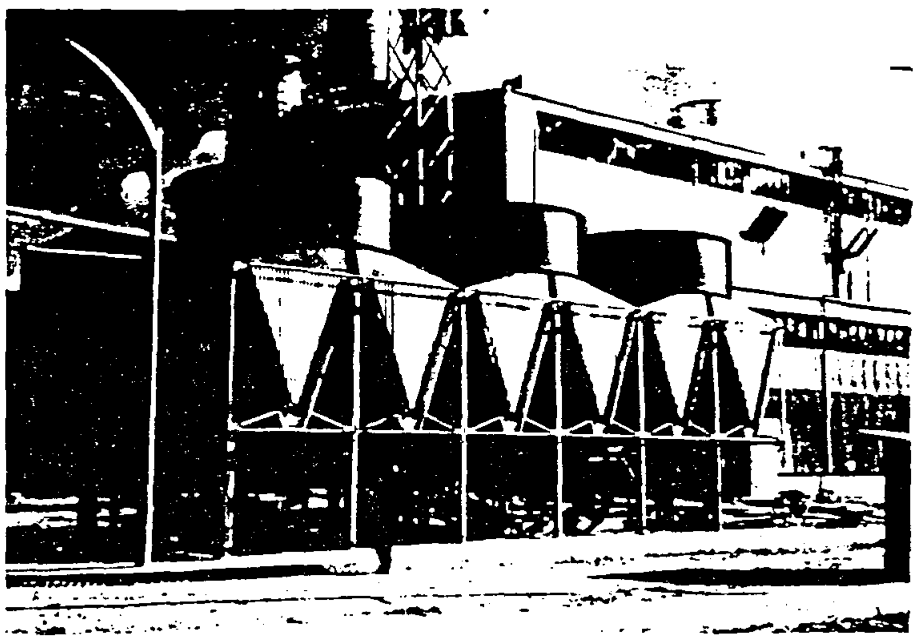

Figure 1.3.3: Mechanical draft dry/wet auxiliary cooler.

The auxiliary dry/wet cooling cells as shown in figure 1.3.3, are required to ensure that effective cooling is maintained even during the hottest peak load periods. These coolers consist of heat exchanger bundles arranged in a V-configuration below an axial flow fan.

The heat exchanger bundles are also made up of Forgo-type perforated plate-fin MBV treated aluminum surfaces, similar to those employed in the dry-cooling deltas, except that the tubes run in the horizontal direction. With a V-inclined angle of approximately 50°, it is found that the plate fins are covered with a fairly thin uniform film of water when deluged from above, along the upper edge of the bundles. The water is collected in trays at the bottom of the "V" from where it is recirculated by deluging pumps, and make-up water is added as required.

Deluge water may be obtained from the main cooling water circuit. Because of the high quality (boilerfeed quality) of this water, it is expensive. Other pretreated water may be considered if regular flushing with circuit water is ensured, to avoid fouling or scaling.

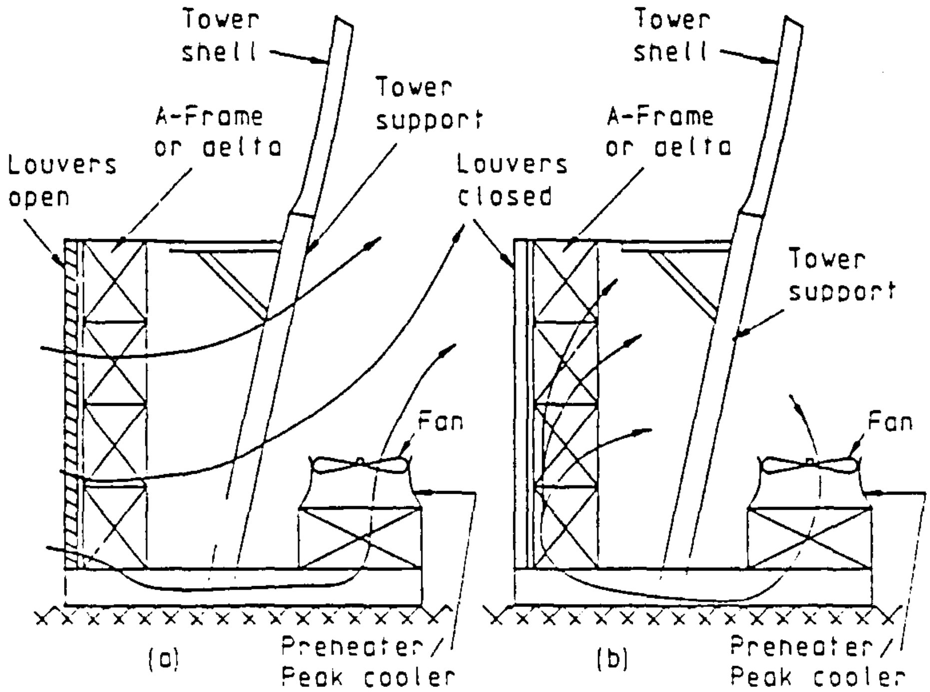

Figure 1.3.4: Preheater/peak coolers inside cooling tower.

Preheater/peak coolers similar to the auxiliary coolers, are installed inside the cooling tower as shown in figure 1.3.4. These water-to-air heat exchangers are also made up of V-bundles consisting of Forgo-type perforated plate-fin MBV treated aluminum surfaces.

The preheater/peak coolers which have an effective area of 5 per cent of the total heat transfer surface area, are connected in parallel with the main cooling deltas and normally operate in the natural draft mode. During the hottest peak periods they enhance the cooling capacity by being deluged with condensate quality water and by operating in an induced mechanical draft mode as shown in figure 1.3.4(a).

During start-up of the cooling plant in cold winter periods, these coolers are used to preheat the cooling deltas before filling. During this operation the rotation of the fan is reversed and the cooling delta louvers are closed as shown in figure 1.3.4(b).

The water flow rate in the preheater/peak coolers is controlled, depending on its mode of operation. During the preheating and deluged peak cooling periods high flow rates are maintained, but this is reduced during normal operation.

Measurements show that a flow of approximately 60 m^3/h deluging water will increase the output of the 100 MW(e) unit by more than 2 MW(e) compared to completely dry operation for an ambient temperature of 38°C. The circuiting in the cooling tower is such that when one of the steam turbines is not in operation, the entire tower is available for cooling the second turbine.

The external surfaces of the vertical cooling deltas can be periodically cleaned by pressurized water jets installed on a 20 m high water distributer which moves on rails along the tower perimeter.

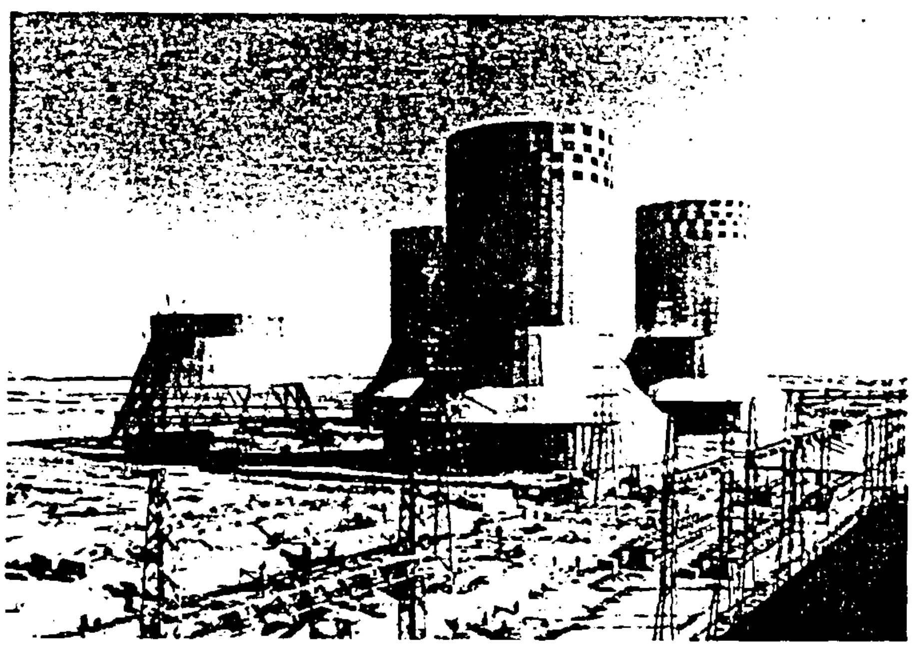

Figure 1.3.5: Isfahan cooling towers during construction, Iran.

Deluge cooling is also incorporated in the cooling towers in the Isfahan power plant in Iran. The four aluminum clad, welded steel cooling towers as shown in figure 1.3.5 are similar to those at the Razdan plant [79KR1].

The dry/wet cooling system at the 500 MW(e) San Juan power plant in New Mexico consists of two induced draft cooling towers. Each tower consists of five cells, each cell containing sixteen air-cooled heat exchangers modules and two evaporative sections. Water in the towers flows in series through the dry heat exchanger to the wet sections, while the flow is in parallel through the dry and wet sections as shown in figure 1.3.6. At design conditions of a dry bulb temperature of 35°C and a wet bulb temperature of 18.9°C, approximately 27 percent of the heat load is discharged as sensible heat. However, at lower ambient temperatures, the wet sections can be bypassed for fully dry operation.

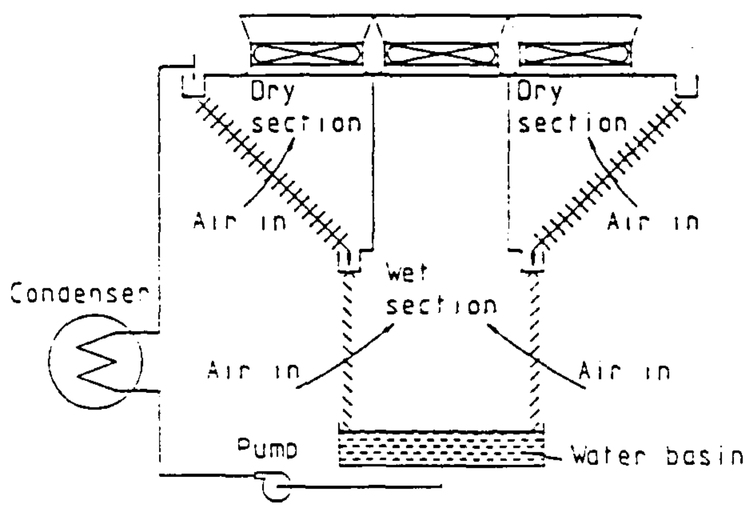

Figure 1.3.6: San Juan dry/wet cooling tower.

Dry/wet cooling using an ammonia phase-change system, designated the Advanced Concepts Test (ACT) was tested at Pacific Gas and Electric Company's Kern Station at Bakersfield.

The facility is capable of condensing approximately 7.5 kg/s of steam from a small house turbine. Details of the facility are given in a number of publications [81EP1, 87EP1].

In the ammonia heat transport system, the exhaust steam from the last stage of the turbine is condensed in a doubly heat-transfer-enhanced steam condenser/ammonia reboiler located directly below the turbine as shown schematically in figure 1.3.7.

Liquid ammonia is boiled as it is pumped through the tubes under a pressure set by the operating temperature in the air-cooled condenser. To avoid substantial reduction in the heat transfer coefficient by complete evaporation of ammonia, the flow rate thereof is set to yield a vapor quality of less than 0.8. This two-phase mixture is passed through a vapor-liquid separator, from which the vapor is sent to the air-cooled condenser, while the liquid is combined with the ammonia condensate from the dry tower and recycled back through the condenser/reboiler.

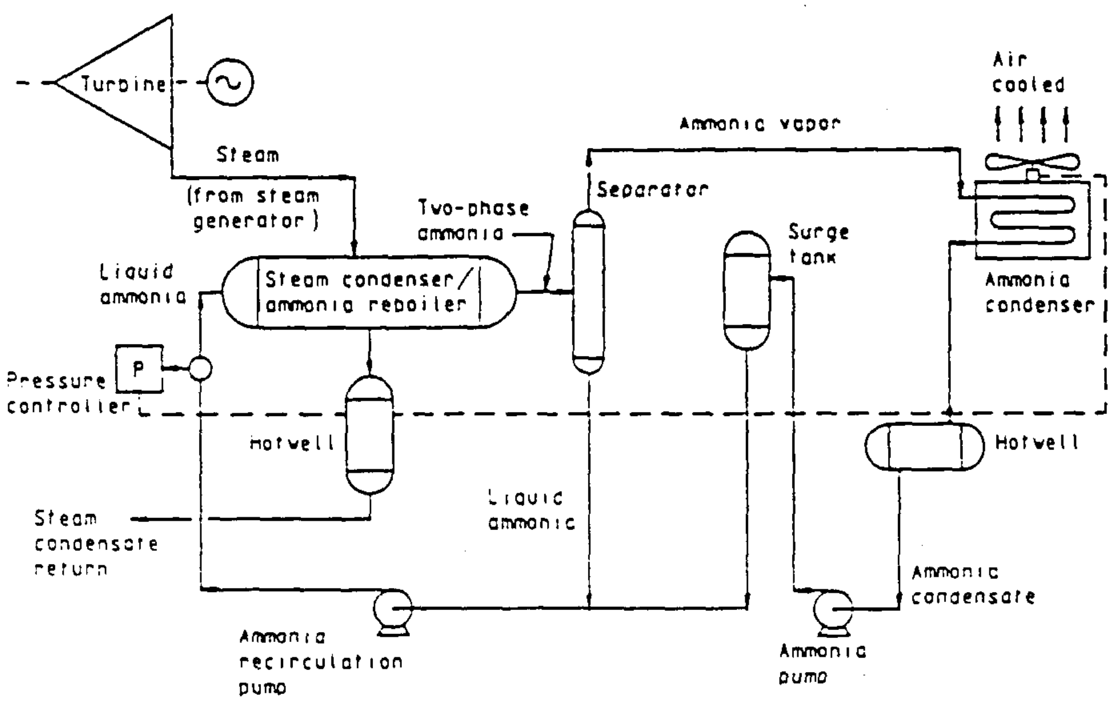

Figure 1.3.7: Schematic of ACT facility.

The reboiler and vapor-liquid separator could be designed to provide thermosyphon recirculation of the ammonia. At the ACT facility a recirculation pump is part of the loop to provide independent control of the liquid flow for experimental purposes.

From the vapor-liquid separator, vapor is transported to the cooling tower by the temperature difference and the associated vapor pressure difference of the saturated ammonia. The ammonia vapor is condensed in the air-cooled (dry) tower. The liquid flows to an ammonia hot well (liquid receiver) and is then returned to the condenser/reboiler. During periods of high ambient air temperature, heat rejection is augmented in one of the following three ways that have been demonstrated at the ACT facility.

1. In the deluge system, water is sprayed over the extended surfaces of the air-cooled heat exchanger (ammonia condenser). The ensuing increase in heat transfer in the presence of an evaporating film on the extended surfaces increases the capability of the heat exchanger to accept the heat load imposed by the condenser/reboiler. The percentage of the heat exchanger surface that is wetted is automatically established by the pressure of the ammonia in the heat transport system.

2. In the augmentation condenser system, a portion of the ammonia vapor from the vapor-liquid separator is routed to a separate evaporative condenser in parallel with the air-cooled ammonia condenser. The fraction of ammonia is controlled by the ammonia pressure in the system.

3. In the capacitive -cooling system, a fraction of the steam from the last stage of the turbine is routed to a parallel water-cooled condenser. The cooling water is modulated to maintain the desired ammonia pressure in the system. The water is in a closed loop with a large storage tank and piped in a fashion that develops a thermocline in the tank, which moves down the tank as water is circulated through the condenser. During periods of lower ambient air temperature and lower loads on the heat rejection system, the hot water in the storage tank is cooled by an ammonia heat pump that rejects heat to the air-cooled tower. During this phase the thermocline moves upwards in the water storage tank.

If operated over the period of a year, each of the dry systems would use only 25 percent of the water normally required to reject this heat load in an evaporative cooling tower. The third would consume no water, the evaporative cooling being replaced by the delayed cooling of the closed system water supply.

The cooling tower, as shown schematically in figure 1.3.8. is provided with two sets of heat exchangers of different types.

1. A deluged all-aluminum plate fin-tube heat exchanger.
2. An aluminum skived-fin-tube heat exchanger.

Located on the long vertical sides of the tower are two all-dry skived-fin heat exchangers sloped 1° toward the outlet to promote drainage. Fourteen dry/wet heat exchangers are arranged in seven A-frame or delta assemblies on the elevated floor of the tower. To allow deluging of the latter, the fin plates are oriented vertically with tubes running horizontally. Deluge water is introduced at a controlled rate, at the apex of the delta configuration from a series of nozzles located in a bonnet running the length of the heat exchanger, which seals off air flow out the ends. The water sprays from the nozzles in a flat pattern, impinges on the ends of the plate fins, flows down the width of the heat exchanger, drains into a collection trough at the bottom and is then recycled. For an apex angle of 50°, the loss of deluge water on the interior face of the bundle was found to be a minimum.

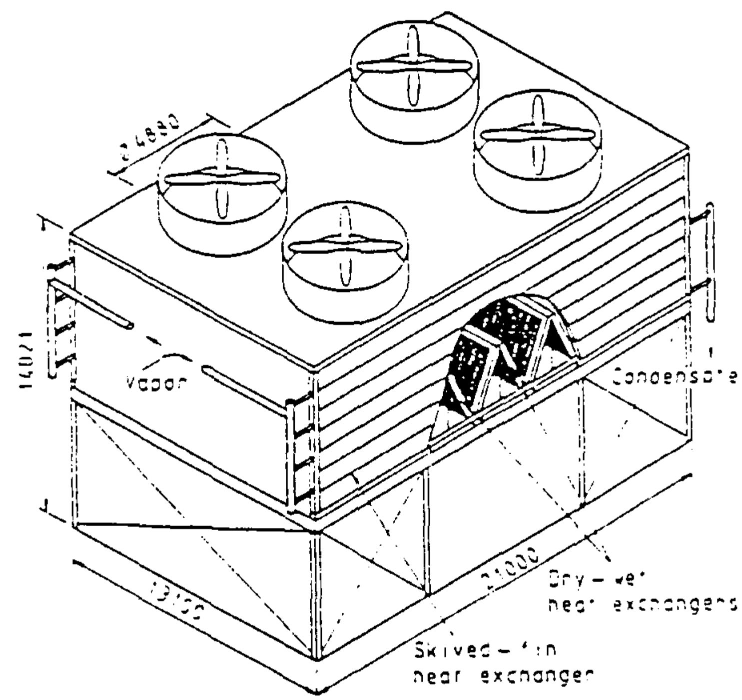

Figure 1.3.8: ACT test facility.

If the ambient temperature exceeds approximately 13°C, and if the tower is at full load, the tower is augmented.

Cooling air is supplied by four 4.88 m diameter axial flow fans with controllable blade pitches. The fan system is able to supply the design air flow rate through each heat exchanger set operated alone. Plywood panels or plastic sheets placed in from of the used set, block off all air flow during tests with individual heat exchanger sets.

In addition to the above, other wet/dry cooling system configurations may be considered for application in power generating plants. A parallel connected dry/wet cooling system employing a divided waterbox condenser and separate dry and wet towers is shown schematically in figure 1.3.9. At maximum ambient temperatures, the dry and wet towers both operate at full capacity. It has been suggested that the dry and the wet-cooling tower be connected in series or in parallel with a conventional surface condenser. This would however require expensive corrosion resistant tubing throughout the condenser and in the dry-cooling tower, unless the open wet-cooling tower is replaced by an evaporative surface cooler.

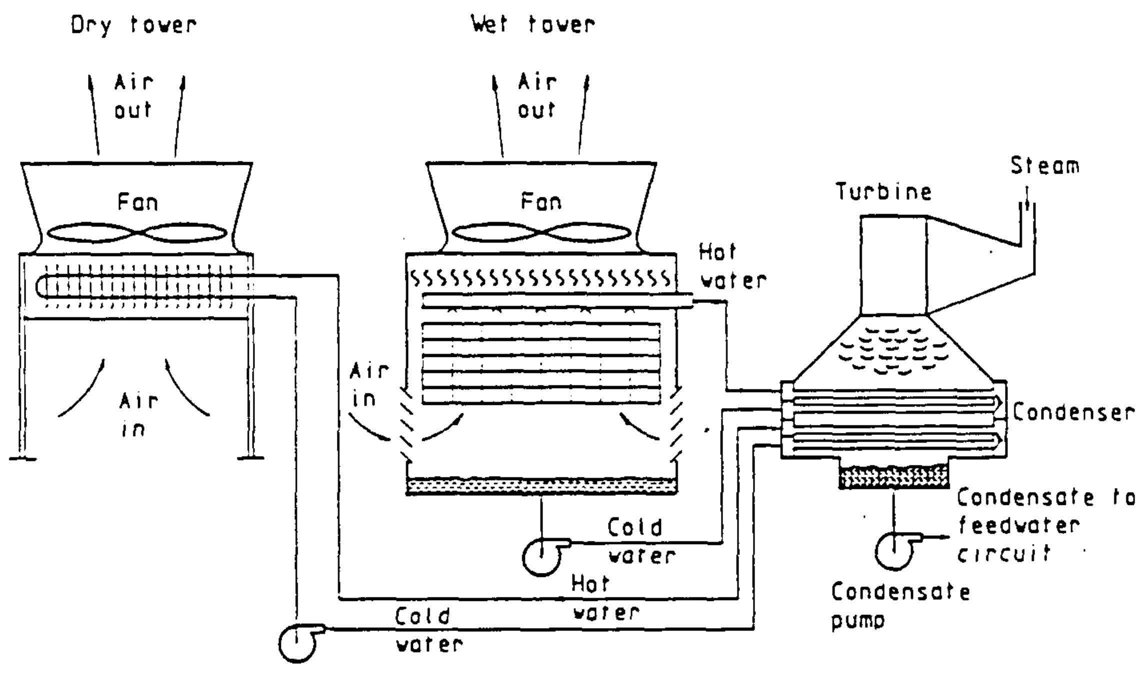

Figure 1.3.9: Parallel connected dry/wet cooling with divided waterbox condenser.

Figure 1.3.10 shows a dry/wet cooling tower system arrangement in which a direct air-cooled condenser is connected in parallel with a wet-cooling tower circuit equipped with a surface condenser. During normal operation all the turbine exhaust steam is condensed in the air-cooled condenser. At high ambient temperatures the wet-cooling tower coupled to a surface condenser improves the cooling capacity of the system. The wet-cooling tower can be replaced by an evaporative cooler.

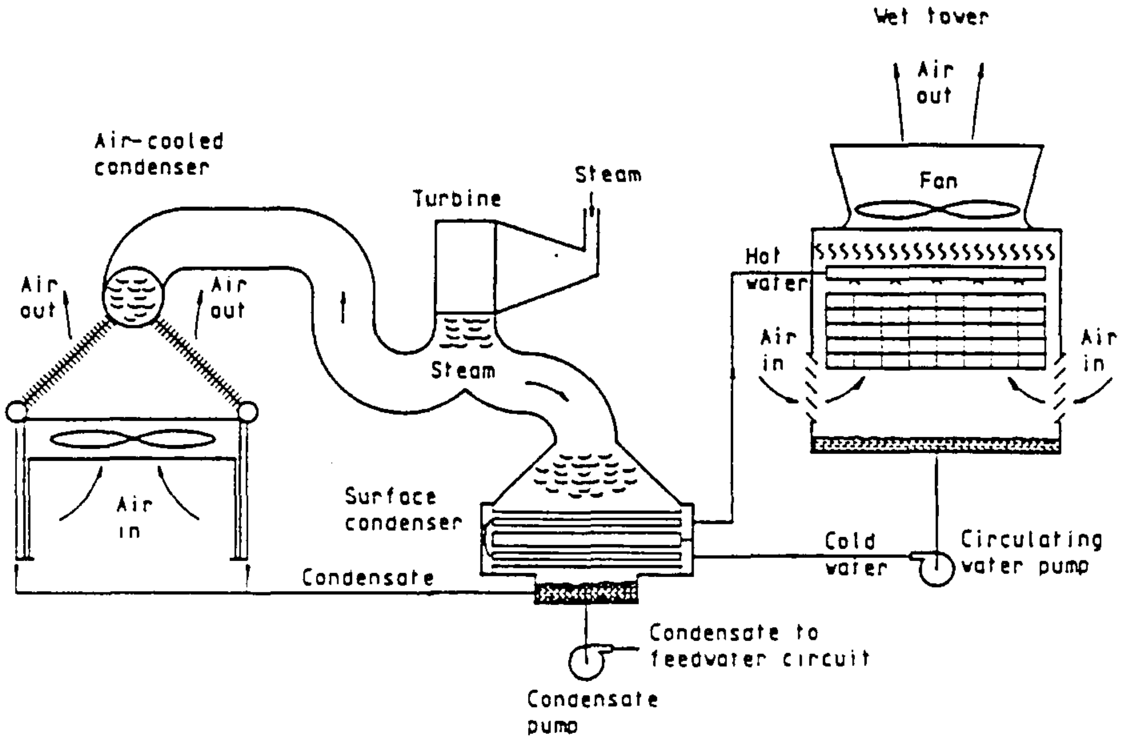

Figure 1.3.10: Air-cooled condenser in parallel with wet-cooling tower.

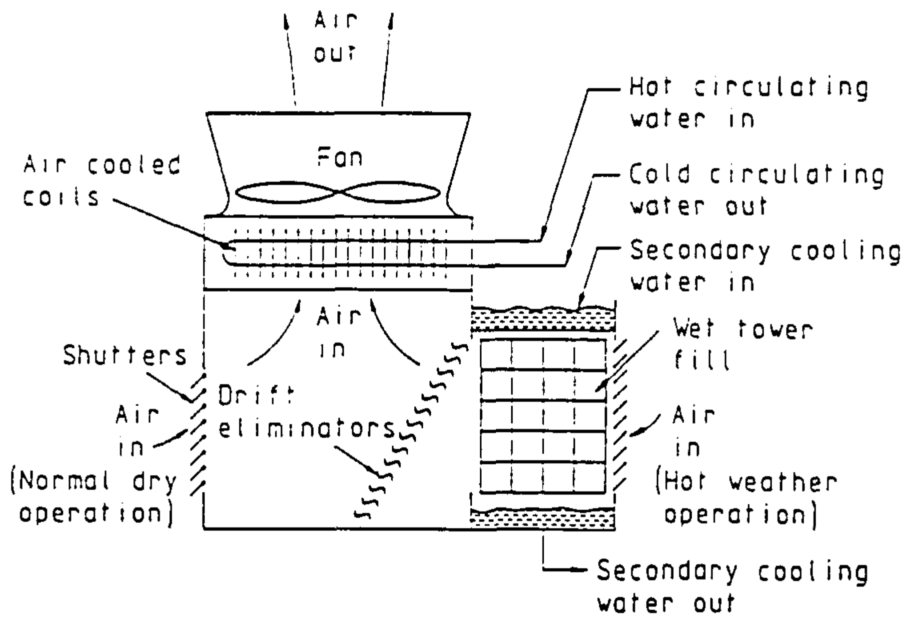

Figure 1.3.11: Dry tower with adiabatic cooling of inlet air.

Precooling by humidification or adiabatic cooling of inlet air prior to its entering a dry tower in order to enhance the performance of the air-cooled heat exchanger during hot weather operation, can be accomplished by spraying water into the air on passing it through wet tower fill as shown in figure 1.3.11. Evaporation of a portion of the secondary cooling water flowing through the spray or fill section cools the air to near its wetbulb temperature.

A number of wet/dry cooling systems have been constructed primarily to reduce visible plumes. These include a 150 MW(e) unit at the BASF petrochemical plant in Ludwigshafen [83KO1] and a 245 MW cooling tower at the Harvard powerplant, U.S.A., which was commissioned in 1977.

The wet/dry cooling system at the 420 MW(e) Altbach/Deizisau power plant was commissioned in 1985 [86AL1, 86MA1]. The system which rejects 558 MW, consists of a concrete cooling tower with a base diameter of 70 m and a height of 45 m. As shown schematically in figure 1.3.12, water flows through the dry elements in one pass from the bottom to the top prior to being distributed through the wet section which is of the conventional type. The air flow arrangement is parallel with dry air blown horizontally into the wet air stream emerging from the next section. In order to mix the two air streams, channels of different lengths are provided for the dry air.

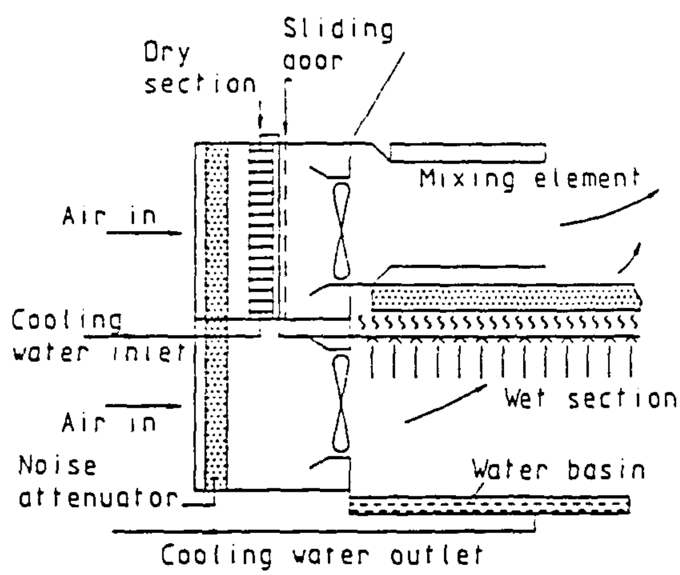

Figure 1.3.12: Altbach wet/dry cooling tower.

The tower can be operated in five main modes:

1. Wet operation at full fan capacity. As the wet section of the tower was designed to dissipate 100 percent of the heat load, it can operate without the dry section at any heat load condition. The sliding gates behind the dry heat exchangers must be closed in order to prevent the recirculation of the plumes through the openings of the fans of the dry section. The formation of visible plumes above the tower is dependent on the temperature and humidity conditions of the atmosphere at that time.

2. Wet operation at reduced fan capacity. This mode of operation can be used at low heat load, particularly in winter. The plume above the cooling tower will be visible.

3. At design conditions of dry bulb temperature of 10°C and relative humidity of 70.8 percent, integrated operation at full fan capacity of both the wet and dry sections. In this mode of operation, the visible plume is eliminated.

4. Integrated operation at reduced fan capacity. This mode should be used during low heat load periods, when the visible plume must eliminated.

5. Dry-cooling operation. At an ambient air temperature of −15°C with the heat load not exceeding 35 percent, the tower can be operated using the dry section only. The wet section of the tower is then bypassed by having the water flow from the heat exchangers to the water basin directly via a bypass line.

The much larger wet/dry tower at the Neckarwestheim power plant has a diameter of 160m and rejects 2500 MW [91AL1].

1.4 CONSERVATION EQUATIONS

The fundamental conservation equations of mass, momentum and energy form the basis for solving fluid flow and heat transfer problems.

The general equation of continuity (conservation of mass) for steady flow through a control volume or stream tube between sections 1 and 2 as shown in figure 1.4.1 is

$$m = \int_{A_1} \rho v \, dA = \int_{A_2} \rho v \, dA \tag{1.4.1}$$

where ρ and v represent the fluid density and velocity respectively while A is the cross-sectional area normal to the velocity.

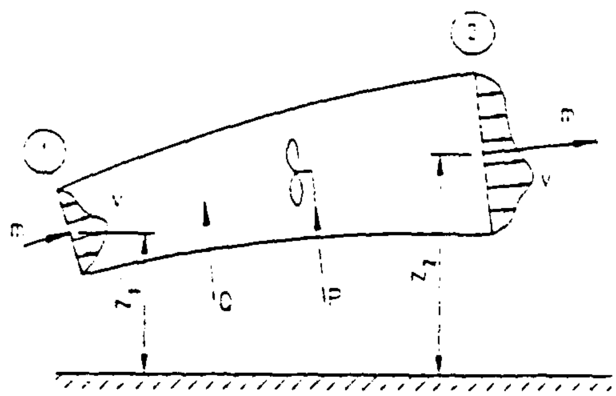

Figure 1.4.1: Control volume.

By applying the first law of thermodynamics (conservation of energy) to a fluid in the control volume between sections 1 and 2, as shown in figure 1.4.1, the resultant energy equation can be expressed as

$$P + Q = m\left[\left(i_2 + \alpha_{e2} v_2^2/2 + g z_2\right) - \left(i_1 + \alpha_{e1} v_1^2/2 + g z_1\right)\right] \tag{1.4.2}$$

where P and Q respectively represent the power or rate of work and the rate of heat input into the fluid.

The enthalpy of a fluid is defined as

$$i = u + p/\rho \tag{1.4.3}$$

where u is the internal energy of the fluid.

In equation (1.4.2) the $\alpha_e v^2/2$ term represents the kinetic energy of the fluid. Since the velocity may vary across a cross-section, a kinetic energy velocity distribution correction factor or *kinetic energy coefficient* is defined as

$$\alpha_e = \frac{1}{m} \int_A (v^2/2)dm/(v_m^2/2) = \int_A v^3 dA/(A v_m^3) \tag{1.4.4}$$

if the density remains constant over the section. The mean velocity at any cross-section is defined as

$$v_m = \int_A v\, dA/A \tag{1.4.5}$$

For a uniform velocity distribution, α_e equals unity.

The potential energy of the fluid may change, depending on its elevation z above any arbitrary datum plane.

1.4.1 GENERAL FEATURES OF ISENTROPIC FLOW

Consider the one-dimensional isentropic (frictionless adiabatic) flow of a fluid through a passage of varying cross-section. For the particular case where the cross-sectional area is infinite, the corresponding fluid velocity is zero and the pressure at this state, p_t, is normally called the isentropic stagnation pressure or the total pressure. The value of the corresponding stagnation enthalpy, i_t, is independent of whether or not entropy changes occur, since it has the same value for all states which are reachable from it adiabatically.

Equation (1.4.2) can be simplified in the particular case where the control surfaces extend between a stagnation section 1 and another section 2 at the same elevation in the duct, for isentropic one-dimensional uniform flow with no work interaction.

$$i_{t1} = i_2 + v_2^2/2 \tag{1.4.6}$$

For a fluid, the change in enthalpy is given by

$$\Delta i = c_p \Delta T \tag{1.4.7}$$

where c_p is the specific heat of the fluid at constant pressure. The value of c_p for some fluids is given in Appendix A.

With this relation, equation (1.4.6) can be written as

$$c_p(T_{t1} - T_2) = v_2^2/2 \tag{1.4.8}$$

Furthermore for a gas

$$c_p - c_v = R \tag{1.4.9}$$

where c_v is the specific heat at constant volume and R is the gas constant.

Since

$$c_p/c_v = \gamma \tag{1.4.10}$$

it follows that

$$c_p = \gamma R/(\gamma - 1) \tag{1.4.11}$$

For a perfect gas, the relation between its pressure, density and temperature is given by.

$$p = \rho RT \tag{1.4.12}$$

If a perfect gas undergoes an isentropic change the following relation holds:

$$p/\rho^{\gamma} = \text{constant} \tag{1.4.13}$$

Substitute equations (1.4.11), (1.4.12) and (1.4.13) into equation (1.4.8) and find

$$p_{t1} = p_2\left[1 + \left(\frac{\gamma - 1}{\gamma}\right)\frac{\rho_2 v_2^2}{2p_2}\right]^{\frac{\gamma}{\gamma - 1}} \tag{1.4.14a}$$

or

$$p_2 = p_{t1}\left[1 - \left(\frac{\gamma - 1}{\gamma}\right)\frac{\rho_{t1} v_2^2}{2p_{t1}}\right]^{\frac{\gamma}{\gamma - 1}} \tag{1.4.14b}$$

Expanding equation (1.4.14) by means of the binomial theorem, the following convenient approximate formula for low speed isentropic flow may be found if the relatively small higher order terms are neglected.

$$p_{t1} = p_2 + \rho_2 v_2^2/2 \tag{1.4.15a}$$

or

$$p_{t1} = p_2 + \rho_{t1} v_2^2/2 \tag{1.4.15b}$$

Similarly if the cross-sectional area at 1 is not infinite find

$$p_1 + \rho_1 v_1^2/2 = p_2 + \rho_1 v_2^2/2 \tag{1.4.16a}$$

or

$$p_1 + \rho_2 v_1^2/2 = p_2 + \rho_2 v_2^2/2 \tag{1.4.16b}$$

Since both approximations are acceptable, corresponding densities and velocities are usually combined to give

$$p_1 + \rho_1 v_1^2/2 = p_2 + \rho_2 v_2^2/2 \tag{1.4.17}$$

This equation is similar to Bernoulli's theorem, which is applicable to any incompressible fluid, i.e.

$$p_1 + \rho\, v_1^2/2 = p_2 + \rho\, v_2^2/2 \tag{1.4.18}$$

Where flow occurs isentropically between two sections that are at different elevations, the energy equation (1.4.2), in the absence of a work interaction, becomes

$$c_p T_1 + v_1^2/2 + gz_1 = c_p T_2 + v_2^2/2 + gz_2 \tag{1.4.19}$$

or following the same procedure as above;

$$(p_1 + \rho_1 v_1^2/2) - (p_2 + \rho_2 v_2^2/2) = \rho_{12} g(z_2 - z_1) \tag{1.4.20}$$

where

$$\rho_{12} = (\rho_1 + \rho_2)/2$$

For the purely hydrostatic case equation (1.4.20) becomes

$$(p_1 - p_2) = \rho_{12} g(z_2 - z_1) \tag{1.4.21}$$

A more accurate expression for the hydrostatic pressure differential between two elevations in the atmosphere is given by equation (10.1.9).

The change in total pressure may similarly be determined for the case where a fan is located between sections 1 and 2 i.e.

$$(p_1 + \rho_1 v_1^2/2) - (p_2 + \rho_2 v_2^2/2) = -\rho_{12}P/m \tag{1.4.22}$$

1.5 REFERENCES

41HA1 Happel, O., Betriebserfahrungen mit einem Luftkondensator, Archiv für Wärmewirtschaft, Vol. 22, No. 12, pp. 265-268, 1941.

50HE1 Heller, H., Condensation by Means of Air for Steam Turbines Equipped with Injection Condensers, 4th World Power Conference, Vol. 3, 1950

59MC1 McKelvey, K.K., The Industrial Cooling Tower, Elsevier Publ. Co., Amsterdam, 1959.

69CH1 Christopher, P.J., and Forster, V.T., Rugeley Dry Cooling Tower System, Proc. Instn. Mech. Engrs., Vol.184, Part 1, No. 11, pp. 197-222, 1969 - 1970.

69SC1 Scherf, O., Die luftgekühlte Kondensationsanlage im 150-MW-Block des Preussag-Kraftwerkes in Ibbenbüren, Energie und Technik, Heft 7, pp. 260-264, 1969.

71HE1 Heeren, H. and Holly, L., Dry Cooling Eliminates Thermal Pollution, Energie, Vol. 23, October and November 1971.

72MA1 March, F. and Schulenberg, F., Air-cooled Condenser for a 160 MW Steam Power Station, Planning of the Plant and Experience Gained in Two Years of Operation, GEA Bochum, 1972.

73HI1 Hirschfelder, G., Der Trockenkühlturm des 300-MW-THTR-Kern- kraftwerkes Schmehausen-Uentrop, VGB Kraftwerktechnik 53, Heft 7, pp.463 - 471, 1973.

73MO1 Moore, F.K., On the Minimum Size of Large Dry Cooling Towers with Combined Mechanical and Natural Draft, Trans. of the ASME, Journal of Heat Transfer, pp. 383-389, August 1973.

74BU1 Buxmann, J. and Heeren, H., Oberflächenkondensator für Trockenkühlung, VGB Kraftwerkstechnik, Vol. 5, pp. 301 - 306, May 1974.

74MA1 Maze, R.W., Air vs. Water Cooling, The Oil and Gas Journal, pp. 74-78, November 1974.

74VA1 Van der Walt, N.T., West, L.A., Sheer T.J. and Kuball, D., The Design and Operation of a Dry Cooling Tower System for a 200 MW Turbo-generator at Grootvlei Power Station, South Africa, 9th World Energy Conference, Detroit, USA, 1974.

75BE1 Berliner, P., Kühltürme, Springer - Verlag, Berlin, 1975.

75ST1 Steele, B.L., Selection of Plant Cooling Source (s), ASME Paper 75-IPWR-6, 1975.

75VG1 VGB Technisch-wissenschaftliche Berichte "Wärmekraftwerke", Heft 5, Kühlturm und Umwelt, Essen, 1975.

76GA1 Gardner, B.R., The Development of the Assisted-draught Cooling Tower, Combustion, pp. 15 - 22, October 1976.

76VO1 Von Cleve, H.-H., Comparison of Different Combinations of Wet and Dry Cooling Towers, ASME Paper 75-WA/Pwr-10, 1976.

77JO1 Jones, W.G., Cooling Water for Power Stations, Proc. Inst. Civil Eng., London, Vol. 62, pp. 373-398, 1977.

77LE1 Lefevre, M., New Technology and Cooling Tower Design Practices, Combustion, pp. 28-32, May 1977.

77SC1 Schulenberg, F., Der Luftkondensator für den 365-MW-Block in Wyoming/USA, Sammelband VGB-Konferenz, 1977.

77SU1 Surface, M.O., System Designs for Dry Cooling Towers, Power Engineering, September 1977.

78EN1 Englesson, G.A., Savage, W. and Hu, M.C., Technical and Economic Feasibilities of Wet/dry Tower Systems for Water Conservation. Paper 2, US papers presented at Symposium of the US–USSR Coordinating Committee on Scientific and Technical Cooperation in the Field of Thermal Power Plant Heat Rejection Systems, November 1978.

78LA1 Larinoff, M.W., Performance and Capital Costs of Wet/dry Cooling Towers in Power Plant Service, Combustion, Vol. 49, No. 11, May 1978.

78VO1 Von Cleve, H.-H., Dry Cooling Tower for the 300 MW THTR at Schmehausen, Germany, AICHE, Symposium Series, No. 174, Vol. 74, pp. 288-292, 1978.

79KR1 Kravets, V.I. and Radionov, N.I., A System of Heat Removal for an Electric Power Station Located in a Dry Subtropical Climate, Report of the Visit of the U.S.A. Delegation of the U.S. - U.S.S.R. Coord. Com. on Sc. and Techn. Coop in the Field of Thermal Power Plant Heat Rejection Systems to the U.S.S.R., eds Neal, J.W. and Savage, W.F., Report DOE/ET-0070 UC-12, U.S. Dept. of Energy, Feb. 1979.

80MC1 McHale, C.E., Jablonka, G.E., Bartz, J.A. and Webster, D.J., New Developments in Dry Cooling of Power Plants, Combustion, pp. 28 - 36, May 1980.

81BA1 Bartz, J.A., and Maulbetsch, J.S., Are Dry-cooled Power Plants a Feasible Alternative? Mechanical Engineering, Vol. 103, No. 10, pp. 34 - 41, October 1981.

81CH1 Cheremisinoff, N.P. and Cheremisinoff, P.N., Cooling Towers: Selection, Design and Practice, Ann Arbor Science Publ. Inc., Ann Arbor, Michigan, 1981.

81EP1 EPRI, Development of an Advanced Concept of Dry/Wet Cooling of Power Generating Plants, Interim Report CS-1668, Feb., 1981.

81KO1 Kosten, G.J., Morgan, K.I., Burns, J.M. and Curlett, P.L., Operating Experience and Performance Testing of the World's Largest Air-cooled Condenser, Paper presented at the American Power Conference, Chicago, April 1981.

83FI1 Fischer, U., Leidenfrost, W. and Li, J., Hybrid Evaporative-Condenser Cooling Tower, Heat Transfer Engineering, Vol. 4, No. 2, June 1983.

83KO1 Kokott, D., Betriebserfahrungen mit einem 150 MW (thermisch) Nass/trockenkühlturm in der BASF, Paper presented at the VGB-Conference, Kühlturm Auslegung und Betrieb 1983, Ludwigshafen und Essen, FRG, May 1983.

84ER1 Ergebnisse der Projektgruppe "Nass-/Trocken - Kühltechnik", VGB Kraftwerkstechnik 64, Vol. 12, December 1984.

84VO1 Von Cleve, H.-H., Die Luftgekühlte Kondensationsanlage des 4000 MW-Kraftwerks Matimba/Südafrika, VGB Kraftwerkstechnik 64, Heft 4, April 1984.

86AL1 Alt, W., Concept Design, Construction and Commissioning of the First Hybrid Cooling Tower for a Heating Power Station with a Net Power Generating Unit Capacity of 420 MW, 5th IAHR Cooling Tower Workshop, Monterey, USA, October 1986.

86BO1 Bodás, J. and Szabó, Z., A Wet/Dry Cooling System for a 600 MW Combined Cycle Power Plant, 5th IAHR Cooling Tower Workshop, Monterey, U.S.A., 1986.

86CR1 Crunden, M.J., The Design and Operation of Evaporative Water Cooling Towers, Int. Build. Serv. Abstr., GB, No. 6, Vol. 21. 1986.

86MA1 Mäule, R., Ernst, G. and Bräuning, G., Results of Experiments on the Performance and the Emmission of the Hybrid Cooling Tower at the Altbach-Deizisau Plant at Neckarwerke, 5th IAHR Cooling Tower Workshop, Monterey, USA, October 1986.

87KN1 Knirsch, H., Design and Construction of Direct Dry Cooling Units, Proc.. VGB

Conference, "South Africa 1987", Vol. 1, pp. 54-69, 1987.

87EP1 EPRI, Wet-dry Cooling Demonstration. A Transfer of Technology, Report CS-5016, Battelle Pacific Northwest Laboratories, Richland, Washington 1987.

87PE1 Pedersen, G.C., Lamkin, V.K. and Seich, M., An Economical Solution to Cooling Tower Drift, Paper TP 87-8, Cooling and Tower Institute Meeting, New Orleans, Louisiana, February, 1987.

87TR1 Trage, B. and Hintzen, F.J., Design and Construction of Indirect Dry Cooling Units, Proc. VGB Conference, "South Africa 1987", Vol. 1, pp. 70-79, 1987.

88BO1 Bodás, J., Szabó, Z . and Awerbach, L., Combined Wet/Dry Dry Cooling Plants "System Heller" of EGI, Paper presented at the ASME Winter Annual Meeting, Chicago, 1988.

88NO1 Nowosad, R.M., A Review of the Development and Application of Industrial Dry/Wet Cooling, Council for Scientic and Industrial Research Report O/DPT1, South Africa, December 1988.

88PE1 Petzel, H.K., 6 Years Operational Experience of Cooling Tower Discharge of Desulphurized Flue Gas, 6th IAHR Cooling Tower Workshop, Pisa, Italy, 1988.

89GO1 Goldwirt, F., Ghuzel, M. and Lemoine, P., Hydraulic Works Study of Golfech Cooling Towers, Proceedings, International Cooling-Tower Conference, EPRI GS- 6317, IAHR Cooling Tower Workshop, Pisa, Italy 1988.

89MI1 Mitchell, R.D., Survey of Water-conserving Heat Rejection Systems, EPRI, Final Report GS-6252, Project 1260 - 59, March 1989.

89TR1 Trage, B. and Hintzen, F.J., Planung und Bau von Anlagen mit indirekter Trockenkühlung, VGB Kraftwerkstechnik, Heft 2, pp. 183 - 189, 1989.

90HI1 Hill, G.B., Pring, E.J. and Osborn, P.D., Cooling Towers, Principles and Practice, Butterworth-Heinemann, London, 1990.

90KN1 Knirsch, H., Design and Construction of Large Direct Cooled Units for Thermal Power Plants, Paper PWR - 26, ASME Joint Power Conference, Boston, 1990.

90TR1 Trage, B., Ham, A.J. and Vicary, Th.C., The Natural Draught, Indirect Dry Cooling System for the 6 x 686 MWe Kendal Power Station, RSA, Paper 90-JPGC/Pwr-25, ASME Joint Power Conference, Boston, 1990.

91AL1 Alt, W. and Damjakob, H., Grosse Hybrid - und Trockenkühltürme an den Beispielen GKN II und KW Kendal, Vorträge VGB-Fachtagung Kühltürme 1991, VGB-Kraftwerkstechnik, Essen, 1991.

91JA1 Jarosi, M., Operational Experiences of the Heller-type Wet/Dry Cooling System Serving the 1200 MWe Trakya CCPP, Paper presented at the Sysmposium on Dry Cooling Towers, Teheran, 1991.

91KN1 Knirsch, H., Dry Cooling Towers at Biggest Coal Fuel Power Station, Modern Power Systems, Ruislip, England, July 1991.

91MI1 Mikovics, A., Water Cooled Condensers in Dry Cooling Systems, Paper presented at the Symposium on Dry Cooling Towers, Teheran, 1991.

91SZ1 Szabo, Z., Why use "Heller System"? Circuitry, Characteristics and Special Features, Paper presented at the Symposium on Dry Cooling Towers, Teheran 1991.

93SM1 Smith, A.R. and Romeister, D., Rye House 700 MW Combined Cycle Power Station, Modern Power Systems, pp. 41-48, November 1993.

93ST1 Staff Report, Dry Cooling Solves GTCC Siting Problems, Modern Power Systems, pp. 39-43, June 1993.

94SP1 Spilko, J., Dry Cooling Enhances Syria's Teshrin Plant Operation, Power

CHAPTER 2

FLUID MECHANICS

2.0 INTRODUCTION

Fluid mechanics is the study of the behavior of fluids at rest and in motion and of the properties of fluids insofar as they affect the fluid motion. The object of this chapter is to introduce the reader to certain terminology, concepts, laws and equations that are directly applicable to the design of air-cooled heat exchangers and cooling towers.

2.1 VISCOUS FLOW

Consider the flow of a fluid over a flat plate as shown in figure 2.1.1.

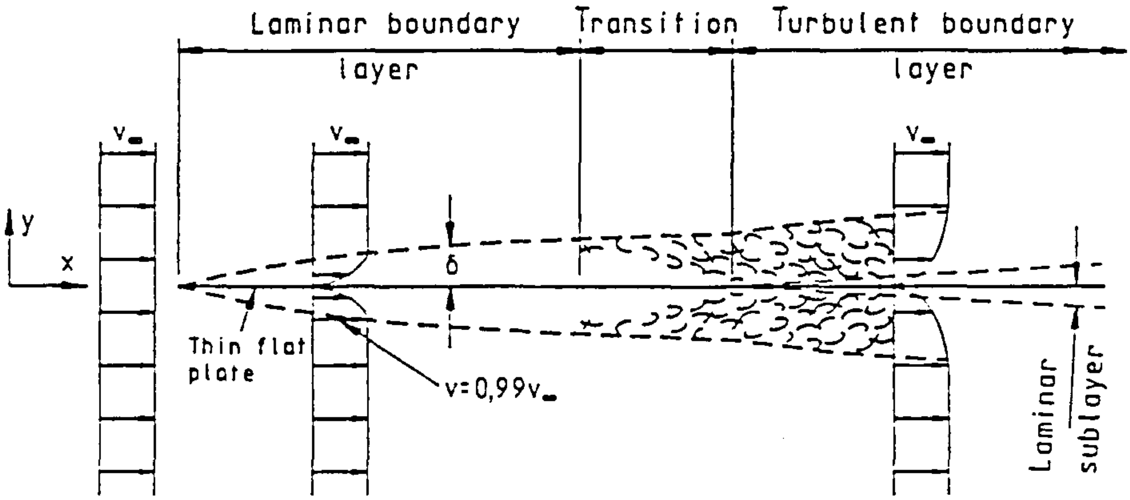

Figure 2.1.1: Boundary layer development along a flat plate.

Beginning at the leading edge of the plate, a region develops where the influence of viscous forces is felt. These viscous forces are described in terms of a shear stress, τ, between the fluid layers. If this stress is assumed to be proportional to the normal velocity gradient, the defining equation for viscosity, known as Newton's equation of viscosity, is

$$\tau = -\mu \frac{dv}{dy} \tag{2.1.1}$$

The constant of proportionality, μ, is called the dynamic viscosity. The values of μ for some fluids are given in Appendix A.

The region of flow which develops from the leading edge of the plate in which the effects of viscosity are observed is called the velocity boundary layer. The y-position where the boundary layer ends is arbitrarily chosen at a point where the velocity becomes 99 per cent of the free stream value. The boundary layer thickness, δ, is defined as the distance between this point and the plate.

Initially, the boundary layer development is laminar, but at some critical distance from the leading edge, depending on the flow field and fluid properties, small disturbances in the flow begin to become amplified and a transition process takes place until the flow becomes turbulent.

The physical mechanism of viscosity is one of momentum exchange. In the laminar portion of the boundary layer, molecules move from one lamina to another, carrying with them momentum corresponding to the velocity of the flow. There is a net momentum transport from regions of high velocity to regions of low velocity, which creates a force in the direction of flow. This force may be expressed in terms of the viscous shear stress as given by equation (2.1.1).

The rate at which the momentum transfer takes place is dependent on the rate at which the molecules move across the fluid layers. In a gas, the molecules would move about with some average speed proportional to the square root of the absolute temperature, since, in the kinetic theory of gases, we identify temperature with the mean kinetic energy of a molecule. The faster the molecules move, the more momentum they will transport. Hence we should expect the viscosity of a gas to be approximately proportional to the square root of temperature, and this expectation is corroborated fairly well by experiment. The viscosities of some typical fluids are given in Appendix A.

The laminar velocity profile is approximately parabolic in shape.

The transition from laminar to turbulent flow occurs typically when

$$\frac{\rho v_\infty x}{\mu} = \frac{v_\infty x}{\nu} \geq 3.2 \times 10^5$$

where v_∞ is the free stream velocity, x is the distance from the leading edge of the plate, and $\nu = \mu/\rho$ is the kinematic viscosity of the fluid. This particular dimensionless group or ratio of inertial force to viscous force is called the Reynolds number:

$$Re_x = \frac{\rho v_\infty x}{\mu} \tag{2.1.2}$$

Although the critical Reynolds number for transition on a flat plate is usually taken as 3.2×10^5 for most analytical purposes, the critical value in a practical situation is strongly dependent on the surface roughness conditions and the "turbulence level" of the free stream. The normal range for the beginning of transition is between 3.2×10^5 and 10^6. With very large disturbances present in the flow, transition may begin with Reynolds numbers as low as 10^5, and for flows which are very free from fluctuations it may not start until $Re_x = 2 \times 10^6$ or more. In reality, the transition process covers a range of Reynolds numbers, with transition being complete and with fully developed turbulent flow usually observed at Reynolds numbers twice the value at which transition began.

A qualitative picture of the turbulent flow process may be obtained by imagining macroscopic chunks of fluid transporting momentum instead of microscopic transport on the basis of individual molecules. The turbulent boundary layer is more complex than the laminar boundary layer because the nature of the flow in the former changes with distance from the plate surface.

The zone immediately adjacent to the wall is a layer of fluid which, because of the stabilizing effect of the wall, remains laminar even though the great majority of the flow in the boundary layer is turbulent. This very thin layer is called the laminar sublayer, and the velocity distribution in this layer is related to the shear stress and viscosity according to Newton's viscosity law.

The flow zone outside the laminar sublayer is turbulent. The turbulence alters the flow regime so much that the shear stress as given by $\tau = -\mu\, dv/dy$ is not significant. What happens is that the mixing action of turbulence causes small fluid masses to be swept back and forth in a direction transverse to the mean flow direction. Thus, as a small mass of fluid is swept from a low-velocity zone next to the sublayer into a higher-velocity zone farther out in the stream, the mass has a retarding effect on the higher-velocity stream. This mass of fluid, through an exchange of momentum, creates the effect of a retarding shear stress applied to a higher-velocity stream. Similarly, a small mass of fluid which originates farther out in the boundary layer in a high-velocity flow zone and is swept into a region of low velocity affects on the low-velocity fluid much like shear stress augmenting the flow velocity. In other words, the mass of fluid with relatively higher momentum will tend to accelerate the lower-velocity fluid in the region into which it moves. Although the process described above is primarily a momentum-exchange phenomenon, it has the same effect as a shear stress applied to the fluid; thus, in turbulent flow, these "stresses" are termed apparent shear stresses, or Reynolds stresses after the British scientist-engineer who first did extensive research on turbulent flow in the late 1800s.

The turbulent velocity profile thus has a nearly linear portion in the sublayer and a relatively flat profile outside this region.

Consider the flow in a tube as shown in figure 2.1.2. A boundary layer develops at the entrance, as shown. Eventually the boundary layer fills the entire tube, and the flow is said to be fully developed. If the flow is laminar, a parabolic velocity profile is experienced as shown in figure 2.1.2(a). When the flow is turbulent, a somewhat blunter profile is observed as in figure 2.1.2(b). In a tube, the Reynolds number based on the mean fluid velocity and the tube diameter is again used as a criterion for laminar and turbulent flow. For $Re_d = \rho v d/\mu \le 2300$ the flow is usually observed to be laminar, whereas for $Re_d \ge 10\ 000$ it is turbulent.

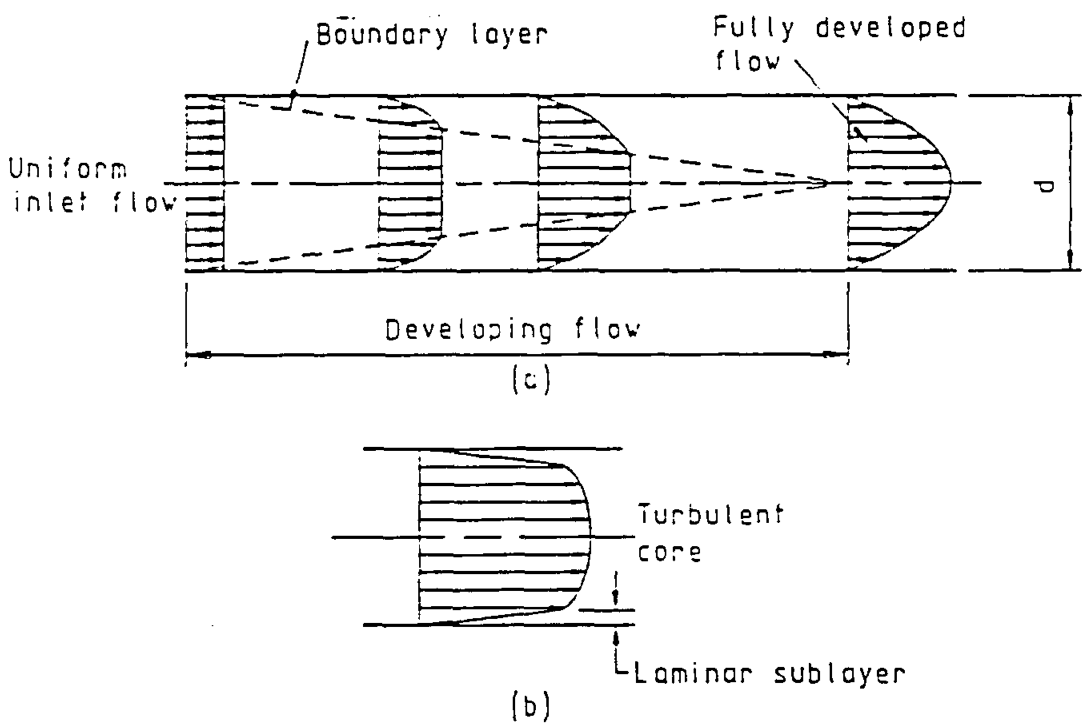

Figure 2.1.2: Velocity profiles in a tube: (a) Laminar flow; (b) turbulent flow.

Again, a range of Reynolds numbers for transition may be observed, depending on the roughness of the pipe and smoothness of the flow. The generally accepted range for transition, also referred to as the critical region, is $2000 < Re_d < 4000$, although laminar flow has been maintained up to Reynolds numbers of 25000 in carefully controlled laboratory conditions.

The continuity relation for one-dimensional flow in a tube is

$$m = \rho v A \tag{2.1.3}$$

where m is the mass rate of flow, v is the mean velocity, and A is the cross-sectional area of the tube.

The mass flux or mass velocity is defined as

$$G = m/A = \rho v \tag{2.1.4}$$

so that the Reynolds number may be written as

$$Re_d = Gd/\mu \tag{2.1.5}$$

Similar flow patterns are observed in channels which are not of circular cross-section. In those cases it is convenient to define the following equivalent or hydraulic diameter for calculating the Reynolds number:

$$d_e = \frac{4 \text{ x cross-sectional flow area}}{\text{wetted perimeter}} \tag{2.1.6}$$

This particular grouping of terms is used because it yields the value of the physical diameter when applied to a circular cross-section.

2.2 FLOW IN DUCTS

In real ducts, flow conditions do not change isentropically as deduced in Chapter 1. The equations can, however, be extended to take into consideration flow losses.

Dimensional analysis shows that for a duct of given geometry and fully developed flow, the pressure drop, Δp, between any two points is related to the duct geometry and fluid properties in the following way:

$$\frac{\Delta p}{\rho v^2/2} = \text{function}\left(\frac{\rho v d_e}{\mu}, \frac{L}{d_e}, \frac{\epsilon}{d_e}\right)$$

The quantity $\rho v^2/2$ is known as the dynamic pressure. The term L/d_e considers the geometry of the duct and ϵ/d_e is a measure of the roughness of the duct surface.

According to the D'Arcy-Weisbach equation, the pressure drop in a circular pipe can be expressed as [00WE01]:

$$\Delta p = f_D\left(\frac{L}{d}\right)\left(\frac{\rho v^2}{2}\right) \tag{2.2.1}$$

The number of velocity heads, $v^2/2$, lost for a given pressure drop, Δp, is expressed by the product of the friction factor f_D and the geometric factor L/d, where L is the length of the pipe. The friction factor under consideration is that corresponding to fully developed velocity profiles, both laminar and turbulent, which are encountered only after 25 or more diameters downstream of a pipe inlet.

This equation is also applicable to ducts other than circular pipes, in which case d is replaced by d_e.

Other definitions of the friction factor appear in the literature. In some cases the right hand side of equation (2.2.1) is divided by a factor 4, giving a friction factor $f = f_D/4$, also referred to as the Fanning friction factor. The friction factor is a function of Re, the cross-sectional shape of the duct and, in the turbulent flow regime, the relative roughness of the duct surface.

2.2.1 LAMINAR FLOW

An extensive summary of fanning friction factors for laminar flow in a variety of ducts is presented by Shah [78SH1]. According to the Hagen-Poiseuille solution for fully developed laminar flow in a circular duct or tube, $f = 16/Re = f_D/4$. The friction factor is independent of the roughness of the surface in the case of laminar flow.

The results for other duct shapes are shown in figure 2.2.1.

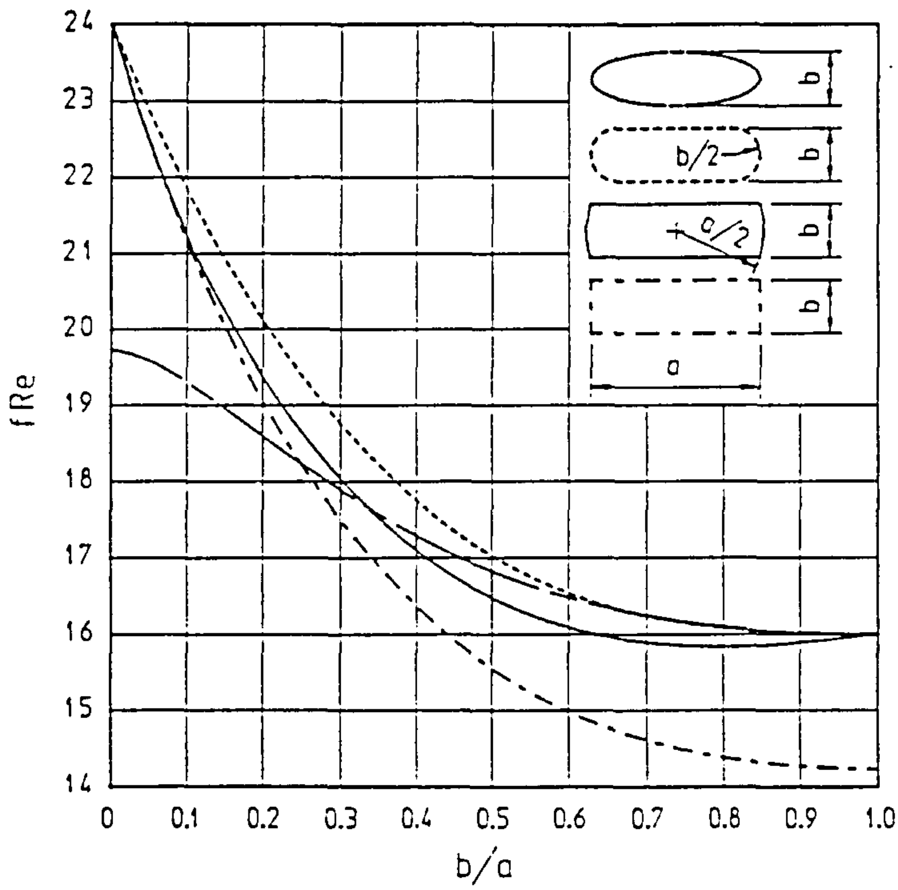

Figure 2.2.1: Friction factors for fully developed flow.

For the rectangular duct the friction curve in figure 2.2.1 may be expressed as

$$fRe = 24\left[1 - 1.3553\left(\frac{b}{a}\right) + 1.9467\left(\frac{b}{a}\right)^2 - 1.7012\left(\frac{b}{a}\right)^3 + 0.9564\left(\frac{b}{a}\right)^4 - 0.2537\left(\frac{b}{a}\right)^5\right] \qquad (2.2.2)$$

A twisted tape is sometimes inserted in a circular tube to establish swirl flow, thereby increasing the heat transfer coefficient in heat exchanger applications. The tape is twisted about its longitudinal axis as shown in figure 2.2.2.

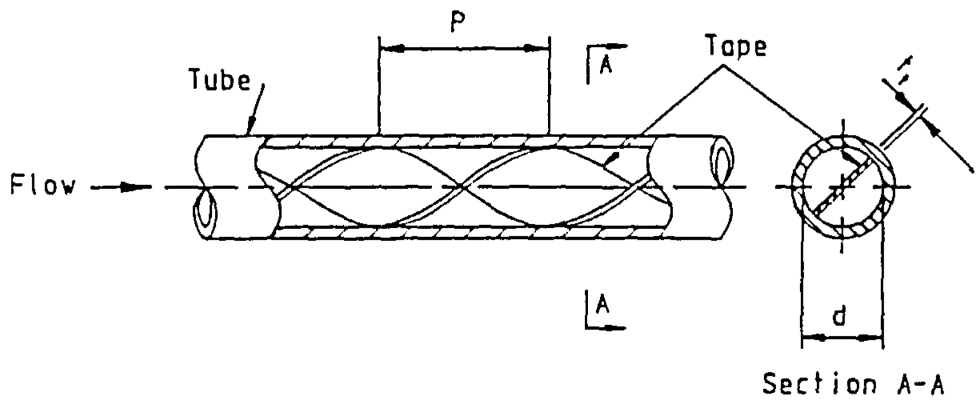

Figure 2.2.2: A circular tube with a twisted tape insert.

According Hong and Bergles [75HO1] the friction factor for fully developed flow is given by

$$f = 45.9/Re \tag{2.2.3}$$

where

$$Re = m/[\mu(\pi d/4 - t_t)]$$

and m is the mass flow rate while t_t is the tape thickness.

A more recent equation for the friction factor was derived numerically by Du Plessis and Kröger [84DU1]:

$$f = a_1 \left[1 + \left\{Re/\left(70(P/d)^{1.3}\right)\right\}^{1.5}\right]^{0.333} \tag{2.2.4}$$

where

$$a_1 = a_2/[Re(15.767 - 0.14706\, t_t/d)]$$
$$a_2 = A_{ts}\, d^2/(a_3 a_4^2)$$
$$a_3 = 2P^2\,(a_6 - 1)/\pi - dt_t$$
$$a_4 = 4a_3/a_5$$
$$a_5 = 2d - 2t_t + \pi d/a_6$$
$$a_6 = [1 + (\pi d/2P)^2]^{0.5}$$
$$A_{ts} = \pi d^2/4$$

This equation is valid for $50 \leq Re \leq 2000$ and for $P/d \geq 2$.

In the case of hydrodynamically developing flow in a duct from an initial uniform velocity distribution, an apparent Fanning friction factor is defined that takes into account both the skin friction and the change in momentum rate (owing to a change in the shape of the velocity profile) in the hydrodynamic entrance region. In a "long duct" the apparent friction factor may be expressed in terms of an incremental pressure drop number K_∞ as

$$f_{app}\, Re = f\, Re + K_\infty\, d_e\, Re/4L \qquad (2.2.5)$$

For a circular duct or pipe

$$f_{app}\, Re = 16 + 0.313\, d\, Re/L \quad \text{for} \quad L/(d\, Re) \geq 0.06 \qquad (2.2.6)$$

Du Plessis [92DU1] proposes the following general correlation which can be applied to developing laminar flow in ducts of various cross sections:

$$f_{app} Re = \left[(fRe)^n + \left\{3.44/\left(L/d_e Re\right)\right\}^n\right]^{1/n} \qquad (2.2.7)$$

The above correlation agrees well with similar correlations by Shah [78SH1].

In equation (2.2.7) fRe is the value for fully developed flow and n is an exponent which is dependant on the duct geometry.

For concentric annular ducts having inner and outer radii of r_i and r_o respectively, values of n are listed in table 2.2.1.

Table 2.2.1: Values of exponent for annular ducts.

r_i/r_o	fRe	n
0	16.00	2.17
0.05	21.57	2.19
0.1	22.34	2.27
0.5	23.81	2.35
0.75	23.97	2.37
1	24.00	2.38

The case $r_i/r_o = 0$ corresponds to a pipe while $r_i/r_o = 1$ can be used for parallel plates.

For rectangular ducts fRe is obtained according to equation (2.2.2). The values for n are listed in table 2.2.2.

Table 2.2.2: Values of exponent for rectangular ducts.

b/a	n
1	2.01
0.5	2.02
0.2	2.17
0	2.38

For isosceles triangular ducts having apex angles of 2θ degrees the values of n are listed in table 2.2.3.

Table 2.2.3: *Values of exponent for isosceles triangular ducts.*

2θ	fRe	n
30°	13.065	1.84
60°	13.333	1.90
90°	13.153	1.97

In general the hydraulic entry length $L_{hy} = x/(d_e Re)$ is the dimensionless length required for the centerline velocity to attain 99 percent of its fully developed value. Values for L_{hy} and K_∞ for different duct sections are listed in table 3.2.1.

When heat is transferred to or from the fluid, all physical properties are evaluated at the bulk mean temperature. For those problems involving large temperature differences, corrections are introduced to provide for the temperature dependence of the fluid properties [83SH1].

In the case of gases, the friction factor evaluated at the bulk mean temperature, is multiplied by one of the following factors:

$$(T_w/T) \text{ for } 1 < (T_w/T) < 3 \text{ (heating)} \tag{2.2.8a}$$

$$(T_w/T)^{0.81} \text{ for } 0.5 < (T_w/T) < 1 \text{ (cooling)} \tag{2.2.8b}$$

For liquids, the friction factor evaluated at the bulk mean temperature is multiplied by one of the following factors to obtain the correct value.

$$(\mu_w/\mu)^{0.58} \text{ for } \mu_w/\mu < 1 \text{ (heating)} \tag{2.2.8c}$$

$$(\mu_w/\mu)^{0.54} \text{ for } \mu_w/\mu > 1 \text{ (cooling)} \tag{2.2.8d}$$

The subscript w refers to the mean value of the duct wall temperature. These relations are also applicable to developing flow.

Example 2.2.1

Air at a pressure of $p = 101025$ N/m^2 and a temperature of $T = 16.87°C$ flows uniformly into a rectangular duct with $a = 50$ mm and $b = 3.5$ mm at a rate of $m = 6.403 \times 10^{-4}$ kg/s. The duct is $L = 200$ mm long. Determine the pressure differential between the inlet and the outlet of the duct.

Solution

According to the perfect gas law given by equation (1.4.12), the density of the air at the specified conditions can be expressed as

$$\rho = \frac{p}{RT} = \frac{101025}{287.08 \times (273.15 + 16.87)} = 1.2134 \text{ kg/m}^3$$

where the gas constant for air is $R = 287.08$ J/kgK

The dynamic viscosity of the air at 16.87°C or $(273.15 + 16.87) = 290.02$ K is according to equation (A.1.3)

$$\mu = 2.287973 \times 10^{-6} + 6.259793 \times 10^{-8}T - 3.131956 \times 10^{-11}T^2 + 8.15038 \times 10^{-15}T^3$$

$$= 2.287973 \times 10^{-6} + 6.259793 \times 10^{-8} \times 290.02 - 3.131956 \times 10^{-11} \times 290.02^2$$

$$+ 8.15038 \times 10^{-15} \times 290.02^3 = 1.8007 \times 10^{-5} \text{ kg/sm}$$

The mean air speed in the duct follows from equation (2.1.3) i.e.

$$v = m/(\rho ab) = 6.403 \times 10^{-4}/(1.2134 \times 0.05 \times 0.0035) = 3.015 \text{ m/s}$$

According to equation (2.1.6) the hydraulic diameter of the duct is

$$d_e = \frac{4ab}{2(a+b)} = \frac{4 \times 0.05 \times 0.0035}{2(0.05 + 0.0035)} = 0.006542 \text{ m}$$

The Reynolds number for the air flowing in the duct is according to equation (2.1.5)

$$Re = \rho\, v\, d_e/\mu = 1.2134 \times 3.015 \times 0.006542/(1.8007 \times 10^{-5}) = 1329.1$$

It follows from equation (2.2.2) that for duct flow

$$fRe = 24\left[1 - 1.3553(0.0035/0.05) + 1.9467(0.0035/0.05)^2 - 1.7012(0.0035/0.05)^3\right.$$

$$\left. + 0.9564(0.0035/0.05)^4 - 0.2537(0.0035/0.05)^5\right] = 21.938$$

For $b/a = 0.0035/0.05 = 0.07$ find from table 2.2.2 $n \approx 2.3$.

Substitute the values for fRe and n into equation (2.2.7) to find

$$f_{app}Re = \left[(21.938)^{2.3} + \left\{3.44/(0.2/0.006542 \times 1329.1)^{0.5}\right\}^{2.3}\right]^{1/2.3} = 30.16$$

or

$$f_{app} = 30.16/1329.1 = 0.02269$$

According to equation (2.2.1) the pressure drop between the inlet and the outlet of the duct is

$$\Delta p = 4 f_{app}\left(\frac{L}{d_e}\right)\frac{\rho v^2}{2} = 4 \times 0.02269\left(\frac{0.2}{0.006542}\right)\left(\frac{1.2134 \times 3.015^2}{2}\right) = 15.3 \text{ N/m}^2$$

2.2.2 TURBULENT FLOW

With fully developed turbulent flow in ducts, the friction loss depends on flow conditions as characterized by the Reynolds number and on the nature of the duct wall surface. The quantity, ϵ, having the dimension of length is introduced as a measure of the surface roughness. From dimensional analysis, it therefore follows in general that the friction factor is a function of the Reynolds number and the relative roughness ϵ/d. The graphical representation of this relationship is known as the Moody diagram [44MO1] and is presented in figure 2.2.3.

As shown, the laminar friction factor for pipe flow is a single straight line and is not influenced by the relative roughness. Reynolds numbers in the range from 2000 to 4000 lie in a critical region where flow can be either laminar or turbulent.

For Reynolds numbers larger than those in the critical region, turbulent flow exists. The two regions, into which the turbulent zone is divided, transition and complete turbulence, categorize the state of the viscous sublayer as influenced by roughness.

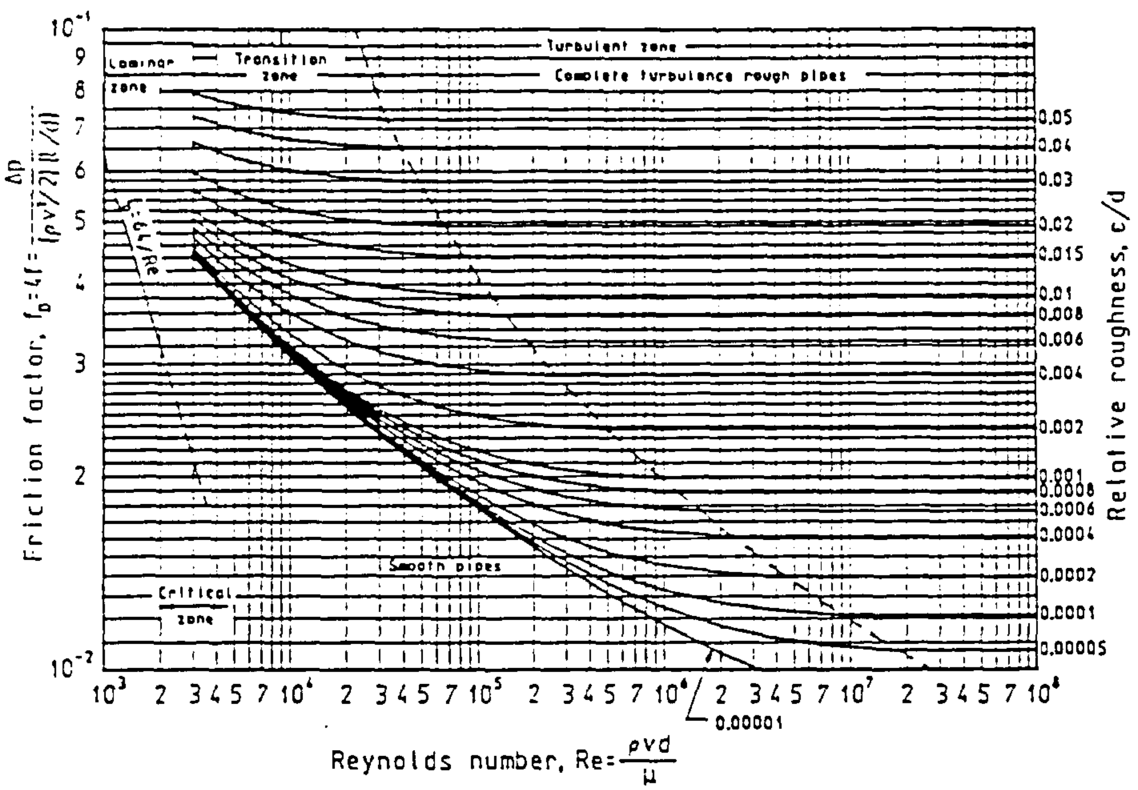

Figure 2.2.3: Friction factors for pipe flow.

Based on Nikuradse's data [32NI1], the following implicit relation is applicable to turbulent flow in smooth pipes:

$$1/f_D^{0.5} = 0.86 \ln (\mathrm{Re}\, f_D^{0.5}) - 0.8 \tag{2.2.9}$$

or according to Filonenko [54FI1],

$$f_D = (1.82 \log_{10} \mathrm{Re} - 1.64)^{-2} \tag{2.2.10}$$

Inspection indicates that for high Reynolds numbers and relative roughness the friction factor becomes independent of the Reynolds number in the region of complete turbulence. Then

$$f_D = [1.14 - 0.86 \ln (\epsilon/d)]^{-2} \tag{2.2.11}$$

Transition between this region and the smooth wall friction factor is represented by an empirical implicit transition function developed by Colebrook [39CO1].

$$\frac{1}{f_D^{0.5}} = \log_{10}\left[\left(\frac{\epsilon/d}{3.7}\right) + \frac{2.51}{\mathrm{Re}\, f_D^{0.5}}\right]^{-2} \tag{2.2.12}$$

For purposes of computation, the following explicit relation is of value [80BE1]:

$$f_D = 0.25\left[\log_{10}\left\{\left(\frac{\epsilon/d}{3.7}\right) + \left(\frac{5.74}{\mathrm{Re}^{0.9}}\right)\right\}\right]^{-2} \tag{2.2.13}$$

Haaland [83HA1] recommends an equation that yields results comparable to the implicit Colebrook equation:

$$f_D = 0.3086\left[\log_{10}\left\{\frac{6.9}{\mathrm{Re}} + \left(\frac{\epsilon/d}{3.75}\right)^{1.11}\right\}\right]^{-2} \tag{2.2.14}$$

for $\epsilon/d > 10^{-4}$. For situations where ϵ/d is very small, Haaland proposes

$$f_D = 2.7778\left[\log_{10}\left\{\left(\frac{7.7}{Re}\right)^3 + \left(\frac{\epsilon/d}{3.75}\right)^{3.33}\right\}\right]^{-2} \qquad (2.2.15)$$

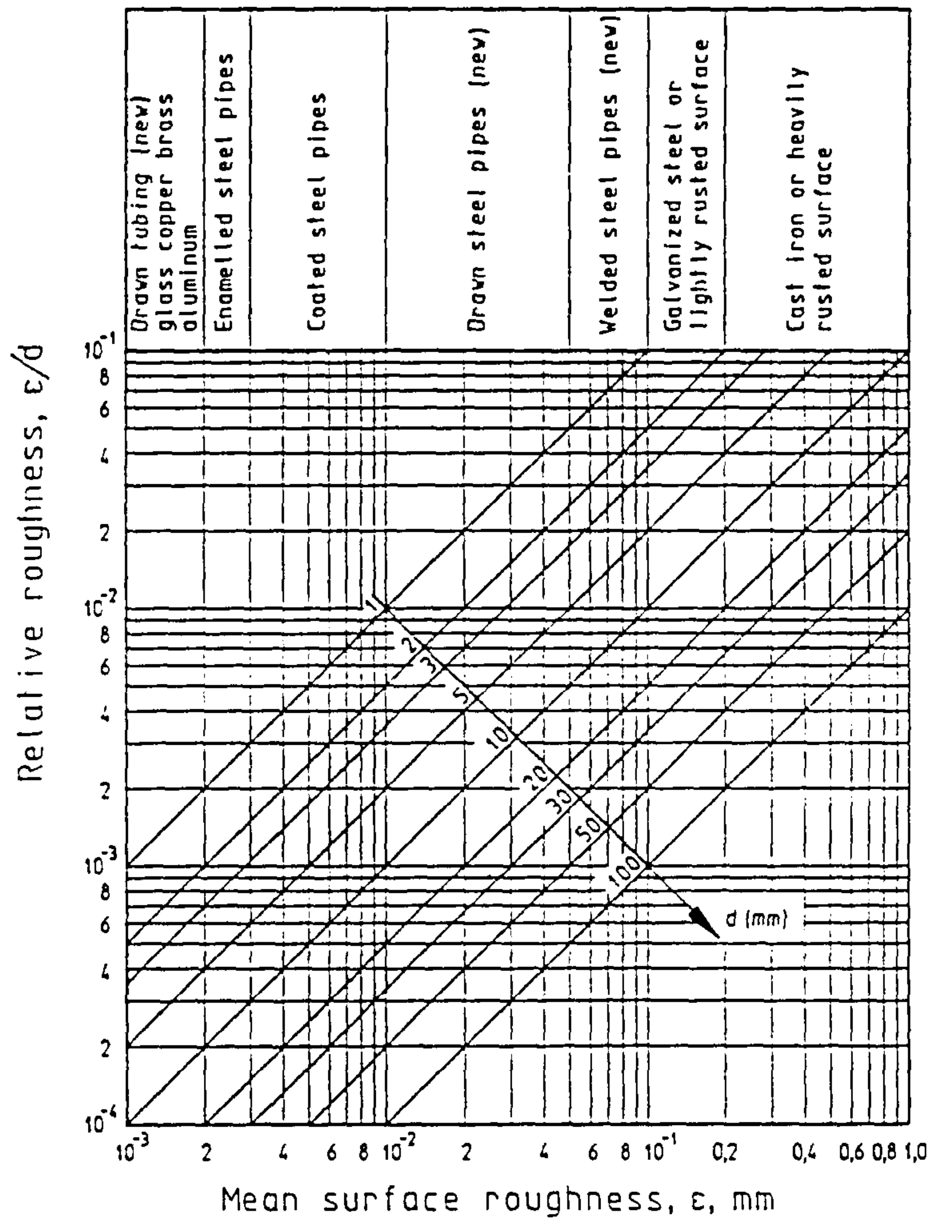

Figure 2.2.4: Surface roughness in pipes [52KI1].

The curves in the turbulent and transitional zones in figure (2.2.3) were drawn employing equation (2.2.11) and the Haaland relations respectively. An approximate indication of the relative roughnesses of typical pipe surfaces encountered in practice are shown in figure 2.2.4.

Although dimensional analysis does not relate the performance of ducts having circular and noncircular cross-sections, the fully turbulent friction factor for noncircular cross-sections (annular spaces, rectangular and triangular ducts, etc.) may be evaluated from the data for circular pipes if the pipe diameter is replaced by an equivalent diameter also referred to as the hydraulic diameter as defined by equation (2.1.6).

The equivalent or hydraulic diameter for an annulus of inner and outer diameter d_i and d_o respectively is

$$d_e = \frac{4(\pi/4)(d_o^2 - d_i^2)}{\pi(d_o + d_i)} = d_o - d_i \qquad (2.2.16)$$

For a rectangular duct having sides a and b it is

$$d_e = 2ab/(a + b) \qquad (2.2.17)$$

Launder and Ying [72LA1] show that for a rectangular duct the secondary velocity distribution gives rise to an increase in the friction factor of about 10 per cent. Even so, their full theory slightly underestimates the measurements of Hartnett et al. [62HA1].

When heat transfer occurs in turbulent duct flow, changes in thermophysical properties should be considered. By multiplying the friction factor, evaluated at the bulk temperature of the fluid, by one of the following appropriate correction factors, this effect is taken into consideration [70PE1]:

$$(7 - \mu/\mu_w)/6 \quad \text{for} \quad (\mu_w/\mu) < 1 \quad \text{(heating)} \qquad (2.2.18)$$

$$(\mu_w/\mu)^{0.24} \quad \text{for} \quad (\mu_w/\mu) > 1 \quad \text{(cooling)} \qquad (2.2.19)$$

for $1.3 < Pr < 10$ and where μ_w is evaluated at the duct wall temperature.

For air and hydrogen

$$(T_w/T)^{\left[-0.6\ +\ 5.6\ (Re_w \rho_w/\rho)^{-0.38}\right]} \quad \text{(heating)} \tag{2.2.20}$$

$$(T_w/T)^{\left[-0.6\ +\ 0.79(Re_w \rho_w/\rho)^{-0.11}\right]} \quad \text{(cooling)} \tag{2.2.21}$$

For developing turbulent flow near the entrance of a duct, the friction factor is considerably higher than that for fully developed flow [55DE1].

2.2.3 TRANSITION LAMINAR - TURBULENT FLOW

In the critical zone in which transition from laminar to turbulent flow takes place, the friction factor is uncertain and there is therefore corresponding uncertainty in pressure drop estimates if the Reynolds number falls in this range, i.e. $2000 \le Re \le 4000$.

A single correlating equation that covers the entire range from the laminar through the critical region to turbulent flow in smooth tubes is proposed by Churchill [77CH1]:

$$f_D = 8\left[\frac{1}{\left\{\left(\frac{8}{Re}\right)^{10} + \left(\frac{Re}{36500}\right)^{20}\right\}^{0.5}} + \left\{2.21\ \ell n\left(\frac{Re}{7}\right)\right\}^{10}\right]^{-0.2} \tag{2.2.22}$$

A more comprehensive equation including the effect of surface roughness is presented by the same author [77CH2]:

$$f_D = 8\left[\left(\frac{8}{Re}\right)^{12} + \frac{1}{(a_1 + a_2)^{1.5}}\right]^{0.0833} \tag{2.2.23}$$

where

$$a_1 = \left[2.457\ \ell n\left\{\frac{1}{(7/Re)^{0.9} + 0.27\epsilon/d}\right\}\right]^{16} \text{ and } a_2 = \left(\frac{37530}{Re}\right)^{16}$$

Example 2.2.1

Calculate the approximate mean D'Arcy friction factor when air at a pressure of p_a = 1.013×10^5 N/m^2 and a bulk temperature of T = 93.33 °C flows through a smooth pipe having an inside diameter of 25.4 mm, at a speed of 6.096 m/s. The inside pipe wall temperature T_w = 426.67 °C. The dynamic viscosity of air at 426.67°C is μ_{aw} = 3.355 x 10^{-5} kg/ms.

Solution

Evaluate the Reynolds number of the air stream at bulk temperature.

According to Appendix A, equation (A.1.1), the density of the air at the bulk temperature of (273.15 + 93.33) = 366.48 K is

$$\rho_a = \frac{p_a}{287.08\ T} = \frac{1.013 \times 10^5}{287.08 \times (273.15 + 93.33)} = 0.9628\ \text{kg/m}^3$$

The dynamic viscosity of the air at this temperature follows from equation (A.1.2).

$$\mu_a = 2.287973 \times 10^{-6} + 6.259793 \times 10^{-8} \times 366.48 - 3.131956 \times 10^{-11} \times 366.48^2$$

$$+ 8.15038 \times 10^{-15} \times 366.48^3 = 2.14236 \times 10^{-5}\ \text{kg/ms}$$

Thus

$$Re = \frac{\rho_a v d}{\mu_a} = \frac{0.9628 \times 6.096 \times 0.0254}{2.14236 \times 10^{-5}} = 6958.61$$

The flow is turbulent and the friction factor for the smooth tube may thus be determined at the bulk temperature according to equation (2.2.10) i.e.

$$f_D = (1.82 \log_{10} 6958.61 - 1.64)^{-2} = 0.03489$$

This factor must be corrected by multiplying it by equation (2.2.20) which includes the Reynolds number of the air evaluated at the wall temperature T_w = 426.67 °C or (273.15 + 426.67) = 699.82 K.

The air density at this temperature is

$$\rho_{aw} = \frac{1.013 \times 10^5}{287.08 \times 699.82} = 0.5042 \text{ kg/m}^3$$

With this density and the specified dynamic viscosity of the air evaluated at the pipe wall temperature, find the corresponding Reynolds number

$$Re_w = \frac{0.5042 \times 6.096 \times 0.0254}{3.355 \times 10^{-5}} = 2326.96$$

The corrected friction factor is thus

$$f_{Dc} = f_D \, (T_w/T)^{[-0.6 + 5.6 \, (Re_w \rho_{aw}/\rho_a)^{-0.38}]}$$

$$= 0.03489 \, (699.82/366.48)^{[-0.6 + 5.6 \, (2326.96 \times 0.5042/0.9628)^{-0.38}]} = 0.03019$$

2.3 LOSSES IN DUCT SYSTEMS

In addition to the frictional resistance experienced during flow in a duct, head losses or losses of mechanical energy may occur at inlets, outlets, abrupt changes in duct cross-sectional area, valves, bends and other appurtenances in such systems.

If the density of the fluid remains constant and there is no change in elevation, a loss coefficient can in general be defined between two cross-sections, 1 and 2 respectively, as

$$K = \frac{\left(p_1/\rho + \alpha_{e1} v_1^2/2\right) - \left(p_2/\rho + \alpha_{e2} v_2^2/2\right)}{v^2/2} \tag{2.3.1}$$

where v usually corresponds to either v_1 or v_2 or some mean value of the two.

Since most loss coefficients are determined experimentally, it is important to specify the velocity on which a loss coefficient for a particular duct element is based, i.e. inlet, outlet, or some mean condition.

If the velocity distribution at sections 1 and 2 is uniform, as is approximately the case in turbulent flow, the kinetic energy coefficient $\alpha_e \approx 1$ and equation (2.3.1) can be written as

$$K = \frac{\left(p_1 + \rho v_1^2/2\right) - \left(p_2 + \rho v_2^2/2\right)}{\rho v^2/2}$$

or

$$K = \left(p_{t1} - p_{t2}\right)/\left(\rho v^2/2\right) \tag{2.3.2}$$

where p_{t1} and p_{t2} are the total pressures at sections 1 and 2 respectively. K is also referred to as the total pressure loss coefficient.

For frictional, fully developed, incompressible flow in a pipe of constant diameter, the pressure drop is given by the empirical D'Arcy-Weisbach equation (2.2.1) and the corresponding loss coefficient according to equation (2.3.1) may be expressed as

$$K_f = \Delta p/(\rho v^2/2) = f_D L/d \tag{2.3.3}$$

The region of influence of an appurtenance or component can be determined experimentally by attaching straight pipe to the exit and entry of the component of sufficient length for fully developed conditions to be attained upstream and downstream. Consider, for example, the pressure distribution along a pipeline containing a bend for incompressible turbulent flow as shown in figure 2.3.1. The variations in static pressure which are present across a section within the bend extend for a diameter or two into the straight pipes upstream or downstream. The constant pressure gradient associated with fully developed flow in a straight pipe is not re-established until 50 or more diameters downstream from the bend.

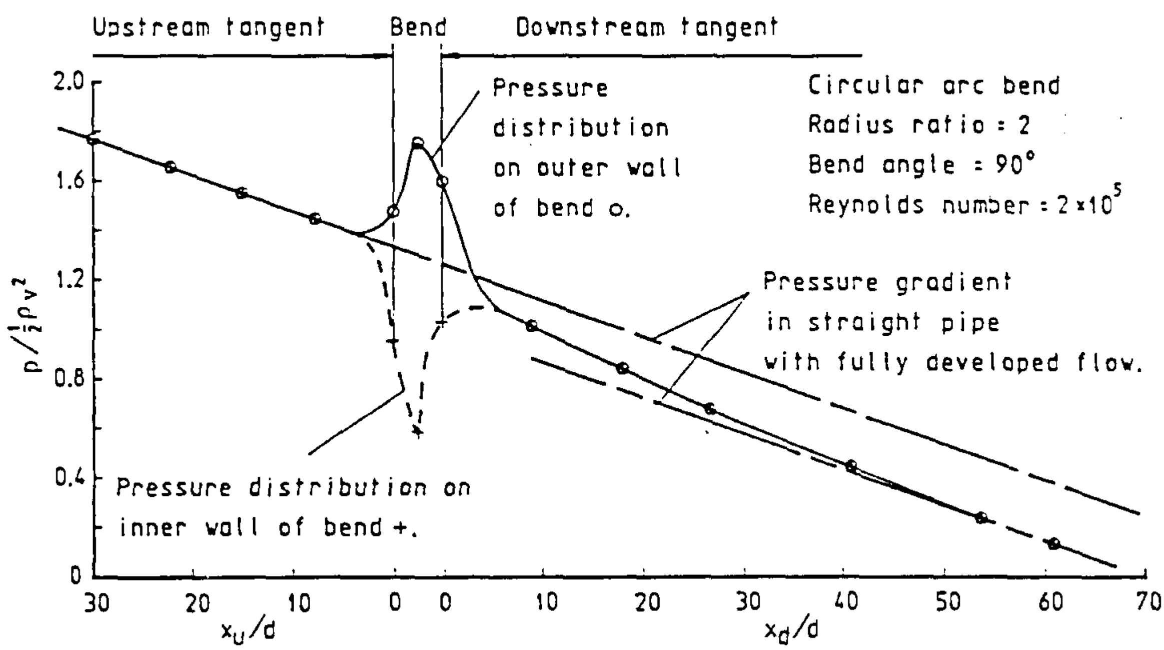

Figure 2.3.1: Pressure distribution in horizontal pipeline containing a bend.

For most other pipework components the variations in static pressure at a cross-section are far less marked than for bends, and the fully developed velocity profile is recovered more quickly. For example, the flow recovers after about five diameters downstream of a sudden enlargement [55HA1].

When the flow upstream and downstream of a component is fully developed, the component is said to be free of interference effects, since its performance is independent of the flow beyond the regions of fully developed flow. In the calculation of system pressure losses it may be necessary to approximate the real situation by using data obtained from tests in interference-free flow. This approach should not lead to large errors, provided that a spacer length of at least 5 diameters - or, in the case of bends, 10 diameters separates one component from another.

In many practical systems, interference exists between the components of the pipe system. This occurs when the regions of influence of two components overlap. The pressure loss through combinations may be higher or lower than the sum of the losses of the components in interference free flow [77ES1].

There are so many possible combinations of components that, at present, the prediction of the performance of a system with interferences can be made with any accuracy only under special circumstances. If the interference in the system is confined to the interactions between a few of the components and data are available for these particular interactions, then, by considering these interacting components as single entities, the principles outlined for interference free flow can be applied. In some circumstances, it may be possible to deduce, by broad physical arguments, that the interference effects will not be important. Consequently the performance of the system can be estimated quite accurately using data obtained under interference-free conditions. Alternatively, there may be one or two particularly large sources of pressure loss in the system, and providing their magnitudes are known with reasonable accuracy, a much lower order of accuracy is acceptable for the other components.

These situations must, however, be regarded as special cases. With the present state of knowledge, if an accurate assessment is required of the performance of a duct flow system in which interferences occur, it is generally necessary to resort to model tests or computer analysis.

Extensive data for loss coefficients of different components in pipe and duct systems is presented in the literature [71MI1, 73HO1, 76CR1, 86ID1, 89FR1, 90MI1].

2.3.1 ABRUPT CONTRACTIONS AND EXPANSIONS

Head or mechanical energy losses occur at abrupt changes in duct flow cross-sectional area. Consider incompressible flow in the duct shown in figure 2.3.2, which includes a contraction at the inlet and a sudden enlargement at the outlet.

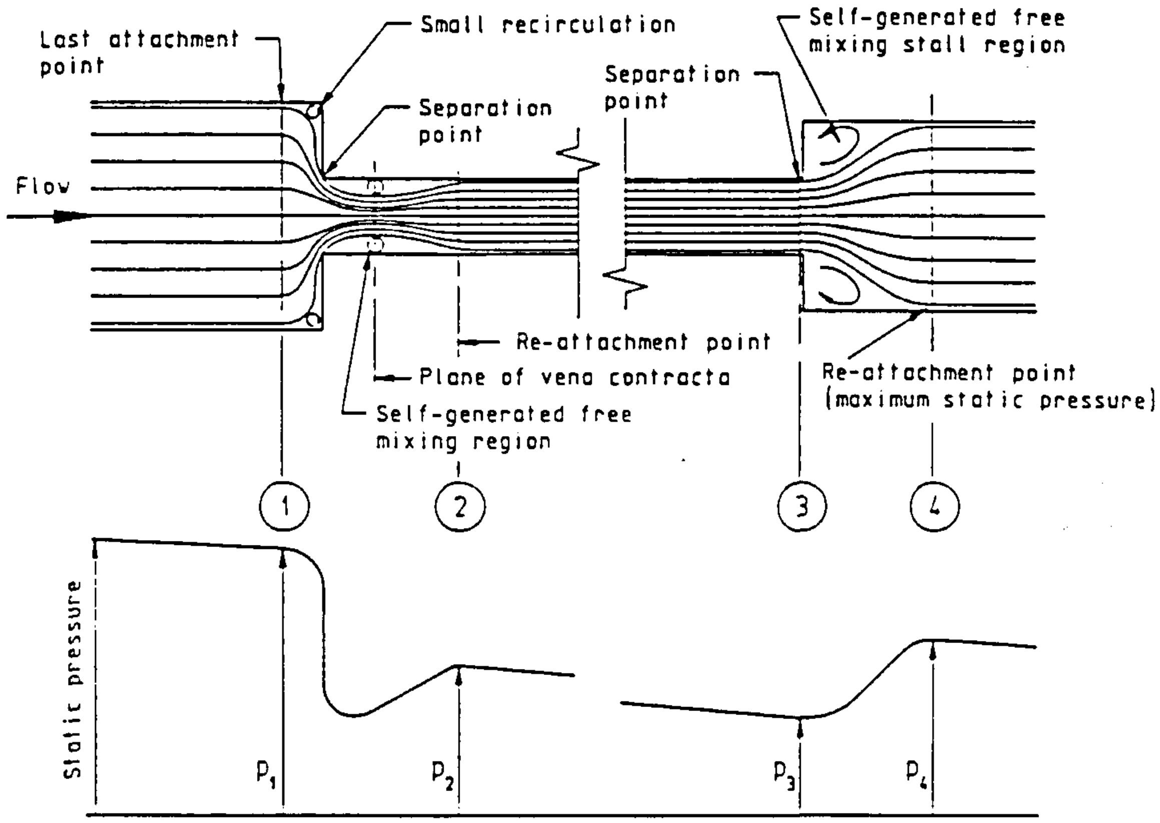

Figure 2.3.2: Static pressure distribution in a duct.

From equation (2.3.2) for uniform velocity distributions, the total inlet pressure drop owing to a reduction in the flow area resulting in an acceleration of the flow and a loss owing to separation of the boundary layer can be expressed as

$$\left(p_1 + \rho v_1^2/2\right) - \left(p_2 + \rho v_2^2/2\right) = K_c \, \rho v_2^2/2 \tag{2.3.4}$$

The corresponding static pressure drop is

$$p_1 - p_2 = (\rho\, v_2^2/2)\left[(1 - \sigma_{21}^2) + K_c\right] \qquad (2.3.5)$$

where $\sigma_{21} = A_2/A_1$. The irreversible loss is contained in the contraction coefficient K_c.

At the outlet of the duct there will be a rise in static pressure owing to the increase in flow area, whereas a loss will occur owing to boundary layer separation and momentum changes following the abrupt expansion.

The resultant change in pressure is

$$p_3 - p_4 = (\rho\, v_3^2/2)\left[K_e - (1 - \sigma_{34}^2)\right] \qquad (2.3.6)$$

where K_e is the expansion coefficient and $\sigma_{34} = A_3/A_4$.

The above loss coefficients are referred to the kinetic energy of the flow in the smaller cross-sectional area and can be expressed by the following two equations respectively [50KA1]:

$$K_c = 1 - 2/\sigma_c + 1/\sigma_c^2 = \left(1 - 1/\sigma_c\right)^2 \qquad (2.3.7)$$

and

$$K_e = (1 - \sigma_{34})^2 \qquad (2.3.8)$$

Equations (2.3.7) and (2.3.8) apply to sharp-edged abrupt changes in cross-section for single tubes or for tube bundles.

The contraction ratio $\sigma_c = A_c/A_2$, as shown graphically in figure 2.3.3 for two-dimensional and three-dimensional circular contractions, is usually determined experimentally [00WE1]. The minimum area of the jet between sections 1 and 2, A_c, is referred to as the vena contracta.

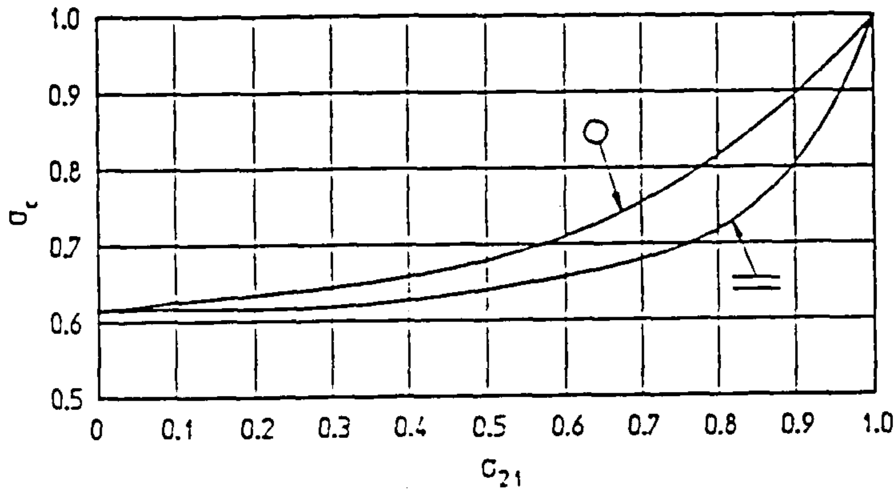

Figure 2.3.3: Contraction ratio for round tubes and parallel plates.

The curves shown in figure 2.3.3 are approximated by the following empirical relations:

$$\sigma_c = 0.61375 + 0.13318\ \sigma_{21} - 0.26095\ \sigma_{21}^2 + 0.51146\ \sigma_{21}^3 \qquad (2.3.9)$$

for round tubes , and

$$\sigma_c = 0.6144517 + 0.04566493\ \sigma_{21} - 0.336651\ \sigma_{21}^2 + 0.4082743\ \sigma_{21}^3$$

$$+ 2.672041\ \sigma_{21}^4 - 5.963169\ \sigma_{21}^5 + 3.558944\ \sigma_{21}^6 \qquad (2.3.10)$$

for parallel plates [46RO1].

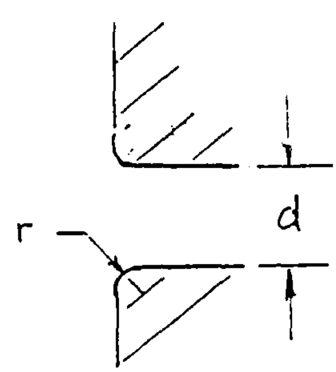

Re > 10000	
r/d	K_c
0.00	0.5
0.02	0.37
0.04	0.26
0.06	0.20
0.08	0.15
0.16	0.06

Figure 2.3.5: Contraction loss coefficient for rounded inlet [89FR1].

It is possible to reduce the contraction loss coefficient for a tube significantly by rounding off the inlet edge. This is illustrated in figure 2.3.5.

For tubes penetrating into a manifold, a higher loss coefficient is applicable, as shown in figure 2.3.6.

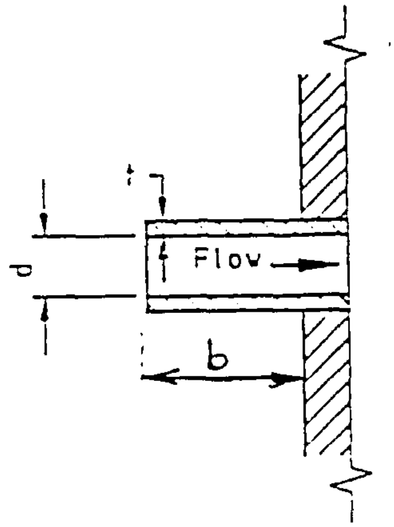

Re > 10000	
b/d = 0.5	
t/d	K_c
0.00	1.00
0.01	0.85
0.02	0.72
0.03	0.61
0.05	0.50

Figure 2.3.6: Contraction loss coefficient for penetrating tube [89FR1].

Example 2.3.1

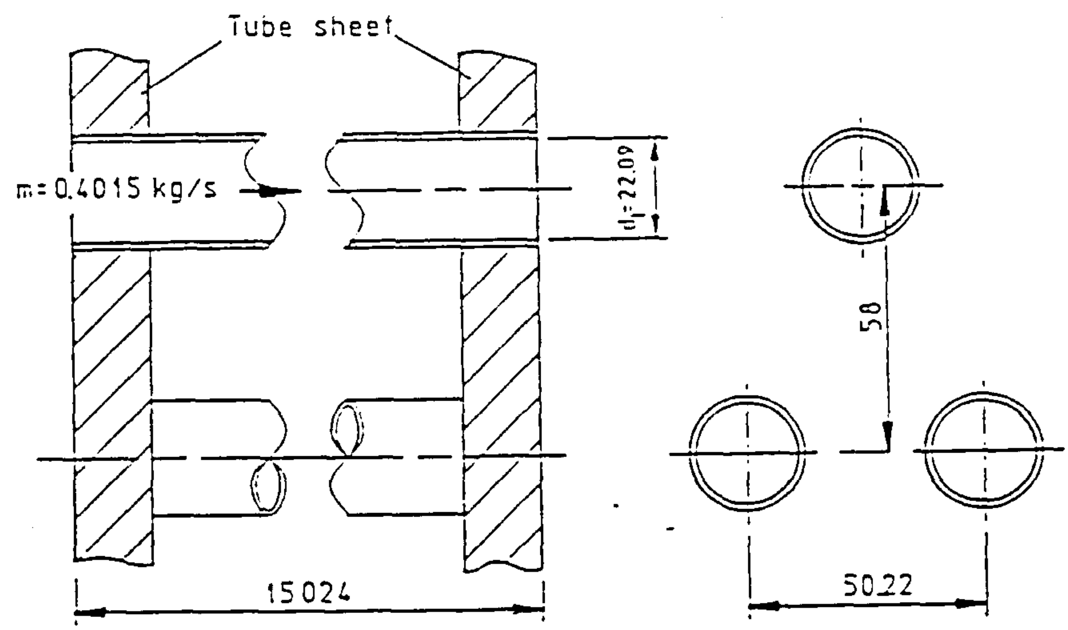

Figure 2.3.7: Tube dimensions and layout.

A heat exchanger bundle consists of tubes having an inside diameter of 22.09 mm and a total length of 15024 mm. The tubes are arranged in a staggered pattern and are welded into tube sheets as shown in figure 2.3.7.

Water at 52.5 °C flows through each tube at a rate of 0.4015 kg/s. The tube inlet has a sharp edge. Determine the difference in static pressure between the headers for a smooth tube and for the case where $\epsilon/d_i = 10^{-3}$.

Solution

The thermophysical properties of water are listed in Appendix A. Evaluate properties at 52.5 °C (325.65 K).

Density of water from equation (A.4.1):

$$\rho_w = (1.49343 \times 10^{-3} - 3.7164 \times 10^{-6} \times 325.65 + 7.09782 \times 10^{-9} \times 325.65^2$$

$$- 1.90321 \times 10^{-20} \times 235.65^6)^{-1} = 986.9767 \text{ kg/m}^3$$

Dynamic viscosity of water from equation (A.4.3):

$$\mu_w = 2.414 \times 10^{-5} \times 10^{247.8/(325.65 - 140)} = 5.21804 \times 10^{-4} \text{ kg/ms}$$

The Reynolds number for the water flowing in the tube is

$$Re = \frac{\rho_w \, v \, d_i}{\mu_w} = \frac{4 \, m}{\pi d_i \, \mu_w} = \frac{4 \times 0.4015 \times 10^7}{\pi \times 22.09 \times 5.21804} = 44349.9$$

The flow in the tube is turbulent. The mean velocity of the water in the tube is determined from

$$v = \frac{4m}{\rho_w \pi d_i^2} = \frac{4 \times 0.4015}{986.9767 \times \pi(0.02209)^2} = 1.06144 \text{m/s}$$

The frictional pressure drop may be determined according to equation (2.2.1).

$$\Delta p_f = f_D \left(\frac{L}{d_i}\right) \frac{\rho_w v^2}{2}$$

For a smooth tube the friction factor follows from equation (2.2.10):

$$f_D = (1.82 \log_{10} 44349.9 - 1.64)^{-2} = 0.021516$$

The frictional pressure drop is thus

$$\Delta p_f = 0.021516 \left(\frac{15024}{22.09}\right) \frac{986.9767 \times 1.06144^2}{2} = 8136.15 \text{ N/m}^2$$

For the rough pipe it follows from equation (2.2.14) that

$$f_D = 0.3086/[\log_{10} \{6.9/44349.9 + (10^{-3}/3.7)^{1.11}\}]^2 = 0.0241234$$

The resultant frictional pressure drop is

$$\Delta p_f = 0.0241234 \left(\frac{15024}{22.09}\right) \frac{986.9767 \times 1.06144^2}{2} = 9122.12 \text{ N/m}^2$$

For the particular tube layout the area ratio for the entering water stream is

$$\sigma = \pi \times 22.09^2/(4 \times 58 \times 50.22) = 0.13158$$

whereas the jet contraction ratio is according to equation (2.3.10)

$$\sigma_c = 0.61375 + 0.13318 \times 0.13158 - 0.26095 \times 0.13158^2 + 0.51146 \times 0.13158^2$$

$$= 0.628$$

For turbulent flow, the inlet contraction loss coefficient may be approximated by equation

(2.3.7), i.e.

$$K_c = 1 - 2/0.628 + 1/0.628^2 = 0.351$$

The corresponding static pressure drop at the inlet to the tube follows from equation (2.3.5):

$$\Delta p_i = 0.5 \text{ x } 986.9767 \text{ x } 1.06144^2 \left[(1 - 0.13158^2) + 0.351\right] = 741.5 \text{ N/m}^2$$

The outlet expansion loss coefficient is approximated by equation (2.3.8):

$$K_e = (1 - 0.13158)^2 = 0.7542$$

The corresponding static pressure drop at the outlet of the tube follows from equation (2.3.6):

$$\Delta p_e = 0.5 \text{ x } 986.9767 \text{ x } 1.06144^2 \left[0.7542 - (1 - 0.13158^2)\right] = -127.0 \text{ N/m}^2$$

For a smooth tube the total static pressure differential between the headers is

$$\Delta p = 8136.15 + 741.5 - 127.0 = 8751 \text{ N/m}^2$$

For the rough tube, the pressure drop is

$$\Delta p = 9122.12 + 741.5 - 127.0 = 9737 \text{ N/m}^2$$

2.3.2 REDUCERS AND DIFFUSERS

When the duct flow area is reduced gradually as shown in figure 2.3.8(a) and (b), the number of velocity heads lost is very small. Based on the smaller flow area, a loss coefficient of $K_{red} = 0.04$, or less, is commonly quoted.

For the conical reducer shown in figure 2.3.8(c), the loss coefficient based on the smaller area may be obtained from the following equation [89FR1]:

$$K_{red} = \left(-0.0125\ \sigma_{21}^4 + 0.0224\ \sigma_{21}^3 - 0.00723\ \sigma_{21}^2 + 0.00444\ \sigma_{21} - 0.00745\right)$$

$$\left(8\ \theta^3 - 4\pi\ \theta^2 - 20\ \theta\right) \qquad (2.3.11)$$

where $\sigma_{21} = A_2/A_1$ and θ is in radians. The loss coefficient is based on the velocity at 2.

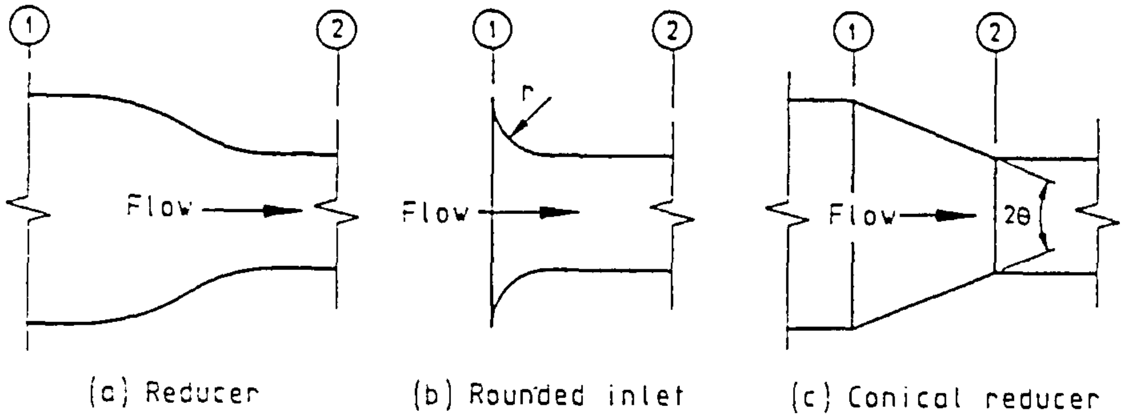

Figure 2.3.8: Reducers.

Whenever it is necessary to increase the flow area of a pipe gradually, the conical diffuser as shown in figure 2.3.9 may be used.

Ideally, in the absence of losses, the total pressure remains constant, i.e.

$$p_{2id} + \rho v_2^2/2 = p_1 + \rho v_1^2/2$$

and the pressure recovery is

$$p_{2id} - p_1 = \rho\left(v_1^2 - v_2^2\right)/2 = \rho v_1^2\left(1 - \sigma_{12}^2\right)/2 \qquad (2.3.12)$$

where $\sigma_{12} = A_1/A_2$ and subscript id refers to ideal conditions.

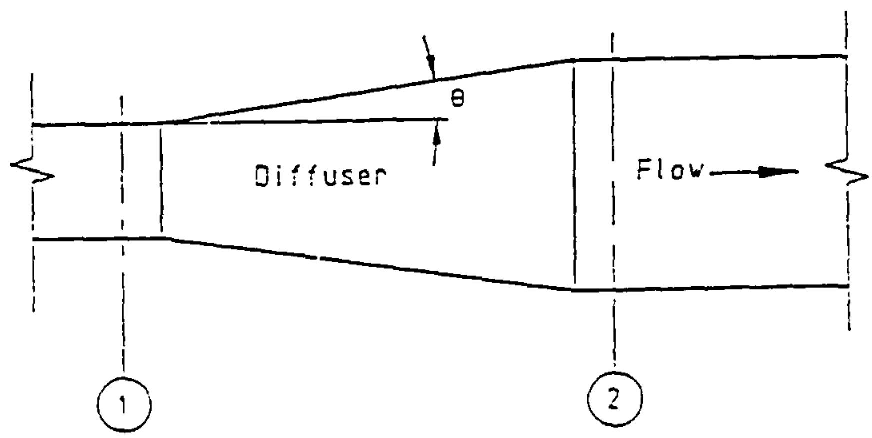

Figure 2.3.9: Conical diffuser.

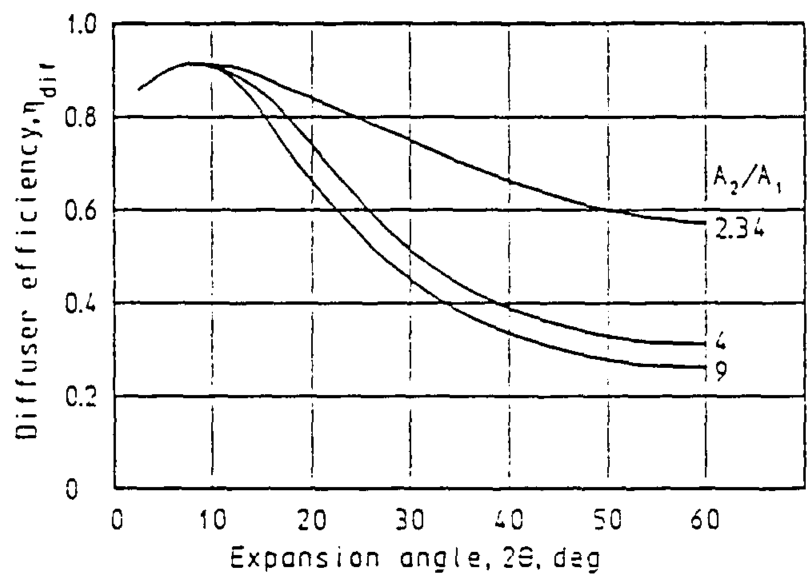

Figure 2.3.10: Conical diffuser efficiencies.

In practical diffusers only a part of this pressure recovery is possible and a diffuser efficiency is defined as

$$\eta_{dif} = \frac{p_2 - p_1}{p_{2id} - p_1} = \frac{p_2 - p_1}{\rho v_1^2 \left(1 - \sigma_{21}^2\right)/2} \qquad (2.3.13)$$

For relatively small expansion angles, the diffuser efficiencies have been determined by Patterson [38PA1] whose results are shown in figure 2.3.10.

The loss coefficient of a diffuser is

$$K_{dif} = \frac{p_{t1} - p_{t2}}{\rho v_1^2/2} = \frac{\left(p_1 + \rho v_1^2/2\right) - \left(p_2 + \rho v_2^2/2\right)}{\rho v_1^2/2} \qquad (2.3.14)$$

Substitute equation (2.3.13) into equation (2.3.14) and find

$$K_{dif} = \left(1 - \eta_{dif}\right)\left(1 - \sigma_{12}^2\right) \qquad (2.3.15)$$

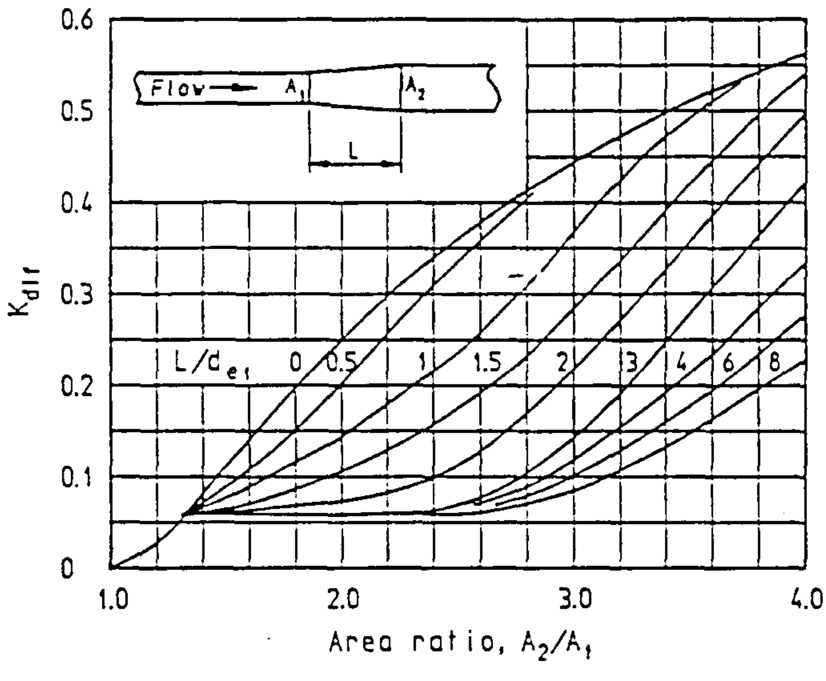

Figure 2.3.11: Losses in duct diffusers.

For practical applications it may be convenient to employ figure 2.3.11 [78DA1].

The losses for open-outlet diffusers are shown in figure 2.3.12. An exceptionally uniform approach velocity (as in a venturi nozzle flow meter) allows more rapid expansion and lower loss, as shown by the broken lines. Extensive data on flat and conical diffusers is presented by Runstadler et al [75RU1].

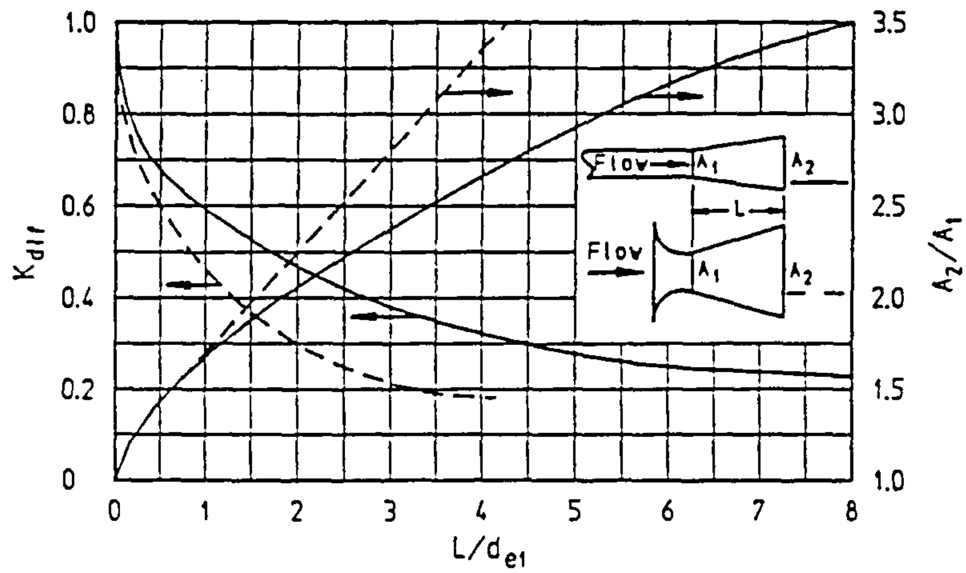

Figure 2.3.12: Losses in open outlet diffusers.

2.3.3 THREE-LEG JUNCTIONS

Pressure loss data for dividing flows through planar three-leg junctions are cited in various reference [73ES1, 74VD1, 78GE1, 90MI1].

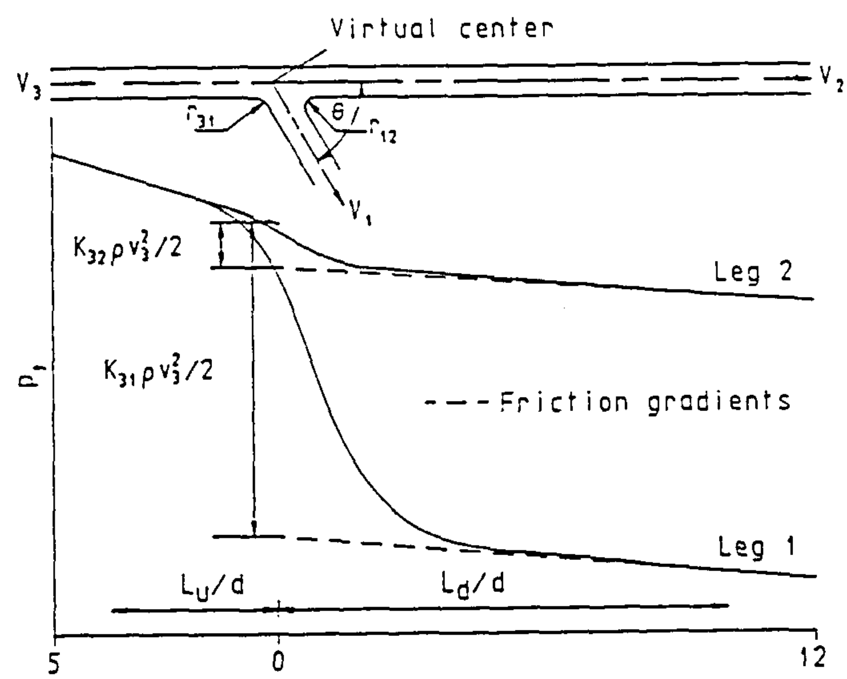

Figure 2.3.13: Variation of total pressure in the vicinity of a junction.

The total pressure differences across pairs of inlet and outlet legs of a junction as shown in figure 2.3.13 are calculated from

$$p_{t3} - p_{t1} = K_{31}\rho v_3^2/2 + f_{D3}L_3\rho v_3^2/2d_3 + f_{D1}L_1\rho v_1^2/2d_1 \qquad (2.3.16)$$

and

$$p_{t3} - p_{t2} = K_{32}\rho v_3^2/2 + f_{D3}L_3\rho v_3^2/2d_3 + f_{D2}L_2\rho v_2^2/2d_2 \qquad (2.3.17)$$

The last two terms on the right-hand side of equations (2.3.16) and (2.3.17) are the straight-pipe friction losses over lengths L_3, L_1 and L_2.

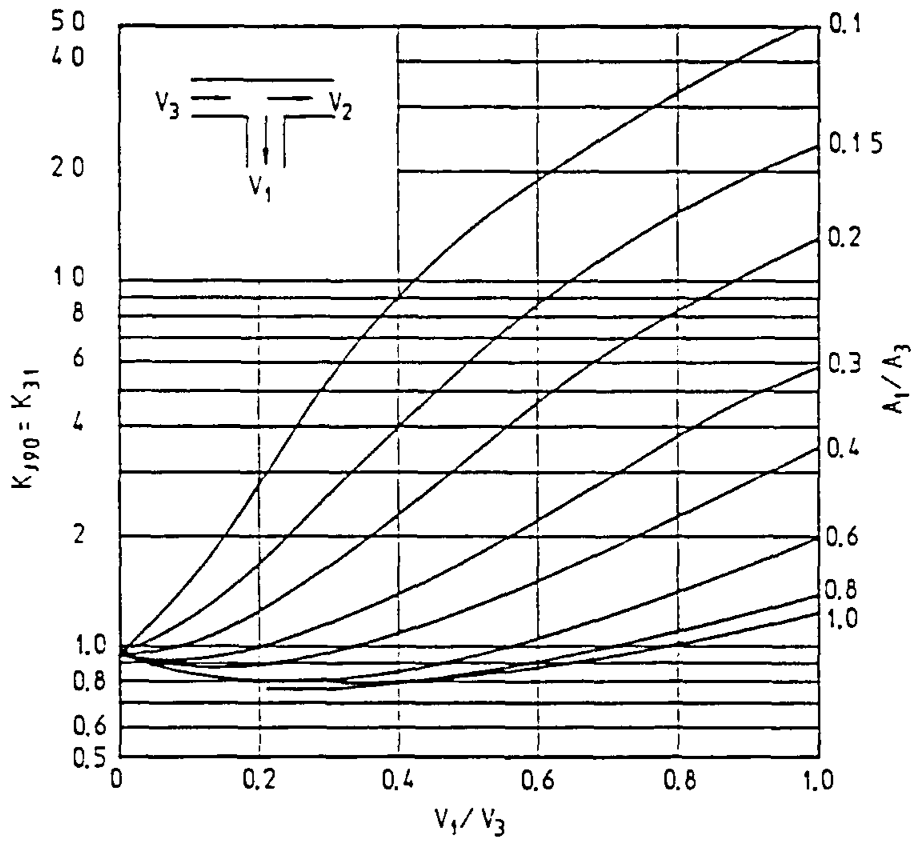

Figure 2.3.14: Loss coefficient for a 90° junction with sharp corners.

The loss coefficient for a 90° junction ($K_{j90} = K_{31}$) with $Re_3 \geq 2 \times 10^5$ between leg 3 and leg 1 is given in figure 2.3.14 for sharp corners ($r_{31} = r_{12} = 0$) as a function of A_1/A_3 and V_1/V_3.

With rounded corners the loss coefficient may be reduced, i.e.

$$K_{31r} = K_{j90r} = K_{j90} - 0.9\left(\frac{V_1/V_3}{A_1/A_3}\right)^2\left(\frac{r_{31}}{d_1}\right)^{0.5} - 0.26\left(\frac{V_1/V_3}{A_1/A_3}\right)^2\left(\frac{r_{12}}{d_1}\right)^{0.5} \tag{2.3.18}$$

for $r_{12}/d_1 < 0.15$ and $r_{31}/d_1 < 0.15$ and

$$K_{31r} = K_{j90r} = K_{j90} - 0.45\left(\frac{V_1/V_3}{A_1/A_3}\right)^2 \tag{2.3.19}$$

for $r_{12}/d_1 > 0.15$ and $r_{31}/d_1 > 0.15$.

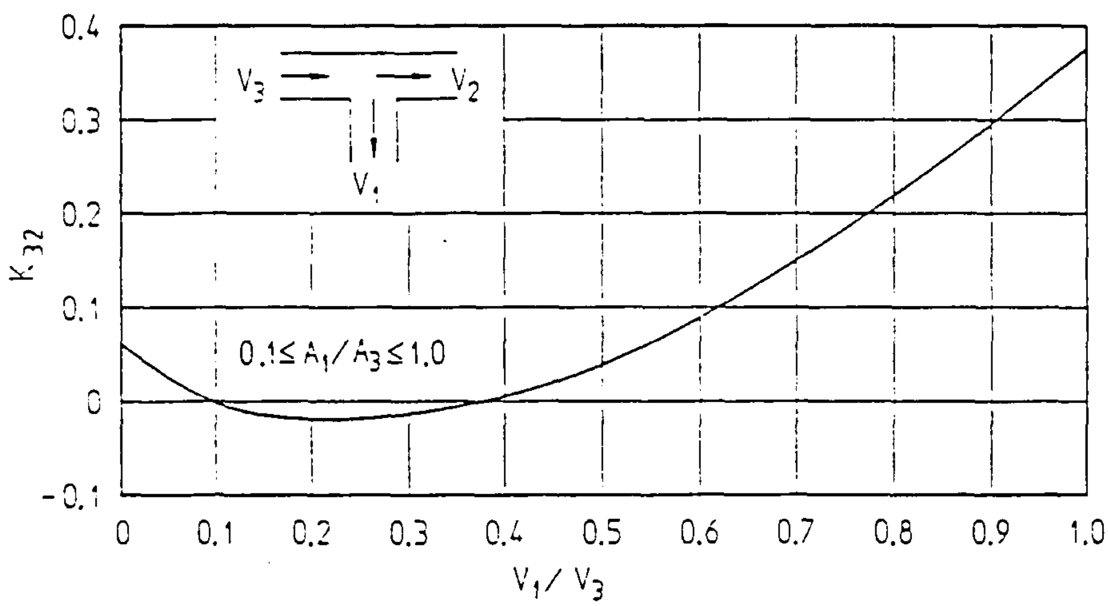

Figure 2.3.15: Loss coefficient K_{32} for a 90 ° junction.

The information strictly applies to junctions where the inlet flow is fully developed and where there is a long downstream duct length, but in practice it can be applied without significant error when there are 15 or more equivalent diameters upstream and at least 4 diameters downstream of the junction.

It is possible to reduce the loss coefficient by installing suitable guide vanes.

The loss coefficient between leg 3 and 2 can be assumed to be unaffected by the geometry of leg 1 and is given in figure 2.3.15 as a function of the flow ratio only. There is no significant change in the loss coefficient, K_{32}, owing to rounding of the junction corners.

In the case of a sharp-edged T-junction ($K_T = K_{31}$) the loss coefficient is as shown in figure 2.3.16.

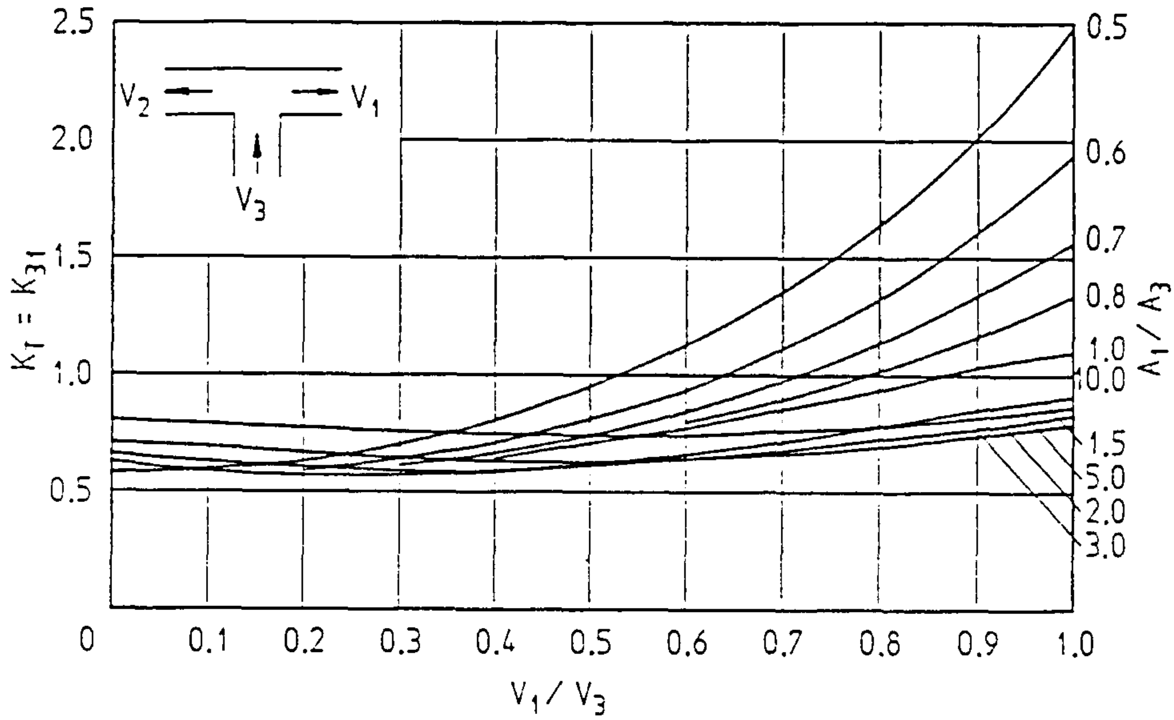

Figure 2.3.16: Loss coefficient for a T-junction with sharp corners.

2.3.4 CURVED DUCTS OR BENDS

A few common types of curved ducts or bends are shown schematically in figure 2.3.17. Pressure-loss data for flow through such bends are available [77ES1]. The pressure loss owing to a sharp bend and, in particular, a miter bend, may be reduced by fitting guide vanes. It is common practice to use a number of guide vanes in a cascade in a miter bend. The vane geometry is not fixed by the bend geometry and a number of designs exist. One example of such a miter bend is shown in figure 2.3.18.

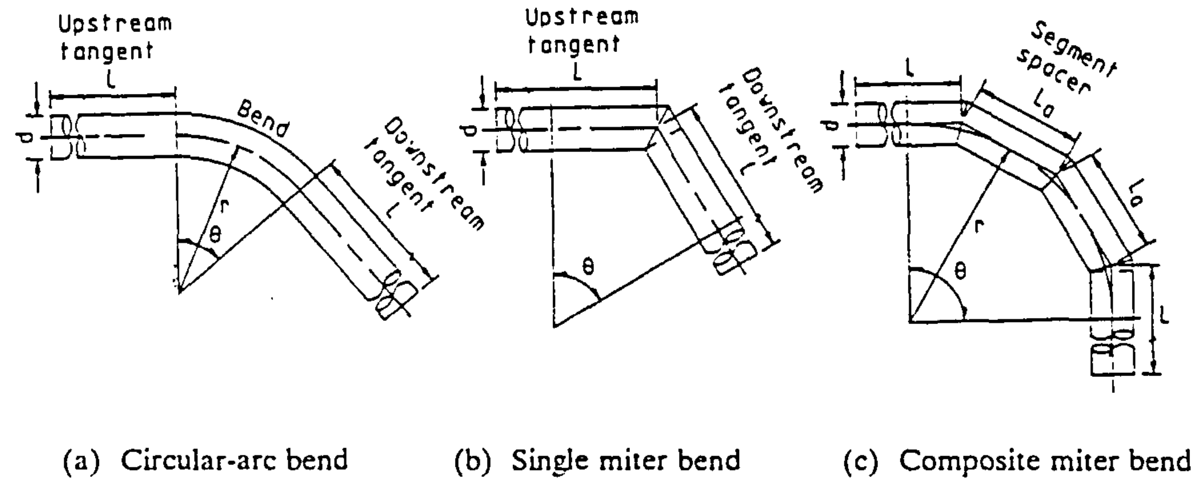

Figure 2.3.17: Bends.

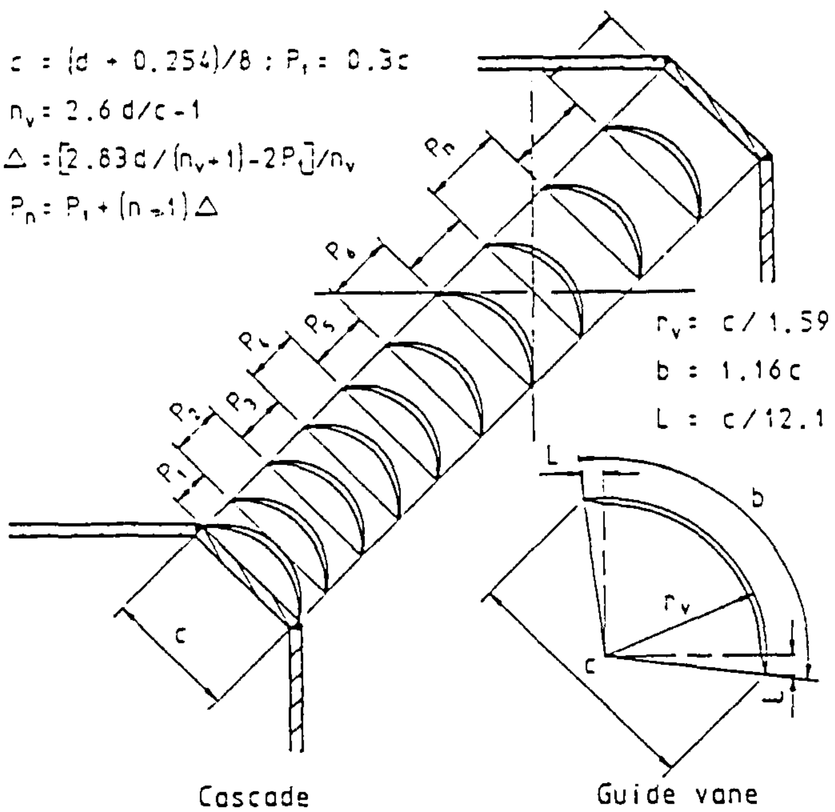

Figure 2.3.18: Miter bend with cascade and circular-arc guide vanes.

Insufficient systematic data exist to provide detailed information on pressure losses in miter bends with cascades as shown in figure 2.3.19. The probable range of the loss coefficient, K_{bm}, is between 0.15 and 0.4, the lower values requiring very careful construction for their achievement. These values compare with a loss coefficient equal to approximately 1.1 for a similar bend without a cascade.

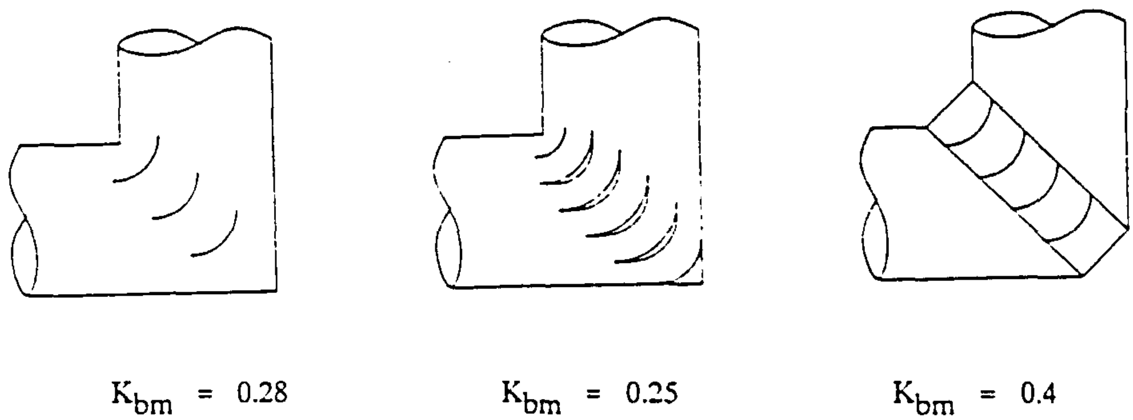

Figure 2.3.19: Miter bends [61JO1].

2.4 MANIFOLDS

The design of manifolds for the distribution or division of a fluid stream into several branching streams, or the formation of a single main stream by the collection or confluence of several smaller streams is of importance in the design of different types of heat exchangers. A manifold basically consists of a main channel (header) to which several smaller conduits (tubes or laterals) are attached at right angles. Manifolds commonly used in flow distribution systems can be classified into five categories, i.e. simple distributing (dividing) or collecting (combining) manifolds, co-current flow (parallel flow) or counter-current flow (reverse flow) manifolds and mixed flow (combined flow) manifolds as shown in figure 2.4.1. The co-current or counter-current flow configurations are also referred to as Z- or U-type heat exchangers.

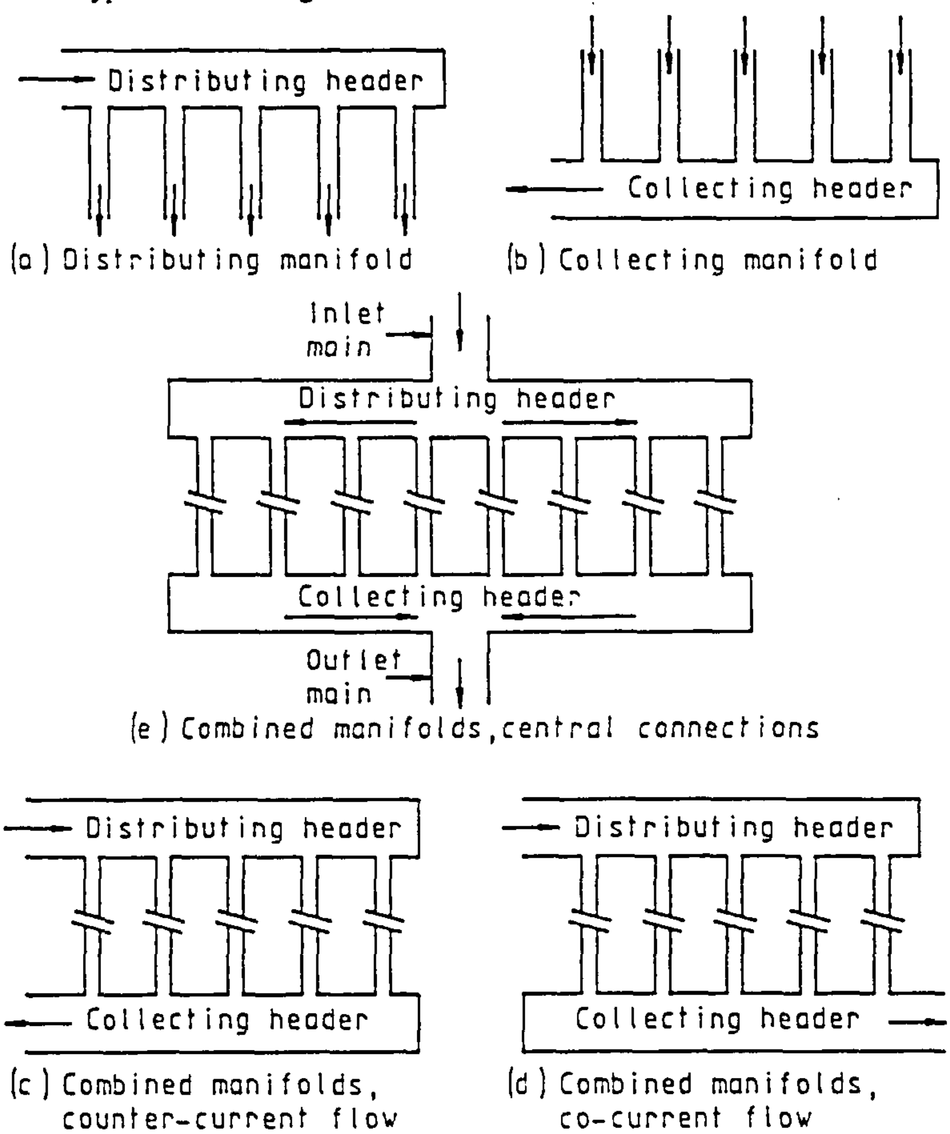

Figure 2.4.1: Types of manifolds.

Often the object of the design is to provide equal flow rates through the branches or laterals. This can usually be achieved approximately if the cross-sectional area of the header is designed such that the fluid velocity and the corresponding pressure in it remains essentially constant.

The variations in fluid pressure in the header are due to frictional effects and changes in momentum. The frictional loss is always in the direction of the flow while the momentum changes cause an increase in pressure in the direction of flow in the distributing header and a decrease in pressure in the direction of flow for the collecting header.

By applying the energy equation to the flow in the header Miller [90MI1] and Hudson [79HU1] quantified the flow and pressure distribution in the header. Enger and Levy [29EN1], Keller [49KE1], Acrivos et al. [59AC1] and Markland [59MA1], based their continuous mathematical model on local momentum balance considerations in the header. Discrete mathematical models based on local momentum balances are derived by Kubo and Euda [69KU1], Majumdar [80MA1] and Datta and Majumdar [80DA1, 83DA1]. Bajura [71BA1] and Bajura and Jones [76BA1] derived continuous mathematical models based on integral momentum balances of the fluid in the header, i.e. the momentum equation in vector form was integrated over a control volume to quantify the flow and pressure distribution. One discrete mathematical model based on an integral momentum balance is due to Nujens [83NU1].

2.5 DRAG

Drag is defined as the force component, parallel to the relative approach velocity exerted on the body by the moving fluid. Mathematically it can be expressed as

$$F_D = C_D A \rho v^2/2 \tag{2.5.1}$$

where A represents the characteristic projected area normal to the flow and the term $\rho v^2/2$ is the dynamic pressure of the main stream. The drag coefficient, C_D, is found by dimensional analysis to be a function of the geometrical configuration of the immersed body, the Reynolds number, the turbulence characteristics of the incoming free stream, and the surface roughness of the body. Experimental data on drag coefficients versus Reynolds numbers for several different two-dimensional bodies are plotted in figure 2.5.1.

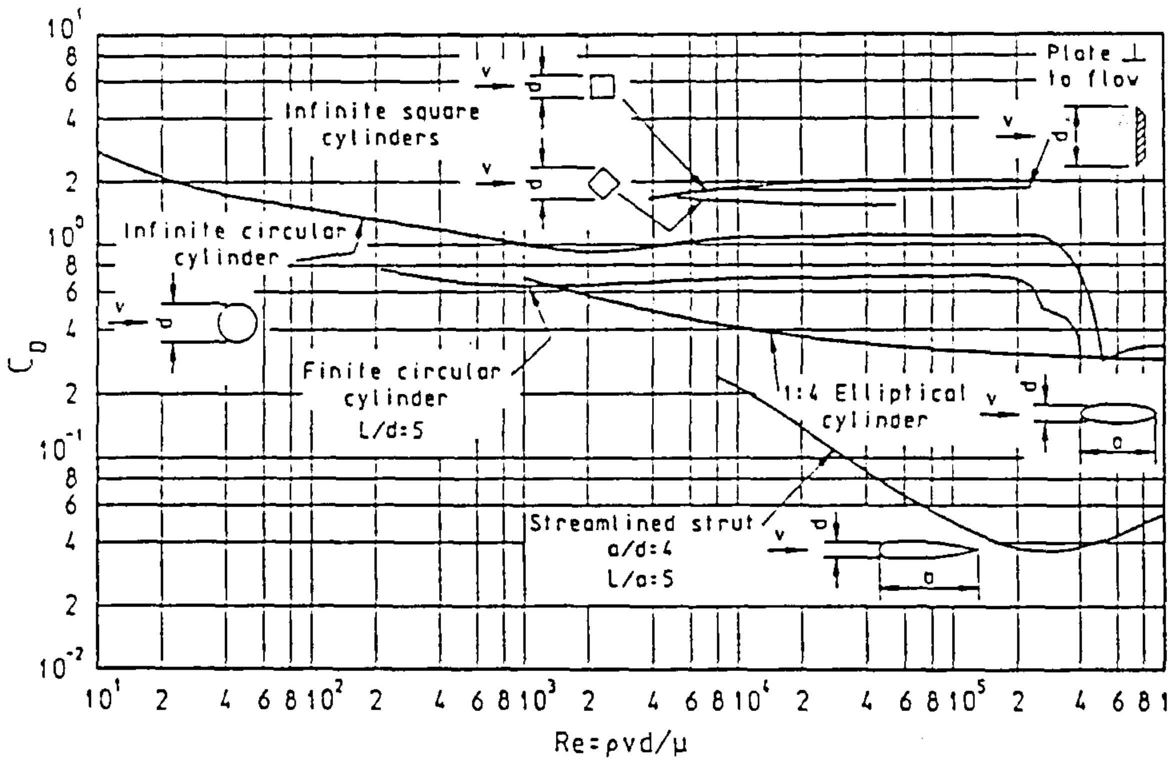

Figure 2.5.1: Coefficient of drag for two-dimensional bodies.

A summary of results on forces associated with flow across circular cylinders is reported by the ESDU [70EN1, 70EN2]. As shown in figure 2.5.1, the drag coefficient remains almost constant at a value or 1.2 for $10^4 < Re < 2 \times 10^5$ in the case of infinitely long cylinders. The drag coefficient is not significantly affected by surfaces roughness or free-stream turbulence for $Re < 3 \times 10^4$. Above this value these effects do, however, become important [70EN1].

If the cylinder axis is rotated through an angle θ_D with respect to the normal approach flow direction, the drag coefficient may be calculated approximately from

$$C_{D\theta} = C_D (\cos \theta_D)^3 \qquad (2.5.2)$$

for $0° < \theta_D < 45°$

Empirical equations based on experimental data have been developed by Hoerner [65HO1] for predicting the drag coefficient about elliptical sections for different Reynolds numbers, i.e.

$$C_D = 2.656 \ (1 + a/d) \ Re^{-0.5} + 1.1 \ (d/a) \qquad (2.5.3)$$

for $10^3 < Re < 10^6$ and where a and d are the dimensions of the major and the minor axes respectively. This relation is plotted in figure 2.5.1.

If the elliptical section is inclined relative to the flow, the drag coefficient is corrected in the same way as for the circular cylinder, i.e. from equation (2.5.2).

The drag coefficient for an infinitely long square section $C_D = 2$ for $Re > 10^4$ according to figure 2.5.1. A very extensive study on square and rectangular sections is presented by the ESDU [78EN1].

The drag coefficients for other two-dimensional structural shapes are listed in table 2.5.1. The drag coefficient for all objects with sharp corners is essentially independent of Reynolds number because the separation points are fixed by the geometry of the object.

A more detailed list of drag coefficients is presented by Sachs [72SA1]. Data for estimating the mean fluid forces acting on lattice frameworks are presented in ESDU Item

Number 75011 [75ES1].

Table 2.5.1: Two-dimensional drag coefficients for structural shapes [77SI1].

Profile and flow direction	C_D	Profile and flow direction	C_D
	1.96 2.01		1.99
	2.04		1.62
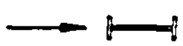	1.81		2.01
	2.00	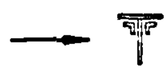	1.99
	1.83		2.19

According to Crowe [77CR1] the drag coefficient for a sphere is given by

$$C_D = 24(1 - 0.15\ Re^{0.687})/Re \tag{2.5.4}$$

for $Re \leq 1000$.

2.6 *FLOW THROUGH SCREENS OR GAUZES*

A screen may be defined as a regular assemblage of elements forming a pervious sheet which is relatively thin in the direction of flow through the screen. Screens of various types may be installed in systems to remove foreign objects from the fluid stream, protect equipment (e.g. against hailstones), reduce fouling or clogging in heat exchangers, smoothen flow or produce turbulence. In such cases the prediction of the total pressure loss caused by the screen is of interest.

An expression for the loss coefficient across a plane screen has been deduced by Cornell [58CO1] for a compressible fluid. Since the losses across screens employed in air-cooled heat exchangers are normally relatively small, the loss coefficient can be expressed approximately in terms of the total pressure difference across the screen and mean free stream conditions, i.e.

$$K_s = 2(p_{t1} - p_{t2})/\rho v^2 \tag{2.6.1}$$

A round-wire screen or gauze of square mesh as shown in figure 2.6.1 is usually specified by the "mesh", defined by the number of openings per unit length $1/P_s$ and by the diameter d_s of the wires.

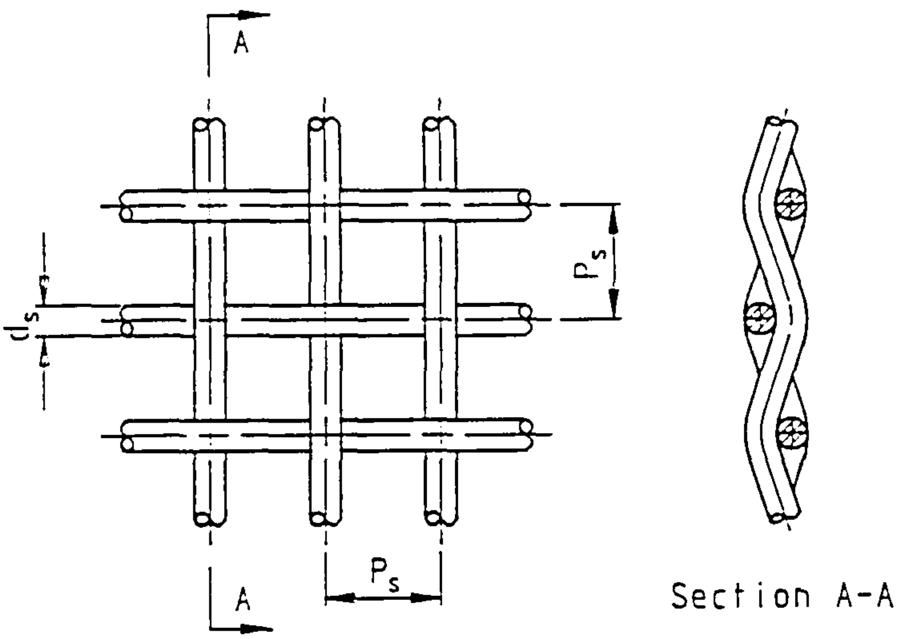

Figure 2.6.1: Geometry of a square-woven screen.

An example of standard mesh data is listed in table 2.6.1.

Table 2.6.1: Standard mesh data.

No. of wire gage	Birmingham wire gage mm	British standard wire gage mm
2	7.21	7.01
4	6.05	5.89
6	5.16	4.88
8	4.19	4.06
10	3.40	3.25
12	2.77	2.64
14	2.11	2.03
16	1.65	1.63
18	1.24	1.22
20	0.89	0.91

The porosity of the screen is defined as

$$\beta_s = \text{area of holes/total area} = (1 - d_s/P_s)^2 \tag{2.6.2}$$

According to Simmons [45SI1], the following equation holds approximately for a screen placed at right angles to an air stream at velocities above about 10 m/s under ambient conditions:

$$K_s = (1 - \beta_s)/\beta_s^2 \tag{2.6.3}$$

This equation can be recommended for application in the case of most screens of practical interest where screen Reynolds numbers exceed 300.

The screen Reynolds number is defined as

$$Re_s = \rho v d_s/(\beta_s \mu) \tag{2.6.4}$$

According to Wieghardt [53WI1] the loss coefficient may be expressed as

$$K_s = 6(1 - \beta_s)\beta_s^{-2} Re_s^{-0.333} \tag{2.6.5}$$

for $60 < Re_s < 1000$.

In figure 2.6.2 equations (2.6.3) and (2.6.5) are compared with the experimental results obtained by various investigators. Since the screen geometry can have a significant influence on the loss coefficient, specific tests should be performed when these losses are of importance.

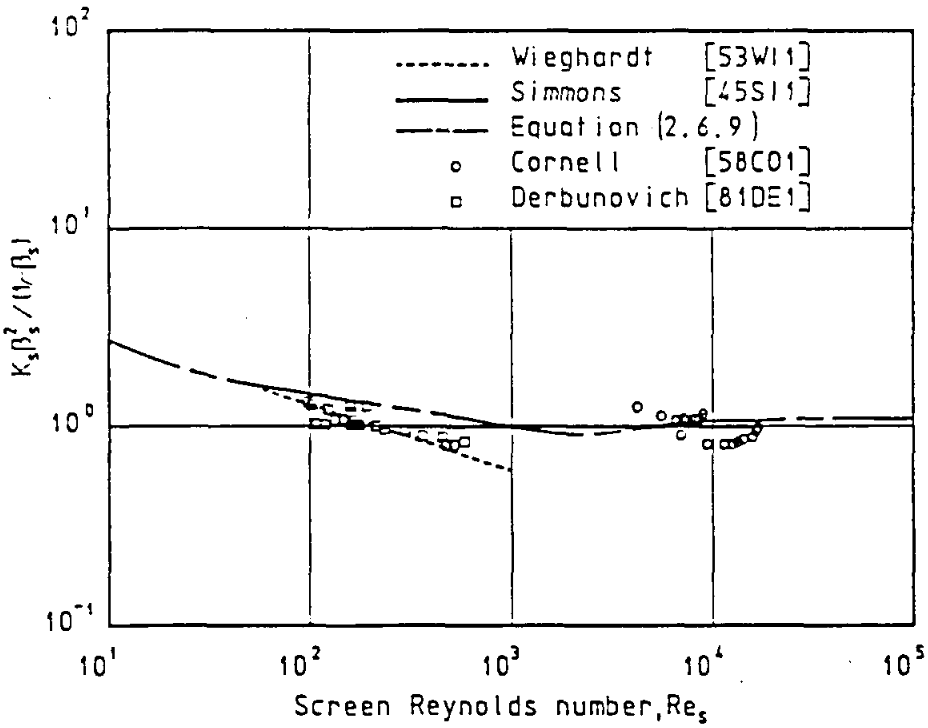

Figure 2.6.2: Screen loss coefficient.

For cases where $d_s/P_s << 1$, the effective drag force per screen area corresponding to one screen opening may, according to equation (2.5.1), be expressed approximately as

$$F_D/A = F_D/[d_s\,(2P_s - d_s)] \approx C_D\,\rho\,v^2/2 \tag{2.6.6}$$

According to equation (2.6.1), the corresponding loss coefficient is

$$K_s = 2F_D/\,(P_s^2\,\rho\,v^2) \tag{2.6.7}$$

Substitute equation (2.6.6) into equation (2.6.7) and find

$$K_s = C_D\,(2\,d_s/P_s - d_s^2/P_s^2) = C_D\,(1 - \beta_s) \tag{2.6.8}$$

Equation (2.6.8) can also be written as

$$K_s\beta_s^2/\,(1 - \beta_s) = C_D\,\beta_s^2 \approx C_D \tag{2.6.9}$$

for $d_s/P_s << 1$.

With the drag coefficient C_D known for an infinitely long cylinder, the approximate relation (2.6.9) can thus be applied over a wide range of Reynolds numbers, as shown in figure 2.6.2.

Fan guards consisting of expanded metal or wire woven mesh are required in most air-cooled heat exchangers. In the petro-chemical industry the recommended openings for woven mesh are usually not more than 2600 mm^2 with a wire diameter of not less than 2.8 mm or 12 Birmingham wire gage (BWG) [78AP1].

2.8 REFERENCES

00WE1 Weisbach, J., Die Experimental-Hydraulik, J.S. Engelhardt, Freiberg, 1855.

29EN1 Enger, M.L. and Levy, M.I., Pressures in Manifold Pipes, Journal of American Water Works Association, May 1929.

32NI1 Nikuradse, J., Gesetzmässigkeiten der turbulenten Strömung in glatten Rohren, Ver. Dtsch. Ing. Forschungsh., Vol. 356, 1932.

38PA1 Patterson, G.N., Modern Diffuser Design, Aircraft Eng., Vol. 10, p. 267, 1938.

39CO1 Colebrook, C.F., Turbulent Flow in Pipes, with Particular References to the Transition Region Between the Smooth and Rough Pipe Laws, J. Inst. Civ. Eng. Lond., Vol. 11, pp. 133-156, 1938 - 1939.

44MO1 Moody, L.F., Friction Factors for Pipe Flow, Trans ASME, Vol. 66, 671, 1944.

45SI1 Simmons, L.F.G., Measurements of the Aerodynamic Forces Acting on Porous Screens, R & M No. 2276, 1945.

46RO1 Rouse, H., Elementary Mechanics of Fluids, John Wiley & Sons, London, 1946.

48MA1 Martinelli, R.C. and Nelson, D.B., Prediction of Pressure Drop During Forced Circulation Boiling of Water, Trans. ASME, Vol. 70, pp. 695-702, 1948.

49KE1 Keller, J.D., The Manifold Problem, Trans. ASME, Vol. 71, pp. 77-85, 1949.

49LO1 Lockhart, R.W. and Martinelli, R.C., Proposed Correlation of Data for Isothermal Two-phase Two-component Flow in Pipes, Chem. Eng. Prog., Vol. 45, No. 1, pp. 39-48, 1949.

50KA1 Kays, W.M., Loss Coefficients for Abrupt Changes in Flow Cross Section with Low Reynolds Number Flow in Single and Multiple-Tube Systems,Trans. ASME, Vol. 72, No. 8, pp. 1067 - 1074, 1950.

52KI1 Kirschmer, O., Kritische Betrachtungen zur Frage der Rohrreibung. Z.VDI 94, 785, 1952.

53WI1 Wieghardt, K.E.G., On the Resistance of Screens, The Aeronautical Quarterly, Vol. 4, pp. 186 - 192, February 1953.

54BA1 Baker, O., Simultaneous Flow of Oil and Gas, Oil and Gas Journal, Vol. 53, pp. 185-195, 1954.

54FI1 Filonenko, G.K., Teploenergetika No. 4, 1954.

55DE1 Deissler, R.G., Turbulent Heat Transfer and Friction in the Entrance Regions of Smooth Passages, ASME Trans., pp. 1221 - 1233, November 1955.

55HA1 Hall, W.B. and Orme, E.M., Flow of Compressible Fluid Through a Sudden Enlargement in a Pipe, Proc. Instn Mech. Engrs, Vol. 169, p. 1007, 1955.

58CO1 Cornell, W.G., Losses in Flow Normal to Plane Screens, Transactions of the ASME, Vol. 80, No. 4, pp. 791 - 799, May 1958.

59AC1 Acrivos, A., Babcock, B.D. and Pigford, R.L., Flow Distribution in Manifolds, Chemical Engineering Science, Vol. 10, pp. 112-124, 1959.

59MA1 Markland, E., Analysis of Flow from Pipe Manifolds, Engineering, Vol. 189, pp. 150-151, 1959.

61JO1 Jorgensen, R., Fan Engineering, Buffalo Forge Co., Buffalo, N.Y., 1961.

61WA1 Wallis, G.B., Flooding Velocities for Air and Water in Vertical Tubes, AEEW - R123, 1961.

62HA1 Hartnett, H.P., Koh, J.C.Y. and McComas, S.T., A Comparis on of Predicted and

Measured Friction Factors for Turbulent Flow through Rectangular Ducts, Trans. ASME, Ser. C, Vol. 84, No. 1, pp. 82-88, 1962.

63SC1 Scott, D.S., Properties of Co-current Gas-liquid Flow, Advances in Chemical Engineering, Vol. 4, pp. 199-277, 1963.

65HO1 Hoerner, S.F., Fluid Dynamic Drag, Hoerner, New Jersey, 1965.

66CL1 Clift, R., Pritchard, C. and Nedderman, R.M., The Effect of Viscosity on the Flooding Conditions in Wetted Wall Columns, Chemical Engineering Science, Vol. 21, pp. 87-95, 1966.

69HE1 Hewitt, G.F. and Roberts, D.N., Studies of Two-phase Flow Patterns by Simultaneous Flash and X-ray Photography, AERE-M2159, 1969.

69KU1 Kubo, T. and Ueda, T., On the Characteristics of Dividing Flow and Confluent Flow in Headers, Bull. of JSME, Vol. 12, No. 52, pp. 802 - 809, 1969.

70BE1 Bell, K.J., Taborek, J. and Fenoglio, F., Interpretation of Horizontal Intube Condensation Heat Transfer Correlation with a Two-phase Flow Regime Map, CEP Symposium Ser. Vol. 66, No. 102, pp. 159-165, 1970.

70EN1 Engineering Sciences Data Unit, Fluid Forces Acting on Circular Cylinders for Application in General Engineering, Item No. 70013, Part 1: Long Cylinders in Two-Dimensional Flow, London 1970.

70EN2 Engineering Sciences Data Unit, Fluid Forces Acting on Circular Cylinders for Application in General Engineering, Item No. 70014, Part 11: Finite-length Cylinders, London, 1970.

70PE1 Pethukov, B.S., Heat Transfer and Friction in Turbulent Pipe Flow with Variable Physical Properties, Advances in Heat Transfer, Vol. 6, eds, Hartnett, J.P., and Irvine, T.F., Academic Press, New York, pp. 503 - 564, 1970.

70PR1 Premoli, A., Di Francesco, D. and Prina, A., An Empirical Correlation for Evaluating Two-phase Mixture Density Under Adiabatic Conditions, European Two-phase Flow Group Meeting, Milan, 1970.

71BA1 Bajura, R.A., A Model for Flow Distribution Manifolds, Trans. ASME, J. Engineering for Power, Paper No. 70-Pwr-3, pp. 7-14, 1971.

71MI1 Miller, D.S., Internal Flow: A Guide to Losses in Pipe and Duct Systems, BHRA, Cranfield, 1971.

72LA1 Launder, B.E. and Ying, W.M., Secondary Flow in Ducts of Square Cross Section, J. Fluid Mech., Vol. 54, Part 2, pp. 289-295, 1972 and Prediction of Flow and Heat Transfer in Ducts of Square Cross-sections, Proc. Inst. Mech. Engrs. Vol. 187, pp. 455-461, 1973.

72SA1 Sachs, F., Wind Forces in Engineering, Pergamon, New York, 1972.

73CH1 Chisholm, D., Pressure Gradients Due to Friction During the Flow of Evaporating Two-phase Mixtures in Smooth Tubes and Channels, Int. J. Heat Mass Transfer, Vol. 16, pp. 347-438, 1973.

73ES1 Engineering Sciences Data Unit, Pressure Losses in Three-leg Pipe Junctions: Dividing Flow, London, 1973.

73HO1 Holms, E., Handbook of Industrial Pipework Engineering, McGraw-Hill Book Co., United Kingdom, 1973.

74OS1 Oschinowo, T. and Charles, M.E., Vertical Two-phase Flow, Canadian J. of Chem. Eng., Vol. 52, pp. 25-35, 1974.

74VD1 Verein Deutscher Ingenieure-Wärmeatlas, VDI, Düsseldorf, 1977.

75ES1 Engineering Sciences Data Unit, Fluid Forces on Lattice Structures, Item No. 75011, London, 1975.

75HO1 Hong, S.W. and Bergles, A.E., Augmentation of Laminar Flow Heat Transfer in Tubes by Means of Twisted-tape Inserts, ASME Paper 75 - HT -44, 1975.

75RU1 Runstadler, P.W., Dolan, F.X. and Dean, R.C., Diffuser Data Book, Creare Inc., Hanover, New Hampshire, USA, 1975.

76BA1 Bajura, R.A. and Jones, E.H., Flow Distribution Manifolds, Trans. ASME, J. Fluid Engineering, Vol. 98, pp. 656 - 666, 1976.

76CR1 Crane, Flow of Fluids Through Valves, Fittings and Pipes, Technical Paper No. 410, 5th ed., Crane Co., New York, 1976.

76TA1 Taitel, Y. and Dukler, A.E., A Model for Predicting Flow Regime Transition in Horizontal and Near Horizontal Gas-liquid Flow, AIChE. J., Vol. 22, No. 1, pp. 47-55, 1976.

77CR1 Crowe, C.T., Sharma, M.P. and Stock, D.E., The Particle-Source-In-Cell Model for Gas-Droplet Flows, Journal of Fluids Engineering, Vol. 99, No. 2, pp. 325 - 332, 1977.

77CH1 Churchill, S.W., Comprehensive Correlating Equations for Heat Mass and Momentum Transfer in Fully Developed Flow in Smooth Tubes, Ind. Eng. Chem., Fundam., Vol. 16, No. 1, 1977.

77CH2 Churchill, S.W., Friction Equation Spans All Fluid Flow Regimes, Chemical Engng., Vol. 84, No. 24, pp. 91 - 92, 1977.

77ES1 Engineering Sciences Data Unit, Pressure Losses in Curved Ducts: Interaction Factors for Two Bends in Series, London, 1977.

77SI1 Simiu, E. and Scanlan, R.H., Wind Effects on Structures; An Introduction to Wind Engineering, J. Wiley, Washington, 1977.

78AP1 American Petroleum Institute (API) Standard 661, Air-cooled Heat Exchangers for General Refinery Services, API, Washington, 1978.

78DA1 Daly, B.B., Woods Practical Guide to Fan Engineering, Essex Telegraph Press Ltd., Colchester, 1978.

78EN1 Engineering Sciences Data Unit, Fluid Forces, Pressures and Moments on Rectangular Blocks, Item No. 71016, London, 1978.

78GE1 General Electric Fluid Flow Data Book, Genium Publishing Corporation, Schenectady, N.Y., 1987.

78SH1 Shah, R.K. and London, A.L., Laminar Flow Forced Convection in Ducts, Academic Press, New York, 1978.

79FR1 Friedel, L., Improved Friction Pressure Drop Correlation for Horizontal and Vertical Two-phase Flow, European Two-phase Flow, Group Meeting, Ispra, Italy, 1979.

79HU1 Hudson, H.E., Uhler, R.B. and Bailey, R.W., Dividing-flow Manifolds with Square Edged Laterals, Journal of Environmental Engineering Division, Proceedings of ASME, Vol. 105, 1979.

79TI1 Tien, C.L. and Liu, C.P., Survey on Vertical Two-phase Counter-current Flooding, EPRI Report NP-984, February 1987.

80BE1 Benedict, R.P., Fundamentals of Pipe Flow, John Wiley, New York, 1980.

80DA1 Datta, A.B. and Majumdar, A.K., Flow Distribution in Parallel and Reverse Flow Manifolds, Int. J. Heat and Fluid Flow, Vol. 2, No. 4, pp. 253 - 262, 1980.

80MA1 Majumdar, A.K., Mathematical Modelling of Flow in Dividing and Combining Flow Manifolds, Applied Mathematical Modelling, Vol. 4, pp. 424 - 431, 1980.

80SP1 Spedding, P.L. and Nguyen, V.T., Regime Maps for Air-water Two-phase Flow, Chem. Eng. Science, Vol. 35, pp. 779-793, 1980.

80TA1 Taitel, Y., Barnea, D. and Dukler, A.E., Modelling Flow Pattern Transition for Steady Upward Gas-liquid Flow in Vertical Tubes, AIChE. Journal, Vol. 26, No. 3, pp. 345-354, 1980.

80WA1 Wallis, G.B., de Sieyes, D.C., Rosselli, R.J. and Lacombe, J., Countercurrent Annular Flow Regimes for Steam and Subcooled Water in a Vertical Tube, Research Project 443-2, EPRI NP-1336, EPRI, California, January 1980.

81CO1 Collier, J.G., Convective Boiling and Condensation, Mc Graw-Hill Book Co., New York, 1981.

81DE1 Derbunovich, G.Q., Zemskaya, A.S., Repik, Ye.U. and Sosedko, Yu.P., Optimum Wire Screens for Control of Turbulence in Wind Tunnels, Fluid Mechanics - Soviet Research, Vol. 10, No. 5, pp. 136 - 147, September-October 1981.

82BA1 Barnea, D. and Brauner, N., Holdup of the Liquid Slug in Two-phase Intermittent Flow, Int. J. Multiphase Flow, Vol. 11, No. 1, pp. 43-49, 1985.

82HE1 Hewitt, G.F., Flow Regimes, Handbook of Multiphase Systems, ed. Hetsroni, G., 1982.

83DA1 Datta, A.B. and Majumdar, A.K., A Calculation Procedure for Two-phase Flow Distribution in Manifolds With and Without Heat Transfer, Int. J. Heat Mass Transfer, Vol. 26, No. 9, pp. 1321 - 1328, 1983.

83HA1 Haaland, S.E., Simple and Explicit Formulas for the Friction Factor in Turbulent Pipe Flow, Trans. ASME J. Fluids Engineering, Vol. 105, No. 3, pp. 89-90, March 1983.

83NU1 Nujens, P.G.J.M., A Discrete Model for Flow Distribution Manifolds, CSIR

Report, Chemical Engineering Research Group, Pretoria, 1983.

83OL1 Olujic, Z., A Method for Predicting Friction Pressure Drop of Two-phase Gas-liquid Flow in Horizontal Pipes, AIChE 75th Annual Meeting, Washington, 1983.

83SH1 Shah, R.K., Fully Developed Laminar Flow Forced Convection in Channels, Low Reynolds Number Flow Heat Exchangers, eds. Kakac, S., Shah, R.K. and Bergles, A.E., Hemisphere Publ. Corp., Washington, 1983.

83TA1 Taitel, Y. and Barnea, B., Counter-current Gas-liquid Vertical Flow, Model for Flow Pattern and Pressure Drop, Int. J. Multiphase Flow, Vol. 9, No. 6, pp. 637-647, 1983.

84DU1 Du Plessis, J.P. and Kröger, D.G., Friction Factor Prediction for Fully Developed Laminar Twisted-tape Flow, Int. J. Heat Mass Transfer, Vol. 27, No. 11, pp. 2095 - 2100, 1984.

84KA1 Kays, W.M. and London, A.L., Compact Heat Exchangers, McGraw-Hill Book Co., New York, 1984.

85CR1 Crawford, T.J., Weinberger, C.B. and Weisman, J., Two-phase Flow Patterns and Void Fraction in Downward Flow, Part 1: Steady-state Flow Patterns, Int. J. Multiphase Flow, Vol. 11, No. 6, pp. 761-782, 1985.

85MC1 Mc Quillan, K.W. and Whalley, P.B., Flow Patterns in Vertical Two-phase Flow, Int. J. Multiphase Flow, Vol. 11, No. 2, pp. 1425-1440, 1985.

85MU1 Mukherjee, H. and Brill, J.P., Empirical Equations to Predict Flow Patterns in Two-phase Inclined Flow, Int. J. Multiphase Flow, Vol. 11, No. 3, pp. 299-315, 1985.

86BA1 Bankoff, S.G. and Lee, S.C., A Critical Review of the Flooding Literature, Multiphase Science and Technology, Vol. 2, pp. 95-180, 1986.

86ID1 Idelchik, I.E., Handbook of Hydraulic Resistance, Hemisphere Publ. Co., Washington, 1986.

86ST1 Stanislav, J.F., Kokal, S. and Nicholson, M.K., Intermittent Gas-liquid Flow in Upward Inclined Pipes, Int. J. Multiphase Flow, Vol. 12, No. 3, pp. 325-335, 1986.

87BA1 Barnea, D., A Unified Model for Predicting Flow Pattern Transitions for the Whole Range of Pipe Inclinations, Int. J. Multiphase Flow, Vol. 13, No. 1, pp.1-12, 1987.

87CI1 Cindric, D.T., Gandi, S.L. and Williams, R.A., Designing Piping Systems for Two-phase Flow, Chem. Eng. Prog., pp. 51-55, March, 1987.

87LI1 Lin, P.Y. and Hanratty, T.J., Effect of Pipe Diameter on Flow Patterns for Air-water Flow in Horizontal Pipes, Int. J. Multiphase Flow, Vol. 13, No. 4, pp. 549-563, 1987.

87JA1 James, P.W. et al, Developments in the Modelling of Horizontal Annular Two-phase Flow, Int. J. Multiphase Flow, Vol. 13, No. 2, pp. 173-198, 1987.

87WH1 Whalley, P.B., Boiling, Condensation, and Gas-liquid Flow, Clarendon Press, Oxford, 1987.

88BR1 Breber, G., Intube Condensation, Heat Transfer Equipment Design, eds. Shah, R.K., Subbarao, E.C. and Mashelkar, R.A., Hemisphere Publ. Co., New York, 1988.

89FR1 Fried, E. and Idelchik, I.E., Flow Resistance: A Design Guide for Engineers, Hemisphere Publ. Co., New York, 1989.

90MI1 Miller, D.S., Internal Flow Systems, 2nd Edition, BHRA Fluid Engineering Series, British Hydraulic Research Association, Cranfield, 1990.

92CA1 Carey, V.P., Liquid-Vapor Phase-Change Phenomena, Hemisphere Publ. Corp., Washington, 1992.

92DU1 Du Plessis, J.P. and Collins, M.R., A New Definition for Laminar Flow Entrance Lengths of Straight Ducts, South African Institution of Mechanical Engineers R + D Journal, pp. 11-16, September 1992.

93HE1 Hewitt, G.F. and Jayanti, S., To Churn or Not to Churn, Int. J. Multiphase Flow, Vol. 19, No. 3, pp. 527-529, 1993.

93JA1 Jayanti, S., Hewitt, G.F., Low, D.E.F. and Hervieu, E., Observation of Flooding in the Taylor Bubble of Co-current Upwards Slug Flow, Int. J. Multiphase Flow, Vol. 19, No. 3, pp. 531-534, 1993.

93MA1 Mao, Z.S. and Dukler, A.E., The Myth of Churn Flow, Int. J. Multiphase Flow, Vol. 19, No. 2, pp. 377-383, 1993.

CHAPTER 3

HEAT TRANSFER

3.0 INTRODUCTION

Engineering thermal science includes thermodynamics and heat transfer. Thermodynamic analyses consider only systems in equilibrium. The role of heat transfer is to supplement thermodynamics, with additional laws that allow the prediction of rates of energy transfer. These laws are based on different modes of heat transfer, namely conduction, convection and radiation.

3.1.1 CONDUCTION

When a temperature gradient exists within a homogeneous substance there is an energy transfer from the high temperature region to the low temperature region, i.e. heat is transferred by conduction and the heat transfer rate per unit area is proportional to the normal temperature gradient, i.e.

$$q = \frac{Q}{A} \propto \frac{dT}{dx}$$

where the heat flux, q, is the ratio of the heat transfer rate, Q, through the area A, and dT/dx is the temperature gradient in the direction of heat flow.

When the proportionality coefficient is inserted,

$$Q = - kA\frac{dT}{dx} \qquad (3.1.1)$$

The positive coefficient k is called the thermal conductivity of the material, and the minus sign is inserted so that the second principle of thermodynamics will be satisfied, i.e. heat must flow downhill on the temperature scale. Equation (3.1.1) is called Fourier's law of heat conduction.

Thermal conductivities of various fluids are given in Appendix A.

Consider the problem of one-dimensional steady-state conduction in a plane wall of homogeneous material having constant thermal conductivity and with each face held at a constant uniform temperature as shown in figure 3.1.1(a).

For the element of thickness, dx, the following energy balance is applicable:

$$Q_x = Q_{x + dx}$$

With equation (3.1.1) this becomes

$$-kA\frac{dT}{dx} = -kA\frac{dT}{dx} + \frac{d}{dx}\left(-kA\frac{dT}{dx}\right)dx$$

or

$$\frac{d}{dx}\left(-kA\frac{dT}{dx}\right) = 0 \qquad (3.1.2)$$

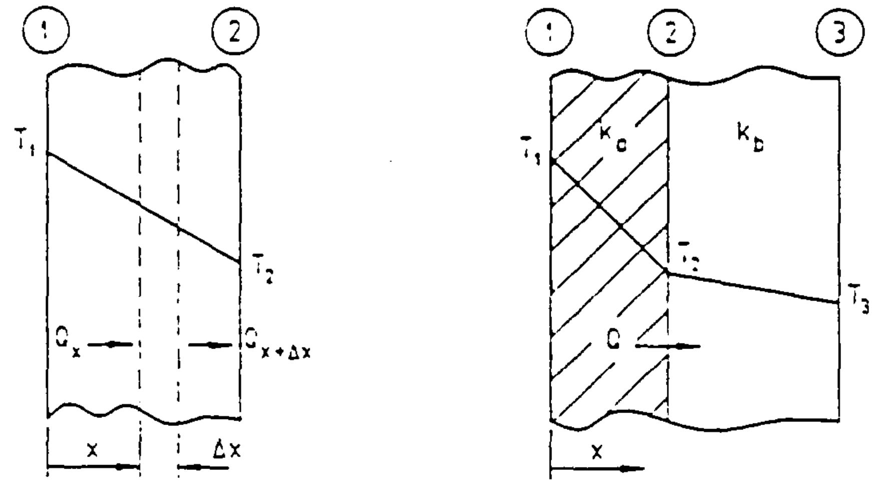

(a) Homogeneous (b) Composite

Figure 3.1.1: One-dimensional heat conduction.

With $T = T_1$ at $x = x_1$ and $T = T_2$ at $x = x_2$, the integration of this relation, assuming a constant value for k, yields the following temperature distribution:

$$T = \frac{(T_2 - T_1)(x - x_1)}{(x_2 - x_1)} + T_1 \qquad (3.1.3)$$

The heat transfer rate may now be determined according to equation (3.1.1), i.e.

$$Q = -kA\frac{dT}{dx} = -\frac{kA(T_2 - T_1)}{(x_2 - x_1)} \qquad (3.1.4)$$

This equation can also be written as

$$Q = \frac{T_1 - T_2}{(x_2 - x_1)/kA} = \frac{\text{thermal potential difference}}{\text{thermal resistance}} \tag{3.1.5}$$

These principles are readily extended to the case of a composite plane wall as shown in figure 3.1.1(b). The steady state heat transfer rate entering the left face is the same as that leaving the right face. Thus

$$Q = \frac{T_1 - T_2}{(x_2 - x_1)/(k_a A)} \quad \text{and} \quad Q = \frac{T_2 - T_3}{(x_3 - x_2)/(k_b A)} \tag{3.1.6}$$

Eliminate T_2 in these relations and find

$$Q = \frac{(T_1 - T_3)}{(x_2 - x_1)/(k_a A) + (x_3 - x_2)/(k_b A)} \tag{3.1.7}$$

Equations (3.1.5) and (3.1.7) illustrate the analogy between conductive heat transfer and electrical current flow, an analogy rooted in the similarity between Fourier's and Ohm's laws. It is convenient to express Fourier's law as

$$\text{conductive heat transfer} = \frac{\text{overall temperature difference}}{\text{summation of thermal resistance}} = \frac{\Delta T \text{ overall}}{\Sigma R_{th}} \tag{3.1.8}$$

where R_{th} are the thermal resistances of the various materials.

In the case of cylindrical co-ordinates, Fourier's law in the radial direction is written as

$$Q = -k A \frac{dT}{dr} \tag{3.1.9}$$

Consider a long cylinder of inside radius r_i and outside radius r_o and length L. If the inside surface of the cylinder is maintained at a temperature T_i and the outside surface at T_o, as shown in figure 3.1.2(a), it may be assumed that the heat flows in the radial direction.

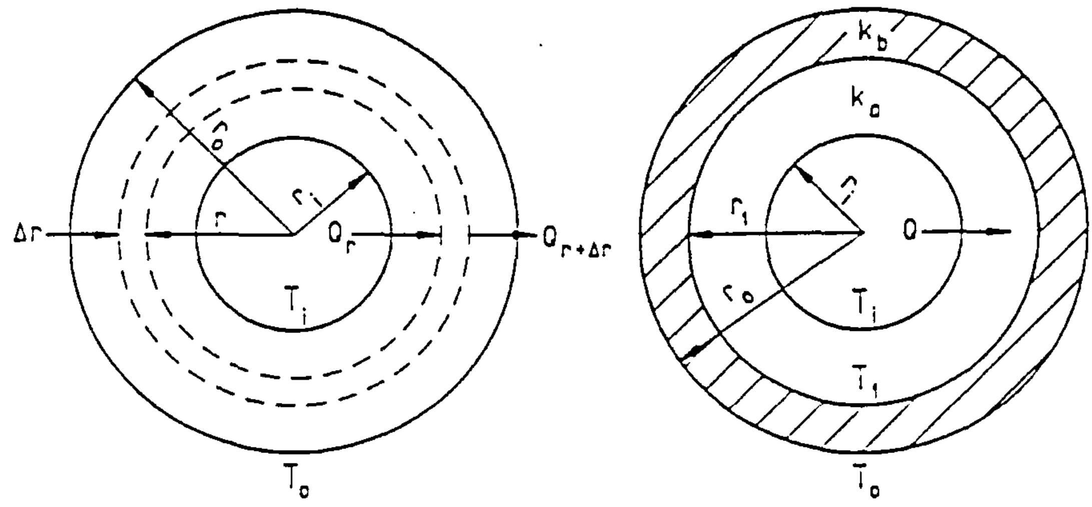

(a) Homogeneous (b) Composite

Figure 3.1.2: Radial heat conduction.

For the elementary cylindrical control volume of thickness Δr, the following energy balance is applicable if steady state conditions are assumed:

$$Q_r = Q_r + dr \tag{3.1.10}$$

With equation (3.1.9) this becomes

$$-2\pi rLk \frac{dT}{dr} = -2\pi rLk \frac{dT}{dr} + \frac{d}{dr}\left(-2\pi rLk \frac{dT}{dr}\right)dr$$

or

$$\frac{d}{dr}\left(-2\pi rLk \frac{dT}{dr}\right) = 0 \tag{3.1.11}$$

With $T = T_i$ at $r = r_i$ and $T = T_o$ at $r = r_o$, the integration of this relation, for a constant value of k, yields the following temperature distribution:

$$T = T_i + (T_o - T_i) \ln (r/r_i)/\ln (r_o/r_i) \tag{3.1.12}$$

The temperature distribution in the cylinder is thus a logarithmic function of the radius. From this relation and equation (3.1.9) the radial heat transfer rate is given by

$$Q = 2\pi Lk(T_i - T_o)/\ln (r_o/r_i) \tag{3.1.13}$$

For the two-layered cylinder shown in figure 3.1.2(b), find the heat transfer rate

$$Q = \frac{2 \pi L (T_i - T_o)}{\ln (r_1/r_i)/k_a + \ln (r_o/r_1)/k_b} \tag{3.1.14}$$

3.1.2 CONVECTION

Convection is a process involving the mass movement of fluids. When a temperature difference produces a density difference which results in the mass movement, the process is called free or natural convection. When a pump or other similar device causes the mass motion to take place, the process is called forced convection.

The heat transferred between a fluid and solid surface when the fluid flows either by free or by forced convection is usually referred to as "heat transfer by convection". In actual fact the fundamental mechanisms of heat transfer in such flows are those of conduction and radiation [61RO1].

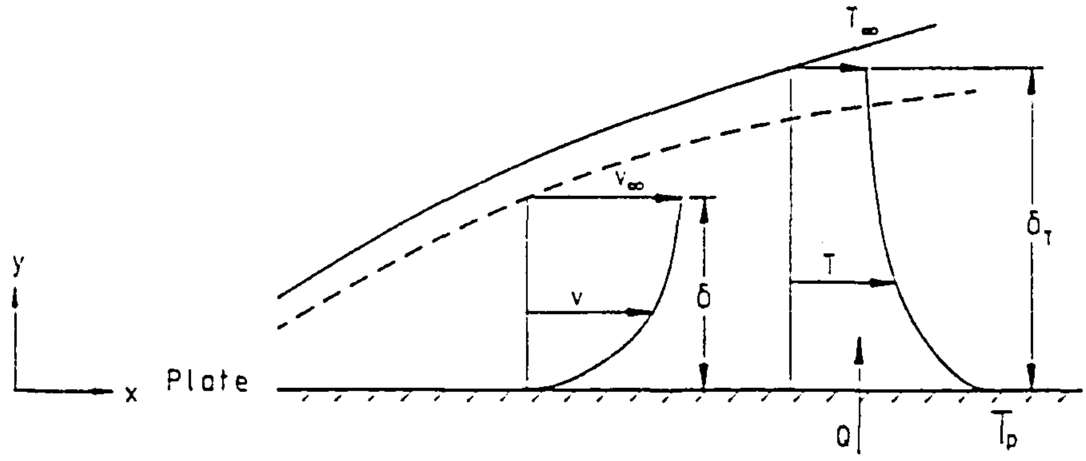

Figure 3.1.3: Convection heat transfer from a plate.

Consider the heated plate shown in figure 3.1.3. The temperature of the plate is T_p and the temperature of the fluid is T_∞. Just as the hydrodynamic boundary layer was defined as that region of the flow where viscous forces are felt, a thermal boundary layer may be defined as that region where temperature gradients are present in the flow. Analogous to the hydrodynamic case, the thermal boundary layer thickness δ_T is defined as that distance from the plate where $T_p - T = 0.99(T_p - T_\infty)$. The thermal boundary layer is not necessarily of the same thickness as the velocity boundary layer.

Since the velocity of the flow at the plate is zero as a result of viscous action, heat is being transferred only by conduction at that point. The temperature gradient is, however, dependent on the rate at which the fluid carries the heat away. To express the overall effect of convection, a quantity, h, called the convection heat transfer coefficient, is defined by the expression

$$Q = h\,A\,(T_p - T_\infty) \tag{3.1.15a}$$

Similarly, in the case of duct flow,

$$Q = h\,A\,(T_w - T_m) \tag{3.1.15b}$$

where T_w is the wall temperature and T_m is the bulk mean fluid temperature.

This equation is known as Newton's law of cooling.

Flow in a two-dimensional duct is designated as thermally fully developed when the dimensionless temperature distribution, as expressed below in brackets, is invariant at a cross-section, i.e. independent of x:

$$\frac{d}{dx}\left(\frac{T_{wm} - T}{T_{wm} - T_m}\right) = 0 \tag{3.1.16}$$

where T_{wm} is the peripheral mean wall temperature and T_m is the bulk mean fluid temperature.

The ratio of the convective conductance or heat transfer coefficient, h, to the molecular thermal conductance, k/L, for flow over a surface or k/d_e for duct flow is defined as a Nusselt number, i.e.

$$Nu = \frac{hL}{k} \quad \text{for a plate} \tag{3.1.17a}$$

or

$$Nu = \frac{hd_e}{k} \quad \text{for a duct} \tag{3.1.17b}$$

The Nusselt number is constant for thermally and hydrodynamically fully developed laminar flow. It is dependent on $x/(d_e RePr)$ for developing laminar temperature profiles, and for developing laminar velocity as well as temperature profiles.

The ratio of momentum diffusivity to thermal diffusivity of the fluid is known as the Prandtl number, i.e.

$$Pr = \nu/\alpha = \mu c_p/k \tag{3.1.18}$$

The product of the Reynolds and Prandtl numbers is known as the Péclet number, i.e.

$$Pe = RePr \tag{3.1.19}$$

whereas the ratio of Nusselt number to Péclet number is referred to as the Stanton number, i.e.

$$St = \frac{Nu}{RePr} = \frac{h}{Gc_p} \tag{3.1.20}$$

3.1.3 OVERALL HEAT TRANSFER COEFFICIENT

It is often convenient to express the heat transfer rate for a combined conductive-convective problem in terms of an overall heat transfer coefficient U.

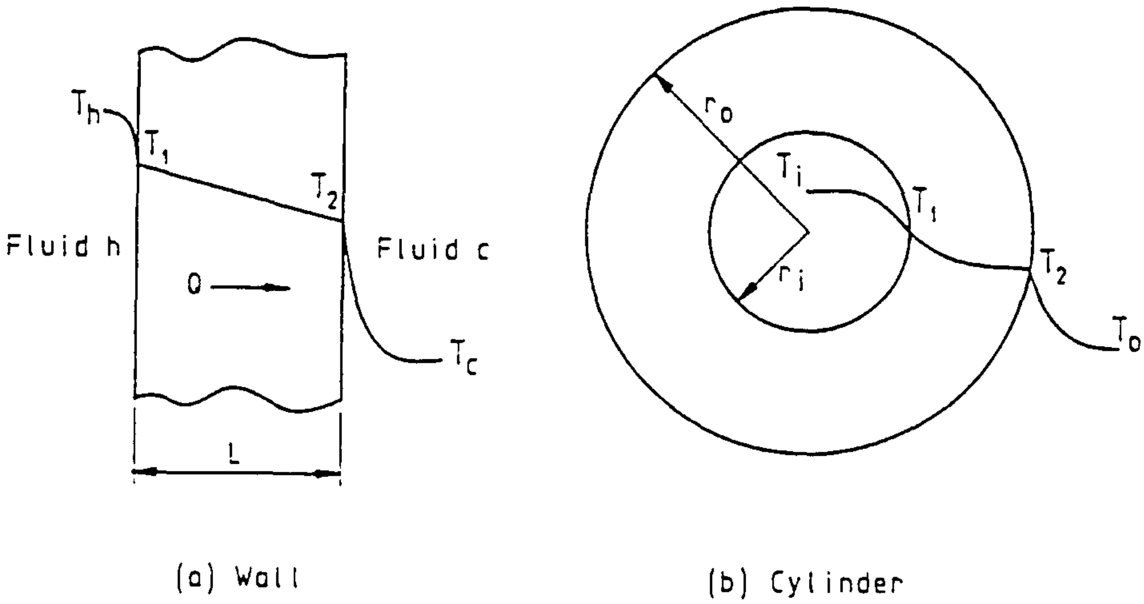

Figure 3.1.4: Conductive-convective geometries.

Consider the plane wall shown in figure 3.1.4(a) exposed to a hot fluid, h, on one side and a cooler fluid, c, on the other side. The heat transfer rate is expressed by

$$Q = h_1 A (T_h - T_1) = kA (T_1 - T_2)/L = h_2 A (T_2 - T_c) \tag{3.1.21}$$

or written in terms of the thermal resistances

$$Q = \frac{T_h - T_1}{1/(h_1 A)} = \frac{(T_1 - T_2)}{L/(kA)} = \frac{(T_2 - T_c)}{1/(h_2 A)} \tag{3.1.22}$$

Upon eliminating T_1 and T_2 in this relation, find

$$Q = \frac{T_h - T_c}{1/(h_1 A) + L/(kA) + 1/(h_2 A)} = UA(T_h - T_c) \tag{3.1.23}$$

This equation defines the overall heat transfer coefficient

$$U = \frac{1}{1/h_1 + L/k + 1/h_2} \tag{3.1.24}$$

In the case of a long cylinder, the radial heat flux through the wall exposed to two fluids at different temperatures, as shown in figure 3.1.4(b), is given by

$$Q = \frac{T_i - T_o}{1/(h_i A_i) + \ell n(r_o/r_i)/(2\pi kL) + 1/(h_o A_o)} \tag{3.1.25}$$

where L is the length of the cylinder. The terms A_i and A_o represent the inside and outside surface areas of the tube. The overall heat transfer coefficient may be based on either the inside or the outside area of the cylinder. Accordingly,

$$U_i = \frac{1}{1/h_i + A_i \ell n(r_o/r_i)/(2\pi kL) + A_i/(A_o h_o)} \tag{3.1.26}$$

or

$$U_o = \frac{1}{A_o/(A_i h_i) + A_o \ell n(r_o/r_i)/(2\pi kL) + 1/(h_o)} \tag{3.1.27}$$

3.2 HEAT TRANSFER IN DUCTS

The heat transfer during the flow of a particular fluid in ducts is determined by the nature of the flow, i.e., laminar, transitional or turbulent. Furthermore, the flow may be fully developed hydrodynamically and thermally or it may be developing in one form or another. In the case of laminar flow, the duct geometry and the thermal boundary conditions have a significant effect on the heat transfer rate. Numerous analytical and numerical solutions have been found for the heat transfer coefficient during laminar flow in various duct geometries. In the region of transitional and turbulent flow, correlations based on experimental measurements are employed to predict heat transfer rates.

3.2.1 LAMINAR FLOW

The heat transfer coefficient during laminar flow in a duct ($Re \leq 2300$) is dependent on a large number of parameters. The complexity of the problem is well illustrated by the extensive summary of results and correlations presented by Shah and London [78SH1]. Different temperature and/or heat flux conditions may occur at the inside wall of the duct. Of these, most commonly encountered are the conditions of constant axial and peripheral temperature which is approximated in certain condensers, evaporators and liquid-to-gas heat exchangers with high liquid flows, and in the case of constant heat flux. A few useful equations will be presented here.

According to Hausen [55KA1] the mean Nusselt number for hydrodynamically fully developed flow in a round tube at a constant wall temperature is

$$Nu_T = 3.66 + \frac{0.0668 \; Re \; Pr \; d/L}{1 + 0.04 \; (Re \; Pr \; d/L)^{0.667}} \qquad (3.2.1)$$

Schlünder [81SC1] proposes the following correlation for these conditions:

$$Nu_T = \left(3.66^3 + 4.2 \; Re \; Pr \; d/L\right)^{0.333} \qquad (3.2.2)$$

A more recent relation was proposed by Gnielinski [89GN1].

$$Nu_T = \left[3.66^3 + 0.7^3 + \left\{1.615\ (Re\ Pr\ d/L)^{0.333} - 0.7\right\}^3\right]^{0.333} \tag{3.2.3}$$

When the inlet velocity distribution to the tube is uniform, Kays [55KA1] recommends the following equation:

$$Nu_T = 3.66 + \frac{0.104\ Re\ Pr\ d/L}{1 + 0.016\ (Re\ Pr\ d/L)^{0.8}} \tag{3.2.4}$$

or according to Churchill and Ozoe [73CH1]

$$Nu_T = \frac{1.2732}{\left[1 + (Pr/0.0468)^{0.667}\right]^{0.25}} \left(\frac{\pi\ Re\ Pr\ d}{4L}\right)^{0.5} \tag{3.2.5}$$

Gnielinski [89GN1] proposes

$$Nu_T = 3.66^3 + 0.7^3 + \left[\left\{1.615\ (Re\ Pr\ d/L)^{0.333} - 0.7\right\}^3\right.$$

$$\left. + \left\{2\ (Re\ Pr\ d/L)^3/(1 + 22\ Pr)\right\}^{0.5}\right]^{0.333} \tag{3.2.6}$$

Under certain operating conditions the heat flux between the tube wall and the fluid may be constant. When this is the case and the inlet velocity distribution is fully developed the mean Nusselt number is [75SH1].

$$Nu_q = 4.364 + 0.0722\ Re\ Pr\ d/L \quad \text{for} \quad L/(Re\ Pr\ d) > 0.03 \tag{3.2.7}$$

$$= 1.953\ (Re\ Pr\ d/L)^{0.333} \quad \text{for} \quad L/(Re\ Pr\ d) \le 0.03 \tag{3.2.8}$$

The duct geometry has a significant influence on the heat transfer coefficient and the friction factor. This is illustrated in table 3.2.1, which lists Nusselt numbers and friction solutions for fully developed flow for several ducts at constant wall temperature and for the case where the heat flux is constant in the axial direction while the temperature is constant peripherally [81SH1].

For a fully developed velocity profile entering between two parallel plates at a constant temperature, the following equations are applicable [75SH1]:

$$Nu_T = 7.541 + 0.0235 \text{ Re Pr } d_e/L \quad \text{for} \quad L/(\text{Re Pr } d_e) > 0.006 \tag{3.2.9}$$

$$= 1.849(\text{Re Pr } d_e/L)^{0.333} + 0.6 \text{ for } 0.0005 < L/(\text{Re Pr } d_e) \leq 0.006 \tag{3.2.10}$$

and in the case of uniform heat flux,

$$Nu_q = 8.235 + 0.0364 \text{ Re Pr } d_e/L \quad \text{for} \quad L/(\text{Re Pr } d_e) \geq 0.01 \tag{3.2.11}$$

$$= 2.236 (\text{Re Pr } d_e/L)^{0.333} + 0.9 \text{ for } 0.001 < L/(\text{Re Pr } d_e) \leq 0.01 \tag{3.2.12}$$

$$= 2.236 (\text{Re Pr } d_e/L)^{0.333} \quad \text{for} \quad L/(\text{Re Pr } d_e) \leq 0.001 \tag{3.2.13}$$

Table 3.2.1: Solutions for heat transfer and friction for fully developed flow in ducts.

Geometry ($L/d_e > 100$)	Nu_T	Nu_q	f Re	K_∞	L_{hy}
○	3.657	4.364	16.000	1.240	0.0380
b, c $\frac{b}{c} = 1$	2.976	3.608	14.227	1.552	0.0324
b, c $\frac{b}{c} = \frac{1}{2}$	3.391	4.123	15.548	1.383	0.0255
b, c $\frac{b}{c} = \frac{1}{8}$	5.597	6.490	20.585	0.879	0.0094
$\frac{b}{c} = 0$	7.541	8.235	24.000		
insulated $\frac{b}{c} = 0$	4.861	5.385	24.000		

In the case where the inlet velocity between the parallel plates is uniform and the wall temperature is constant, the Nussalt number is given by Stephan [59ST1] as

$$Nu_T = 7.55 + \frac{0.024\ (Re\ Pr\ d_e/L)^{1.14}}{1 + 0.0358\ (Re\ Pr\ d_e/L)^{0.64}\ Pr^{0.17}} \tag{3.2.14}$$

The tabulated values for rectangular ducts are shown graphically in figure 3.2.1. Curves through these points are given by the following equations [78SH1]:

$$Nu_T = 7.541\ [1 - 2.610\ b/a + 4.970\ (b/a)^2 - 5.119\ (b/a)^3 + 2.702\ (b/a)^4 - 0.548\ (b/a)^5] \tag{3.2.15}$$

For a uniform heat flux,

$$Nu_q = 8.235\ [1 - 2.0421\ b/a + 3.0853\ (b/a)^2 - 2.4765\ (b/a)^3 + 1.0578\ (b/a)^4 - 0.1861\ (b/a)^5] \tag{3.2.16}$$

With these equations it is possible to determine the limiting values for any rectangular duct.

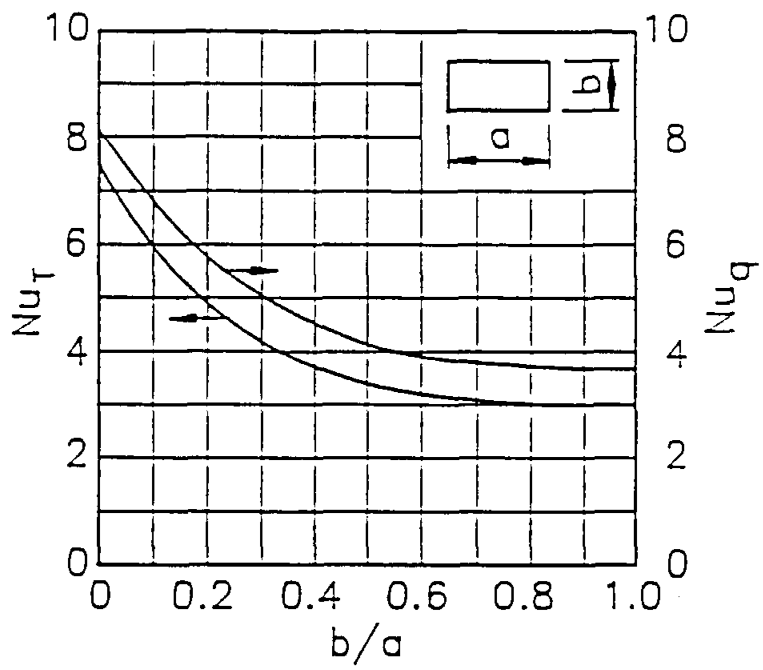

Figure 3.2.1: Heat transfer for fully developed flow through rectangular ducts.

When L/d is less than 0.0048Re in tubes and when L/d_e is less than 0.0021Re in ducts of a rectangular cross-section for both constant wall temperature conditions and uniform heat flux conditions,

$$Nu = \frac{Re\ Pr\ d_e}{4L} \ln \left[\frac{1}{1 - 2.654/\{Pr^{0.167}\ (Re\ Pr\ d_e/L)^{0.5}\}} \right] \tag{3.2.17}$$

This equation has been found useful for ordinary liquids and gases [80KR1].

Jamil [67JA1], Cheng and Jamil [70CH1] and Zarling [76ZA1] analyzed the problem of fully developed flow in noncircular ducts as shown in table 3.2.2 for the case of uniform heat flux. These results are compared to those of a rectangular duct in figure 3.2.2.

Table 3.2.2: Solutions for heat transfer and friction for fully developed flow in ducts.

				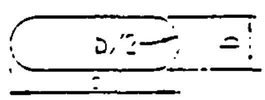		
2θ	b/a	Nu_q	fRe	b/a	Nu_q	fRe
0	0	8.235	24.000	0	8.24	24.00
10	0.087	-	21.551	0.150	6.59	20.94
20	0.174	6.020	19.822	0.200	6.16	20.13
40	0.342	4.991	17.603	0.250	5.77	19.41
60	0.500	4.483	16.475	0.333	5.28	18.40
100	0.766	4.269	15.842	0.500	4.72	17.03
140	0.940	4.335	15.933	0.667	4.45	16.32
180	1	4.364	16.000	1	4.36	16.00

Various investigators have analyzed the problem of fully developed flow in elliptical ducts at constant wall temperature as well as for the case of a uniform heat flux [78SH1]. The results are listed in table 3.2.3. Abdel-Wahed et al [84AB1] report the results of experimental studies.

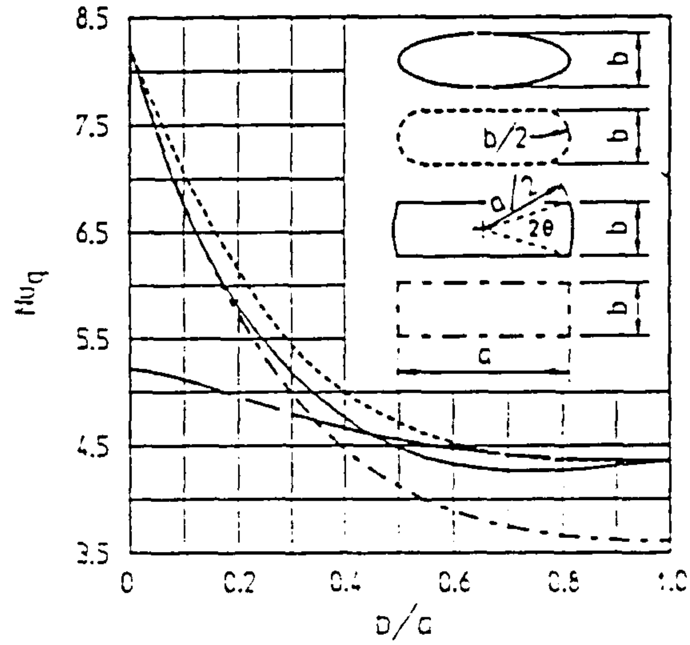

Figure 3.2.2: Heat transfer for fully developed flow in ducts.

Table 3.2.3: Solutions for heat transfer and friction for fully developed flow in elliptical ducts.

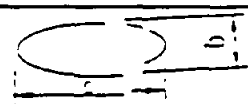

b/a	Nu_T	Nu_q	fR_e
1.00	3.658	4.364	16.000
0.80	3.669	4.387	16.098
0.50	3.742	4.558	16.823
0.25	3.792	4.880	18.240
0.125	3.725	5.085	19.146
0.063	3.647	5.176	19.536
0.00	3.488	5.225	19.739

Hydrodynamically and thermally developing flows at the inlets to heat exchanger ducts or across interrupted surfaces generally tend to lead to higher heat transfer coefficients when compared to fully developed flow. Solutions for many of these problems appear in the literature [83KA1].

At very low Reynolds numbers, or if high temperature differences are employed , or if the passage geometry has a large hydraulic diameter, free-convection effects may become important. For horizontal tubes, free convection sets up secondary flows at a cross-section that aid the convection process. Hence the heat transfer coefficient for the combined convection is higher than that for the pure forced convection. Metais and Eckert [64ME1] have classified free, mixed and forced convection regimes as shown in figure 3.2.3(a) for horizontal tubes with the axially constant wall temperature boundary condition. The limits of the forced and mixed convection regimes are defined in such a manner that free convection effects contribute only about 10 percent to the heat flux. Figure 3.2.3(a) may therefore be used as a guide to determine whether or not free convection is important.

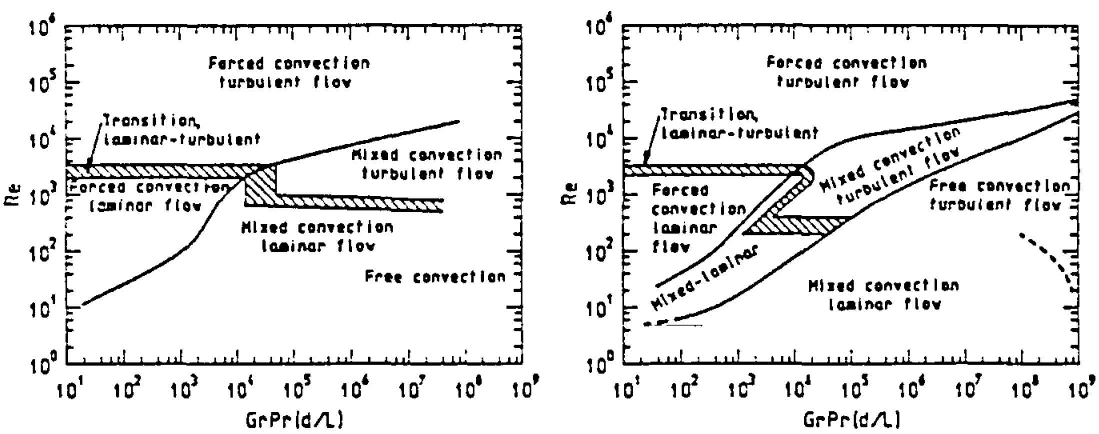

(a) Horizontal tube (b) Vertical tube

Figure 3.2.3: Free, forced and mixed convection ($10^{-2} < Pr\ d/L < 1$).

Among others Brown and Thomas [65BR1] and Oliver [86HO1] present heat transfer equations for laminar combined free and forced convection inside horizontal tubes having a constant wall temperature. According to Oliver [86HO1]:

$$Nu_T = 1.75\,[Gz + 0.0083\,(GrPr)^{0.75}]^{0.333}\,(\mu/\mu_w)^{0.14} \qquad (3.2.18)$$

where $Gz = Re\,Pr\,d/L$ and $Gr = g\rho^2 d^3 \beta\,(T_w - T)/\mu^2$

All of the fluid properties are evaluated at the fluid bulk mean temperature except μ_w which is evaluated at the wall temperature.

The effect of superimposed free convection for vertical tubes, unlike horizontal tubes is dependent upon the flow direction and on whether or not the fluid is heated or cooled. The flow regime chart of Matais and Eckert [64ME1] for vertical tubes, as shown in figure 3.2.3(b), provides guidelines to determine the significance of the superimposed free convection.

Laminar flow generally results in relatively low heat transfer coefficients. Variable fluid property effects, which are predominantly due to viscosity and density variation, tend to increase heat transfer coefficients. The need for more effective heat transfer systems has stimulated interest in techniques to augment or enhance heat transfer.

The various techniques to augment heat transfer inside tubes are generally classified as passive or active. With passive techniques no external energy other than pump work is required to produce the augmentation. These techniques are further classified as surface roughness, internal extended surface, displaced promotors, swirl flow, additives and compound techniques in which more than one of these techniques are employed. With active techniques, external energy is required to produce the augmentation. These techniques include mechanical aids, heated surface vibration, fluid pulsation, electrostatic fields and suction or injection.

Surveys [78BE1] and evaluations [83BE1] of augmentation techniques appear in the literature.

Hong and Bergles [76HO1] present an equation for fully developed laminar flow in a circular uniformly heated tube with a twisted tape insert as shown in figure 2.2.2.

$$Nu = 5.172[1 + 0.00548\,Pr^{0.7}\,(Re\,d/P)^{1.25}]^{0.5} \qquad (3.2.19)$$

where the Nu and Re numbers are based on the inside diameter of the tube. Other correlations are presented by Manglik and Bergles [86MA1].

A more complex correlation for thermally developing flow was presented by Du Plessis and Kröger [87DU1].

Considerable test data are available for internally finned tubes [78SH1,74CA1].

The following correlations of Watkinson et al [75WA1] are applicable in the case of laminar flow:

Spirally finned tubes:

$$Nu = 19.2\ Re^{0.26}\ (Pr\ d_e/L)^{0.333}\ (L_f/P_f)^{0.5}\ /\ \phi \tag{3.2.20}$$

where

$$\phi = 2.25\ (1 + 0.01\ Gr^{0.333})/\log_{10} Re \tag{3.2.21}$$

and L_f is the average distance between fins. In this equation the Grashof number is defined as

$$Gr = g\rho^2\ d^3\ \beta\ (T_w - T)\ /\ \mu^2$$

Straight-finned tubes:

$$Nu = 2.43\ Re^{0.46}\ (Pr\ d_e/L)^{0.333}\ (1/n_f)^{0.5}/\phi \tag{3.2.22}$$

These correlations are based on data for oil in horizontal tubes having an approximately uniform temperature. Other data for both water and ethylene glycol in both steam-heated and electrically heated tubes are in approximate agreement with these correlations [78MA1].

A configuration consisting of a combination of internal fins and spiral tapes may be considered to improve the effective heat transfer coefficient when cooling viscous media [78VA1, 79JE1].

In some of the above equations it is assumed that the fluid properties are constant and they are evaluated at the bulk mean temperature. According to Shah [83SH1] no corrections for temperature-dependent property effects are required when the above heat transfer equations are applied to gases and if temperature differences are not excessive.

For liquids, where only the viscosity is strongly temperature-dependent, the following relations are adequate for both heating and cooling:

$$\frac{Nu}{Nu_{cp}} = \left(\frac{\mu}{\mu_w}\right)^{0.14} \tag{3.2.23}$$

Bergles presents surveys of analytical solutions [83BE2] and experimental studies [83BE3, 86BE1] that evaluate the influence that variable transport properties may have on the heat transfer rate in laminar duct flows.

Example 3.2.1

Oil flows at a rate of $m_o = 0.11094$ kg/s in a 1 m long horizontal tube having an inside diameter of $d_i = 13.5$ mm. The flow entering the tube is hydrodynamically fully developed. The tube-wall is at a constant temperature of $T_w = 99.105$ °C. The mean temperature of the oil in the tube is $T_o = 44.1958$ °C. Determine the Nusselt number applicable to this flow.

The thermophysical properties of the oil are:

Volume coefficient of expansion	$\beta_o = 7.47 \times 10^{-4}\ K^{-1}$
Density	$\rho_o = 880.5 - 0.613T$ kg/m^3
Thermal conductivity	$k_o = 0.13428 - 7.185 \times 10^{-5}\ T$ W/mK
Specific heat	$c_{po} = 3.642\ T + 1809$ J/kg K
Dynamic viscosity	

In the range 5°C < T < 50°C, $\mu_o = \exp[-0.3948\,(\ln T)^2 + 1.2709\,(\ln T) - 2.8523]$ kg/ms
In the range 50°C ≤ T ≤ 100°C, $\mu_o = 38.876/T^{1.9325}$ kg/ms

where T is in °C

Solution

Evaluate the thermophysical properties of the oil at T_o = 44.1958 °C, i.e.

ρ_o = 880.5 - 0.613 x 44.1958 = 853.408 kg/m^3
k_o = 0.13428 - 7.185 x 10^{-5} x 44.1958 = 0.1311 W/mK
c_{po} = 3.642 x 44.1958 + 1809 = 1969.961 J/kg K
$\mu_o = \exp[-0.3948\,(\ln 44.1958)^2 + 1.2709 \ln 44.1958 - 2.8523]$ = 0.02462 kg/sm

At a wall temperature of T_w = 99.105 °C find the dynamic viscosity

$\mu_{ow} = 38.876/(99.105)^{1.9325}$ = 0.0053979 kg/ms

For the given oil mass flow rate find the corresponding Reynolds number.

$$Re_o = \frac{4m_o}{\pi d_i \mu_o} = \frac{4 \times 0.11094}{\pi \times 13.5 \times 10^{-3} \times 0.02462} = 424.99$$

i.e. the flow is laminar.

The Prandtl number of the oil at its mean temperature is

$$Pr_o = \mu_o c_{po}/k_o = 0.02462 \times 1969.961/0.1311 = 369.9499$$

To evaluate the influence that free convection effects may have on the Nusselt number, determine the Grashof number for the flow inside the tube.

$$Gr_o = g\rho_o^2\, d_i^3\, \beta_o\, (T_w - T_o)/\mu_o^2$$

$$= 9.8 \times 853.408^2 \times 0.0135^3 \times 7.47 \times 10^{-4} (99.105 - 44.1958)/0.02462^2 = 1188.3$$

Thus

$$Gr_o Pr_o d_i/L = 1188.3 \times 369.9499 \times 0.0135 = 5934.8$$

According to figure 3.2.3 (a) flow conditions are close to the dividing line between forced convection laminar flow and mixed convection laminar flow for $Re_o = 424.99$ and $Gr_o Pr_o d_i/L = 5934.8$. Equations ignoring free convection effects and those taking into consideration free convection are thus applicable.

It follows from equation (3.2.1) and equation (3.2.23) which corrects for temperature-dependent properties that

$$N_T = \left[3.66 + \frac{0.0668 \times 424.99 \times 369.9499 \times 13.5 \times 10^{-3}}{1 + (0.04 \times 424.99 \times 369.9499 \times 13.5 \times 10^{-3})^{0.667}}\right]\left(\frac{0.02462}{0.0053979}\right)^{0.14}$$

$$= 27.579$$

Similarly according to equations (3.2.2) and (3.2.23) find

$$Nu_T = (3.66^3 + 4.2 \times 424.99 \times 369.9499 \times 13.5 \times 10^{-3}) (0.02462/0.0053979)^{0.14}$$

$$= 25.69$$

From equation (3.2.3) and (3.2.23) it follows that

$$Nu_T = \left[3.66^3 + 0.7^3 + \left\{1.615(424.99 \times 369.9499 \times 0.0135)^{0.333} - 0.7\right\}^3\right]^{0.333}$$

$$\times (0.02462/0.0053979)^{0.14} = 24.7135$$

Equation (3.2.18) can also be applied in this case.

$$Nu_T = 1.75\,[424.99 \times 369.9499 \times 13.5/1000$$

$$+ 0.0083\,(1188.3 \times 369.9499)^{0.75}]^{0.333}\,(0.02462/0.0053979)^{0.14} = 28.346$$

This latter value is preferred since it makes provision for free convection effects which tend to increase the effective heat transfer coefficient.

3.2.2 TURBULENT FLOW

In 1930 Dittus and Boelter [62HS1] summarized the available heat transfer data for turbulent flow in tubes and plotted them in a single graph. The various experiments described in thirteen papers were done with fluids which covered a wide range of viscosities. The fluids were heated or cooled. The resultant equations, which have since found wide application in the design of heat transfer equipment, are

$$Nu = 0.0243\,Re^{0.8}\,Pr^{0.4} \tag{3.2.24}$$

for heating and

$$Nu = 0.0265\,Re^{0.8}\,Pr^{0.333} \tag{3.2.25}$$

for cooling. The thermophysical properties are evaluated at the arithmetic mean bulk temperature.

An improved equation that considers flow development, was proposed by Hausen in 1959 and modified by him in 1974 [59HA1, 74HA1]:

$$Nu = 0.0235\,(Re^{0.8} - 230)\,(1.8\,Pr^{0.3} - 0.8)\left[1 + \left(\frac{d}{L}\right)^{0.667}\right]\left(\frac{\mu}{\mu_w}\right)^{0.14} \tag{3.2.26}$$

For fully developed turbulent flow Petukhov developed an equation that was subsequently modified [70PE1]:

$$Nu = \frac{(f_D/8)\,Re\,Pr}{1.07 + 12.7\,(f_D/8)^{0.5}\,(Pr^{0.667} - 1)}\left(\frac{\mu}{\mu_w}\right)^{b} \tag{3.2.27}$$

where b = 0.11 for $T_w > T$ or b = 0.25 for $T_w < T$ for liquids and b = 0 for uniform heat flux or for gases. All properties are evaluated at the bulk temperature of the fluid except for $T\mu_w$ which is evaluated at T_w. For smooth tubes the recommended friction factor is according to equation (2.2.10)

$$f_D = (1.82 \log_{10} Re - 1.64)^{-2} \tag{3.2.28}$$

Equation (3.2.27) is applicable in the following ranges:

$0.5 < Pr < 200$ for 6 per cent accuracy

$0.5 < Pr < 2000$ for 10 per cent accuracy

$10^4 < Re < 5 \times 10^6$

$0 < \mu/\mu_w < 40$

On the basis of the earlier work of Hausen and Petukhov as well as on most of the available experimental data, Gnielinski [75GN1] proposes the following equation:

$$Nu = \frac{(f_D/8)\ (Re - 1000)\ Pr\ [1 + (d/L)^{0.67}]}{1 + 12.7\ (f_D/8)^{0.5}\ (Pr^{0.67} - 1)} \tag{3.2.29}$$

Equation (3.2.29) is valid for the ranges, $2300 < Re < 10^6$, $0.5 < Pr < 10^4$, and $0 < d/L < 1$.

All thermophysical properties are evaluated at the bulk mean temperature of the fluid.

Care should be taken when applying this equation at low Reynolds numbers and to very short tubes.

Variations in the properties of the fluid may be taken into consideration by multiplying the right-hand side of equation (3.2.29) with a correction factor [70PE1]. For liquids

$(Pr/Pr_w)^{0.11}$ (heating)

$(Pr/Pr_w)^{0.25}$ (cooling)

for $0.1 < (Pr/Pr_w) < 10$, and for gases

$(T/T_w)^{0.45}$ (heating)

$(T/T_w)^{0.36}$ (cooling)

Cain et al [73CA1] investigated the heat transfer characteristics of flow in elliptical ducts and found existing equations to be in good agreement with experimental results for Re > 20000.

3.2.3 TRANSITIONAL FLOW

The transitional region between laminar and turbulent flow has not been extensively examined, and methods for determining the extent of this region and obtaining heat transfer coefficients may be unreliable. For round tubes Hausen [43HA1] proposed the following equation:

$$Nu = 0.116\,(Re^{0.667} - 125)\,Pr^{0.333}\,[1 + (d/L)^{0.667}] \tag{3.2.30}$$

for $2100 < Re > 10000$

Barrow and Roberts [70BA1] recommend a relation for elliptical ducts in the range of $4000 < Re < 20000$ i.e.

$$Nu = 0.00165\,Re^{1.06}\,Pr^{0.4} \tag{3.2.31}$$

Metais and Eckert [64ME1] attempt to establish certain criteria that define the limits of different transfer regimes in transitional flow as shown in the modified plot in figure 3.2.4.

The heat transfer coefficients for the cooling of oil at a constant tube wall temperature were determined for the ranges $550 < Re < 2800$ and $132 < Pr < 642$ [81RO1]. With the transfer regions divided as given in figure 3.2.4, correlating equations have been obtained for each regime.

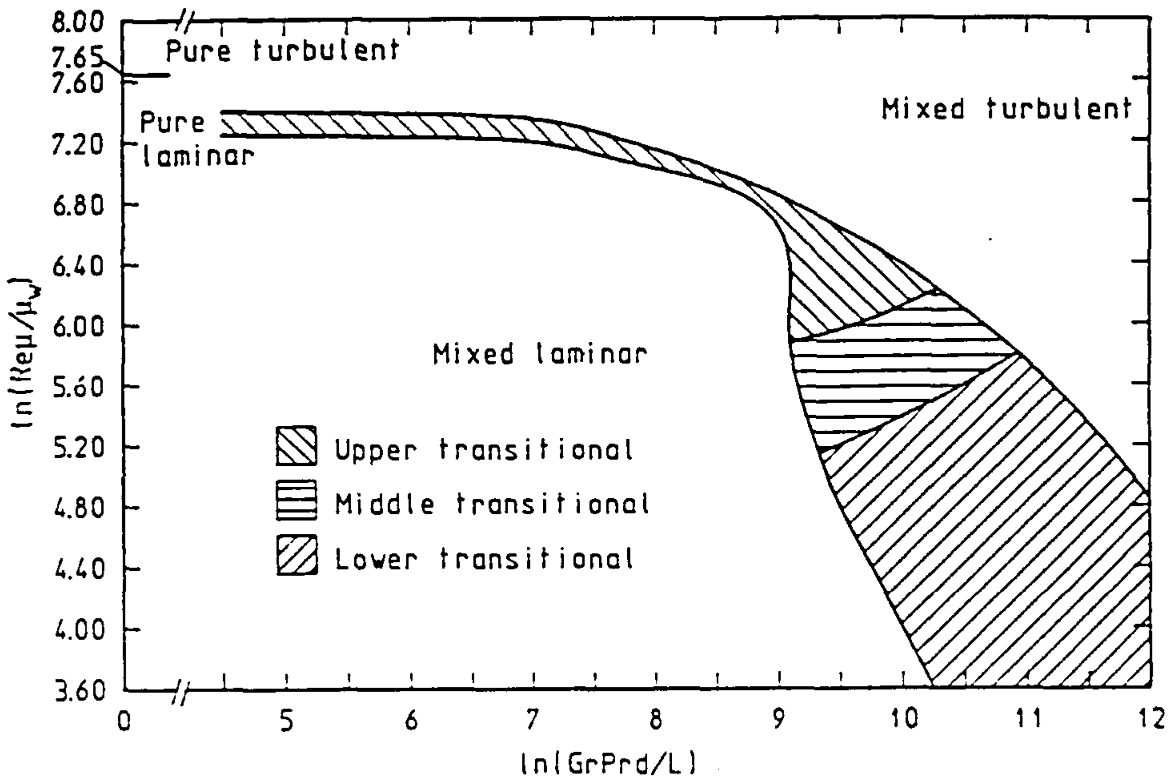

Figure 3.2.4: Modified Metais and Eckert plot.

Mixed turbulent:

$$Nu = 0.0184(Re^{0.8} - 213.9)(1.8\,Pr^{0.333} - 0.8)[1 + (d/L)^{0.67}](\mu/\mu_w)^{0.14} \qquad (3.2.32)$$

Upper transitional:

$$Nu = 0.0277\,(Re^{0.8} - 272.5)\,(1.8\,Pr^{0.333} - 0.8)\,[1 + (d/L)^{0.67}]\,(\mu/\mu_w)^{0.14} \qquad (3.2.33)$$

Middle transitional:

$$Nu = 0.0176\,(Re^{0.8} - 106.1)(1.8\,Pr^{0.333} - 0.8)[1 + (d/L)^{0.67}](\mu/\mu_w)^{0.14} \qquad (3.2.34)$$

Mixed laminar:

$$Nu = 0.002\ Re^{1.42}\ Pr^{0.333}\ (\mu/\mu_w)^{0.14} \tag{3.2.35}$$

No suitable equation has been found to correlate the data in the lower transitional regime.

A single correlating equation that covers the entire range from the laminar through the transitional to the turbulent regime in smooth tubes is proposed by Churchill [77CH1]. The behavior for all Reynolds and Prandtl numbers for developed or developing conditions is represented by

$$Nu^{10} = Nu_l^{10} + \left[\frac{\exp\{(2200 - Re)/365\}}{Nu_{lc}^2} + \left\{ \frac{1}{Nu_0 + \dfrac{0.02793\ Re\ Pr\ f_D^{0.5}}{(1 + Pr^{0.8})^{0.833}}} \right\}^2 \right]^{-5} \tag{3.2.36}$$

where Nu_l is the Nusselt number for laminar flow, Nu_{lc} is the Nusselt number at Re = 2100 and Nu_0 is the value which the Nusselt number approaches as Re Pr approaches zero. The latter is approximately 4.8 for flow at a constant wall temperature and 6.3 for a uniform heat flux. For flow in a tube at a constant wall temperature, Nu_l may be approximated by

$$Nu_{lT} = 3.657 \left[1 + \left(\frac{Re\ Pr\ d/L}{7.60} \right)^{2.67} \right]^{0.125} \tag{3.2.37}$$

and at a uniform heat flux by

$$Nu_{lq} = 4.364 \left[1 + \left(\frac{Re\ Pr\ d/L}{7.3} \right)^{2} \right]^{0.167} \tag{3.2.38}$$

The value for Nu_{lc} is obtained by substituting Re = 2100 into equation (3.2.37) or (3.2.38). For a smooth tube the friction factor, f_D, can be determined according to equation (2.2.18).

Taborek [90TA1] notes that data in the transition region can be plotted approximately as a straight line on a linear scale between the limits $2000 \le Re \le 8000$. Using a value of the Nusselt number for laminar and turbulent flow, Nu_l and Nu_t respectively at these boundary Reynolds numbers, the linear proration results in

$$Nu = (1.333 - Re/6000)Nu_l + (Re/6000 - 0.333)Nu_t \tag{3.2.39}$$

Example 3.2.2

If in example 2.3.1 heat is removed from the water at a uniform rate (constant heat flux), determine the Nusselt number for the case where the tube wall is smooth. Compare the values obtained according to equations (3.2.25), (3.2.26), (3.2.27), (3.2.29) and (3.2.36) respectively.

Solution

Since $Re_w = 44349.9 > 2300$ the flow is turbulent.

In addition to the thermophysical properties of water at 52.5°C (325.65 K), evaluated in Example 2.3.1, find:

The specific heat of water follows from equation (A.4.2)

$$c_{pw} = 8.15599 \times 10^3 - 2.80627 \times 10 \times 325.65 + 5.11283 \times 10^{-2} \times 325.65^2 - 2.17582 \times 10^{-13} \times 325.65^6 = 4179.926 \text{ J/kgK}$$

The thermal conductivity of water from equation (A.4.4)

$$k_w = -6.14255 \times 10^{-1} + 6.9962 \times 10^{-3} \times 325.65 - 1.01075 \times 10^{-5} \times 325.65^2 + 4.74737 \times 10^{-12} \times 325.65^4 = 0.64556 \text{ W/mK}$$

The Prandtl number is

$$Pr_w = \mu_w c_{pw}/k_w = 5.21804 \times 10^{-4} \times 4179.926/0.64556 = 3.379$$

For cooling, according to the Dittus and Boelter, equation (3.2.25) gives,

$$Nu = 0.0265 \times 44349.9^{0.8} \times 3.379^{0.333} = 207.42$$

The Hausen equation (3.2.26) for small differences in wall and fluid temperature gives

$$Nu = 0.0235\,(44249.9^{0.8} - 230)(1.8 \times 3.379^{0.3} - 0.8)\,[1 + 22.09/15024^{0.667}] = 212.56$$

Similarly, according to the Petukhov equation (3.2.27)

$$Nu = \frac{0.021516 \times 44349.9 \times 3.379/8}{1.07 + 12.7(0.021516/8)^{0.5}(3.379^{0.667} - 1)} = 212.68$$

Gnielinski's equation (3.2.29) gives

$$Nu = \frac{(0.021516/8)(44349.9 - 1000)3.379\left[1 + (22.09/15024)^{0.67}\right]}{1 + 12.7(0.021516/8)^{0.5}\,(3.379^{0.67} - 1)} = 217.94$$

Applying Churchill's equation, it follows from equation (3.2.38) that

$$Nu_{lq} = 4.364\left[1 + \left(\frac{44349.9 \times 3.379 \times 22.09}{7.3 \times 15024}\right)^2\right]^{0.167} = 13.621$$

Furthermore,

$$Nu_{lc} = 4.364\left[1 + \left(\frac{2100 \times 3.379 \times 22.09}{7.3 \times 15024}\right)^2\right]^{0.167} = 5.255$$

The friction factor follows from equation (2.2.18), i.e.

$$f_D = 8\left[\frac{1}{\left\{\left(\frac{8}{44349.9}\right)^{10} + \left(\frac{44349.9}{36500}\right)^{20}\right\}^{0.5}} + \left\{2.21 \ln\left(\frac{44349.9}{7}\right)\right\}^{10}\right]^{-0.2} = 0.02137$$

Substitute these values into equation (3.2.36) and find

$$Nu^{10} = 13.621^{10} + \left[\frac{\exp\{(2200 - 44349.9)/365\}}{5.255^2}\right.$$

$$\left. + \left\{\frac{1}{6.3 + \frac{0.02793 \times 44349.9 \times 3.379 \times 0.02137^{0.5}}{(1 + 3.379^{0.8})^{0.833}}}\right\}^2\right]^{-5}$$

or

$$Nu = 214.59$$

3.3 EXTENDED SURFACES

In the design and construction of various types of heat transfer equipment, shapes such as cylinders, bars and plates are used to implement the flow of heat between source and sink. They provide heat-absorbing or heat-rejecting surfaces, and each is known as a prime or base surface. When the prime surface is extended by appendages intimately connected with it, the additional surface is known as an extended surface. The elements used to extend prime surfaces are referred to as fins.

3.3.1 FIN EFFICIENCY OR EFFECTIVENESS

Consider an essentially one-dimensional plate fin of uniform thickness, t_f, exposed to the surrounding fluid at a temperature, T_∞, as shown in figure 3.3.1. The temperature at the root of the fin is T_r.

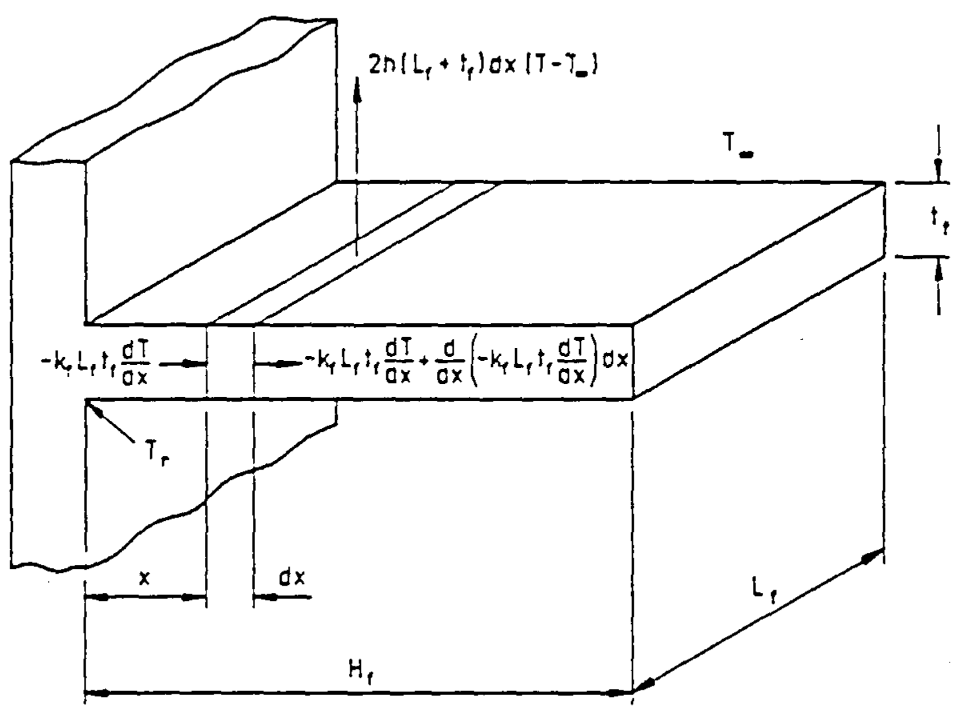

Figure 3.3.1: Schematic drawing of a longitudinal fin of rectangular profile.

Neglecting radiation effects, apply an energy balance to an elementary length of the fin and find that the difference between the heat conducted into the control volume and that conducted out is equal to the heat transferred by convection to the surrounding fluid:

$$\frac{d}{dx}\left(k_f\, L_f\, t_f\, \frac{dT}{dx}\right) dx \;=\; 2h\,(L_f + t_f)\, dx\,(T - T_\infty) \tag{3.3.1}$$

or, assuming constant thermal conductivity k_f,

$$\frac{d^2T}{dx^2} - \frac{2h(L_f + t_f)}{k_f\, L_f\, t_f}(T - T_\infty) \;=\; 0 \tag{3.3.2}$$

This equation assumes that the heat transfer coefficient is uniform and that substantial temperature gradients occur only in the x-direction. The latter assumption will be satisfied if the fin is thin. This is a reasonable approximation in practice.

Assume, furthermore, that $t_f << L_f$, and substitute $\theta = T - T_\infty$ into equation (3.3.2) to give

$$\frac{d^2\theta}{dx^2} - \frac{2h\theta}{k_f t_f} \;=\; 0 \tag{3.3.3}$$

Let

$$b^2 \;=\; 2h/(k_f\, t_f) \tag{3.3.4}$$

and find the general solution for equation (3.3.3), i.e.

$$\theta \;=\; a_1\, e^{-bx} + a_2\, e^{bx} \tag{3.3.5}$$

At the fin root or base $x = 0$ and $\theta = \theta_r = (T_r - T_\infty)$, whereas at the fin tip heat is lost owing to convection. To simplify the problem it is assumed that the heat loss at the fin tip is negligible, or $dT/dx = d\theta/dx = 0$ at $x = H_f$.

Thus

$$\theta_r = a_1 + a_2$$

and

$$0 = -a_1 b e^{-bH_f} + a_2 b e^{bH_f}$$

Solve for a_1 and a_2 and find

$$\frac{\theta}{\theta_r} = \frac{e^{-bx}}{1 + e^{-2bH_f}} + \frac{e^{bx}}{1 + e^{2bH_f}} = \frac{\cosh [b(H_f - x)]}{\cosh \left(bH_f\right)} \tag{3.3.6}$$

With this equation it is possible to calculate the heat transfer through the fin, i.e.

$$Q = -k_f L_f t_f \left.\frac{dT}{dx}\right)_{x = 0} = -k_f L_f t_f \left.\frac{d\theta}{dx}\right)_{x = 0} \tag{3.3.7}$$

$$= k_f L_f t_f \theta_r b \left[\frac{e^{-bH_f}}{e^{-bH_f} + e^{bH_f}} - \frac{e^{bH_f}}{e^{bH_f} + e^{-bH_f}}\right]$$

$$= (2h/k_f t_f)^{0.5} L_f (T_r - T_\infty) \tanh \left(bH_f\right) \tag{3.3.8}$$

The effectiveness of a fin transferring heat is also known as the fin efficiency and is defined as the ratio of the actual heat transferred by the fin, to the heat that would be transferred if the entire fin were at the root temperature.

$$\eta_f = \frac{(2h/k_f t_f)^{0.5} L_f (T_r - T_\infty) \tanh \left(bH_f\right)}{2h H_f L_f (T_r - T_\infty)} = \frac{\tanh \left(bH_f\right)}{bH_f} \tag{3.3.9}$$

For the same boundary conditions as above it can be shown that the efficiency of a radial fin of rectangular profile is

$$\eta_f = \frac{2/\xi}{(1 + d_f/d_r)} \left[\frac{I_1(a_1 \xi) K_1(a_2 \xi) - I_1(a_2 \xi) K_1(a_1 \xi)}{I_1(a_1 \xi) K_o(a_2 \xi) + I_o(a_2 \xi) K_1(a_1 \xi)} \right] \tag{3.3.10}$$

where $\xi = [(d_f - d_r)/2]\,(2h/k_f t_f)^{0.5}$, $a_1 = 1/(1 - d_r/d_f)$ and $a_2 = a_1 d_r/d_f$ in the modified Bessel functions I and K.

The efficiencies of longitudinal and radial fins having rectangular profiles are shown in figure 3.3.2. An extensive study of extended surface characteristics is presented by Kern and Kraus [72KE1].

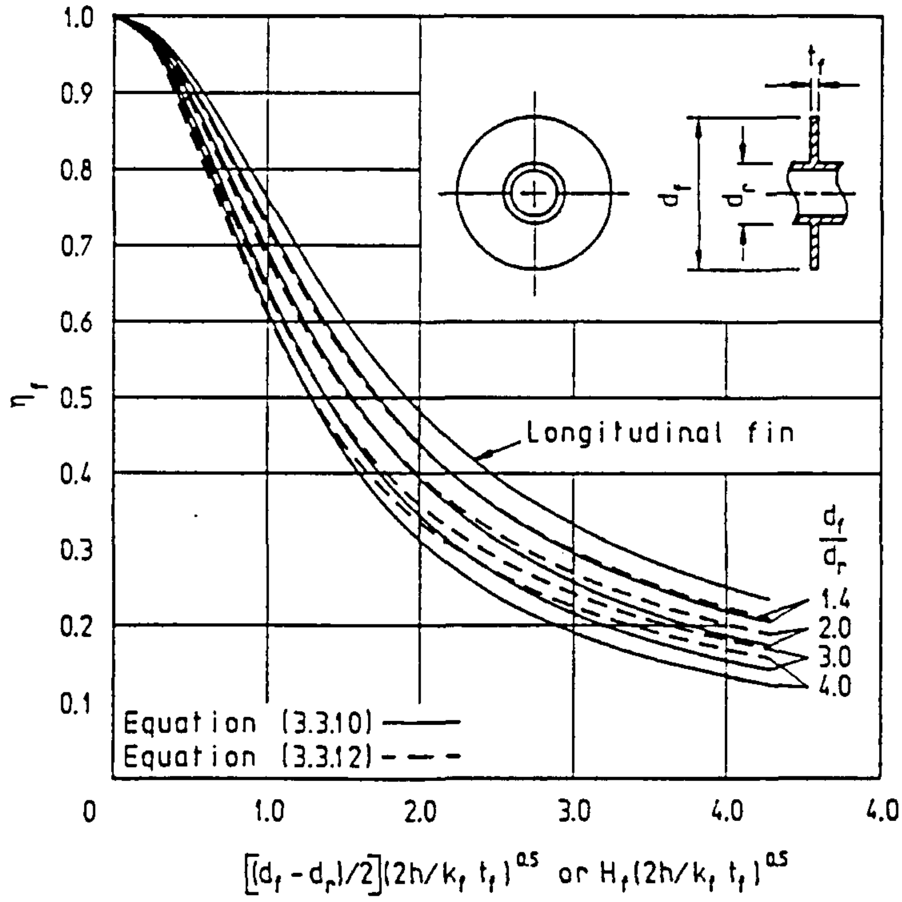

Figure 3.3.2: Efficiencies of radial and longitudinal fins having rectangular profiles.

In a practical radial fin the local heat transfer coefficient is not uniform and the corresponding efficiency differs from the value predicted by equation (3.3.10), in particular at low fin efficiencies [93HU1].

The definition of surface effectiveness as the actual heat transfer from the fin and the free base surface, divided by the heat transfer from those surfaces when the entire fin is at the root or base temperature, is of practical interest, i.e.

$$e_f = \frac{h\, A_r\, (T_r - T_\infty) + h\, A_f\, \eta_f\, (T_r - T_\infty)}{h\, (A_r + A_f)\, (T_r - T_\infty)} = \frac{A_r + A_f\, \eta_f}{A_r + A_f}$$

$$= 1 - A_f\, (1 - \eta_f)/(A_r + A_f) = 1 - A_f\, (1 - \eta_f)/A \qquad (3.3.11)$$

where A_r is the exposed root area, A_f is the fin area, and $A = A_r + A_f$.

3.3.2 SIMPLIFIED EQUATIONS

Other approximate methods for determining the fin efficiency for different finned surfaces have been proposed [46SC1, 55ZA1, 66RI1]. The empirical method described by Schmidt [46SC1] is relatively simple but accurate enough for application in most practical cases [94ZE1].

For a radial fin of uniform thickness he finds

$$\eta_f = \tanh\,(b\, d_r\, \phi/2)/(b\, d_r\, \phi/2) \qquad (3.3.12)$$

where $b = [2h/(k_f t_f)]^{0.5}$ as defined in equation (3.3.4) and

$$\phi = (d_f/d_r - 1)\,[1 + 0.35\, \ell n\, (d_f/d_r)] \qquad (3.3.13)$$

The fin root diameter, d_r, is replaced by the outside tube diameter, d_o, if the fin has no shoulder at its root. The results of this analysis are compared to the more accurate solution in figure 3.3.2 (broken lines). For most practical fins having an efficiency of more than fifty per cent, the difference is less than 1.6 percent.

In the case of a continuous plate fin having a rectangular tube array as shown in figure 3.3.3(a), an equivalent circular fin diameter, d_{fe}, that has the same fin efficiency as the rectangular fin is determined.

$$d_{fe}/d_r = 2.56(L_1/d_r)(L_2/L_1 - 0.2)^{0.5} \tag{3.3.14}$$

L_1 and L_2 are defined in figure 3.3.3, where L_2 is always selected to be greater than or equal to L_1. The parameter ϕ given by equation (3.3.13) is computed using d_{fe} instead of d_f. With the computed value of ϕ, the efficiency is calculated employing equation (3.3.12).

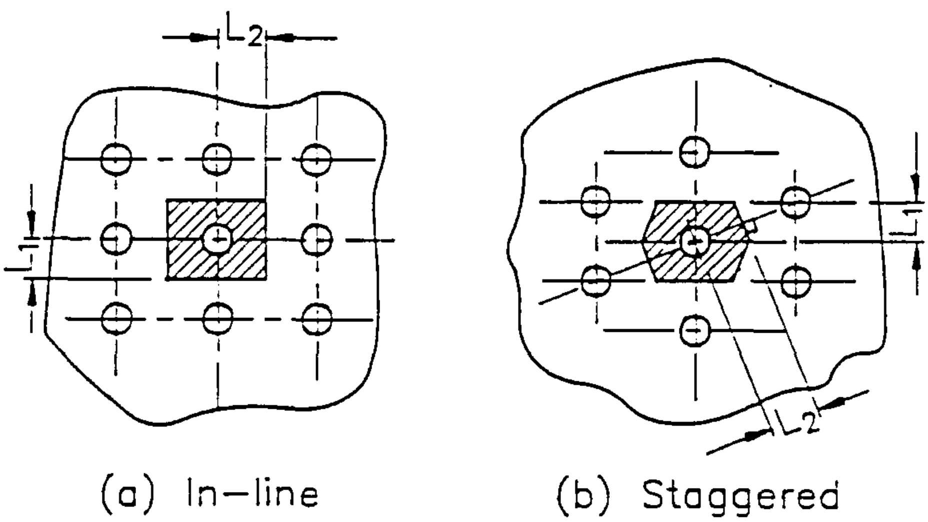

Figure 3.3.3: Tube arrangements.

When the tubes are arranged in a staggered layout as shown in figure 3.3.3(b), the following empirical relation gives a circular fin that has the same efficiency as the illustrated hexagonal fin.

$$d_{fe}/d_r = 2.54\ (L_1/d_r)\ (L_2/L_1 - 0.3)^{0.5} \tag{3.3.15}$$

L_1 and L_2 are defined in figure 3.3.3(b) with $L_2 \geq L_1$.

3.4 CONDENSATION

In all power and refrigeration cycles, vapor condensation occurs on cooled surfaces. If the liquid or condensate wets the surface, a film forms and the process is called film condensation. A temperature gradient exists in the film, and the film presents thermal resistance to heat transfer. If the liquid does not wet the surface, droplets are formed and the process is called dropwise condensation. Under such conditions a large portion of the area of the surface is directly exposed to the vapor, with the result that relatively high heat transfer rates may be experienced. Although the heat transfer rates in dropwise condensation may be as much as ten times higher than in film condensation and would thus be preferred to film condensation in practical condensers, this mode of condensation is difficult to maintain since wetting of the surface usually occurs after an extended period of time. The presence of traces of noncondensable gases in the vapor reduces the rate of heat transfer [92CA1]. This can be particularly detrimental in low pressure steam condensers where air leaking into the system must be purged continuously.

3.4.1 FILM CONDENSATION

Consider a vertical plate of height H and width W which is exposed to a saturated vapor as shown in figure 3.4.1. If the plate temperature, T_p, is less than the saturation temperature of the vapor, T_v, condensation will occur.

In the case of film condensation, a film of thickness δ will flow downwards under the action of gravity. For all practical purposes the temperature distribution through the film will be linear, with the temperature at the liquid-vapor interface equal to the saturation temperature of the vapor. If it is assumed that the shear at the liquid-vapor interface, the buoyancy force owing to displaced vapor, and momentum effects in the film are negligible, a force balance applied to the elementary control volume shown in figure 3.4.1 gives

$$\mu \frac{dv}{dy} = \rho g(\delta - y) \tag{3.4.1}$$

Integrating and applying the boundary condition with $v = 0$ at $y = 0$ yields

$$v = \rho g(\delta y - y^2/2)/\mu \tag{3.4.2}$$

The film flow rate per unit width, is then determined as follows:

$$m/W = \rho\int_0^\delta v\,dy = \rho^2 g\,\delta^3/(3\mu)$$

from which it follows that the film thickness is

$$\delta = \left[3\mu m/\left(W\rho^2 g\right)\right]^{0.333} \tag{3.4.3}$$

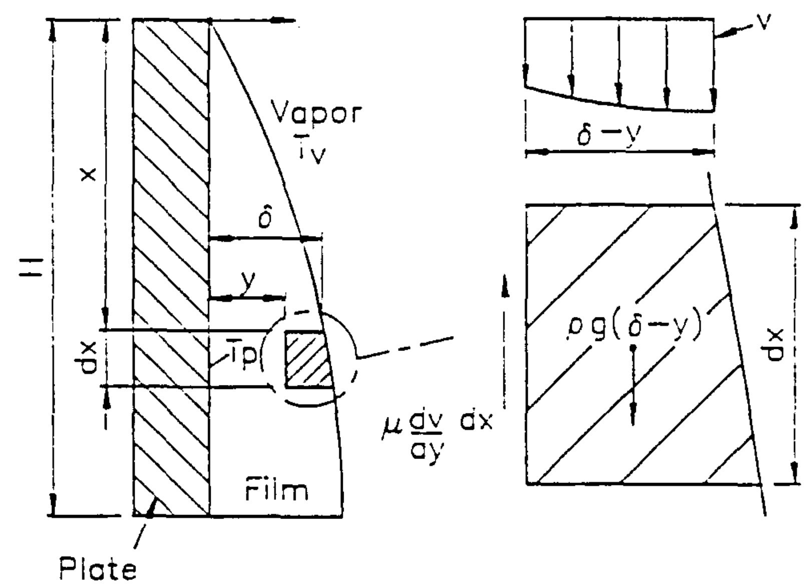

Figure 3.4.1: Film condensation on a vertical flat plate.

The change of m with x, which is due to the condensing vapor, may be expressed as

$$dm/dx = kW\left(T_v - T_p\right)/\left(\delta i_{fg}\right) \tag{3.4.4}$$

if the temperature distribution through the film is linear.

Substitute equation (3.4.3) into equation (3.4.4) and find

$$\left[i_{fg}/(kW)\right]\left[3\mu m/\left(W\rho^2 g\right)\right]^{0.333} dm = \left(T_v - T_p\right)dx \tag{3.4.5}$$

By ingrating this equation over the plate height the condensate flow rate can be determined at x = H if m = 0 at x = 0 i.e.

$$m_H = 0.9428\ W\left[k^3\ \rho^2\ g\ H^3\left(T_v - T_{pm}\right)^3/\left(\mu i_{fg}^3\right)\right]^{0.25} \tag{3.4.6}$$

where the mean temperature difference across the film over the plate height is given by

$$T_v - T_{pm} = \int_0^H \left(T_v - T_p\right)dx/H \tag{3.4.7}$$

The heat transfer rate to the plate can be expressed in terms of this mass flow rate or in terms of a mean heat flux q, or the mean heat transfer coefficient h.

$$Q = qWH = m_H\ i_{fg} = hWH\left(T_v - T_{pm}\right) \tag{3.4.8}$$

Substitute equation (3.4.6) into equation (3.4.8) and find

$$h = 0.9428\left[k^3\ \rho^2\ g\ i_{fg}/\left\{\mu\ H\left(T_v - T_{pm}\right)\right\}\right]^{0.25} \tag{3.4.9}$$

The mean heat transfer coefficient can also be expressed in terms of the condensate flow rate by substituting equation (3.4.8) into equation (3.4.9).

$$h = 0.9245\left[k^3\ \rho^2\ g\ W/\left(\mu m_H\right)\right]^{0.333} \tag{3.4.10}$$

or

$$h = 0.9245 \left[k^3 \rho^2 g/\left(\mu^2 Re_H\right)\right]^{0.333} \tag{3.4.11}$$

where the film Reynolds number at the lower edge of the plate is given by

$$Re_H = m_H/(\mu W) \tag{3.4.12}$$

In his pioneering analysis of condensation heat transfer in 1916, Nusselt [16NU1] assumed a constant plate temperature and found the heat transfer coefficient as given by equation (3.4.9) with $T_{pm} = T_{pc}$.

The particular case of film condensation where the heat flux through the film is uniform was originally studied by Parr [21PA1]. The resultant condensation heat transfer coefficient may be obtained by replacing m_H in equation (3.4.10) by the constant heat flux q_c as related by equation (3.4.8).

$$h_q = 0.9245 \left[k^3 \rho^2 g\ i_{fg}/\left(\mu q_c H\right)\right]^{0.333} \tag{3.4.13}$$

Most practical laminar film condensation occurs at neither constant heat flux nor constant wall temperature but at some intermediate condition.

More refined analyses of film condensation are presented by Rohsenow [73RO2]. The laminar condensation equations presented above, match experimental data well as long as the film remains smooth. In practice it has been found that ripples will develop on the condensate film for Reynolds numbers as low as 8, and it becomes turbulent at a Reynolds number of approximately 350. Experiments have revealed that the heat transfer rate in the wavy and turbulent sections is considerably larger than the estimate based on the above-mentioned equations [72WA1]. The sizeable record of experimental data and correlations on condensation heat transfer in the wavy and turbulent regimes was reviewed by Chen, Gerner and Tien [87CH2] and Chun and Kim [90CH1].

The above equations can also be applied to vertical tubes if the condensate film thickness is small compared to the tube diameter and vapor shear effects are negligible.

3.4.2. CONDENSATION IN DUCT

In modern air-cooled steam condensers, inclined finned elliptical or flattened tubes or ducts having a relatively large cross-section find application. Consider a vapor that condenses filmwise on the inside surface of such a long inclined ($0° \leq \phi \leq 60°$) flattened tube as shown in figure 3.4.2. This analysis is applicable only to that part of the tube where the vapor velocity and the corresponding shear stress on the condensate film is negligible.

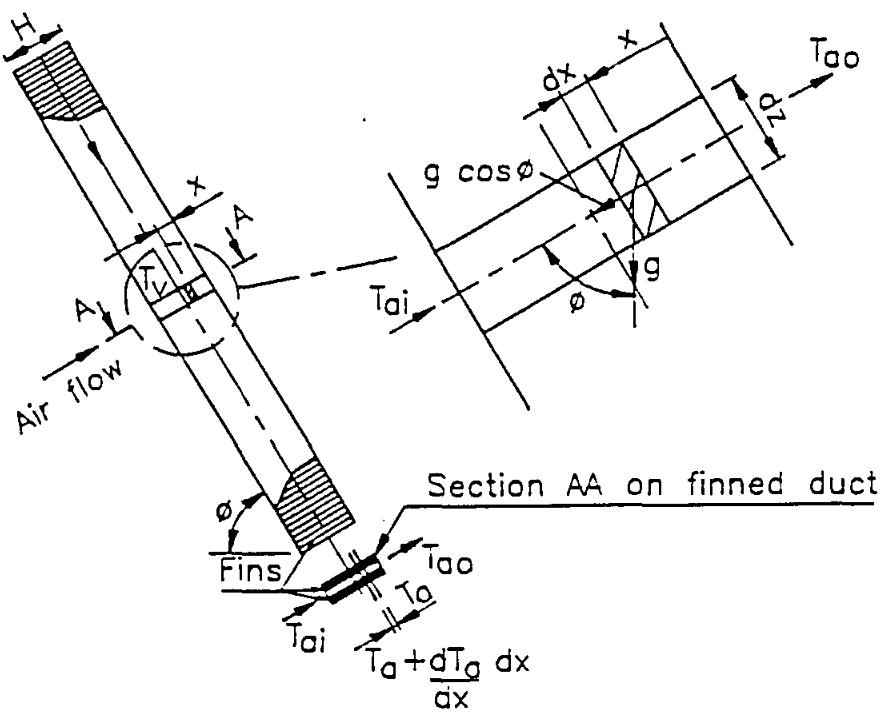

Figure 3.4.2: Condensation in flattened tube.

The tube wall is cooled externally by an air stream flowing across it. If the saturation vapor temperature, T_v, and the overall heat transfer coefficient, U, based on the inside surface area are assumed to be essentially constant at a section of the tube (U << h for most air-cooled steam condensers), the local heat flux can be expressed approximately as

$$q_x = U(T_v - T_a) = - \dot{m}_a c_{pa} (dT_a/dx)/dz \qquad (3.4.14)$$

where m_a is the air mass flow rate corresponding to the elementary tube length dz.

In this equation $U \approx h_{ae}A_a/A_i = Nyk_aA_{fr}Pr_a^{0.333}/A_i$.

Rewrite equation (3.4.14) and integrate.

$$\int_{T_{ai}}^{T_{ax}} \frac{dT_a}{(T_v - T_a)} = -\int_{H}^{x} \frac{Udz}{m_a c_{pa}}\, dx$$

or

$$T_v - T_{ax} = (T_v - T_{ai}) \exp\left[Udz(x - H)/\left(m_a c_{pa}\right)\right] \qquad (3.4.15)$$

where T_{ai} is the temperature of the entering air stream and T_{ax} is the temperature of the air at x.

Substitute equation (3.4.15) into equation (3.4.14) and find that the local heat flux varies as a function of x, as follows:

$$q_x = U(T_v - T_{ai}) \exp\left[Udz(x - H)/\left(m_a c_{pa}\right)\right] \qquad (3.4.16)$$

This local heat flux can be expressed in terms of the change in condensate flow rate i.e.

$$q_x = i_{fg}\,(dm/dx)/dz = U\left(T_v - T_{ai}\right) \exp\left[Udz(x - H)/\left(m_a c_{pa}\right)\right] \qquad (3.4.17)$$

Integrate equation (3.4.17) between the top of the condensing surface at x = 0 and x to find

$$m = \left(T_v - T_{ai}\right)m_a c_{pa}\left[\exp\left\{Udz(x - H)/\left(m_a c_{pa}\right)\right\} - \exp\left\{-\,UdzH/\left(m_a c_{pa}\right)\right\}\right]/i_{fg}$$

(3.4.18)

The local heat flux through the film can also be expressed as

$$q_x = k\left(T_v - T_t\right)/\delta = U\left(T_v - T_{ai}\right)\exp\left[Udz(x - H)/\left(m_a c_{pa}\right)\right] \tag{3.4.19}$$

where T_t is the tube-wall temperature.

With the component of the gravitational force $g\cos\phi$ acting on the condensate film in the x-direction, find as in section 3.4.1.

$$\delta = \left[3\mu m/\left(dz\rho^2 g\cos\phi\right)\right]^{0.333} \tag{3.4.20}$$

Substitute equations (3.4.18) and (3.4.20) into equation (3.4.19) and find

$$\begin{aligned}\left(T_v - T_t\right) = {} & U\left(T_v - T_{ai}\right)^{1.333}\left(\frac{3\mu m_a c_{pa}}{dz\rho^2 g\cos\phi k^3 i_{fg}}\right)^{0.333}\exp\left[Udz(x-H)/\left(m_a c_{pa}\right)\right] \\ & \left[\exp\left\{Udz(x - H)/(m_a c_{pa})\right\} - \exp\left\{-UdzH/(m_a c_{pa})\right\}\right]^{0.333}\end{aligned} \tag{3.4.21}$$

To find the mean temperature difference across the condensate film, integrate equation (3.4.21) over the tube height i.e. from $x = 0$ to $x = H$.

$$\left(T_v - T_{tm}\right) = \left(\frac{1.267\mu}{H^3\rho^2 g\cos\phi k^3 i_{fg}}\right)^{0.333}\left[\frac{m_a c_{pa}\left(T_v - T_{ai}\right)\left\{1 - \exp\left[-UdzH/\left(m_a c_{pa}\right)\right]\right\}}{dz}\right]^{1.333} \tag{3.4.22}$$

Replace the gravitational acceleration in equation (3.4.9) by $g\cos\phi$ and substitute equation (3.4.22) into equation (3.4.9) to find an approximate mean local condensation heat transfer coefficient

$$h = 0.9245\left[\frac{k^3\rho^2 g\cos\phi i_{fg} dz}{\mu m_a c_{pa}\left(T_v - T_{ai}\right)\left[1 - \exp\left\{-UdzH/\left(m_a c_{pa}\right)\right\}\right]}\right]^{0.333} \tag{3.4.23}$$

If the vapor temperature T_v does not change significantly along the length of the tube the mean condensation heat transfer coefficient is essentially equal to the local mean value as given by equation (3.4.23). In a practical finned tube, conduction in the fin in the air flow direction will have some influence on T_t.

3.4.3 CONDENSATION ON CYLINDER

Consider unit length of the elementary control volume in the condensate film on a horizontal tube or pipe as shown in figure 3.4.3. An essentially stagnant saturated vapor condenses on the cooler outer surface of the tube.

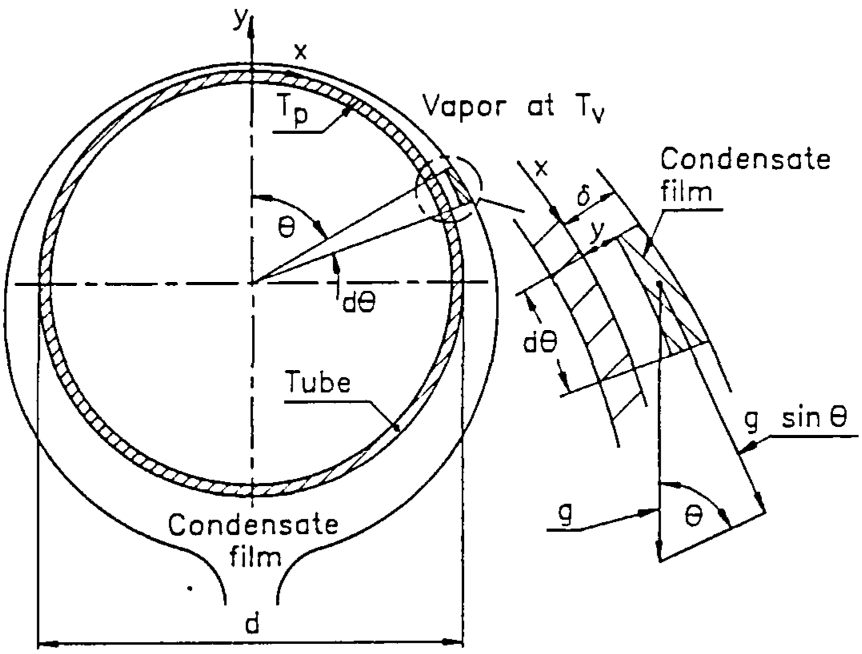

Figure 3.4.3: Condensation on tube.

By following a procedure similar to that in section 3.4.1 it can be shown that

$$\delta = \left[3\mu m / \left(\rho^2 g \sin\theta\right)\right]^{0.333} \tag{3.4.24}$$

if $\delta << d$ and effects due to surface tension and the accumulation of condensate at the base of the tube can be ignored.

Furthermore according to equation (3.4.5) it follows that for the condensate film on the tube

$$\frac{i_{fg}}{k}\left(\frac{3\mu m}{\rho^2 g}\right)^{0.333} dm = \left(T_v - T_t\right)\sin\theta^{0.333}\, dx$$

$$= \left(T_v - T_t\right) d\sin\theta^{0.333}\, d\theta/2 \tag{3.4.25}$$

where T_t is the temperature of the tube or pipe wall.

Equation (3.4.25) is readily integrated for the case where the tube wall temperature is constant i.e.

$$\int_o^{m_\pi} m^{0.333} dm = \frac{dk}{2i_{fg}}\left(\frac{\rho^2 g}{3\mu}\right)^{0.333}\left(T_v - T_{tc}\right)\int_o^{\pi} \sin\theta^{0.333}\, d\theta \tag{3.4.26}$$

The integral on the right hand side of the equation can be expressed in terms of Gamma functions [90BR1] to give

$$m_\pi = 1.1437\left[\frac{dk}{i_{fg}}\left(\frac{\rho^2 g}{\mu}\right)^{0.333}\left(T_v - T_{tc}\right)\right]^{0.75} \tag{3.4.27}$$

The mean condensation heat transfer coefficient on the outside of the tube is related to this mass flow rate.

$$h_{\Delta T}\, \pi\, d\left(T_v - T_{tc}\right)/2 = m_\pi\, i_{fg}$$

or with equation (3.4.27)

$$h_{\Delta T} = 0.728\left[k^3\rho^2 g\, i_{fg}/\left\{\mu d\left(T_v - T_{tc}\right)\right\}\right]^{0.25} \tag{3.4.28}$$

If the rate of condensation is uniform around the circumference of the tube i.e. the heat flux is constant it follows that

$$k\left(T_v - T_t\right)/\delta = q_c$$

or

$$T_v - T_t = q_c\delta/k \qquad (3.4.29)$$

The condensate mass flow rate can be expressed as

$$m = \left(q_c x\right)/i_{fg} = q_c\ \theta d/\left(2i_{fg}\right) \qquad (3.4.30)$$

Substitute equations (3.4.24) and (3.4.30) into equation (3.4.29) and find

$$T_v - T_t = \left(q_c/k\right)\left[3\mu q_c\ \theta d/\left(2\rho^2 g i_{fg}\sin\theta\right)\right]^{0.333} \qquad (3.4.31)$$

Integrate this equation to find the mean temperature difference

$$\left(T_v - T_{tm}\right) = \left(\frac{q_c}{\pi k}\right)\left(\frac{3\mu q_c d}{2\rho^2 g\ i_{fg}}\right)^{0.333}\int_0^{\pi}\left(\frac{\theta}{\sin\theta}\right)^{0.333}d\theta \qquad (3.4.32)$$

or

$$T_v - T_{tm} = 1.636\ q_c\left(\mu q_c d/k^3\rho^2 g\ i_{fg}\right)^{0.333} \qquad (3.4.33)$$

where the integral on the right hand side of equation (3.4.32) is found to have a value of 4.49.

The mean heat transfer coefficient can be found from the following relation:

$$h_q\left(T_v - T_{tm}\right) = q_c \tag{3.4.34}$$

Substitute equation (3.4.33) into equation (3.4.34) and find

$$h_q = 0.611\left[k^3\rho^2 g\ i_{fg}/\left(\mu q_c d\right)\right]^{0.333} \tag{3.4.35}$$

The above equations can also be applied where condensation occurs inside a near horizontal tube if the condensate is effectively drained at the bottom of the tube. In practice the accumulated condensate at the bottom of the tube tends to reduce the mean heat transfer coefficient. Chato [62CH1] and Kröger [77KR1] report test results for condensing refrigerants at low vapor velocities inside horizontal or slightly inclined tubes. For inlet vapor Reynolds numbers of less that 35000, the former proposes the following equation for the heat transfer coefficient:

$$h_{\Delta T} = 0.555\left[k^3\rho^2 g\ i_{fg}/\left\{\mu d\left(T_v - T_{tm}\right)\right\}\right]^{0.25} \tag{3.4.36}$$

Chen and Kocamustafaogullari [87CH1] present a more detailed analysis of condensation in a horizontal tube taking into consideration the flow of the condensate at the bottom of the tube.

3.4.4 CONDENSATION CORRELATIONS

The problems associated with the determination of flow patterns, heat transfer and pressure drop during condensation in practical condenser tubes and ducts are manifold. Although flow pattern maps developed for no-phase-change, two-phase flow are generally used to determine conditions during condensation, their applicability in such cases has not always been confirmed. Potentially applicable maps are evaluated by Breber [80BR1].

Typical changing flow patterns encountered during condensation have been observed visually in a 6.7 m long glass tube having an inside diameter of 22 mm as shown in figure 3.4.4 [79PA1, 80BR1]. The figure shows that there are two distinct groups of patterns for condensation inside a horizontal tube i.e. vapor shear-controlled flow and gravity controlled flow. Flow patterns associated with high vapor shear are basically mist, annular, and a mist-annular combination. As condensation proceeds, the condensate flow rate increases and the vapor flow rate correspondingly decreases and the effect of gravity on the flow pattern becomes more important. In a limiting case, as analyzed in the previous section, axial forces are negligible and condensate formed on the walls drains vertically to the bottom of the tube. Actually, there is nearly always some axial shear force present causing phase boundary disturbances. Basic flow patterns associated with gravity-controlled flow are wavy and stratified flow. However, with a high liquid loading, the waves may form frothy surges or may bridge the tube to give slug flow.

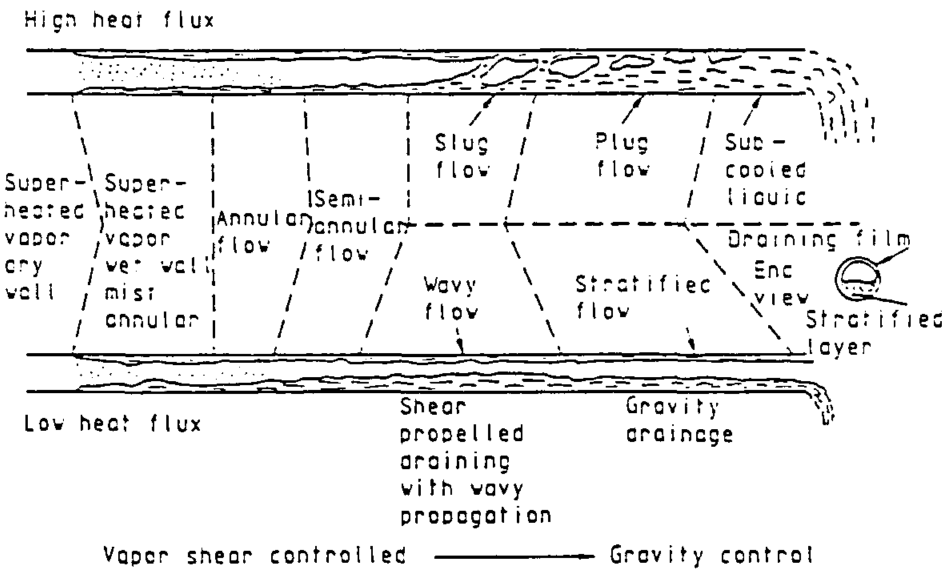

Figure 3.4.4: Schematic illustration of flow patterns in tubeside condensation.

The flow patterns between the limiting regimes of shear-controlled and gravity controlled flow are difficult to characterize quantitatively as a number of different patterns may exist sequentially or even simultaneously.

Typical flow patterns observed during condensation with flow downward inside a vertical tube are shown schematically in figure 3.4.5.

Hewitt [79HE1] shows that in the case of condensation during co-current upflow in a vertical tube various flow patterns are observed including bubble, slug or plug, churn, annular and wispy annular. A variety of complex flow patterns are similarly anticipated during counter-current or reflux condensation in a vertical tube.

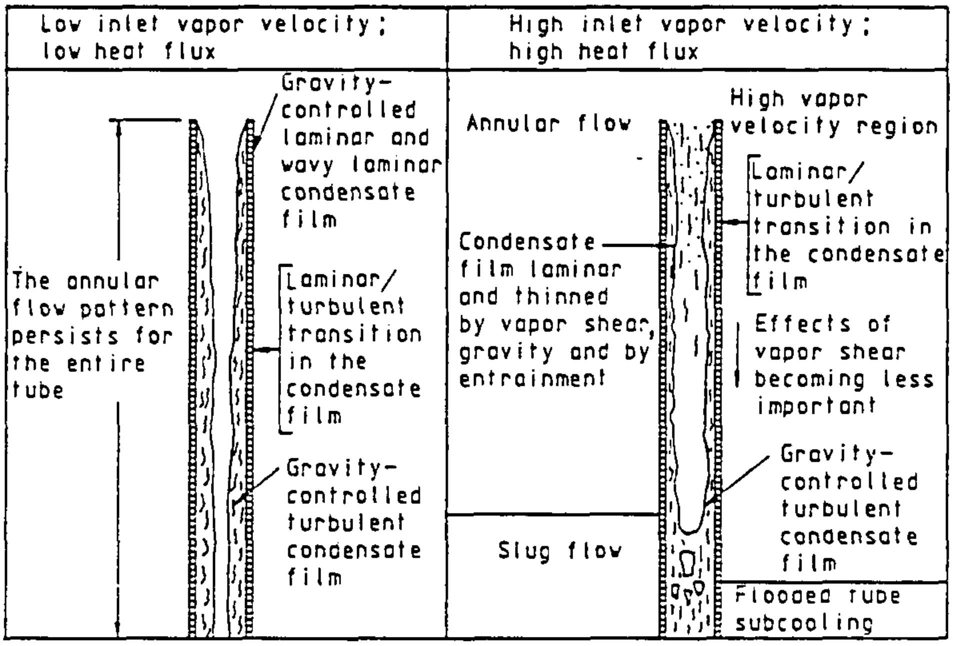

Figure 3.4.5: Flow patterns during downflow condensation inside vertical tubes.

During two-phase flow with condensation of a vapor inside inclined tubes, the axial pressure gradient, dp_{vtp}/dz is made up of contributions due to frictional, dp_{vf}/dz, accelerational, dp_{vm}/dz and gravitational, dp_{vs}/dz, effects as given by equation (2.7.12).

$$\frac{dp_{vtp}}{dz} = \frac{dp_{vf}}{dz} + \frac{dp_{vm}}{dz} + \frac{dp_{vs}}{dz}$$

$$= \frac{dp_{vf}}{dz} + G^2 \frac{d}{dz}\left[\frac{(1-x)^2}{(1-x)\rho_c} + \frac{x^2}{\alpha\rho_v}\right] + \left[\alpha\,\rho_v + (1-\alpha)\rho_c\right] g \sin\phi \qquad (3.4.37)$$

To predict the pressure drop during condensation inside tube, equations developed for adiabatic two-phase flows are employed although they may not necessarily accurately predict the measured pressure distribution due to among others the fact that they neglect a change of the interfacial shear stress, τ_i, caused by the effect of mass transfer from the vapor to the liquid. Owen, Sardesai et al. [81OW1, 82SA1] tried to solve this problem for an annular flow pattern using an annular flow model of the type developed by Whalley et al. [82WH1]. The authors suggest that the adiabatic frictional pressure gradient be corrected by a factor γ_f such that

$$dp_{vfc}/dz = \left(dp_{vf}/dz\right)\gamma_f \tag{3.4.38}$$

where

$$\gamma_f = \left[G_c\left(v_v - v_i\right)/\tau_i\right]/\left[1 - \exp\left\{G\left(v_i - v_v\right)/\tau_i\right\}\right] \tag{3.4.39}$$

and where dp_{vf}/dz is the frictional pressure gradient in the absence of mass transfer, G_c is the condensing mass flux and v_v and v_i are the axial velocities of the vapor-phase and the vapor-liquid interface respectively.

A systematic and practical approach to the problem is presented by Carey [92CA1].

It was shown in the previous sections that it is possible to predict the condensation heat transfer coefficient approximately in gravity controlled flows where shear stresses are negligible. Numerous equations for predicting the local and mean heat transfer coefficient during annular flow are available in the literature [51CA1, 60AL1, 71KO1, 72MU1, 73RO2]. Their limitations should be clearly noted and they should only be used within their particular range of application.

Other useful equations that do not require a high level of computational effort include those due to Boyko and Kruzhilin [67BO1], Soliman et al. [68SO1], Schulenberg [69SC1], Chawla [72CH1], Traviss et al. [73TR1] and Shah [79SH1].

According to Akers et al. [58AK1] the mean condensation heat transfer inside a tube can be expressed approximately by the following empirical expression:

$$\frac{h_c d_i}{k_c} = 0.026\ Pr_c^{0.333}\ Re_m \tag{3.4.40}$$

where $Pr_c = \mu_c c_{pc}/k_c$ and the mixture Reynolds number is defined as

$$Re_m = d_i \left[m_c + m_v (\rho_c/\rho_v)^{0.5} \right] / (\mu_c A_{ts})$$

In this expression A_{ts} is the tube cross-sectional area and m_c and m_v are the condensate and vapor mass flow rates respectively.

Shah [79SH1] conducted an extensive survey of existing condensation heat transfer data and proposes the following correlating equation for the local heat transfer coefficient:

$$Nu_{cx} = \frac{h_{cx} d_i}{k_c}$$

$$= 0.023\ Re_c^{0.8}\ Pr_c^{0.4} \left[(1 - x_{vx})^{0.8} + \frac{3.8 x_{vx}^{0.76} (1 - x_{vx})^{0.04}}{p_r^{0.38}} \right] \tag{3.4.41}$$

In this equation $Re_c = m d_i/(A_{ts}\mu_c)$ and $p_r = p_v/p_{cr}$, where p_{cr} is the critical pressure of the fluid and x_{vx} is the local quality of the vapor.

By integrating equation (3.4.41), the mean condensation coefficient for the case where the vapor quality variation is linear with length is found.

$$Nu_c = \frac{0.023\ Re_c^{0.8}\ Pr_c^{0.4}}{(x_{vo} - x_{vi})} \left[-\frac{(1 - x_v)^{1.8}}{1.8} + \frac{3.8}{p_r^{0.38}} \left(\frac{x_v^{1.76}}{1.76} - \frac{0.04\ x_v^{2.76}}{2.76} \right) \right]_{x_{vi}}^{x_{vo}}$$

For the case of $x_{vi} = 1$ to $x_{vo} = 0$, this equation yields

$$Nu_c = 0.023\ Re_c^{0.8}\ Pr_c^{0.4}\ (0.55 + 2.09/p_r^{0.38}) \tag{3.4.42}$$

A general approximation for the mean condensation coefficient is given by

$$Nu_c = \frac{h_c d_i}{k_c} = 0.023\, Re_c^{0.8}\, Pr_c^{0.4} \left[(1 - x_v)^{0.8} + \frac{3.8 x_v^{0.76} (1 - x_v)^{0.04}}{p_r^{0.38}} \right] \tag{3.4.43}$$

assuming that the vapor quality variation is linear with length. In this equation, x_v is the arithmetic mean vapor fraction, i.e. $x_v = 0.5\,(x_{vi} + x_{vo})$

This equation is applicable under the following conditions:

$7\text{mm} < d_i < 40\text{ mm}$
$0.002 < p_r < 0.44$
$350 < Re_c < 63000$
$21°C < T_v < 310°C$
$3\text{ m/s} < m/(A_{ts}\rho_v) < 300\text{ m/s}$
$11\text{ kg/m}^2\text{s} < m/A_{ts} < 211\text{ kg/m}^2\text{s}$
$1 < Pr_c < 13$
$158\text{ W/m}^2 < Q/A < 1893000\text{ W/m}^2$

Schulenberg [69SC1, 70SC1] studied the particular problem of heat transfer and pressure drop during the condensation of low-pressure steam in inclined tubes. For vertical tubes he proposed the following equation for determining the mean heat transfer coefficient:

$$Nu_c = \frac{h_c d_i}{k_c} = 0.683 \left[Ku_c\, Pr_c \left(\frac{\mu_v}{\mu_c}\right)^2 \left(\frac{\rho_c}{\rho_v}\right) \left(\frac{d_i}{L}\right) \right]^{0.333} Re_v^{0.55} \tag{3.4.44}$$

The Kutateladze number is defined as

$$Ku_c = i_{fg}/[c_{pc}\,(T_v - T_t)] \tag{3.4.45}$$

where T_t is the inside tube-wall temperature.

The Reynolds number in this equation is expressed in terms of the mean superficial vapor velocity, $v_{vs} = m_v/\rho_v A_{ts}$, i.e.

$$Re_v = \rho_v v_{vs} d_i/\mu_v = m_v d_i/A_{ts}\mu_v \tag{3.4.46}$$

where m_v is the arithmetic mean vapor mass flow rate and A_{ts} is the cross-sectional area of the tube. This equation is applicable when $2500 < Re_v < 20\,000$ and $2830\ N/m^2 < p_v < 26446\ N/m^2$.

For inclined tubes, Schulenberg proposes the following equation:

$$Nu_c = \frac{h_c d_i}{k_c} = 1.04 \left[Ku_c\, Pr_c \left(\frac{\mu_v}{\mu_c}\right)^2 \left(\frac{\rho_c}{\rho_v}\right) \left(\frac{d_i \sin^2\theta}{L}\right)\right]^{0.333} \left(\frac{Re_v}{\sin\theta}\right)^{0.55} \tag{3.4.47}$$

where $5° < \theta < 90°$ is the angle of inclination with respect to the vertical. This equation is applicable when $10950 < Re_v < 14150$ and $6525\ N/m^2 < p_v < 8085\ N/m^2$.

If all the steam entering the tube were to condense, the total heat transfer rate can be expressed as

$$Q = h_c\, \pi\, d_i\, L\left(T_v - T_t\right) = \rho_v\, v_{vi}\, \pi\, d_i^2\, i_{fg}/4 \tag{3.4.48}$$

where v_{vi} is the velocity of the steam entering the tube.

Substitute equation (3.4.45) into equation (3.4.44) and find

$$Nu_c = 1.197\, (\sin\theta)^{0.1755} \left(\rho_c/\mu_c\right)^{0.5} \left(\mu_v/\rho_v\right)^{0.5} Re_{vi}^{0.325} \tag{3.4.49}$$

Roth [84RO2] and Fürst [89FU1] report the results of condensation heat transfer tests conducted on inclined elliptical tubes.

3.4.5 PRESSURE AND TEMPERATURE DISTRIBUTION INSIDE DUCT

During condensation of a flowing vapor in an air-cooled finned tube or duct, a change in pressure will occur along the duct due to frictional and momentum effects. This change in pressure will result in a corresponding change in vapor temperature and heat transfer rate.

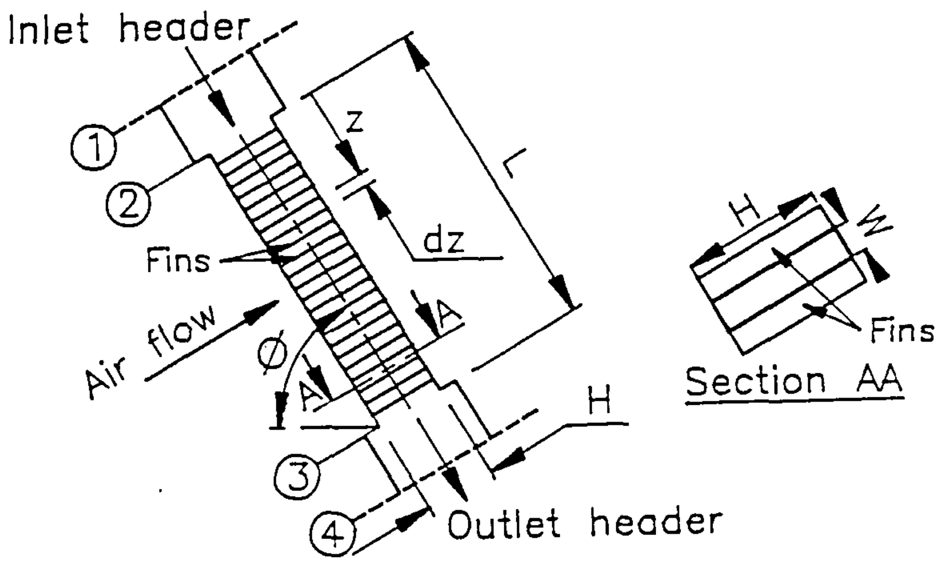

Figure 3.4.6: Inclined air-cooled condenser tube or duct.

Consider the case where dry low-pressure steam condenses completely inside an inclined flattened air-cooled finned tube, located between two headers as shown in figure 3.4.6. If the geodetic pressure is neglected, the incremental change in pressure in the tube is according to equation (2.7.10)

$$dp_v = dp_{vf} + dp_{vm} \tag{3.4.50}$$

The frictional pressure loss may be modelled in terms of an effective interfacial friction factor, f_{De}, that takes into consideration the effect of condensate wave formation as well as the distortion of the vapor velocity profile due to the flow of vapor towards the condensing surface if the flow is assumed to be essentially stratified i.e. according to equation (2.2.1)

$$dp_{vf} = f_{De}\rho_v v_v^2 \, dz/(2d_e) \tag{3.4.51}$$

where d_e is the hydraulic diameter of the duct.

For adiabatic co-current stratified gas-liquid flow in a high aspect ratio flattened tube the two-phase interfacial friction factor corresponds closely to the single-phase smooth tube D'Arcy friction factor i.e. it is little influenced by wave formation.

When condensation occurs, the effective friction factor that takes into consideration the vapor velocity distortion due to flow towards the condensing surface [GROENE], is approximated, for a high aspect ratio flattened tube, by

$$f_{De} = f_D(1 + 6.56 \times 10^{-4} Re^2_{vn}) \tag{3.4.52}$$

for laminar flow, where $f_D = 96/Re_v$ between parallel plates, $Re_v = \rho_v v_v d_e/\mu_v \le 2300$ and d_e is the hydraulic diameter of the tube.

If the rate of condensation along the tube length is uniform the vapor velocity decreases linearly from the inlet to the outlet of the tube i.e.

$$v_v = v_{v2}(1 - z/L) \tag{3.4.53}$$

The local vapor Reynolds number may thus be expressed as

$$Re_v = \rho_v v_{v2}(1 - z/L)d_e/\mu_v = Re_{v2}(1 - z/L) \tag{3.4.54}$$

The mass flow rate of vapor per unit length of tube normal to the condensing surface is approximately

$$m_{vn} = 2\rho_v v_{vn} H = \rho_v WH(- dv_v/dz) = \rho_v WH v_{v2}/L$$

or

$$v_{vn} = v_{v2}W/(2L) \tag{3.4.55}$$

The corresponding Reynolds number for this vapor flow towards the condensing surface is defined as

$$Re_{vn} = 2\rho_v v_{vn} W/\mu_v = \rho_v v_{v2} W^2/(\mu_v L) \approx Re_{v2} W/(2L) \tag{3.4.56}$$

For turbulent vapor flow

$$f_{De} = f_D(a_1 + a_2/Re_v) \tag{3.4.57}$$

where

$$a_1 = 1.0649 + 1.041 \times 10^{-3} Re_{vn} - 2.011 \times 10^{-7} Re_{vn}^3$$

$$a_2 = 290.1479 + 59.3153 Re_{vn} + 1.5995 \times 10^{-2} Re_{vn}^3$$

for $0 \le Re_{vn} \le 40$. Instead of employing equations (2.2.9) or (2.2.10) it is convenient to express the friction factor very approximately as $f_D = 0.3164 Re_v^{-0.25}$ in the range $2300 \le Re_v \le 10^5$.

Groenewald and Kröger [93GR1] show that for a practical air-cooled steam condenser the change in pressure in the region of laminar duct flow is negligible compared to that in the turbulent region. The frictional pressure drop in the duct can thus be approximated according to equation (2.2.1) with equation (3.4.57) by

$$dp_{vf} = \int_{Re_{v2}}^{2300} f_{De} \left(\frac{\rho_v v_v^2}{2}\right) \frac{dz}{d_e} = - \frac{0.1582 \mu_v^2 L}{\rho_v d_e^3 Re_{v2}} \int_{Re_{v2}}^{2300} \left(a_1 Re_v^{1.75} + a_2 Re_v^{0.75}\right) dRe_v$$

$$= \frac{0.1582 \mu_v^2 L}{\rho_v d_e^3 Re_{v2}} \left[\frac{a_1}{2.75}\left(Re_{v2}^{2.75} - 2300^{2.75}\right) + \frac{a_2}{1.75}\left(Re_{v2}^{1.75} - 2300^{1.75}\right)\right]$$

$$\approx \frac{0.1582\mu_v^2 L}{\rho_v d_e^3 Re_{v2}}\left(\frac{a_1}{2.75} Re_{v2}^{2.75} + \frac{a_2}{1.75} Re_{v2}^{1.75}\right) \tag{3.4.58}$$

if $Re_{v2} >> 2300$.

In equation (3.4.58) it is assumed that changes in thermophysical properties are negligible. During condensation of the vapor laminarization of the flow will tend to occur at $Re_v >$ 2300 but this has a negligible influence on dp_f in practical air-cooled condenser tubes.

The change in pressure due to accelerational effects can be expressed directly in terms of the momentum of the vapor entering the tube i.e.

$$dp_{vm} = -\rho_v v_{v2}^2 \tag{3.4.59}$$

This equation assumes that the velocity distribution of the entering vapor is uniform and that no vapor flows out of the tube.

In addition to the frictional and momentum effects, the loss at the inlet to the tube is significant in a condenser tube. According to equation (2.3.5)

$$p_{v1} - p_{v2} = (\rho_v v_{v2}^2/2)[\,(1 - \sigma_{21}^2) + K_c] \tag{3.4.60}$$

If all steam entering the tube condenses the change in pressure between the inlet and the outlet manifolds can be expressed in dimensionless form by adding equations (3.4.58) (3.4.59) and (3.4.60) and dividing by $\rho_v v_{v2}^2/2$ i.e.

$$\frac{p_{v1} - p_{v4}}{\rho_v v_{v2}^2/2} = (K_c - \sigma_{21}^2 - 1) + \frac{0.3164\ L}{Re_{v2}^2 d_e}\left(\frac{a_1}{2.75}\ Re_{v2}^{2.75} + \frac{a_2}{1.75}\ Re_{v2}^{1.75}\right) \tag{3.4.61}$$

The frictional pressure differential between the inlet and any other section of the duct is given by

$$dp_{vf} = p_{v2} - p_{vf} = \int_{Re_{v2}}^{Re_v} f_{De}\left(\frac{\rho_v v_v^2}{2}\right)\frac{dz}{d_e}$$

$$= \frac{0.1582\mu_v^2 L}{\rho_v d_e^3 Re_{v2}}\left[\frac{a_1}{2.75}\left(Re_{v2}^{2.75} - Re_v^{2.75}\right) + \frac{a_2}{1.75}\left(Re_{v2}^{1.75} - Re_v^{1.75}\right)\right] \tag{3.4.62}$$

while the corresponding pressure differential due to accelerational effects is

$$dp_{vm} = \rho_v\left(v_v^2 - v_{v2}^2\right) \tag{3.4.63}$$

To find the mean static pressure in the tube, integrate the sum of equation (3.4.61) and equation (3.4.62) over the entire tube length and find

$$\int_0^L \left[(p_{v2} - p_{vf}) + \rho_v\left(v_v^2 - v_{v2}^2\right)\right]\frac{dz}{L}$$

or

$$p_{vm} \approx p_{v2} - \frac{0.1582\mu_v^2 L}{\rho_v d_e^3 Re_{v2}}\left(0.267a_1 Re_{v2}^{2.75} + 0.364a_2 Re_{v2}^{1.75}\right) + \frac{2}{3}\rho_v v_{v2}^2 \tag{3.4.64}$$

The temperature of saturated steam can be expressed approximately in terms of the saturation pressure as

$$T_v = 5149.6889682/\left[\ell n\left(1.020472843\text{x}10^{11}/p_v\right)\right] \tag{3.4.65}$$

for 3500 $N/m^2 \leq p_v \leq 75000$ N/m^2 and where T_v is in K.

If the steam condensing inside the duct remains essentially saturated, there will be in addition to the pressure drop, a corresponding change in temperature. The mean steam temperature can be determined approximately by substituting the value of p_{vm} into equation (3.4.65).

The above procedure can also be followed to determine the pressure change during condensation in a tube. In that case the coefficients in equation (3.4.57) are respectively [GROEN],

$$a_1 = 1.0046 + 1.719 \times 10^{-3} Re_{vn} - 9.7746 \times 10^{-6} Re_{vn}^2$$

$$a_2 = 574.3115 + 24.2891 Re_{vn} + 1.8515 Re_{vn}^2$$

For condensers employed in the petro-chemical industry the vapor inlet velocity to the condenser tubes is usually limited to 30 m/s [73RO3] which is considerably lower than that encountered in low-pressure steam condensers. Depending on the nature of the flow in the former case, other equations for determining the pressure drop may be appropriate e.g. Baroczy [66BA1].

3.5 HEAT EXCHANGERS

The principles of heat transfer are applied to the design of heat transfer equipment. Depending on the particular application, the geometry and performance characteristics of heat exhangers may differ significantly.

3.5.1 LOGARITHMIC MEAN TEMPERATURE DIFFERENCE

Consider a simple heat exchanger consisting of two concentric pipes as shown in figure 3.5.1. One fluid flows on the inside of the smaller pipe while the other fluid flows in the annular region between the two pipes.

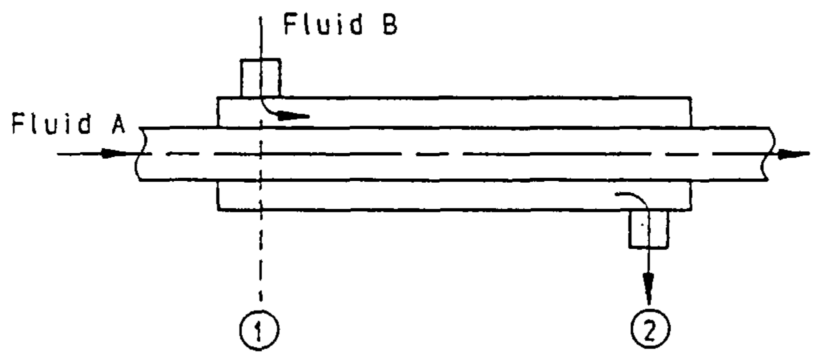

Figure 3.5.1: Double pipe heat exchanger.

The fluids may flow in the same direction as shown in figure 3.5.1, which is referred to as parallel flow, or they may flow in opposite directions or counterflow. Examples of the corresponding fluid temperature profiles are shown schematically in figure 3.5.2.

In order to determine how much heat is transferred from the hot to the cold fluid, an expression for the mean temperature difference between the two streams must be determined.

For the parallel flow heat exchanger as shown in figure 3.5.2(a), the heat transferred through an element of tube area dA is expressed as

$$dQ = U(T_h - T_c)dA \tag{3.5.1}$$

where U is the overall heat transfer coefficient referred to the tube area and the subscripts h and c designate the hot and cold fluids respectively. For purposes of this analysis it will be assumed that the overall heat transfer coefficient is constant. In certain practical cases this assumption is a reasonable approximation. Where significant entrance effects and changes in physical properties occur, a numerical step-by-step integration of equation (3.5.1) may be necessary.

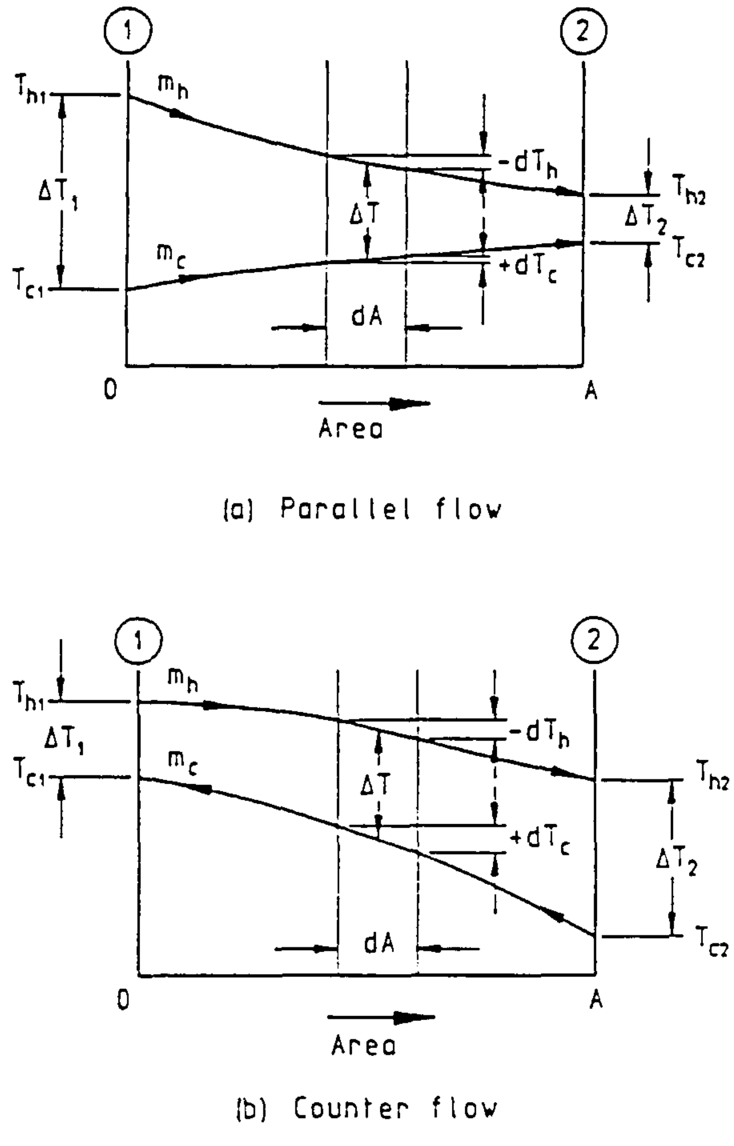

Figure 3.5.2: Temperature profiles.

The heat transfer can also be expressed as

$$dQ = -m_h c_{ph} dT_h = m_c c_{pc} dT_c \tag{3.5.2}$$

From equation (3.5.2) it follows that

$$dT_h - dT_c = -dQ \left(\frac{1}{m_h c_{ph}} + \frac{1}{m_c c_{pc}} \right) \tag{3.5.3}$$

By substituting equation (3.5.1) into equation (3.5.3), find

$$\frac{d(T_h - T_c)}{(T_h - T_c)} = -U \left(\frac{1}{m_h c_{ph}} + \frac{1}{m_c c_{pc}} \right) dA \tag{3.5.4}$$

If constant specific heats are assumed, this equation may be integrated between the ends of the heat exchanger:

$$\ln \left(\frac{T_{h2} - T_{c2}}{T_{h1} - T_{c1}} \right) = -UA \left(\frac{1}{m_h c_{ph}} + \frac{1}{m_c c_{pc}} \right) \tag{3.5.5}$$

Similarly, integration of equation (3.5.2) between the same limits gives

$$Q = -m_h c_{ph} (T_{h2} - T_{h1}) = m_c c_{pc} (T_{c2} - T_{c1}) \tag{3.5.6}$$

Substitute the values of mc_p from equation (3.5.6) into equation (3.5.5) and find

$$Q = UA \frac{(T_{h2} - T_{c2}) - (T_{h1} - T_{c1})}{\ell n \left[(T_{h2} - T_{c2})/(T_{h1} - T_{c1}) \right]} = UA \, \Delta T_{\ell m} \tag{3.5.7}$$

where

$$\Delta T_{\ell m} = \frac{(T_{h2} - T_{c2}) - (T_{h1} - T_{c1})}{\ell n \left[(T_{h2} - T_{c2})/(T_{h1} - T_{c1}) \right]} = \frac{\Delta T_2 - \Delta T_1}{\ell n(\Delta T_2/\Delta T_1)} \tag{3.5.8}$$

This is known as the logarithmic mean temperature difference (LMTD). Equation (3.5.8) is also applicable in the case of counterflow conditions, or when the temperature of one of the fluids is constant during condensation or boiling.

The mean hot fluid temperature for the parallel flow heat exchanger can be found by integrating equation (3.5.4) over only a part of the heat exchanger area A_x from section 1, to give

$$T_{hx} = T_{cx} + (T_{h1} - T_{c1}) \exp\left[- UA_x\left(\frac{1}{m_h c_{ph}} + \frac{1}{m_c c_{pc}}\right)\right] \tag{3.5.9}$$

Integrate equation (3.5.2) between the same limits.

$$-m_h\, c_{ph}\, (T_{hx} - T_{h1}) = m_c\, c_{pc}\, (T_{cx} - T_{c1})$$

or

$$T_{cx} = T_{c1} - m_h\, c_{ph}\, (T_{hx} - T_{h1})/(m_c\, c_{pc}) \tag{3.5.10}$$

Substitute equation (3.5.10) into equation (3.5.9) and find

$$T_{hx} = \frac{T_{c1} + \dfrac{m_h c_{ph} T_{h1}}{m_c c_{pc}} + (T_{h1} - T_{c1})\exp\left[-UA_x\left(\dfrac{1}{m_h c_{ph}} + \dfrac{1}{m_c c_{pc}}\right)\right]}{\left[1 + m_h c_{ph}/(m_c c_{pc})\right]} \tag{3.5.11}$$

The mean temperature of the hot fluid is obtained by integrating equation (3.5.11) over the entire heat exchanger, i.e.

$$T_{hm} = \frac{1}{A}\int_0^A T_{hx}\, dA$$

$$= \frac{T_{c1} + \dfrac{m_h c_{ph}\, T_{h1}}{m_c\, c_{cp}}}{(1 + m_h c_{ph}/m_c c_{pc})} - \frac{(T_{h1} - T_{c1})\left[\exp\left\{-UA\left(\dfrac{1}{m_h c_{ph}} + \dfrac{1}{m_c c_{pc}}\right)\right\} - 1\right]}{UA(1+m_h c_{ph}/m_c c_{pc})(1/m_h c_{ph}+1/m_c c_{pc})} \qquad (3.5.12)$$

Similarly the mean temperature of the cold fluid is found to be

$$T_{cm} = \frac{T_{h1} + \dfrac{m_c c_{pc} T_{c1}}{m_h c_{ph}}}{1+m_c c_{pc}/m_h c_{ph}} + \frac{(T_{h1}-T_{c1})\left[\exp\left\{-UA\left(\dfrac{1}{m_h c_{ph}} + \dfrac{1}{m_c c_{pc}}\right)\right\} - 1\right]}{UA(1+m_h c_{ph}/m_c c_{pc})(1/m_h c_{ph}+1/m_c c_{pc})} \qquad (3.5.13)$$

The corresponding mean temperatures for a counterflow heat exchanger are

$$T_{hm} = \frac{T_{c1} - \dfrac{m_h c_{ph} T_{h1}}{m_c c_{pc}}}{(1-m_h c_{ph}/m_c c_{pc})} - \frac{(T_{h1}-T_{c1})\left[\exp\left\{-UA\left(\dfrac{1}{m_h c_{ph}} - \dfrac{1}{m_c c_{pc}}\right)\right\} - 1\right]}{UA(1+m_h c_{ph}/m_c c_{pc})(1/m_h c_{ph}-1/m_c c_{pc})} \qquad (3.5.14)$$

and

$$T_{cm} = \frac{T_{h1} - \dfrac{m_c c_{pc} T_{c1}}{m_h c_{ph}}}{1-m_c c_{cp}/m_h c_{ph}} + \frac{(T_{h1}-T_{c1})\left[\exp\left\{-UA\left(\dfrac{1}{m_h c_{ph}} - \dfrac{1}{m_c c_{pc}}\right)\right\} - 1\right]}{UA(1-m_h c_{ph}/m_c c_{pc})(1/m_h c_{ph}-1/m_c c_{pc})} \qquad (3.5.15)$$

Crossflow heat exchangers are commonly used in air-cooling applications. An example of such an exchanger is shown in figure 3.5.3(a), where the fluid flows inside the tubes while cooling air flows across the tube bundles. In this exchanger the hot fluid, which is confined to the separate tubes, is said to be "unmixed", whereas the air stream, which can move about freely as it flows through the bundle, is said to be mixed. Unmixed conditions also occur when both streams are confined to specific channels, as in the finned tube heat exchanger shown in figure 3.5.3(b).

For crossflow heat exchangers having mixed and unmixed flow, the mathematical derivation of an expression for the mean temperature difference becomes quite complex [40BO1, 83TA1, 84RO1]. The usual procedure is to modify the simple counterflow LMTD by a correction factor F_T determined for a particular arrangement. The product of F_T and $\Delta T_{\ell m}$ is called the corrected mean temperature difference.

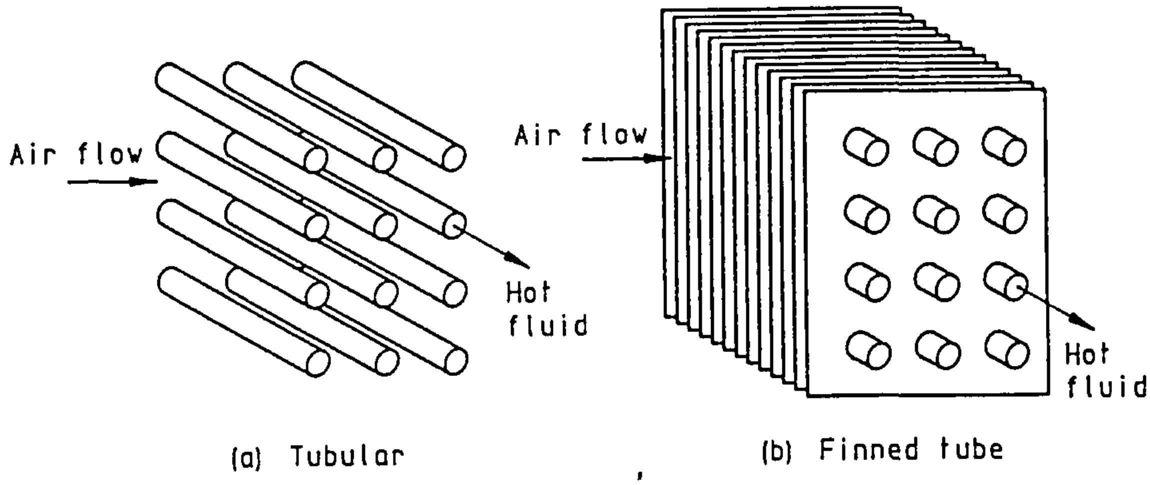

Figure 3.5.3: Crossflow heat exchangers.

The heat transfer equation then takes the form

$$Q = UAF_T \Delta T_{\ell m} \tag{3.5.16}$$

The temperature correction factor for an unmixed singlepass crossflow heat exchanger is shown in figure 3.5.4. Methods for evaluating F_T for other heat exchangers are presented in Appendix C.

Equation (3.5.7) is useful when all terminal temperatures for the evaluation of the logarithmic mean temperature difference are known. There are, however, numerous occasions when the fluid outlet temperatures are not known. This type of problem is encountered in the selection of a heat exchanger or when the unit has been tested at one flow rate, but service conditions require different flow rates for one or both fluids. The outlet temperatures and the rate of heat transfer can then be found only by an iterative procedure. To avoid this problem, the effectiveness - NTU (Number of Transfer Units) method as presented in the following section may be a more appropriate approach in such a case.

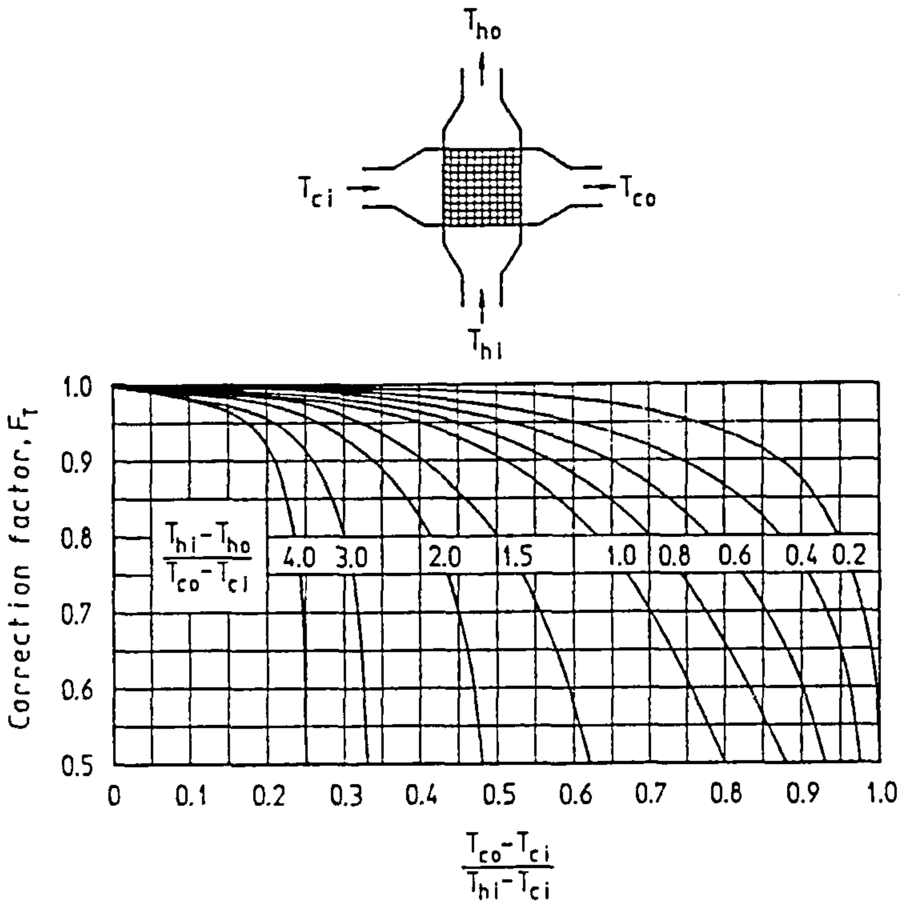

Figure 3.5.4: Correction factor for singlepass crossflow heat exchanger, both fluids unmixed.

3.5.2 EFFECTIVENESS - NTU METHOD

The effectiveness - NTU (Number of Transfer Units) method of heat exchanger analysis is of value when variables other than the stream temperatures are specified. Furthermore, this method makes it possible to compare various types of heat exchangers, so that the one best suited to accomplishing a particular heat transfer objective can be selected.

The effectiveness of a heat exchanger, e, is defined as the ratio of the actual rate of heat transfer in a given heat exchanger to the maximum possible rate of heat exchange. The latter would be obtained in a counterflow heat exchanger of infinite heat transfer area, where in the absence of heat losses to the environment the outlet temperature of the colder fluid equals the inlet temperature of the hotter fluid when $m_c\, c_{pc} < m_h\, c_{ph}$ or the outlet temperature of the warmer fluid equals the inlet temperature of the colder one when $m_h c_{ph} < m_c c_{pc}$.

Depending on which of the heat capacity rates is smaller, the effectiveness for the parallel flow exchanger may be expressed as

$$e = C_h(T_{h1} - T_{h2})/\left[C_{min}(T_{h1} - T_{c1})\right] \tag{3.5.17}$$

or

$$e = C_c(T_{c2} - T_{c1})/\left[C_{min}(T_{h1} - T_{c1})\right] \tag{3.5.18}$$

where the heat capacity rates are defined as $C_h = m_h c_{ph}$ and $C_c = m_c c_{pc}$, and C_{min} is the smaller of these values.

The method of deriving an expression for the effectiveness of a heat exchanger is illustrated by applying it to a parallel flow arrangement.

Rewrite equation (3.5.5) with equation (3.5.17) and (3.5.18) to obtain

$$\ln\,(1 - eC_{min}/C_h - eC_{min}/C_c) = -UA(1/C_h + 1/C_c)$$

or

$$1 - e\,(C_{min}/C_h + C_{min}/C_c) = \exp\left[-UA\,(1/C_h + 1/C_c)\right] \tag{3.5.19}$$

Solving for e yields

$$e = \frac{1 - \exp\,[-UA(1/C_h + 1/C_c)]}{(C_{min}/C_h + C_{min}/C_c)} \tag{3.5.20}$$

From this relation it follows that in general for parallel flow

$$e = \frac{1 - \exp[-UA/C_{min}\,(1 + C_{min}/C_{max})]}{1 + C_{min}/C_{max}} \qquad (3.5.21)$$

This derivation illustrates how the effectiveness for a given flow arrangement can be expressed in terms of two dimensionless parameters, the heat capacity rate ratio C_{min}/C_{max} and the ratio of the overall conductance to the smaller heat capacity rate, UA/C_{min}. The latter of the two parameters is called the number of transfer units, or NTU. The number of heat transfer units is a measure of the heat transfer size of the exchanger. The larger the value of NTU, the closer the heat exchanger approaches its thermodynamic limit.

In the case of condensation, where the fluid temperature stays essentially constant or the fluid acts as if it had infinite specific heat, C_{min}/C_{max} approaches zero, and the effectiveness relation for all heat exchanger arrangements becomes

$$e = 1 - \exp(-UA/C_{min}) \qquad (3.5.22)$$

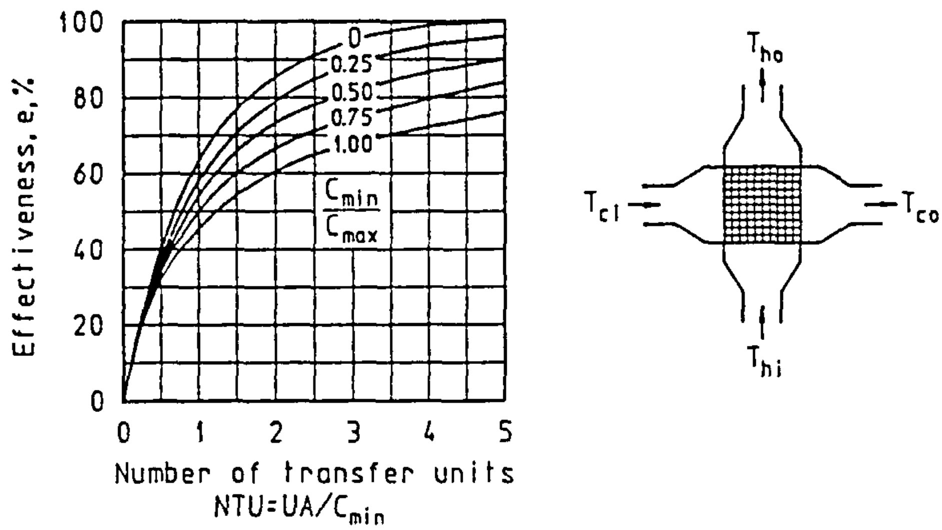

Figure 3.5.5: Effectiveness for crossflow exchanger with fluid unmixed.

By analyses similar to the one presented here for parallel flow, the effectiveness may be evaluated for most flow arrangements of practical interest. The effectiveness of a crossflow heat exchanger with both streams unmixed is shown in figure 3.5.5.

Table 3.5.1 summarizes effectiveness relations for a number of different types of heat exchangers [84KA1]. Other geometries are presented in the literature [87ES1].

Table 3.5.1: Heat exchanger effectiveness relations.

$$N = NTU = UA/C_{min}; \quad C = C_{min}/C_{max}$$

Flow geometry	Relation
Double pipe parallel flow	$e = \dfrac{1 - \exp[-N(1 + C)]}{(1 + C)}$
Double pipe counterflow	$e = \dfrac{1 - \exp[-N(1 - C)]}{1 - C\exp[-N(1 - C)]}$
Double pipe counterflow, C = 1	$e = \dfrac{N}{N + 1}$
Crossflow with both streams unmixed	$e = 1 - \exp\left[N^{0.22}\left\{\exp\left(-CN^{0.78}\right) - 1\right\}/C\right]$
Crossflow with both streams mixed	$e = \left[\dfrac{1}{1 - \exp(-N)} + \dfrac{C}{1 - \exp(-NC)} - \dfrac{1}{N}\right]^{-1}$
Crossflow with C_{max} mixed, C_{min} unmixed	$e = [1 - \exp\{-C(1 - \exp^{-N})\}]/C$
Crossflow with C_{max} unmixed, C_{min} mixed	$e = 1 - \exp[-\{1 - \exp(-NC)\}/C]$
All exchangers with C = 0	$e = 1 - \exp(-N)$

For a multipass overall-counterflow arrangement with the fluids mixed between passes the effectiveness is given by [81SH1].

3.6 REFERENCES

16NU1 Nusselt, W., Die Oberflächen Kondensation des Wasserdampfes, Zeit, Ver. Deut. Ing., Vol. 60, pp. 541 - 546, 569, 1916.

21PA1 Parr, P.H., The Water Film on Evaporating and Condensing Tubes, The Engineer, Vol. 113, pp. 559 - 561, 1921.

40BO1 Bowman, R.A., Mueller, A.C. and Nagle, W.M., Mean Temperature Difference in Design, ASME Trans., Vol. 62, 1940.

43HA1 Hausen, H., Z. VDI, Beih. Verfahrenstech., Vol. 4, No. 91, 1943.

46SC1 Schmidt, T.E., La Production Calorifique des Surfaces Munies Dailettes, Annexe Du Bulletin De L'Institut International Du Froid, Annex G-5 1945 - 1946.

49BE1 Bergelin, O.P., Kegel, P.K., Carpenter, F.G. and Gazley, C., Co-current Gas-liquid Flow. Flow in Vertical Tubes, Meeting at Berkely, Cal., USA, ASME Heat Transfer and Fluid Mechanics Institute, pp. 19-28, June 1949.

51CA1 Carpenter, E.F. and Colburn, A.P., The Effect of Vapor Velocity on Condensation Inside Tubes, Proc. Inst. Mech. Engrs and ASME Gen. Disc. on Heat Transfer, pp. 20-26, London, 1951.

55KA1 Kays, W.M., Numerical Solution for Laminar Flow-Heat Transfer in Circular Tubes, Trans. ASME, Vol. 77, pp. 1265 - 1274, 1955.

55ZA1 Zabronsky, H., Temperature Distribution and Efficiency of a Heat Exchanger Using Square Fins on Round Tubes, ASME Trans., J. Applied Mechanics, Vol. 77, 1955.

58AK1 Akers, W.W., Deans H.A. and Crosser, O.K., Condensing Heat Transfer Within Horizontal tubes, Chem. Eng. Prg. Symp. Series, Vol. 55, No. 29, pp. 171 - , 1958.

58BR1 Brauer, H., Wärmeübergang bei der Filmkonsation reiner Dämpfe an lotrechten Wänden, Forsch. Ing. Wes., Vol. 24, pp. 105-117, 1958.

59HA1 Hausen, H., Neue Gleichungen für die Wärmeübertragung bei freier oder erzwungener Konvektion, Allg. Wärmetechn., Vol. 9, pp. 75-79, 1959.

59ST1 Stephan, K., Wärmeübergang und Druckabfall bei nicht ausgebildeter Laminarströmung in Rohren und in Ebenen Spalten, Chem. -Ing. -Techn., Vol. 31, pp. 773 - 778, 1959.

60AL1 Altman, M., Stanle, F.W. and Norris, R.H., Local Heat Transfer and Pressure Drop for Refrigerant - 22 Condensing in Horizontal tubes, Third Natl. Heat Transfer Conf., CEP Symp. Series, Vol. 56, No. 30, p. 157, 1960.

61RO1 Rohsenow, W.M. and Choi, H.Y., Heat Mass and Momentum Transfer, Prentice Hall Inc., Englewood Cliffs, New Jersey 1961.

62HS1 Hsu, S.T., Engineering Heat Transfer, D. van Nostrand Co. Inc., Princeton, 1962.

62CH1 Chato, J.C., Laminar Condensation Inside Horizontal and Inclined Tubes, ASHRAE Jnl, pp. 52 - 60, 1962.

64ME1 Metais, B. and Eckert, E.R.G., Forced, Mixed and Free Convection Regimes, J. Heat Transfer, Vol. 86, pp. 295 - 296, 1964.

65BR1 Brown, A.R. and Thomas, M.A., Combined Free and Forced Convection Heat Transfer for Laminar Flow in Horizontal Tubes, J. Mech. Eng. Sci., Vol. 7, pp. 440 - 448, 1965.

66BA1 Baroczy, C.J., A Systematic Correlation for Two-phase Pressure Drop, Chem. Eng. Prog. Symp. Ser., Vol. 62, No. 64, pp. 232-249, 1966.

66RI1 Rich, D.G., The Efficiency and Thermal Resistance of Angular and Rectangular Fins, Proc. Int. Heat Transfer Conference, 1966.

67BO1 Boyko, L.D. and Kruzhilin, G.N., Heat Transfer and Hydraulic Resistance During Condensation of Steam in a Horizontal Tube and in a Bundle of Tubes, Int. J. Heat Mass Transfer, Vol. 10, pp. 361-373, 1967.

67JA1 Jamil, M., Laminar Forced Convection in Non-circular Ducts, M.S. Thesis, Mech. Eng. Dept., University of Alberta, Edmonton, 1967.

68SO1 Soliman, M., Schuster, J.R. and Berenson, P.J., A General Heat Transfer Correlation for Annular Flow Condensation, Trans. ASME, J. of Heat Transfer, Vol. 90, pp. 267-276, May, 1986.

69SC1 Schulenberg, F.J., Wärmeübergang und Druckänderung bei der Kondensation von Strömenden Dampf in geneigten Rohren, Dr. -Ing. thesis, Universität Stuttgart, 1969.

70BA1 Barrow, H. and Roberts A., Flow and Heat Transfer in Elliptical Ducts, 4th Int. Heat Transfer Conf., Versailles, Sept. 1970.

70CH1 Cheng, K.C. and Jamil, M., Laminar Flow and Heat Transfer in Circular Ducts with Diametrically Opposite Flat Sides and Ducts of Multiply Connected Cross Sections, Can. J. Chem. Eng., Vol. 48, pp. 333 - 334, 1970.

70PE1 Petukhov, B.S., Heat Transfer and Friction in Turbulent Pipe Flow with Variable Physical Properties, Advances in Heat Transfer, Vol. 6, eds Hartnett J.P., and Irvine, T.F., Academic Press, New York, pp. 504 - 564, 1970.

70SC1 Schulenberg, F., Wärmeübergang und Druckverlust bei der Kondensation von Kältemitteldämpfen in Luftgekühlten Kondensatoren, Kältetechnik-Klimatisierung, Vol. 3, pp. 75-81, 1970.

71KO1 Kosky, P.G. and Staub, F.W., Local Condensing Heat Transfer Coefficients in the Annular Flow Regime, AIChE Journal, Vol. 17, pp. 1037-1043, 1971.

72CH1 Chawla, J.M., Wärmeübergang in Durchströmten Kondensator-Rohren, Kältetechnik-Klimatisierung, Vol. 24, pp. 233-240, 1972.

72KE1 Kern, D.Q. and Kraus, A.D., Extended Surface Heat Transfer, McGraw Hill Book Co., New York, 1972.

72MU1 Murthy, V.N. and Sarma, P.K., Condensation Heat Transfer Inside Horizontal tubes, The Canadian J. of Chem. Eng., Vol. 50, pp. 547-549, 1972.

72WA1 Walt, J. v.d. and Kröger, D.G., Heat Transfer During Film Condensation of Saturated and Superheated Freon-12, Progress in Heat and Mass Transfer, Vol. 6, pp. 75-97, 1972.

73CA1 Cain, D., Roberts, A. and Barrow, H., An Experimental Investigation of Turbulent Flow and Heat Transfer in Elliptical Ducts, Wärme und Stoffübertragung, Vol. 2, 1973.

73CH1 Churchill, S.W. and Ozoe, H., Correlations for Laminar Forced Convection in Flow over an Isothermal Flat Plate and in Developing and Fully Developed Flow in an Isothermal Tube, J. Heat Transfer, Vol. 95, pp. 416 -419, 1973.

73RO1 Roetzel, W., Laminar Film Condensation in Tubes: Calculation of Local Film Resistance and Local Adiabatic Mixing Temperature, Int. J. of Heat and Mass Transfer, Vol. 16, pp. 2297-2304, 1973.

73RO2 Rohsenow, W.M., Handbook of Heat Transfer, Mc Graw Hill Book Co., New York, 1973.

73RO3 Rose, J.C., Wilson, D.J. and Cowan, G.H., The Performance of Air-cooled Heat Exchangers, Part II. Air-cooled Heat Exchanger Performance Specification, Heat Transfer and Fluid Flow Service, Harwell, 1973.

73TR1 Traviss, D.P., Rohsenow, W.M. and Baron, A.B., Forced Convection Condensation in Tubes: A Heat Transfer Correlation for Condenser Design, ASHRAE Trans., Vol. 30, Part 1, pp. 157-165, 1973.

74CA1 Carnavos, T.C., Some Recent Developments in Augmental Heat Elements, Heat Exchangers: Design and Theory Sourcebook, eds Afgan, N.H., and Schlünder, E.U., Scripta Book Company, Washington, pp. 441 - 489, 1974.

74HA1 Hausen, H., Extended Equation for Heat Transfer in Tubes at Turbulent Flow, Wärme und Stoffübertragung, Vol. 7, pp. 222 - 225, 1974.

75GN1 Gnielinski, V., Forsch. Ing. Wesen, Vol 41, No. 1, 1975.

75SH1 Shah, R.K., Thermal Entry Length Solutions for the Circular Tube and Parallel Plates, Proc. 3rd Natl. Heat Mass Transfer Conf., Indian Inst. Technol., Bombay, Vol. 1, Pap. No. HMT-11-75, 1975.

75WA1 Watkinson, A.P., Miletti, D.C. and Kubanek, G.R., Heat Transfer and Pressure Drop of Internally Finned Tubes in Laminar Oil Flow, ASME Paper No. 75-HT-41, 1975.

76HO1 Hong, S.W. and Bergles, A.E., Augmentation of Laminar Flow Heat Transfer by Means of Twisted-tape Inserts, J. Heat Transfer, Vol. 98, pp. 251 -256, 1976.

76ZA1 Zarling, J.P., Application of the Schwarz-Newmann Technique to Fully Developed Laminar Heat Transfer in Non-circular Ducts, ASME Paper 76 - WA/HT-49, 1976.

77CH1 Churchill, S.W., Comprehensive Correlating Equations for Heat Mass and Momentum Transfer in Fully Developed Flow in Smooth Tubes, Ind. Eng. Chem., Fundam., Vol. 16, No. 1, 1977.

77KR1 Kröger, D.G., Laminar Condensation Heat Transfer Inside Inclined Tubes, AICHE Symposium Series, Vol. 73, No. 164, pp. 256 - 260, 1977.

78BE1 Bergles, A.E., Enhancement of Heat Tranfer, Heat Transfer 1978, Proc. of the Sixth International Heat Tranfer Conference, Vol. 6, pp. 89-108, Hemisphere Publishing Corporation, Washington, 1978.

78MA1 Marner, W.J. and Bergles, A.E., Augmentation of Tubeside Laminar Flow Heat Transfer by Means of Twisted - tape Inserts, Static-mixer Inserts and Internally finned Tubes, Heat Transfer 1978, Vol. 2, pp.583 - 588, Hemisphere Publishing Corporation, Washington, 1978.

78SH1 Shah, R.K. and London, A.L., Laminar Flow Forced Convection in Ducts, Academic Press, New York, 1978.

78VA1 Van Rooyen, R.S. and Kröger, D.G., Laminar Flow Heat Transfer in Internally Finned Tubes with Twisted Tape Inserts, Proc. 6th Int. Heat Transfer Conference, Paper FC(a) - 16, Toronto, August 1978.

79HE1 Hewitt, G.F., Two-phase Flow, Two-phase Heat Transfer in Steady and Transient States, Course presented at Stanford, 1979.

79JE1 Jesch, J., Lutcha, J. and Michal, V., The Use of Air Coolers for Viscous Media, Int. Chem. Engineering, Vol. 19, No. 4, pp. 680-688, 1979.

79PA1 Palen, J.W., Breber, G. and Taborek, J., Prediction of Flow Regimes in Horizontal Tubeside Condensation, Heat Transfer Engineering, Vol. 1, No. 2, pp. 47-57, 1979.

79SH1 Shah, M.M., A General Correlation for Heat Transfer During Film Condensation Inside Pipes, Int. J. Heat Mass Transfer, Vol. 22, pp. 547 - 556, 1979.

80BR1 Breber, G., Palen, J.W. and Taborek, J. Prediction of Horizontal Tubeside Condensation of Pure Components Using Flow Regime Criteria, Trans. ASME, Vol. 102, pp. 471-476, 1980.

80KR1 Kreith, F., Basic Heat Transfer, Harper and Row Publishers, New York, 1980.

81OW1 Owen, R.G., Sardesai, R.S. and Butterworth, D., Two-phase Pressure Drop for Condensation Inside a Horizontal Tube, Symp. on Advancement in Heat Exchangers, Int. Centre for Heat and Mass Transfer, Dubrovnik, 1981.

81RO1 Rogers, D.G., Experimental Heat Transfer Coefficients for the Cooling of Oil in Horizontal Internal Forced Convective Transitional Flow, CSIR, South Africa, Report CENG 371, 1981.

81RO2 Rohsenow, W.M., Why Laminar Flow Heat Exchangers can Perform Poorly, in Heat Exchangers, Thermal-Hydraulic Fundamentals and Design, eds. Kakac, S., Bergles, A.E. and Mayinger, F., pp. 1057-1071, McGraw Hill, New York, 1981.

81SC1 Schlünder, E.-U., Einführung in die Wärme - und Stoffübertragung, Vieweg, Braunschweig, 1972.

81SH1 Shah, R.K., Compact Heat Exchangers, in Heat Exchangers, Thermal-Hydraulic Fundamentals and Design, eds Kakac, S., Bergles, A.E. and Mayinger, F., pp.111 - 151, McGraw Hill, New York, 1981.

82BL1 Blangetti, F., Krebs, R. and Schlünder, E.U., Condensation in Vertical Tubes - Experimental Results and Modelling, Chem. Eng. Fund., Vol. 1, No. 2, pp. 20 - 63, 1982.

82SA1 Sardesai, R.S., Owen, R.G. and Pulling, D.J., Pressure Drop for Condensation of a Pure Vapor in Downflow in a Vertical Tube, Proc. 7th Int. Heat Transfer Conf., Paper Cs 23, Vol. 5, pp. 139-145, München, 1982.

82WH1 Whalley, P.B., Azzopardi, B.J., Hewitt, G.F. and Owen, R.G., A Physical Model for Two-phase Flows with Thermodynamic and Hydrodynamic Non-equilibrium, Proc. 7th Int. Heat Transfer Conf., Paper Cs 29, München, 1982.

83BE1 Bergles, A.E. and Joshi, S.D., Augmentation Techniques for Low Reynolds Number In-tube Flow, Low Reynolds Number Flow Heat Exchangers, eds Kakac, S., Shah, R.K., and Bergles, A.E., Hemisphere Publishing Corporation, Washington, 1983.

83BE2 Bergles, A.E., Prediction of the Effects of Temperature - Dependent Fluid Properties on Laminar Heat Transfer, Low Reynolds Number Flow Heat

Exchangers, eds Kakac, S., Shah, R.K., and Bergles, A.E., Hemisphere Publishing Corporation, Washington, 1983.

83BE3 Bergles, A.E., Experimental Verification of Analyses and Correlation of the Effects of Temperature - Dependent Fluid Properties on Laminar Heat Transfer, Low Reynolds Number Flow Heat Exchangers, eds Kakac, S., Shah, R.K., and Bergles, A.E., Hemisphere Publishing Corporation, Washington, 1983.

83KA1 Kakac, S. and Yener, Y., Laminar Forced Convection in Combined Entrance Region of Ducts, Low Reynods Number Flow Heat Exchangers, eds Kakac, S., Shah, R.K., and Bergles, A.E., Hemisphere Publishing Corporation, Washington, 1983.

83SH1 Shah, R.K., Fully Developed Laminar Flow Forced Convection in Channels, Low Reynolds Number Flow Heat Exchangers, ed. Kakac, S., Shah, R.K. and Bergles, A.E., Hemisphere Publishing Corporation, Washington, 1983.

83TA1 Taborek, J., Mean Temperature Difference, Heat Exchanger Design Handbook, Vol. 1, Hemisphere Publ. Corp., Washington, 1983.

84AB1 Abdel-Wahed, R.M., Attia, A.E. and Hifni, M.A., Experiments on Laminar Flow and Heat Transfer in an Elliptical Duct, Int. J. Heat Mass Transfer, Vol. 27, No. 12, 1984.

84KA1 Kays, W.M. and London, A.L., Compact Heat Exchangers, Mc Graw - Hill Book Co., New York, 1984.

84RO1 Roetzel, W., Berechnung von Wärmeübertragern, VDI-Wärmeatlas, pp. Ca1 - Ca31, VDI Verlag GmbH, Düsseldorf, 1984.

84RO2 Roth, J.E., Wärmeübertragung bei der Kondensation in geneigten ovalen Rohren, Fortschr. - Ber. VDI, Vol. 6, No. 145, Düsseldorf, 1984.

86BE1 Bergles, A.E., Experimental Verification of Analyses and Correlation of the

Effects of Temperature-dependent Fluid Properties on Laminar Heat Transfer, Heat Exchanger Sourcebook, ed. Palen, J.W., Hemisphere Publishing Corporation, Washington, 1986.

86HO1 Holman, J.P. Heat Transfer, Mc Graw Hill Book Co., New York, 1986.

86MA1 Manglik, R.M., and Bergles, A.E., An Analysis of Laminar Flow Heat Transfer in Uniform Temperature Circular Tubes with Tape Inserts, Technical Report ERI Project 1744, Department of Mechanical Engineering, Iowa State University, Ames, 1986.

87CH1 Chen, I.Y. and Kocamustafaogullari, G., Condensation Heat Transfer Studies for Stratified, Co-current Two-Phase Flow in Horizontal Tubes, Int. J. Heat Mass Transfer, Vol. 30, No. 6, pp. 1133 - 1148, 1987.

87CH2 Chen, S.L. Gerner, F.M. and Tien C.L., General Film Condensation Correlations, Experimental Heat Transfer, Vol. 1, pp. 93-107, 1987.

87DU1 Du Plessis, J.P. and Kröger, D.G., Heat Transfer Correlation for Thermally Developing Laminar Flow in a Smooth Tube with a Twisted-tape Insert, Int. J. Heat Mass Transfer, Vol. 30, No. 3, pp. 509-515, 1987.

87ES1 Engineering Sciences Data Unit, Effectiveness - NTU Relationships for the Design and Performance Evaluation of Multi-pass Crossflow Heat Exchangers, Item No. 87020, London 1987.

89DI1 Di Giovanni, M.A. and Webb, R.L., Uncertainty in Effectiveness - NTU Calculations for Crossflow Heat Exchangers, Heat Transfer Engineering, Vol. 10, No. 3, pp. 61-70, 1989.

89FU1 Fürst, J., Kondensation in geneigten ovalen Rohren, Fortschr. - Ber. VDI, Vol. 19, No. 36, Düsseldorf, 1989.

89GN1 Gnielinski, V., Zur Wärmeübertragung bei laminarer Rohrströmung und konstanter Wandtemperatur, Chem. - Ing. - Tech., Vol. 61, No. 2, pp. 161 - 163, 1989.

90BR1 Bronstein, I.N. and Semendjajew, K.A., Taschenbuch der Mathematik, eds. Grosche, G., Ziegler, V. and Ziegler, D., Verlag Harri Deutsch, Thun und Frankfurt/Main, 1990.

90CH1 Chun, M.H. and Kim K.T., Assessment of New and Existing Correlations for Laminar and Turbulent Film Condensation on a Vertical Surface, Int. Comm. Heat Mass Transfer, Vol. 17, pp. 431-441, 1990.

90TA1 Taborek, J., Design Method for Tube-side Laminar and Transition Flow Regime with Effects of Natural Convection, Paper presented at Open Forum Session, 9th Int. Heat Transfer Conf., Jerusalem, 1990.

92CA1 Carey, V.P., Liquid-vapor Phase-change Phenomena, Hemisphere Publ. Corp., Washington, 1992.

92RO1 Roetzel, W., Laminare Filmkondensation an einer senkrechten ebenen Wand mit örtlich veränderlicher Oberflächentemperatur, Wärme- und Stoffübertragung, Vol. 27, pp. 173-175, 1992.

93HU1 Hu, X. and Jacobi, A.M., Local Heat Transfer Behaviour and Its Impact on a Single-row, Annularly Finned Tube Heat Exchanger, Trans. of the ASME, Journal of Heat Transfer, Vol. 115, pp. 66-74, February 1993.

CHAPTER 4

MASS TRANSFER AND EVAPORATIVE COOLING

4.0 INTRODUCTION

Psychrometry is the study of the properties of mixtures of air and water vapor. The subject is important in cooling system practice because atmospheric air is not completely dry but a mixture of air and water vapor. In certain cooling systems water is added to the air-water-vapor mixture. Psychrometric principals will be applied in this and later chapters, to the performance evaluation of cooling towers, evaporative coolers and systems incorporating adiabatic pre-cooling of the air.

Since there is usually both a heat and mass transfer process between the air and some wetted surface, information on mass transfer is presented. Because of the analogy that exists between momentum heat and mass transfer there is a similarity in the equations employed.

4.1.1 MASS TRANSFER

When a mixture of gases or liquids is contained such that there exists a concentration gradient of one or more of the constituents or components across the system, there will be mass transfer on a microscopic level as a result of diffusion from regions of high concentration to regions of low concentration. Not only may mass transfer occur on a molecular basis, but also in turbulent flow systems accelerated diffusion rates will occur as a result of rapid-eddy mixing processes, just as these mixing processes created increased heat transfer and viscous action in turbulent flow.

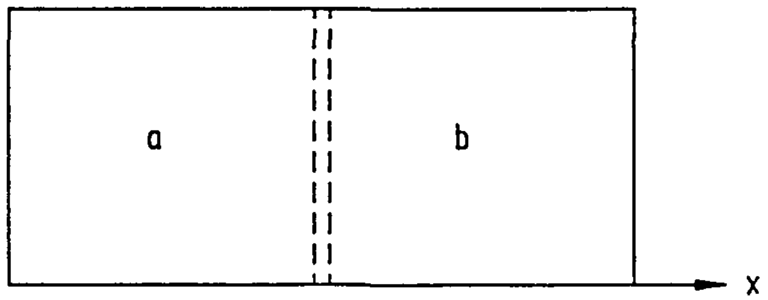

Figure 4.1.1: Diffusion of components.

Consider the system shown in figure 4.1.1. A thin partition separates two gases a and b. When the partition is removed, the two gases diffuse through one another until equilibrium is established and the concentration of the gases is uniform throughout the container. The diffusion rate is given by Fick's law of diffusion which states that the mass flux of a constituent per unit area is proportional to the concentration gradient. Thus

$$\frac{m}{A} = -D\frac{dc}{dx} \tag{4.1.1}$$

where the constant of proportionality, D, is called the diffusion coefficient, and has the units of m^2/s. The concentration c is the mass of a constituent per unit volume. Notice the similarity between equation (4.1.1), Newton's equation of viscosity, equation (2.1.1) and Fourier's law of heat conduction, equation (3.1.1). The diffusion equation describes the transport of mass while the equation of viscosity describes the transport of momentum and the conduction equation describes the transport of energy.

To understand the physical mechanism of diffusion, consider the imaginary plane shown by the dashed line in figure 4.1.2.

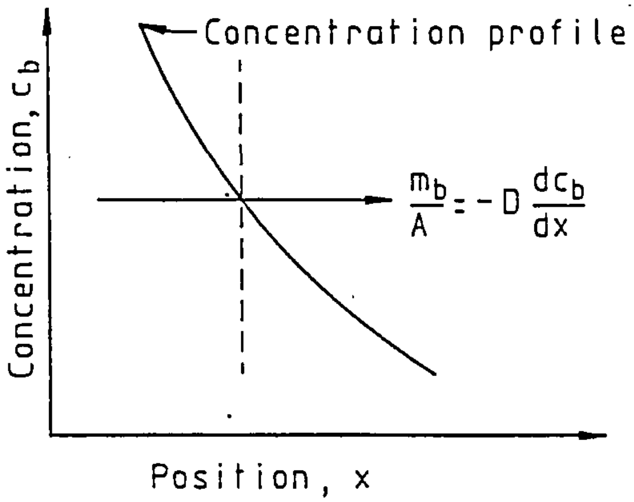

Figure 4.1.2: Sketch showing diffusion dependence on concentration profile.

The concentration of constituent b is greater on the left side of this plane than on the right side. A higher concentration means that there are more molecules per unit volume. If the system is a gas or a liquid, the molecules move about in a random fashion, and the higher the concentration, the more molecules will cross a given plane per unit time. Thus, on the average, there are more molecules moving from left to right across the plane than in the opposite direction. This results in a net mass transfer from the region of high concentration to the region of low concentration . The fact that the molecules collide with each other influences the diffusion process strongly. In a mixture of gases there is a decided difference between a collision of like molecules and a collision of unlike molecules. The collision between like molecules does not appreciably alter the basic molecular movement because the two molecules are identical and it does not make any difference whether one or the other of the two molecules crosses a certain plane. The collision of two unlike molecules, say, molecules a and b, might result in molecule b crossing some particular plane instead of molecule a. The molecules would, in general have different masses; thus the mass transfer would be influenced by the collision.

By using the kinetic theory of gases it is possible to predict analytically the diffusion rates for some systems by taking into account the collision mechanism and molecular weights of the constituent gases. In gases the diffusion rates are clearly dependent on the molecular speed, and consequently we should expect a dependence of the diffusion coefficient on temperature since the temperature indicates the average molecular speed. Gilliland [34GI1] has proposed a semi-empirical equation for the diffusion coefficients in gases:

$$D = 0.04357\, T^{1.5} \left(1/M_a + 1/M_b\right)^{0.5} \Big/ \left[p\left(V_a^{0.333} + V_b^{0.333}\right)^2\right],\ m^2/s \tag{4.1.2}$$

where V_a and V_b are the molecular volumes of gases a and b, and M_a and M_b are the corresponding molecular masses respectively while T is in Kelvin and p is the total system pressure. For air $V_a = 29.9$ and $M_a = 28.97$, while for water vapor $V_v = 18.8$ and $M_v = 18.016$.

Equation (4.1.2) offers a convenient expression for calculating the diffusion coefficient for various compounds and mixtures, but it should not be used as a substitute for experimental values of the diffusion coefficient when they are available for a particular system.

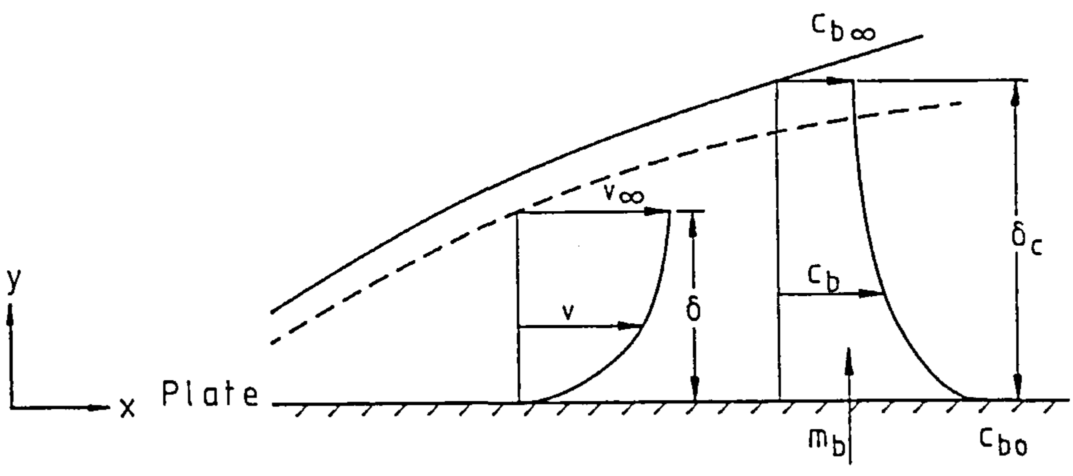

Figure 4.1.3: Velocity and concentration boundary layer on a flat plate.

Calculation of momentum and heat transfer rates at a solid-fluid interface by the appropriate rate equation require a knowledge of the velocity and the temperature profiles within the boundary layer. Similarly, mass transfer at an interface is determined by the concentration boundary-layer profile. Figure 4.1.3 shows a fluid mixture, with free-stream velocity and concentration designated respectively by v_∞ and $c_{b\infty}$, flowing over a flat plate; if the plate surface is maintained at a concentration $c_{bo} > c_{b\infty}$, mass m_b diffuses from the surface into the fluid stream. A concentration boundary layer grows from the leading edge in the same way that a velocity or a thermal boundary layer grows, and the thickness of the concentration boundary-layer, δ_c, is defined as the distance from the plate where $(c_{bo} - c_b) = 0.99\,(c_{bo} - c_{b\infty})$.

By analogy with heat transfer, a mass transfer coefficient h_D is defined by

$$m_b = h_D\, A \left(c_{bo} - c_{b\infty}\right) \tag{4.1.3}$$

The relative rates of growth of the velocity and concentration boundary layers are determined by the Schmidt number of the fluid i.e.

$$Sc = \mu/(\rho D) = \nu/D \tag{4.1.4}$$

The Schmidt number is analogous to the Prandtl number in heat transfer. A dimensionless mass transfer number called the Sherwood number corresponding to the Nusselt number for heat transfer may be defined as

$$Sh = h_D\, L/D \text{ for a plate} \tag{4.1.5a}$$

or

$$Sh = h_D\, d_e/D \text{ for a duct} \tag{4.1.5b}$$

If a temperature difference exists between the plate and the free stream in addition to the concentration difference, a thermal boundary layer will grow concurrently with the velocity and the concentration boundary layers. The relative rate of growth of the thermal and concentration boundary layers are determined by the Lewis number.

$$Le = k/\left(\rho c_p\, D\right) = \alpha/D = Sc/Pr \tag{4.1.6}$$

The temperature and concentration profiles will coincide when $Le = 1$. Similarities between the governing equations of heat, mass and momentum transfer suggest that empirical correlations for mass transfer would be similar to those for momentum and heat transfer.

The Reynolds analogy for mass transfer over a smooth flat plate becomes [86HO1]

$$h_D\, Sc^{0.667}/v_\infty = 0.332\, Re_x^{0.5} \text{ for laminar flow} \tag{4.1.7}$$

$$h_D\, Sc^{0.667}/v_\infty = 0.0296\, Re_x^{-0.2} \text{ for turbulent flow} \tag{4.1.8}$$

while for turbulent pipe flow

$$h_D\, Sc^{0.667}/v_m = f/8 \tag{4.1.9}$$

Gilliland [41GI1] presents an equation for the vaporization of liquids into air inside circular columns where the liquid wets the surface and the air is forced through the column.

$$Sh = h_D\, d/D = 0.023\, Re^{0.83}\, Sc^{0.44} \tag{4.1.10}$$

This equation is valid for $2000 < Re < 35000$ and $0.6 < Sc < 2.5$.

Frössling [38FR1] presents a semi-empirical correlation for the mass transfer coefficient from a single spherical water droplet suspended in an air stream.

$$Sh = h_D\, d/D = 2 + 0.552\, Re^{0.5}\, Sc^{0.33} \tag{4.1.11}$$

for $2 \le Re \le 800$.

When evaluating the mass transfer coefficients for an air-water-vapor mixture, the thermophysical properties of the mixture are determined according to the equations listed in Appendix A.3.

In air-water-vapor systems, the concentration of the water vapor in the air is often expressed in terms of the humidity ratio w, which is defined as the ratio of the mass of water vapor per unit mass of dry air. When moist air is considered to be a mixture of independent perfect gases, dry air and water vapor, each is assumed to obey the perfect gas equation of state and it follows [72AS1, 82ST1] that

$$w = \frac{\text{kg of water vapor}}{\text{kg of dry air}} = \frac{p_v V/R_v T}{p_a V/RT} = \left(\frac{R}{R_v}\right)\frac{p_v}{(p - p_v)} = \left(\frac{287.08}{461.52}\right)\frac{p_v}{(p - p_v)} = \frac{0.622 p_v}{(p - p_v)} \tag{4.1.12}$$

where p_v is the partial pressure of the water vapor, p_a is the partial pressure of the air, $p = p_a + p_v$ is the total mixture pressure and V is an arbitrary volume of the air-vapor mixture. The gas constant for air is $R = 287.08$ J/kgK and for water vapor $R_v = 461.52$ J/kgK. For air that is saturated with water vapor, the corresponding partial pressure of the water vapor can be determined according to equation (A.2.1). For unsaturated conditions it is in practice however more convenient to employ equation (A.3.5) to determine the humidity ratio.

If the plate in figure 4.1.3 were thus to be replaced by a water surface exposed to an air stream the mass transfer coefficient can be defined by the following equation:

$$m_w = h_d A \left(w_{so} - w_\infty\right) \tag{4.1.13}$$

At the water-air interface, the humidity ratio corresponding to saturation conditions is according to equation (4.1.12)

$$w_{so} = 0.622\, p_{vs} / \left(p - p_{vs}\right) \tag{4.1.14}$$

Equate equation (4.1.3) and equation (4.1.13) to find

$$h_d = h_D \left(c_{bo} - c_{b\infty}\right) / \left(w_{so} - w_\infty\right) \tag{4.1.15}$$

Noting that the species or constituent concentration c_b is equivalent to the partial density of the substance, ρ_b, and introducing the perfect gas law, equation (4.1.15) for an air-water-vapor system yields (the subscript b refers to constituent or component b which is the water vapor in this case)

$$h_d = h_D \left(\frac{p_{vso}}{R_v T_{so}} - \frac{p_{v\infty}}{R_v T_\infty} \right) / \left(w_{so} - w_\infty \right) \tag{4.1.16}$$

From equation (4.1.12) it follows that

$$p_v = pw / (0.622 + w) \tag{4.1.17}$$

Substitute equation (4.1.17) into equation (4.1.16) and find

$$h_d = \frac{h_D\, p}{R_v} \left[\frac{w_{so}}{T_{so} \left(w_{so} + 0.622 \right)} - \frac{w_\infty}{T_\infty \left(w_\infty + 0.622 \right)} \right] / (w_{so} - w_\infty) \tag{4.1.18}$$

This equation is not only limited to flow over flat plates but can also be extended to other geometries where water is exposed to an air stream i.e.

$$h_d = \frac{h_D\, p}{R_v} \left[\frac{w_s}{T_s \left(w_s + 0.622 \right)} - \frac{w}{T(w + 0.622)} \right] / (w_s - w) \tag{4.1.19}$$

Poppe [84PO1] derived the following expression for the mass transfer coefficient under isothermal conditions:

$$h_d = \frac{h_D\, p}{R_v T} \ln \left[\left(w_s + 0.622 \right) / (w + 0.622) \right] / \left(w_s - w \right) \tag{4.1.20}$$

It is sometimes convenient to express the mass transfer coefficient in terms of the relative humidity. The latter is defined as the ratio of the mole fraction of water vapor in a given moist air sample to the mole fraction in an air sample which is saturated at the same temperature and pressure [72AS1]. For perfect gas relationships another expression for the relative humidity is

$$\phi = p_v/p_{vs} \tag{4.1.21}$$

With this relation and equation (4.1.19) it can be shown that for isothermal conditions [86HA1]

$$h_d = \frac{h_D\, p}{RT}\left(1 - \frac{p_{vs}}{p}\right)\left(1 - \frac{\phi\, p_{vs}}{p}\right) \tag{4.1.22}$$

4.1.2 PSYCHROMETRIC CHART

Psychrometric properties of air-water-vapor mixtures can be presented in the form of equations or graphically. Psychrometric charts are a useful and widely accepted tool for design and analysis of processes of heat and mass exchange involving moist air [82ST1].

Unfortunately, no universal chart exists which is suitable for all applications. This is because firstly, a given chart is only valid for the particular barometric pressure for which it was drawn; and secondly, depending on the application, different ranges of temperature and moisture content of the air may be required so that the necessary clarity and accuracy of the chart is maintained [82JO1].

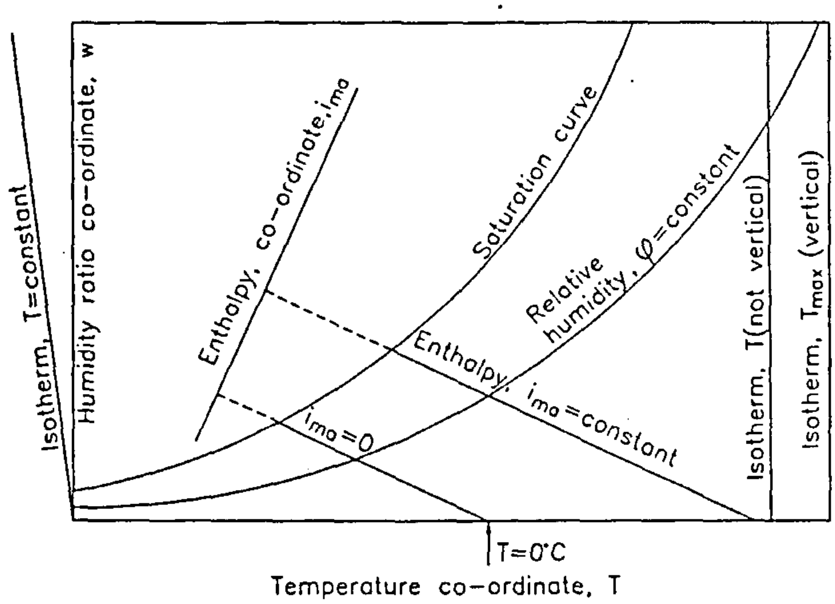

Figure 4.1.4: Psychrometric chart co-ordinates

The conventional psychrometric chart has a vertical co-ordinate for humidity ratio and an inclined co-ordinate for enthalpy both with linear scales as shown in figure 4.1.4. The abscissa shows the drybulb temperature.

The enthalpy of a mixture of dry air and water vapor is the sum of the enthalpy of the dry air and the enthalpy of the water vapor. Enthalpy values are always based on some reference value, and the zero value of dry air is usually chosen as air at 0°C. The zero value of water vapor is saturated liquid water at 0°C, the same reference value that is used for steam.

An equation for the approximate enthalpy of a mixture of air and water vapor is

$$i_{ma} = c_{pa}T + w(i_{fgwo} + c_{pv}T), \text{ J/kg dry air} \tag{4.1.23}$$

where the specific heats are evaluated at T/2°C and the latent heat of vaporization is obtained from equation (A.4.5) at 0°C. This equation is listed in Appendix A.3 as equation (A.3.6b) together with equation (A.3.6a) which expresses the enthalpy per kg of air-water-vapor mixture. In certain processes it is useful to employ the equation based on dry air since the latter does not change. If the mass of the mixture were used as the basis, an iterative method of solving the problem would usually be required since the mass of the mixture changes during the process.

It is evident from the above equation for enthalpy that the isotherms will not be parallel lines. The maximum temperature isotherm is usually chosen as vertical. The saturation curve is obtained with the aid of equation (A.2.1). Lines of constant relative humidity are found with aid of equations (4.1.21) and (A.2.1) while lines of constant wetbulb temperature are determined by means of equation (A.3.5).

A detailed psychrometric chart for moist air at a barometric pressure of 101325 N/m^2 is shown in figure 4.1.5.

Figure 4.1.5: Phsychrometric chart

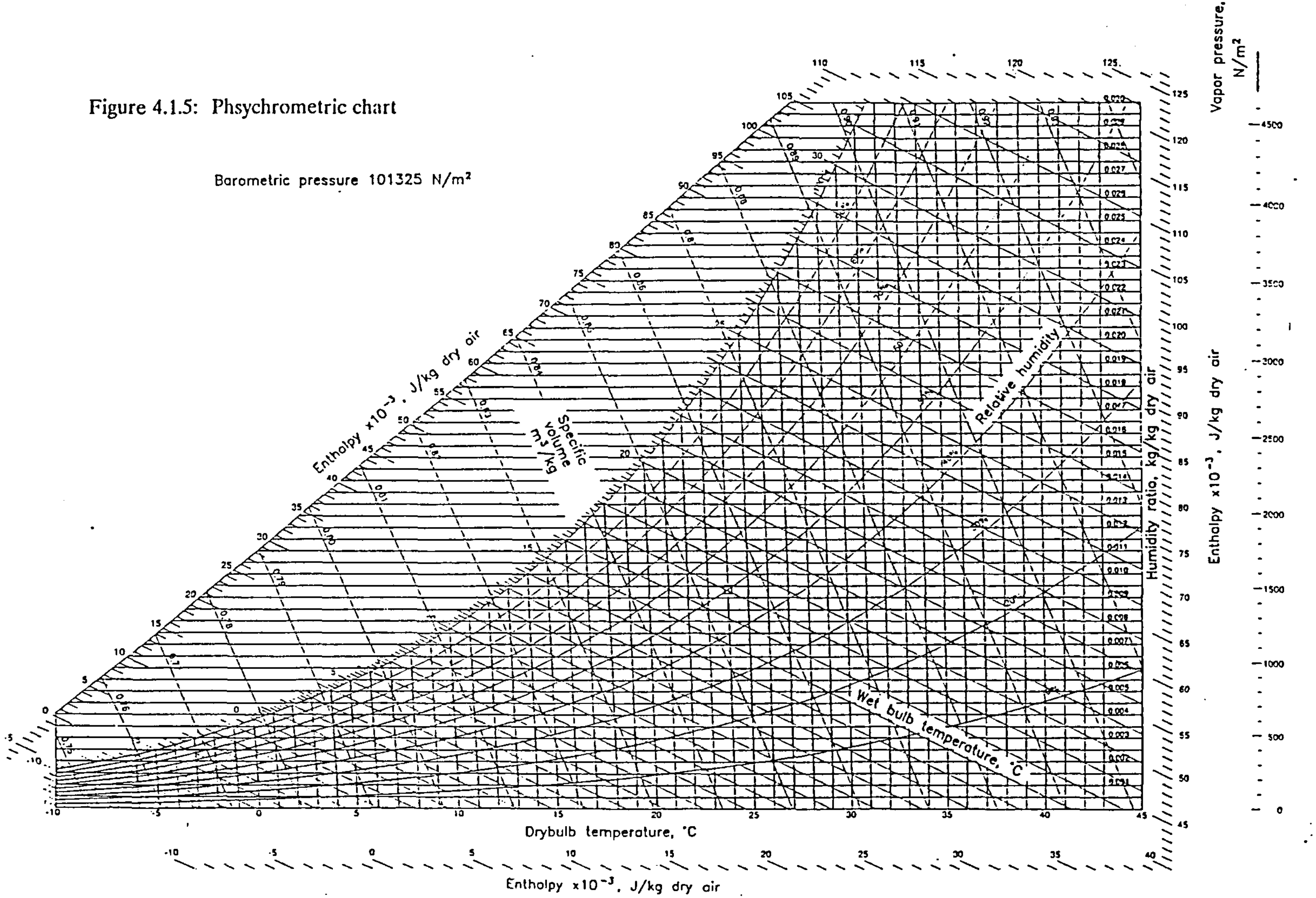

4.2 HEAT AND MASS TRANSFER IN WET-COOLING TOWERS

Consider an elementary control volume in the fill or packing of a counterflow wet-cooling tower as shown in figure 4.2.1. Evaporation of the downward flowing water occurs at the air-water interface where the air is saturated with water vapor. The vapor subsequently diffuses into the free stream air which has a lesser vapor concentration.

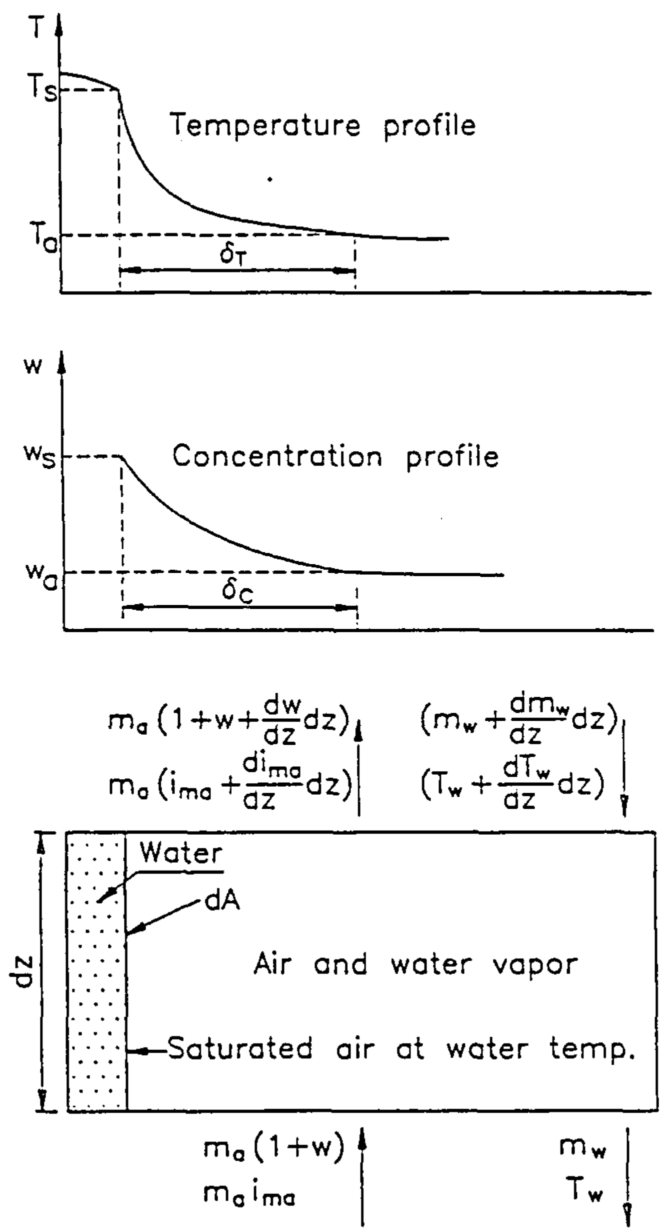

Figure 4.2.1: Control volume for derivation of governing equations for counterflow fill.

It will be assumed that the interface water temperature is essentially the same as the bulk water temperature. The effect of this assumption on the transfer process has been investigated by a number of researchers [61BA1, 88WE1, 91MA1]. Air and water properties at any horizontal cross-section are furthermore assumed to be constant and the area dA for heat and mass transfer is identical.

A mass balance for the control volume yields,

$$m_a\,(1 + w) + \left(m_w + \frac{dm_w}{dz}\,dz\right) = m_a\left[1 + \left(w + \frac{dw}{dz}dz\right)\right] + m_w$$

or

$$\frac{dm_w}{dz} = m_a\,\frac{dw}{dz} \qquad (4.2.1)$$

where m_a is the mass flow rate of the air constituent.

An energy balance for the control volume yields

$$m_a i_{ma} + \left(m_w + \frac{dm_w}{dz}\,dz\right) c_{pw}\left(T_w + \frac{dT_w}{dz}dz\right) = m_a\left(i_{ma} + \frac{di_{ma}}{dz}dz\right) + m_w c_{pw} T_w$$

(4.2.2)

where T_w is in °C.

Neglecting second order terms, equation (4.2.2) simplifies to

$$m_w\,c_{pw}\,\frac{dT_w}{dz} + c_{pw}\,T_w\,\frac{dm_w}{dz} = m_a\frac{di_{ma}}{dz} \qquad (4.2.3)$$

where i_{ma} refers to the enthalpy of the air-water vapor mixture per unit mass of dry air, which according to equation (A.3.6b) is expressed as

$$i_{ma} = c_{pa} T_a + w \left(i_{fgwo} + c_{pv} T_a \right) \tag{4.2.4}$$

and where i_{fgwo} is evaluated at 0°C and c_{pa} and c_{pv} at $T_a/2$°C.

Substitute equation (4.2.1) into equation (4.2.3) to find

$$\frac{dT_w}{dz} = \frac{m_a}{m_w} \left(\frac{1}{c_{pw}} \frac{di_{ma}}{dz} - T_w \frac{dw}{dz} \right) \tag{4.2.5}$$

The total enthalpy transfer at the air-water interface consists of an enthalpy transfer associated with the mass transfer and the heat transfer due to the difference in vapor concentration and temperature respectively.

Accordingly, one has

$$dQ = dQ_m + dQ_c \tag{4.2.6}$$

where the subscripts m and c refer to the enthalpies associated with mass transfer and convective heat transfer respectively. The enthalpy transfer associated with the mass transfer at the interface is expressed by

$$\frac{dm_w}{dz} dz = h_d \left(w_s - w \right) dA \tag{4.2.7}$$

where w_s is the saturation humidity ratio of air evaluated at the local bulk water temperature.

The corresponding enthalpy transfer is

$$dQ_m = i_v \frac{dm_w}{dz} dz = i_v h_d (w_s - w) dA \tag{4.2.8}$$

where h_d is the mass transfer coefficient. Furthermore, i_v is the enthalpy of the water vapor, which is given by

$$i_v = i_{fgwo} + c_{pv} T_w$$

where T_w is in °C and c_{pv} is evaluated at $T_w/2$ °C.

The convective transfer of sensible heat at the interface is given by

$$dQ_c = h(T_w - T_a)dA \tag{4.2.9}$$

The enthalpy of the saturated air evaluated at the local bulk water temperature is given by

$$i_{mas} = c_{pa} T_w + w_s (i_{fgwo} + c_{pv} T_w) = c_{pa} T_w + w_s i_v$$

which may be re-written as

$$i_{mas} = c_{pa} T_w + w i_v + (w_s - w) i_v \tag{4.2.10}$$

where c_{pa} is evaluated at $T_w/2$°C

Subtract equation (4.2.4) from equation (4.2.10). To simplify the analysis it is convenient to evaluate the specific heats c_{pa} and c_{pv} at $T_a/2$°C.

$$i_{mas} - i_{ma} = (c_{pa} + w\, c_{pv}) (T_w - T_a) + (w_s - w)\, i_v$$

or

$$T_w - T_a = \left[\left(i_{mas} - i_{ma}\right) - \left(w_s - w\right) i_v\right] / c_{pma} \tag{4.2.11}$$

where $c_{pma} = c_{pa} + w\, c_{pv}$.

Substitute equations (4.2.8), (4.2.9) and (4.2.11) into equation (4.2.6) to find upon re-arrangement.

$$dQ = h_d \left[\frac{h}{c_{pma} h_d} \left(i_{mas} - i_{ma} \right) + \left(1 - \frac{h}{c_{pma} h_d} \right) i_v \left(w_s - w \right) \right] dA \tag{4.2.12}$$

where $h/(c_{pma}\,h_d) = Le_f$, which is known as the Lewis factor, and is an indication of the relative rates of heat and mass transfer in an evaporative process. Bosnjakovic [65BO1] proposed the following equation to express the Lewis factor for air-water-vapor systems:

$$Le_f = 0.866^{0.667} \left(\frac{w_s + 0.622}{w + 0.622} - 1 \right) / \ln \left(\frac{w_s + 0.622}{w + 0.622} \right) \tag{4.2.13}$$

Noting that the enthalpy transfer must be equal to the enthalpy change of the air stream, one has from equation (4.2.12)

$$\frac{di_{ma}}{dz} = \frac{1}{m_a} \frac{dQ}{dz} = \frac{h_d\, a_{fi}\, A_{fr}}{m_a} \left[Le_f \left(i_{mas} - i_{ma} \right) + \left(1 - Le_f \right) i_v \left(w_s - w \right) \right] \tag{4.2.14}$$

for a one-dimensional model of the cooling tower fill, where the available area for heat and mass transfer is the same at any horizontal section through the fill. This area for a section dz deep, is given by

$$dA = a_{fi}\, A_{fr}\, dz$$

where a_{fi} is the wetted area divided by the corresponding volume of the fill (area density) and A_{fr} is the corresponding frontal area.

The heat and mass transfer in the fill of an evaporative cooling tower is governed by equations (4.2.1), (4.2.5), (4.2.7) and (4.2.14).

When the ambient humidity is high enough, the air becomes saturated with water vapor prior to its exit from the fill. In this case, the abovementioned equations fail to describe the evaporative process in the fill. Since the temperature of the saturated air at the interface is still higher than the temperature of the now saturated free stream air, a potential for heat and mass transfer will still exist. The excess water vapor transferred to the free stream air will condense as a mist.

Assume that the heat and mass transfer coefficients for the mist zone will be the same as those for unsaturated air as is proposed by Bourillot [83BO1] and Poppe and Rögener [91PO1]. The evaporation rate in the mist zone will depend on the difference in moisture content of the saturated air at the interface, that is at the local bulk water temperature, and the moisture content of the free stream air, thus

$$\frac{dm_w}{dz} = h_d\, a_{fi}\, A_{fr} \left[w_s - w_{sa}\right] \quad . \tag{4.2.15}$$

where w_{sa} is the humidity ratio of saturated air at temperature T_a.

Since the excess water vapor will condense, the enthalpy of supersaturated air is expressed by

$$i_{ss} = c_{pa}\, T_a + w_{sa}\, (i_{fgwo} + c_{pv}\, T_a) + (w - w_{sa}) c_{pw}\, T_a \tag{4.2.16}$$

Proceeding along the same lines as in the case of unsaturated air, find

$$\frac{di_{ma}}{dz} = \frac{h_d\, a_{fi} A_{fr}}{m_a}\left[Le_f(i_{mas} - i_{ma}) + (1 - Le_f) i_v (w_s - w_{sa}) + Le_f (w - w_{sa}) c_{pw} T_a\right] \tag{4.2.17}$$

In addition to the assumption stated earlier, Merkel [25ME1] assumes that the Lewis factor is equal to unity and that the evaporation loss is negligible. Introducing these two assumptions, the governing equations (4.2.14) and (4.2.5) simplify respectively to

$$\frac{di_{ma}}{dz} = \frac{h_d\, a_{fi}\, A_{fr}}{m_a}\left(i_{mas} - i_{ma}\right) \tag{4.2.18}$$

and

$$\frac{dT_w}{dz} = \frac{m_a}{m_w}\,\frac{1}{c_{pw}}\,\frac{di_{ma}}{dz} \tag{4.2.19}$$

With only the above equations, it is impossible to calculate the state of the air leaving the fill, since to achieve this at least two properties must be known. Hence, the exit air temperature, which is essential to calculate the air flow rate through a natural draft tower, is unknown. Merkel assumes that the air leaving the fill is saturated with water vapor, which enables him to determine the temperature and density of the air and the draft accordingly. In most practical cases, this assumption will yield reasonable results.

Traditionally, equations (4.2.18) and (4.2.19) are combined to yield upon integration

$$\frac{h_d\, a_{fi}\, A_{fr}\, L_{fi}}{m_w} = \frac{h_d a_{fi} L_{fi}}{G_w} = \int_{T_{wo}}^{T_{wi}} \frac{c_{pw}\, dT_w}{(i_{mas} - i_{ma})} \tag{4.2.20}$$

which is commonly referred to as Merkel's equation. The non-dimensional term $h_d a_{fi} L_{fi}/G_w$, is known as the Merkel number or transfer characteristic.

The implications of some of the approximations made in deducing equation (4.2.20) are evaluated by Lefevre [84LE1].

4.3 FILLS OR PACKS

Cooling tower fills or packs have been developed from the simple timber splash bar to the modern vacuum formed or injection molded plastic fills which are now in common use. Fills should be structurally strong, chemically inactive, fire resistant, resistant to fouling and erosion and have a low air flow resistance. A critical comparative study, the main objective of which is to identify the deficiencies of seven different plastic fill materials, is presented by Monjoie [94MO1]. Among others, properties concerning forming, assembly, fire, chemical, thermal, recycling and environmental impact are evaluated. Examples of some plastic fills are shown in figure 4.2.2. Further examples of fills are shown in figure 4.2.3. PVC can be used to a water temperature of about 50°C, CPVC up to 62°C while higher temperatures would require polypropylene or stainless steel [94BU1]. In some

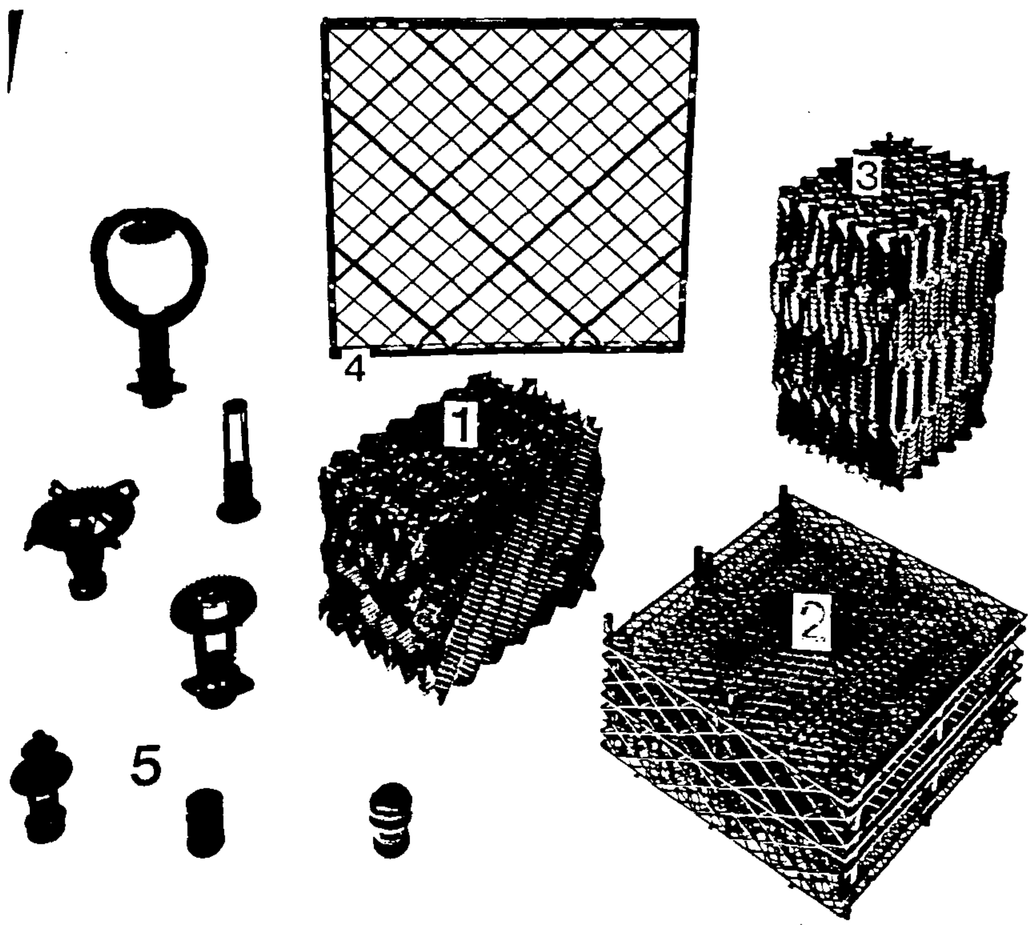

Figure 4.3.1: Plastic fills and spray nozzles; (1) and (3) film, (2) trickle grid, (4) splash, (5) spray nozzles.

applications fill materials that can be recycled may be preferred. Many of the deficiencies of plastic fills may be avoided by employing stainless steel fills.

Water is introduced via spray nozzles (a few examples are shown in figure 4.3.1) located above the fill. Nozzles should be designed and arranged in such a manner that they provide an even flow of water droplets above the fill. In a counterflow cooling tower approximately 15 percent of the cooling may actually occur in this region above the fill. The spray may be directed downwards or upwards. In the case of the latter the longer droplet residence time improves the transfer process in the spray zone. The spray produced by practical nozzles in cooling towers has a distribution of droplet sizes with an average droplet diameter of about 4 mm [74SC1]. The lightest drops (less than about 0.3 mm) are carried upwards by the air to the droplet eliminators where most are collected and returned downwards to the fill in the form of larger drops.

1. Splash fill

The splash type fill or pack is designed to break the mass of water falling through the cooling tower into a large number of drops, thus increasing the water surface area exposed to cooling air and, as a result, the amount of heat transferred to the surrounding air by conduction, convection, radiation and evaporation. As water falls through the fill, droplets collide with successive layers of splash bars which causes redistribution of water and heat due to the formation of fresh droplets. A further benefit is that the retention time of water falling through the tower is prolonged by contact with the fill which extends the period during which the water is exposed to cooling air. The disadvantage of splash fill is that by its very nature a large volume of fill material is required to break up the water flow, which in turn necessitates large towers. There is a natural tendency for free falling droplets to agglomerate, so splash bars are generally arranged in layers some 200 to 600 mm apart, frequently resulting in fill heights of perhaps 5 to 8 m in the largest towers.

The effectiveness of a particular splash type fill is governed by its ability to form droplets, but its efficiency also depends upon its air resistance and, to a lesser extent, on economical use of material. Treated timber is frequently used due to its easy availability, structural strength, relative cheapness and long working life under most conditions. Injection molded

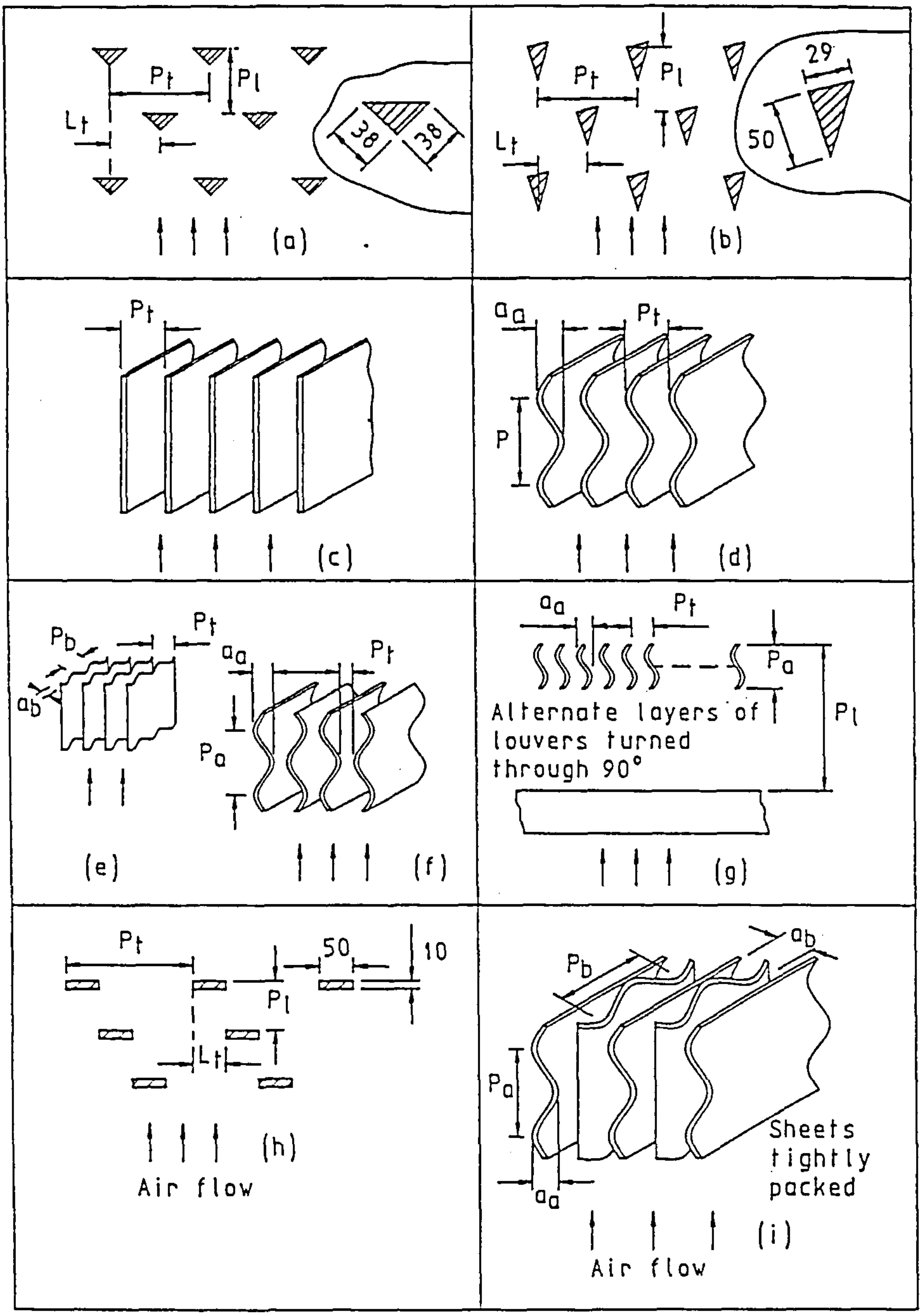

Figure 4.3.2: Fills. (a) (b) and (h), splash; (c) (d) (e) (f) (g) and (i), film [61LO1].

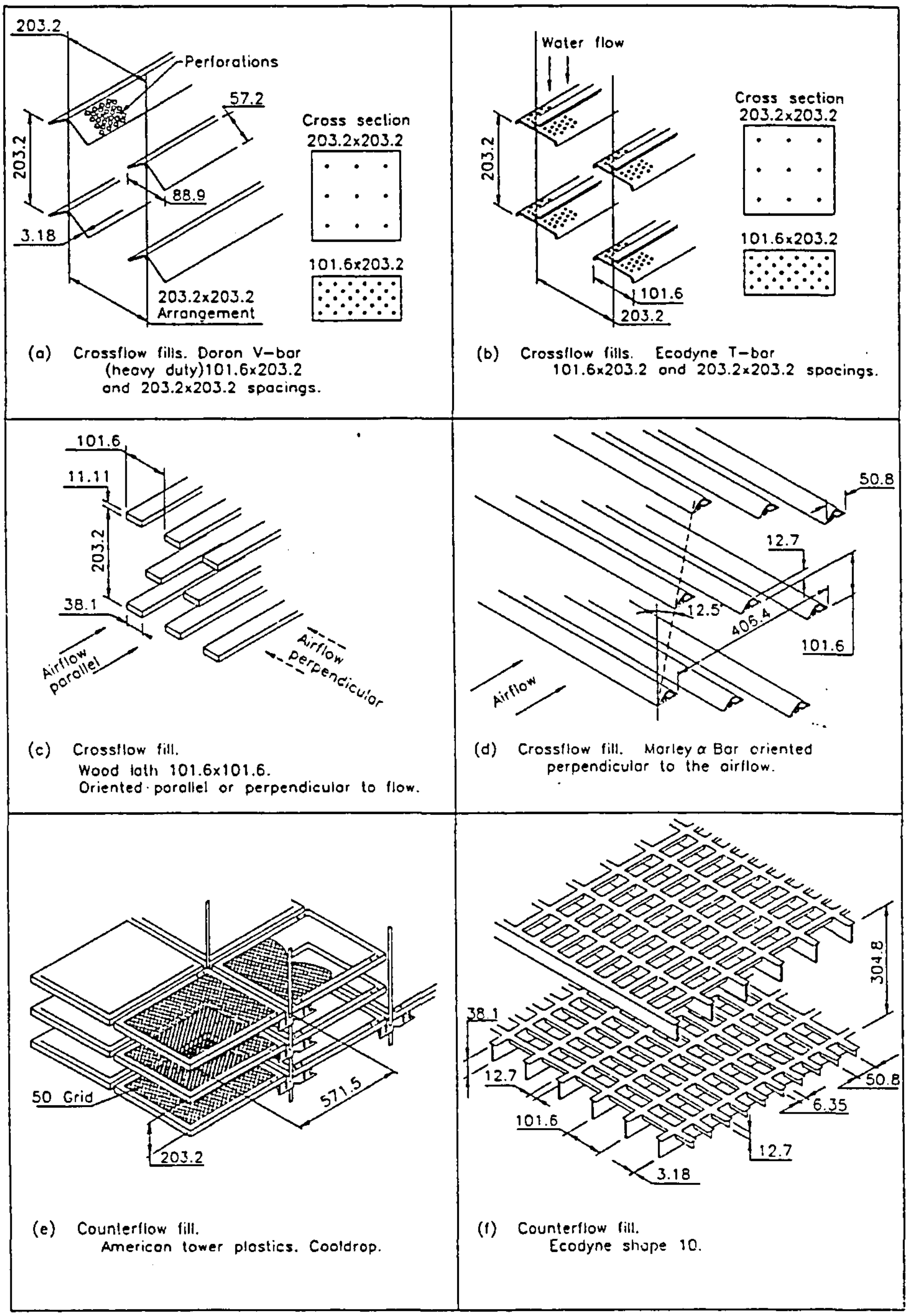

Figure 4.3.3 (a): Fills [89JO1].

plastic fills have been in service now for some years.

Splash fills tend to produce more carry-over than other types of fill particularly if high air rates are used. Efficient spray eliminators are employed to overcome this potential disadvantage. However, the increased air resistance of the complete tower demands additional draft or fan capacity and consequently an increase in running costs.

The inherent disadvantages of splash fills have created a demand for the development of film type fills which are more compact and hence generally preferred. The latter require less material and water pumping power due to the lower fill height.

2. Trickle grid

Trickle grids are much finer than splash packs and are made up of fine plastic or metal grids onto which the water is sprayed. It subsequently runs down the grid rather than splashing. This type of fill has been introduced over recent years with the considerable advances in plastic injection molding which have taken place. Because of the much finer mesh than the splash type fill, they tend to clog more easily and have a greater pressure drop.

3. Film fill

Film fills differ from splash fills in that although the purpose is again to produce a large water surface area, this is not achieved by the formation of droplets but by allowing the water to spread itself thinly over a large area of fill. This difference largely eliminates the problem of carry-over of water droplets into the atmosphere and allows higher air velocities to be used.

Fill types may be placed in several categories, the simplest of which is the timber grid. This consists of a series of closely spaced slats placed in tightly packed layers, each layer at right angles to the previous layer. This arrangement provides good water distribution over a large area but air resistance is high. Thin timber sections have low structural strength and limited resistance to chemical attack and distortion. Corrugated or flat asbestos sheeting was frequently used in the past while resin impregnated cardboard, metal

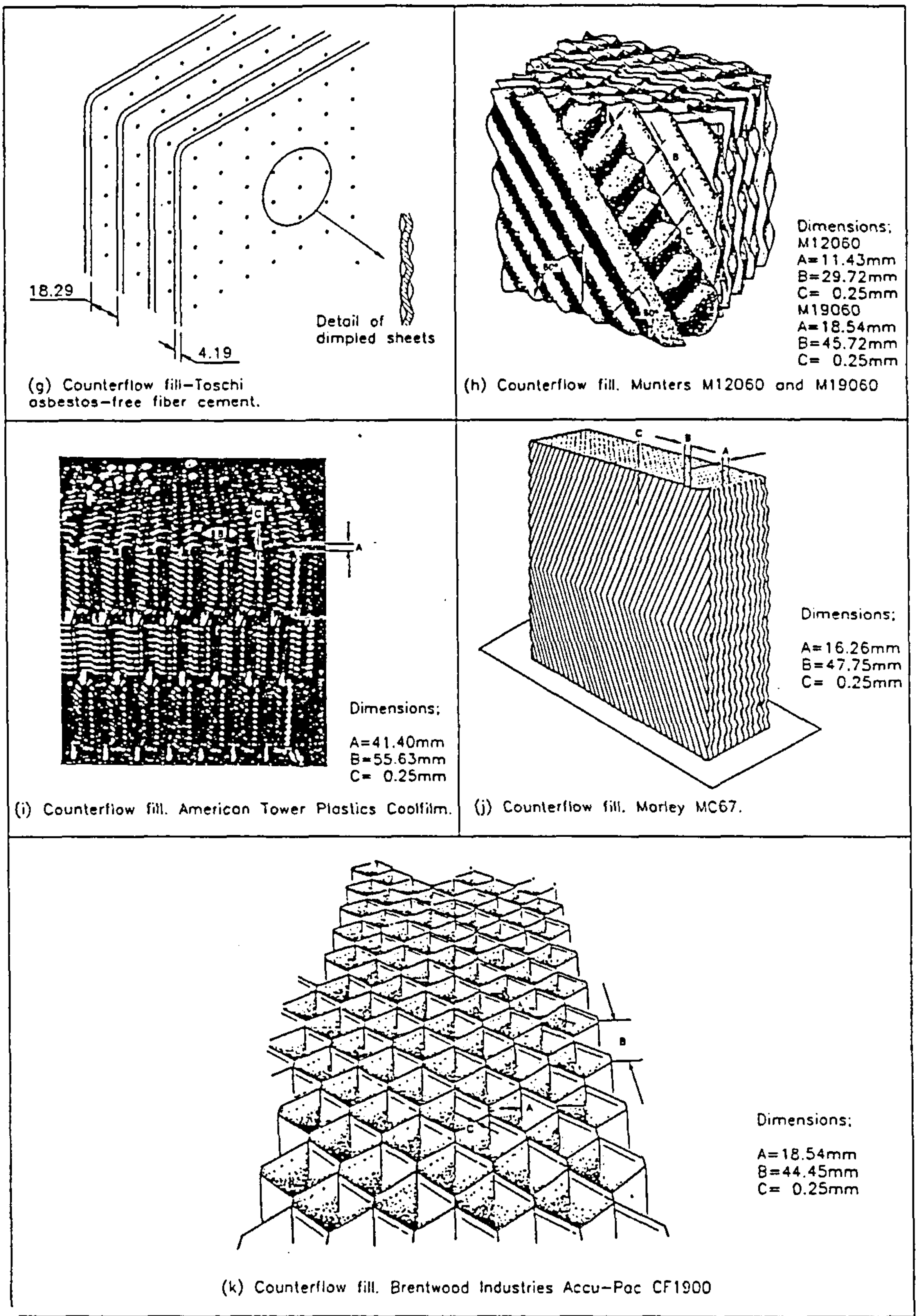

Figure 4.3.3 (b): Fills [89JO1].

and particularly the more effective plastics are preferred presently.

A theoretical examination [56KE1] suggests that a fill consisting of a series of close parallel vertical film surfaces would give good transfer with low pressure drop. Various manufacturers have designed packs along these lines but found that in practice they were not reliable due to a tendency towards uneven water distribution which considerably reduces heat transfer effectiveness..Fouling is more of a problem in this fill than in the splash type.

4. Extended film fills

Although problems were encountered with early thermo-plastic film type fills these difficulties have been largely overcome and there are now a wide variety of pressed or vacuum formed fills available. These vary considerably in design but generally have high transfer characteristics, low weight, acceptable strength and adequate durability. The problems of water and air distribution have been reduced by the development of geometrical designs which incorporate interconnected channels and secondary profiles. Both these features improve water and air distribution and encourage greater mixing of the layer of saturated air which forms adjacent to the water layer and the bulk of air travelling through the fill, thus further improving transfer.

A large variety of proprietary cooling tower fills are produced by commercial manufacturers. The results of studies on the performance characteristics of fills have been reported in the literature [61LO1, 67CO1, 76KE1, 82CA1, 88FU1, 89JO1]. Some of the more recent studies [89JO1] have critically evaluated test facilities and methods of data evaluation. Thermal and pressure drop data obtained in one facility does not always agree with that obtained in another facility. Distorted flow patterns, test facility edge effects, influences due to the type of spray nozzle and spray or rain zone [88FU1], different test temperatures and pressures, changes in fill wetting patterns (the degree of wetting of the fill surface may change with time) and errors in measurement are some of the reasons for these discrepancies. In large modern test facilities where the cross-section of the fill is up to 7m x 7m, these problems can be greatly reduced [88FA1]. It is also important to elaborate on the method employed in evaluating the test data i.e. Merkel, Poppe or other. Where the Merkel method is employed it is convenient to present the transfer and pressure drop characteristics per meter of fill height respectively as follows:

$$h_{d1}\, a_{fi}\, A_{fr}/m_{wm} = h_{d1}\, a_{fi} / G_{wm} = a_d \left(G_{wm}/G_{avm}\right)^{-b_d} \tag{4.3.1}$$

and

$$K_{fi1} = a_p \left(G_{wm}/G_{avm}\right) + b_p \quad . \tag{4.3.2}$$

where mean mass flow rates through the fill are given by $G_{wm} = m_{wm}/A_{fr}$ and $G_{avm} = m_{avm}/A_{fr}$. The subscript refers to one meter height of the fill. In most fill performance characteristics presented in the literature, G_{wm} and G_{avm} are not rigorously defined. This may lead to errors especially when evaluating the draft equation in the case of a natural draft wet-cooling tower.

Other forms for approximating the above characteristics empirically are as follows:

$$h_{d1}\, a_{fi} / G_{wm} = a_d\, G_{wm}^{b_d}\, G_{avm}^{c_d} \tag{4.3.3}$$

or

$$h_{d1}\, a_{fi} / G_{wm} = a_d \left(G_{wm}/G_{avm}\right)^{-b_d} L_{fi}^{c_d} \tag{4.3.4}$$

and

$$K_{fi1} = a_p\, G_{wm}^{b_{pa}}\, G_{avm}^{b_{pb}} \tag{4.3.5}$$

where the values of a_d, a_p, b_d and b_p are determined experimentally in each case.

These relatively simple correlations can obviously not take into consideration all variables with the result that there is usually considerable scatter of test data and this may lead to correspondingly less reliable cooling system designs. Ideally fill performance tests for a particular cooling tower should thus be conducted under conditions similar to those specified for the tower design operating point.

The performance characteristics of a few fills are listed in table 4.3.1 [61LO1]. A more

Table 4.3.1: Data for counterflow fills (Merkel's theory) [61LO1].

Mass transfer per meter of fill height $h_{d1}\, a_{fi}/G_{wm} = a_d\, (G_{wm}/G_{avm})^{-b_d}$

Loss coefficient per meter of fill height $K_{fi1} = a_p\, (G_{wm}/G_{avm}) + b_p$

Fill type	Description	Fig. no. 4.3.2	Dimensions				Mass Transfer		Pressure	
			a_a m	P_a m	P_t m	P_l m	a_d	b_d	a_p	b_p
1	Triangular splash bar	a	Staggered		0.1524	0.2286	0.2950	0.50	2.62	5.00
2	Triangular splash bar	a	Staggered		0.1524	0.1524	0.3084	0.50	2.73	9.15
3	Triangular splash bar	a	Staggered		0.1524	Altern 0.1270 0.3302	0.3150	0.45	1.57	4.5
4	Triangular splash bar	a	Staggered		0.1524	0.3048	0.246	0.42	1.89	3.0
5	Triangular splash bar	a	Staggered		0.1143	0.4572	0.236	0.47	2.16	3.75
6	Flat asbestos sheets	c			0.0444		0.2887	0.70	0.725	1.37
7	Flat asbestos sheets	c			0.0381		0.361	0.72	0.936	1.30

Fill type	Description	Fig. no. 4.3.2	Dimensions				Mass Transfer		Pressure	
			a_a m	P_a m	P_t m	P_l m	a_d	b_d	a_p	b_p
8	Flat asbestos sheets	c			0.0318		0.394	0.76	0.77	1.70
9	Flat asbestos sheets	c			0.0254		0.459	0.73	0.89	1.70
10	Triangular splash bar (Bar upside down)	a	Staggered		0.1524	0.2286	0.276	0.49	4.15	6.35
11	Corrugated asbestos sheets	d	0.054	0.1461	0.0445		0.69	0.69	1.93	7.80
12	Corrugated asbestos sheets	d	0.054	0.1461	0.03175		0.72	0.61	3.61	8.10
13	Corrugated asbestos sheets	d	0.054	0.1461	0.0572		0.59	0.68	1.39	1.50
14	Corrugated asbestos sheets	e	a_b = 0.054	P_b = 0.1461	0.0445		0.36	0.66	1.93	0.44

Fill type	Description	Fig. no. 4.3.2	Dimensions				Mass Transfer		Pressure	
			a_a m	P_a m	P_t m	P_l m	a_d	b_d	a_p	b_p
15	Corrugated asbestos sheets	f	0.054	0.1461	0.0254		0.56	0.58	1.74	12.4
16	Triangular splash bar	b	In line		0.1016	0.2032	0.24	0.52	2.51	0.35
17	Triangular splash bar	b	Staggered		0.1016	0.2032	0.29	0.55	2.18	1.55
18	Triangular splash bar	b	Staggered		0.1016	0.2540	0.26	0.58	1.69	1.45
19	Triangular splash bar	b	In line		0.1016	0.2540	0.24	0.54	1.61	1.45
20	Triangular splash bar	b	Staggered		0.1016	0.1950	0.31	0.53	2.35	1.50
21	Triangular splash bar	b	Staggered		0.1016	0.1524	0.32	0.54	2.32	2.80
22	Triangular splash bar	b	Staggered		0.1270	0.2032	0.31	0.46	2.10	1.30
23	Triangular splash bar	b	Staggered		0.0508	0.1524	0.61	0.65	4.08	11.0
24	Triangular splash bar	b	Staggered		0.1270	0.1905	0.31	0.49	2.59	1.00

	Description	Fig. no. 4.3.2	Dimensions				Mass Transfer		Pressure	
			a_a m	P_a m	P_t m	P_l m	a_d	b_d	a_p	b_p
25	Triangular splash bar	b	Staggered		0.1524	0.1905	0.29	0.47	2.64	0.60
26	Asbestos louvers	g	0.0254	0.1461	0.0254	0.2731	0.67	0.70	1.08	7.55
27	Asbestos louvers	g	0.0254	0.1461	0.0254	0.1715	0.94	0.68	2.78	12.0
28	Asbestos louvers	g	0.0254	0.1461	0.0254	0.5271	0.39	0.69	1.06	4.30
29	Asbestos louvers	g	0.0254	0.1461	0.0254	0.4001	0.51	0.67	1.41	5.05
30	Abestos louvers	g	0.0381	0.1334	0.0254	0.1588	1.15	0.66	3.71	25.0
31	Asbestos louvers	g	0.0381	0.1334	0.0381	0.1588	0.81	0.66	4.04	17.6
32	Asbestos louvers	g	0.0381	0.1334	0.0381	0.3874	0.55	0.65	2.55	11.5
33	Asbestos louvers	g	0.0381	0.1334	0.0381	0.5144	0.33	0.63	2.22	6.20
34	Rectangular splash bar	h	L_t = 0.05		0.2032	0.2286	0.28	0.52	2.08	5.40

Fill type	Description	Fig. no. 4.3.2	Dimensions				Mass Transfer		Pressure	
			a_a m	P_a m	P_t m	P_l m	a_d	b_d	a_p	b_p
35	Rectangular splash bar	h	L_t = 0.05		0.2032	0.3048	0.26	0.53	1.90	3.40
			Corrugations horizontal		Corrugations vertical					
36	Corrugated asbestos sheets	i	0.0540	0.1461	a_b = 0.0540	P_b = 0.1461	0.61	0.73	1.82	9.70
37	Corrugated asbestos sheets	i	0.0270	0.0730	0.0270	0.0730	1.01	0.80	2.75	24.6
38	Corrugated asbestos sheets	i	0.0270	0.0730	0.0540	0.1461	0.68	0.79	1.90	8.0

Fill type	Description	Fig. no. 4.3.2	Dimensions				Mass Transfer		Pressure	
			a_a m	P_a m	a_b m	P_b m	a_d	b_d	a_p	b_p
39	Corrugated asbestos sheets	i	0.0540	0.1461	0.0270	0.0730	0.81	0.79	3.18	31.2
40	Corrugated asbestos sheets	i	0.0603	0.1778	0.0603	0.1778	0.53	0.71	2.71	10.8
41	Corrugated asbestos sheets	i	0.0270	0.0730	0.2220	0.0746	0.44	0.72	2.60	3.60

Table 4.3.2 (a): Data for crossflow fills (Merkel's theory) [89JO1].

Mass transfer per meter of air travel distance (ATD) in fill $h_{d1}a_{fi}/G_{wm} = a_d(G_{wm}/G_{avm})^{-b_d}$ where ATD = air travel distance Loss coefficient per meter of air travel distance (ATD) in fill $K_{fi1} = a_p G_{wm}^{b_{pa}} G_{avm}^{b_{pb}}$									
Fig 4.3.3	Description, spacing [mm]	Airflow orientation	Fill configuration	Size(s) tested, HxWxATD [m]	a_d	b_d	a_p	b_{pa}	b_{pb}
a	Doron V-bar, 101.6x203.2	Parallel	Staggered	3.658x2.438x1.829 3.658x2.438x2.438	0.268	0.56	0.751	0.66	-0.73
a	Doron V-bar, 203.2x203.2	Parallel	In-line	3.658x2.438x1.829 3.658x2.438x2.438	0.239	0.38	0.985	0.72	-0.82
b	Ecodyne T-bar, 101.6x203.2	Parallel	Staggered	3.658x2.438x1.829 3.658x2.438x2.438	0.263	0.34	0.112	1.30	-0.22
b	Ecodyne T-bar, 203.2x203.2	Parallel	In-line	3.658x2.438x1.829 3.658x2.438x2.438	0.245	0.35	0.206	0.89	-0.069
c	Wood lath, 101.6x101.6	Parallel	Staggered	3.658x2.438x1.829 3.658x2.438x2.438	0.274	0.45	1.437	0.76	-0.80

Fig 4.3.3	Description, spacing [mm]	Airflow orientation	Fill con-figuration	Size(s) tested, HxWxATD [m]	a_d	b_d	a_p	b_{pa}	b_{pb}
c	Wood lath, 101.6x101.6	Perpendicular	Staggered	3.658x2.438x1.829 3.658x2.438x2.438	0.358	0.57	1.828	0.71	-0.59
d	Marley Alpha-bar, 101.6x406.4	Perpendicular	Staggered	3.658x2.438x1.829 3.658x2.438x2.438	0.307	0.052	1.816	0.71	-0.85

Table 4.3.2 (b): Data for counterflow fills (Merkel's theory) [89JO1].

Mass transfer per meter of fill height $h_d a_{fi}/G_{wm} = a_d(G_{wm}/G_{avm})^{b_{da}} ATD^{b_{db}}$ where ATD = air travel distance Loss coefficient per meter of fill height $K_{fi} = a_p(G_{wm})^{b_{pa}}(G_{avm})^{b_{pb}} ATD^{b_{pc}}$									
Fig 4.3.3	Description	Size(s) tested, H,W,ATD [m]	a_d	b_{da}	b_{db}	a_p	b_{pa}	b_{pb}	b_{pc}
e	American Tower Plastics Cool Drop	HxW=2.438x2.438 ATD=2.0,2.8 and 3.4	0.710	-0.42	-0.50	2.880	0.85	-0.600	0.17
f	Ecodyne Shape10	HxW=2.438x2.438 ATD=1.829,2.438 and 3.353	0.605	-0.35	-0.42	1.103	1.10	-0.640	0.32
g	Toshi Fiber Cement (Dimpled and Unslotted)	HxW=2.438x2.438 ATD=1.22,1.62 and 2.03	1.169	-0.64	-0.51	0.621	0.99	-0.350	0.17

Fig 4.3.3	Description	Size(s) tested, H,W,ATD [m]	a_d	b_{da}	b_{db}	a_p	b_{pa}	b_{pb}	b_{pc}
h	Munters 12060	HxW=2.438x2.438 ATD=0.609,0.914 and 1.524	2.490	-0.67	-0.062	15.845	0.34	-0.19	0.017
h	Munters 19060	HxW=2.438x2.438 ATD=0.914,1.524 and 2.134	1.597	-0.59	-0.19	6.875	0.31	-0.048	0.014
i	American Tower Plastics Cool Film	HxW=2.438x2.438 ATD=1.0,1.5 and 2.0	2.138	-0.56	-0.38	7.821	0.23	-0.039	0.038
j	Marley MC67	HxW=2.438x2.438 ATD=0.914,1.219 and 1.524	1.495	-0.63	-0.35	7.089	0.27	-0.140	0.005
k	Brentwood Ind Accu-Pak CF1900	HxW=2.438x2.438 ATD=0.914,1.524 and 2.134	1.664	-0.62	-0.27	3.691	0.31	-0.099	0.45

recent publication on counterflow and crossflow fill performance data is presented by Johnson et al. [89JO1]. Four methods or codes for determining the transfer coefficients were evaluated i.e. FACTS [83BE1], TEFERI [83BO1, 83BO2], VERA 2D [83MA1] and ESC [57ZI1, 84BA1]. They note that the value of the mass transfer coefficient calculated by these methods varied as much as ten percent from each other and stress the importance of using the same method to predict cooing tower performance as was used to derive the characteristics of a particular fill. The complete data listing of the calculated mass transfer coefficients, the resulting correlations and the confidence limits associated with the correlations, and the statistical summary of the capability of the codes to predict large scale cooling tower performance are provided. Some of the results are listed in tables 4.3.2 (a) and 4.3.2 (b). Dreyer [94DR1] presents a mathematical model with which the performance characteristics of splash fill material can be predicted and lists extensive experimental performance data.

Combinations of different types of fill may be installed in a particular cooling tower to achieve a desired performance or to enhance the performance and reduce fouling in an existing tower [94PH1].

Fouling of fills due to biological growths such as algae and bacteria, transported colloidal materials in the recirculating water, airborne dirt or particles, silt or suspended solids in the make-up water and scaling due to dissolved materials carried in solution can significantly reduce the performance of the fill when installed in a cooling tower [94AU1, 94CO1, 94GI1, 94MO1, 94NE1, 94PU1]. Certain fills tend to be more susceptible to fouling than others.

When selecting a particular fill for a cooling system it is very important not only to consider its initial performance characteristics and cost but also its long term structural, performance and fouling characteristics since they can have significant cost implications on plant performance or output.

4.4 EFFECTIVENESS - NTU METHOD APPLIED TO EVAPORATIVE SYSTEM

Jaber and Webb [87JA1] developed the equations necessary to apply the effectiveness - NTU method directly to counterflow or crossflow wet-cooling towers. The approach is particularly useful in the latter case and simplifies the method of solution when compared to a more conventional numerical procedure.

Consider the equation for heat transfer in an evaporative process as given by equation (4.2.12) which may be written as

$$dQ = h_d\left[Le_f(i_{mas} - i_{ma}) + (1 - Le_f)i_v(w_s - w)\right]dA \tag{4.4.1}$$

With the assumption of Merkel that the Lewis factor is equal to unity, equation (4.4.1) reduces to

$$dQ = h_d(i_{mas} - i_{ma})dA \tag{4.4.2}$$

where $(i_{mas} - i_{ma})$ is the enthalpy driving potential used by the effectiveness - NTU method in the case of evaporative cooling.

It follows from equations (4.2.14) and (4.2.19) that for the control volume shown in figure 4.2.1

$$dQ = m_w c_{pw} dT_w = m_a di_{ma} \tag{4.4.3}$$

It is convenient to relate dQ to the slope of the saturated air enthalpy-temperature, T_w, curve. Equation (4.4.3) is thus written as

$$dQ = m_w c_{pw} di_{mas}/(di_{mas}/dT_w) = m_a di_{ma} \tag{4.4.4}$$

from which it follows that

$$di_{mas} = dQ(di_{mas}/dT_w)/(m_w c_{pw}) \tag{4.4.5}$$

With $di_{ma} = dQ/m_a$ from equation (4.4.3) and writing $(di_{mas} - di_{ma}) = d(i_{mas} - i_{ma})$ one obtains

$$d(i_{mas} - i_{ma}) = dQ\left[(di_{mas}/dT_w)/(m_w c_{pw}) - 1/m_a\right] \tag{4.4.6}$$

From equations (4.4.6) and (4.4.2) it follows that

$$\frac{d(i_{mas} - i_{ma})}{(i_{mas} - i_{ma})} = h_d\left(\frac{(di_{mas}/dT_w)}{m_w c_{pw}} - \frac{1}{m_a}\right)dA \tag{4.4.7}$$

This equation which is applicable in an evaporative system, will correspond to heat exchanger design equation (3.5.4) if one defines the air capacity rate (cold fluid) as m_a and the water capacity rate (hot fluid) as $m_w c_{pw}/(di_{mas}/dT_w)$.

The maximum theoretical amount of heat that can be transferred, is Q_{max} = (minimum capacity rate) $(i_{masi} - i_{mai})$, where i_{masi} is the saturated air enthalpy at the water inlet condition and i_{mai} denotes air inlet enthalpy.

There are two possible cases to be considered:

Case 1: $m_w c_{pw}/(di_{mas}/dT_w) < m_a$

where consistent with heat exchanger design terminology $C_{emin} = m_w c_{pw}/(di_{mas}/dTw)$ and $C_{emax} = m_a$ and the evaporative capacity rate ratio for this particular case is given by

$$C_e = C_{emin}/C_{emax} = m_w c_{pw}/\left[(di_{mas}/dT_w)m_a\right]$$

Substitute C_e into equation (4.4.7) to find

$$\frac{d(i_{mas}-i_{ma})}{(i_{mas}-i_{ma})} = \frac{h_d(di_{mas}/dT_w)(1-C_e)dA}{m_w c_{pw}} \tag{4.4.8}$$

The analogous definition for NTU in this particular evaporative system or wet-cooling tower is

$$NTU_e = h_d A(di_{mas}/dT_w)/(m_w c_{pw}) \tag{4.4.9}$$

where A is the total wetted transfer area.

The heat exchange effectiveness is defined as

$$e_e = Q/Q_{max} \tag{4.4.10}$$

where

$$Q_{max} = m_w c_{pw}(i_{masi} - i_{mai})/(di_{mas}/dT_w) \tag{4.4.11}$$

Integrating equation (4.4.8) between the entering and leaving air states, i_{ai} and i_{ao} respectively and substituting equation (4.4.9), gives

$$(i_{maso} - i_{mai})/(i_{masi} - i_{mao}) = \exp[-NTU_e(1 - C_e)] \tag{4.4.12}$$

where i_{maso} refers to saturated air enthalpy at water outlet condition.

Integration of equation (4.4.3) between inlet and outlet conditions gives

$$Q = m_w c_{pw}(T_{wi} - T_{wo}) = m_a(i_{mao} - i_{mai}) \tag{4.4.13}$$

The gradient of the saturated air enthalpy-temperature T_w curve over the control volume, is

$$\frac{di_{mas}}{dT_w} = \frac{i_{masi} - i_{maso}}{T_{wi} - T_{wo}} \tag{4.4.14}$$

It follows from equations (4.4.10), (4.4.11), (4.4.13) and (4.4.14) that

$$e_e = (i_{masi} - i_{maso})/(i_{masi} - i_{mai}) \tag{4.4.15}$$

and from equations (4.4.10), (4.4.11) and (4.4.13) that

$$C_e e_e = (i_{mao} - i_{mai})/(i_{masi} - i_{mai}) \tag{4.4.16}$$

From equations (4.4.15) and (4.4.16) it follows that

$$\frac{e_e - 1}{e_e C_e - 1} = \frac{i_{maso} - i_{mai}}{i_{masi} - i_{mao}} \tag{4.4.17}$$

Equating equations (4.4.12) and (4.4.17) gives the effectiveness - NTU equation for a counterflow evaporative system or cooling tower

$$e_e = \frac{1 - \exp[-NTU_e(1 - C_e)]}{1 - C_e\exp[-NTU_e(1 - C_e)]} \tag{4.4.18}$$

which is similar to the effectiveness - NTU expression for a counterflow heat exchanger.

Case 2: $m_a < m_w c_{pw} / (di_{mas}/dT_w)$

In this case

$$C_e = m_a (di_{mas}/dT_w)/(m_w c_{pw})$$

Keeping in mind that the direction of the minimum fluid has reversed and following the same procedure as in Case 1, again obtain equation (4.4.18).

The effectiveness - NTU method is subject to approximations involved in linearizing the i_{mas} versus T_w curve as a straight line. The accuracy of the method can be increased by breaking up the design into a number of increments.

An analytical method was developed by Berman [61BE1] to improve the approximation of the i_{mas} versus T_w curve as a straight line. He proposed a correction factor λ given by

$$\lambda = (i_{maso} + i_{masi} - 2i_{mas}) / 4 \tag{4.4.19}$$

where i_{mas} denotes the enthalpy of the saturated air at the mean water temperature $T_{wm} = (T_{wi} + T_{wo})/2$.

This factor is used to correct Q_{max} as follows:

$$Q_{max} = C_{emin}(i_{masi} - \lambda - i_{mai}) \tag{4.4.20}$$

The use of the correction factor essentially gives a two-increment design.

The effectiveness - NTU equations described above show that the effectiveness - NTU equations for a counterflow heat exchanger can be applied directly to a counterflow cooling tower.

Similarly, the equations for a crossflow heat exchanger can be applied to a crossflow cooling tower. Jaber and Webb [87JA1] recommend the use of the unmixed/unmixed effectiveness - NTU equation as listed in tabel 3.5.1.

4.5 EVAPORATIVE COOLER

In a so-called evaporative cooler, an example of which is shown in figure 1.3.1, cooling of a process fluid flowing in tubes is achieved by spraying water onto the tubes essentially deluging them and forming a film of water which flow downwards under the action of gravity. As the water flows down the surface of the tube, it is evaporated by air flowing over it, resulting in cooling of the process fluid.

One of the earliest useful analytical treatments of close circuit evaporative coolers was due to Parker and Treybal [61PA1]. The method was derived before low cost computing facilities were generally available and used Merkel's approximation for the heat-mass transfer process. One of the most significant features of this work is that the recirculating water temperature was not assumed constant and it was therefore the first solution which described the variation of this temperature as the water ran over the tubes. In addition the enthalpy of the saturated air was assumed to be a linear function of temperature, making it possible to integrate the simultaneous differential equations over the height of the coil.

Mizushina and Miyashita [68MI1] using a similar approach to Parker and Treybal integrated their equations numerically using a computer. At the same time the above two authors [67MI1] carried out some useful experiments to determine the applicable heat and mass transfer coefficients in a smooth tube bundle with triangular spacing.

Perez-Blanco and Bird [82PE1] did an analysis on the performance of a rather idealized vertical counterflow evaporative cooling unit, but used the correct thermodynamic equations without any approximations.

Kreid et al [78KR1] presented an approximate method of analyzing deluged heat exchangers with fins using an effective overall heat transfer coefficient based on log mean enthalpy difference. They practically demonstrated the method to predict heat transfer rates within 5 per cent of the actual values.

Leidenfrost and Korenic [79LE1, 82LE1] presented a rigorous analysis of finned tube evaporative condensers which could be applied to cross- or counterflow devices and did not make use of Merkel's approximation of a Lewis factor of unity. Their analysis can even accommodate partially dry heat exchangers. They proposed the use of a stepwise integration process using a graphic method originally derived by Bosnjakovic [60BO1] to determine the exit state of the air and water leaving an element which amounts to a computerization of that method.

Some useful software was developed by Webb [84WE1] to approximate the performance of various types of evaporative cooling devices using a unified approach for the air side. It is stated that the prediction accuracy is in the order of 3 per cent of the manufacturer's data on several devices. However, the evaporative cooler program is limited to vertical counterflow equipment. Erens and Dreyer [88ER1] present a general approach to the performance evaluation of evaporative coolers based on the methods of Poppe [91PO1] and Bourillot [83BO1].

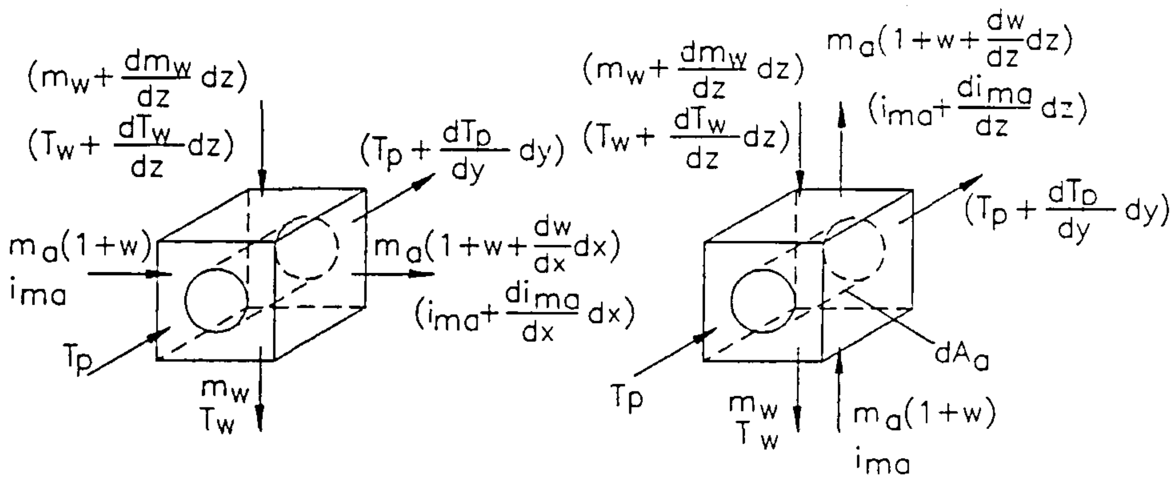

(a) Crossflow (b) Counterflow

Figure 4.5.1: Control volume of tube evaporative cooler.

Consider an elementary control volume of a tube evaporative cooler as shown in figure 4.5.1.(b). Water is sprayed over the tubes to deluge them and then falls down through an upwards flowing air stream. A waterfilm forms on the smooth or finned tube outside surface. In order to derive the governing equations for the evaporative cooler, the following assumptions are made.

1. The waterfilm throughout the cooler is at a constant mean film temperature. Since the deluge water is recirculated, its inlet temperature is equal to its outlet temperature, often with a relatively small deviation in temperature as it flows through the tube bank or bundle [67MI1]. In certain cases this assumption is however not acceptable [74FI1].

2. The air/water interface area is approximately the same as the outer surface area of the tube bundle, i.e. the waterfilm on the tubes is very thin such that the area exposed to the air stream dA_a is essentially the same as outside surface area of the tubes.

3. The deluge water is evenly distributed between the different tube rows and the outside tube surface area is totally wetted.

4. The Lewis factor is equal to unity and the evaporation loss is negligible.

Following the same procedure as in section 4.2, the governing equations for the evaporative cooler are:

$$di_{ma} = h_d \left(i_{mas} - i_{ma}\right) dA_a/m_a \tag{4.5.1}$$

$$dT_w = -\left(m_a di_{ma} + m_p c_{pp} dT_p\right)/(m_w c_{pw}) \tag{4.5.2}$$

Equation (4.5.1) corresponds to equation (4.2.18) and equation (4.5.2) to equation (4.2.19).

For the evaporative cooler a third variable, the process fluid temperature T_p is present and therefore a third governing equation is necessary.

$$dT_p = -U_a \left(T_p - T_w\right) dA_a/(m_p c_{pp}) \tag{4.5.3}$$

U_a is the overall heat transfer coefficient between the process fluid inside the tubes and the deluge water film on the outside.

$$U_a = \left[\frac{1}{h_w e_f} + \frac{A_a}{A_p h_p} + \sum_n \frac{A_a}{A_n} R_n \right]^{-1} \tag{4.5.4}$$

In this equation h_w is the heat transfer coefficient between the waterfilm and the tube outer surface while h_p is the heat transfer coefficient on the inside of the tube. R_n includes all other resistances (tube wall, fouling, contact resistance if the outer surface is finned, etc.) between the waterfilm and the process fluid whereas e_f is the effectiveness of a finned surface.

By making the assumption that the deluge water film has a constant mean temperature, T_{wm}, throughout the cooler, equation (4.5.2) is eliminated.

Integrate equation (4.5.1) between i_{ai} an i_{ao}

$$i_{mao} = i_{masm} - (i_{masm} - i_{mai}) \exp(-NTU_a) \tag{4.5.5}$$

where

$$NTU_a = A_a h_d / m_a$$

Similarly equation (4.5.3) can be integrated between the inlet and outlet process fluid temperatures to give

$$T_{po} = T_{wm} + (T_{pi} - T_{wm}) \exp(-NTU_p) \tag{4.5.6}$$

where

$$NTU_p = A_a U_a / (m_p c_{pp})$$

The heat transfer rate of the evaporative cooler is given by the following equation

$$Q = m_a(i_{mao} - i_{mai}) = m_p c_{pp} (T_{pi} - T_{po}) \tag{4.5.7}$$

Substitute equations (4.5.5) and (4.5.6) into equation (4.5.7) and simplify

$$m_a\left[i_{masm} - (i_{masm} - i_{ai}) \exp(-NTU_a) - i_{mai}\right]$$

$$= m_p c_{pp}\left[T_{pi} - T_{wm} - (T_{pi} - T_{wm}) \exp(-NTU_p)\right]$$

or

$$T_{wm} = T_{pi} - \frac{m_a (i_{masm} - i_{mai}) [1 - \exp(-NTU_a)]}{m_p c_{pp} [1 - \exp(-NTU_p)]} \tag{4.5.8}$$

From equation (4.5.8) the mean deluge water film temperature can be determined iteratively. The outlet conditions can be determined from equations (4.5.5) and (4.5.6). The outlet air is assumed to be saturated with water vapor.

Numerous correlations for the mass transfer coefficient, h_d, between the cooling water flowing downwards over banks of horizontal tubes and the upwards flowing air stream are found in the literature.

Parker and Treybal [61PA1] tested tube banks consisting of 19mm outside tubes arranged on a $2d_o$ triangular pitch and found

$$h_d = 0.04935\left[(1 + w)(m_a/A_c)\right]^{0.905} \approx 0.04935(m_{avm}/A_c)^{0.905} \tag{4.5.9}$$

where A_c is the minimum cross-sectional air flow area between the tubes. The air mass velocity was in the range of $0.68 < (m_{avm}/A_c) < 5$.

Mitzushina et al. [67MI1] tested bundles having 12 - 40mm outside diameter tubes arranged on a $2d_o$ triangular pitch and found

$$h_d = 5.5439 \times 10^{-8}\, Re_{avm}^{0.9}\, Re_{wm}^{0.15}\, d_o^{-1.6} \tag{4.5.10}$$

This equation is valid for $1.2 \times 10^3 < Re_{avm} = m_{av}d_o/(A_c\mu_a) < 1.4 \times 10^4$ and $50 < Re_{wm} = m_{wm}d_o/(A_c\mu_{wm}) = 4\,\Gamma_m/\mu_{wm} < 240$. The deluge water mass flow rate per unit length over one half of a cooling tube can in general be expressed as $\Gamma_m = m_{wm}d_o/(2Afr)$.

Nitsu et al. [69NI1] tested banks of both plain and finned tubes and found that above a critical Γ_m/d_o value of 0.7, the mass-transfer coefficient was in all cases independent of water flowrate. The correlations obtained were for:

1. Plain tubes, 16mm outside diameter with $P_\ell/d_o = 2.38$ and $P_t/d_o = 2.34$

$$h_d = 0.076(m_{avm}/A_c)^{0.8} \tag{4.5.11}$$

for $1.5 \le (m_{avm}/A_c) \le 5$

2. Finned (42.6mm fin diameter) tubes having a 16mm outside diameter and arranged with $P_\ell/d_o = 2.38$ and $P_t/d_o = 2.34$ and $1.5 < (m_{avm}/A_c) < 5$.

$$h_d = 0.0135(m_{avm}/A_c)^{1.25} \tag{4.5.12}$$

for a fin spacing of 11mm

$$h_d = 0.0112(m_{avm}/A_c)^{1.25} \tag{4.5.13}$$

for a fin spacing of 6.1mm.

Dreyer and Erens [90DR1] studied a crossflow evaporative cooler having 38.1mm outside diameter tubes arranged in a $2d_o$ mm triangular pattern. Based on the Merkel method of analysis they find

$$h_d = 5.5749 \times 10^{-5}\, Re_{avm}^{0.64}\, Re_{wm}^{0.2} \tag{4.5.14}$$

for $2500 < Re_{avm} = m_{avm}d_o/(\rho_{av}\mu_{avm}A_c) < 13500$ and $230 < Re_{wm} = 4\Gamma_m/\mu_{wm} <$

1100.

Various correlations are also found in the literature with which the heat transfer coefficient between the waterfilm and the tube outer surface can be determined.

Parker and Treybal [61PA1] give the following expression for this coefficient on the outside of smooth tubes:

$$h_w = 704\ (1.3936 + 0.02214\ T_{wm})\ (\Gamma_m/d_o)^{0.333} \tag{4.5.15}$$

where T_{wm} is in °C.

This equation is valid for water in the temperature range 15°C to 70°C and is based on data obtained on tubes having an outside diameter of 19mm and an equilateral $2d_o$ pitching. Γ_m/d_o values covered, were from 1.4 to 3kg/m^{2}s and the maximum air Reynolds number $(m_{avm}d_o/A_c\mu_{avm})$ was approximately 5000.

According to Mitzushina et al. [67MI1].

$$h_w = 2102.9(\Gamma_m/d_o)^{0.333} \tag{4.5.16}$$

This expression is valid for $0.2 < (\Gamma_m/d_o) < 5.5$ kg/m^{2}s and airside Reynolds numbers in the range 1500 to 8000. Tube diameters varied from 12.7mm to 40mm arranged on a $2d_o$ equilateral pitching.

Leidenfrost and Korenic [82LE1] obtained a similar equation namely

$$h_w = 2064(\Gamma_m/d_o)^{0.252} \tag{4.5.17}$$

for a bank of in-line tubes having a 15.9mm outside diameter and with $P_t/d_o = 2$ and $P_\ell/d_o = 2.4$ in the range $2 < \Gamma_m/d_o < 5.6$.

For staggered banks of plain tubes having a 16mm outside diameter, Nitsu et al. [69NI1] obtained the correlation

$$h_w = 990(\Gamma_m/d_o)^{0.46} \tag{4.5.18}$$

for $P_t/d_o = 2.34$, $P_\ell/d_o = 2.38$ and $0.5 < (\Gamma_m/d_o) < 3.2$.

For banks of finned tubes having a tube diameter of 16mm, a fin diameter of 42.6mm, and fin spacings of 6.1 and 11mm, the correlation

$$h_w = 430(\Gamma_m/d_o)^{0.4} \tag{4.5.19}$$

was obtained for $0.5 < \Gamma_m/d_o < 3.2$.

Dreyer and Erens [90DR1] find the following correlation for crossflow conditions:

$$h_w = 2843(\Gamma_m/d_o)^{0.384} \tag{4.5.20}$$

in the range $0.038889 < \Gamma_m < 0.180556$. This equation is applicable to smooth tubes having an outside diameter of 38.1mm.

It should be stressed that the above correlations were evaluated by following a particular analytical evaluation procedure in each case. Thus when employing the correlations to design an evaporative cooler the same method of analysis should preferably be followed and the cooler geometry and operating conditions should ideally be close to those of the test equipment for which the correlation was obtained.

When designing an evaporative cooler it is important that the desired air flow rate through the tube bundle be achieved. Airside pressure loss information is required for this purpose.

A comprehensive study of the airside pressure loss in both plain and finned tube evaporative coolers is reported by Nitsu et al. [69NI1] and Tezuka et al. [77TE1]. Data obtained over a range of air and water flowrates showed that pressure loss dependence on water flowrate was weak. Generally the water loading Γ_m/d_o should not be less than 0.8

kg/m^2s through plain tubes to ensure a good distribution.

The data obtained by Nitsu et al. [69NI1] are correlated by the following equations:

1. Plain tube banks where $2 \leq (m_{avm}/A_c) \leq 6$ and $1.3 \leq \Gamma_m/d_o \leq 3.5$.

$$\Delta p = 4.9 n_r P_\ell (m_{avm}/A_c)^{1.85} (\Gamma_m/d_o)^{0.285} \tag{4.5.21}$$

2. Finned (fin diameter 42.6mm) tube banks where $2 \leq (m_{avm}/A_c) \leq 6$ and $0.16 \leq \Gamma_m/d_o \leq 1.8$

$$\Delta p = 11\, n_r P_\ell (m_{avm}/A_c)^{1.94} (\Gamma_m/d_o)^{0.12} \tag{4.5.22}$$

for a fin pitch of 6.1mm.

$$\Delta p = 7.1\, n_r P_\ell (m_{avm}/A_c)^{1.94} (\Gamma_m/d_o)^{0.12} \tag{4.5.23}$$

for a fin pitch of 11mm.

For smooth tubes in crossflow Dreyer and Erens [90DR1] find

$$\Delta p = 1.5482 \times 10^{-4} \Delta p_a/(a + 9.25 \times 10^{-5}) - 0.32773 \tag{4.5.24}$$

where

$a = m_{wm}/[(m_{avm} + m_{wm}\rho_{avm}/\rho_{wm})Re_{avm}]$ and $Re_{avm} = (m_{avm} + m_{wm})d_o/(\mu_{avm}A_c)$, for $2.15 \times 10^{-5} < a < 19 \times 10^{-5}$, $0.0278 < \Gamma_m < 0.175$ and $0.85 < m_{avm}/A_{fr} < 2.5$. Furthermore, Δp_a is the pressure drop as determined for only air flowing through the bank at a rate of $(m_{avm} + m_{wm})$.

4.6 RAIN ZONE

In any detailed analysis of the performance characteristics of a wet counterflow cooling tower, the transfer processes in the spray or rain zone may not be ignored. Earlier studies considered the transfer processes in the rain zone to be relatively unimportant or too complex to analyze. Rish [61RI1] was one of the first to include the rain zone in his comprehensive analysis of counterflow cooling towers. He ignores variations in drop sizes in the spray or rain regions above and below the fill.

Lowe and Christie [61LO1] derive the mass transfer and pressure drop for counterflow conditions, assuming that no drop collisions or agglomeration occur. Their data is applicable to small drops only, where the drops fall at their terminal velocity in the major part of the flow field. In most real towers, large drops may not even attain their terminal velocity prior to reaching the pond.

With the aid of modern computers it is attempted to solve the momentum and energy equations for air-drop flows numerically [83MA1, 86BE1, 86BE2]. These methods are essentially two-dimensional, and describe the interaction between the air (continuous phase) and the drops (dispersed phase) but neglect the effect of the drops on the turbulence modelling. Benton and Rehberg [86BE2] conducted a numerical investigation of the rain zone. Their results are restricted to either counterflow or pure crossflow conditions. The rain zone of a natural draft counterflow tower is however essentially a combination of the two.

Numerical methods tend to be relatively expensive and time consuming. The equation of Rish [61RI1], on the other hand, is simple to understand and use, but lacks generality. The following analysis by Hoffmann and Kröger [90HO1] is a compromise between the above extremes.

To analyze the flow pattern and the processes in the rain zone of a wet cooling tower, consider the inlet section of a circular natural draft tower as shown in figure 4.6.1. In the absence of cross-winds, the flow in the inlet section is essentially axially symmetrical, and the problem is reduced to two dimensions in a cylindrical polar coordinates set.

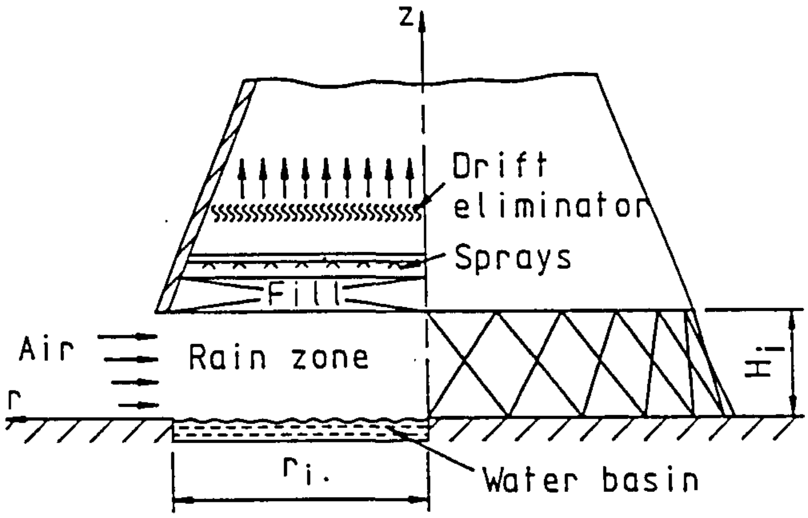

Figure 4.6.1: Schematic presentation of inlet section of counter-flow cooling tower.

If the resistance to air flow in the fill is high enough, or if the fill thickness is varied, such that the flow through the fill may be assumed to be approximately uniform, the following boundary conditions are applicable.

$v_z(r,0)$ = 0; impervious surface
$v_r(0,z)$ = 0; tower axis is line of symmetry
$v_z(r,H_i)$ = constant; flow through fill is uniform

If one assumes radial inflow of ambient air at the inlet, a fourth boundary condition is obtained.

$$v_z(r_i,z) = 0$$

In practice this can only be achieved approximately with a well rounded inlet to the tower and in the absence of inclined louvers and support struts.

The equation of continuity for steady, axi-symmetric, incompressible flow in a set of polar coordinates is

$$\frac{\partial v_r}{\partial r} + \frac{v_r}{r} + \frac{\partial v_z}{\partial z} = 0 \tag{4.6.1}$$

If one defines a potential function $\phi(r,z)$, the radial and axial velocity vectors may be expressed respectively by

$$v_r = -\partial\phi/\partial r \tag{4.6.2a}$$

and

$$v_z = -\partial\phi/\partial z \tag{4.6.2b}$$

Equation (4.6.1) may be written in terms of the potential function ϕ and solved by the method of separation of variables. The solution of this equation, with the set of boundary conditions provided, is

$$\phi(r,z) = \sum_{n=1}^{\infty} \frac{-2v_{zi}}{\lambda_n^2 r_i} \frac{J_0(\lambda_n r)}{J_1(\lambda_n r_i)} \frac{\cosh(\lambda_n z)}{\sinh(\lambda_n H_i)} \tag{4.6.3}$$

with the eigenvalues λ_n such that $(\lambda_n r_i)$ are the roots of $J_0(\lambda r_i) = 0$

An example of the resultant vector diagram of the potential flow field for a particular cooling tower [90HO1], is shown in figure 4.6.2. It is noted that in the major part of the flow field, the two components of the velocity vectors (axial and radial) can be predicted approximately by a simple linear model. The only significant deviation from this simplified model exists in the vicinity of the lower edge of the tower shell. Compared to the entire flow field, this region is however relatively small.

Thus, for all practical purposes

$$v_r = a_r r \tag{4.6.4a}$$

and

$$v_z = a_z z \quad (4.6.4b)$$

where a_r and a_z are constants.

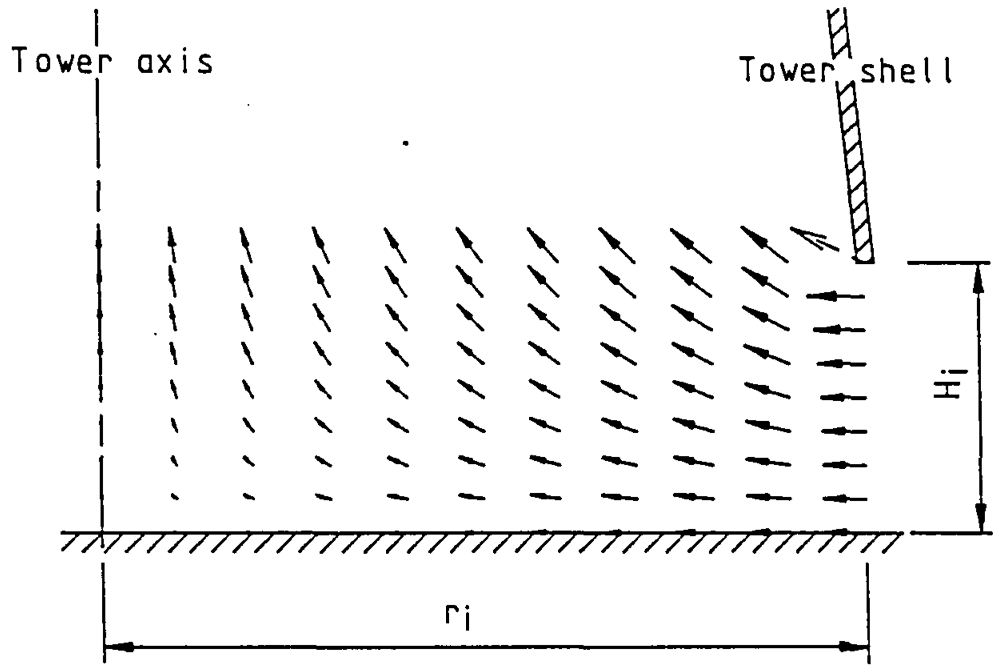

Figure 4.6.2: Velocity vectors for irrotational inlet flow to cooling tower.

The drag coefficient for drops is lower than that for rigid spheres due to internal circulation and drop deformation. Furthermore, the internal circulation tends to enhance the heat and mass transfer processed by increasing the mixing in the dispersed phase. For this analysis, it is assumed that the drops in the rain zone are essentially spherical and furthermore their diameters do not change in view of the relatively small evaporation rate. It is also assumed that no drop agglomeration will occur.

For spherical drops, equation (2.5.4) by Crowe et al [77CR1] gives the drag coefficient:

$$C_D = 24\left(1 + 0.15\ Re^{0.687}\right)/Re \quad (4.6.5)$$

for Reynolds numbers up to 1000.

The radial and axial components of the drag force on a single drop are respectively

$$F_{D,r} = C_D A_d \rho_a \left(v_r - v_{d,r}\right)^2/2 \tag{4.6.6a}$$

and

$$F_{D,z} = C_D A_d \rho_a \left(v_z - v_{d,z}\right)^2/2 \tag{4.6.6b}$$

where A_d is the cross-sectional area of the drop.

With these values it can be shown that the corresponding forces on an elementary annular control volume in the rain zone are·

$$dF_r = \frac{3 \pi C_D \rho_a G_w}{2 \rho_w d_d v_{d,z}} \left(v_r - v_{d,r}\right)^2 r \, dr \, dz \tag{4.6.7a}$$

in the radial direction and

$$dF_z = \frac{3 \pi C_D \rho_a G_w}{2 \rho_w d_d v_{d,z}} \left(v_z - v_{d,z}\right)^2 r \, dr \, dz \tag{4.6.7b}$$

in the axial direction. G_w is the water mass flow rate per unit area through the fill.

Upon integration of equation (4.6.7), the rain zone pressure loss coefficient based on the frontal area of the fill is found to be

$$K_{rz} = 2 \left[\left(\frac{F_r}{\pi d_i H_i} \right)^2 + \left(\frac{4 F_z}{\pi d_i^2} \right)^2 \right]^{0.5} / \left(\rho_a v_z^2 \left(r, H_i\right) \right) \tag{4.6.8}$$

According to the above relation, the pressure drop across the rain zone is dependent on certain independent variables, i.e.

$$\Delta p = f\left(d_d, d_i, H_i, \rho_a, \rho_w, \mu_a, v, v_w\right)$$

If μ_a is approximately constant, i.e. when the air temperature T_a does not change significantly, find upon application of a dimensional analysis

$$\Delta p = f\left[d_r, \left(d_i/H_i\right), \left(G_w/G_a\right)\right]$$

where the ratio $d_r = d_d/d_c$. G_a is the air mass flow rate per unit area through the fill.

In the above equation, the drop diameter is non-dimensionalized by introducing the critical drop falling in air. According to Clift et al [78CL1] the critical drop diameter is

$$d_c = \left[16\ \sigma_w/\left\{g\left(\rho_w - \rho_a\right)\right\}\right]^{0.5} \quad . \tag{4.6.9}$$

At an arbitrarily chosen reference temperature of 20°C the critical drop diameter is 10.92mm. Larger drops will break up into one large drop, containing about 75 per cent of the original drop mass, and a number of smaller droplets. This phenomenon coincides with a Reynolds number of approximately 1000.

An empirical correlation for the rain zone pressure loss coefficient based upon these dimensionless groups, is given by

$$K_{rz} = \left[3.1724 - 0.1643\left(d_i/H_i\right) + 0.007004\left(d_i/H_i\right)^2\right]\left(G_w/G_a\right)/d_r^{1.2} \tag{4.6.10}$$

for $10 \le (d_i/H_i) \le 15$. Equation (4.6.10) is accurate within 4 per cent in the range of $0°C \le T_a \le 40°C$ if μ_a is evaluated at 20°C.

Frössling [38FR1] proposed a semi-empirical correlation for the mass transfer coefficient for a single spherical water droplet falling in an air stream i.e.

$$Sh = h_D\ d_d/D = 2 + 0.552\ Re^{0.5}\ Sc^{0.33} \tag{4.6.11}$$

for $2 \le Re \le 800$. D is the diffusion coefficient for water vapor in air. The Schmidt number, Sc is defined as ν_a/D.

According to Poppe [84PO1], the relation between the mass transfer coefficients h_d and h_D as given by equation (4.1.20) is

$$h_d = \left(h_D p / R_v T\right) \ln\left[\left(w_s + 0.622\right)/\left(w + 0.622\right)\right] / \left(w_s - w\right) \tag{4.6.12}$$

The evaporation rate from a single drop is

$$\dot{m}_d = h_d A_d \left(w_s - w\right) = h_d \pi d_d^2 \left(w_s - w\right) \tag{4.6.13}$$

The mass transfer for the elementary annular control volume in the rain zone is

$$dm_{cv} = \sum_{j=1}^{n_{cv}} dm_d \tag{4.6.14}$$

where n_{cv} refers the number of droplets in the control volume.

On the assumption of a uniform drop diameter equal to the mass drop diameter, equation (4.6.14) becomes

$$dm_{cv} = n_{cv}\, dm_d \tag{4.6.15}$$

Equation (4.6.15) may be integrated to obtain the mass transfer for the rain zone. The mean mass transfer coefficient for the rain zone is

$$h_{drz}\, a_{rz} = \frac{1}{H_i r_i} \int_0^{H_i} \int_0^{r_i} h_d\, n_{cv}\, A_d \tag{4.6.16}$$

where a_{rz} is the surface area of the drops divided by the corresponding volume of the rain zone (area density). It is normal practice to write the mass transfer coefficient and the area density as a product since it is usually very difficult to determine the area density of a complex fill geometry.

It follows from equation (4.6.11) through (4.6.16) that the mean mass transfer coefficient is dependent on the following independent variables

$$h_{drz}\, a_{rz} = f\left(d_d, d_i, H_i, v, v_w, \rho_a, \rho_w, \mu_a, D\right)$$

If the variation in the air temperature is not too large, the viscosity, μ_a, and the diffusion coefficient, D, is approximately constant.

Upon application of a dimensional analysis, find

$$h_{drz}\, a_{rz} = f\left[d_r, \left(d_i/H_i\right), \left(G_a/G_w\right)\right]$$

where the ratio $d_r = d_d/d_c$.

This coefficient, which is referred to the frontal area of the fill, can be expressed by the following empirical relation in terms of the appropriate dimensionless groups.

$$h_{drz}\, a_{rz} = \left[5.81684 \times 10^{-3}/d_r^2 + 6.04223 \times 10^{-4}\left(d_i/H_i\right)\right]\left(G_w/G_a\right) \tag{4.6.17}$$

An accuracy of 2 percent in the range of $0°C \leq T_a \leq 40°C$ is achieved if μ_a and D are evaluated at 20°C.

A more detailed expression for the transfer coefficient in the rain zone of a round cooling tower is given by Conradie [93CO1].

$$\frac{h_{drz}a_{rz}H_i}{\rho_{ai}v_{ao}} = 3.15\left(\frac{H_i}{d_d}\right)^{1.64}\left(\frac{\rho_{ai}v_{ao}H_i}{\mu_{ai}}\right)^{2.244}\left(\frac{d_i}{H_i v_{ao}}\right)^{2.764}\left(\frac{p_a}{\rho_{ai}v_{ao}^2}\right)^{1.483}$$

$$\left(\frac{v_{wo}}{v_{ao}}\right)\exp\left[\frac{\left\{\ln\left(gH_i/v_{ao}^2\right)-8.222\right\}^2}{26.626}\right]\left(\frac{v_{ao}^2}{R_v T_{wo}}\right)^{1.497}\left[0.205 + 0.00131\left(\frac{d_i}{H_i}\right) + \right.$$

$$\left. 0.0699w_o - 0.191w_i - 1.3 \times 10^{-5}\left(\frac{\rho_{wo}}{\rho_{ai}}\right) + 0.188\left(\frac{\sigma_{wo}}{H_i\rho_{ai}v_{ao}^2}\right)\right] \tag{4.6.18}$$

where v_{ao} is the air velocity based on the frontal area of the fill. The subscript o refers to conditions at the outlet of the rain zone or inlet to the fill. Equation (4.6.18) is applicable in the range 80 m $\leq d_i \leq$ 120 m, 4m $\leq H_i \leq$ 12m, 0.00075 m/s $\leq v_w \leq$ 0.003 m/s, 1 m/s $\leq v_a \leq$ 3 m/s.

For a rectangular cooling tower the following expression is recommended:

$$\frac{h_{drz} a_{rz} H_i}{\rho_{ai} v_{ao}} = 340.76 \times 1.007^{(W_i/H_i)} \left(\frac{\rho_{ai} v_{ao} H_i}{\mu_{ai}} \right)^{0.359} \left(\frac{d_i}{H_i v_{ao}} \right)^{1.0986}$$

$$\left(\frac{p_a}{\rho_{ai} v_{ao}^2} \right) 0.409^{w_o} 0.365^{w_i} (0.9996)^{(\rho_{wo}/\rho_{ai})} \left(\frac{v_{wo}}{v_{ao}} \right) \left(\frac{v_{ao}^2}{R_v T_{wo}} \right)^{0.95} \left(\frac{H_i \rho_{ai} v_{ao}^2}{\sigma_{wo}} \right)^{0.165}$$

$$\exp\left[0.01835536 \left\{ \ell n \left(gH_i/v_{ao}^2 \right) - 13.46 \right\}^2 + 0.1208605 \left\{ \ell n \left(d_d/H_i \right) - 0.0324 \right\}^2 \right] \tag{4.6.19}$$

where W_i is the inlet distance from the symmetry line to the outer edge of the heat exchanger platform. This equation is applicable in the range 4 m $\leq W_i \leq$ 40 m, 2m $\leq H_i \leq$ 8 m, 0.001 m/s $\leq v_{wo} \leq$ 0.006 m/s, 1 m/s $\leq v_{ao} \leq$ 7.5 m/s.

Equations (4.6.18) and (4.6.19) are furthermore limited to the following temperature ranges:

$0°C \leq T_{ai} \leq 40°C$
$0°C \leq T_{wb} \leq 22°C$
$0°C \leq T_{wo} \leq 40°C$

No attempt is made to determine the statistical distribution of drop sizes in the rain zone, but drop sizes ranging from 3 mm to 8 mm are frequently encountered [76YA1, 86BE2, 86MI1]. The pressure loss and mass transfer coefficients given by equations (4.6.10) and (4.6.17) respectively, will only yield information regarding the mass mean drop diameter. A mean drop diameter of 5 mm yields results that agree well with the data of Rish

[86RI1], and is recommended if no further information on the drop size is available. It should however be stressed that this mean drop diameter is not necessarily physically meaningful except in cases where the drop sizes are quite uniform. In most rain zones a wide spectrum of drop sizes are present. Reliable rain zone performance characteristics for a given fill can in practice only be obtained by tests performed in large facilities.

4.7 DRIFT ELIMINATORS

In the use of wet-cooling towers for heat rejection, drift or mist refers to the small droplets of circulating water that are carried out of the cooling tower by the saturated exhaust air. The droplets usually contain chemicals and other impurities that pollute the environment. Inertial impaction separators, known as drift or droplet eliminators or separators, are employed to remove the water droplets from the warm exhaust air, thereby conserving water and corrosion and algae control chemicals.

In this type of separator, the two-phase exhaust flow is forced to abruptly change direction. This causes the dense drift droplets to hit the eliminator walls and become trapped inside the cooling tower.

Drift eliminators have evolved from the early single-pass wood lathe to multiple-pass wood and then to sinusoidal-wave shapes. These were followed by combinations of sinusoidal and honeycomb shapes, as reported by Holmberg [74HO1]. Currently, various styles of cellular drift eliminator packs are constructed from thermoformed sheets of polyvinylchloride (PVC) an example of which is shown in figure 4.7.1.

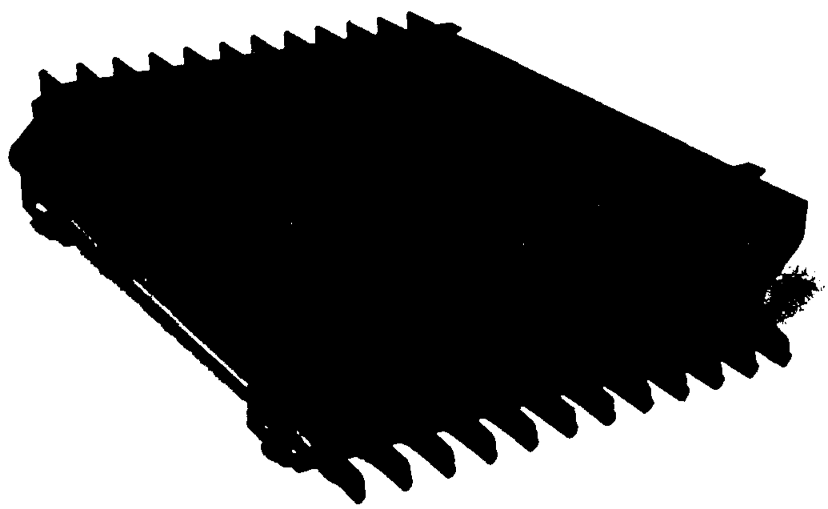

Figure 4.7.1: Drift eliminator.

The performance of these drift eliminators is measured by primarily two criteria: droplet collection efficiency and pressure loss.

Chilton [52CH1] constructed an apparatus to test different counterflow fill and eliminator schemes for resistance to air flow and drift elimination. Foster et al. [74FO1] theoretically and experimentally investigated the variation in collection efficiency with drop size for two types of eliminators. Chan and Golay [76CH1] developed a numerical model to calculate the collection efficiency for various droplet sizes using different eliminator geometries. They also compared the results of their numerical model to results obtained in laboratory model tests [77CH1]. Yao and Schrock [76YA2] devised a numerical technique for optimizing the aerodynamic design of counterflow drift eliminators. Becker and Burdick [92BE1, 93BE1, 94BE1] investigated the characteristics of two styles of commercially available crossflow cooling tower drift eliminators (types T and Z) and stress the importance of considering not only the measured pressure losses as shown in figure 4.7.2, but also the interaction of the drift eliminators with the flow pattern through the entire system especially in the case of a mechanical draft unit where the flow approach to the fan is affected.

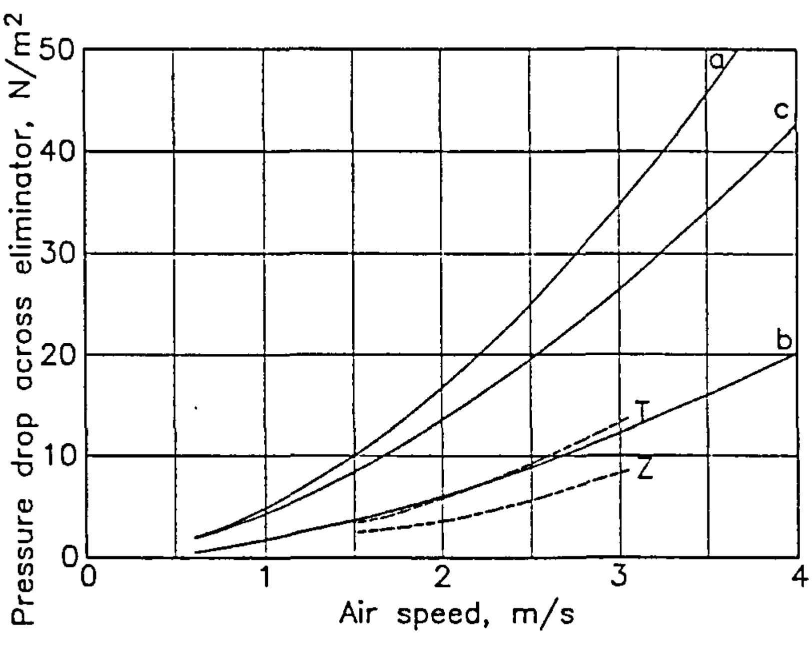

Figure 4.7.2: Comparison of pressure drop across eliminator packs.

The pressure drop across three other (a, b and c) commercially available eliminators including the type shown in figure 4.7.1 are also shown in figure 4.7.2. The pressure drop results for these three eliminators are also presented in terms of a loss coefficient in figure 4.7.3.

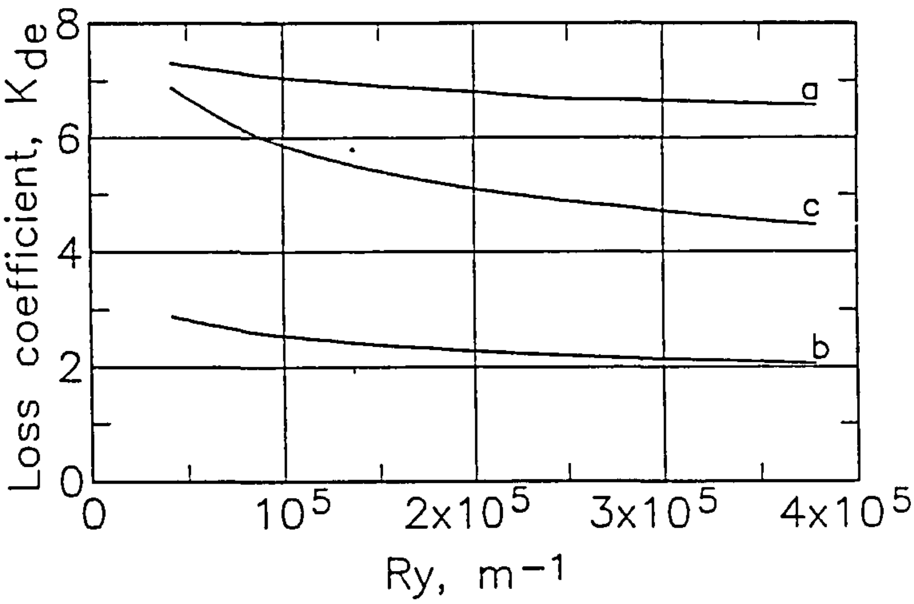

Figure 4.7.3: Loss coefficient for drift eliminators.

The drift eliminator loss coefficient can be expressed by a relation of the type

$$K_{de} = a_{de} Ry^{b_{de}} \tag{4.7.1}$$

where a_{de} and b_{de} are constants.

It is noted that the pressure drop can vary significantly for different drift eliminators at the same air speed. Certain drift eliminators having a higher resistance are more effective than those with the lower resistance although this is not necessarily always the case. The efficiency of a drift eliminator is determined by the measurable residual water load behind it. Practical eliminators have residual loads compared to the cooling water volume flow rate of 0.01 percent or less. The degree of separation achievable depends among others on the droplet size distribution and the air approach velocity. An example of the effectiveness of a typical separator is shown in figure 4.7.4 [84VG1]. It is noted that droplets having a diameter of more than 150 x 10^{-6} m are almost completely separated.

Drift eliminators are most effective at upstream air speeds of 2 m/s to 4 m/s. At higher speeds there is a danger that flooding may occur in the eliminator pack.

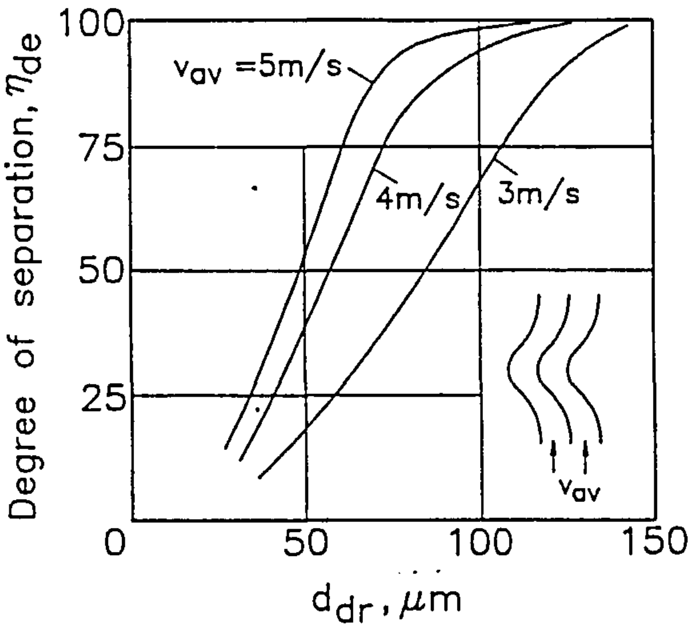

Figure 4.7.4: Effectiveness of droplet eliminator.

4.8 SPRAY AND ADIABATIC COOLING

The performance of air-cooled heat exchangers can be considerably enhanced by spraying droplets of water directly onto a part of the air-side heat transfer surface or into the air-stream approaching the heat exchanger. Spray droplets may be quite large causing significant wetting of the heat transfer surface or they may be quite small (mist) resulting in a relatively thin water film to form where wetting does occur [70FI1, 73SE1, 74SI1, 75YA1, 84SI1, 88HA1, 88NA1, 91KR1, 94LE1].

If the water is introduced into the inlet air stream of an air-cooled heat exchanger or dry cooling tower in the form of a very fine spray or mist such that all droplets evaporate before reaching the heat exchanger, the effective dry bulb temperature of the air will be reduced, while its humidity increases as the water evaporates. For all practical purposes the ambient air is cooled down, following essentially the line of constant wetbulb temperature from its original state at 1 to the final state at 2 i.e., $T_{wb2} = T_{wb1}$, as shown schematically on the phsychromatic chart, figure 4.8.1 [82ST1].

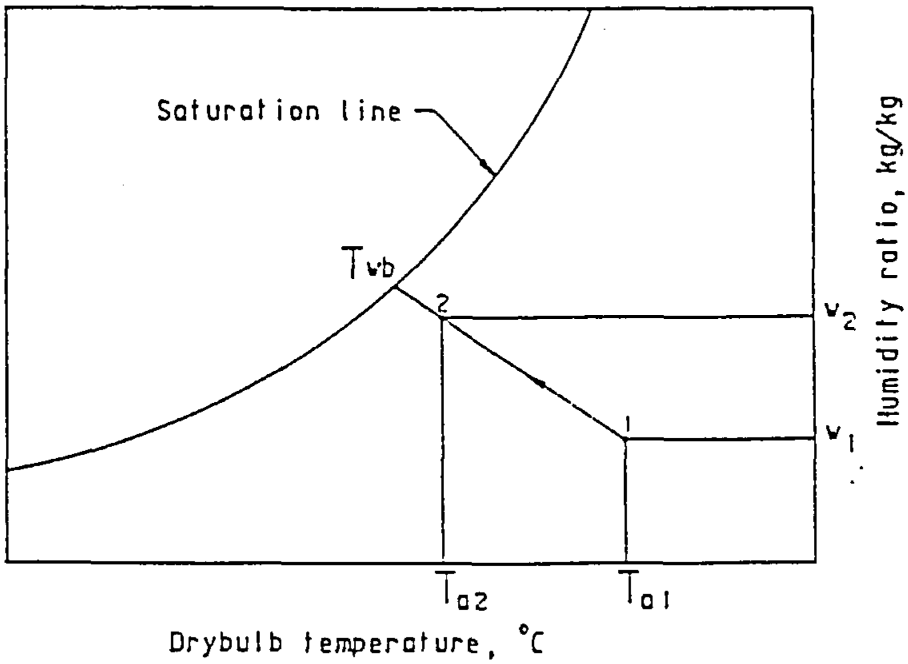

Figure 4.8.1: Adiabatic cooling.

The spray may be introduced into the air stream at a fixed or variable rate depending on the system requirements. The particular ambient temperature at which the spray is switched on depends to a large extent on the ultimate total cost of the spray relative to the cost of the product delivered by the plant e.g. power, chemical substance etc.

The spray may be introduced at such a rate that the relative humidity (defined by equation (4.1.21)) of the air entering the heat exchanger bundles, does not exceed a prescribed relative humidity.

If the air is cooled from state 1 to state 2 as shown in figure 4.8.1, the drybulb temperature, T_{a2}, can be determined iteratively from equations (4.1.17),(4.1.21),(A.2.1) and (A.3.5). The humidity ratios w_1 and w_2 are determined according to equation (A.3.5). Thus the mass of water evaporated per unit mass of air entering the heat exchanger is $(w_2 - w_1)$.

Small deviations from the constant wetbulb temperature line do occur in practice, if the water spray temperature does not correspond to the wet bulb temperature of the inlet air.

The adiabatic cooling of air by injecting water droplets into the stream, has been investigated extensively [81BL1], however only relatively small air-cooled heat exchangers have to date been fitted with devices to facilitate this in order to increase the desired cooling capacity.

4.9 REFERENCES

25ME1 Merkel, F., Verdunstungskühlung, VDI-Zeitschrift, Vol. 70, No. 70, pp. 123-128, January 1925.

34GI1 Gilliland, E.R., Diffusion Coefficients in Gaseous Systems, Ind. Eng. Chem., Vol. 26, pp. 681, 1934.

38FR1 Frössling, N., Über die Verdunstung Fallender Tropfen, Gerlands, Beiträge zur Geophysik, Vol. 25, pp. 170-216, 1938.

52CH1 Chilton, H., Elimination of Carryover from Packed Towers with Special Reference of Natural Draft Water Cooling Towers, Trans. of the London Inst. of Chem. Engrs, Vol. 30, pp. 235-250, London, England, 1952.

56KE1 Kelly, N.W. and Swenson, L.K., Comparative Performance of Cooling Tower Packing Arrangements, Chem, Eng. Progress, Vol. 25, No. 7, p. 263, 1956.

57ZI1 Zivi, S.M. and Brand, B.B., An Analysis of the Crossflow Cooling Tower, Refrigeration Engineering, Vol. 64, pp. 31-34, 90-92, 1957.

60BO1 Bosnjakovic, F., Technical Thermodynamics, translated by P.L. Blackshear, pp. 1-80, Holt, Reinhart and Winston, New York, 1960.

61BA1 Baker, D.R. and Shryock, H.A., A Comprehensive Approach to the Analysis of Cooling Tower Performance, ASME Journal of Heat Transfer, pp. 339-350, 1961.

61LO1 Lowe, H.J. and Christie, D.G., Heat Transfer and Pressure Drop Data on Cooling Tower Packings and Model Studies of the Resistance of Natural Draft Towers to Airflow, Proc. of the Int. Heat Transfer Conf. Boulder, Colorado, 1961.

61PA1 Parker, R.O. and Treybal, R.E., The Heat, Mass Transfer Characteristics of Evaporative Coolers, Chemical Engineering Progress Symposium Series, Vol. 57, No.32, pp. 138-149, 1961.

61RI1 Rish, R.F., The Design of a Natural Draught Cooling Tower, Proceedings of the 2nd International Heat Transfer Conference, Boulder, Colorado, 1961.

65BO1 Bosnjakovic, F., Technische Thermodinamik, Theodor Steinkopf, Dresden, 1965.

67CO1 Cooling Tower Institute, Cooling Tower Institute Performance Curves, CTI, Houston, Texas. 1967.

67MI1 Mizushina, T., Ito, R. and Miyashita, H., Experimental Study of an Evaporative Cooler, International Chemical Engineering, Vol. 7, No.4, pp. 727 - 732, October 1967.

68MI1 Mizushina, T., Ito, R. and Miyashita, H., Characteristics and Methods of Thermal Design of Evaporative Coolers, International Chemical Engineering, Vol. 8, No. 3, pp. 532 - 538, July 1968.

69NI1 Nitsu, Y., Naito, K. and Anzai, T., Studies on Characteristics and Design Procedure of Evaporative Coolers, Journal of SHASE Japan, Vol. 41, No. 12, 1967, Vol. 41, No. 13, 1967 and Vol. 43, No. 7, 1969.

70FI1 Finlay, I.C. and McMillan, T., Pressure Drop, Heat and Mass Transfer During Air-water Mist Flow Across a Bank of Tubes, National Engineering Laboratory Report No. 474, East Kilbride, Glasgow, 1970.

72AS1 ASHRAE Handbook of Fundamentals, American Society of Heating Refrigerating and Air-conditioning Engineers Inc., New York, 1972.

73SE1 Sen, G.N., Heat Transfer During Air-water Mist Flow Across Annular Finned-tube Banks, Ph.D. thesis, University of Strathclyde, 1973.

74FI1 Finlay, I.C. and Grant, W.D., The Accuracy of Some Simple Methods of Rating Evaporative Coolers, NEL Report No. 584, East Kilbride, Glasgow, NEL, 1974.

74FO1 Foster, P.M., Williams, M.J. and Winter, R.J., Droplet Behaviour and Collection by Counterflow Cooling Tower Eliminators, Atmospheric Environment, Vol. 8, pp. 349-360, 1974.

74HO1 Holmberg, J., Drift Management in the Chalk Point Cooling Tower, Mission, Kansas: The Marley Co., 1974.

74SC1 Scriven, R.A., Morton, V.M. and Newlands, A.G., Production of Airborne Droplets in Cooling Towers, Atmospheric Environment, Vol. 8, pp. 337-347, 1974.

74SI1 Simpson, H.C., Beggs, G.C. and Sen, G.N., Heat Transfer from Extended Surface Tubes to an Air-water Mist, International Chemical Engineering-Symposium Series, Vol. 11. No. 38, Paper No. H3, 1974.

75YA1 Yang, W-J. and Clark, D.W., Spray Cooling of Compact Heat Exchangers, International Journal of Heat and Mass Transfer, Vol. 18, pp. 311-317, 1975.

76CH1 Chan, J. and Golay, M., Numerical Simulation of Cooling Tower Drift Eliminator Performance, Numerical / Laboratory Computer Methods in Fluid Mechanics, ed. Pouring, A.A., ASME, pp. 229-241, New York, 1976.

76KE1 Kelly, N.W., Kelly's Handbook of Crossflow Cooling Tower Performance, N.W. Kelly and Assoc., Kansas City, MO, 1976.

76YA1 Yao, S.C. and Schrock, V.E., Heat and Mass Transfer from Freely Falling Drops, Journal of Heat Transfer, Vol. 98, No. 1, pp. 102-126, 1976.

76YA2 Yao, S.C. and Schrock, V.E., Aerodynamic Design of Cooling Tower Drift Eliminators, Trans. of the ASME, Journal of Engineering for Power, pp. 450-456, Oct., 1976.

77CH1 Chan, J. and Golay, M., Comparative Performance Evaluation of Current Design Evaporative Cooling Tower Drift Eliminators, Atmospheric Environment, Vol. 11, pp. 775-781, 1977.

77CR1 Crowe, C.T., Sharma, M.P. and Stock, D.E., The Particle-Source-In-Cell Model for Gas-Droplet Flows, Journal of Fluid Engineering, Vol. 99, No. 2, pp. 325 - 332, 1977.

77TE1 Tezuka, S., Kasai, S. and Nakamura, T., Performance of an Evaporative Cooler, Heat Transfer, Japanese Research, Vol. 6, No. 1, pp. 1 - 18, 1977.

78CL1 Clift, R., Grace, J.R. and Weber, M.E., Bubbles, Drops, and Particles, Academic Press, New York, 1987.

79LE1 Leidenfrost, W. and Korenic, B., Analysis of Evaporative Cooling and Enhancement of Condenser Efficiency and of Coefficient of Performance, Wärme und Stoffübertragung, Vol. 12, pp. 5-23, 1979.

82CA1 Cale, S.A., Development of Evaporative Cooling Packing, Commission of European Communities, Report EUR 7709 EN, Luxembourg, 1982.

82JO1 Johannsen, A., Plotting Psychrometric Charts by Computer, The South African Mechanical Engineer, Vol. 32, pp. 154-162, July 1982.

82LE1 Leidenfrost, W. and Korenic, B., Evaporative Cooling and Heat Transfer Augmentation Related to Reduced Condenser Temperatures, Heat Transfer Engineering, Vol. 3, No. 3-4, pp. 38 - 59, 1982.

82PE1 Perez-Blanco, H. and Bird, W.A., Study of Heat and Mass Transfer in Evaporative Coolers, ORNL/TM 8150, 1982.

82ST1 Stoecker, W.F. and Jones, J.W., Refrigeration and Air Conditioning, McGraw-Hill Book Co., Singapore, 1982.

83BE1 Benton, D.J., A Numerical Simulation of Heat Transfer in Evaporative Cooling Towers, Tennessee Valley Authority, Report WR28-1-900-110, 1983.

83BO1 Bourillot, C., TEFERI, Numerical Model for Calculating the Performance of an

Evaporative Cooling Tower, EPRI Report CS-3212-SR, August 1983.

83BO2 Bourillot, C., On the Hypothesis of Calculating the Water Flowrate Evaporated in a Wet Cooling Tower, EPRI Report CS-3144-SR, 1983.

83MA1 Majumdar, A.K. and Singhal, A.K., VERA2D: Program for 2-D Analysis of Flow, Heat, and Mass Transfer in Evaporative Cooling Towers, EPRI Report CS 2923, March 1983.

84BA1 Baker, D., Cooling Tower Performance, Chemical Publ. Co., pp. 122-133, New York, 1984.

84FI1 Finlay, I.C. and Harris, D., Evaporative Cooling of Tube Banks, Int. Journal of Refrigeration, Vol. 7, No. 4, pp. 214-224, 1984.

84LE1 Lefevre, M.R., Eliminating the Merkel Theory Approximations - Can it Replace the Empirical Temperature Correction Factor?, Paper TP-84-18, Cooling Tower Institute Annual Meeting, 1984.

84PO1 Poppe, M. and Rögener, H., Berechnung von Rückkühlwerken, VDI-Wärmeatlas, 4th ed., pp. Mh1 - Mh15, VDI-Verlag, Düsseldorf, 1984.

84SI1 Simpson, H.C., Beggs, G.C. and Raouf, M.I.N., Air-water Mist Flow Over Extended Surface Tube Banks, First UK National Heat Transfer Conference, University of Leeds, pp. 745-760, 1984.

84VG1 VGB, Rezirkulation mitgerissenen Kühlwassers in Zellenkühlern mit saugenden Ventilatoren, VGB-TW 105, VGB, Essen, March 1984.

84WE1 Webb, R.L., A Unified Theoretical Treatment for Thermal Analysis of Cooling Tower Evaporative Condensers and Fluid Coolers, ASHRAE Publication KC-84-07, No. 3 (RP-322), 1984.

86BE1 Benocci, C., Buchlin, J.M. and Weinacht, P., Predicting the Air/droplet

Interaction in the Inlet Section of a Natural Draft Cooling Tower, Proceedings of the 5th IAHR Cooling Tower Workshop, Monterey, October 1986.

86BE2 Benton, D.J. and Rehberg, R.L., Mass Transfer and Pressure Drop in Sprays Falling in a Freestream at Various Angles, Proceedings of the 5th IAHR Cooling Tower Workshop, Monterey, October 1986.

86HA1 Hauenschild, R., Übereinstimmung zwischen Theorie und Praxis bei Merkel-zahl nachgewiesen, BWK, Bd. 38, No. 6, June 1986.

86HO1 Holman, J.P., Heat Transfer, Mc Graw-Hill Book Co., New York, 1986.

86LE1 Leidenfrost, W. and Korenic, B., Principles of Evaporative Cooling and Heat Transfer Augmentaton, Handbook of Heat and Mass Transfer, pp. 1025 - 1063, Gulf Publishing Co., Houston, 1986.

86MI1 Missimer, J.R. and Brackett, C.A., Model Tests of the Rain Zone of a Counterflow Natural Cooling Tower, Proceedings of the 5th IAHR Cooling Tower Workshop, Monterey, October 1986.

88ER1 Erens, P.J. and Dreyer, A.A., An Improved Procedure for Calculating the Performance of Evaporative Closed Circuit Coolers, AIChE Symposium Series, No. 263, Vol. 84, pp. 140-145, 1988.

88FA1 Fabre, L. and Legrand, G., Mistral New Test Bench for Cooling Tower Components, Paper presented at the 6th IAHR Cooling Tower Workshop, Pisa, Italy, 1988.

88FU1 Fulkerson, R.D., Comparative Evaluation of Counterflow Cooling Tower Fills, Journal of the Cooling Tower Institute, Vol. 9, No. 2, 1988.

88HA1 Hayashi, Y. and Takimoto, A., Convective Heat Transfer with Evaporation of Suspended Spray Droplets (2nd Report: Experiments for a Vertical Flat Plate), Heat Transfer - Japanese Research, Vol. 2, pp. 22-38, March-April 1988.

88NA1 Nakayama, W., Kuwahara, H. and Hirasawa, S., Heat Transfer from Tube Banks to Air-water Mist Flow, International Journal of Heat and Mass Transfer, Vol. 31, No.2, pp. 449-460, 1988.

88RE1 Renksizbulut, M. and Haywood, R.J., Transient Droplet Evaporation with Variable Properties and Internal Circulation at Reynolds Numbers, International Journal of Multiphase Flow, Vol. 14, No. 2, pp. 189 - 202, 1989.

88WE1 Webb, R.L., A Critical Evaluation of Cooling Tower Design Methodology, Heat Transfer Design, eds. Shah, R.K., Subbarao, E.C. and Mashelkar, R.F., pp. 547-558, Hemisphere Publ. Co., New York, 1988.

89JO1 Johnson, B.M. (ed.), Cooling Tower Performance Prediction and Improvement, Volume 1, Applications Guide, EPRI GS-6370, Volume 2, Knowledge Base, EPRI GS-6370, EPRI, Palo Alto, 1989.

90DR1 Dreyer, A. and Erens, P., Heat and Mass Transfer Coefficient and Pressure Drop Correlations for a Crossflow Evaporative Cooler, ASME IHTC, Jerusalem, 19-EN-20, pp. 233-238, 1990.

90HO1 Hoffmann, J.E. and Kröger, D.G., Analysis of Heat Mass and Momentum Transfer in the Rain Zone of a Natural Draft Counterflow Cooling Tower, Proceedings of the 9th International Heat Transfer Conference, Jerusalem, Israel, August 1990.

91KR1 Kriel, D.E., M.Eng. thesis, Prediction and Measurement of the Performance of Spray Cooled Heat Exchangers, University of Stellenbosch, Stellenbosch, South Africa, 1991.

91MA1 Marseille, T.J., Schliesing, J.S., Bell D.M. and Johnson, B.M., Extending Cooling Tower Thermal Performance Prediction Using a Liquid-side Film Resistance Model, Heat Transfer Engineering, Vol. 12, No. 3, pp. 19-30, 1991.

91OS1 Osterle, F., On the Analysis of Counterflow Cooling Towers, Int. J. Heat Mass

Transfer, Vol. 34, No. 4/5, pp. 1313-1316, 1991.

91PO1 Poppe, M. and Rögener, H., Berechnung von Rückkühlwerken, VDI-Wärmeatlas, pp. Mi1-Mi15, VDI-Verlag, Düsseldorf, 1991.

92BE1 Becker, B.R. and Burdick, L.F., Effect of Drift Eliminator Design on Cooling Tower Performance, Trans. of the ASME, Journal of Engineering for Gas Turbines and Power, Vol. 114, pp. 632-642, 1992.

93BE1 Becker, B.R. and Burdick, L.F., Drift Eliminators and Cooling Tower Performance, ASHRAE Journal, pp. 28-36, June 1993.

93CO1 Conradie, C.F.G., Die Verkoelingsvermoë van Nat Koeltorings en Droë/Nat Stelsels by Kragstasies, M.Eng thesis, University of Stellenbosch, South Africa, June 1993.

94AU1 Aull, R.J., Evaluation of Anti-fouling Replacement Fills in Utility Cooling Service, Paper presented at the EPRI Cooling Towers and Advanced Cooling Systems Conference, St. Petersburg Beach, Florida, August, 1994.

94BE1 Becker, B.R. and Burdick L.F., The Aerodynamic Effects of Drift Eliminator Design, Paper presented at the 9th IAHR Cooling Tower and Spraying Pond Symposium, von Karman Institute, Brussels, Belgium, 1994.

94BU1 Burger, R., Cooling Towers, The Overlooked Energy Conservation Profit Center, Paper presented at the EPRI Cooling Tower and Advanced Cooling Systems Conference, St. Petersburg Beach, Florida, August 1994.

94CO1 Combaz, P., Scaling in Nuclear Power Plant Cooling Towers, Paper presented at the 9th IAHR Cooling Tower and Spraying Pond Symposium, von Karman Institute, Brussels, Belgium, September 1994.

94GI1 Gill, J.S., Yorke, M.A., Donlan, R.M., Gibbon, D.L. and McClung, B., A Mechanistic Approach to the Development of Chemical Solutions for Fouling of

Cooling Tower Film Fills, Paper presented at the EPRI Cooling Towers and Advanced Cooling Systems Conference, St. Petersburg Beach, Florida, August 1994.

94LE1 Lee, S.L., Yang, Z.H. and Hsyua, Y., Cooling of a Heated Surface by Mist Flow, Journal of Heat Transfer, Vol. 116, pp. 167-172, February 1994.

94MO1 Monjoie, M., Plastic Material Selection for Cooling Tower Film Fill, Paper presented at the 9th Int. Ass. for Hydraulic Research Cooling Tower and Spraying Pond Symposium, von Karman Institute for Fluid Dynamics, Brussels, September 1994.

94NE1 Newton, M.T., Noble, R.T., Philpot, E.F. and Eastis, J.H., Pilot Scale Cooling Tower Fouled Fill Treatment, Paper presented at the EPRI Cooling Towers and Advanced Cooling Systems Conference, St. Petersburg Beach, Florida, August 1994.

94PH1 Phelps, P.M. and Minett, T.O., Combination Film/splash Fill for Overcoming Film Fouling, Paper presented at the EPRI Cooling Towers and Advanced Cooling Systems Conference, St. Petersburg Beach, Florida, August 1994.

94PU1 Puckorius, P.R., Fouling of Cooling Tower Film Fill: Causes, Cleanup Techniques and Operating Guidelines, Paper presented at the EPRI Cooling Towers and Advanced Cooling Systems Conference, St. Petersburg Beach, Florida, August 1994.

CHAPTER 5

HEAT TRANSFER SURFACES

5.0 INTRODUCTION

The most expensive and most critical component of any air-cooled heat exchanger is the heat transfer surface area. Owing to the relatively low heat transfer coefficient on the air-side, extended surfaces or fins are required to increase the surface area density, thereby improving the overall conductance, resulting in a lighter and more compact heat exchanger.

These reductions of heat exchanger mass and volume are particularly important for propulsive plants (automobile, truck, aircraft, etc.), cryogenic, refrigeration and air-conditioning systems. In air-cooled heat exchangers as found in power plants and chemical processing complexes, it is important to have low-cost finned surfaces that resist corrosion, can be readily cleaned, and have adequate mechanical strength. A service life of more than 25 years should be guaranteed. Although non-metallic materials have been evaluated for possible use in air-cooled heat exchangers, no large unit incorporating such materials has been built [81PO1, 84GU1].

5.1 FINNED SURFACES

Finned tubes may be round, elliptical, flattened or otherwise streamlined to reduce the flow resistance on the air side. Different types and shapes of fins are either an integral part of the tube or attached to the tube by mechanical means only, or by soldering, brazing, galvanizing or welding.

To improve the heat transfer characteristics, the fin surface may be roughened, cut, corrugated or perforated. In certain applications, sections of the surface are stamped out to create spaces separating the adjacent fins. Examples of finned surfaces are shown in figure 5.1.1 [88KR1].

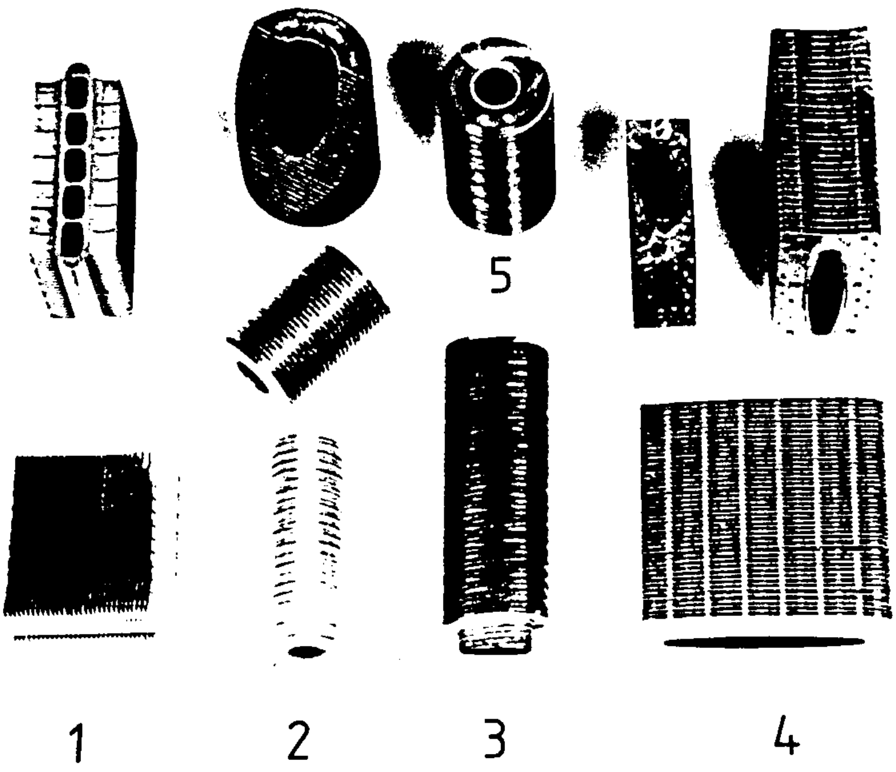

Figure 5.1.1: Finned tubes. (1) Integrally finned tube (skived fin); (2) extruded bimetallic finned tube; (3) helically wound galvanized steel finned tube; (4) galvanized plate finned tube; (5) helically wound bimetallic finned tube.

Round tubes with smooth helical fins are encountered in many industrial air-cooled systems.

These tubes are readily mass-produced in great lengths at a minimum cost. An aluminum, steel or other metal tape is tension-wound onto the tube to form the fins as shown in figure 5.1.2 (a). The wavy fin in figure 5.1.2 (b) improves the thermal contact. If required the contact may be further improved by soldering, brazing or welding. The above-mentioned types of extended surfaces are also known as I-fin and IW-fin respectively.

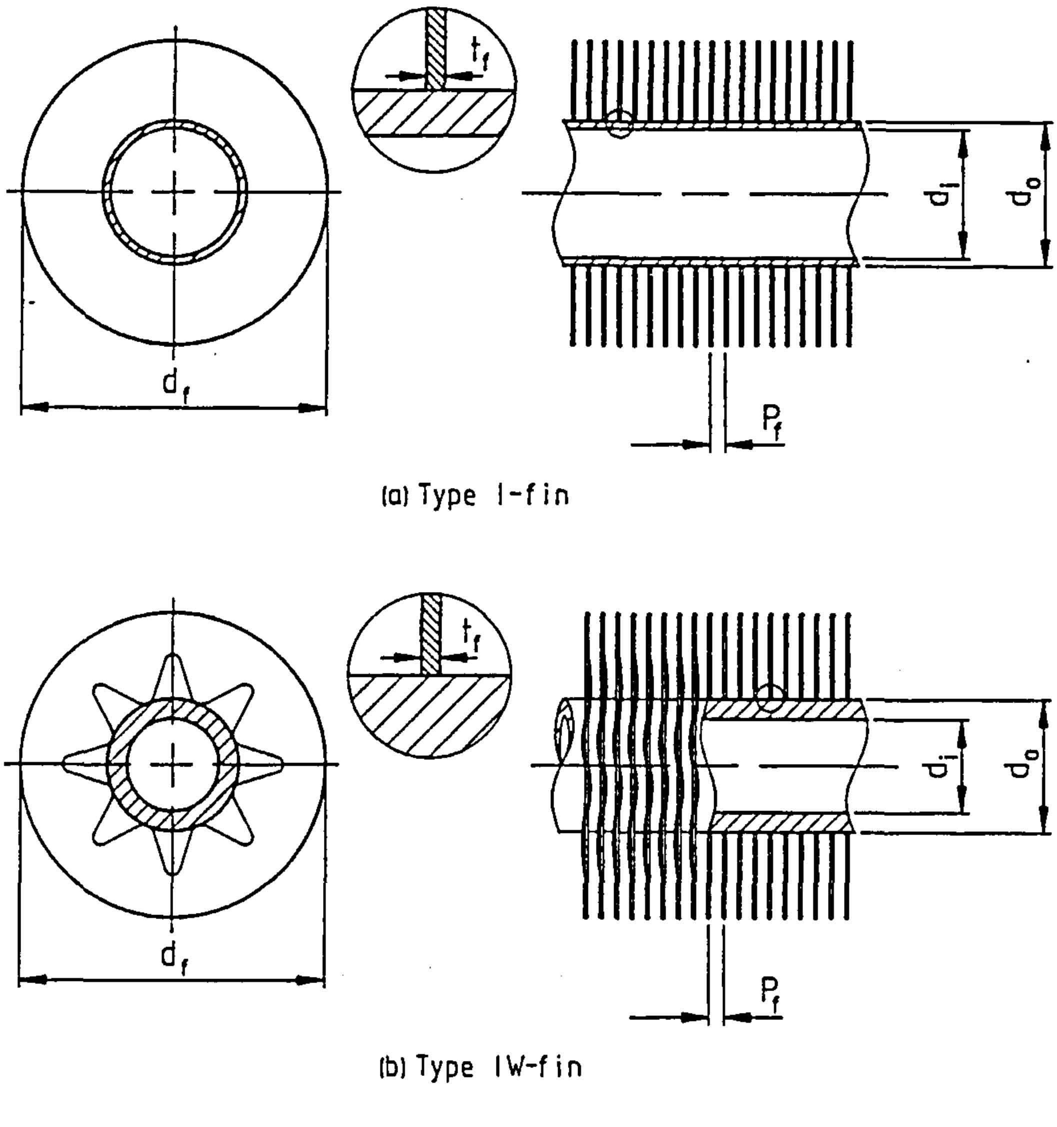

Figure 5.1.2: Type I and type IW-finned tube.

Good thermal contact is also obtained in the L-fin tube shown in figure 5.1.3(a). Where the fin material is aluminum and the core tube is steel, this geometry is less subject to corrosion than in the case of the I-type tube. The overlapped or double L-fin shown in figure 5.1.3(b) is even more protective. These aluminum finned tubes should preferably not be employed where the tube-wall temperature exceeds 120° C. Owing to the difference between the thermal expansion coefficients of the two materials, the thermal contact resistance becomes prohibitive above this temperature (see section 5.8). If the fins are tension-wound onto externally knurled core tubes, thermal contact is enhanced and higher operating temperatures are possible.

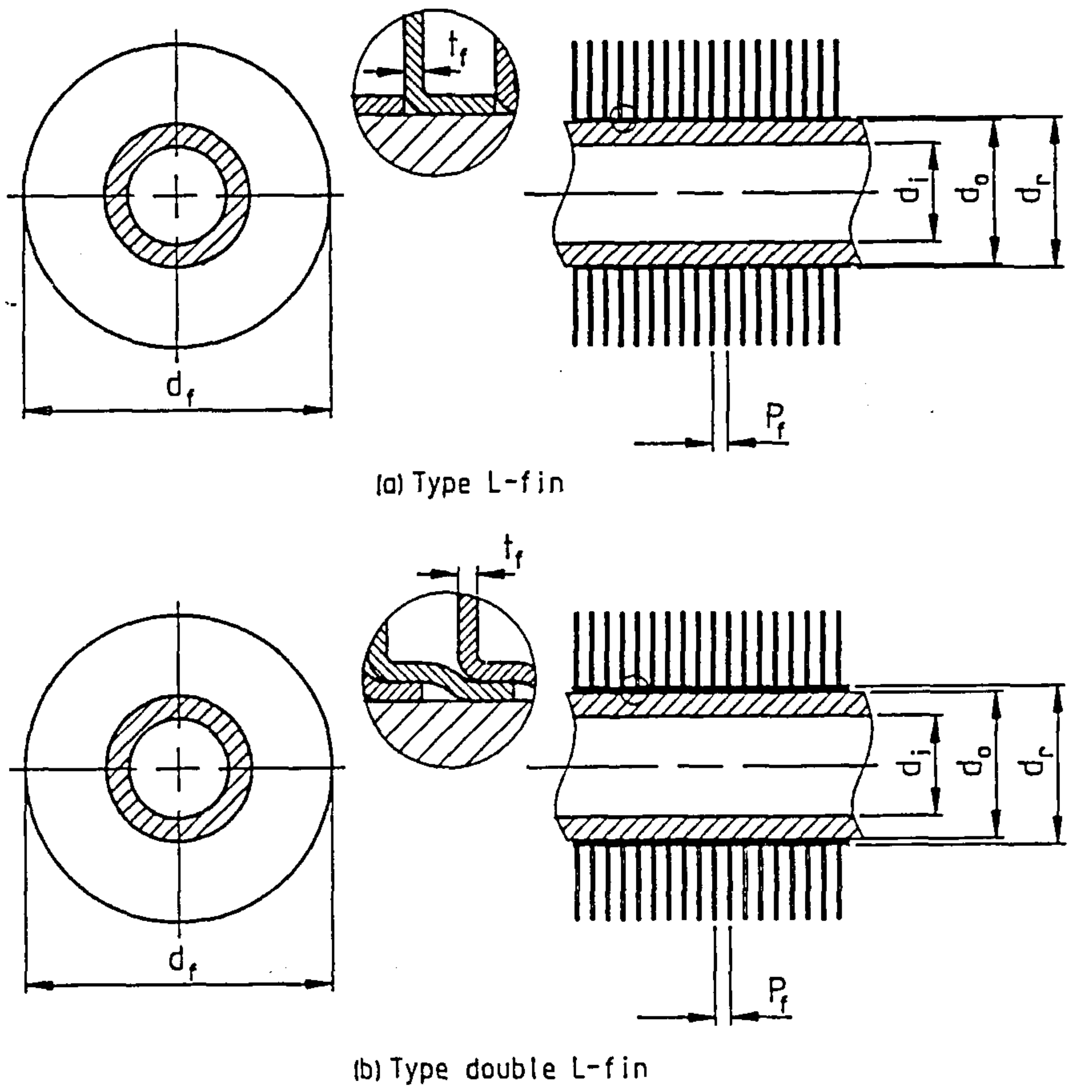

Figure 5.1.3: L- and double L-finned tube.

Elliptical steel tubes with tension-wound steel IW or L fins are available. These finned tubes are galvanized and find application where a low air-flow resistance is required in addition to good thermal contact and corrosion resistance.

For operating at temperatures of up to a tube-wall temperature of 400° C, helically wound aluminum G-fins as shown in figure 5.1.4(a) are acceptable. The core tube is provided with a groove into which the fin is rolled, whereafter the groove is peened back against the sides of the fin material.

Where corrosion is a major consideration, an extruded bimetallic E-fin tube as shown in figure 5.1.4(b) is recommended for tube-wall temperatures up to 200° C. The finned surface is obtained by plastically deforming an outer aluminum muff onto an internal steel tube during a rolling process. The fins can also be extruded from materials other than aluminum.

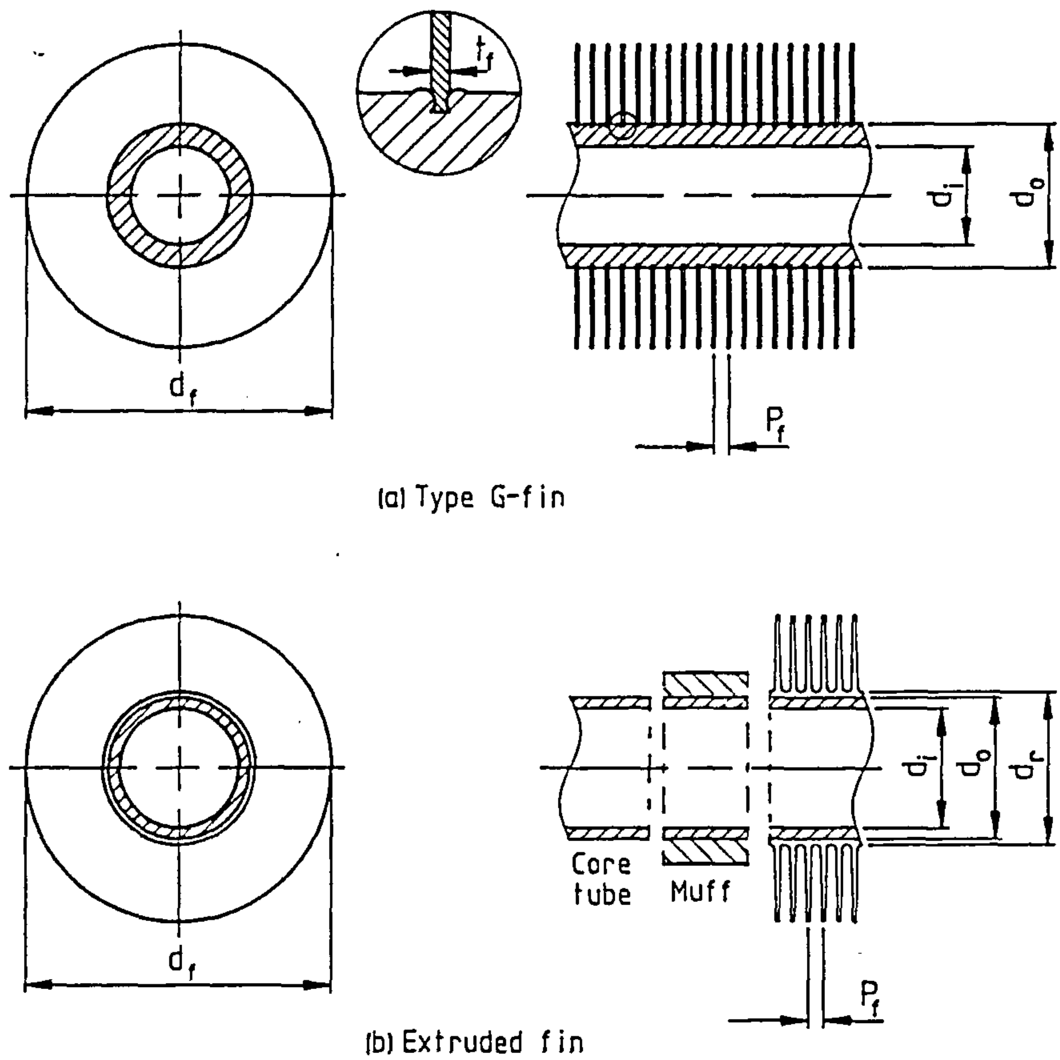

Figure 5.1.4: Grooved and extruded finned tubes.

Tubes made of copper, cupronickel, aluminum or other materials may be extruded directly to form an integrally finned tube with no core tube. This is known as a K-fin tube.

Modified surfaces are obtained by partially or fully cutting the helical fins or slotting or punching the surface as shown in figure 5.1.5.

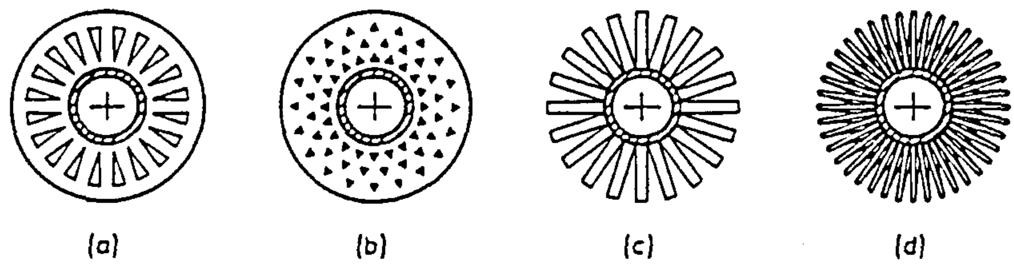

Figure 5.1.5: Augmented fin geometries. (a) Slotted fin; (b) punched and bent triangular projections; (c)segmented fin; (d) wire-loop extended fin.

Serrated or segmented finned tubes are made by helically winding a continuous strip of metal that has been partially cut into narrow sections. Upon winding, these sections "separate" to form protrusions extending from the fin root. The fins are attached to the tube by continuous arc-welding.

Helically wound wire-loop fins are found in limited application. Studded fins are made by welding individual studs around the base of the tube. The shape of the studs as well as the number of studs can vary.

Although the heat transfer characteristics of these surfaces are improved [90FI1], problems of increased pressure drop, fouling, cost, etc., often detract from the potential advantages.

Various forms of annular finned tubes are found in practice. These fins are made of discs or plates of various shapes which are separated from each other by spacers. The spacers are in the form of tube collars at the base of the tube or protrusions stamped out of the finned surface. Examples of such finned tubes are shown schematically in figure 5.1.6.

Round tubes may be expanded mechanically or hydraulically to ensure an acceptable fin-tube bond.

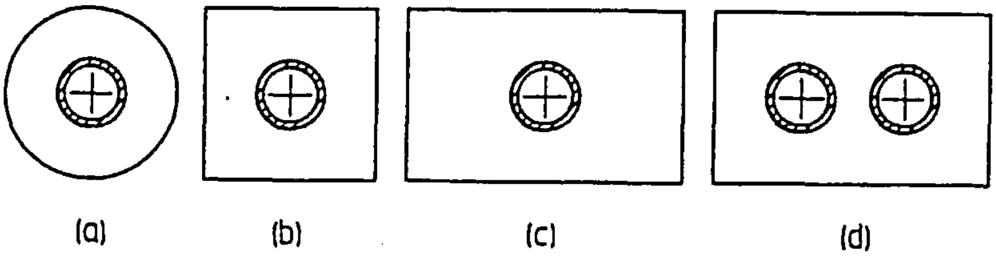

Figure 5.1.6: Annular finned tube. (a) Radial fin; (b) square fin; (c) and (d) rectangular fin.

An elliptical steel tube with a rectangular steel-plate fin is shown in figure 5.1.7. The finned tube is galvanized after assembly to ensure good thermal contact. The fin may contain bent triangular projections or turbulators to enhance the heat transfer [66SC1, 88GE1].

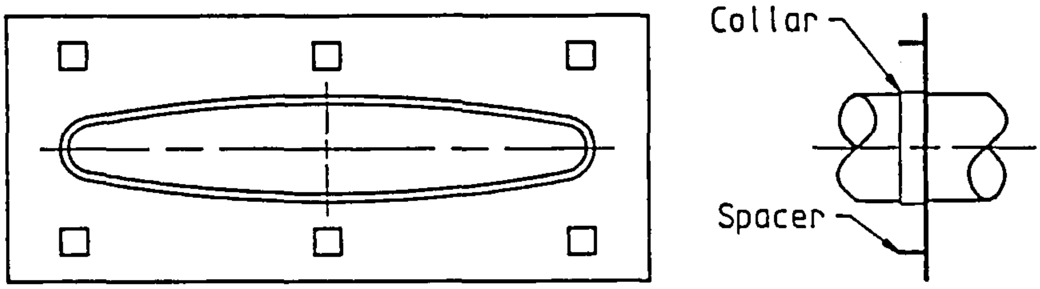

Figure 5.1.7: Elliptical tube with rectangular plate fin.

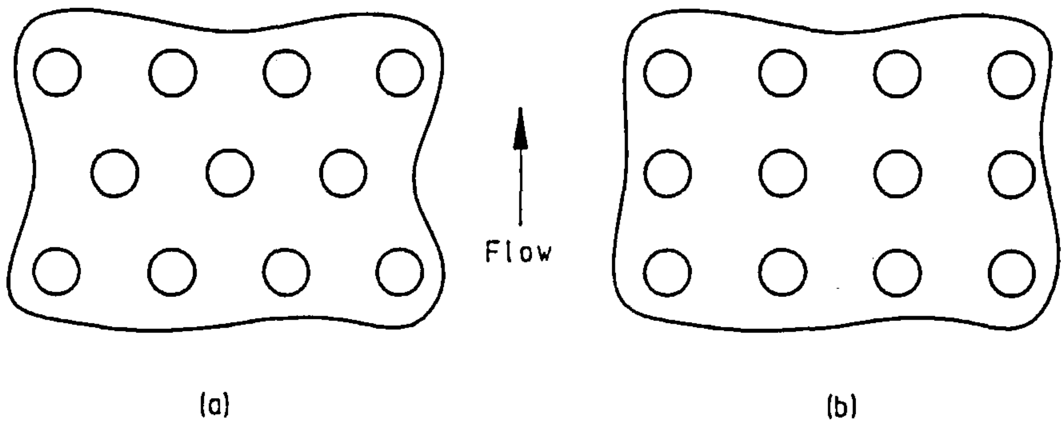

Figure 5.1.8: Continuous plate fin. (a) Staggered tube arrangement; (b) aligned tube arrangement.

An example of a continuous plate fin is shown in figure 5.1.8. The tubes may be arranged in a staggered or aligned pattern.

Forgo-type all-aluminum slotted plate finned heat exchanger bundles have been installed in numerous dry-cooling towers. Since 1976 a modified manufacturing technology has been used to produce the flat plate fin with integral spacer collars as shown in figure 5.1.9.

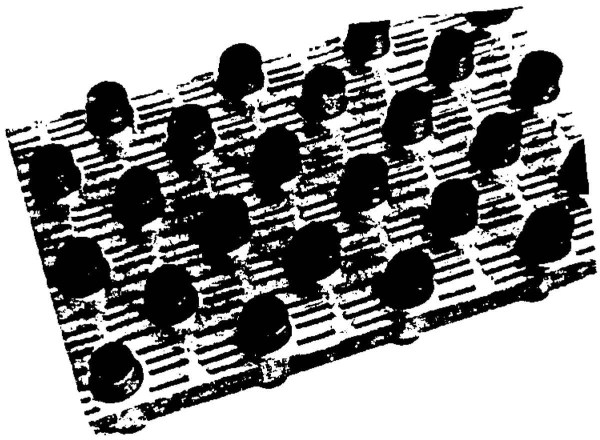

Figure 5.1.9: All aluminum Forgo-type finned tube.

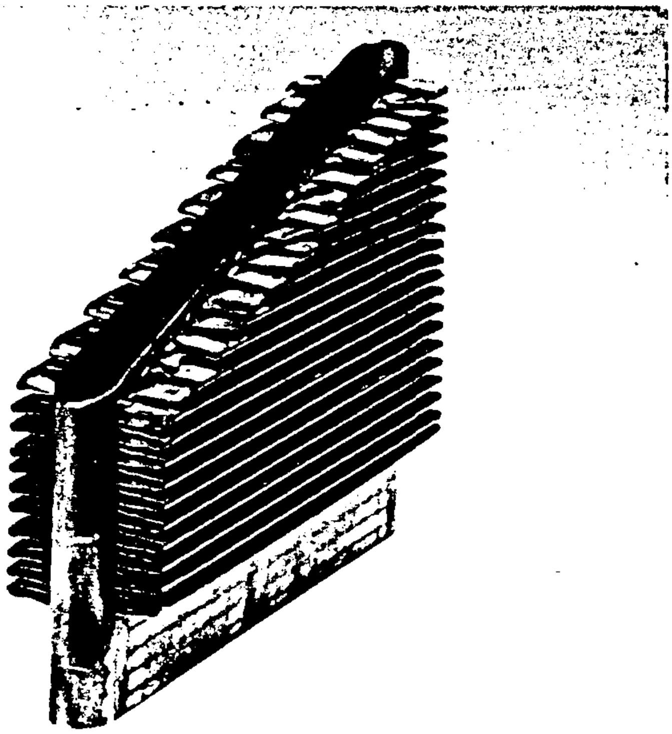

Figure 5.1.10: Wavy-finned flattened tube.

Typically, the plate fins are 1200 mm long and 150 mm wide and make provision for six-rows of round, staggered tubes. The fins are mechanically bonded to the tubes and for this reason are made of a tough aluminum which will also resist high-pressure jet cleaning. Corrosion resistance is improved by MBV treatment (modified Bauer-Vogel process) [88PA1].

The flattened, externally aluminized steel tube onto which wavy aluminum fins are bonded as shown in figure 5.1.10, has very good performance characteristics. It is particularly suited for application in air-cooled condensers where only a single row of these tubes may replace two or more rows of elliptical or round tubes. The flat tube may also consist of an extruded aluminum core tube.

Other enhanced heat transfer surfaces are shown in figure 5.1.11. Continuing research and development will undoubtedly lead to further improvements in performance characteristics of finned tubes [91RE1].

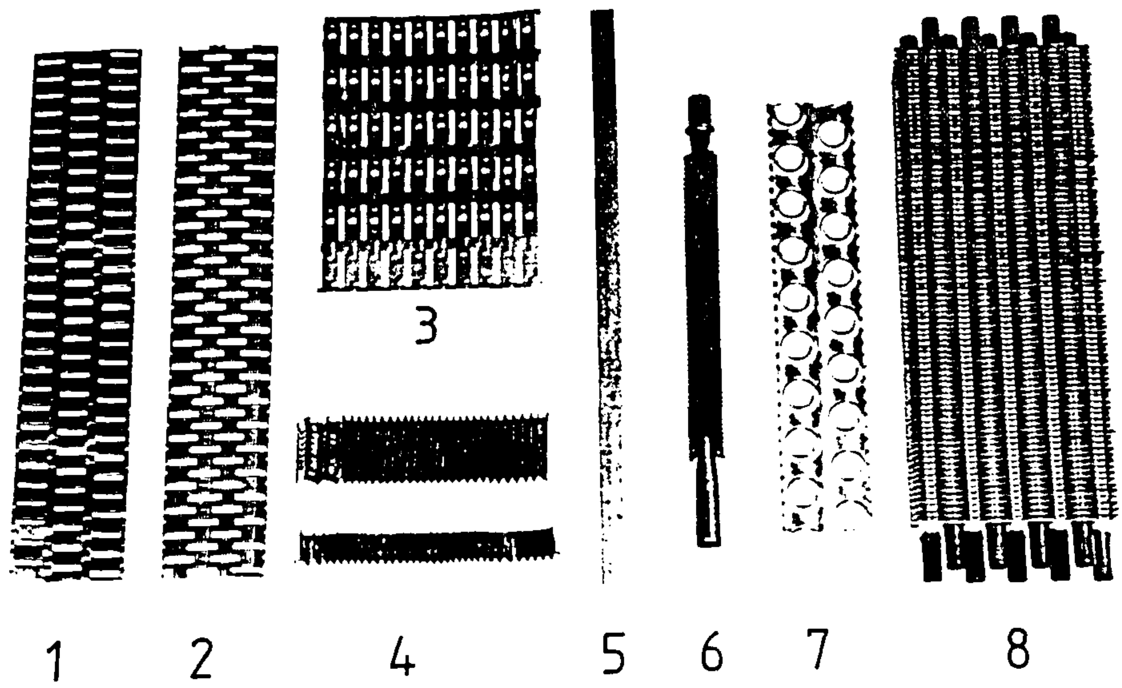

Figure 5.1.11: Enhanced plate-fin surfaces. (1) Plate fin; (2) louvered fin; (3) dimpled fin with reinforced leading edge; (4) louvered C-T fin; (5) flat tube; (6) flattened tube with louvered C-T fin; (7) wavy fin; (8) perforated plate fin with round tubes.

5.2 TEST FACILITIES AND PROCEDURES

The performance characteristics of extended surfaces are normally determined under idealized conditions in windtunnels designed specifically for this purpose. An example of an atmospheric open-loop induced draft tunnel is shown schematically in figure 5.2.1 [47WI1].

A radial fan 8 draws air uniformly through the rounded inlet section, where its wet- and drybulb temperature as well as the turbulence level is measured, and then across the heat exchanger bundle 1 which is heated by a fluid flowing inside the tubes. The static pressure difference is measured across the bundle at points located in the duct wall 3. Depending on the type of bundle to be tested, care should be taken that the outlet pressure tap is in a position where it will not be influenced by flow distortions immediately after the bundle. After the heat exchanger, the air passes through an insulated connecting section 2 and two sets of air mixers 4, followed by a venturi in which a sampling tube is located.

The air discharged from the heat exchanger may have a non-uniform temperature distribution together with a non-uniform velocity distribution. The most accurate means of measuring the mean temperature of the air stream under these conditions, is to introduce air mixers and then sample the stream at a number of points. Air mixers may consist of a series of vanes arranged to divide the air flow into many small streams which are diverted across each other. The venturi arrangement after the mixers tends to minimize the non-uniformity of the air-stream velocity. The sampling tube 5 permits the withdrawal of air from numerous points across the venturi throat and conveys it to a convenient location where the mean dry- and wetbulb temperature may be measured.

The air flow is determined by measuring the pressure drop across one or more elliptical nozzles mounted in a plate 7 located between two perforated plates 6. The corresponding mass flow rate is given by

$$m = C_n \phi_g Y \alpha A_n (2\rho_n \Delta p_n)^{0.5} \tag{5.2.1}$$

The nozzle coefficient of discharge, C_n, is a function of the nozzle Reynolds number. For $30000 < Re_n < 100000$,

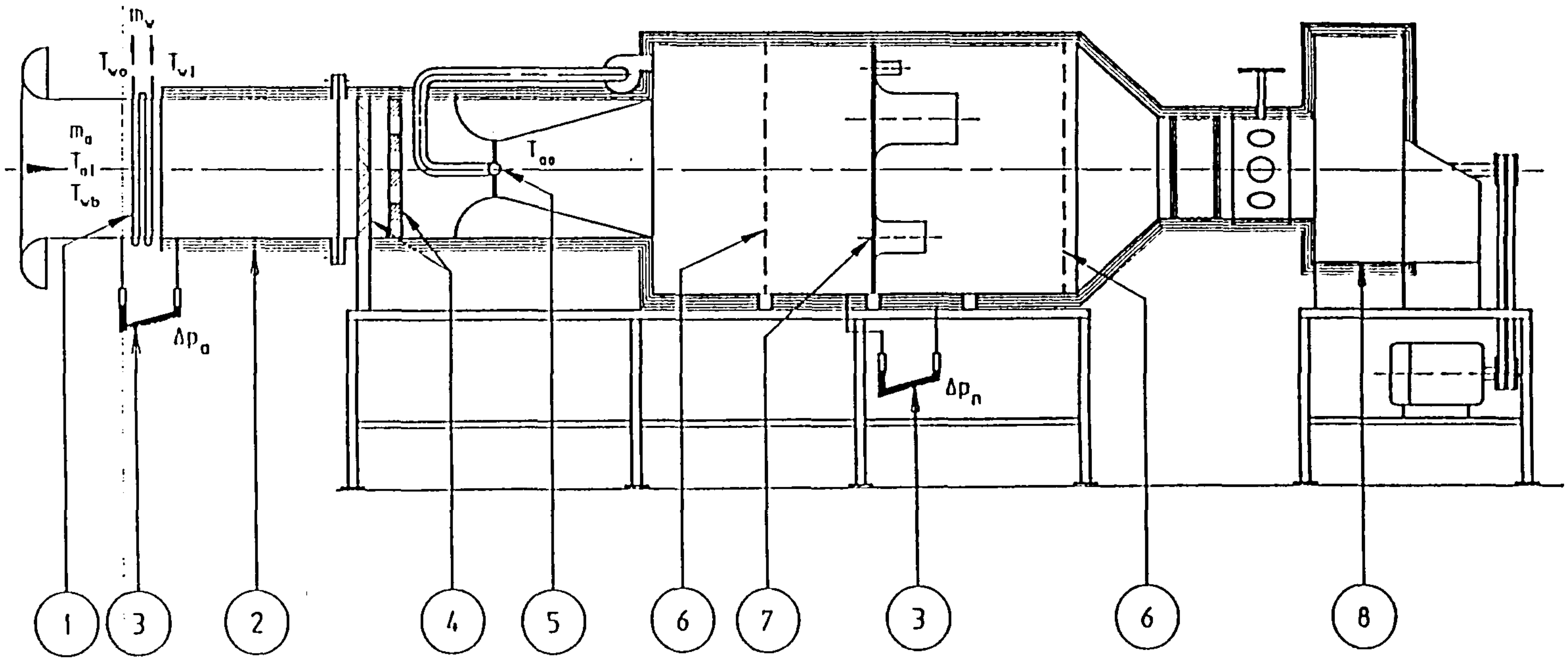

Figure 5.2.1: Test windtunnel.

$$C_n = 0.954803 + 6.37817 \times 10^{-7}\ Re_n - 4.65394 \times 10^{-12}\ Re_n^{\ 2} + 1.33514 \times 10^{-17}\ Re_n^{\ 3} \tag{5.2.2a}$$

For $100000 < Re_n < 350000$

$$C_n = 0.9758 + 1.08 \times 10^{-7}\ Re_n - 1.6 \times 10^{-13}\ Re_n^{\ 2} \tag{5.2.2b}$$

and for $Re_n > 350000$, $C_n = 0.994$.

The gas expansion factor ϕ_g may be approximated by the following relation:

$$\phi_g = 1 - 3\ \Delta p_n/(4\ p_u\ c_p/c_v) \tag{5.2.3}$$

where $c_p/c_v = 1.4$ for air and p_u is the upstream pressure.

For a compressible fluid, it can be shown that the approach velocity factor is approximately

$$Y = 1 + 0.5\ (A_n/A_{tus})^2 + 2(A_n/A_{tus})^2\ \Delta p_n/(p_u\ c_p/c_v) \tag{5.2.4}$$

Values for the thermal expansion coefficient, α, depend on the material from which the nozzle is manufactured.

Warm water, steam or some other heated fluid is passed through the tubes. Where warm water is employed, a uniform distribution of flow must be ensured through each of the tube passes. This can be achieved by the correct design of the manifolds. Air-water counterflow conditions are normally preferred. Since the difference between the inlet and outlet water temperature is usually small, it is recommended that these differences be measured by connecting sets of inlet and outlet thermocouples in series. These sets of thermocouples are readily calibrated before and after testing by operating the system under isothermal conditions with no air flow. The absolute water temperatures are measured independently.

When planning the experiments, estimates concerning the outlet air temperatures should be made to ensure that these are not too close to the inlet water temperature, since this may lead to significant errors in determining the heat transfer coefficient especially if the core is thick. Whenever possible, tests should be conducted under conditions similar to those experienced during practical operating conditions.

Methods of testing and test equipment are prescribed by various standards, including ARI Standard 410 [72AR1] and ASHRAE Standard 33-78 [78AS1].

5.3 INTERPRETATION OF EXPERIMENTAL DATA

Consider for example an experimental air-cooled cross-flow heat exchanger bundle consisting of externally finned tubes in which warm water is to be cooled as shown in figure 5.2.1. The following energy balance is applicable if it is assumed that heat losses from the bundle to the environment are negligible:

$$m_a(i_{ao} + v_{ao}^2/2) + m_w(i_{wo} + v_{wo}^2/2) = m_a(i_{ia} + v_{ai}^2/2) + m_w(i_{wi} + v_{wi}^2/2) \quad (5.3.1)$$

or

$$m_a[(i_{ao} - i_{ai}) + (v_{ao}^2 - v_{ai}^2)/2] = m_w [(i_{wi} - i_{wo}) + (v_{wi}^2 - v_{wo}^2)/2] \quad (5.3.2)$$

The change in kinetic energy of both the air and the water stream is normally negligible when compared to the change in corresponding enthalpy in a practical heat exchanger and equation (5.3.2) may be simplified to read

$$Q = m_a (i_{ao} - i_{ai}) = m_w(i_{wi} - i_{wo}) \quad (5.3.3)$$

or expressed in terms of temperatures

$$Q = m_a c_{pa} (T_{ao} - T_{ai}) = m_w c_{pw} (T_{wi} - T_{wo}) \quad (5.3.4)$$

where Q is the rate of heat transfer from the water to the air stream. Since the respective air and water mass flow rates and the inlet and outlet temperatures are measured, the quality of the data can to a large extent be determined by the energy balance as given by equation (5.3.4), i.e. the increase in air-stream energy must be equal to the heat transferred from the water.

It is also possible however to express the heat transfer rate in terms of the overall heat transfer coefficient as given by equation (3.5.16).

$$Q = U_a A_a F_T \Delta T_{\ell m} \quad (5.3.5)$$

where in general

$$U_a = \left(\frac{1}{h_a e_f} + \frac{A_a}{h_w A_w} + \sum_n \frac{A_a}{A_n} R_n \right)^{-1} \tag{5.3.6}$$

and where, according to equation (3.3.11), the effectiveness of the finned surface is

$$e_f = 1 - A_f (1 - \eta_f)/A_a$$

The summation term represents the thermal resistances other than those owing to the convective effects on the air and water side respectively.

Substitute equation (5.3.6) into equation (5.3.5), rearrange and find

$$h_a = \left[e_f A_a \left(\frac{F_T \Delta T_{\ell m}}{Q} - \frac{1}{h_w A_w} - \sum_n \frac{R_n}{A_n} \right) \right]^{-1} \tag{5.3.7}$$

All parameters in the denominator of equation (5.3.7) are either specified or available from experimental data except e_f, which is also a function of h_a. Equation (5.3.7) can thus be solved iteratively to find the air-side heat transfer coefficient under particular test conditions.

In equation (5.3.7) the R_n/A_n terms may include the resistance owing to the tube wall, fouling, and a thermal contact resistance between the tube and the fin. The latter is usually poorly defined, and it is thus convenient to re-write equation (5.3.7) as follows:

$$\frac{1}{h_a e_f A_a} + \sum_n \frac{R_n}{A_n} = \frac{F_T \Delta T_{\ell m}}{Q} - \frac{1}{h_w A_w} \tag{5.3.8}$$

A new effective heat transfer coefficient h_{ae} based on the air-side surface area is defined as

$$h_{ae} A_a = \left(\frac{1}{h_a e_f A_a} + \sum_n \frac{R_n}{A_n} \right)^{-1} = \left(\frac{F_T \Delta T_{\ell m}}{Q} - \frac{1}{h_w A_w} \right)^{-1} \tag{5.3.9}$$

The air-side static pressure drop measured across a heat exchanger bundle is generally due to a number of effects. To illustrate this, consider a parallel plate core heat exchanger model as shown in figure 5.3.1.

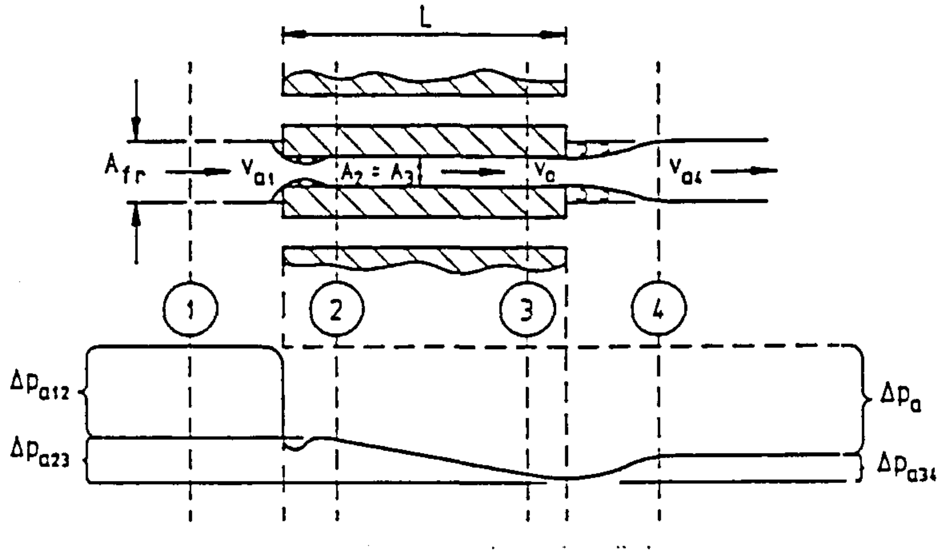

Figure 5.3.1: Pressure variation and losses through parallel plate core.

As the air flow enters the plates the static pressure initially drops, owing to a decrease in cross-sectional flow area. This is followed by a loss owing to the irreversible free expansion that follows the abrupt contraction through boundary-layer separation and the consequent pressure change owing to a change of momentum rate associated with changes in velocity profile downstream from the vena contracta. Thus

$$\Delta p_{a12} = \frac{G_{a2}^2}{2\rho_{a1}}\left[(1 - \sigma^2) + K_c\right] \tag{5.3.10}$$

where $\sigma = A_2/A_{fr}$ and K_c is the entrance contraction loss coefficient. The mass velocity G_{a2} is based on the minimum free flow area A_2, thus $G_{a2} = m_a/A_2$. The change in density between 1 and 2 is usually negligible so that $\rho_{a1} \approx \rho_{a2}$.

The pressure drop between 2 and 3 is due to flow acceleration and surface friction. The former is due to the air being heated. If the duct area between 2 and 3 does not change,

$$\Delta p_{a23} = \frac{G_{a2}^2}{2\rho_{a1}}\left[2\left(\frac{\rho_{a1}}{\rho_{a4}} - 1\right) + f_{app}\frac{A_a\rho_{a1}}{A_2\rho_{am}}\right] \tag{5.3.11}$$

where ρ_{am} is the mean air density.

At the outlet a partial pressure recovery occurs owing to the increase in flow area. However, a pressure loss occurs owing to the irreversible free expansion.

$$\Delta p_{a34} = \frac{G_{a2}^2}{2\rho_{a4}}[-(1 - \sigma^2) + K_e] \tag{5.3.12}$$

It is assumed that there is practically no change in density between 3 and 4, i.e. $\rho_{a3} \approx \rho_{a4}$.

The static pressure loss across the heat exchanger is thus the sum of equations (5.3.10), (5.3.11) and (5.3.12).

$$\Delta p_a = \frac{G_{a2}^2}{2\rho_{a1}}\left[(1 - \sigma^2 + K_c) + 2\left(\frac{\rho_{a1}}{\rho_{a4}} - 1\right) + f_{app}\frac{A_a\,\rho_{a1}}{A_2\,\rho_{am}}\right.$$

$$\left. - (1 - \sigma^2 - K_e)\frac{\rho_{a1}}{\rho_{a4}}\right] \tag{5.3.13}$$

Values for different contraction and expansion loss coefficients are determined as discussed in section 2.3.1.

Generally, the core frictional pressure drop is the dominating term accounting for about 90 percent or more of Δp_a. In the case of a finned tube core the friction factor, f_{app}, is an apparent factor which takes into account both the skin friction and form drag effects in the core. For flow over tube banks, normal fins on individual tubes, longitudinal fins on individual fins, and screen matrices, the inlet and outlet losses may thus for all practical purposes be accounted for by the friction factor, so that equation (5.3.13) becomes

$$\Delta p_a = \frac{G_{a2}^2}{2\,\rho_{a1}}\left[(1-\sigma^2) + 2\left(\frac{\rho_{a1}}{\rho_{a4}} - 1\right) + f_{app}\,\frac{A_a\,\rho_{a1}}{A_2\,\rho_{am}} - (1-\sigma^2)\,\frac{\rho_{a1}}{\rho_{a4}}\right]$$

or

$$\Delta p_a = \frac{G_{a2}^2}{2}\left[\frac{f_{app}\,A_a}{\rho_{am}\,A_2} + (1+\sigma^2)\left(\frac{1}{\rho_{a4}} - \frac{1}{\rho_{a1}}\right)\right] \tag{5.3.14}$$

From this equation it follows that the effective friction factor is

$$f_{app} = \rho_{am}\,\frac{A_2}{A_a}\left[\frac{2\Delta p_a}{G_{a2}^2} - (1+\sigma^2)\left(\frac{1}{\rho_{a4}} - \frac{1}{\rho_{a1}}\right)\right] \tag{5.3.15}$$

All parameters in equation (5.3.15) are specified or available in the form of experimental data, so that the friction factor may be determined.

The correct mean air density is obtained by integration:

$$\frac{1}{\rho_{am}} = \frac{1}{A_a}\int_0^A \frac{1}{\rho_a}\,dA_a \tag{5.3.16}$$

For the counterflow heat exchanger in which C_{min}/C_{max} is unity, stream temperatures vary linearly with area; so that the harmonic mean density may be determined from

$$\frac{1}{\rho_{am}} = 0.5\left(\frac{1}{\rho_{a1}} + \frac{1}{\rho_{a4}}\right) \tag{5.3.17}$$

This relation is a fair approximation for any flow arrangement other than parallel flow.

In the particular case where the wall temperature is approximately constant, as in a condenser, the mean density is a function of the logarithmic mean temperature difference between the streams.

$$\frac{1}{\rho_{am}} = 2\ R_a \left(\frac{T_{const} - \Delta T_{lm}}{p_{a1} + p_{a2}}\right) \tag{5.3.18}$$

Under isothermal conditions equation (5.3.14) reduces to

$$\Delta p_{a_{iso}} = G_{a2}^2\ f_{appiso} A_a/(2\ \rho_a\ A_2) \tag{5.3.19}$$

or

$$f_{appiso} = 2\rho_a\ \Delta p_{aiso}\ A_2\ /(G_{a2}^2\ A_a) \tag{5.3.20}$$

In certain applications it is convenient to express the pressure drop in terms of the mass velocity based on the frontal area of the core, i.e. $G_{afr} = m_a/A_{fr}$. Equations (5.3.14) may thus be written as

$$\Delta p_a = \frac{G_{afr}^2}{2\sigma^2}\left[\frac{f_{app}\ A_a}{\rho_{am}\ A_2} + (1 + \sigma^2)\left(\frac{1}{\rho_{a4}} - \frac{1}{\rho_{a1}}\right)\right] \tag{5.3.21}$$

In the above equations subscripts 1 and 4 may be replaced by i and o, referring to inlet and outlet conditions respectively.

5.4 PRESENTATION OF DATA

Different methods for presenting the heat transfer and pressure drop characteristics of finned tubes are found in the literature. Generally the heat transfer coefficient is presented in the form of the dimensionless Nusselt number, i.e.

$$Nu = hd_e/k \tag{5.4.1}$$

where d_e is some equivalent diameter. Similarly, the pressure differential may be represented by the dimensionless Euler number

$$Eu = \Delta p/\rho v^2 = \rho \Delta p/G^2 \tag{5.4.2}$$

or a loss coefficient defined as

$$K = 2\Delta p_t/\rho v^2 = 2\rho \Delta p_t/G^2 \tag{5.4.3}$$

where Δp_t is the change in total pressure across the heat exchanger. The mass velocity may be based on the minimum flow area through the heat exchanger, or the frontal area of the heat exchanger.

Other methods of presentation may, however, be preferred for various reasons [84KA1, 84KR1, 86KR1].

5.4.1 COLBURN J- AND FRICTION FACTOR

Kays and London [84KA1] present their heat transfer data for many different finned surfaces in dimensionless form according to a method originally proposed by Colburn [33CO1],

$$j = St\,Pr^{0.67} = \frac{Nu\,Pr^{0.67}}{Re\,Pr} = \frac{h\,Pr^{0.67}}{G_c\,c_p} = \text{function of Re} \tag{5.4.4}$$

where j is known as the Colburn j-factor. The mass velocity, G_c, is evaluated on the basis of the minimum free flow area A_c, i.e. $G_c = m/A_c$. The Reynolds and Nusselt numbers are based on the equivalent diameter defined as

$$d_e = 4 A_c L/A \tag{5.4.5}$$

where L is the flow length of the heat exchanger, A_c is the minimum flow cross-sectional area, and A is the total heat transfer area. For flow normal to tube banks, L is an equivalent flow length measured from the leading edge of the first tube row to the leading edge of a tube row that would follow the last tube row.

The Reynolds number is

$$Re = 4G_c A_c L/(\mu A) = 4mL/(\mu A) \tag{5.4.6}$$

With h obtained from equation (5.3.7) and the corresponding value of G_c known, the j-factor and the Reynolds number can be determined with the aid of equations (5.4.4) and (5.4.6).

The friction factor, f, can also be expressed in terms of the Reynolds number:

$$f = \text{function of Re} \tag{5.4.7}$$

From experimental data and other specified parameters, f_{app} is obtained from equation (5.3.15) for a particular flow condition.

All physical properties are evaluated at the arithmetic mean temperature $T_m = (T_i + T_o)/2$. According to Kays and London [84KA1], the above correlations are satisfactory over a limited range of temperatures and no corrections are required for variations in properties. Some uncertainty still exists however, concerning correction factors that take into consideration variations in thermophysical properties during flows through heat exchanger bundles.

The calculated values of j and f_{app} as functions of the Reynolds number are presented graphically in figure 5.4.1 for a particular heat exchanger core configuration.

The above method of presenting the data is also employed in a very extensive survey of finned-tube performance characteristics undertaken by PFR Engineering Systems Inc. [76PF1].

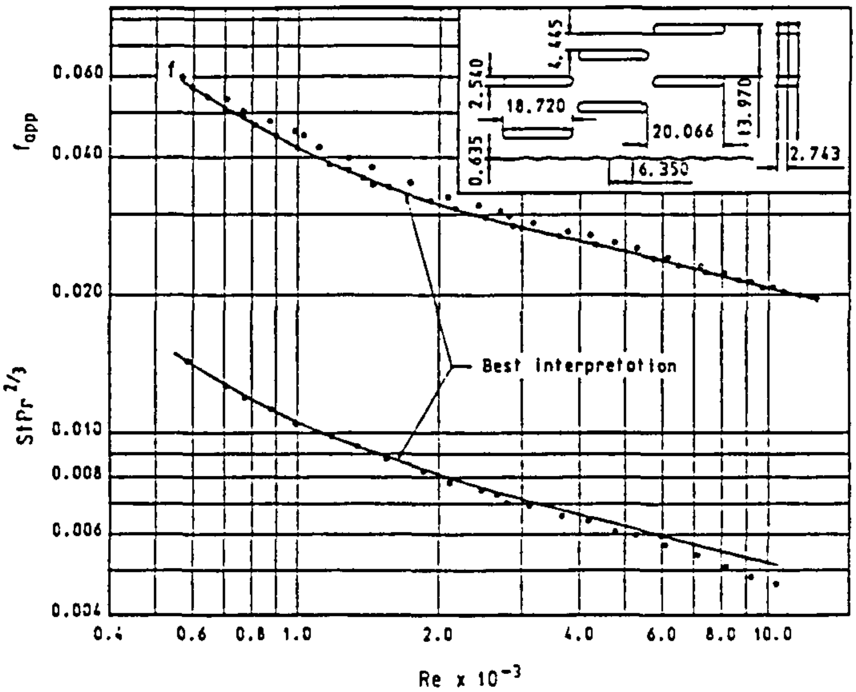

Fin pitch = 366 per m
Flow passage hydraulic diameter = 4.12×10^{-3} m
Fin metal thickness (copper) = 0.102×10^{-3} m
Free flow area/frontal area = 0.788
Total heat transfer area/total volume = 748 m^2/m^3
Fin area/total area = 0.814

Figure 5.4.1: Performance characteristics of heat exchangers.

5.4.2 CHARACTERISTIC HEAT TRANSFER AND PRESSURE DROP PARAMETER

Another method for presenting the experimentally obtained performance data of finned tubes which has particular merit in the case of industrial finned-tube heat exchangers is evaluated by Kern [80KE1] and is presented in a modified form in this section [86KR1].

According to equation (5.4.4), the heat transfer coefficient under conditions of forced convection through finned surfaces may be expressed in terms of dimensionless parameters as

$$Nu/(Re\ Pr^{0.333}) = f\ (Re) \qquad (5.4.8)$$

or

$$Nu = a_1\ Re^{b1}\ Pr^{0.333} \qquad (5.4.9)$$

The coefficient a_1 and the exponent b_1 are not necessarily constant over a wide range of the Reynolds number.

Both the Nusselt number and the Reynolds number contain an equivalent or hydraulic diameter. Because of the relatively arbitrary nature or the definition of this quantity for finned surfaces, different definitions are found in the literature. In practice this often leads to confusion and makes any comparison of performance characteristics of different types of finned surfaces meaningless.

In the absence of the equivalent diameter, equation (5.4.9) may be written as

$$h/k = a_2\ Ry^{b_2}\ Pr^{0.333} \qquad (5.4.10)$$

where

$$Ry = G_{fr}/\mu = m/(\mu\ A_{fr}) \qquad (5.4.11)$$

is known as a characteristic flow parameter.

The effective finned surface area and the heat exchanger frontal area play a major role in comparing and optimizing heat exchangers. These parameters are introduced into equation (5.4.10) such that

$$Ny_h = h\ e_f\ A/(k\ A_{fr}\ Pr^{0.333}) = a_{Ny_h}\ Ry^{b_{Ny\,h}} \qquad (5.4.12)$$

where Ny_h is known as a characteristic heat transfer parameter.

For most industrial finned surfaces that have been performance tested, the actual finside heat transfer coefficient, h, or the finned surface effectiveness, e_f, is of no particular interest. For this reason the use of an effective heat transfer coefficient as defined by equation (5.3.9) may be preferred to define a corresponding heat transfer parameter:

$$Ny = h_e A/(k A_{fr} Pr^{0.333}) = a_{Ny} Ry^{b_{Ny}} \tag{5.4.13}$$

All physical properties are evaluated at the arithmetic mean temperature $Tm = (T_i + T_o)/2$.

The pressure drop across a finned-tube heat exchanger during isothermal flow conditions may also be expressed in dimensionless form based on the free stream conditions as

$$Eu_{iso} = \Delta p_{iso}/\rho v^2 = a_3 Re^{b_3} \tag{5.4.14}$$

If the equivalent diameter is not included in this equation it may be written as

$$Eu_{iso} = \frac{\Delta p_{iso}}{\rho v^2} = a_4 \left(\frac{G_{fr}}{\mu}\right)^{b_4} = a_4 Ry^{b_4} \tag{5.4.15}$$

or in terms of a characteristic pressure drop parameter defined as

$$Ey_{iso} = \frac{\rho \Delta p_{iso}}{\mu^2} = a_{Ey} Ry^{b_{Ey}} = Eu_{iso} Ry^2 \tag{5.4.16}$$

During non-isothermal operation, however, there is in addition to the frictional loss a further term owing to acceleration effects as shown in equation (5.3.21), i.e.

$$\Delta p_{acc} = \frac{G_{fr}^2}{2}\left(\frac{1}{\sigma^2} + 1\right)\left(\frac{1}{\rho_o} - \frac{1}{\rho_i}\right) \tag{5.4.17}$$

where σ is the ratio of the minimum air-side flow area between the tubes divided by the corresponding frontal area.

By introducing the characteristic flow parameter Ry, this equation may be modified to read as follows:

$$\frac{\rho_m \Delta p_{acc}}{\mu^2} = \frac{\rho_m Ry^2}{2}\left(\frac{1}{\sigma^2} + 1\right)\left(\frac{\rho_i - \rho_o}{\rho_i \rho_o}\right) \tag{5.4.18}$$

Substitute the mean density from equation (5.3.17) into equation (5.4.18), and find

$$\frac{\rho_m \Delta p_{acc}}{\mu^2} = Ry^2\left(\frac{1}{\sigma^2} + 1\right)\left(\frac{\rho_i - \rho_o}{\rho_i + \rho_o}\right) \tag{5.4.19}$$

The non-isothermal characteristic pressure drop parameter is thus defined as

$$Ey = Ey_{iso} + \frac{\rho_m \Delta p_{acc}}{\mu^2} = \frac{\rho \Delta p}{\mu^2}$$

$$= a_{Ey}\, Ry^{\,b_{Ey}} + Ry^2\left(\frac{1}{\sigma^2} + 1\right)\frac{(\rho_i - \rho_o)}{(\rho_i + \rho_o)} \tag{5.4.20}$$

From this equation it also follows that the non-isothermal static pressure drop can be expressed as

$$\Delta p = \rho_m v_m^2 \left[a_{Ey}\, Ry^{(b_{Ey} - 2)} + \left(\frac{1}{\sigma^2} + 1\right)\left(\frac{\rho_i - \rho_o}{\rho_i + \rho_o}\right)\right] \tag{5.4.21}$$

A corresponding loss coefficient based on the total pressure difference across the heat exchanger and the mean density can be defined as

$$K_{he} = \frac{\Delta p_t}{\rho_m v_m^2/2} = \frac{\Delta p + \rho_i v_i^2/2 - \rho_o v_o^2/2}{\rho_m v_m^2/2}$$

5.5 HEAT TRANSFER AND PRESSURE DROP CORRELATIONS:

Although numerous heat transfer and pressure drop correlations for flow through bundles of finned tubes have been reported in the literature, all have their limitations and great care should be taken when applying them to a particular design. In the following equations all thermophysical properties are evaluated at the mean air temperature unless specified otherwise.

5.5.1 HEAT TRANSFER CORRELATIONS FOR STAGGERED CIRCULAR FINNED TUBES

Some of the early empirical relations applicable to bundles of staggered circular finned tubes are proposed by Jameson [45JA1], Katz and Young [54KA1], Kutateladze and Borishaniskii [58KU1] and Schmidt [63SC1].

The heat transfer correlations proposed by Briggs and Young [63BR1] are based on a wide range of data. Their general equation for six-row, equilaterally arranged, finned tube bundles can be recommended:

$$\frac{hd_r}{k} = 0.134\ Pr^{0.33}\ Re^{0.681} \left[\frac{2(P_f - t_f)}{d_f - d_r}\right]^{0.2} \left(\frac{P_f - t_f}{t_f}\right)^{0.1134} \qquad (5.5.1)$$

where $Re = G_c\, d_r/\mu$

This equation is valid within the following limits:

$1000 < Re < 18000$

$11.13\ mm < d_r < 40.89\ mm$

$1.42\ mm < (d_f - d_r)/2 < 16.57\ mm$

$0.33\ mm < t_f < 2.02\ mm$

$1.30\ mm < P_f < 4.06\ mm$

$24.49\ mm < P_t < 111\ mm$

Brauer [64BR1] investigated the heat transfer and pressure drop characteristics of round and elliptical finned tubes for staggered and in-line arrangement but did not develop any new empirical equations to correlate his data.

Schulenberg [65SC1] proposed a correlation in which the exponent of the Reynolds number is a function of the finned surface area. In 1966 Vampola [66VA1] proposed an equation based on an extensive study of different finned tubes. For more than three tube rows,

$$\frac{h\, d_e}{k} = 0.251\ Re^{0.67} \left(\frac{P_t - d_r}{d_r}\right)^{-0.2} \left(\frac{P_t - d_r}{P_f - t_f} + 1\right)^{-0.2} \left(\frac{P_t - d_r}{P_d - d_r}\right)^{0.4} \qquad (5.5.2)$$

when $(P_t - d_r)/(P_d - d_r) > 1$. For all other values of the latter term, it is replaced by unity in the above equation. The diagonal pitch is given by

$$P_d = [(P_t/2)^2 + P_l^2]^{0.5}$$

The Reynolds number is defined as

$$Re = G_c\, d_e/\mu$$

where

$$d_e = \frac{A_{re}\, d_r + A_f\, (A_f/2n_f)^{0.5}}{A_f + A_{re}}$$

all values being calculated for a one-meter length of tube, A_f being the fin surface area and A_{re} the corresponding exposed root area.

This equation is valid within the following limits:

$1000 < R_e < 10000$
$10.67\ \text{mm} < d_r < 26.01\ \text{mm}$
$5.20\ \text{mm} < (d_f - d_r)/2 < 9.70\ \text{mm}$
$0.25\ \text{mm} < t_f < 0.70\ \text{mm}$

$2.28 \text{ mm} < P_f < 5.92 \text{ mm}$

$20.32 \text{ mm} < P_l < 52.40 \text{ mm}$

$24.78 \text{ mm} < P_t < 49.55 \text{ mm}$

$16.20 \text{ mm} < d_e < 34.00 \text{ mm}$

$0.48 \text{ mm} < (P_t - d_r)/d_r < 1.64$

$4.34 < (P_t - d_r)/(P_f - t_f) + 1 < 25.2$

$0.45 < (P_t - d_r)/(P_d - d_r) < 2.50$

Further correlations were proposed by Zozulya et al [70ZO1] and Kuntysh [71KU1]. In 1974 Mirković [74MI1] proposed the following correlation for an eight-row tube bundle:

$$\frac{hd_{et}}{k} = 0.224 \ Pr^{0.33} \ Re^{0.662} \left(\frac{P_t - d_r}{d_r}\right)^{0.1} \left(\frac{d_r}{P_l - d_r}\right)^{0.15} \left[\frac{2(P_f - t_f)}{d_f - d_r}\right]^{0.25} \qquad (5.5.3)$$

where

$$Re = G_c \, d_{et}/\mu$$

and

$$d_{et} = A_1/\pi(d_f - d_r + P_f)$$

A_1 is the area exposed to the airstream by one fin and its corresponding exposed root area.

This equation is valid within the following limits:

$3000 < Re < 56\,000$

$25.40 \text{ mm} < d_r < 50.80 \text{ mm}$

$9.53 \text{ mm} < (d_f - d_r)/2 < 15.88 \text{ mm}$

$1.27 \text{ mm} < t_f < 2.03 \text{ mm}$

$4.23 \text{ mm} < P_f < 8.47 \text{ mm}$

$60 \text{ mm} < P_l < 80 \text{ mm}$

$100 \text{ mm} < P_t < 120 \text{ mm}$

Other correlations include those of Zhukauskas [74ZH1], Elmahdy and Biggs [79EL1], Hofmann [76HO1], Biery [81BI1], Gianolio and Cuti [81GI1], Brandt and Wehle [83BR1], ESDU [86ES1] and Nir [91NI1]. Weierman [76WE1] correlated performance data for finned tubes and presented his findings in graphic form.

Ganguli et al [85GA1] propose the following correlation for three or more rows of finned tubes:

$$\frac{h\ d_r}{k} = 0.38\ Re^{0.6}\ Pr^{0.333}\ (A/A_r)^{-0.15} \tag{5.5.4}$$

where

$Re = G_c d_r/\mu$

The ratio of the total air-side area to the root area A_r if no fins are present, is given by

$$(A_f + A_{re})/A_r = \left[(d_f^2 - d_r^2)/2 + d_f t_{ft} + d_r(P_f - t_{fr})\right]/(d_r P_f)$$

This correlation is valid for:

$11.176\ mm < d_r < 50.8\ mm$
$5.842\ mm < (d_f - d_r)/2 < 19.05\ mm$
$2.3\ mm < P_f < 3.629\ mm$
$0.254\ mm < t_f < 0.559\ mm$
$27.432\ mm < P_t < 98.552\ mm$
$1800 < Re < 100000$
$1 < (A_f + A_{re})/A_r \leq 50$

The above correlations are applicable to bundles having three or more rows of finned tubes and are based on tests performed in windtunnels where the turbulence levels of the incoming airstream are generally low, as would be the case in many induced-draft heat exchangers. These equations should, therefore be multiplied by a row correction factor, F_r, when the bundle consists of fewer tube rows.

Information in the literature for bundles less than six rows deep is inconsistent. Brauer [62BR1] found heat transfer stability by the second row, Ward and Young [59WA1] by the fourth to sixth row, and Mirković [74MI1] by the eighth row. Eckels and Rabas [85EC1] also found stability by the fourth row.

Ward and Young [59WA1] found the row-effect to be a function of the air velocity, v_c, through the smallest cross-section of the finned tube bundle as shown in figure 5.5.1. According to Gionolio and Cuti [81GI1] this trend is correlated approximately by

$$h_{nr} = h_6 \left(1 + v_c/n_r^2\right)^{-0.14} \tag{5.5.5}$$

where h_6 is the mean heat transfer coefficient for a six-row bundle and n_r is the number of tube rows in the flow direction.

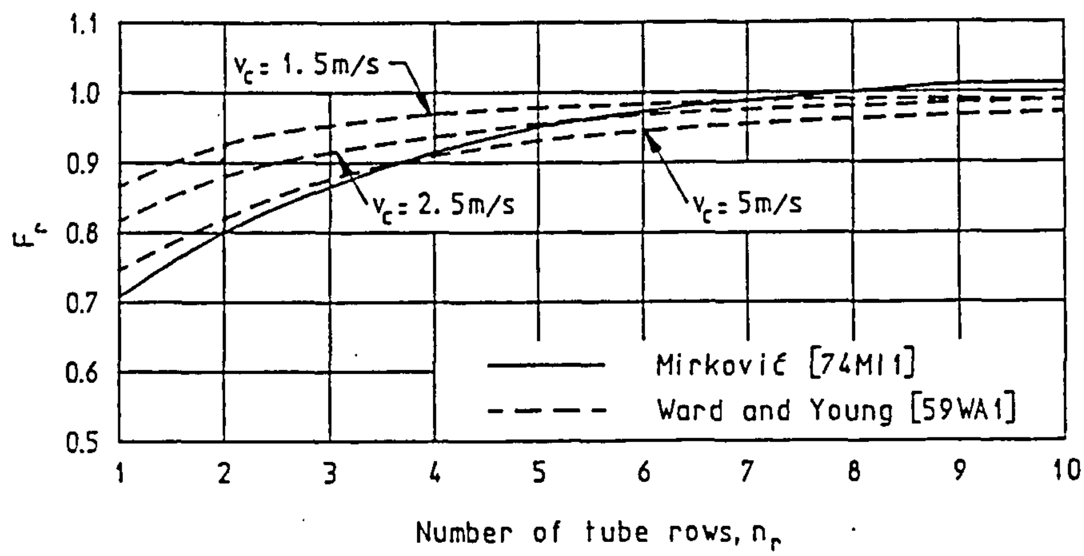

Figure 5.5.1: Tube row correction factor.

Because of this row-effect, it is recommended that the heat transfer performance characteristics of individual tube rows in a bundle be determined in windtunnel tests for the accurate design of certain types of heat exchangers, e.g. induced-draft condensers.

Where the turbulence levels of the incoming airstream are high, such as in forced-draft heat exchangers, other correction factors are recommended (see section 5.9).

The above equations are given not because they are necessarily better than others referred to but because they represent a wide spectrum of data and have been applied in the design of practical systems.

It is obvious from this extensive yet incomplete summary of references that no single correlation exists that can accurately predict the heat transfer characteristics of circular finned tubes arranged in a staggered pattern.

Extensive surveys of finned tube performance characteristics are presented by PFR Engineering Systems Inc. [76PF1], Stasiulevicius and Srinska [88ST1], and Zukauskas and Ulinskas [88ZU1].

Where uncertainties exist, or where the limits of applicability are exceeded, the results of different equations should be compared for a particular design. When a more sophisticated analysis is required, laboratory tests must be conducted on a bundle of the particular finned tubes to be employed.

5.5.2 PRESSURE DROP CORRELATIONS FOR STAGGERED CIRCULAR FINNED TUBES

Numerous correlations with which the static pressure drop through bundles of staggered circular finned tubes can be predicted are reported in the literature. Gunter and Shaw [45GU1], Jameson [45JA1] and Ward and Young [59WA1] presented some of the earlier correlations.

A frequently used equation is that due to Robinson and Briggs [66RO1] for tubes arranged in a staggered (equilateral) pattern:

$$Eu = \frac{\rho\,\Delta p}{G_c^2} = 18.93\, n_r\, Re^{-0.316} \left(\frac{P_t}{d_r}\right)^{-0.927} \left(\frac{P_t}{P_d}\right)^{0.515} \tag{5.5.6}$$

for n_r tube rows and where

$$Re = G_c\, d_r/\mu$$

and the diagonal pitch can be found from

$$P_d = \left[(P_t/2)^2 + P_l^2\right]^{0.5}$$

This equation is valid for

$2000 < Re < 50000$

$18.64 \text{ mm} < d_r < 40.89 \text{ mm}$

$39.68 \text{ mm} < d_f < 69.85 \text{ mm}$

$10.52 \text{ mm} < (d_f - d_r)/2 < 14.48 \text{ mm}$

$42.85 \text{ mm} < P_t < 114.3 \text{ mm}$

$37.11 \text{ mm} < P_l < 98.99 \text{ mm}$

$2.31 \text{ mm} < P_f < 2.82 \text{ mm}$

$1.8 < P_t/d_r < 4.6$

Vampola [66VA1] proposes the following empirical relation for the pressure drop:

$$Eu = \frac{\rho\,\Delta p}{G_c^2} = 0.7315\, n_r\, Re^{-0.245} \left(\frac{P_t - d_r}{d_r}\right)^{-0.9} \left(\frac{P_t - d_r}{P_f - t_f} + 1\right)^{0.7} \left(\frac{d_e}{d_r}\right)^{0.9} \quad (5.5.7)$$

where the definition of Re and the limits of applicability of this equation are similar to those of equation (5.5.2).

Based on a series of tests conducted by Mirković [74MI1],

$$Eu = \frac{\rho\,\Delta p}{G_c^2} = 3.96\, n_r\, Re^{-0.31} \left(\frac{P_t - d_r}{d_r}\right)^{0.14} \left(\frac{d_r}{P_l - d_r}\right)^{0.18} \left[\frac{d_f - d_r}{2(P_f - t_f)}\right]^{0.2} \quad (5.5.8)$$

where

$$Re = G_c\, d_{eh}/\mu$$

5.6 OBLIQUE FLOW THROUGH HEAT EXCHANGERS

In large air-cooled systems, heat exchanger bundles are often arranged in the form of A-frames, deltas or V-arrays to conserve space. The general flow pattern through two finned tube bundles of an A-frame or a V- or A-frame array heat exchanger system is sketched in figure 5.6.1.

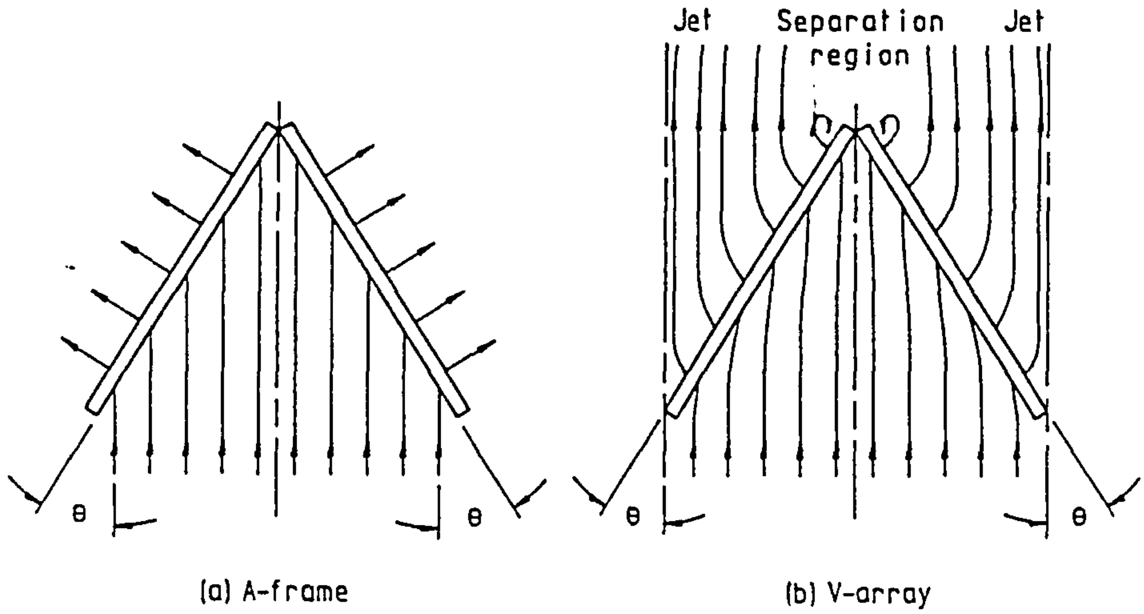

Figure 5.6.1: General picture of the flow through inclined finned tube bundles.

On passing through the bundles in the V- or A-frame array, the streamlines will emerge in a direction almost perpendicular to the downstream face if the loss coefficient of the finned tube bundle is high, and will then converge into a jet with severe separation at the downstream corners of the bundle face, forming distorted velocity profiles. As the downstream streamlines are curved, the pressure is not uniform along the downstream face of the bundle, and this in turn causes the velocity through the bundle to vary with position. The result is that the upstream flow may approach the bundle with greater obliquity than it would if this flow were uniform. Thus, the obliquity of the incoming flow to the bundle front face and the jet formed at the downstream face may be regarded as two inter-related effects which cause a considerable loss that contributes significantly to overall aerodynamic losses and hence will affect the performance of the cooling system.

5.6.1 OBLIQUE FLOW ANALYSIS

The inlet pressure loss for oblique or inclined flow through a finned tube heat exchanger bundle may be analyzed by a simplified model proposed by Moore and Torrence [77MO2]. Consider a set of parallel thin sheets of negligible thickness as shown in figure 5.6.2.

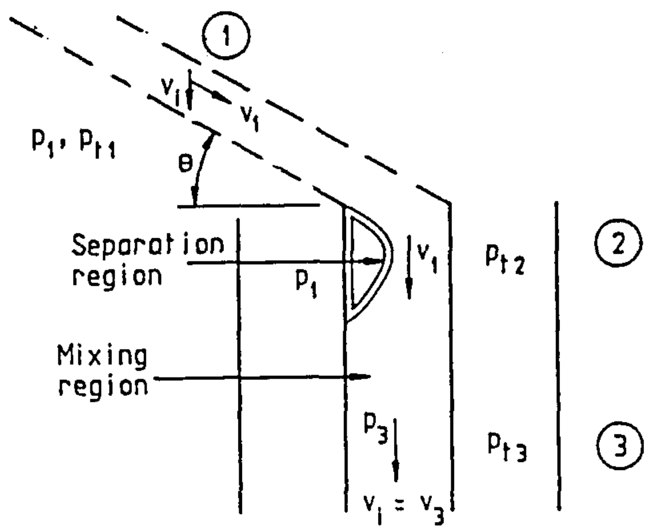

Figure 5.6.2: Behavior of the flow at the entrance of a parallel thin sheet bundle.

Incoming flow streamlines approach the upstream face with an angle θ and the flow is constrained to leave normally. The entering flow tends to separate on the thin sheet leading edge upon entering and a jet is formed. Referring to figure 5.6.2, the velocity of the flow is assumed uniform over the cross section at 1. After turning, the flow evolves into a parallel flow at 2, and since the flow is potential between 1 and 2, the velocity at 2 can be assumed to be essentially uniform. It is also assumed that the static pressure within the initial separation region is approximately constant and is therefore equal to the upstream static pressure, p_1. Thus by Bernoulli's equation the velocity at the minimum cross-section must be equal to the upstream velocity, v_1. The flow then mixes downstream from this minimum cross-section and attains the velocity v_3 and static pressure p_3. The drop in total pressure difference between positions 2 and 3 is given by the following equation:

$$p_{t1} - p_{t3} = \Delta p_{it} = p_1 - p_3 + \rho\,(v_1^2 - v_3^2)/2 \qquad (5.6.1)$$

Applying the momentum equation between 2 and 3 one obtains

$$p_1 - p_3 = \rho v_3(v_3 - v_1) \qquad (5.6.2)$$

Substitution of equation (5.6.2) into equation (5.6.1) yields

$$\Delta p_{it} = \rho v_3^2 - \rho v_3 v_1 + \rho v_1^2/2 - \rho v_3^2/2$$

which can be written as

$$\Delta p_{it} = \rho v_3^2(v_1/v_3 - 1)^2/2 \qquad (5.6.3)$$

Since $v_1/v_3 = 1/\sin\theta$, by continuity, i.e. the contraction coefficient is equal to $\sin\theta$, and by introducing the definition

$$K_{i\theta} = \Delta p_{it}/(\rho v_3^2/2) \qquad (5.6.4)$$

the above equation may be written as

$$K_{i\theta} = \left(\frac{1}{\sin\theta} - 1\right)^2 \qquad (5.6.5)$$

Mohandes [79MO1, 84MO1] proposes the following modified expression for the loss coefficient based on experimental observations with bundles of finned tubes or sheets having a finite thickness:

$$K_{i\theta} = \left(K_{ci}^{0.5} + \frac{1}{\sin\theta} - 1\right)^2 \qquad (5.6.6)$$

where K_{ci} is the entrance contraction loss coefficient for the normal flow condition, based on the normal approach free stream velocity. For turbulent flow between flat sheets $K_{ci} = K_c/\sigma_{21}^2$ where K_c is given by equation (2.3.13).

The loss coefficient for the complete bundle is

$$K_{he\theta} = K_{i\theta} + K_f + K_{ei} = \Delta p_t/(\rho v_i^2/2) \qquad (5.6.7)$$

where K_f and K_{ei} represent respectively the friction and outlet expansion losses respectively and v_i is the mean normal inlet velocity.

Substitute equation (5.6.6) into equation (5.6.7) and find

$$K_{he\theta} = \left(K_{ci}^{0.5} + \frac{1}{\sin\theta} - 1\right)^2 + K_f + K_{ei}$$

$$= K_{he} + \left(\frac{1}{\sin\theta} - 1\right)\left[\left(\frac{1}{\sin\theta} - 1\right) + 2\,K_{ci}^{0.5}\right] \qquad (5.6.8)$$

where K_{he} is the loss coefficient for normal flow through the bundle and includes the contraction and expansion losses under these conditions.

In the case of a single inclined bundle located in a duct of constant cross-section or in an array of V- or A-frames the stream leaving the bundle in an approximately normal direction is redirected as shown in figure 5.6.3.

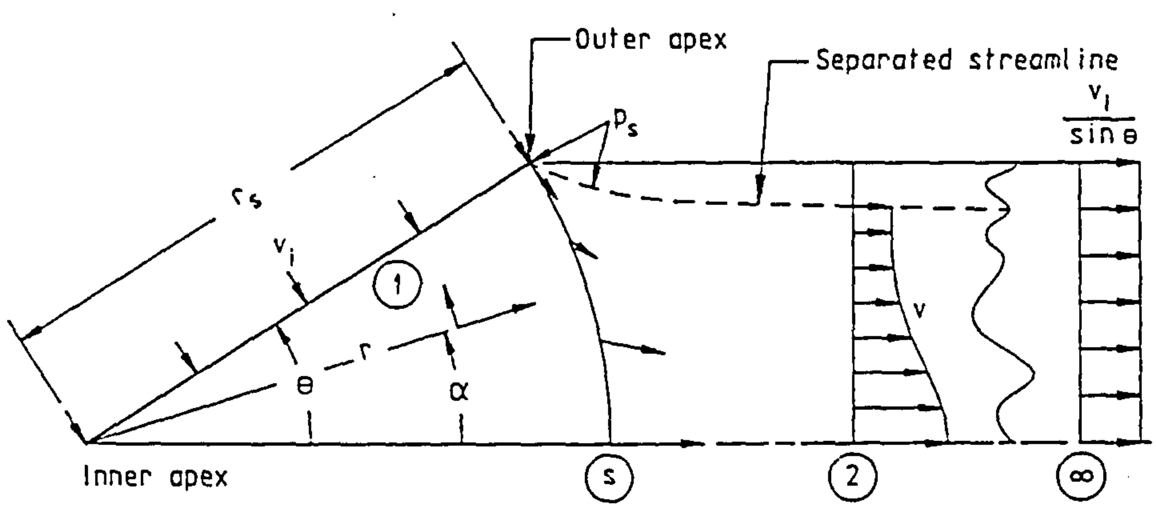

Figure 5.6.3: Sketch of the co-ordinate system and flow process.

The total pressure drop after the inclined bundle is due first to the turbulent decay of the jet near the centerline which occurs directly downstream in the "V" region from position 1 to position 2, and the second part of the loss occurs between 2 and ∞, owing to the final mixing process which is responsible for smoothing out the velocity profile [79MO3]. The downstream loss coefficient is given by

$$K_d = (p_{t1} - p_{t\infty})/(\rho_1 v_i^2/2) \tag{5.6.9}$$

where p_{t1} is the mean total pressure immediately downstream of the bundle, v_i is the mean velocity normal to the bundle at this point, and ρ_1 is the corresponding density. The value of this coefficient for different angles is shown graphically in figure 5.6.4 and may be expressed in terms of the following empirical relation [86KO1]:

$$K_d = \exp(5.488405 - 0.2131209\,\theta + 3.533265 \times 10^{-3}\theta^2 - 0.2901016 \times 10^{-4}\theta^3) \tag{5.6.10}$$

where the apex semi-angle θ is given in degrees.

The jetting loss alone, may be expressed as [86KO2]:

$$K_{dj} = \exp(5.32262 - 0.22888\theta + 4.193055 \times 10^{-3}\theta^2 - 4.082383 \times 10^{-5}\theta^3) \tag{5.6.11}$$

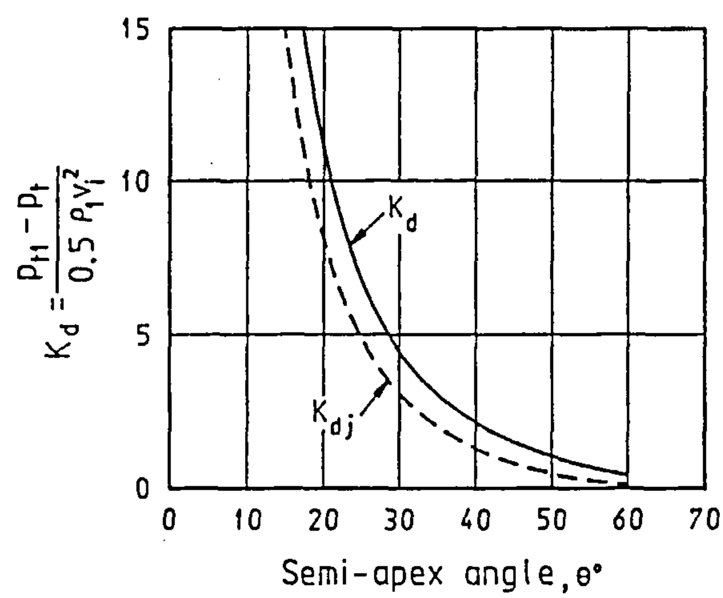

Figure 5.6.4: Overall downstream losses.

The total loss coefficient for the bundle with inlet and downstream losses owing to oblique flow is obtained by the addition of equations (5.6.8) and (5.6.9).

$$K_{he\theta} = K_{he} + \left(\frac{1}{\sin\theta_m} - 1\right)\left[\left(\frac{1}{\sin\theta_m} - 1\right) + 2 K_{ci}^{0.5}\right] + K_d \tag{5.6.12}$$

where θ_m is the mean flow incidence angle.

Owing to the flow distortion downstream of the bundle, the actual mean flow incidence angle will not be uniform along the bundle face and is generally smaller than θ as shown in figure 5.6.5. This effect should be taken into account when evaluating the inlet loss in equation (5.6.12). The curve shown in figure 5.6.5 is represented approximately by the following empirical relation:

$$\theta_m = 0.0019\,\theta^2 + 0.9133\,\theta - 3.1558 \tag{5.6.13}$$

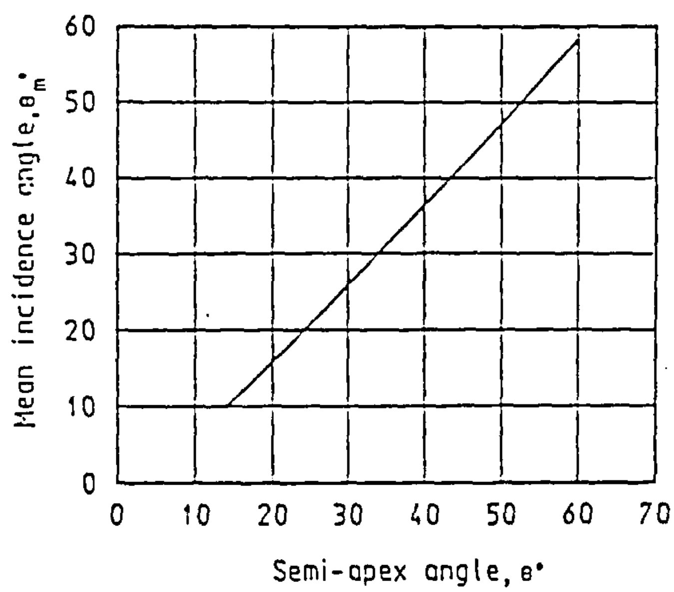

Figure 5.6.5: Mean flow incidence angle as function of the semi-apex angle.

It follows from equation (5.6.12) that the change in total pressure is

$$\Delta p_{t\theta} = \frac{0.5}{\rho}\left(\frac{m}{A_{fr}}\right)^2 \left[K_{he} + \left(\frac{1}{\sin\theta_m} - 1\right)\left\{\left(\frac{1}{\sin\theta_m} - 1\right) + 2 K_{ci}^{0.5}\right\} + K_d\right] \tag{5.6.14}$$

When heat is transferred to the air stream the total pressure drop across an inclined heat exchanger bundle is

$$\Delta p_{t\theta} = 0.5\left(\frac{m}{A_{fr}}\right)^2\left[\frac{K_{he}}{2}\left(\frac{1}{\rho_i}+\frac{1}{\rho_o}\right)+\frac{1}{\rho_i}\left(\frac{1}{\sin\theta_m}-1\right)\left\{\left(\frac{1}{\sin\theta_m}-1\right)\right.\right.$$

$$\left.\left.+\,2\,K_{ci}^{0.5}\right\}+\frac{K_d}{\rho_o}\right] \tag{5.6.15}$$

where K_{he} is obtained from equation (5.4.22) or (5.4.23).

The corresponding loss coefficient is

$$K_{he\theta} = K_{he}+\frac{2\,\rho_o}{(\rho_o+\rho_i)}\left(\frac{1}{\sin\theta_m}-1\right)\left[\left(\frac{1}{\sin\theta_m}-1\right)+2\,K_{ci}^{0.5}\right]$$

$$+\,\frac{2\,\rho_i\,K_d}{(\rho_o+\rho_i)} \tag{5.6.16}$$

The loss coefficient given by equation (5.6.12) may be determined directly in an experimental test and expressed in terms of the flow parameter Ry. In the case of non-isothermal conditions the resultant loss coefficient is approximately

$$K_{he\theta} = a_{K_\theta}\,Ry^{\,b_{K_\theta}}+\frac{2}{\sigma^2}\left(\frac{\rho_i-\rho_o}{\rho_i+\rho_o}\right) \tag{5.6.17}$$

5.6.2 OBLIQUE FLOW EXPERIMENTS

Kotzé et al [86KO1] compare equations (5.6.8) and (5.6.12) to isothermal experimental results obtained on single inclined three-, four- and eight-tube row bundles. Details of their finned tubes and tube arrangement in the test bundle are given in example 5.4.1.

As shown in figure 5.6.6, good agreement between theory and experiment is obtained for the eight-row bundle, which has a relatively high flow resistance. Although equation (5.6.8) also predicts the pressure drop quite accurately for the remaining bundles where the flow approaches obliquely but leaves the bundle normally, some discrepancy is observed when equation (5.6.12) is applied to bundles where the outlet flow is directed by the duct walls.

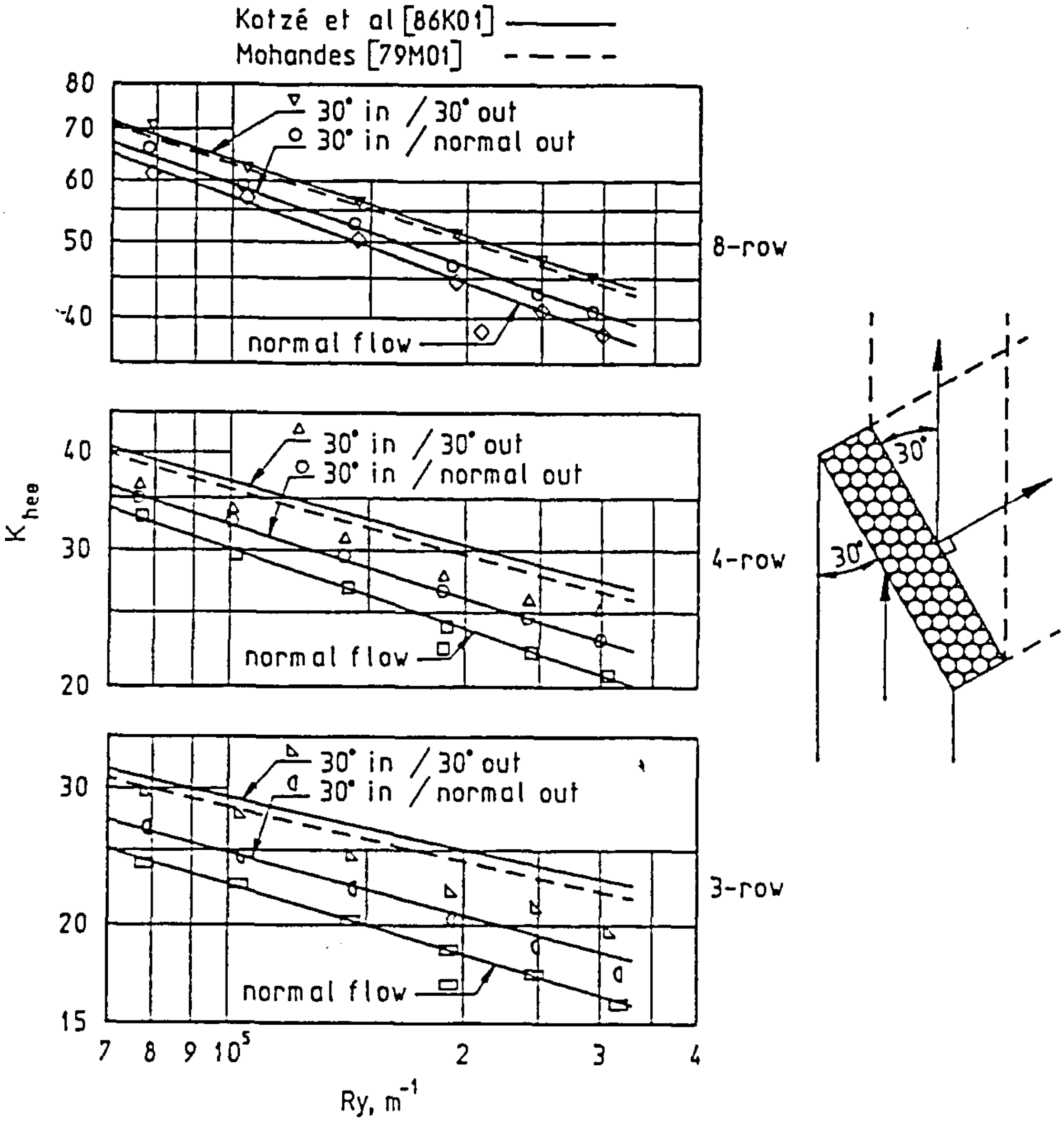

Figure 5.6.6: Pressure drop across heat exchanger.

When the total pressure drop across an inclined bundle is determined experimentally under isothermal conditions, losses under non-isothermal conditions can be predicted only approximately, since the inlet and outlet losses which are dependent on the respective densities are not known.

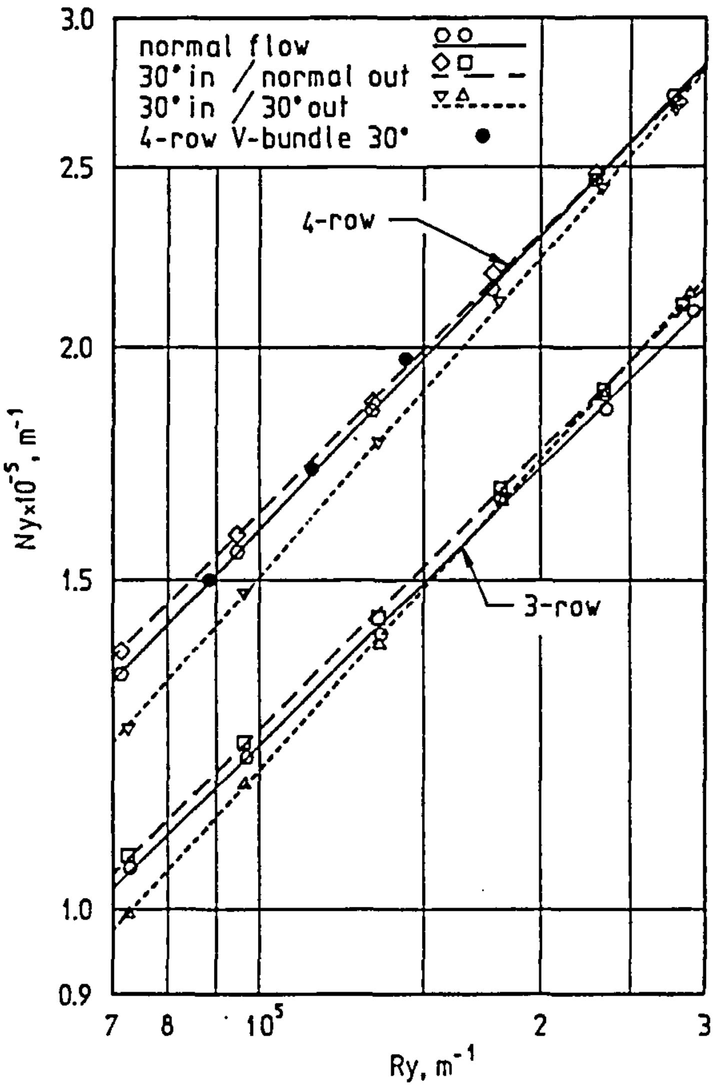

Figure 5.6.7: Heat transfer in 3- and 4-row heat exchangers.

The heat transfer characteristics of the single three- and four-row heat exchanger bundles are shown in figure 5.6.7. There is a small increase in heat transfer rate compared to normal flow conditions when the flow enters obliquely but leaves the bundle in a normal direction.

A reduction is, however, observed where the flow enters and leaves the bundle at 30°. Experimental results obtained by Becker [84BE1] are in agreement with this trend. In the case of the four-row V-bundle arrangement, the heat transfer coefficient is similar to that obtained under normal flow conditions.

The results of the isothermal pressure drop measurements across a two-row plate finned heat exchanger are shown graphically in figure 5.6.8. Based on a curve that is fitted through the normal flow data the losses for other arrangements are predicted. Good agreement is obtained between theory and experiment up to inclination angles of 25°.

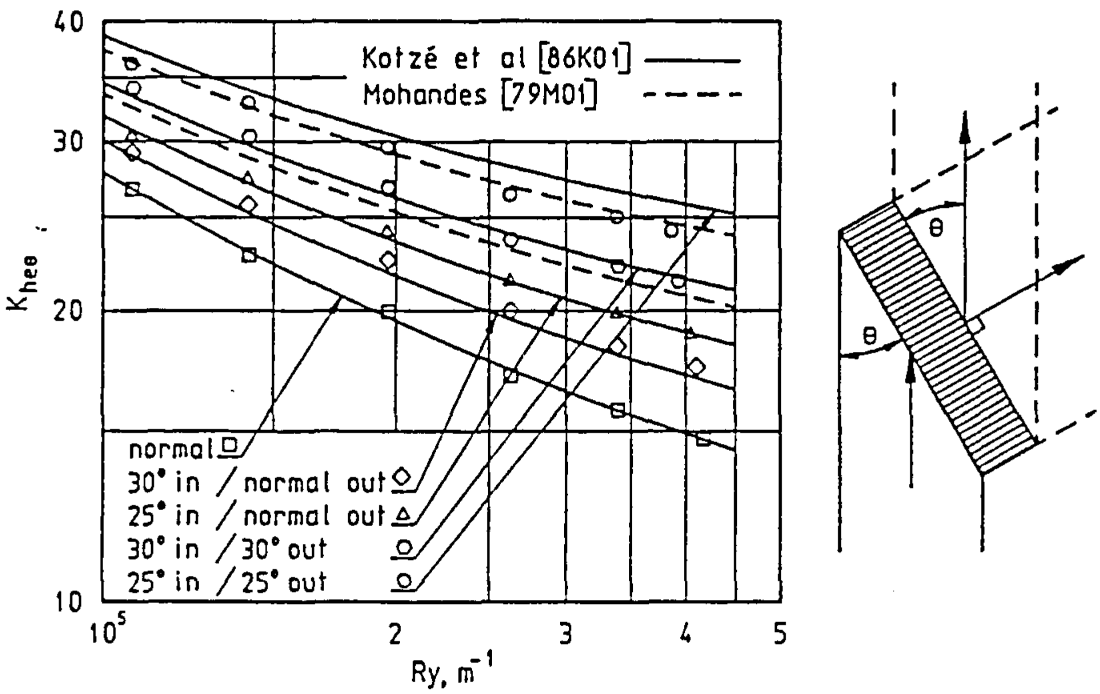

Figure 5.6.8: Pressure drop across plate-finned heat exchanger.

The corresponding heat transfer results are shown in figure 5.6.9. Where the inlet flow only is inclined, there is an increase in the heat transfer rate as was observed in the round-tube bundles. Although to a lesser extent, there is also a higher heat transfer rate compared to the normal flow conditions when both the inlet and the outlet flows are inclined.

The enhanced heat transfer may be due to eddy shedding and boundary layer development near the leading edge of the tilted fins. Samie and Sparrow [86SA1] have observed significant increases in the Nusselt number during flow across a single yawed finned tube, and Somerton et al [85SO1] observed similar trends in the case of inclined radiator cores.

Additional test results are reported by Fisher and Bucher [81FI1, 84FI1] and Monheit and Freim [86MO1]. In view of their method of testing, care should be taken when interpreting their pressure drop data.

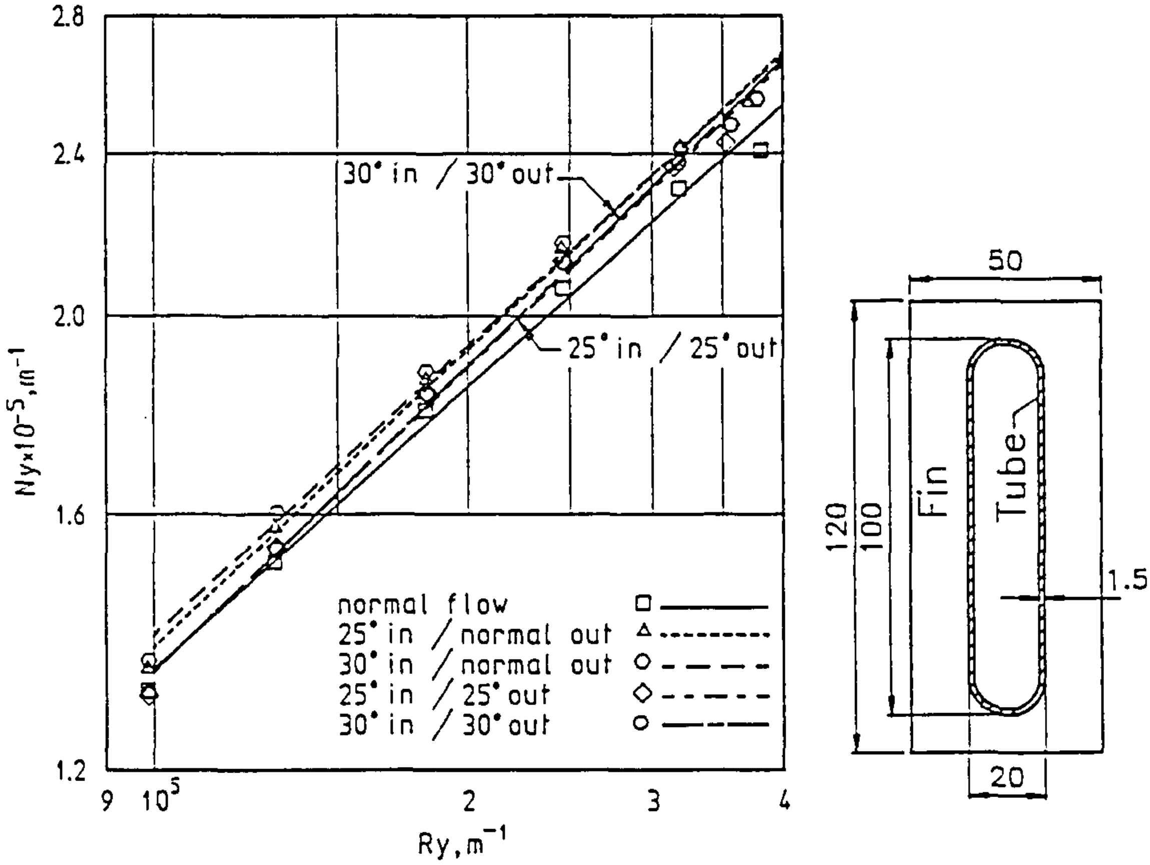

Figure 5.6.9: Heat transfer in plate-finned heat exchanger.

Van Aarde and Kröger [93VA1], obtained test results for flow losses in heat exchanger arrangements as shown in figure 5.6.10, incorporating process fluid ducts and walkways such as found in air-cooled condensers. They define a total loss coefficient that includes kinetic energy losses at the outlet of an A-frame array i.e.

$$K_{\theta t} = \left[\left(p_1 + \rho v_1^2/2\right) - p_a\right] / \rho v_i^2/2 = K_{i\theta} + K_f + K_e + K_{dj} + K_o$$

$$= K_{he} + \left(\frac{1}{\sin\theta_m} - 1\right)\left[\left(\frac{1}{\sin\theta_m} - 1\right) + 2\,K_{ci}^{0.5}\right] + K_{dj} + K_o \qquad (5.6.18)$$

or for non-isothermal flow

$$K_{\theta t} = K_{he} + \frac{2}{\sigma_{min}^2}\left(\frac{\rho_1 - \rho_2}{\rho_1 + \rho_2}\right) + \frac{2\,\rho_2}{(\rho_1 + \rho_2)}\left(\frac{1}{\sin\theta_m} - 1\right)\left[\left(\frac{1}{\sin\theta_m} - 1\right) + 2\,K_{ci}^{0.5}\right]$$

$$+ (K_{dj} + K_o)\,2\,\rho_1/(\rho_1 + \rho_2) \qquad (5.6.19)$$

θ_m is given by equation (5.6.13) while K_{he} is obtained from equation (5.4.23).

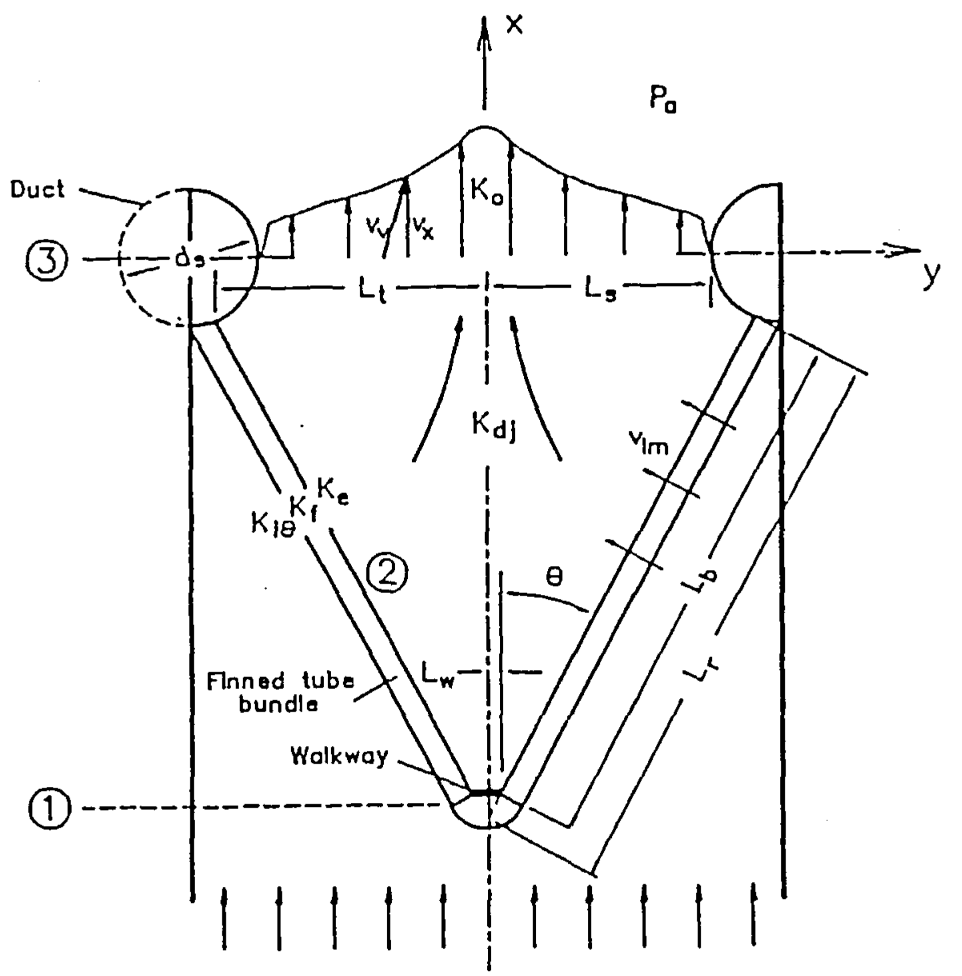

Figure 5.6.10: Section of an array of A-frames.

The inlet contraction loss coefficient based on the normal upstream velocity for turbulent flow between plates follows from equation (2.3.7).

$$K_{ci} = \left[\left(1 - 1/\sigma_c\right)/\sigma \right]^2 \tag{5.6.20}$$

where σ is the ratio of the flow area between the fins at their leading edge to the corresponding area immediately upstream of the fins. For plate fins, σ_c is given by equation (2.3.11).

The jetting loss coefficient is expressed by the following relation:

$$K_{dj} = \left[\left\{ -2.89188 \left(\frac{L_w}{L_b}\right) + 2.93291 \left(\frac{L_w}{L_b}\right)^2 \right\} \left(\frac{L_b}{L_s}\right) \left(\frac{L_t}{L_s}\right) \left(\frac{28}{\theta}\right)^{0.4} \right.$$

$$\left. + \left\{ \exp\left(2.36987 + 5.8601 \times 10^{-2}\theta - 3.3797 \times 10^{-3}\,\theta^2\right) \left(\frac{L_s}{L_t}\right) \right\}^{0.5} \left(\frac{L_b}{L_r}\right) \right]^2 \tag{5.6.21}$$

where θ is in degrees.

The outlet loss coefficient is given by

$$K_o = \left[\left\{ -2.89188 \left(\frac{L_w}{L_b}\right) + 2.93291 \left(\frac{L_w}{L_b}\right)^2 \right\} \left(\frac{L_s}{L_t}\right)^3 \right.$$

$$\left. + 1.9874 - 3.02783 \left(\frac{d_s}{2L_t}\right) + 2.0187 \left(\frac{d_s}{2L_t}\right)^2 \right] \left(\frac{L_b}{L_s}\right)^2 \tag{5.6.22}$$

These equations are valid for $K_{he} \geq 30$, semi-apex angles of $20° \leq \theta \leq 35°$ and for $0 \leq d_s/(2L_t) \leq 0.17886$ and $0 \leq (L_w/L_b) \leq 0.09033$. Equation (5.6.19) is conservative at low air velocities through the heat exchanger.

When applying equations (5.6.12) (5.6.16) (5.6.18) and (5.6.19) to tubes where the fins do not cover the entire effective frontal area as shown in figure 5.6.11 (b), the second term on the right hand side of these equations must theoretically be multiplied by the square of the relevant area ratio i.e. $[P_t/(P_t - d)]^2$. In practice this tends to give an inlet loss coefficient that is higher than measured.

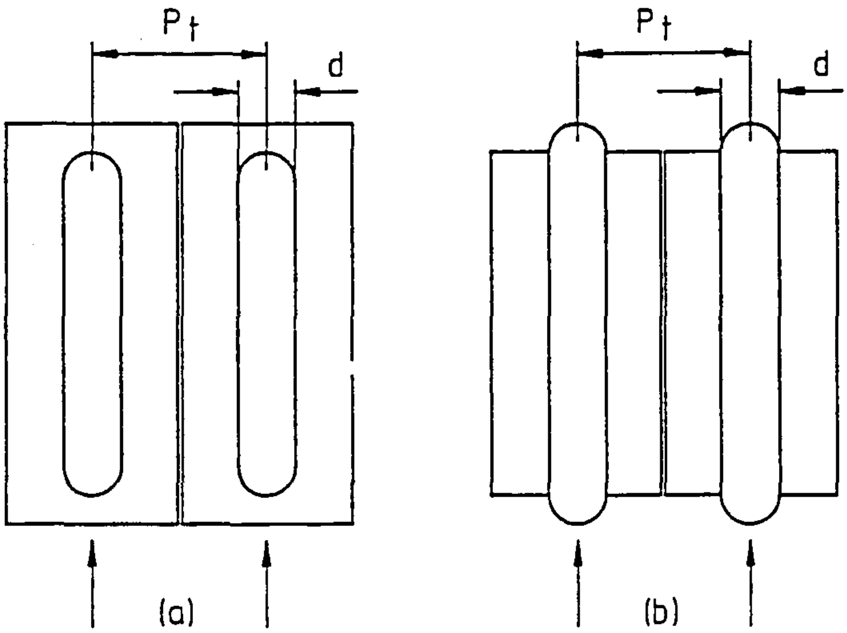

Figure 5.6.11: Finned tubes.

It is noted that the air flow distribution through the heat exchanger bundles is not uniform as shown in figure 5.6.12 due to losses. Measured bundles velocities follow trends predicted by Moore [79MO2].

Various methods have been proposed to reduce the additional pressure loss during flow through inclined bundles. These include the introduction of guide vanes or airfoils [78MO1, 79MO2, 84FI1] or the use of formed plate fins [73PH1] as shown in figure 5.6.13. The latter not only reduce the total pressure drop but also improve the heat transfer owing to a more uniform flow through the bundle.

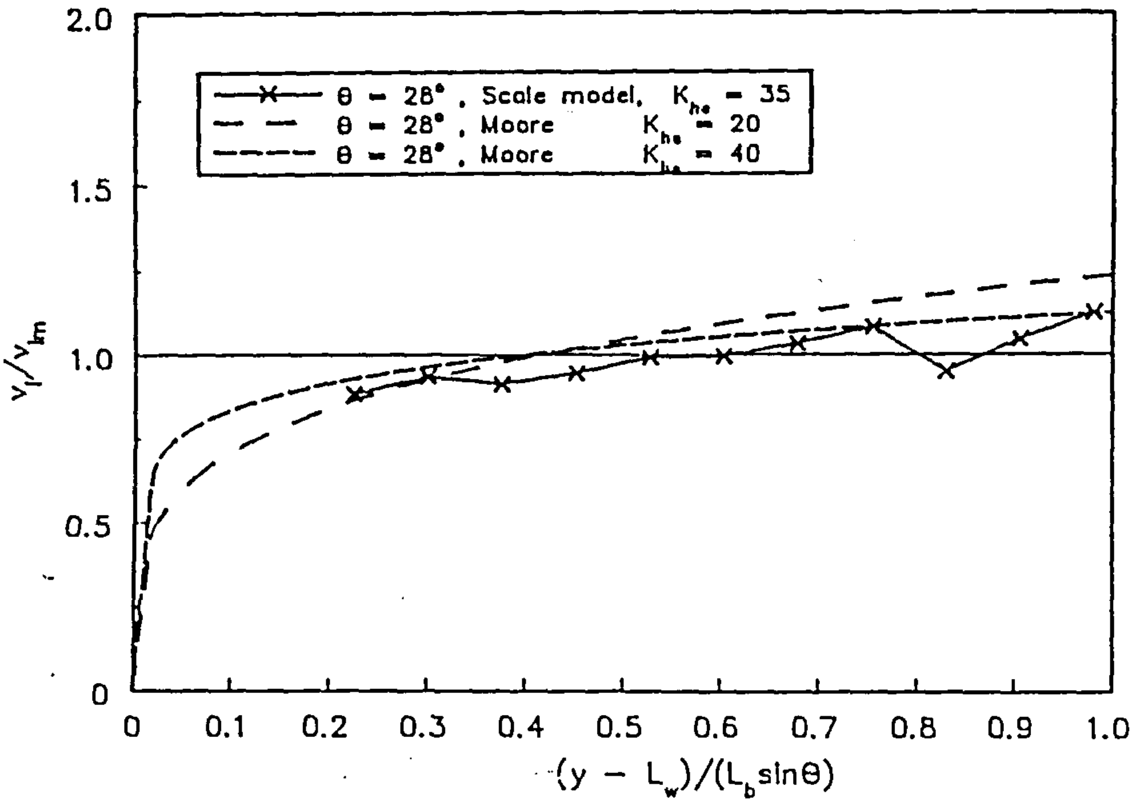

Figure 5.6.12: Dimensionless velocity distribution through bundle.

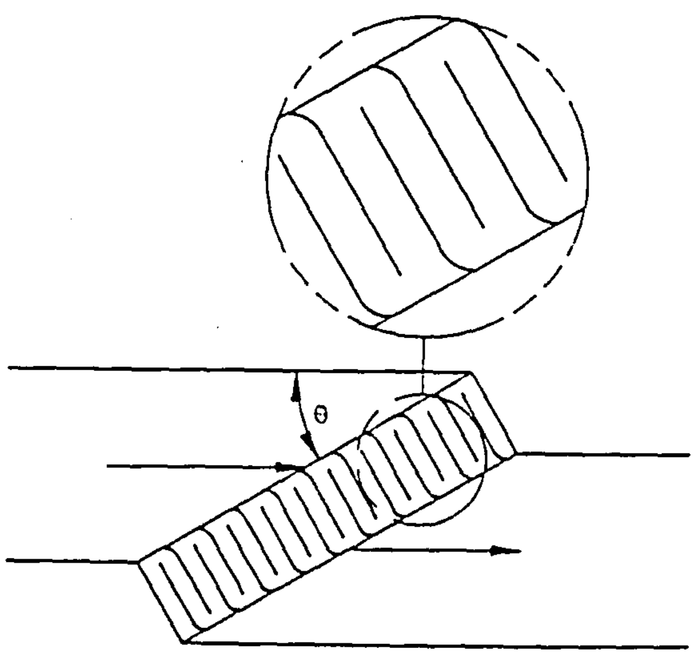

Figure 5.6.13: Formed plate fins.

5.7 CORROSION, EROSION AND FOULING

A finned tube heat exchanger may have to be erected in an area in which the environment is particularly corrosive or harsh. Corrosive atmospheres may contain gases including sulphur dioxide, chlorine compounds, carbon monoxide, carbon dioxide and NO_x. These impurities combined with moisture, rain, hailstones, snow and ice and other airborne inorganic materials such as dust, fly-ash, coal dust, etc., tend to encourage the corrosion and erosion of finned surfaces in such a heat exchanger. Physical damage during erection, poor maintenance and ineffective cleaning will accelerate this trend.

Corrosion problems have been experienced by a few large air-cooled heat exchangers in different parts of the world. The natural draft Ibbenbüren tower in Germany was fitted with aluminum finned tubes. Irregular cleaning, poor maintenance and polluted air owing to the industrial environment have been cited as the major causes for the deterioration of the finned tubes. The dry Rugeley tower in England was fitted with the same type of all-aluminum tube as the Ibbenbüren tower. Owing to intermittent operation, high moisture content and extreme chlorine concentrations in the atmosphere, serious corrosion of the aluminum was experienced. Some corrosion has been observed on the surface of the unprotected steel core tube in the Grootvlei 6 tower in South Africa. Galvanized surfaces may be attacked by atmospheres containing sulfides, especially when these collect in suspensions on the fin [66SC1].

Many laboratory and field tests have been conducted to determine the characteristics of different types of finned tubes subjected to corrosive atmospheres.

An extensive survey of materials and corrosion performance in dry-cooling applications was conducted by Battelle's Pacific Northwest Laboratories [76BA1]. The experience gained over many years of operation of industrial plants is summarized and some of the major causes of corrosion are identified. For example, the service life of galvanized coatings subjected to different types of atmospheric environments is shown in figure 5.7.1.

Other air-side corrosion tests were conducted on six different types of finned tubes employed in dry-cooling towers in the period from 1977 to 1983 by the Vereinigung der Grosskraftwerksbetreiber (VGB) in collaboration with three utilities and five producers of finned tubes, including Alesa Alusuisse, Zürich; Balcke - Dürr, Ratingen; GEA, Bochum; Linde, München; and Transelektro/EGI, Budapest [84VG1, 85SU1].

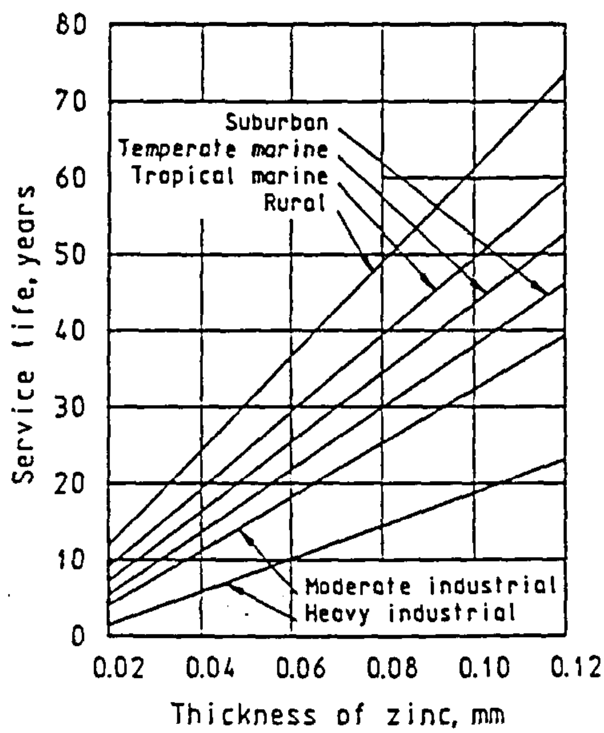

Figure 5.7.1: Service life or zinc coatings versus zinc thickness.

In a paper on heat exchanger materials for dry-cooling towers, Bodás [88BO1] refers to galvanized structural surfaces that show signs of corrosion after 5 to 6 years of exposure to a polluted industrial atmosphere. Palfalvi [88PA1] also refers to the corrosion of galvanized surfaces in the polluted environment at the Gargarin power station, where the average thickness of the zinc layer on the heat exchanger support frames and louvers was significantly reduced after more than 12 years of operation. It is noted by Bodás [88BO1] that, if such a reduction in zinc thickness were to occur on a galvanized finned surface, the fin efficiency would be correspondingly reduced. It would appear that the observed corrosion occurs primarily on the cold outside surfaces of the bundle frames.

The VGB study concluded that galvanized (50 to 80 μm zinc) steel surfaces offered satisfactory corrosion resistance. Where the protective zinc coating was locally damaged, adequate cathodic protection was maintained. It is noted that the loss in zinc was found to be considerably less in surfaces operated under continuous warm conditions in a cooling tower than in samples tested at ambient temperatures.

The VGB study further concluded that unprotected aluminum was not likely to offer adequate corrosion resistance when installed in a cooling tower for a period of 25 to 30 years. Coated aluminum surfaces are, however, acceptable. Where the coating is damaged, corrosion tends to occur primarily near the inlet of the heat exchanger bundle. Aluminum finned tubes have been installed in numerous dry-cooling towers, and good performance characteristics have been maintained for many years [88BO1, 91BO1]. Finned tubes protected by an electrophoretic coating [79HO1] are claimed to have enhanced performance characteristics [81FI1].

Extruded bimetallic finned tubes as shown in figure 5.1.1 ensure protection of the steel core tube except at the ends, where additional protection is required after welding. In extreme cases the fins should preferably be coated, since they may suffer intergranular corrosion owing to the substantial deformation during the manufacturing process [77BA1].

Wrapped-on aluminum finned tubes, as shown in figure 5.1.3, were installed at the Grootvlei cooling towers in South Africa. In Grootvlei 5 the outside surface of the steel core tube was galvanized and no corrosion problems were experienced after 15 years of operation. In the case of Grootvlei 6, where the core tube was not galvanized, corrosion occurred particularly on the upper tubes, reducing the effective overall heat transfer coefficient by approximately 10 per cent [88HA1].

Although some corrosion has occurred in a few air-cooled heat exchangers exposed to particularly harsh environments, it is unlikely that similar problems will be experienced in future plants. Practice has shown that both galvanized steel and chemically oxidized (modified Bauer-Vogel process MBV) or otherwise protected [88BO1, 91BO1] aluminum surfaces are suitable for use in air-cooled heat exchangers and dry-cooling towers with a specified service life of more than 25 years. Continuous operation at temperatures higher than ambient tend to reduce galvanic corrosion and the removal of zinc. Regular cleaning further extends the service life. Where the environment is particularly corrosive it may be advisable to erect a corrosion test stand at the particular site several years before selecting a specific heat transfer surface [88BO1]. Such a unit can also be used to monitor fouling characteristics.

Corroded finned surfaces and fin deformation [89PA1] generally cause the air-side flow resistance to increase.

Erosion of finned surfaces has been observed particularly in areas where sandstorms are common. Adjustable louvers may be required in such cases to protect the heat exchangers. Erosion is not uncommon in mechanical draft systems operating in dry sandy areas.

Fouling of the finned surface of an air-cooled heat exchanger tends to increase the thermal and the flow resistance on the air-side, resulting in a net reduction in the heat transfer rate. Although the effect of dirt deposits on the overall heat transfer coefficient is usually small, the reductions in air-flow rate and mean temperature difference may significantly reduce performance. An increase in pressure drop of 20 per cent owing to fouling has been reported by Rose [70RO1], while Preece et al [70PR1] observed a 52 per cent increase in pressure drop owing to corrosion of fins, and Russell [79RU1] suggests that pressure drop increases of up to 40 per cent were not unrealistic in practical designs. Clearly, exact figures depend on the heat exchanger type and the type and magnitude of the fouling layer, but marked increases of pressure drop and hence of fan power requirements may occur. Russel has also indicated that reducing fan speeds to reduce noise and loading the fans near to the maximum can lead to the disastrous consequence of stalling the fan if the pressure drop increases beyond a certain level.

Laboratory experiments conducted by Hunn [74HU1], in which different samples of dry and wet coal dust were introduced into the air stream which flowing through finned tube geometries characteristic of dry-cooling tower applications, showed that increases in pumping power of up to 45 per cent are required to maintain the same rate of heat transfer, while the fouling layer thickness increases to the point where 48 per cent blockage of the freeflow area occurs.

In general much uncertainty exists concerning the effect of fouling on the performance of practical systems. One of the reasons for this uncertainty is the fact that the nature of the material which causes fouling on extended surfaces can be diverse, ranging from normal atmospheric dust to organic matter, products of corrosion, soot, or insects. Furthermore, fouling tends to be a transient phenomenon.

Based on the deposition model from Kern and Seaton [59KE1], Bemrose and Bott [84BE2] postulate the following relationship for the friction factor on the finned side as a measure of fouling at a time τ:

$$f = f_o [1 + a(1 - e^{-b\tau})] \tag{5.7.1}$$

where f_o is the friction factor corresponding to the original clean surface at a time τ equal to zero, and a and b are constants.

Fouling tests were conducted by Bemrose and Bott [81BE1, 83BO1] in a test rig containing one- to four-row bundles of spirally wound finned tubes. Calcium dust with a particle median diameter of 14 μm was introduced into the air stream over a range of air velocities. The increase in friction factor generally followed the predicted trend given by equation (5.7.1).

As observed in practical heat exchangers subjected to dustladen air streams, more foulant was seen to deposit on the front and rear faces than in the middle of the bank of tubes.

The trend predicted by equation (5.7.1) is not necessarily representative of all types of fouling, and increases in flow resistance following quite a different function have been observed.

Since most fouling in air-cooled systems occurs at the inlet to the heat exchanger, or at the first two tube rows in a multi-row tube bundle, cleaning is usually best done from the outlet side by means of jets of compressed air or water. Rinsing or low-pressure jets are used where lightweight slightly fouled fins are encountered, and pressures of 50 bar to 200 bar are not uncommon in the case of galvanized steel tubes. At some sites soap is added to the water jet, and in extreme cases fly ash or fine sand may be introduced, although care must be taken not to erode the protective coating or the fin itself. Steam cleaning is also used in some extreme cases. Aircraft jet engines have been used to remove particulates from finned surfaces in dry-cooling towers in the USSR [79NE1]. At Grootvlei, a gradual build-up of impurities over a number of years formed a tough layer on the finned surface that could not be removed completely by the above-mentioned methods.

In practice it is advisable to evaluate the potential for fouling in a particular area by exposing various types of finned tube heat exchanger bundles to a stream of ambient air over an extended period. In addition to pollutants generated in industrial areas , both the local flora and fauna may lead to fouling. During the flowering season or in the fall fouling may be more pronounced particularly during windy periods. The presence of seeds and other plant matter, especially during harvest time, may further encourage fouling. Alternating periods of dust and rain will cause a build-up of material on the finned surface.

Flies, butterflies, moths, locusts and other insects, especially during breeding and hatching periods, tend to clog up the system. Unless essential, all lights in the vicinity of the finned surfaces, or of the ducts leading to them should be extinguished so as not to attract insects at night. Warm heat exchanger surfaces tend to attract insects, which may be followed by birds, with the result that fluff and feathers accumulate on the inlet side of the finned surface. The orientation of the plant should take into account the location of potential sources of pollutants (e.g. coal or ash) and wind direction.

The frequency of cleaning is determined by the type and rate of fouling that occurs in a particular application. Semi-annual or annual cleaning is sufficient to control fouling at many locations [66SC1]. The installation of a suitable screen may be of value in the control of certain types of fouling. Screens are also installed in areas where damage by hailstones may occur.

5.8 THERMAL CONTACT AND GAP RESISTANCE

Finned tubes used in air-cooled heat exchangers may be broadly classified under four headings descriptive of the nature of the junction between tube and fins, i.e. integral fins, embedded fins, soldered, galvanized or brazed fins, and interference fit fins. Edge tension and footed tension wound helical fins, helically extruded finned muff and expanded plate fins are examples of the latter. The finned tube types rely upon residual radial stresses owing to the finning operation to maintain intermetallic heat transfer contact between them. Under these circumstances the tube wall has a lesser diameter and the fin base a greater diameter than either would have in the absence of the contact pressure. The sum of both displacements is the "interference".

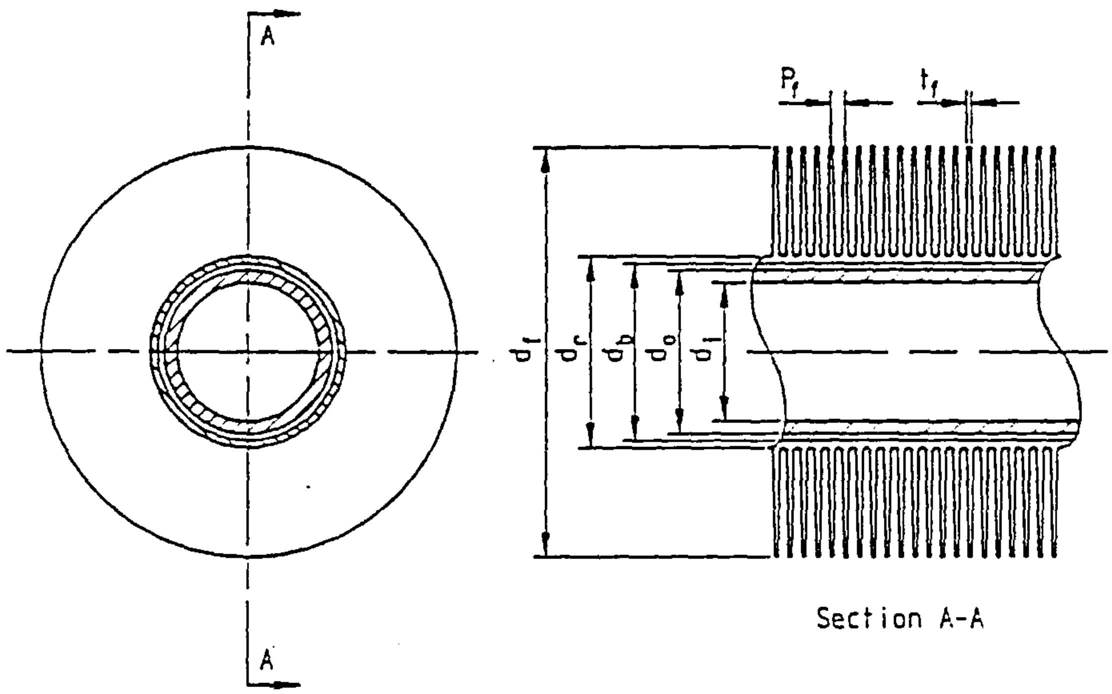

Figure 5.8.1: Extruded bimetallic finned tube.

Most interference fit finned tubes are bimetallic, aluminum being the most common fin material. At elevated temperatures the fins will tend to expand away from the tube walls of lesser thermal expansion coefficients with a corresponding possible loss of thermal contact, even though the fins in air-cooled equipment are necessarily at a temperature lower than that of the tube. The imperfect metal-to-metal contact results in a resistance to heat transfer known as the contact resistance. In poor-quality finned tubes, or at high temperatures when practically no metal-to-metal contact exists and when no contact pressure is exerted, a gap exists between the surfaces, and the resistance to heat transfer is referred to as the gap resistance. Figure 5.8.1 defines various dimensions of an extruded finned tube under these conditions.

5.8.1. ANALYSIS OF CONTACT AND GAP RESISTANCE

To analyze the above problem, Gardner and Carnavos [60GA1] considered an annular disk subjected to a uniform radial load and heat flux. They derived the following expression for the radial gap, g, between the fin base and the tube wall upon elastic relaxation from a state of residual stress brought about by the finning operation:

$$g = \frac{d_o}{2}\left[(\alpha_f - \alpha_t)(T_i - T_p) - \left\{\alpha_f\left(1 - \frac{R_a/e_f}{R_{ta} + R_{cga}}\right) - \alpha_t\left(\frac{R_{ia}}{R_{ta} + R_{cga}}\right)\right\}\right.$$

$$\left. \times \quad (T_i - T_a) + a\,(p_c - p_{cp})\right] \tag{5.8.1}$$

where T_i is the temperature of the fluid inside the tube, T_p is the fin and tube temperature during production, and T_a is the ambient fluid or air bulk temperature. The contact pressure between the fin base and the tube is p_c, while p_{cp} represents the contact pressure during original production, and α is the thermal expansion coefficient.

Furthermore,

$$a = \frac{1}{E_f}\left(\frac{d_f^2 + d_o^2}{d_f^2 - d_o^2} + v_f\right) + \frac{t_f}{E_t\,P_f}\left[\frac{d_o^2 + (d_o - 2t_t)^2}{d_o^2 - (d_o - 2t_t)^2} - v_t\right] \tag{5.8.2}$$

where E is the elastic modules and v is Poisson's ratio.

The total heat transfer resistance in the absence of any gap resistance is

$$R_{ta} = R_a/e_f + R_{ia} \tag{5.8.3}$$

where the fin effectiveness is according to equation (3.3.11)

$$e_f = 1 - A_f(1 - \eta_f)/A_a$$

and R_a is the thermal resistance on the outside or finned side while R_{ia} includes the resistances owing to the fluid film inside the tube as well as the tubewall, all referred to the total outside surface area.

Similarly, the sum of any contact and gap resistance based on the outside surface area is

$$R_{cga} = R_{ca} + R_{ga} \tag{5.8.4}$$

Negative values of the gap, g, are not possible; only zero or positive values have significance.

When g = 0, fins and core tube are in contact with no gap resistance, and the corresponding contact pressure may thus be obtained from equation (5.8.1).

$$p_c = p_{cp} - \frac{1}{a}\left[(\alpha_f - \alpha_t)(T_i - T_p)\right.$$

$$\left. - \left\{\alpha_f\left(1 - \frac{R_a/e_f}{R_{ta} + R_{ca}}\right) - \frac{\alpha_t R_{ia}}{R_{ta} + R_{ca}}\right\}(T_i - T_a)\right] \tag{5.8.5}$$

The subject of thermal metal-to-metal contact resistance has been studied by numerous investigators [87LE1]. Contact correlations developed by Shlykov and Ganin [64SH1] and more recently by Yovanovich [81YO1] appear to be the most reliable. The former presents a simple mathematical model of parallel resistance between the places of actual contact of the two surfaces and the voids existing between them. For two dissimilar materials they derived the following expression for contact resistance:

$$R_c = \frac{1}{\left[\frac{k_a}{\epsilon} + 4.2 \times 10^4 \left(\frac{p_c}{s_t b_p}\right)\left(\frac{k_f k_t}{k_f + k_t}\right)\right]}$$

or, based on the outside surface area in the case of a finned tube,

$$R_{ca} = \frac{d_f^2 - d_o^2}{2 d_o P_f \left[\frac{k_a}{\epsilon} + 4.2 \times 10^4 \left(\frac{p_c}{s_t b_p}\right)\left(\frac{k_f k_t}{k_f + k_t}\right)\right]} \tag{5.8.6}$$

where ϵ is the arithmetic mean value of the height of the micro roughness of the surfaces in contact and k_a is the thermal conductivity of gases or air entrapped among roughness asperities between the surfaces. The value of b_p is a function of the cold workability of the metal. A value of 3 is recommended for aluminum, whereas the value for copper is approximately 5. The yield stress of the tube material which is taken equal to the ultimate stress is represented by s_t.

According to Gardner and Carnavos [60GA1] the initial contact pressure p_{cp} is estimated to be approximately 0.67 of the yield stress of the fin material as originally cold worked. In the extreme case of fully annealed aluminum this value is approximately 24.1×10^6 N/m^2. Tests performed by Young and Briggs [65YO1] suggest that this value is a good approximation. Smith, Gunther and Victory [66SM1] performed a series of strain gauge tests in order to determine initial contact pressures on commercial tubes available at that stage. They obtained values of up to almost 30×10^6 N/m^2. It would appear that even higher values are possible for good quality tubes [86CO1].

Under certain conditions the contact pressure p_c may become zero, in which case, according to equation (5.8.6), the contact resistance becomes

$$R_{ca} = \epsilon(d_f^2 - d_o^2)/(2\, k_a\, d_o\, P_f) \tag{5.8.7}$$

Any further increase in the inside fluid temperature, T_i, will result in the formation of a gap between the tube wall surface and the base of the finned section. The thermal resistance of the gap alone, based on the outside surface area, is

$$R_{ga} = g(d_f^2 - d_o^2)/(2k_a\, d_o\, P_f) \tag{5.8.8}$$

The total thermal resistance under these conditions is obtained by the addition of equations (5.8.7) and (5.8.8)

$$R_{cga} = (d_f^2 - d_o^2)\,(\epsilon + g)/(2k_a\, d_o\, P_f) \tag{5.8.9}$$

Substitute g from equation (5.8.1) into equation (5.8.9) and find

$$R_{cga} = \left(\frac{d_f^2 - d_o^2}{4k_aP_f}\right)\left[\frac{2\epsilon}{d_o} + (\alpha_f - a_t)\,(T_i - T_p)\right.$$

$$\left. - \left\{\alpha_f\left(1 - \frac{R_a/e_f}{R_{ta} + R_{cga}}\right) - \frac{\alpha_t R_{ia}}{R_{ta} + R_{cga}}\right\}(T_i - T_a) - ap_{cp}\right]$$

or

$$R_{cga}^2 + R_{cga}\frac{\left(d_r^2 - d_o^2\right)}{4k_a\,P_f}\left[\frac{4\,R_{ta}\,k_a\,P_f}{\left(d_f^2 - d_o^2\right)} - \frac{2\epsilon}{d_o} - (\alpha_f - \alpha_t)\,(T_i - T_p)\right.$$

$$\left. + \alpha_f\,(T_i - T_a) + a\,p_{cp}\right] + R_{ta}\left[\left(d_f^2 - d_o^2\right)/\left(4k_a\,P_f\right)\right]$$

$$\times\left[\alpha_f\,(T_i - T_a) - (\alpha_f - \alpha_t)\,(T_i - T_p) + a\,p_{cp} - 2\epsilon/d_o\right]$$

$$- \left[\left(d_f^2 - d_o^2\right)/\left(4\,k_a\,P_f\right)\right](T_i - T_a)\left[\alpha_f\,R_a/e_f + \alpha_t\,R_{ia}\right] = 0 \tag{5.8.10}$$

In general this equation gives satisfactory results if the value of p_{cp} is known. Kulkarni and Young [66KU1] present graphically the contact and gap resistances for specific cases based on these equations.

The above analysis is applied to a particular finned tube under given operating conditions as shown in figure 5.8.2. Initially the thermal resistance increases relatively gradually until g = 0, after which there is a very rapid increase. From the results it is obvious that the initial contact pressure will have a significant influence on the contact and gap resistances between the aluminum fin and the steel tube. Limited experimental results are in excellent agreement with this trend.

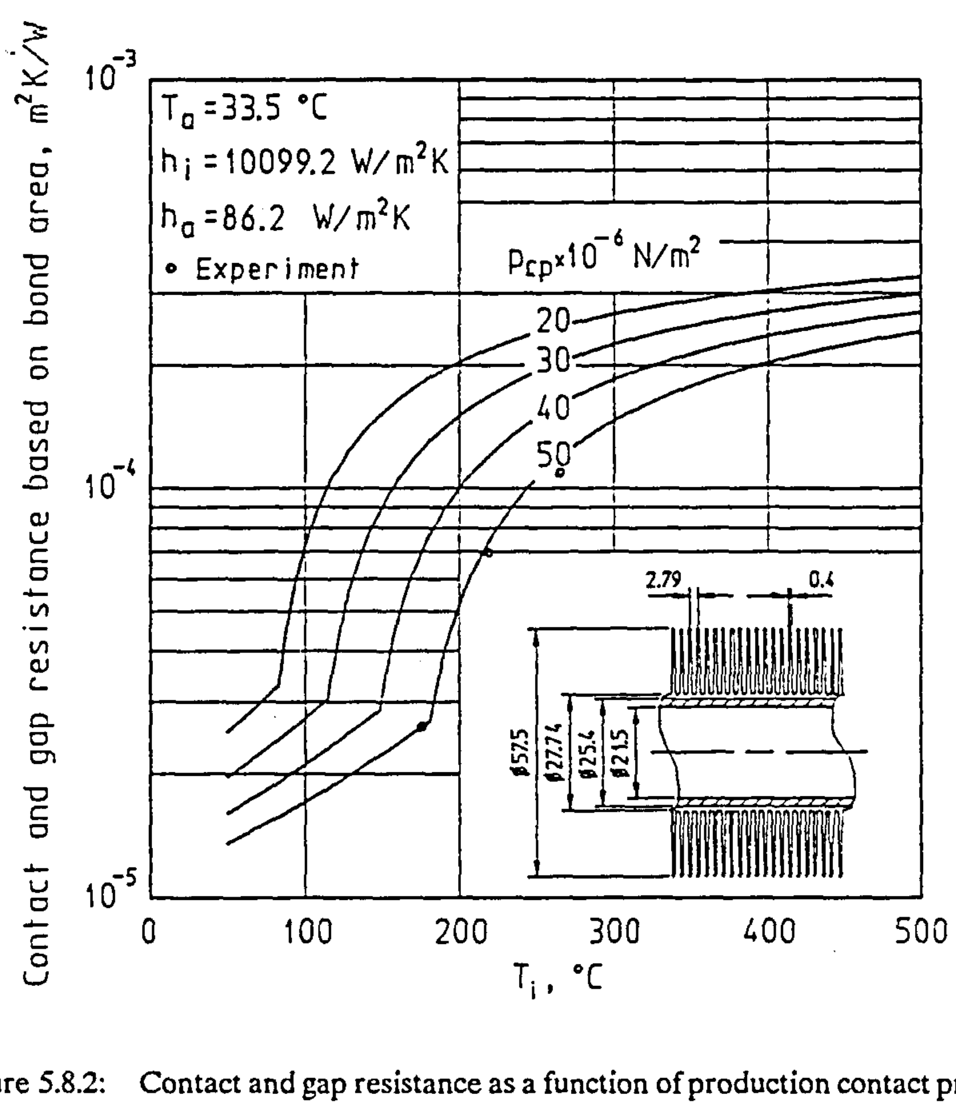

Figure 5.8.2: Contact and gap resistance as a function of production contact pressure p_{cp} [86CO1].

If the heat transfer coefficient on the outside surface of the particular finned tube is increased, while other conditions remain unchanged, the contact and gap resistances tend to decrease as shown in figure 5.8.3. An initial contact pressure of 30 x 10^6 N/m^2 is assumed.

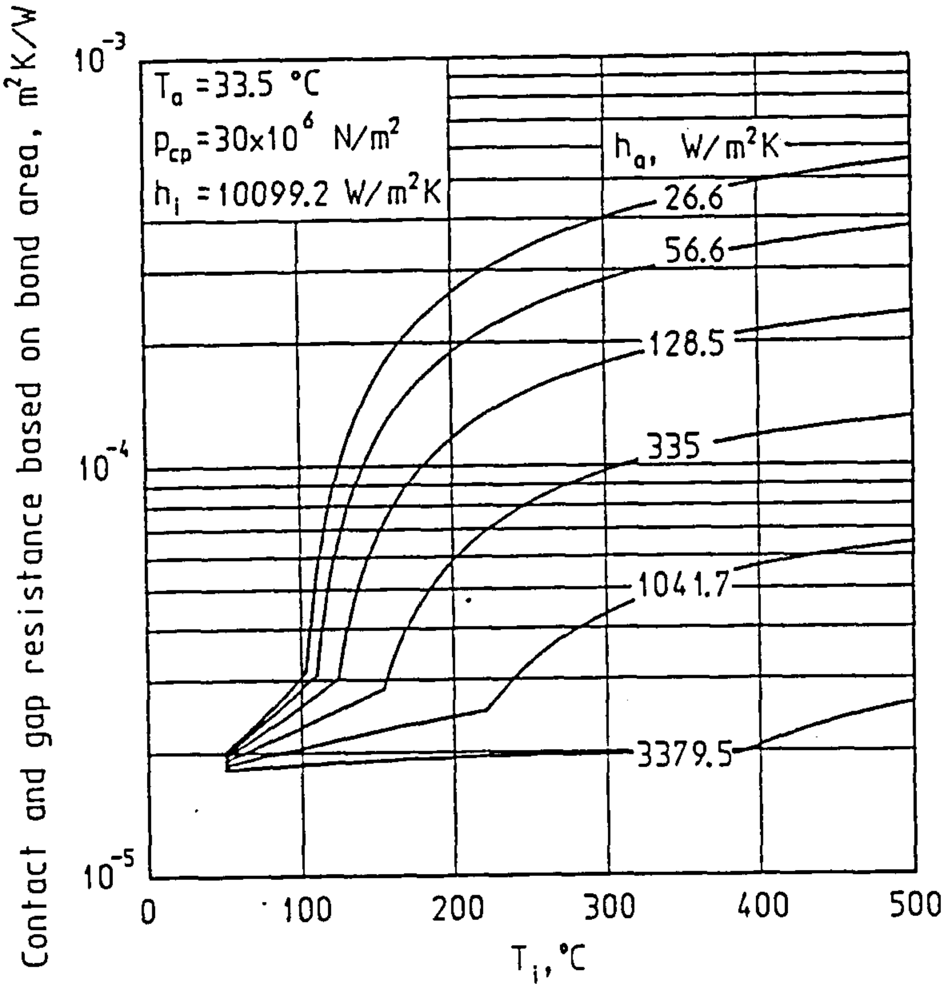

Figure 5.8.3: Contact and gap resistance as a function of outside heat transfer coefficient h_a.

An increase in thermal resistance can be expected when the fluid temperature on the outside surface is increased, other parameters being the same. This is illustrated in figure 5.8.4.

Example 5.8.1

Air at a temperature of 33.4915°C flows across an extruded bimetallic finned tube as shown in figure 5.8.2. Saturated steam at 100.7°C condenses inside the tube. The air-side heat transfer coefficient h_a = 86.2 W/m^2 K while the condensation heat transfer coefficient inside the tube h_i = 10099.21 W/m^2 K. The elastic module of the aluminum fin material is 6.945665 x 10^{10} N/m^2 and that of the steel tube is 1.940773 x 10^{11} N/m^2.

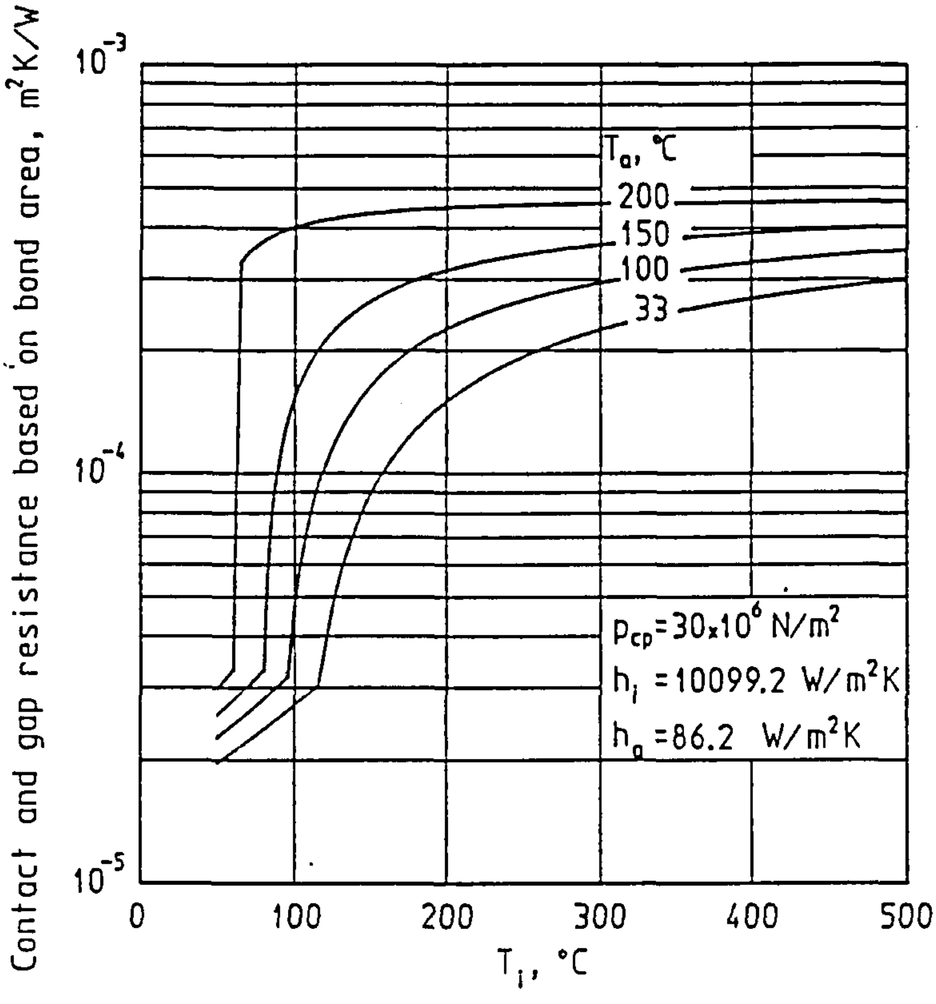

Figure 5.8.4: Contact and gap resistance as a function of ambient temperature T_a.

The corresponding thermal expansion coefficients are 2.36516 x 10^{-5} K^{-1} and 1.156774 x 10^{-5} K^{-1} respectively, and the respective thermal conductivities are 227.7142 W/mK and 52.42969 W/mK. For aluminum the Poisson ratio is 0.334 and for steel 0.292. At a production or fabrication temperature of 21.11°C the contact pressure is found to be 38.2 x 10^6 N/m^2. The arithmetic mean value of the height of the micro roughness of the surfaces in contact is 10^{-6} m. The yield stress of the steel tube material is 5.4 x 10^8 N/m^2. Determine the thermal contact resistance between the fin root and the core tube, based on the bond area.

Solution

The approximate surface area of a single fin is found from

$$A_f = \frac{\pi}{2}(d_f^2 - d_r^2) = \frac{\pi}{2}(57.5^2 - 27.74^2)10^{-6} = 3.985 \times 10^{-3} m^2$$

The corresponding exposed root area is approximately

$$A_r = \pi\, d_r(P_f - t_f) = \pi \times 27.74(2.79 - 0.4) \times 10^{-6} = 0.2083 \times 10^{-3} m^2$$

By adding the above values, the total effective air-side area around one fin is found:

$$A_a = 4.1933 \times 10^{-3}\ m^2$$

The corresponding area inside the tube is

$$A_i = \pi\, d_i P_f = \pi \times 21.5 \times 2.79 \times 10^{-6} = 0.18845 \times 10^{-3}\ m^2$$

The thermal resistance owing to the fluid film inside the tube as well as the tubewall resistance, all referred to the total outside surface area, is given by

$$R_{ia} = (1/h_i + R_t)A_a/A_i = \left[\frac{1}{h_i} + \frac{\ell n\ (d_o/d_i)A_i}{2\ \pi\ k_t\ P_f}\right]\frac{A_a}{A_i}$$

$$= \left[\frac{1}{10099.21} + \frac{\ell n(25.4/21.5)\pi \times 21.5}{2\pi \times 52.42969 \times 1000}\right]\frac{4.1933}{0.18845} = 2.9638 \times 10^{-3}\ m^2\ K/W$$

For a given heat transfer coefficient the corresponding fin efficiency may be calculated. According to equation (3.3.13),

$$\phi = \left(\frac{57.5}{27.74} - 1\right)\left[1 + 0.35\,\ell n\left(\frac{57.5}{27.74}\right)\right] = 1.346515$$

and, furthermore,

$$b = [2 \times 86.2/(227.7142 \times 0.4 \times 10^{-3})]^{0.5} = 43.505441$$

The fin efficiency follows from equation (3.3.12):

$$\eta_f = \frac{\tanh\,(43.505441 \times 27.74 \times 1.346515/2000)}{(43.505441 \times 27.74 \times 1.346515/2000)} = 0.8258$$

According to equation (3.3.11) the surface effectiveness is

$$e_f = 1 - 3.985\,(1 - 0.8258)/4.1933 = 0.8345$$

From equation (5.8.3) it follows that

$$R_{ta} = 1/(h_a e_f) + R_{ia} = 1/(86.2 \times 0.8345) + 2.9638 \times 10^{-3} = 1.6865 \times 10^{-2}\,m^2K/W$$

According to equation (5.8.2),

$$a = \frac{1}{6.945665 \times 10^{10}}\left(\frac{57.5^2 + 25.4^2}{57.5^2 - 25.4^2} + 0.334\right)$$

$$+ \frac{0.4}{1.940733 \times 10^{11} \times 2.79}\left[\frac{25.4^2 + (25.4 - 2 \times 1.95)^2}{25.4 - (25.4 - 2 \times 1.95)^2} - 0.292\right]$$

$$= 3.044423 \times 10^{11}\ m^2/N$$

The desired contact pressure is found by solving equations (5.8.5) and (5.8.7) simultaneously. This is most readily done by following an iterative procedure. Assuming arbitrarily a value of $R_{ca} = 4.152 \times 10^{-4}\ m^2\ K/W$ and substituting this into equation (5.8.5), find

$$p_c = 38.2 \times 10^6 - \frac{10^{11}}{3.044423}\Bigg[(2.36516 - 1.156774)10^{-5}\ (100.7 - 21.11)$$

$$- 2.36516 \times 10^{-5}\left(1 - \frac{1}{86.2 \times 0.8345\ (1.6865 \times 10^{-2} + 4.152 \times 10^{-4})}\right)$$

$$- \frac{1.156774 \times 10^{-5} \times 2.9638 \times 10^{-3}}{1.6865 \times 10^{-2} + 4.152 \times 10^{-4}}\ (100.7 - 33.4915)\Bigg] = 1.2438 \times 10^7\ N/m^2$$

The thermal conductivity of the air entrapped between the surfaces asperities at the bond interface is evaluated according to equation (A.1.4) at 100,7°C and found to be 3.148×10^{-2} W/mK.

Substitute the above values of p_c and k_a into equation (5.8.6) and find

$$R_{ca} = \frac{1}{2 \times 25.4 \times 2.79}$$

$$\times \frac{(57.5^2 - 25.4^2)}{\left[\dfrac{3.148 \times 10^{-2}}{10^{-6}} + 4.2 \times 10^4 \left(\dfrac{1.2438 \times 10^7}{5.4 \times 10^8 \times 3}\right)\left(\dfrac{227.7142 \times 52.42969}{227.7142 + 52.42969}\right)\right]}$$

$$= 4.152 \times 10^{-4}\ m^2\ K/W$$

Based on the surface area the approximate contact resistance is

$$R_c = R_{ca} \times 2\ d_o P_f/(d_f^2 - d_o^2) = 4.152 \times 10^{-4} \times 2 \times 25.4 \times 2.79/(57.5^2 - 25.4^2)$$

$= 2.21 \times 10^{-5} m^2 K/W$

5.8.2 MEASURING CONTACT AND GAP RESISTANCE

Gardener and Carnavos [60GA1] present the results of experimental studies on contact and gap resistance, in which the heat transfer rate is measured in a four-row bundle of finned tubes installed in a wind tunnel. Because of the major thermal resistance on the air-side, this method of testing is reliable only in a laboratory environment, especially where good quality tubes with a small contact resistance are tested. Furthermore, the method of testing is expensive.

Young and Briggs [65YO1] tested single-finned tubes of the extruded muff type in a concentric pipe heat exchanger. The test fluids were recirculating streams in axial counterflow, the one through the tube being Mobiltherm 600 and the one through the annular space between the shell and the finned tube Mobiltherm Light. Heat was provided to the tube stream by an electrical resistance heater and discharged from the shell stream through a water-cooled heat exchanger. One reason for using a heat transfer oil rather than air on the finned side of the tube was to reduce the heat transfer resistance on that side, thus making the contact or gap resistance a reasonably large fraction of the overall resistance.

Smith, Gunter and Victory [66SM1] tested single extruded muff and footed tension-wound tubes in an apparatus originally developed for industrial manufacturing control purposes. Air is blown across the finned surface while steam condenses inside the tube. It is unlikely that this particular type of facility can guarantee repeatable quantitative results when good quality tubes are being tested in an industrial environment, primarily because of the relatively high thermal resistance on the air-side [86CO1].

Other studies include those of Young et al [57YO1], Dart [59DA1], Eckels [77EC1] Christensen and Fernandes [83CH2], and Sheffield et al [85SH1]. Electrical methods to determine the contact resistance have been considered but found to be impractical. In another indirect method of testing, the core tube is withdrawn mechanically from a specified length of finned tubing. The force required to achieve this and the thermal contact resistance are supposed to be related. This is not necessarily true, however, since the former tends to be very sensitive to the mechanical and geometric characteristics of the contact surfaces [85ER1].

In view of the limitations of the above-mentioned test equipment, Coetzee and Kröger [86CO1] recommend a test method for good quality extruded bimetallic finned tubes, in which saturated steam is condensed on the outside finned surface at approximately 100°C while hot water flows inside the tube. The method is accurate and can readily be applied in practice by simply measuring the difference between the steam and the water temperatures and the condensate flow rate.

The thermal contact resistance will also tend to increase in finned tubes subjected to thermal cycles or excursions. Although no theoretical method is available for predicting the performance degradation under such conditions, experimental studies have been carried out.

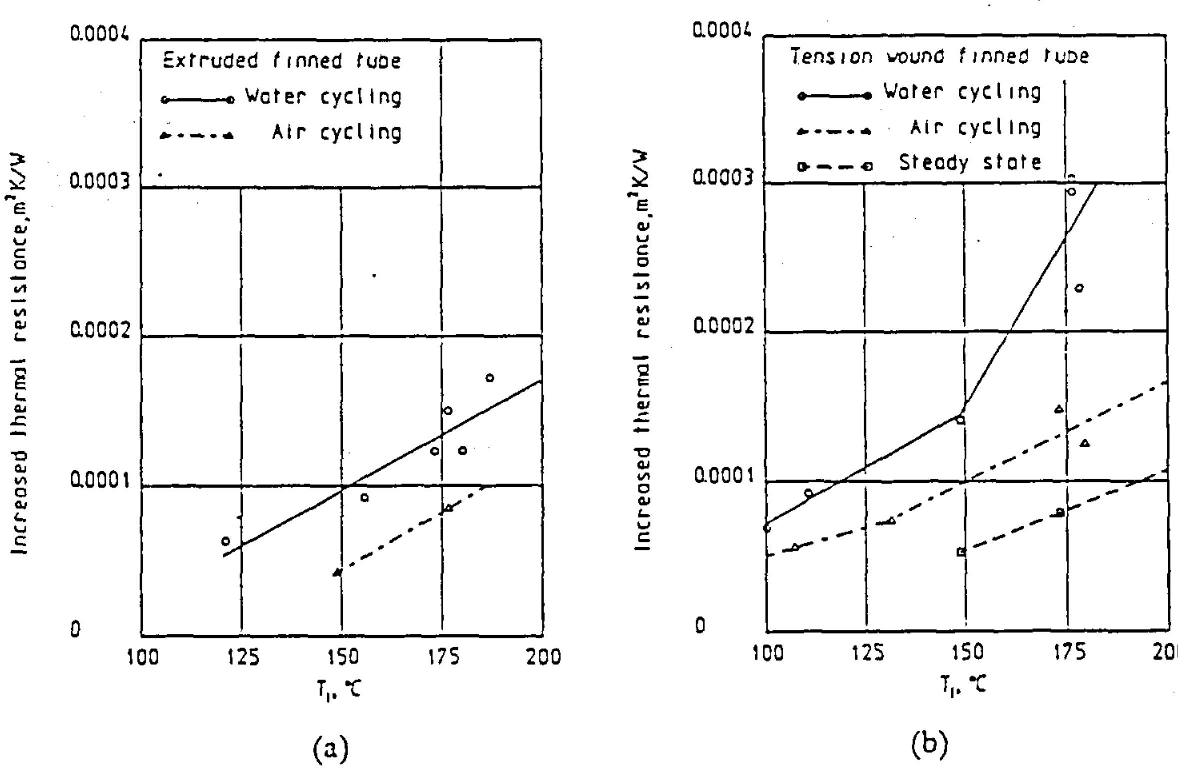

Figure 5.8.5: Increased resistance owing to thermal cycling [66SM1].

5.9 FREE STREAM TURBULENCE

The air-side heat transfer and pressure drop characteristics of heat exchangers are obtained experimentally in windtunnels in which the air upstream of the heat exchanger has a low level of turbulence (1 to 3 per cent). Where the heat exchanger consists of bundles of plain or finned tubes the heat transfer coefficient in the first rows is lower than further downstream, owing to the higher levels of turbulence that exist in the wake stream. In real air-cooled heat exchangers the level of turbulence in the inlet air stream may, however, be considerably higher, owing to the absence of smooth inlets or the presence of flow-control devices, turning vanes, louvers, bar grids, grills or screens. In a forced-draft unit the wake of the fan introduces a degree of turbulence.

Baines and Peterson [51BA1] experimentally investigated the establishment and decay of turbulence downstream from biplane lattices or screens and compared the decay to theoretical expressions derived by other investigators. They found that the approximate expression of Frenkiel [48FR1] most closely represents the true decay, i.e.

$$Tu = 1.12\,(d_s/x_s)^{5/7} \tag{5.9.1}$$

where x_s is the downstream distance from the screen and d_s the wire diameter. Experiments indicate that a distance of 5 to 10 times the wire pitch or mesh length downstream from any screen is necessary to ensure reasonably good flow establishment. The maximum intensity of turbulence is reached within 2 or 3 mesh lengths from the screen.

Equation (5.9.1) can be used in practical designs to predict the turbulence downstream from a screen if the Reynolds number based on the free stream velocity, i.e. $Re = \rho v d_s/\mu$, exceeds 100.

In the case of a bar grid, vortices separate from the cylindrical bars and move downstream in the fluid. At larger distances from the grid it is possible to discern a regular pattern of vortices which move alternatively clockwise and counter-clockwise, known as the von Kármán vortex street. This vortex street moves with a velocity which is smaller than the free flow stream velocity before the grid. Another feature of these fluctuations is that

Smith et al [66SM1] used a multipurpose cycling apparatus capable of operation with the heating medium always flowing in the tubes and either steady or intermittent air flow, or intermittent water spray on the finned side. In the case of air cycling between 24°C and 47°C, the air flow was continued for 1.5 minutes and the total cycle time was approximately 5 minutes. For water cycling between 47°C and 115°C, the spray time was 45 seconds and the total cycle time was 5 to 6 minutes. The finned tubes were 6.1 m long and of the extruded muff and L-footed tension-wound types. A minimum of 500 cycles were run on each tube. The results of these tests are shown in figure 5.8.5.

In properly galvanized steel-finned tubes as shown in figure 5.8.6(a), the thermal contact resistance should be negligible. Poor temperature control or impurities in the zinc bath may, however, result in the formation of cavities, poor penetration and an irregular coating thickness as shown in figure 5.8.6(b).

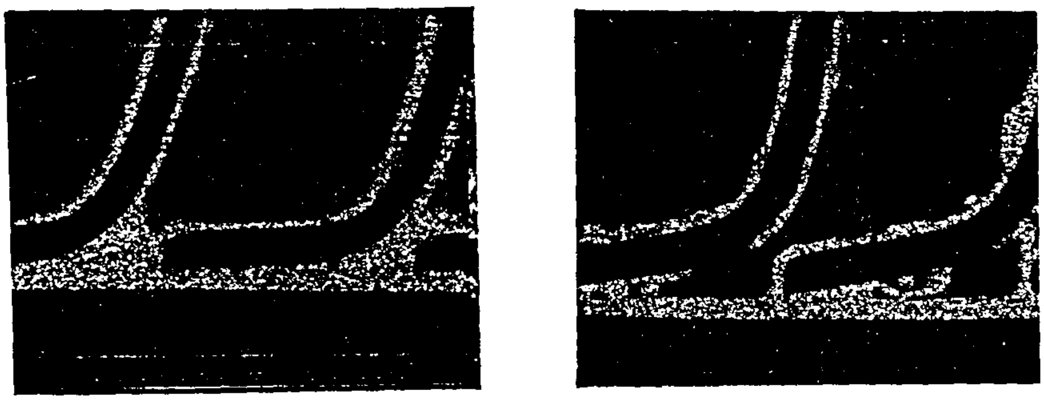

(a) Good quality (b) Poor quality

Figure 5.8.6: Galvanized finned tube.

Taborek [87TA1] evaluates accepted industrial practices and notes the lack of progress in the standardization of test procedures for determining the thermal contact resistance in finned tubes.

they are oriented in one plane, creating fluctuations only along the direction of free stream movement and perpendicularly to the cylindrical bars of the grid.

Correlations of turbulence intensity as measured by Fourie and Kröger [87FO1] as a function of Reynolds number and grid position, together with the frequency of vortex shedding based on the measurements of Blenk et al [35BL1], are shown in figure 5.9.1.

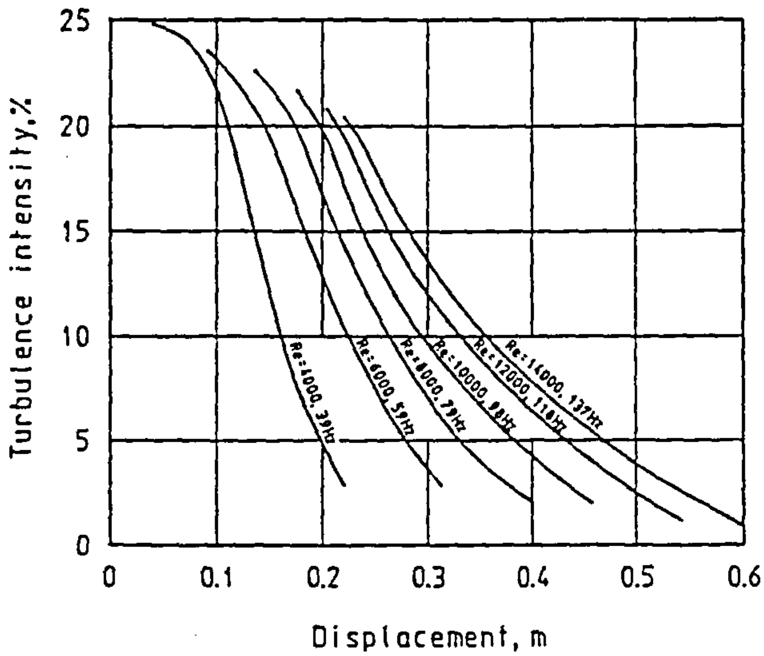

Figure 5.9.1: Measured turbulence intensity and corresponding frequency of vortex shedding behind bar grid.

Stephan and Traub [86ST1] determined the influence of turbulence intensity on heat transfer and pressure drop in bundles consisting of in-line and staggered plain tube banks. The tube diameter was 28 mm and the longitudinal pitch-to-diameter ratio was maintained at 1.54 while the transversal ratio was varied between 1.54 and 3.07. The air-side Reynolds number based on the tube diameter and the mean velocity through the minimum flow area ranged from 2×10^4 to 1.5×10^5. Different turbulence intensities were generated with the aid of wire screens having wire diameters from 1 mm to 2.5 mm and pitches from 3.5 mm to 12 mm and a biplanar grid consisting of a 6 mm wide bar at a pitch of 30 mm. It was possible to generate turbulence levels of 3.3 per cent to 7 per cent with the screens and 25 per cent with the grid, 90 mm downstream of the screens or the grid. Generally their turbulence measurements were in agreement with the values predicted by equation (5.9.1).

The correlation of heat transfer tests for bundles consisting of one to five rows of in-line plain tubes is shown in figure 5.9.2 in the form of a reduced Nusselt number, Nu/Nu_o, where Nu_o denotes the Nusselt number for the same bundle, but without a grid, as a function of the inlet turbulence level.

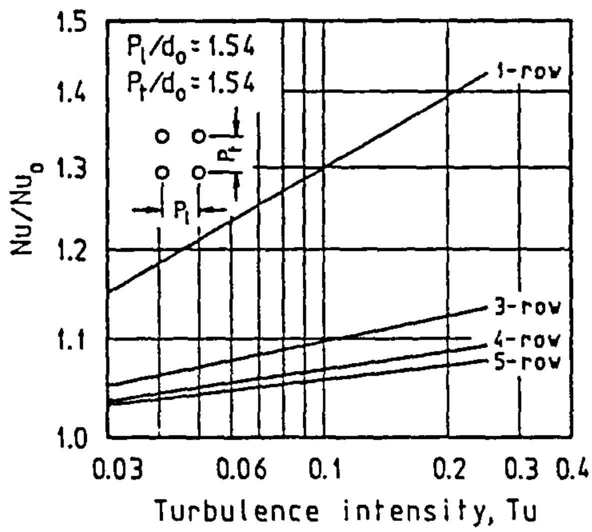

Figure 5.9.2: Increased heat transfer in an in-line tube bundle.

The enhancement of the mean heat transfer coefficient for bundles with five rows is up to 8 per cent, with four rows 9.5 per cent, with three rows 13.5 per cent, and for the single row 42 per cent at a turbulence intensity of 25 per cent.

The drag coefficients or friction factors for these bundles are found to be almost independent of the free stream turbulence level over a wide range of Reynolds numbers. Only for very high turbulence levels and high Reynolds numbers is a decrease in flow resistance observed for the single row bundle owing to a downstream shift in the boundary-layer separation point.

Zozulya et al [73ZO1] studied the influence of free stream turbulence on staggered finned tubes. The outside tube diameter was 22 mm with fins having a diameter of 38 mm, a thickness of 0.8 mm and an interfin spacing of 3.8 mm. The transversal tube pitch was

53mm and that in the longitudinal direction was 30 mm. The turbulence level of the incoming air stream was adjusted by installing orthogonal steel strips 6, 12 and 25 mm wide at pitches of 12, 24 and 45 mm respectively. As shown in figure 5.9.3, an increase in the flow turbulence to 22 - 25 per cent, has the greatest effect on the heat transfer coefficient for the first row, with an increase of 20 per cent at v_c = 5 m/s and 35 per cent at v_c = 15 m/s. No change is observed in the fourth row.

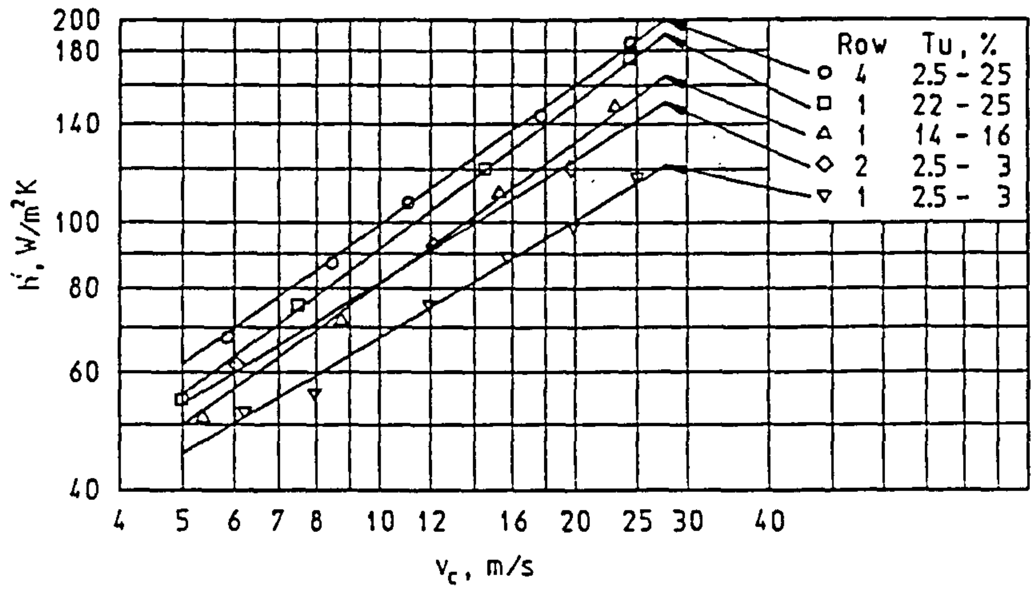

Figure 5.9.3: Change in heat transfer owing to turbulence.

Tests were conducted by Fourie and Kröger [87FO1] on bundles of staggered finned tubes having root diameters of 27.2 mm. The mean fin thickness was 0.37 mm at a 2.54 mm pitch. Tube pitches were 55 mm in the longitudinal direction and 66.7 mm in the transversal direction respectively. Free stream air speeds were varied from 2 m/s to 10 m/s resulting in corresponding Reynolds numbers, based on the tube root diameter and the minimum flow area in the bundle, of 6500 and 32500 respectively. Square screens having wire diameters of 0.5 mm (fine), 1.5 mm (medium) and 3 mm (coarse) at corresponding pitches of 1.85, 6.3 and 16 mm respectively and a bar grid consisting of 12.7 mm bars having a pitch of 25.4 mm were installed at different positions upstream of the bundles.

The results of their heat transfer tests with the coarse screen located in different positions before one-, two-, and three-row bundles are shown in figure 5.9.4. The largest increase

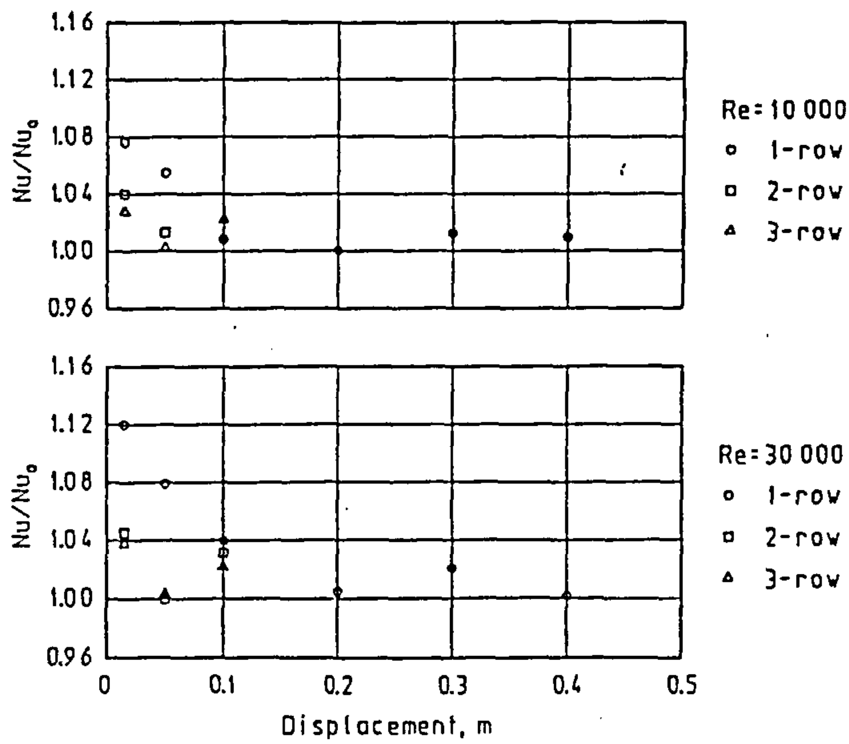

Figure 5.9.4: Change of heat transfer with coarse screen upstream of finned tube bundle.

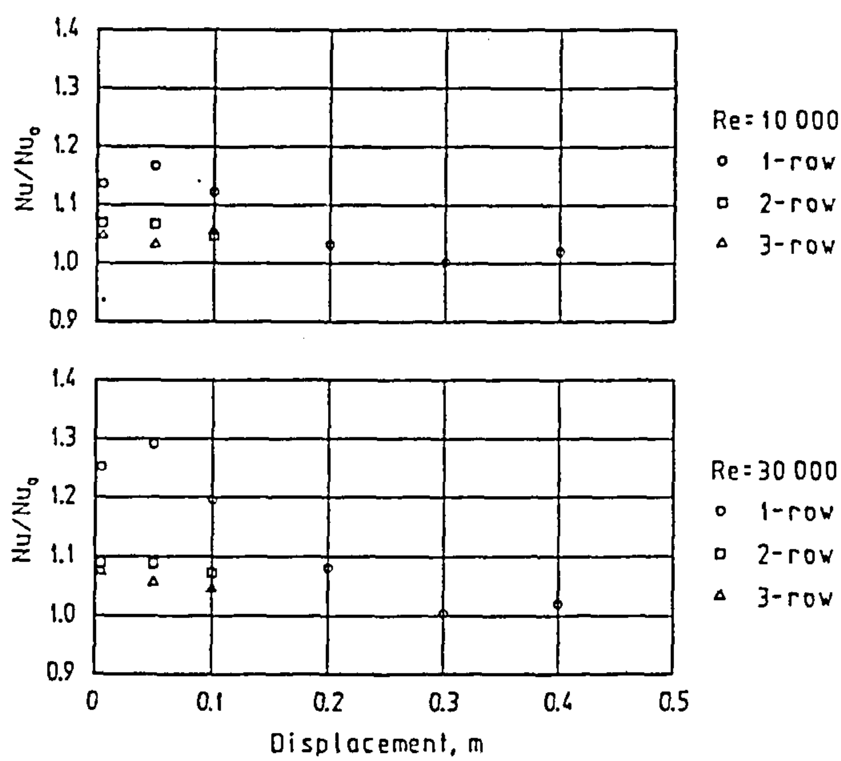

Figure 5.9.5: Change of heat transfer with bar grid upstream of finned tube bundle.

in heat transfer coefficient is observed when the screen is located relatively close to the bundle at the higher Reynolds number. No corresponding change in pressure differential across the bundle was observed.

Less enhancement was achieved with the finer screens.

As shown in figure 5.9.5, a maximum enhancement of 30 per cent was observed in the single-row bundle with the bar grid located 50 mm upstream. For this particular case a reduction in pressure drop was observed as shown in figure 5.9.6.

The turbulence levels for the various tests can be determined with the aid of equation (5.9.1) or from figure 5.9.2 for the bar grid. No measurable change in heat transfer was observed for bundles having more than three tube rows.

Nirmalan and Junkhan [82NI1] studied the influence of free stream turbulence intensity on five configurations of plate and louvered fin, single-pass, crossflow heat exchanger surfaces, geometric details of which are given in table 5.9.1.

Streamwise turbulence intensities of up to 16 per cent were obtained with three planar grids 6.4, 12.7 and 19 mm wide at pitches of 25, 50 and 75 mm respectively. Turbulence intensities generated by these grids were measured and found to be in good agreement with the equation of Baines and Peterson [51BA1]. Free stream air velocities ranged from 3 m/s to 15.3 m/s, resulting in corresponding Reynolds numbers, based on conditions at the minimum free flow area, ranging from 900 to 10000 [77JU1]. Exchangers 1 and 2 presented similar responses to the effects of inlet turbulence intensity. The Stanton number ratio versus Reynolds number curves indicates some augmentation. The maximum improvement, as shown in figure 5.9.7(a), is about 6 per cent for exchanger 1.

This relatively small increase in performance suggests that only the finned region near the inlet was affected by turbulence. Further downstream the wake flow generated by the staggered tube arrangement produces mixing effects that are essentially unaffected by upstream turbulence.

In exchanger 2 the louvered fins and high fin density promote mixing, and fin boundary layers, unaffected by turbulence, are maintained.

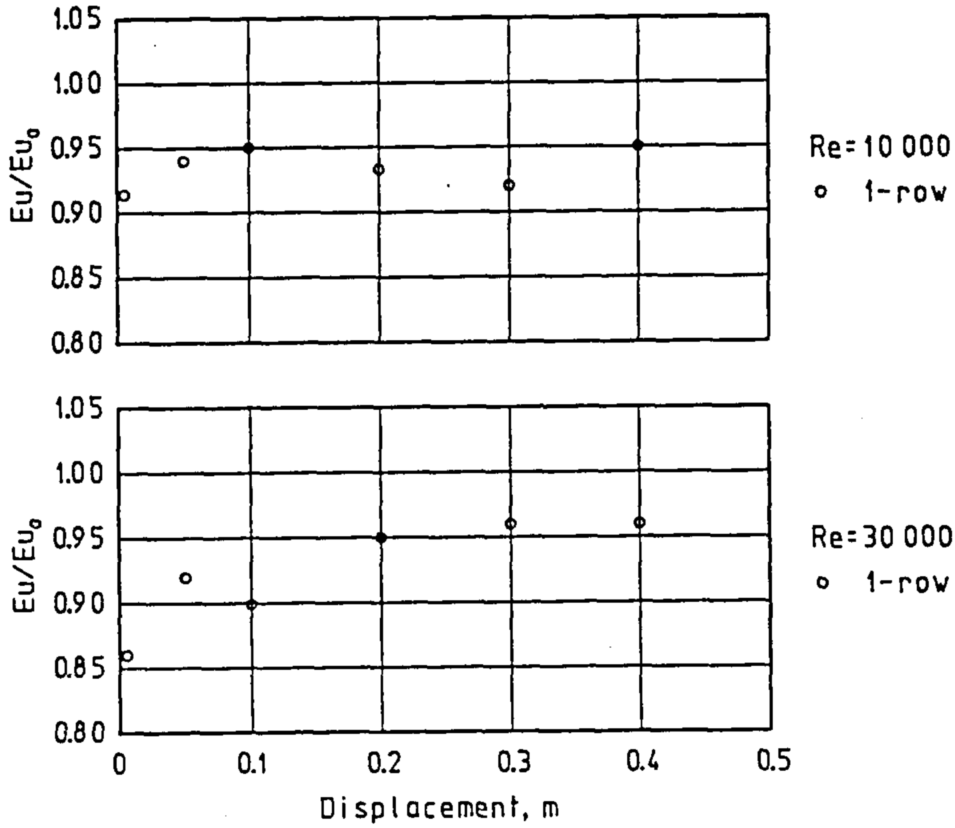

Figure 5.9.6: Change of pressure differential with bar grid upstream.

Table 5.9.1: Heat exchanger bundle geometries.

Exchanger No.	Fin type	Tube rows	Tube configuration	Longitudinal pitch (m)	Transversal pitch (m)	Fin density (fins/m)	Bundle thickness (m)
1	Flat	3	Staggered	0.0193	0.0177	315	0.055
2	Louvered	2	In-line	0.0171	0.0116	551	0.033
3	Flat	3	In-line	0.0257	0.0121	157.5	0.076
4	Flat	6	In-line	0.0257	0.0121	157.5	0.152
5	Flat	6	In-line	0.0257	0.0121	315	0.152
Tube size for exchanger 1,3,4 and 5: 0.0185 m x 0.0026 m							
Tube size for exchanger 2: 0.0133 m x 0.0026 m							

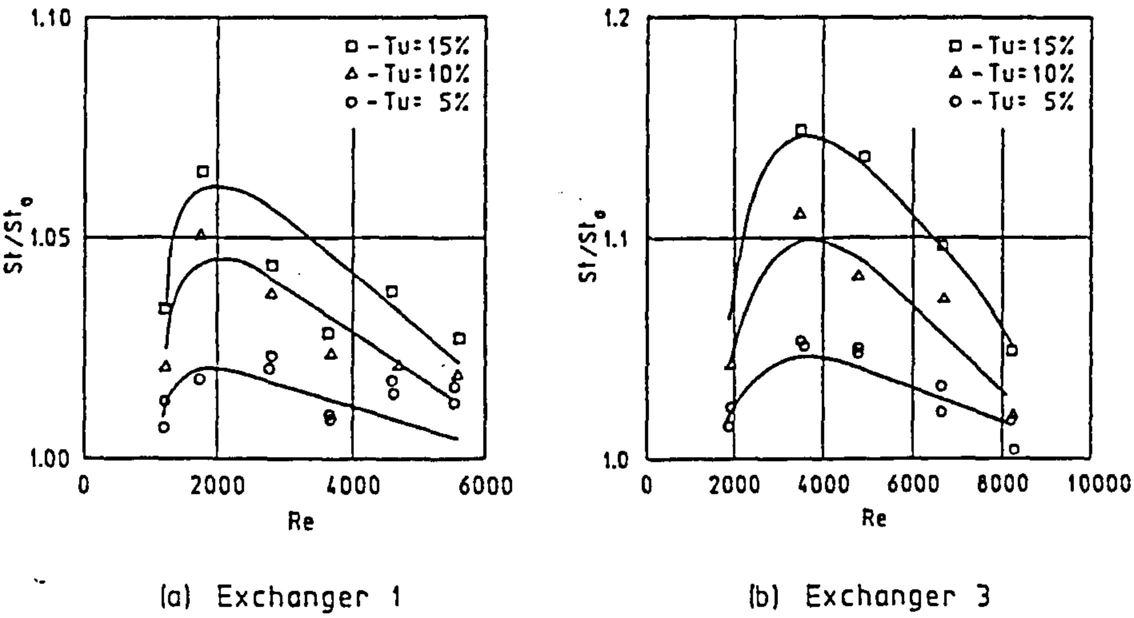

Figure 5.9.7: Stanton number increase.

As shown in figures 5.9.7(b), 5.9.8(a) and 5.9.8(b), more enhancement is achieved in exchangers 3, 4 and 5 owing to less effective mixing in the wake of the in-line tube arrangement. With the lower fin density the resultant thicker boundary layer is more strongly affected by free stream turbulence.

Gianolio and Cuti [81GI1] describe performance tests conducted on a pilot plant simulating an air-cooled heat exchanger that can be operated in both the induced-draft and forced draft modes. Under forced-draft conditions the velocity of the air stream approaching the finned tube heat exchanger bundle has, in addition to the axial component, a tangential component. The resultant oblique approach velocity and the turbulence in the fan wake [84KO1] tend to improve the heat transfer coefficient, particularly on the upstream tube rows, when compared to a six-row bundle, as is shown in figure 5.9.9. This enhancement is exceptionally high and not typical of all forced draft heat exchangers.

The degree of turbulence will also be influenced by other disturbances, such as support structures, walkways, screens etc. located upstream and downstream of the fan. In such forced draft systems a row correction factor of unity is recommended for all tube rows [85HU1].

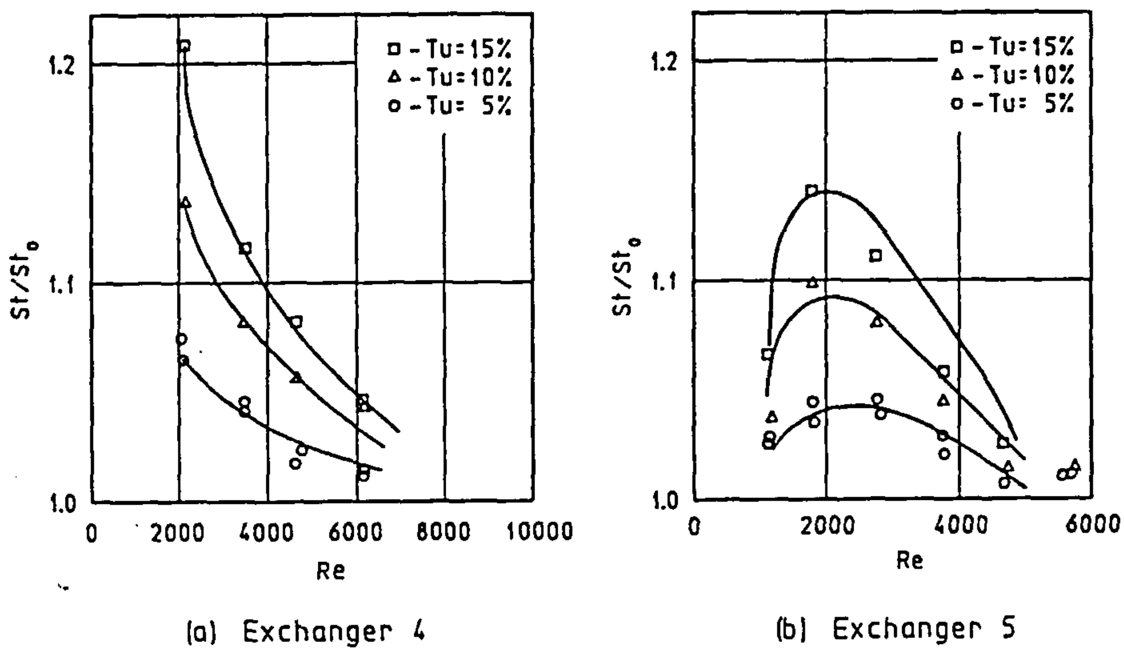

Figure 5.9.8: Stanton number increase.

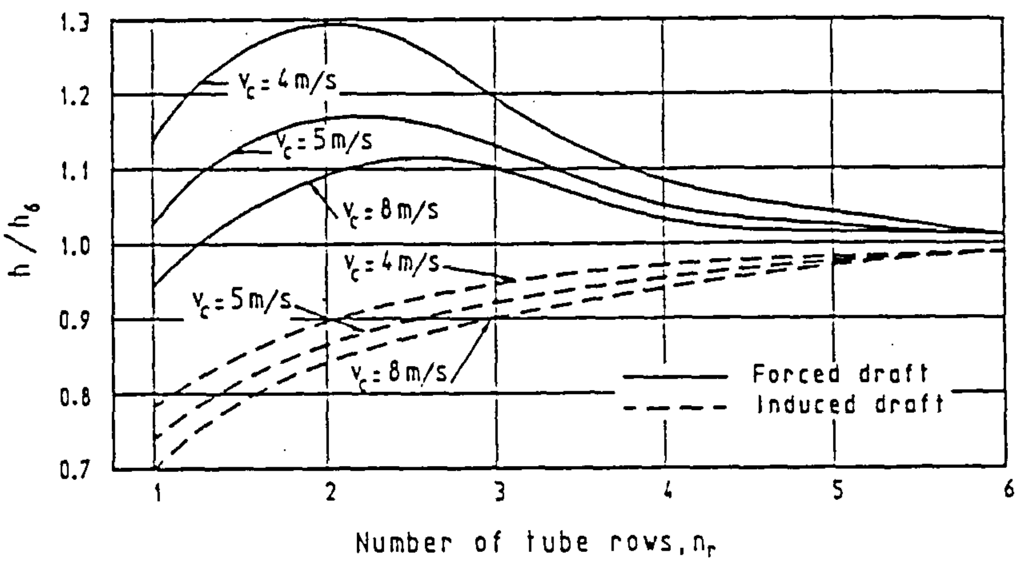

Figure 5.9.9: Comparison of heat transfer coefficient for induced and forced flow.

No general equation exists with which the enhancement in heat transfer owing to free stream turbulence at different Reynolds numbers can be quantified in specific heat exchanger bundles.

From available experimental data, however, it is concluded that free stream turbulence may enhance heat transfer in relatively thin heat exchanger cores or bundles in which little active internal mixing occurs owing to the geometric design of finned surfaces. In addition to the level of turbulence, the nature of the turbulence in the approach air stream undoubtedly affects the degree of enhancement that will be achieved. The influence on the pressure drop is in most cases small.

5.10 NON-UNIFORM FLOW AND TEMPERATURE DISTRIBUTION

An extensive review of the causes and effects of non-uniform or maldistributed flow and temperature distribution on the performance of different types of heat exchangers is presented by Mueller and Chiou [87MU1] [88MU1] and Kitto and Robertson [89KI1].

The causes of maldistribution in air-cooled heat exchangers include designs of headers and inlet and outlet duct systems, upstream and downstream appurtenances, manufacturing tolerances of flow passages through the heat exchanger [70LO1, 77MO1, 78BE1, 80SH1], variations in fluid viscosity, thermo-acoustic oscillations, fouling or blockage [82SP1], corrosion, recirculation and wind.

An early study of McDonald and Eng [63MC1] showed that the effect of tubeside maldistribution in a crossflow heat exchanger was small and resulted in a maximum thermal performance reduction of about four per cent. Chiou [78CH1, 78CH2, 79CH1, 80CH1, 80CH2, 82CH1, 82CH2, 83CH1] and Solar et al [83SO1] evaluated the effect of non-uniform flow and/or temperature distribution on the thermal performance of crossflow heat exchangers by using one and / or two-dimensional finite difference techniques to solve the governing differential equation.

Using numerical integration, Dobryakov et al [73DO1] and Fagan [80FA1] analyzed the effects of air-flow maldistribution on heat exchanger performance. Rabas [87RA1] extended their integral approach to both one- and two-dimensional nonuniform flow and temperature distributions as found in air-cooled condensers.

5.11 REFERENCES

33CO1 Colburn, A.P., A Method of Correlating Forced Convection Heat Transfer Data and a Comparison with Fluid Friction, Trans. Am. Inst. Chem. Eng., Vol. 29, pp. 174-210, 1933; reprinted in Int. J. Heat Mass Transfer, Vol. 7, pp. 1359 - 1384, 1964.

35BL1 Blenk, H., Fuchs, D. and Liebert, L., Über die Messung von Wirbelfrequenzen, Luftfahrtforschung Vol. 12, pp. 38 - 41, 1935.

45GU1 Gunter, A.Y. and Shaw, W.A., A General Correlation of Friction Factors for Various types of Surfaces in Crossflow, Trans. ASME, Vol. 67, pp. 643 - 660, 1945.

45JA1 Jameson S.L., Tube Spacing in Finned Tube Banks, Trans. ASME, Vol. 67, pp. 633 - 642, 1945.

47WI1 Wile, D.D., Air Flow Measurement in the Laboratory, ASRE, Refrigerating Engineering, pp. 515 - 521, June, 1947.

48FR1 Frenkiel, F.N., Trans, ASME, Vol. 70. pp. 311, 1948.

51BA1 Baines, W.D. and Peterson, E.G., An Investigation of Flow Through Screens, Trans. ASME, Vol. 73, pp. 467 - 480, 1951.

54KA1 Katz, D.L., Young, E.H., Williams, R.B., Balekjian, G. and Williamson, R.P., Correlation of Heat Transfer and Pressure Drop for Air Flowing Across Banks of Finned Tubes, Univ. Mich. Eng. Res. Inst. Report on Project M592, Aug. 1954.

57YO1 Young, E.H., Fleming, J.R. and Conroy, W.F., Development of an Apparatus for Measurement of Low Bond Resistance in Finned and Bare Duplex Tubes, University of Michigan, Eng. Res. Inst. Proj. 1592, Report 48, 1957.

58KU1 Kutateladze, S.S. and Borishaniskii, V.M., A Concise Encyclopedia of Heat Transfer, Moscow, 1958, English ed., 1966.

59DA1 Dart, D.M., Effect of Fin Bond on Heat Transfer, ASHRAE J., pp. 67 - 71, 1959.

59KE1 Kern, D.Q. and Seaton, R.E., A Theoretical Analysis of Thermal Surface Fouling, Brit. Chem. Eng., Vol. 4, pp. 258 - 262, May 1959.

59WA1 Ward, D.J. and Young, E.H., Heat Transfer and Pressure Drop of Air in Forced Convection Across Triangular Pitch Banks of Finned Tubes, Chem. Eng. Progr. Symp. Ser. Vol. 55, No. 29, pp. 37 - 44, 1959.

60GA1 Gardner, K.A. and Carnavos, T.C., Thermal-Contact Resistance in Finned Tubing, J. Heat Transfer, Trans. ASME, Ser. C, Vol. 82, No. 2, pp. 279 - 293, 1960.

62BR1 Brauer, H., Heat Transfer and Flow Resistance with In-line and Staggered Finned Tubes, Dechema Monograph, Vol. 40, pp. 61 - 76, 1962.

63BR1 Briggs, D.E. and Young, E.H., Convective Heat Transfer and Pressure Drop of Air Flowing Across Triangular Pitch Banks of Finned Tubes, Chem. Eng. Progr. Symp. Ser., Vol. 59, No. 41, pp. 1 - 10, 1963.

63MC1 McDonald, J.S. and Eng, K.V., Tube Side Flow Distribution Effects on Heat Exchanger Performance, Chemical Engineering Progress Symposium Series, Vol. 59, pp. 370-378, 1963.

63SC1 Schmidt, T.E., Der Wärmeübergang an Rippenrohre und Berechnung von Rohrbündelnwärmeaustauschern, Kältetechnik, Vol. 15, No. 4, Part 1 and Part 11, pp. 370 - 378, 1963.

64BR1 Brauer, H., Compact Heat Exchangers, Chemical and Process Engineering, pp. 451 - 460, August 1964.

64SH1 Shlykov, Y.P. and Ganin, Y.A., Thermal Resistance of Metallic Contacts, Int. J. Heat and Mass Transfer, Vol. 7, pp. 921 - 929, 1964.

65SC1 Schulenberg, F.J., Wahl der Bezugslänge zur Darstellung von Wärmübergang und Druckverlust in Wärmetauschern, Chemie-Ing-Techn. Vol. 37, 1965.

65YO1 Young, E.H. and Briggs, D.E., Bond Resistance of Bimetallic Finned Tubes, Chem. Eng. Prog., Vol. 61, No. 7, pp. 71 - 78, 1965.

66KU1 Kulkarni, M.V. and Young, E.H., Bimetallic Finned Tubes, Chem. Eng. Prog., Vol. 62, No. 7, pp. 68 - 71, 1966.

66RO1 Robinson, K.K. and Briggs, D.E., Pressure Drop of Air Flowing Across Triangular Pitch Banks of Finned Tubes, Chem. Eng. Progr. Symp. Ser., Vol. 62, No. 64, pp. 177 - 184, 1966.

66SC1 Schulenberg, F.J., Finned Elliptical Tubes and Their Application in Air-cooled Heat Exchangers, ASME. Trans., Journal of Engineering for Industry, pp. 179-190, May 1966.

66SM1 Smith, C.E., Gunter, A.Y. and Victory, S.P., Evaluation of Fin Tube Performance under Steady-state and Thermal Cycling Conditions, Chem. Eng. Progr., Vol. 62, No. 7, 1966.

66VA1 Vampola, J., Heat Transfer and Pressure Drop in Flow of Gases Across Finned Tube Banks, Strojirenstvi, Vol. 7, pp. 501 - 507, 1966.

70LO1 London, A.L., Laminar Flow Gas Turbine Regenerators - The Influence of Manufacturing Tolerances, Trans. of the ASME, Journal of Engineering for Power. pp. 46-56, Jan. 1970.

70PR1 Preece, R.J., Lis, J. and Hitchcock, J.A., Comparative Performance Characteristics of Some Extended Surfaces for Air Cooler Applications, Conf.

on Air Coolers, Inst. Mech. Engrs., London, pp. 41 - 60, 24 Sept, 1970.

70RO1 Rose, J.C., Some Problems Associated with the Operation and Testing of Air-cooled Heat Exchangers, Conference on Air-coolers, Inst. Mech. Engrs. London, pp. 77 - 87, 24 Sept, 1970.

70ZO1 Zozulya, N.V., Kalinin, B.L. and Khavin, A.A., Influence of the Layout of a Bank of Finned Aluminium Tubes on Heat Transfer, Teploenergetika, Vol. 17, No. 6, 1970.

71KU1 Kuntysh, V.B. and Iokhvedor, F.M., Effect of Relative Interfin Distance on the Thermal Convective Heat Transfer in Finned Tube Bundles and on Augmenting of Heat Transfer, Heat Transfer, Soviet Research, Vol. 3, No. 2, pp. 50 - 61, 1971.

72AR1 ARI, Standard for Forced Circulation Air-Cooling and Air-Heating Coils, Standard 410, ARI, Arlington, Virginia, 1972.

73DO1 Dobrykov, B.A. et al., The Calculation of Heat Exchange Equipment with Cross-flow of the Heat Transfer Agents, Int. Chem Engineering. Vol 13, No. 1, pp. 81 - 84, 1973.

73PH1 Phillips, N.V., Gloeilampenfabrieken, Eindhoven, Patent No. 7314929, Netherlands, 1973.

73ZO1 Zozulya, N.V., Vorobyev, Yu.P. and Khavin, A.A., Effect of Flow Turbulization on Heat Transfer in a Finned-Tube Bundle, Heat Transfer - Soviet Research, Vol. 5, No.1, pp. 154 - 156, 1973.

74HU1 Hunn, B.D., Effects of External Fouling on Dry Cooling Tower Performance, Proc. Front of Power Techn. Conf., Okla. State Univ., 1974.

74MI1 Mirković, Z., Heat Transfer and Flow Resistance Correlation for Helically

Finned and Staggered Tube Banks in Crossflow, in Heat Exchangers: Design and Theory Source Book, eds. N.H. Afgan and E.U. Schlünder, McGraw Hill Book Co., pp. 559 - 584 1974.

74ZH1 Zhukauskas, A.A., Investigation of Heat Transfer in Different Arrangements of Heat Exchanger Surfaces, Teploenergetika, Vol. 21, No. 5, pp. 24 - 29, 1974.

76BA1 Battelle Pacific Northwest Laboratories, A Survey of Materials and Corrosion Performance in Dry Cooling Applications, BNWL-1958, UC - 12, 1976.

76HO1 Hofmann, H., Möglichkeiten zur Berechnung des Wärmeübergangs und des Druckverlustes von Rippenrohrbündeln, Luft und Kältetechnik, Vol. 12, pp. 136 - 139, 1976.

76PF1 Rozenman, T., Momoh, S.K. and Pundyk J.M., Heat Transfer and Pressure Drop Characteristics of Dry Tower Extended Surfaces, Part 1, PFR Report no. BNWL-PFR-7-100, PFR Eng. Systems Inc. California, 1976.

76WE1 Weierman, C., Correlations Ease the Selection of Finned Tubes, The Oil and Gas Journal, Vol. 74, No. 36, pp. 94 - 100, Sept., 1976.

77BA1 Battelle Pacific Northwest Laboratories, Aluminum Alloy Performance Under Dry Cooling Tower Conditions, 1977.

77EC1 Eckels, P.W., Contact Conductance of Mechanically Expanded Plate Finned Heat Exchangers, ASME Paper 77-HT-24, 1977.

77JU1 Junkhan, G.H., Bergles, A.E. and Jensen, M.K., Heat Exchanger Core Testing, Data Analysis, and Performance Prediction, Heat Transfer Lab. Rep., HTL - 14, USU-ERI-AMES-78189, Iowa State Univ., Ames, Iowa, Nov. 1977.

77MO1 Mondt, J.R., Effects of Nonuniform Passages on Deepfold Heat Exchanger Performance, Trans of the ASME, Journal of Engineering for Power, pp. 657 - 663, 1977.

77MO2 Moore, F.K., and Torrence, K.E., Air Flow in Dry Natural-Draught Cooling Towers Subject to Wind, Cornell Energy Report, Final Report to ERDA, Ithaca, New York, 1977.

78AS1 ASHRAE Standard 33 - 78, Methods for Testing Forced Circulation Air Cooling and Air Heating Coils, ASHRAE, New York, 1978.

78BE1 Bell, K.J. and Kegler W.H., Analysis of Bypass Flow Effects in Tube Banks and Heat Exchangers, AICHE Symposium Series, Vol. 74, No. 174.

78CH1 Chiou, J.P., Thermal Performance Deterioration in Crossflow Heat Exchanger Due to Flow Nonuniformity of Both Hot and Cold Sides, Proc. 6th Int. Heat Transfer Conf., Vol. 4, Paper HX-16, pp. 279 - 284, 1978.

78CH2 Chiou, J.P., The Thermal Performance Deterioration in Crossflow Heat Exchanger Due to Flow Nonuniformity, ASME Journal of Heat Transfer, Vol. 100, pp. 580-587, 1978.

78MO1 Moore, F.K., Aerodynamics of the Heat Exchangers and Their Arrangement in Large Dry Cooling Towers, ASME Paper 78-WA/HT-19, 1978.

79CH1 Chiou, J.P., The Effect of Nonuniform Fluid Flow Distribution on Thermal Performance of Crossflow Heat Exchanger, ASME paper 79-WA/HT-3, 1979.

79EL1 Elmahdy, A.H. and Biggs, R.C., Finned Tube Heat Exchanger: Correlation of Dry Surface Heat Transfer Data, ASHRAE Trans., Vol. 85, 1979.

79HO1 Höfling, E. and Maly. Z., Umfassende Korrosionsschutzsystem für Lamellenkühler, Schweizerische Aluminium Rundschau, Vol. 6, 1979.

79MO1 Mohandes, M.A., The Flow through Heat Exchanger Banks, Ph.D. thesis, Oxford University, 1979.

79MO2 Moore, F.K., Flow Fields and Pressure Losses of V-Bundles with Finite

Resistance, ASME Paper 79-WA/HT-4, 1979.

79MO3 Moore, F.K. and Ristorcelli, J.R., Turbulent Flow and Pressure Losses Behind Oblique High-drag Heat Exchangers, Int. J. Heat Mass Transfer, Vol. 22, pp. 1175 - 1186, 1979.

79NE1 Neal, J.W. and Savage, W.F., Report of the Visit of the United States of America Delegation of the U.S. - U.S.S.R. Co-ordinating Committee on Scientific and Technical Co-operation in the Field of Thermal Power Plant Heat Rejection Systems to the Union of Soviet Socialistic Republics, DOE/ET-0078, U.S. Dept. of Energy, 1979.

79RU1 Russell, C.M.B., The Effect on the Thermal Performance of External Corrosion of Fin Tubes, Nat. Heat Transfer Conf., San Diego, Aug. 1979.

79SC1 Schack, K., Berechnung des Druckverlustes in Querstrom von Rippenrohrbündeln, Chem. -Ing. -Technik, 51, pp. 986 - 987, 1979.

80CH1 Chiou, J.P., The Effect of the Flow Nonuniformity on the Sizing of the Engine Radiator, SAE Technical Paper 800035, 1980.

80CH2 Chiou, J.P., The Advancement of Compact Heat Exchanger Theory Considering the Effects of Longitudinal Heat Conduction and Flow Nonuniformity, Compact Heat Exchangers History, Technical Advancement and Mechanical Design Problems, ASME HTD - Vol. 10, pp. 101 - 102, 1980.

80FA1 Fagan, T.F., The Effects of Air Flow Maldistribution on Air - to Refrigerant Heat Exchanger Performance, ASHRAE Trans., Vol. 86, Pt 2, 1980.

80KE1 Kern, J., Zur Bewertung von Kompakt-Wärmeaustauschern, Wärme-und Stoffübertragung, Vol. 13, pp. 205 - 215, 1980.

80SH1 Shah, R.K. and London, A.L., Effects of Nonuniform Passages on Compact Heat Exchanger Performances, Trans. of the ASME, Journal of Engineering for

Power, Vol. 102, pp. 653 - 659, July 1980.

81BE1 Bemrose, C.R. and Bott, T.R., Studies of Gas-side Fouling in Heat Exchangers, Progress in the Prevention of Fouling in Industrial Plant Conf., Univ. of Nottingham, pp. 2 - 20, April, 1981.

81BI1 Biery, J.C., Prediction of Heat Transfer Coefficients in Gas Flow Normal to Finned and Smooth Tube Banks, Journal of Heat Transfer, ASME Trans., Vol. 103, pp. 705 - 714, 1981.

81FI1 Fischer, O. and Bucher, K.H., Analytical and Thermal-Hydraulic Optimization of Finned Tube Bundle Heat Exchangers for Dry Cooling Towers, in Heat Exchangers, Thermal-Hydraulic Fundamentals and Design, eds. Kakac, S., Bergles A.E., and Mayinger, F., pp. 765 - 777, McGraw - Hill, 1981.

81GI1 Gianolio, E. and Cuti, F., Heat Transfer Coefficients and Pressure Drops for Air Coolers with Different Numbers of Rows Under Induced and Forced Draft, Heat Transfer Eng., Vol. 3, No. 1, pp. 38 - 47, 1981.

81PO1 Pollack, H., Wärme und strömungstechnische Untersuchungen an Kunststoffwärmeaustauschern für Trockenkühltürme, Report No. BMFT-FB-T 81-004, Bundesministerium für Forschung und Technologie, Bonn, 1991.

81YO1 Yovanovich, M.M., New Contact and Gap Conductance Correlations for Conforming Rough Surfaces, AIAA, Paper No. 81 - 1164, AIAA 16th Thermophysics Conf., Palo Alto, Calif., June 1981.

82CH1 Chiou, J.P., Effect of Nonuniformities of Inlet Temperatures of Both Fluids on the Thermal Performance of a Crossflow Heat Exchanger, ASME Paper 82-WA/HT-42, 1982.

82CH2 Chiou, J.P., The Effect of Nonuniformities of Inlet Fluid Temperature on the Thermal Performance of Crossflow Heat Exchanger, Proc. 7th Int. Heat Transfer Conf., Paper HX3, pp. 179-184, 1982.

82KA1 Kast, W., and Eberhard, V., Verfahren zur Berechnung des Druckverlustes in Rippenrohrbündeln, Verfahrenstechnik, Vol. 16, 1982.

82NI1 Nirmalan, V. and Junkhan, G.H., Effects of Turbulence Parameters on Heat Transfer of Cross Flow Heat Exchangers, Proc. 7th Int. Heat Transfer Conf., Vol. 6, pp. 233 - 238, München, 1982.

82SP1 Sparrow, E.M. and Ruiz, R., Effect of Blockage-induced Flow Maldistribution on the Heat Transfer and Pressure Drop in a Tube Bank, Trans. of the ASME, Journal of Heat Transfer, Vol. 104, pp. 691-699, Nov. 1982.

83BO1 Bott, T.R. and Bemrose, C.R., Particulate Fouling on the Gas-side of Finned Tube Heat Exchangers, J. Heat Transfer, Vol. 105, No. 1, pp. 178 - 183, Feb. 1983.

83BR1 Brandt, F. and Wehle, F., Eine zusammenfassende Darstellung des Wärmeübergangs an Rohrbündeln mit glatten Rohren und Rippenrohren, VGB-Konferenz, 1983.

83CH1 Chiou, J.P., The Effect of the Air Flow Nonuniformity on the Thermal Performance of an Automobile Air Conditioning Condenser, SAE Trans., Vol. 97, pp. 2587-2600, 1983.

83CH2 Christensen, R.N. and Fernandes, H.V., Contact and Fouling Resistances in Finned Tube Heat Exchangers, ASME Paper 83-HT-39, 1983.

83SO1 Solar, A.I., Singh, K.P. and Ng, T.L., Effect of Nonuniform Inlet Flow and Air Cooler Heat Exchange Performance, Proc. ASME-JSME Thermal Engineering Joint Conference, Vol. 1, pp. 537-542, 1983.

84BE1 Becker, N., Druckverlust und Wärmeübertragung von Rippenrohrbündeln für Naturzug-Trockenkühltürme, Dr. Ing. thesis, Technische Hochschule, Aachen, 1984.

84BE2 Bemrose, C.R. and Bott, T.R., Correlations for Gas-side Fouling of Finned Tubes, 1st U.K. National Conference on Heat Transfer, Vol. 1, pp. 357 - 367, Pergamon Press, London, 1984.

84FI1 Fischer, O., Experimental Investigations of Forgo-type Dry Cooling Elements, Paper presented at the 4th IAHR Cooling Tower Workshop, Interlaken, Switzerland, 1984.

84GU1 Guyer, E.C., Mullen, G.P. and Brownell, D.L., Nonmetallic Heat Exchangers: A Survey of Current and Potential Designs for Dry-Cooling Systems, Report CS-3454, Res. Proj. 1260-29, Dynatech Co., Cambridge, Mass., 1984.

84KA1 Kays, W.M. and London, A.L., Compact Heat Exchangers, McGraw-Hill Book Co., New York, 1984.

84KO1 Kotb, M.A., Experimental Investigation of 3-D Turbulent Free Shear Flow Propellors and Windmills, Ph.D thesis, Virginia Polytechnic Institute and State University, Blacksburg, Virginia, 1984.

84KR1 Kröger, D.G., Radiator Characterization and Optimization, SAE Paper 840380, 1984.

84MO1 Mohandes, M.A., Jones, T.V. and Russel, C.M.B., Pressure Loss Mechanism in Resistances Inclined to an Air Flow with Application to Fintubes, Paper presented at the First National Heat Transfer Conference, Leeds, 1984.

84VG1 VGB-TW 504, Vergleichende Korrosionsversuche an Trockenkühl-Elementen für Trockenkühltürme, VGB Kraftwerkstechnik GMBH, Essen 1984.

85EC1 Eckels, P.W. and Rabas, T.J., Heat Transfer and Pressure Drop of Typical Air Cooler Finned Tubes, J. Heat Transfer, Vol. 107, No. 1, pp. 198 - 204, 1985.

85ER1 Ernest, T.L., Sheffield, J.W. and Sauer, H.J., Finned Tube Contact Conductance: Characterizing the Integrity of Mechanical Bond, ASHRAE Trans., Vol. 91, Pt.

2, 1985.

85GA1 Ganguli, A., Tung, S.S. and Taborek, J., Parametric Study of Air-cooled Heat Exchanger Finned Tube Geometry, AIChE Symposium Series, Vol. 81, No. 245, pp. 122 - 128, 1985.

85HU1 Huber, F.V. and Rabas, T.J., The Effect of Geometry on the Heat Transfer Row Correction for Typical Finned Tube Bundles, AICHE Natl. Heat Transfer Conf., Denver, Co., 1985.

85SH1 Sheffield, J.W., Abu-Ebid, M. and Sauer, H.J., Finned Tube Contact Conductance: Empirical Correlation of Thermal Conductance, ASHRAE Trans., Vol. 91, Pt 2, 1985.

85SO1 Somerton, C., Bridges, R.D., Callihan, R.W., and Taff, C., Heat Transfer Analysis of an Inclined Radiator, ASME Paper 85-WA/HT-24, 1985.

85SU1 Süthoff, Th. and Reichel, H.-H., Vergleichende Korrosionsversuche an Trockenkühlelementen für Trockenkühltürme, VGB Kraftwerkstechnik 65, Heft 9, pp. 835 - 844, September, 1985.

86CO1 Coetzee, D. and Kröger, D.G., Analysis and Measurement of Contact and Gap Resistances in Extruded Bi-metallic Finned Tubes, Heat Recovery Systems, Vol. 6., No., 6, pp. 503 - 513, 1986.

86ES1 ESDU, High-fin Staggered Tube Banks: Heat Transfer and Pressure Drop for Turbulent Single Phase Gas Flow, Eng. Sciences Data Item No. 86022, London, 1986.

86KO1 Kotzé, J.C.B., Bellstedt, M.O. and Kröger, D.G., Pressure Drop and Heat Transfer Characteristics of Inclined Finned Tube Heat Exchanger Bundles, Proc. 8th Int. Heat Transfer Conf., San Francisco, 1986.

86KO2 Kotzé, J.C.B., Ontwerp van Droë Direk Geforseerde en Indirek Natuurlike

Konveksie Koeltorings, M.Eng. Thesis, University of Stellenbosch, Stellenbosch, 1986.

86KR1 Kröger, D.G., Performance Characteristics of Industrial Finned Tubes Presented in Dimensional Form, Int. J. Heat Mass Transfer, Vol. 29, No. 8, 1986.

86MO1 Monheit, M. and Freim, J., Effect of Tube Bank Inclination on the Thermal Hydraulic Performance of Air Cooled Heat Exchangers, Proc. 8th Int. Heat Transfer Conf., San Francisco, pp. 2927 - 2732, 1986.

86SA1 Samie, F. and Sparrow, M., Heat Transfer from a Yawed Finned Tube, Jnl. of Heat Transfer, ASME Trans., Vol. 108, pp. 479 - 482, 1986.

86ST1 Stephan, K. and Traub, D., Influence of Turbulence Intensity on Heat Transfer and Pressure Drop in Compact Heat Exchangers, Proc. 8th Int. Heat Transfer Conf., San Francisco, pp. 2739 - 2744, Aug. 1986.

87FO1 Fourie, J.G. and Kröger, D.G., Influence of Turbulence on Performance of Circular Helically Finned Tubes, Proc. 17th Int. Congress for Refrigeration, Vol. B, pp. 856 - 863, Vienna, 1987.

87LE1 Lemczyk, T.F. and Yovanovich, M.M., New Models and Methodology for Predicting Thermal Contact Resistance in Compound Cylinders and Finned Tubes, Heat Transfer Engineering, Vol. 8, No. 2, pp. 35-48, 1987.

87MU1 Mueller, A.C. and Chiou, J.P., Review of Various Types of Flow Maldistribution in Heat Exchangers, ASME HDT-Vol. 75, 24th National Heat Transfer Conference, eds Kitto, J.B. and Robertson, L.M., New York, 1987.

87RA1 Rabas, T.J., The Effect of Nonuniform Inlet Flow and Temperature Distributions on the Thermal Performance of Air-Cooled Condensers, ASME Report HTD.-Vol. 75, Maldistribution of Flow and its Effect on Heat Exchanger Performance, eds Kitto, J.B. and Robertson, J.M., 1987.

87TA1 Taborek, J., Bond Resistance and Design Temperatures for High-finned Tubes - A Reappraisal, Heat Transfer Engineering, Vol. 8, No. 2, pp. 26 - 34, 1987.

88BO1 Bódás, J., Guidelines in Selecting Heat Exchanger Materials for Dry Cooling Plants of Large Capacity Steam Turbines, 6th IAHR Cooling Tower Workshop, Pisa, 1988.

88GE1 GEA Luftkühlergesellschaft GmbH, Bochum, Patent No. 88/8258, Fed. Rep. Germany.

88HA1 Ham, A.J. and West, L.A., ESKOM Fortschritte in der Trockenkühlung, VGB Kraftwerkstechnik 68, Heft 9, pp. 912 - 917, September 1988.

88KR1 Kröger, D.G., Untersuchung von Trockenkühlsystemen, VGB Kraftwerkstechnik, Vol. 10, No. 68, October 1988.

88MU1 Mueller, A.C. and Chiou, J.P., Review of Various Types of Flow Maldistribution in Heat Exchangers, Heat Transfer Engineering, Vol. 9, No. 2, 1988.

88PA1 Palfalvi, G., Experience with Aluminium Air Coolers in Power Plants, 6th IAHR Cooling Tower Workshop, Pisa, 1988.

88ST1 Stasiulevicius, J. and Srinska, A., Heat Transfer of Finned Tube Bundles in Crossflow, Hemisphere Publ. Corp., New York, 1988.

88ZU1 Zukauskas, A. and Ulinskas, R., Heat Transfer in Tube Banks in Crossflow, Hemisphere Publ. Corp., New York, 1988.

89KI1 Kitto, J.B. and Robertson, J.M., Effects of Maldistribution of Flow on Heat Transfer Equipment Performance, Journal of Heat Transfer Engineering Vol. 10, No. 1, pp. 18 - 25, 1989.

89PA1 Paikert, P., Werkstoffauswahl für luftgekühlte Wärmeaustauscher, Chem.-Ing.-Tech., Vol. 61, No. 8, pp. 590 - 596, 1989.

90FI1 Fiebig, M., Mitra, N.K. and Dong. Y., Einfluss ausgestanzter Deltaflügel - Wirbelzeuger auf Wärmeübergang und Strömungswiderstand von Rippenrohren, Wärme und Stoffübertragung, Vol. 25, No. 1, pp. 33 - 43, 1990.

91BO1 Bódás, J., Heat Exchanger Materials for Dry Cooling Plants, Paper prsented at the Symposium on Dry Cooling Towers, Teheran, 1991.

91NI1 Nir, A., Heat Transfer and Friction Factor Correlations for Crossflow Over Staggered Finned Tube Banks, Heat Transfer Engineering, Vol. 12, No. 1, pp. 43-58, 1991.

91RE1 Reay, D.A., Heat Transfer Enhancement - A Review of Techniques and Their Possible Impact on Energy Efficiency in the U.K., Heat Recovery Systems and CHP, Vol. 11, No. 1, pp. 1-40, 1991.

93VA1 Van Aarde, D.J. and Kröger, D.G., Flow Losses Through an Array of A-frame Heat Exchangers, Heat Transfer Engineering, Vol. 14, No. 1, pp. 43-51, 1993.

CHAPTER 6

FANS

6.0 INTRODUCTION

Different types of fans find application in air-cooled heat exchangers and evaporative coolers including axial-, centrifugal-, mixed- and cross-flow types. When selecting a fan for a particular application, factors such as cost, performance (stability of operation, ease of control, power consumption, flow range), mechanical arrangement (convenience of installation), self cleaning blade properties and noise emission characteristics are usually considered. The effective operation of such a fan in a system may be influenced by various structural and aerodynamic factors. Numerous books on the subject have been published [61JO1, 73EC1, 78DA1, 83WA1]. Guides as to the selection of appropriate fans for a particular application are also available [79ES1]. In this chapter certain characteristics of axial flow fans which find general application in air-cooled heat exchangers are highlighted.

Modern axial flow fans are usually made by extruding aluminum or molding fiberglass blades as shown in figure 6.0.1. Extruded aluminum blades are by nature always of uniform chord width (sections may however be welded onto the extrusion) while molded fiberglass blades can have any desired shape.

One of the basic criteria for blade design is to produce, if possible, a uniform air flow over the entire plane of the fan. It follows that as one moves from the tip of the blade to the hub the tangential velocity decrease and in order to produce uniform airflow the blade width and twist must increase. The air vectors at the inboard sections of the blade may actually reverse direction. In a fan designed with a hub seal disc this effect is reduced. An example that illustrates performance differences due to blade shape and backflow is shown in figure 6.0.2 [79MO1]. In the absence of a bell inlet the fan performance is measurably reduced.

Axial flow fans are usually provided with four to eight blades. Both the fan cost and the air volume supplied at a given fan speed increase with increasing blade number. For a specified air volume flow rate the rotational speed can be reduced with increasing blade numbers. This has the favourable effect of reducing noise and increasing efficiency but also cost.

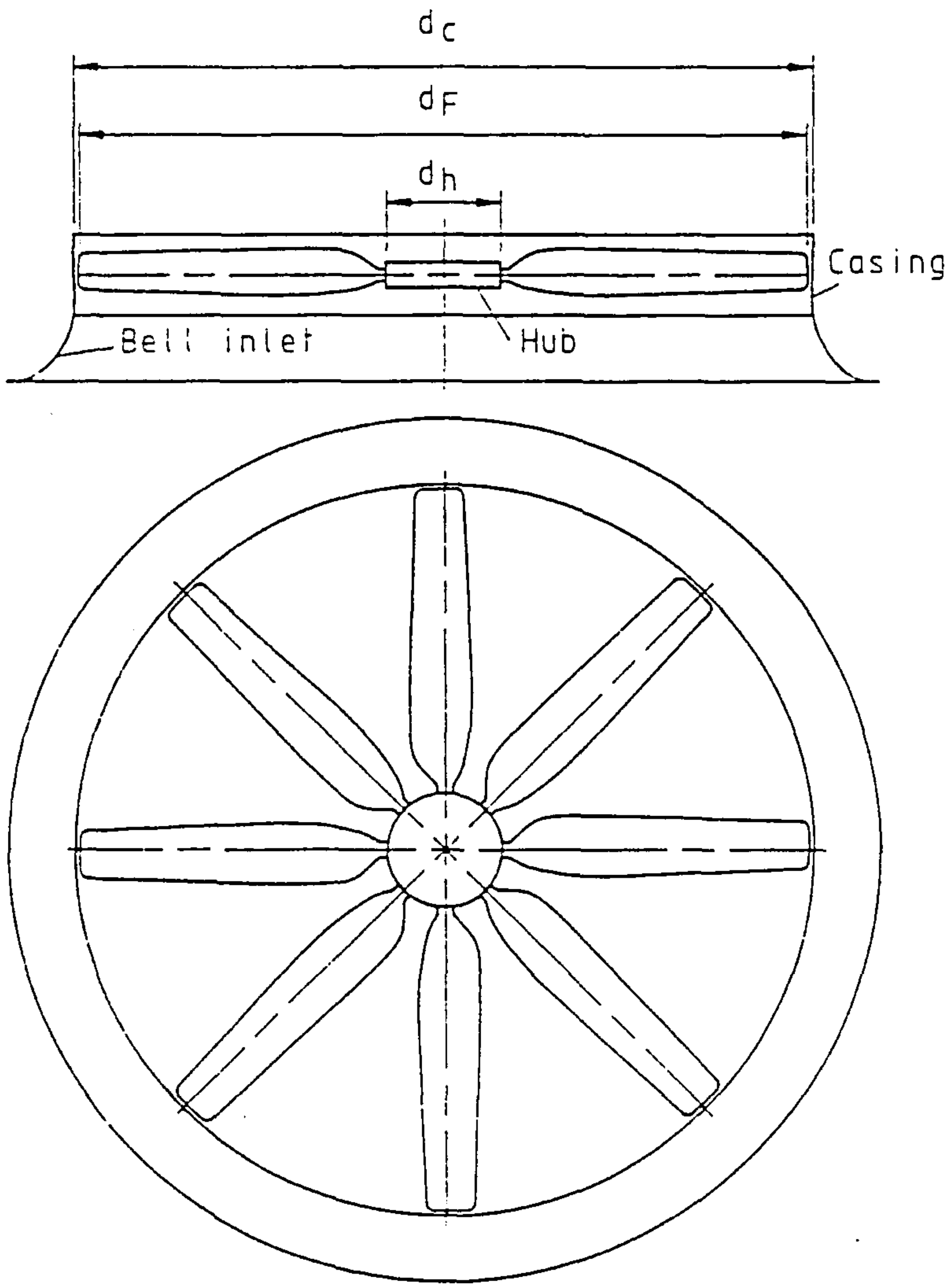

Figure 6.0.1: Eight bladed axial flow fan in casing with bell-type inlet.

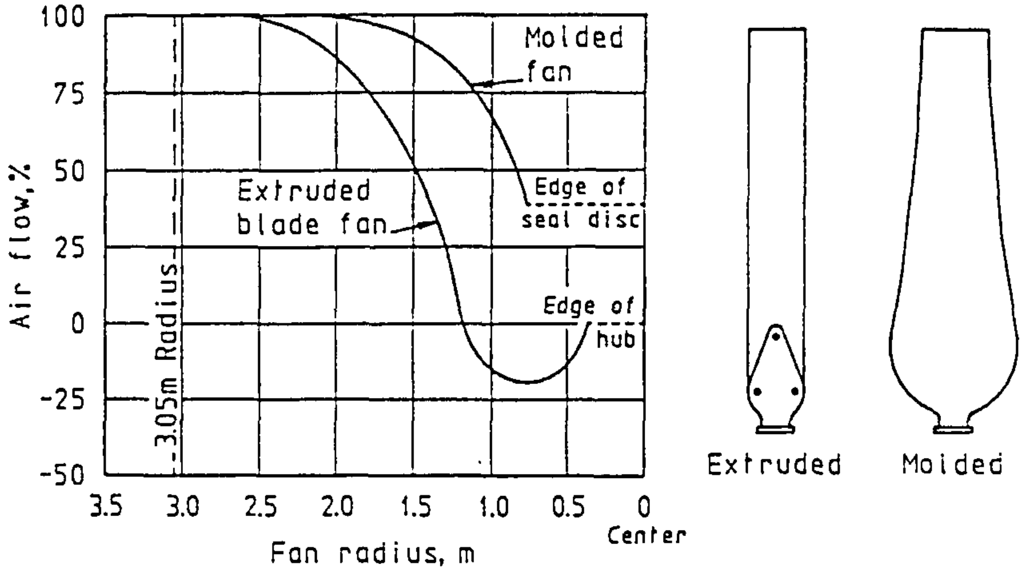

Figure 6.0.2: Air-flow distribution through fan.

6.1 TEST FACILITIES AND PROCEDURES

The performance characteristics of fans are determined in test facilities that must comply with specifications as set out in one of many codes or standards. For axial flow fans, existing standards [46AS1, 66VD1, 74AM1, 75AS1, 80AS1, 80BS1, 85DE1, 85DE2] are to a certain extent related [84RO1], although the modern versions are more comprehensive [84DE1] and are regularly updated.

It has been agreed by the International Organization for Standardization (ISO) that four standard fan installation types should by recognized.

1. Installation type A: free inlet, free outlet.
2. Installation type B: free inlet, ducted outlet.
3. Installation type C: ducted inlet, free outlet.
4. Installation type D: ducted inlet, ducted outlet.

Free inlet or outlet, signifies that the air enters or leaves the fan directly from or to the unobstructed free atmosphere except that in installations of type A, a partition in which the fan is mounted, may support a pressure difference between the inlet and the outlet sides. Ducted inlet or outlet signifies that the air enters or leaves the fan through a long, straight duct directly connected to, and of the same cross-sectional area as the fan inlet or outlet respectively.

Standardized airways designed for type A installation tests may be adapted to provide tests for type B, C or D installations.

An example of a type A test installation is shown in figure 6.1.1. The air mass flow rate through this installation is determined by measuring the pressure in the wall of a calibrated inlet venturi nozzle or bellmouth 1. The general expression for the mass flow rate through this type of nozzle is as follows:

$$m = C_n \epsilon_n A_n (2 \rho_n \Delta p_n)^{0.5} \tag{6.1.1}$$

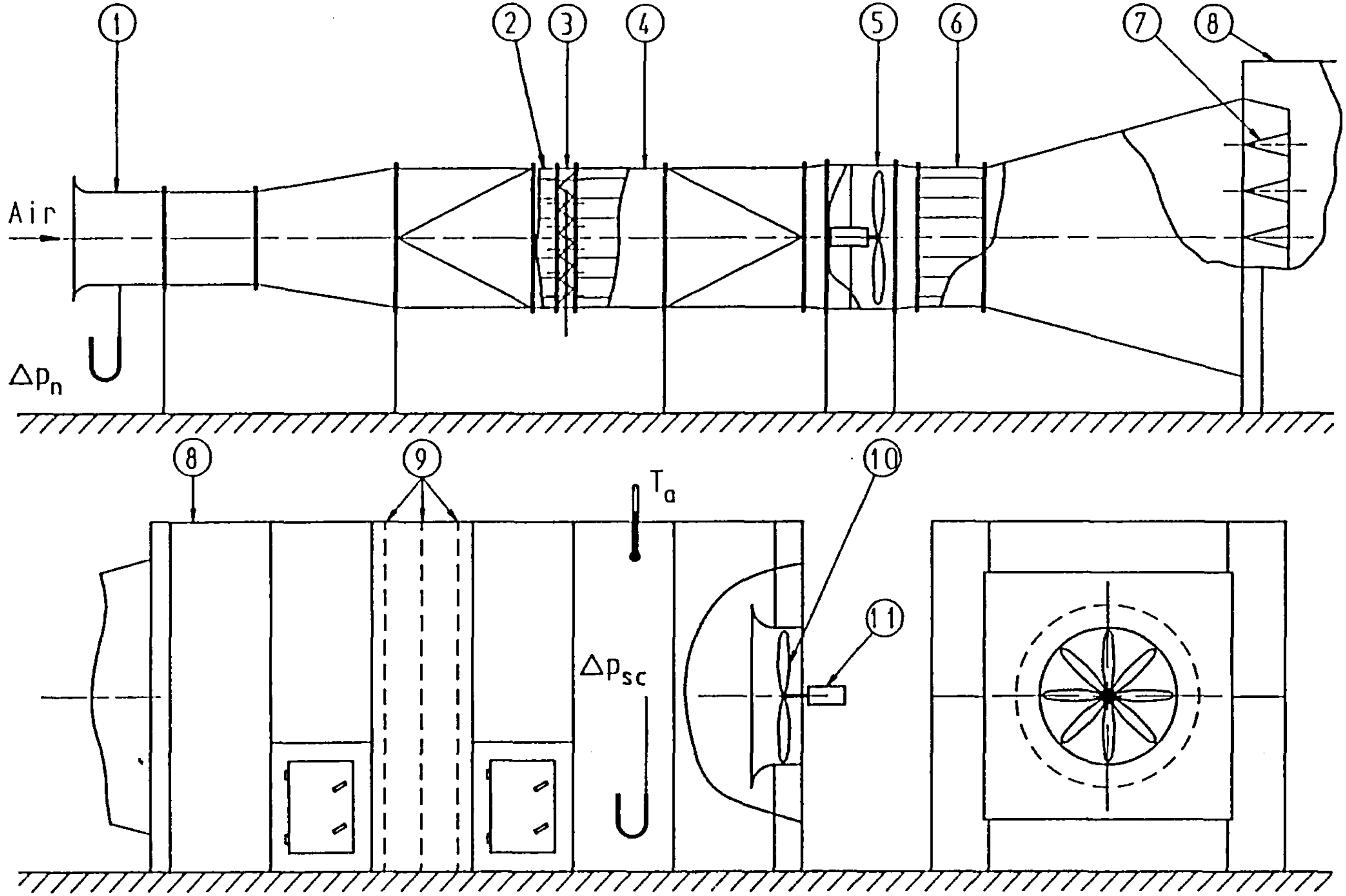

Figure 6.1.1: Fan test facility.

where C_n is the flow coefficient and ϵ_n is the expansibility factor. The product of $C_n\epsilon_n$ for a particular nozzle can be determined experimentally by doing a velocity traverse with the aid of a pitot-static tube.

An adjustable louver flow control device 3 is preceded and followed by respectively flow straighteners 2 and 4. The auxiliary fan 5 is installed to overcome the flow resistance of the test airways under certain operating conditions. Any swirl after the auxiliary fan is eliminated by the flow straighteners 6.

A set of flow guide vanes 7 ensures a relatively even flow distribution into the settling chamber 8. The wire screens 9 further improve the air flow through the settling chamber.

Temperature and static pressure measuring points are located after the screens to define fan inlet conditions. The static pressure, Δp_{sc}, is defined as that absolute pressure measured at the inside surface of the settling chamber wall, minus the reference atmospheric pressure. The density of the air in the settling chamber, ρ_T, can be determined from the perfect gas relation i.e.

$$\rho_T = (p_a + \Delta p_{sc})/RT_a \tag{6.1.2}$$

The air volume flow rate through the fan is thus

$$V_T = m/\rho_T \tag{6.1.3}$$

Although the air velocity in the settling chamber immediately upstream of the fan is small, it is not necessarily negligible, and the dynamic pressure associated with it may be determined from

$$p_{dT} = 0.5(m/A_{sc})^2/\rho_T \tag{6.1.4}$$

The fan is mounted in an appropriate casing or housing at the outlet of the settling chamber. Details of the type of inlet employed during tests must be specified. Care should be taken to avoid the presence of any obstruction which might significantly modify air flow immediately before or after the fan. The fan should preferably be operated at a speed close to that specified. It may be driven by a variable speed electric or hydraulic drive. The torque, M_T, in the shaft at the impeller and the rotational speed, N_T, are monitored during testing. The power input to the fan can be determined with these values according to

$$P_{FT} = 2 \pi M_T N_T \tag{6.1.5}$$

For this test, a fan static pressure is defined as

$$\Delta p_{FsT} = -\Delta p_{sc} - p_{dT} \tag{6.1.6}$$

In some cases it may be preferred to present the fan pressure characteristics in terms of the fan total pressure which is defined as the difference in total pressure at fan inlet and outlet i.e.

$$\Delta p_{FtT} = \Delta p_{FsT} + (m/A_c)^2/(2\rho_T) \tag{6.1.7}$$

for the type A test, where A_c is the gross area at the outlet of the casing, without deduction for motors fairings or other obstructions. In some standards Δp_{FtT} is based on the net outlet area [85DE1].

Fan static efficiency is defined as

$$\eta_{FsT} = V_T \Delta p_{FsT} / P_{FT} \tag{6.1.8}$$

and fan total efficiency as

$$\eta_{FtT} = V_T \Delta p_{FtT} / P_{FT} \tag{6.1.9}$$

The total efficiency is always larger than the static efficiency.

Examples of the other standardized test airways are shown schematically in figure 6.1.2. The installation type or types selected for testing a particular fan, depends on the intended application of the fan. Although fans are sometimes installed in duct systems similar to one of the standard installation types, this is not always the case. If the fan system geometry deviates considerably from one of the standard installations, performance tests should be conducted on the system or a model thereof.

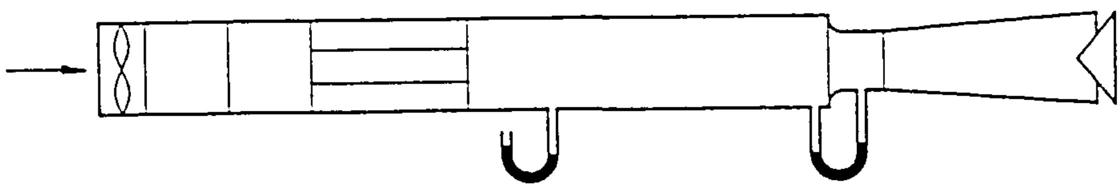

(a) Standardized airways for free inlet, ducted outlet, type B installation.

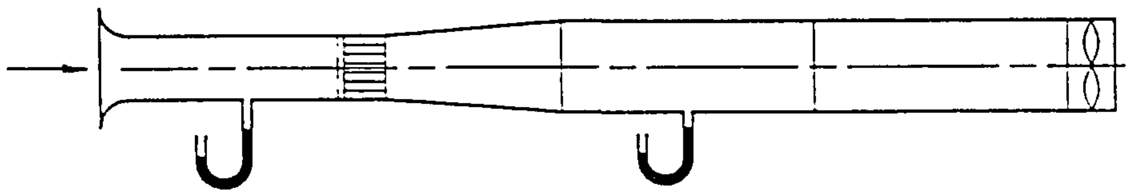

(b) Standardized airways for ducted inlet, free outlet, type C installation.

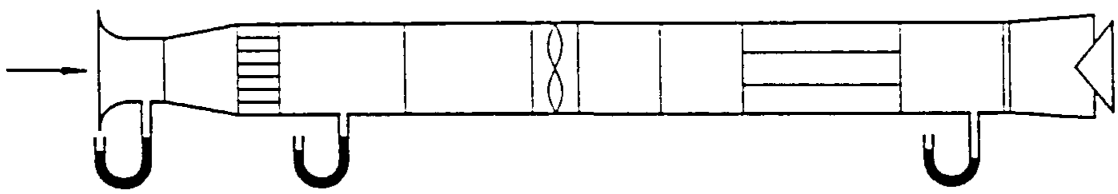

(c) Standardized airways for ducted inlet, ducted outlet, type D installation.

Figure 6.1.2: Standardized airways.

6.2 PRESENTATION OF DATA AND RESULTS

Since it is often not possible to carry out fan tests at exactly the speed or density specified, conversion rules also known as fan laws are used to determine the fan performance at the specified rotational speed, N, and the fan inlet density, ρ, i.e.

Volume flow rate:

$$\frac{V}{V_T} = \frac{N}{N_T} \tag{6.2.1}$$

Pressure:

$$\frac{\Delta p_{Ft}}{\Delta p_{FtT}} = \frac{\Delta p_{Fs}}{\Delta p_{FsT}} = \frac{p_{Fd}}{p_{FdT}} = \left(\frac{N}{N_T}\right)^2 \left(\frac{\rho}{\rho_T}\right) \tag{6.2.2}$$

Power:

$$\frac{P_F}{P_{FT}} = \left(\frac{N}{N_T}\right)^3 \left(\frac{\rho}{\rho_T}\right) \tag{6.2.3}$$

Efficiency:

$$\eta_{Ft} = \eta_{FtT} \text{ and } \eta_{Fs} = \eta_{FsT} \tag{6.2.4}$$

The actual test results, or the results after conversion according to the above rules may be plotted as a series of test points against inlet volume flow. Rotational speeds are referred to a constant stated speed, N, and densities are referred to a constant stated density, ρ, which is usually chosen to be 1.2 kg/m^3.

Adjustable duty fan characteristics are required for a fan having means for altering its performance due to variable pitch blades. A family of constant speed characteristics at 1.2 kg/m^3 inlet density is recommended, selected at suitable steps of adjustment. Efficiencies may be shown by means of smooth contours drawn through points of equal efficiency on the fan pressure characteristics. An example is shown in figure 6.2.1 for an 8-bladed axial

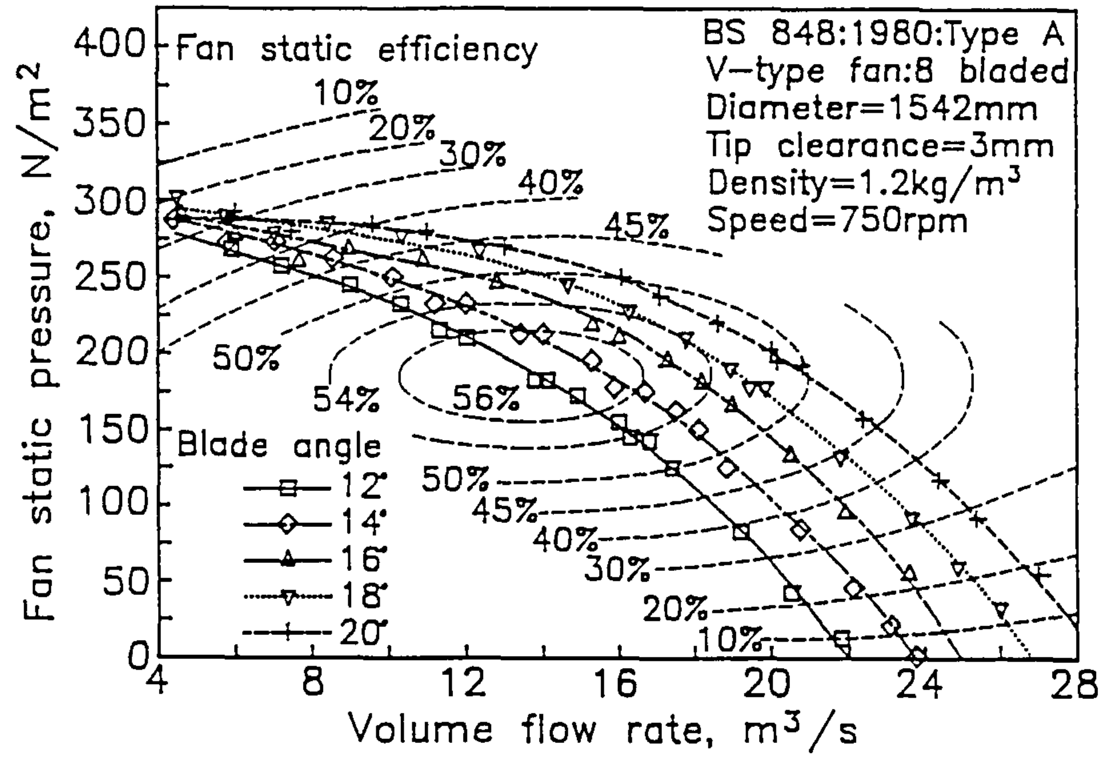

Figure 6.2.1: Fan static pressure and efficiency.

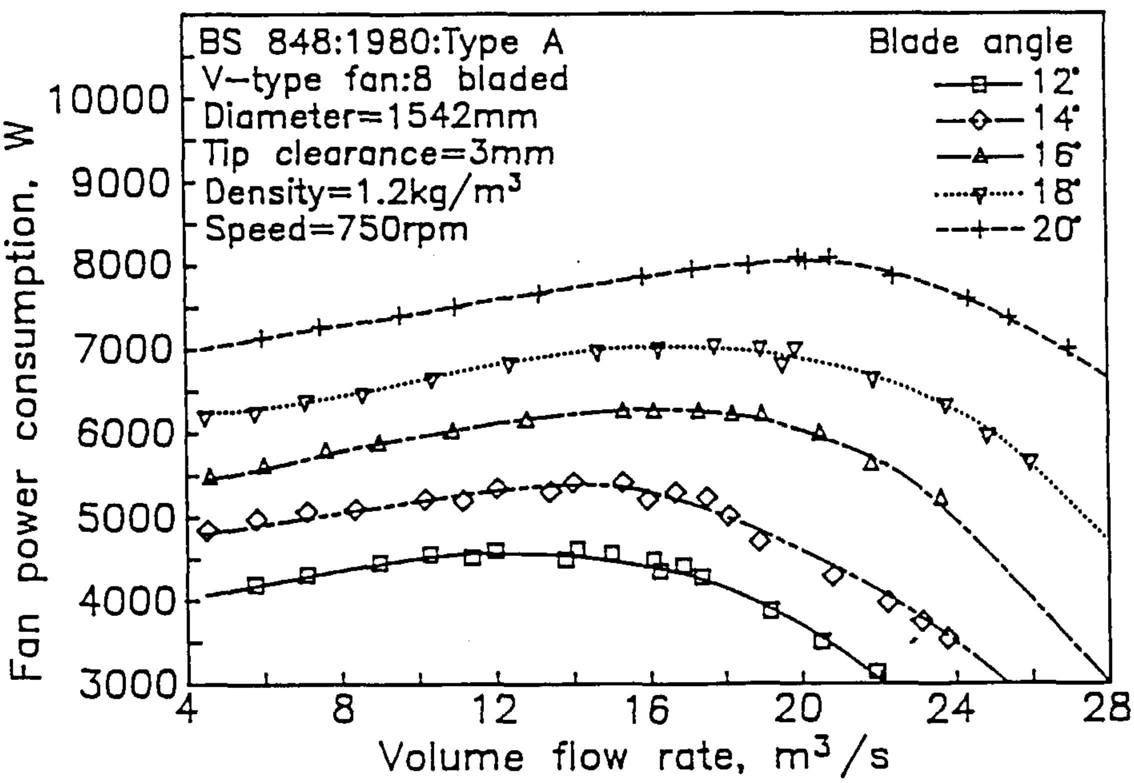

Figure 6.2.2: Fan power.

flow fan (as shown schematically in figure 6.0.1 with a bell inlet) installed in a 1542 mm diameter casing.

The corresponding fan power and static efficiency is shown respectively in figures 6.2.2 and 6.2.3.

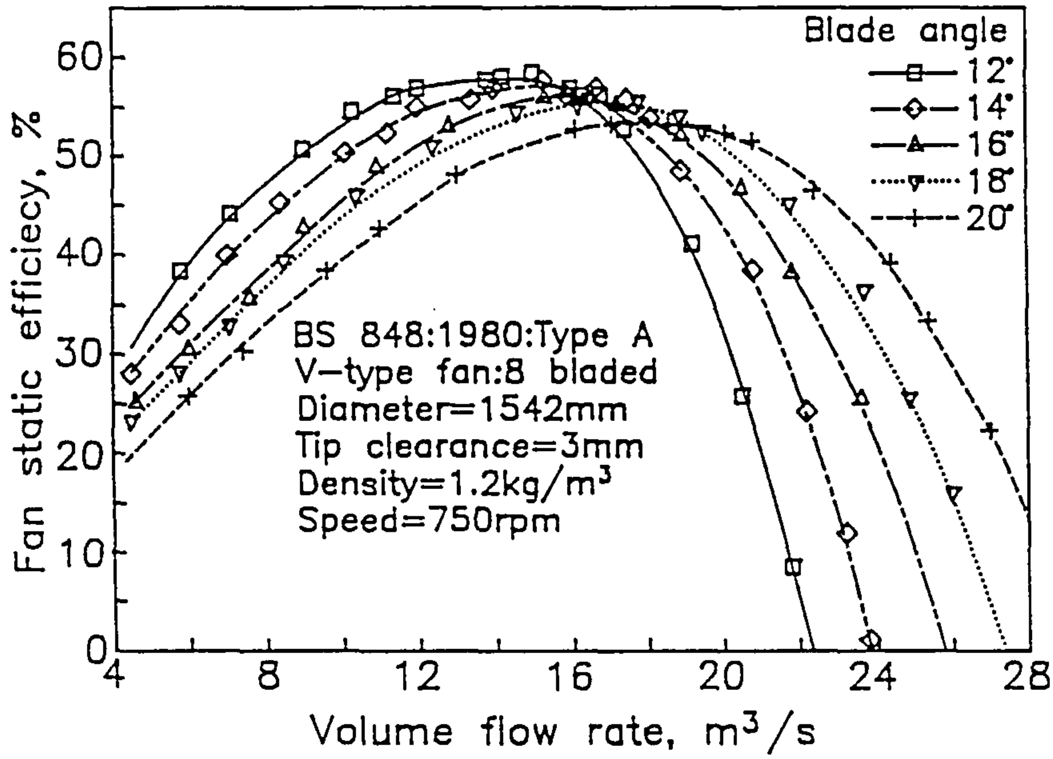

Figure 6.2.3: Fan static efficiency.

Very large diameter axial flow fans find application in industry. Since suitable test facilities for such service fans are unavailable, geometrically similar smaller models are tested in standardized airways.

The following conversion rules may be applied to model tests:

Volume flow rate:

$$\frac{V_l}{V} = \frac{N_l}{N}\left(\frac{d_{Fl}}{d_F}\right)^3 \tag{6.2.5}$$

Pressure:

$$\frac{\Delta p_{Ftl}}{\Delta p_{FT}} = \frac{\Delta p_{Fsl}}{\Delta p_{Fs}} = \frac{p_{Fdl}}{p_{Fd}} = \left(\frac{N_l}{N}\right)^2 \left(\frac{d_{Fl}}{d_F}\right)^2 \left(\frac{\rho_1}{\rho}\right) \tag{6.2.6}$$

Power:

$$\frac{P_{Fl}}{P_F} = \left(\frac{N_l}{N}\right)^3 \left(\frac{d_{Fl}}{d_F}\right)^5 \left(\frac{\rho_l}{\rho}\right) \tag{6.2.7}$$

Efficiency:

$$\eta_{Ftl} = \eta_{Ft} \text{ and } \eta_{Fsl} = \eta_{Fs} \tag{6.2.8}$$

Service fans much larger than the test model may be expected to show a slight improvement in efficiency, but no allowance for this scale effect should be made according to most standards unless otherwise agreed, upon adequate evidence, between manufacturer and purchaser.

According to VDI standards [66VD1], it is noted that if the Reynolds number based on fan diameter of the test fan and that of a larger fan are different, the dependence of the frictional losses on this number should be considered. A possible approximate relation between the efficiencies of two such fans is

$$\eta_{F1} = 1 - 0.5(1 - \eta_F)\left[1 + (Re_F/Re_{Fl})^{0.2}\right] \tag{6.2.9}$$

where $Re_F = \rho v_t d_F/\mu$ and v_t is the blade tip speed. Fan blade tip speeds of 60 m/s or less are recommended in areas where relatively low noise levels must be maintained.

The VDI standard gives the following conversion rule for tip clearance in fans of different diameters:

6.3 TIP CLEARANCE

An increase in the gap between the fan blade tip and the casing, also referred to as the fan blade tip clearance, results in a reduction of the fan efficiency [79MO1, 83WA1, 92VE1]. This is primarily due to air leakage from the higher pressure fan outlet stream to the lower pressure inlet region around the tips of the fan blades. In practical systems a recommended difference between casing diameter and fan diameter is of the order of 0.5 to 1.0 per cent or less of the fan diameter i.e.

$$s_F/d_F \approx s_F/d_c \approx (d_c - d_F)/(2d_c) = 0.005 \text{ to } 0.01$$

In the petro-chemical industry a radial clearance between the fan tip and the casing of 0.5 percent of the fan diameter or 19 mm, whichever is smaller, is recommended [78AP1].

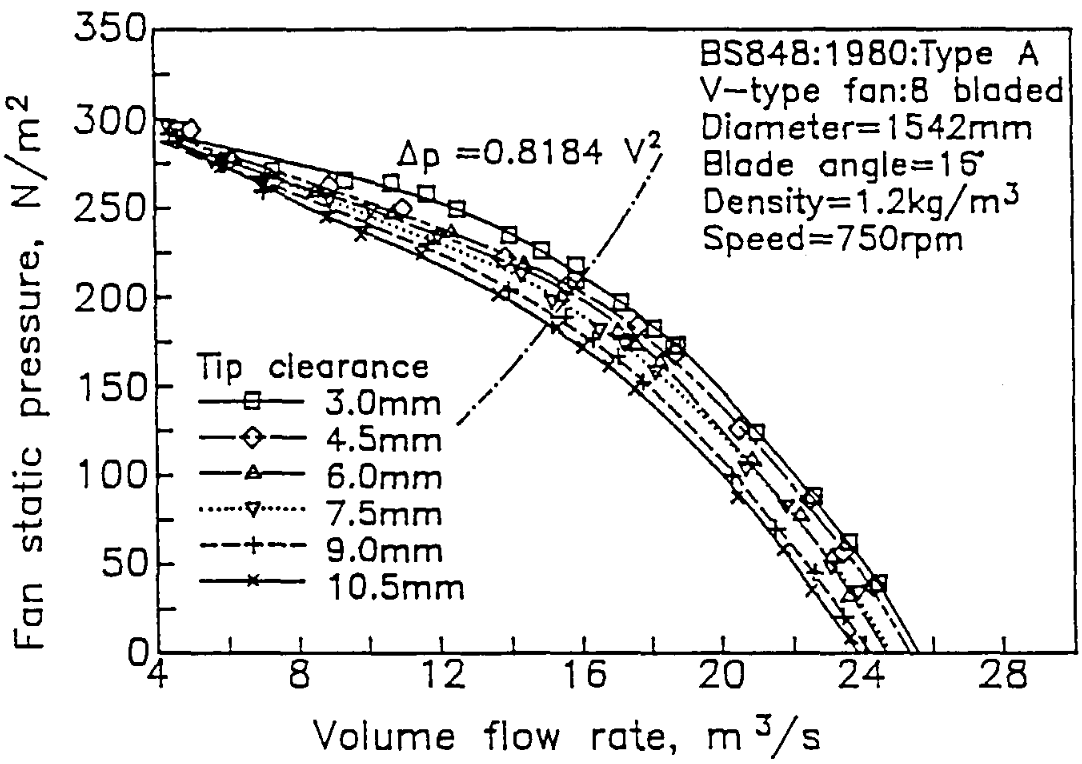

Figure 6.3.1: Effect of tip clearance on fan pressure.

According to Wallis [83WA1] the loss in fan efficiency due to tip clearance can be expressed as

$$\text{Efficiency loss} = 2\left(\frac{\text{tip clearance}}{\text{blade span}} - 0.01\right) \tag{6.3.1}$$

Ruden (44RU1) found that there is a measurable reduction in pressure rise across the fan as the tip clearance increases.

Figure 6.3.1. shows the effect of increasing tip clearance on the fan static pressure for the V-fan. Venter and Kröger [92VE1] find that over the practical operating range of this fan i.e. in the region of maximum efficiency both the fan pressure and the air volume flow rate through the fan decrease linearly with increasing tip clearance as shown in figure 6.3.2 if the system loss coefficient is essentially constant over that range.

It should be noted that the data due to Monroe [79MO1] is for a constant air volume flow rate through the fan. For a given installation, this form of presentation is not realistic since it does not reflect the actual trend in air flow as the tip clearance increases.

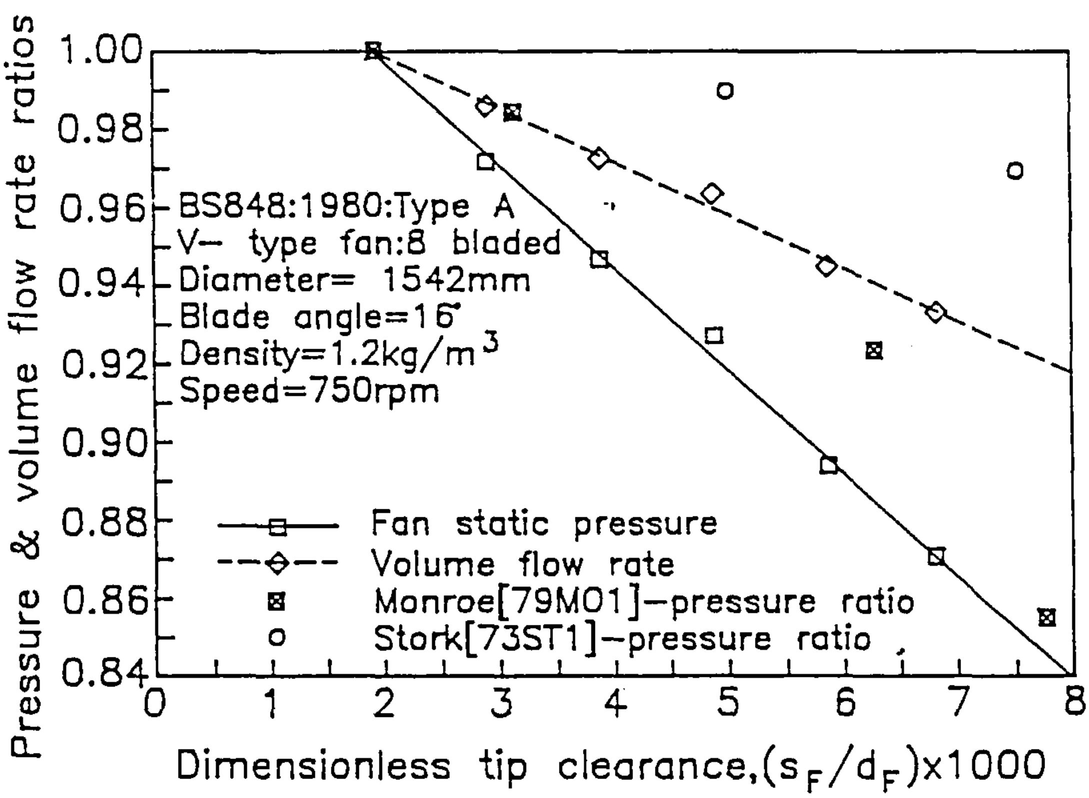

Figure 6.3.2: Effect of tip clearance on fan performance.

Noise levels generally increase with increasing tip clearance [92HV1]. In view of the demand for high efficiency and quiet operation small tip clearances are desirable.

Reverse flow usually occurs in the vicinity of the hub of an axial flow fan [79MO1]. The magnitude of this phenomenon increases progressively with increasing system flow resistance. By designing the fan with profiled blades or locating a disc on the downstream side of the hub, this problem can be reduced. A reduction in backflow and a corresponding small improvement in performance may also be achieved in certain cases by retrofitting an existing fan with a disc.

6.4 FAN SYSTEM

The interaction between the fan and the installation flow resistances (known as the system or installation effect) has been recognized and investigated by a number of authors [79NO1, 81GR, 82CO1, 83OC1, 90WO1, 90RI1, 94KR1]. Available literature covers only a sector of the complete range of all applications in industry. Beard [80BE1] and Hay et al [72HA1] explored the system effects associated with inlet shrouds and with the distance between radiator and fan in vehicle cooling systems. The systems effect associated with elbows, diffusers and contractions, both at the fan inlet and outlet, is examined by a number of authors [84DA2, 84DE1, 84RO1, 90ZA1]. Studies by Cory [82CO1] and Coward [83CO1] are relevant to the same range of fan applications. The effect of fan plenums on the fan performance is presented by Lambert et al [72LA1], Stone and Wen [73ST1] and Russel and Berryman [78RU1, 87BE1]. In view of the complexity of the flow in some systems it may be prudent to perform model tests on such systems.

6.4.1 SYSTEM LOSSES

Venter and Kröger [91VE1] conducted experiments on the V-type fan described in the previous sections to determine the influence that flow resistances located immediately upstream and downstream thereof have on its performance. The resistances included support structures, screens and walkways. They conclude that for a reasonably uniformly distributed resistance, the so-called bulk method [85VE1] satisfactorily predicts effective pressure loss coefficients. The loss coefficients based on the velocity through the fan, for resistances created by obstacles located on the upstream or suction side and the downstream or discharge side of the fan are shown in figures 6.4.1 and 6.4.2 respectively. These coefficients are a function of the projected area of the obstacle, A_{ob}, and the distance x from the fan.

The upstream obstacle loss coefficient can be expressed as

$$K_{up} = 2\Delta p_{up}/\left(\rho v^2\right) = 2\rho\Delta p_{up}/\left(m_a/A_e\right)^2 = f\left(x/d_c, A_{ob}/A_c\right) \qquad (6.4.1)$$

where $A_e = A_c - A_h$, with A_c the casing cross-sectional area and A_h the hub cross-sectional area.

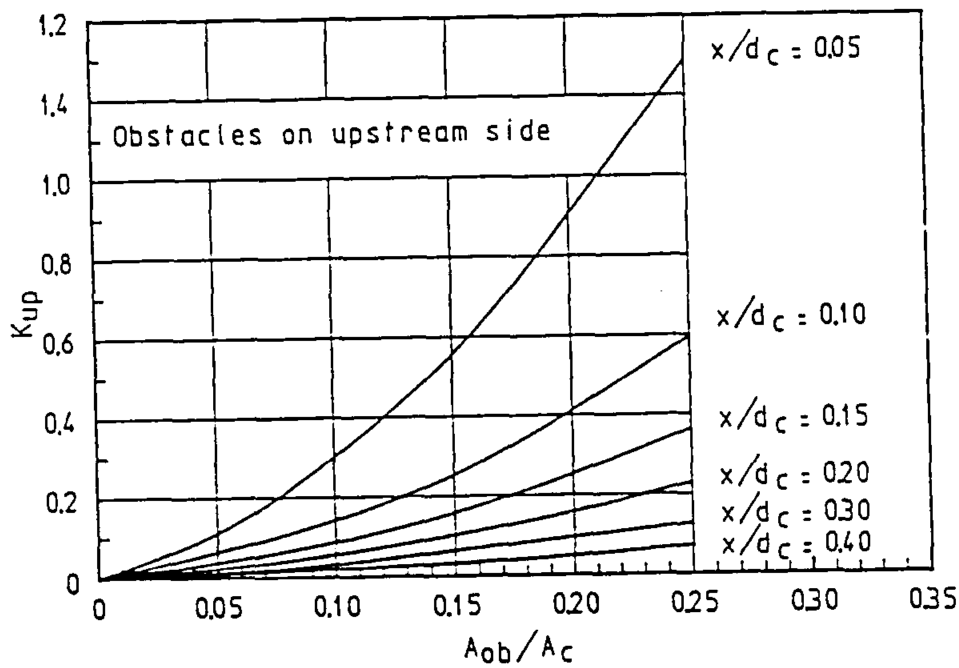

Figure 6.4.1: Upstream loss coefficient due to obstacles.

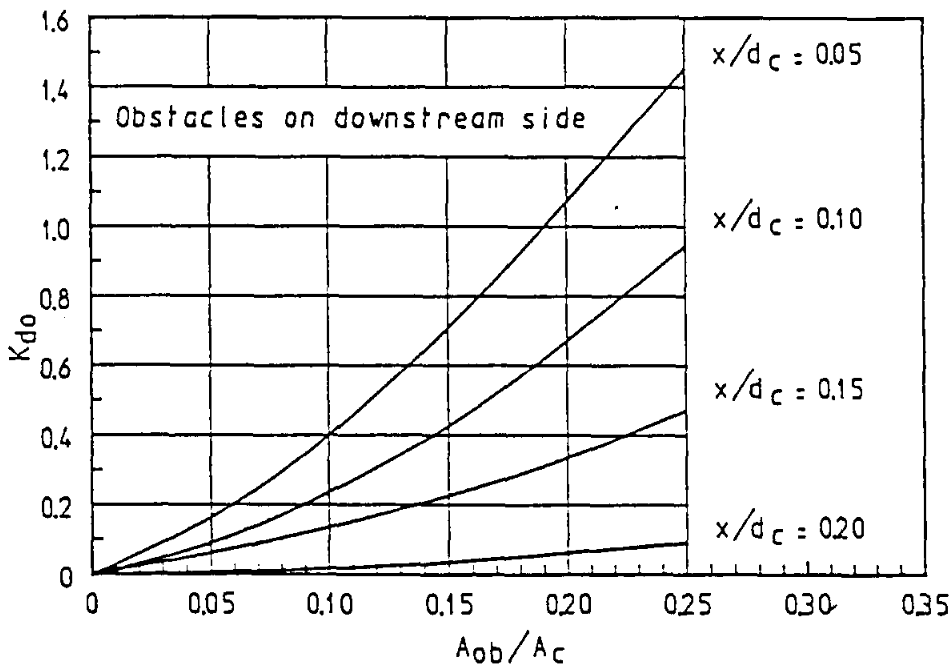

Figure 6.4.2: Downstream loss coefficient due to obstacles.

Similarly the downstream loss coefficient can be expressed as

$$K_{do} = 2\Delta p_{do}/(\rho v^2) = 2\rho\Delta p_{do}/(m_a/A_e)^2 = f(x/d_c, A_{ob}/A_c) \tag{6.4.2}$$

6.4.2 PLENUM LOSSES

The complexity of the flow in a plenum is illustrated by a few studies [75TU1, 78RU1, 87BE1].

Examples of typical plenum arrangements found in the petro-chemical industry are shown in figure 6.4.3 [78AP1].

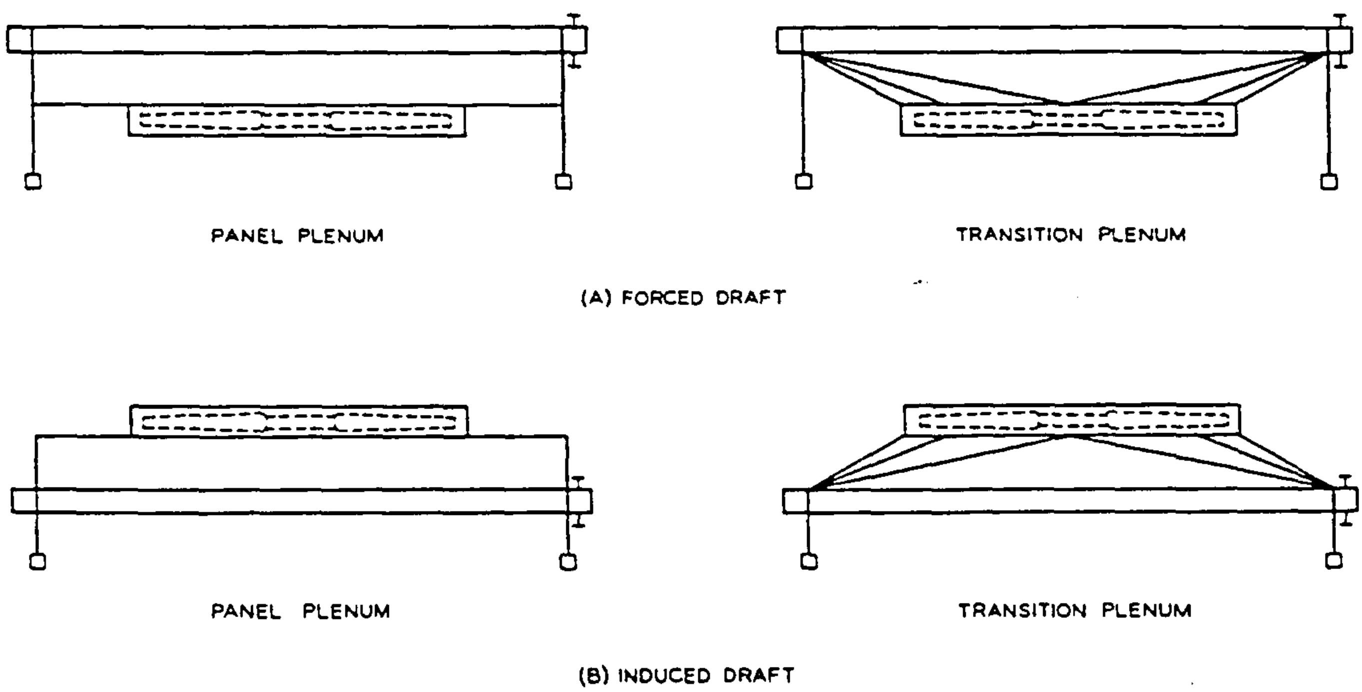

Figure 6.4.3: Plenum arrangements.

Fans are generally sized so that the area covered by the fan is a minimum of 40 percent of the bundle face area served by that fan [83PA1]. Monroe [79MO1] suggests that the area of coverage shall not be less than 40 percent of the bundle face area for induced draft units and 50 percent for forced draft units. Although coverage as low as 30 percent for induced draft units is possible [73RO1] the larger values are preferred.

When the fan is installed in an induced draft air-cooled heat exchanger as shown in figure 1.2.2 where the ratio of the fan area to heat exchanger frontal area, $A_F/A_{fr} \approx 0.6$, and the ratio of the plenum height to fan diameter, $H_{pl}/d_F \approx 0.45$, and the fan is fitted with a rounded or bell-type inlet, the plenum loss coefficient based on the mean velocity through the fan is negligible and the velocity distribution of the air flowing through the heat exchanger is quite uniform.

In a forced draft configuration as shown in figure 1.2.1 for $A_F/A_{fr} \approx 0.6$ and $H_{pl}/d_F \approx 0.45$ the loss coefficient $K_{pl} \approx 0.75\, \alpha_{eF}$ where $1.5 \leq \alpha_{eF} \leq 2.5$ (molded blades) and the fan operates near its maximum efficiency. For this particular case the kinetic energy coefficient at the outlet of the heat exchanger bundle $\alpha_{he} \approx 1.13$. It should be noted that K_{pl} is a complex function of the system geometry and performance characteristics. The loss coefficient is higher for smaller values of A_F/A_{fr} and H_{pl}/d_F [78RU1] and extruded blades.

For the A-frame configuration shown in figure 1.2.3 where the fan is supported by an overhead bridge and the apex angle is approximately 60° and the area ratio of the fan to the total frontal heat exchanger area $A_F/A_{fr} \approx 0.3$, the effective plenum loss coefficient based on the mean velocity through the fan, is approximately equal to the kinetic energy coefficient i.e. $K_{pl} \approx \alpha_{eF}$ as measured at the outlet of the fan when tested near its maximum efficiency according to British Standard BS848, test type A, ($1.5 \leq \alpha_{eF} \leq 2.5$ for molded blades). This result is obtained if losses through the A-frame are determined according to equation (5.6.19).

By minimizing system losses and introducing "low noise fans", noise levels can be significantly reduced [94VA1]. In many areas passive methods of noise control are however required. Active noise cancellation systems will find increased application in future air-cooled heat exchangers [91OC1].

6.5 REFERENCES.

44RU1 Ruden, P., Investigation of Single Stage Axial Flow Fans, NACA Tech. Mem. No. 1062, 1944.

46AS1 American Society of Mechanical Engineers, Test Code for Fans PTC 11-1946, New York, 1946.

61BA1 Barna, P.S., Estimation of Scale Effects in Axial Flow Fans, Aircraft Engineering, Nov. 1961.

61JO1 Jorgensen, R., ed., Fan Engineering, Buffalo Forge Company, New York, 1961.

66VD1 Verein Deutscher Ingenieure, VDI-Richtlinien, Abname - und Leistungs-versuche an Ventilatoren, VDI 2044, Berlin und Köln, 1966.

72HA1 Hay, N. and Taylor, S.R.G., The Effects of Vehicle Cooling Systems Geometry on Fan Performance, Conference on Fan Technology and Practice, Inst. Mech. Engrs, pp. 176-192, London, April 1972.

72LA1 Lambert, P.C., Cowan, G.H. and Bott, T.R., Flow Characteristics in a Box-shaped Plenum Chamber Associated with an Air-cooled Heat Exchanger, United Kingdom Atomic Energy Authority, Harwell, 1972.

73EC1 Eck, B., Fans - Design and Operation of Centrifugal, Axial - Flow and Crossflow Fans, Pergamon Press, Fed. Rep. Germany, 1973.

73ST1 Stone, R.D. and Wen, S.H., Airflow Characteristics of Buildt-up Fan Plenums and Performance of Airflow Correction Devices, ASHRAE Semi-annual Meeting, Chicago, January, 1973.

74AM1 Air Moving and Conditioning Association, Laboratory Methods of Testing Fans for Rating Purposes, AMCA Standard 210-74, 1974.

75AS1 American Society of Heating Refrigerating and Air-Conditioning Engineers, Laboratory Methods of Testing Fans for Rating Purposes, ASHRAE Standard 51-75, 1975.

75TU1 Turner, J.T., The Aerodynamics of Forced Draught Air Cooled Heat Exchangers, Int. Symp. on Cooling Systems, BHRA Fluid Engineering, Cranfield, England, 1975.

77CH1 Cheremisinoff, P.N. and Chercmisinoff, P.P., Industrial Noise Control Handbook, Ann Arbor Science, 1977.

78AP1 American Petroleum Institute (API) Standard 661, Air-cooled Heat Exchangers for General Refinery Services, API, Washington, 1978.

78DA1 Daly, B.B., Woods Practical Guide to Fan Engineering, Woods of Colchester Ltd., 1978.

78RU1 Russell, C.M.B. and Berryman, R.J., The Calculation of Pressure Losses in Air-cooled Heat Exchanger Air Inlets and Plenum Chambers, ASME Heat Transfer Division, HTD Vol. 96, pp.429-234, New York, 1978.

79ES1 Engineering Sciences Data Unit, A Guide to Fan Selection and Performance, Item No. 79037, ESDU, London, 1980.

79MO1 Monroe, R.C., Improving Cooling Tower Fan System Efficiencies, Combustion Magazine, Vol. 50, No. 11, pp. 20-26, May 1979.

79NO1 Nowakowski, J.K., Pressure Losses in the Inlet and Outlet Channels of High-pressure Single-and tow-stage Axial-flow Fans, Proc. 6th Conf. Fluid Machinery, pp. 760-769, Hungary, 1979.

80AS1 American Society of Mechanical Engineers, Performance Test Codes - General Instructions, PCT 1, 1980.

80BE1 Beard, R.A., Truck Radiator Technology, Part II, Product Application Technology, Heat Transfer Division, Covrad Ltd., Conventry, England, 1980.

80BS1 British Standards Institution, Fans for General Purposes, Part 1, Methods of Testing Performance, BS 848, 1980.

81GR1 Graham, J.B., Fan Selection and Application Considerations, Symp. Proc. Power Plant Fans - State of the Art, Indianapolis, Oct. 1981.

82LO1 Cory, W.T.W., Fan Performance Testing the Effects of the System, BHRA Int. Conf. Fan Design and Applications, Guildford, Sept. 1982.

83CO1 Coward, C.W., A Summary of Pressure Loss Values for Various Fan Inlet and Outlet Duct Fittings, ASHRAE Trans., Vol. 89, 1983.

83OC1 O'Connor, J.F., The System Effect on how it Changes Fan Performance, ASHRAE Trans., Vol. 89, 1983.

83PA1 Paikert, P., Air-cooled Heat Exchangers, Handbook for Heat Exchanger Design, 1983.

83WA1 Wallis, R.A., Axial Flow Fans and Ducts, John Wiley and Sons, New York, 1983.

84DA1 Daly, B.B., Interaction between the Fan and the System, Installation Effects in Ducted Fan Systems, Inst. of Mech. Engrs, Conference Publication No. C110/84, pp. 1-7, 1984.

84DE1 Deeprose, W.M. and Smith, T.W., The Usefulness of BS848 Part 1: 1980 in Establishing the Installed Performance of a Fan, Inst. of Mech. Engrs. Conference Publication, No. C115/84, pp. 9-20, 1984.

84RO1 Roslyng, O., Installation Effect on Axial Flow Fan Caused by Swirl and Non-Uniform Velocity Distribution, Institution of Mechanical Engineers, Proceedings, Vol. C114/84, pp. 21-28, 1984.

85DE1 Deutsche Norm, Ventilatoren; Leistungsmessung, Normkennlinien, Deutsches Institut für Normung, Berlin, DIN 24 163, Teil 1, 1985.

85DE2 Deutsche Norm, Ventilatoren; Leistungsmessung, Normkennlinien, Deutsches Institut für Normung, Berlin, DIN 24 163, Teil 2, 1985.

85MO1 Monroe, R.C., Minimizing Fan Energy Costs, Chemical Engineering, pp. 141-142, May 1985.

85MO2 Monroe, R.C., Minimizing Fan Energy Costs, Chemical Engineering, pp.57-59, June 1985.

85VE1 Ventilatoren Stork Hengelo, General Instructions for E-type Fans, V.960874, 1985.

86BA1 Bass, R.M., Small Scale Wind Tunnel Testing of Model Propellers, AIAA-86-0392, 1986.

86OW1 Owen, D.T., Hurst, D.W. and Methven. P., Wind Tunnel Testing of Pressure Tapped Model Propellers, Paper No. 21, Proc. Royal Aeronautical Society, Aerodynamics at Low Reynolds numbers, Oct. 1986.

87BE1 Berryman, R.J. and Russell, C.M.B., Airflow in Air-cooled Heat Exchangers, Heat Transfer Engineering, Vol. 8, No.4, pp. 40-44, 1987

90BO1 Bolton, A.M., Gray, A.J. and Margetts, E.J., Installation Effects in Fan Systems, Proc. Inst. Mech. Eng. Eur. Conf. London, March 1990.

90RI1 Riera-Ubiergo, J.A. and Charbonelle, F., Installation Effects in Fan Systems, Proc. Inst. Mech. Eng. Eur. Conf. London, March 1990.

90TH1 Thiart, G.D., A Numerical Procedure for Predicting the Effects of Distorted Inflow Conditions on the Performance of Axial Flow Fans, Ph.D-thesis, University of Stellenbosch, South Africa, 1990.

90VE1 Ventilatoren Stork Howden B.V., Fan Performance Catalog, Hengelo, Nederland, 1990.

90WO1 Woods Ballard, W.R., Fans in Air Handling Units, Installation Effects in Fan Systems, Proc. Inst. Mech. Eng. Eur. Conf. London, March 1990.

90ZA1 Zaleki, T.H., System Effect Factors for Axial Flow Fans, Installation Effects on Fan Systems, Proc. Inst. Mech. Eng. Eur. Conf. London, March 1990.

91OC1 O'Connor, L., Putting a Lid on Noise Pollution, Mechanical Engineering, Vol. 113, No. 6, pp. 46-51, ASME, June 1991.

91TH1 Thiart, G.D., Personal Communication from G.D. Thiart, Department of Mechanical Engineering, University of Stellenbosch, South Africa, 1991.

91VE1 Venter, S.J. and Kröger, D.G., An Evaluation of Methods to Predict the System Effect Present in Air-cooled Heat Exchangers, Heat Recovery Systems and CHP, Vol. 11, No. 5, pp. 431-440, 1991.

92HU1 Hunnabal, P.J., Control of Tonal Noise Generation in Axial Flow Fans by Optimising Geometry of Fixed and Rotating Components, Proc. Int. INCE Symp., pp. 475-482, CETIM, Senlis, France, Sept. 1992.

92VE1 Venter, S.J. and Kröger, D.G., The Effect of Tip Clearance on the Performance of an Axial Flow Fan, Energy Convers. Mgmt, Vol. 33, No. 2, pp. 89-97, 1992.

94KR1 Kröger. D.G., Fan Performance in Air-cooled Steam Condensers, Heat Recovery Systems and CHP, Vol. 14, No. 4, pp. 391-399, 1994.

94VA1 Van der Speck, H.F., Advanced Low Noise Cooling Fans, Paper presented at the IAHR 9th Cooling Tower and Spraying Pond Symposium, von Karman Institute, Brussels, Belgium, September 1994.

CHAPTER 7

NATURAL DRAFT COOLING TOWERS

7.0 INTRODUCTION

Natural draft cooling towers are found in power and chemical plants throughout the world. Different shapes and types of structures exist, but their fundamental function is the same, i.e. to create, by means of buoyancy effects, the flow of air through the fill or bundles of finned tube heat exchangers.

The hyperbolic concrete tower which is normally operated in the wet mode is also effectively employed as a dry-cooling tower if designed specifically for this purpose. Other towers may be made of aluminum clad steel or wood. The main dimensions of cooling towers are usually determined by performance, structural [77NI1] and economic considerations [84AL1, 84KR1] although aerodynamic and thermal factors should not be ignored [92GR1]. In areas of the world where seismic activity is prevalent, aluminum clad steel towers may be preferred. Cost structures may also be such that this type of dry-cooling tower is cheaper than a concrete tower.

The performance of any natural draft cooling tower is influenced by the characteristics of the fill or the finned tube heat exchanger bundles at the base of the tower, the tower geometry and ambient conditions, such as temperature, pressure, winds, inversions and precipitation [76MO2, 79HE1].

7.1 DRY-COOLING TOWER

Consider the example of a hyperbolic natural draft dry-cooling tower as shown in figure 7.1.1. The heat exchanger bundles are located horizontally at the inlet cross-section of the tower. The density of the heated air inside the tower is less than that of the atmosphere outside the tower, with the result that the pressure inside the tower is less than the external pressure at the same elevation. This pressure differential causes air to flow through the tower at a rate which is dependent on the various flow resistances encountered, the cooling tower dimensions and the heat exchanger characteristics [74BU1, 74MO1, 75MO1, 76MO1, 80MO1, 84BE1].

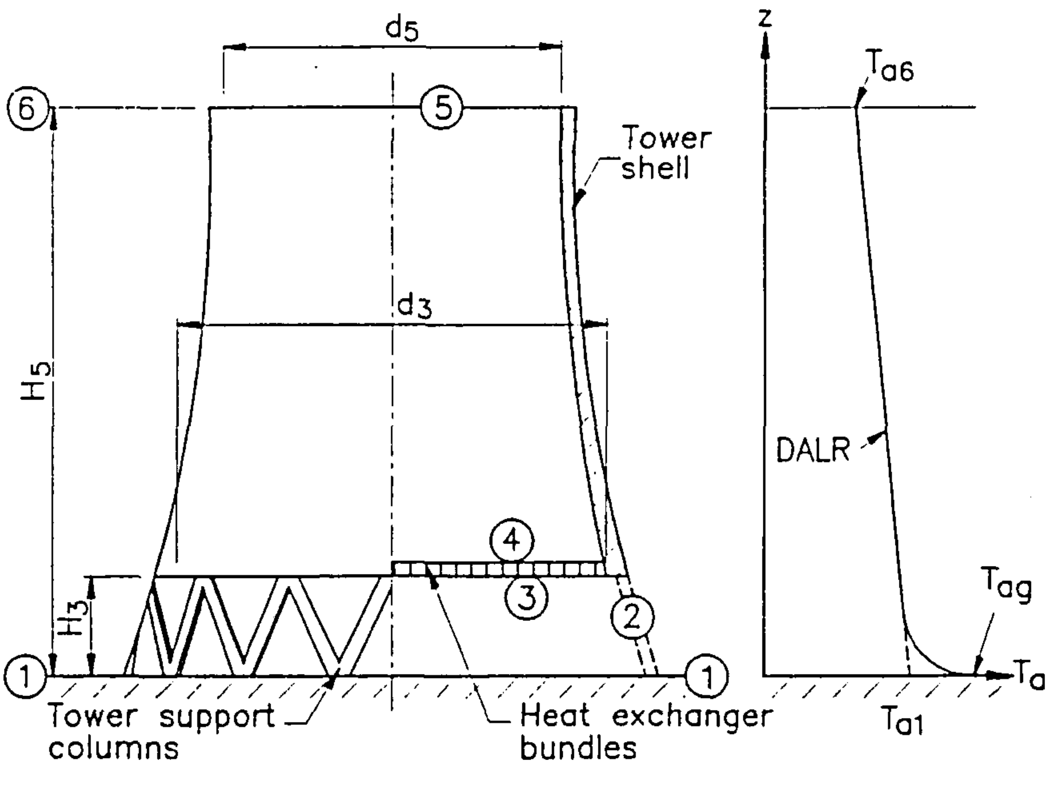

Figure 7.1.1: Natural draft cooling tower with horizontal heat exchanger.

To evaluate the performance characteristics of such a cooling tower, both the energy equation and the draft equation must be satisfied. The following analysis has been found to give results that accurately predict the performance of large practical dry-cooling towers.

Ambient conditions influence the performance of the cooling tower. As shown in figure

10.1.3 significant changes in temperature may occur near ground level during any 24-hour period. During a clear day, a temperature lapse rate of -0.00975 Km^{-1}, also known as the dry adiabatic lapse rate (DALR), is observed in the region of the surface boundary layer (SBL). Significant deviations do however occur at ground level, which, if not taken into consideration, may lead to erroneous design specifications or the incorrect interpretation of cooling tower acceptance test data. More complex temperature distributions are discussed in chapter 10.

For this analysis the specified ambient air temperature at any elevation z will be assumed to be as given by equation (10.1.7b), i.e.

$$T_a = T_{a1} - 0.00975\ z$$

where T_{a1} is the temperature at ground level, obtained by extrapolating the measured DALR to that elevation. T_{a1} will usually differ from the actual temperature, T_{ag}, measured at ground level as shown schematically in figure 7.1.1.

At the elevation 6, which corresponds to the top of the cooling tower, the temperature of the ambient air is thus

$$T_{a6} = T_{a1} - 0.00975 H_5 \tag{7.1.1}$$

The heat transfer characteristics of the heat exchangers in the cooling tower can be expressed according to equations (3.5.6) and (3.5.16) respectively as

$$Q = m_a c_{pa}(T_{a4} - T_{a3}) = m_w c_{pw}(T_{wi} - T_{wo}) \tag{7.1.2}$$

and

$$Q = \frac{UA\ F_T\left[(T_{wi} - T_{a4}) - (T_{wo} - T_{a3})\right]}{\ln\left[(T_{wi} - T_{a4})/(T_{wo} - T_{a3})\right]} \tag{7.1.3}$$

It follows from equation (1.4.19), that the approximate inlet temperature to the heat exchanger located at an elevation H_3 above ground level is given by

$$T_{a3} = T_{a1} - \left(v_{a3}^2/2 + g\, H_3\right)/c_{pa}$$

For natural draft cooling towers, $v_{a3}^2/2 \ll g\, H_3$, with the result that

$$T_{a3} \approx T_{a1} - g\, H_3/c_{pa} = T_{a1} - g(\gamma - 1)H_3/(\gamma R) = T_{a1} - 0.000975H_3 \tag{7.1.4}$$

where $g = 9.8 m/s^2$, $\gamma = 1.4$ and $R = 287.08$ J/kgK.

The approximate pressure differential between the outside and the inside of the tower at the mean heat exchanger elevation, that causes the air to flow through the tower, may be determined with the aid of equation (1.4.21) [80MO1].

$$\Delta p_a \approx \left(\rho_{ao} - \rho_{ai}\right) g \left[H_5 - \left(H_3 + H_4\right)/2\right] = \sum \text{flow losses} \tag{7.1.5}$$

where ρ_{ao} and ρ_{ai} are respectively the densities outside and inside the tower at the elevation of the heat exchanger. This is also known as the draft equation.

Although this approximate relation is often used in cooling tower designs it is inadequate in many cases. A more detailed approach is followed in the present analysis.

For dry air, find according to equation (10.1.9b), the pressure at 6 external to the tower i.e.

$$p_{a6} = p_{a1}(1 - 0.00975\, H_5/T_{a1})^{3.5} \tag{7.1.6}$$

where $H_6 = H_5$ is the tower height.

The difference in pressure between 1 at ground level and 5 at the outlet of the tower, may be expressed in terms of the losses experienced by the air stream as it flows through various resistances in the tower as shown schematically in figure 7.1.2.

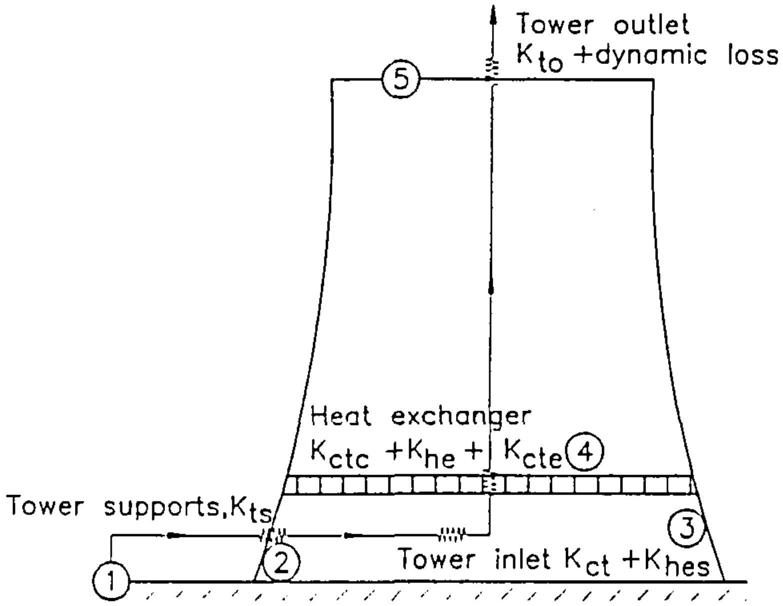

Figure 7.1.2: Losses through cooling tower.

The stagnant ambient air at 1 accelerates to flow through the tower supports at 2, where it experiences certain losses (K_{ts}) before flowing through the heat exchanger bundles from 3 to 4. Upstream of the heat exchanger, losses are experienced due to separation and re-direction of the flow at the lower edge of the tower shell (K_{ct}), and the presence of the heat exchanger supports (K_{hes}). Contraction (K_{ctc}), form and frictional (K_{he}) and expansion (K_{cte}) losses are experienced across the heat exchanger. The flow is essentially isentropic from 4 to 5 with a further loss in kinetic energy at the outlet of the tower. The resultant total pressure difference is found by adding the resistances between 1 and 5.

$$p_{a1} - \left[p_{a5} + \alpha_{e5}(m_a/A_5)^2/(2\rho_{a5})\right]$$

$$= \left(K_{ts} + K_{ct} + K_{hes} + K_{ctc} + K_{he} + K_{cte}\right)_{he} \left(m_a/A_{fr}\right)^2/(2\rho_{a34})$$

$$+ \; p_{a1}\left[1 - \{1 - 0.00975(H_3 + H_4)/(2T_{a1})\}^{3.5}\right]$$

$$+ \; p_{a4} \left[1 - \{1 - 0.00975(H_5 - H_3/2 - H_4/2)/T_{a4}\}^{3.5} \right] \tag{7.1.7}$$

where m_a is the air mass flow rate through the tower. The subscript he implies that all loss coefficients are referred to the frontal area of the heat exchanger and the mean density of the air flowing through it. This form of the equation is useful for comparing the relative magnitudes of the flow losses. The frontal area is the projection of the effective finned surface as viewed from the upstream side. Stiffening beams, straps or other obstructions located up against the finned surface, thereby impeding flow through the heat exchanger must be considered when evaluating the effective frontal area, A_{fr}. The last two terms on the right hand side of equation (7.1.7) are analogous to equation (7.1.6) and take into consideration static pressure differentials due to elevation between ground level and the mean heat exchanger elevation and the latter and the tower outlet respectively.

Du Preez and Kröger [94DU1] studied the velocity and pressure distribution in the outlet plane of hyperbolic natural draft cooling towers. They find that for $1/Fr_D \leq 3$, the velocity distribution is almost uniform i.e. $\alpha_{e5} \approx 1$ for dry-cooling towers where the heat exchangers are located in the cross-section near the base of the tower and even for wet counterflow towers where the flow through the fill may be more distorted due to its lower flow resistance. The mean pressure at the outlet plane is found to be slightly less than that of the ambient air at the same elevation i.e.

$$p_{a5} = p_{a6} + \Delta p_{a56} = p_{a6} + K_{to}(m_a/A_5)^2/(2\rho_{a5}) \tag{7.1.8}$$

For a hyperbolic tower with a cylindrical outlet the loss coefficient is given by

$$K_{to} = \Delta p_{a56} \; / \; (\rho_{a5} \, v_{a5}^2 \; / \; 2) = 2\rho_{a5} \, \Delta p_{a56} \; / \; (m_a \; / \; A_5)^2$$

$$= - \, 0.28 \, Fr_D^{-1} + 0.04 \, Fr_D^{-1.5}$$

where $Fr_D = (m_a/A_5)^2/[\rho_{a5}(\rho_{a6} - \rho_{a5})gd_5]$. This equation is valid for $0.5 \leq d_5/d_3 \leq 0.85$ and $5 \leq K_{he} \leq 40$.

According to equation (1.4.19) the temperature at the tower outlet can be approximated by

$$T_{a5} = T_{a4} + \left[\left(v_{a4}^2 - v_{a5}^2\right)/2 + g\left(H_4 - H_5\right)\right]/c_{pa} \approx T_{a4} + g\left(H_4 - H_5\right)/c_{pa}$$

$$= T_{a4} - g(\gamma - 1)\left(H_5 - H_4\right)/(\gamma R) = T_{a4} - 0.00975\left(H_5 - H_4\right) \qquad (7.1.10)$$

since $(v_{a4}^2 - v_{a5}^2) << g(H_4 - H_5)$ for natural draft cooling towers. From the perfect gas relation it thus follows that for $p_{a5} \approx p_{a6}$, the density at the outlet of the tower is

$$\rho_{a5} = p_{a6}/[R\,\{T_{a4} - 0.00975\,(H_5 - H_4)\}] \qquad (7.1.11)$$

where p_{a6} is obtained from equation (7.1.6).

The density of the ambient air at elevation 6 follows from

$$\rho_{a6} = p_{a6}/RT_{a6} \qquad (7.1.12)$$

where T_{a6} is given by equation (7.1.1).

If dynamic effects are neglected, an approximate expression for p_{a4} may similarly be obtained.

$$p_{a4} \approx p_{a1}\left[1 - 0.00975\left(H_3 + H_4\right)/\left(2T_{a1}\right)\right]^{3.5}$$

$$- \left(K_{ts} + K_{ct} + K_{ctc} + K_{he} + K_{cte}\right)_{he}\left(m_a/A_{fr}\right)^2/(2\rho_{a34}) \qquad (7.1.13)$$

Substitute equations (7.1.6), (7.1.8) and (7.1.13) into equation (7.1.7) and find with α_{e5} = 1,

$$p_{a1}\left[\left\{1 - 0.00975\left(H_3 + H_4\right)/\left(2T_{a1}\right)\right\}^{3.5}\right.$$

$$\times \left\{\left[1 - 0.00975\left(H_5 - H_3/2 - H_4/2\right)/T_{a4}\right]^{3.5} - \left(1 - 0.00975\, H_5/T_{a1}\right)^{3.5}\right]$$

$$= \left(K_{ts} + K_{ct} + K_{hes} + K_{ctc} + K_{he} + K_{cte}\right)_{he}\left(m_a/A_{fr}\right)^2/\left(2\rho_{a34}\right)$$

$$\times \left[1 - 0.00975\left(H_5 - H_3/2 - H_4/2\right)/T_{a4}\right]^{3.5} + \left(1 + K_{to}\right)\left(m_a/A_5\right)^2/\left(2\rho_{a5}\right) \qquad (7.1.14)$$

This equation is known as the draft equation for a natural draft cooling tower where the heat exchangers are arranged horizontally in the base of the tower. If the heat exchangers are arranged in the form of A-frames or V-arrays, K_{he} is replaced by $K_{he\theta}$. The latter can be determined according to equation (5.6.16).

In determining the dry air density after the heat exchanger, the specified pressure at ground level can be employed in the perfect gas relation, i.e.

$$\rho_{a4} \approx p_{a1}/RT_{a4} \qquad (7.1.15)$$

Furthermore, for all practical purposes

$$\rho_{a3} \approx p_{a1}/RT_{a3} \qquad (7.1.16)$$

The harmonic mean density of the dry air flowing through the heat exchanger follows from:

$$1/\rho_{a34} = 0.5(1/\rho_{a3} + 1/\rho_{a4}) = 0.5R(T_{a3} + T_{a4})/p_{a1} \qquad (7.1.17)$$

The loss coefficient through the tower supports, K_{ts}, is based on the drag coefficient of the particular support geometry.

$$C_{Dts} = 2F_{Dts}/\left(\rho_{a1} v_{a2}^2 A_{ts}\right) \qquad (7.1.18)$$

A list of drag coefficients for different geometries is given in section 2.5. With equation (7.1.18) the effective pressure drop across the tower supports is given approximately by

$$\Delta p_{ats} = n_{ts} F_{Dts}/A_2 = n_{ts} F_{Dts}/\left(\pi d_3 H_3\right) = \rho_{a1} v_{a2}^2 C_{Dts} L_{ts} d_{ts} n_{ts}/\left(2\pi d_3 H_3\right) \tag{7.1.19}$$

where L_{ts} is the support length and d_{ts} is its effective diameter or width, and n_{ts} is the number of tower supports. The corresponding loss coefficient based on the conditions at the tower supports 2 is

$$K_{ts} = 2\Delta p_{ats}/\left(\rho_{a1} v_{a2}^2\right) = C_{Dts} L_{ts} d_{ts} n_{ts}/\left(\pi d_3 H_3\right) \tag{7.1.20}$$

For substitution into equation (7.1.14), this loss coefficient is required to be based on conditions at the heat exchanger, i.e.

$$K_{tshe} = 2\Delta p_{ats} \rho_{a34}/(m_a/A_{fr})^2 = \frac{C_{Dts} L_{ts} d_{ts} n_{ts} A_{fr}^2}{(\pi d_3 H_3)^3} \left(\frac{\rho_{a34}}{\rho_{a1}}\right) \tag{7.1.21}$$

It is assumed that the air density and the velocity distribution through the supports is uniform. Since the distance between the tower supports is finite, the above approach tends to underestimate the magnitude of the loss coefficient.

Due to separation at the lower edge of the cooling tower shell and distorted inlet flow patterns, a cooling tower loss coefficient K_{ct}, based on the tower cross-sectional area 3, can be defined to take these effects into consideration. Empirical equations for this coefficient are presented in section 7.3.

The cooling tower inlet loss coefficient based on conditions at the heat exchanger is

$$K_{cthe} = K_{ct} \left(\rho_{a34}/\rho_{a3}\right) \left(A_{fr}/A_3\right)^2 \tag{7.1.22}$$

The heat exchanger support structure consists of pillars and beams that offer limited flow resistance. These resistances can be expressed in terms of a loss coefficient K_{hes}.

Depending on the heat exchanger bundle arrangement in the cooling tower base, only a portion of the available area is effectively covered due to the rectangular shape of the bundles. This reduction in effective flow area results in contraction, and subsequent expansion losses. These losses may be respectively approximated by equations (2.3.13) and (2.3.14) based on the effective reduced flow area A_{e3}

$$K_{ctc} = 1 - 2/\sigma_c + 1/\sigma_c^2 \tag{7.1.23}$$

and

$$K_{cte} = \left(1 - A_{e3}/A_3\right)^2 \tag{7.1.24}$$

The effective area, A_{e3}, corresponds to the frontal area of the heat exchanger bundles if they are installed horizontally. In the case of an array of A-frames, A_{e3} corresponds to the projected frontal area of the bundles. Because of the essentially porous nature of the bundles, the actual contraction loss coefficient will be less than the value given by equation (7.1.23). However, if the flow resistance of the heat exchanger support structure (K_{hes}) is not considered separately, this value is not unrealistic.

Based on the conditions at the heat exchanger, the above expressions become

$$K_{ctche} = \left(1 - 2/\sigma_c + 1/\sigma_c^2\right)\left(\rho_{a34}/\rho_{a3}\right)\left(A_{fr}/A_{e3}\right)^2 \tag{7.1.25}$$

and

$$K_{ctehe} = \left(1 - A_{e3}/A_3\right)^2\left(\rho_{a34}/\rho_{a4}\right)\left(A_{fr}/A_{e3}\right)^2 \tag{7.1.26}$$

Similar equations may be deduced for a tower as shown in figure 7.1.3, where the heat exchangers are arranged vertically around the circumference at the base of the tower. For a DALR the mean inlet air temperature to the heat exchangers is

$$T_{a2} \approx T_{a1} - 0.00975\ H_4/2 \tag{7.1.27}$$

The relevant heat transfer equations are:

$$Q = m_a c_{pa} (T_{a3} - T_{a2}) = m_w c_{pw} (T_{wi} - T_{wo}) \tag{7.1.28}$$

and

$$Q = \frac{UA\, F_T \left[(T_{wi} - T_{a3}) - (T_{wo} - T_{a2}) \right]}{\ln \left[(T_{wi} - T_{a3}) / (T_{wo} - T_{a2}) \right]} \tag{7.1.29}$$

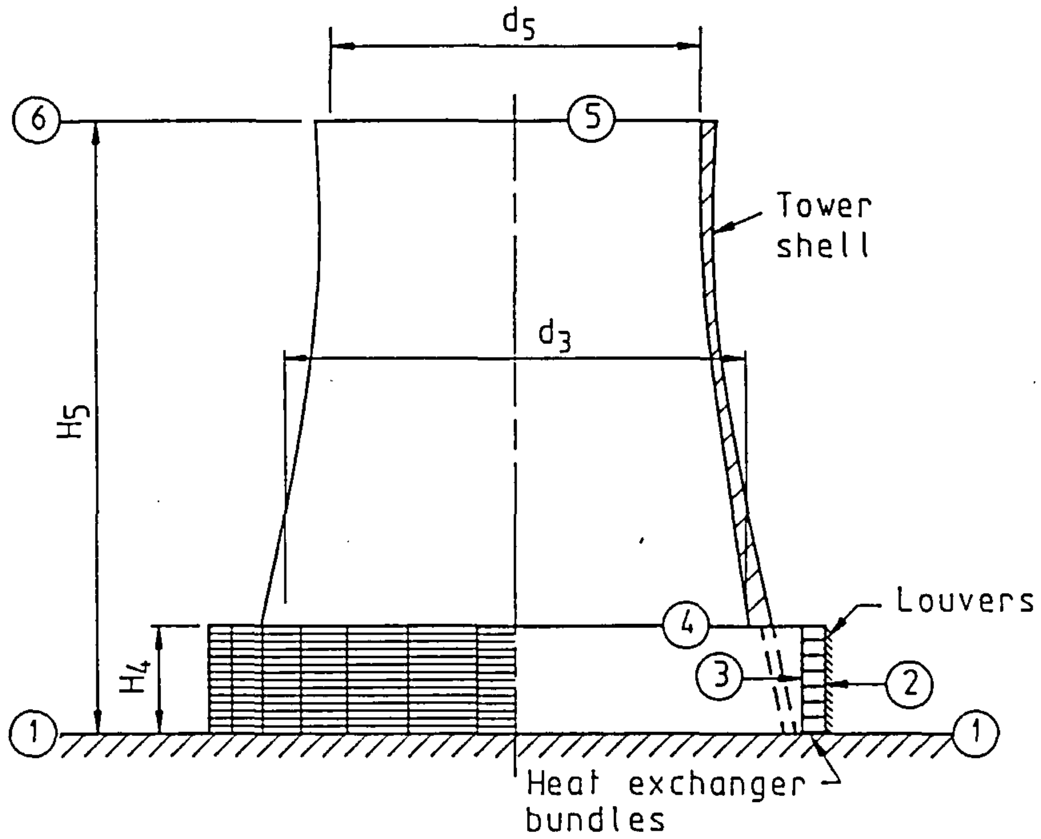

Figure 7.1.3: Natural draft cooling tower with vertical heat exchangers.

Similarly, the corresponding draft equation for dry air is

$$p_{a1}\left[(1 - 0.00975\ H_4/2T_{a1})^{3.5}(1 - 0.00975\ (H_5 - H_4/2)/T_{a3})^{3.5}\right.$$

$$\left. - \ (1 - 0.00975\ H_5/T_{a1})^{3.5}\right]$$

$$= \left(K_{i\ell} + K_{ctc} + K_{he} + K_{cte} + K_{ct}\right)_{he} \left(m_a/A_{fr}\right)^2/\left(2\rho_{a23}\right)$$

$$x \left[1 - 0.00975 \left(H_5 - H_4/2\right)/T_{a3}\right]^{3.5} + \left(K_{to} + \alpha_{e5}\right)\left(m_a/A_5\right)^2/\left(2\rho_{a5}\right) \qquad (7.1.30)$$

where $K_{i\ell}$ is the inlet louver loss coefficient based on A_{fr}. The velocity distribution at the outlet of this type of tower is less uniform than in the case where the heat exchangers are installed horizontally. A velocity distribution correction factor, α_{e5}, takes this effect into consideration. Du Preez and Kröger [94DU1] determined the value of α_{e5} numerically and propose the following empirical relations:

$$\alpha_{e5} = 1.004 + 5.8\left(d_5/d_3\right)^9 + \left[0.007 + 0.043\left(d_5/d_3\right)^{2.5}\right]Fr_D^{-1.5} \qquad (7.1.31)$$

while the tower outlet loss coefficient is correlated by

$$K_{to} = -0.129\left(Fr_D\ d_5/d_3\right)^{-1} + 0.0144\left(Fr_D\ d_5/d_3\right)^{-1.5} \qquad (7.1.32)$$

for $1/Fr_D \le 3$, $0.49 \le d_5/d_3 \le 0.69$ and $5 \le K_{he} \le 40$.

If the heat exchanger bundles are arranged in the form of deltas or A-frames, K_{he} is replaced by $K_{he\theta}$. All loss coefficients are based on conditions at the heat exchanger.

The air density at the outlet of the tower is

$$\rho_{a5} = p_{a6}/\left[R\left\{T_{a3} + 0.00975\left(H_4/2 - H_5\right)\right\}\right] \qquad (7.1.33)$$

When the air contains water vapor, this can be taken into consideration in the evaluation of all thermo-physical properties. Furthermore the draft equation as given by equation (7.1.14) for the horizontal bundle layout is extended as follows.

$$p_{a1}\left[\{1 - 0.00975 \left(H_3 + H_4\right)/2T_{a1}\}^{3.5(1+w)\{1-w/(w + 0.62198)\}}\right.$$

$$x \{1 - 0.00975 \left(H_5 - H_3/2 - H_4/2\right)/T_{a4}\}^{3.5(1+w)\{1-w/(w + 0.62198)\}}$$

$$- \left(1 - 0.00975\ H_5/T_{a1}\right)^{3.5(1+w)\{1-w/(w\ +\ 0.62198)\}}\Big]$$

$$= \left(K_{ts} + K_{ct} + K_{hes} + K_{ctc} + K_{he} + K_{cte}\right)_{he} \left(m_a/A_{fr}\right)^2/\left(2\rho_{a34}\right)$$

$$\times \left[1 - 0.00975 \left(H_5 - H_3/2 - H_4/2\right)/T_{a4}\right]^{3.5(1+w)\{1-w/(w\ +\ 0.62198)\}}$$

$$+ \left(1 + K_{to}\right)\left(m_a/A_5\right)^2/\left(2\rho_{a5}\right) \tag{7.1.34}$$

where w is the humidity ratio and the pressure at the outlet of the tower, p_{a6}, required to determine the density, ρ_{a5}, according to equation (7.1.28) is given by

$$p_{a6} = p_{a1} \left(1 - 0.00975\ H_5/T_{a1}\right)^{3.5(1+w)\{1-w/(w\ +\ 0.62198)\}} \tag{7.1.35}$$

Similarly for the case where the bundles are arranged vertically around the base of the tower, the draft equation (7.1.30) may be extended as follows, to take into consideration the presence of water vapor:

$$p_{a1}\Big[\left(1 - 0.00975\ H_4/2T_{a1}\right)^{3.5(1+w)\{1-w/(w\ +\ 0.62198)\}}$$

$$\times\ \{1 - 0.00975 \left(H_5 - H_4/2\right)/T_{a3}\}^{3.5(1+w)\{1-w/(w+0.62198)\}}$$

$$- \left(1 - 0.00975\ H_5/T_{a1}\right)^{3.5(1+w)\{1-w/(w\ +\ 0.62198)\}}\Big]$$

$$= \left(K_{i\ell} + K_{ctc} + K_{he} + K_{cte} + K_{ct}\right)_{he}\left(m_a/A_{fr}\right)^2/\left(2\rho_{a23}\right)$$

$$\times \left[1 - 0.00975\left(H_5 - H_4/2\right)/T_{a3}\right]^{3.5(1+w)\{1-w/(w\ +\ 0.62198)\}}$$

$$+ \left(K_{to} + \alpha_{e5}\right)\left(m_a\ /\ A_5\right)^2\ /\ \left(2\rho_{a5}\right) \tag{7.1.36}$$

The presence of water vapor in the air usually has a negligible influence on the performance of a dry-cooling tower.

7.2 WET-COOLING TOWER

Consider the example of a hyperbolic natural draft wet-cooling tower as shown in figure 7.2.1. The fill is located horizontally at the inlet cross-section of the tower. The density of the warm moist air inside the tower is less than that of the atmosphere outside the tower, hence the pressure inside the tower is less than the external pressure at the same elevation. This pressure differential causes air to flow through the tower at a rate that is dependent on the various flow resistances encountered, the cooling tower dimensions and the transfer characteristics of the fill and the rain zone.

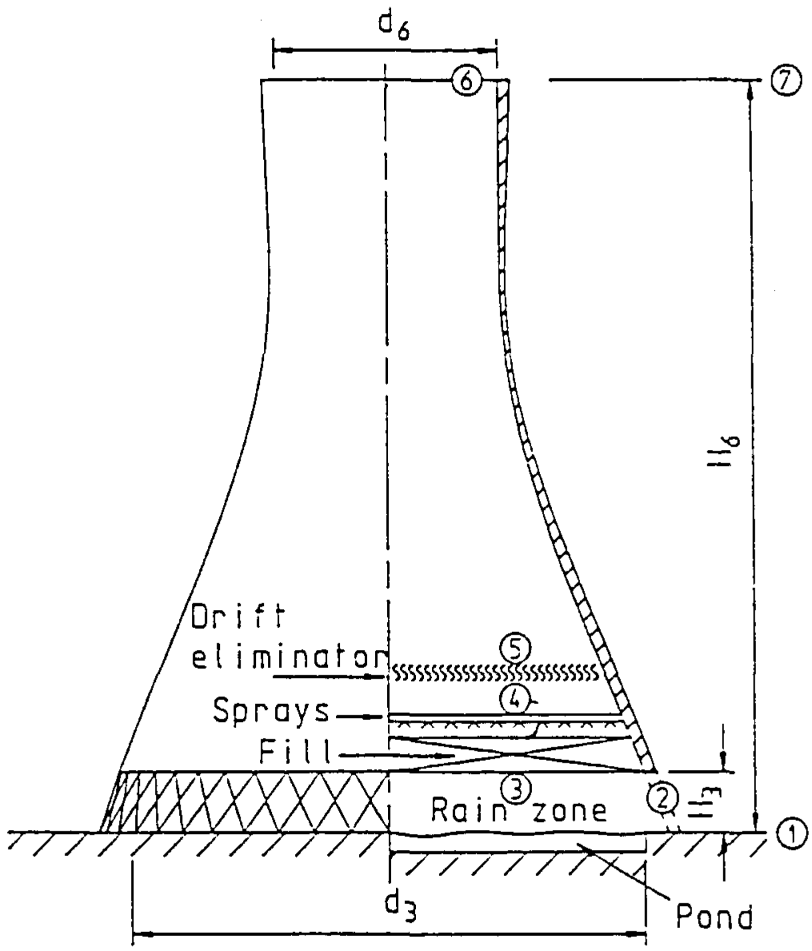

Figure 7.2.1: Natural draft cooling tower with horizontal fill.

Different approaches for evaluating the performance characteristics of such a cooling tower, appear in the literature [26ME1, 52CH1, 61LO1, 61RI1, 67SI1, 72ZI1, 73ME1, 74YA1, 75NA1, 77NA1, 78PA1, 83BO1, 83MA1, 83SU1, 85MA1, 91PO1]. In practice the classical Merkel method [26ME1] or the more detailed method due to Poppe [72PO1, 91PO1] are most commonly employed in the performance evaluation of wet-cooling towers.

Two- and three-dimensional mathematical models have been developed to determine the performance characteristics of wet-cooling towers. The 2-d models include TEFERI [83BO1], VERA 2 D [83MA2], STAR [87CA1], ETHER [90GR1] and others [94LI1], while TACT [88RA1] is a 3-d model. Even in the most sophisticated of these programs, use is made of empirical or experimental data e.g. fill performance characteristics, etc. and simplifying assumptions are made to avoid excessive complexity. The results obtained with these multi-dimensional codes are thus not necessarily always better than those obtained by the application of simpler point models.

In the following analysis, which is to some extent similar to that applied to the dry-cooling tower in the previous section, a procedure is presented showing how the performance of a counterflow wet-cooling tower, having a fill of uniform thickness, can be determined to a relatively high degree of accuracy.

Neglecting the evaporation loss (typically of the order of one to three per cent), an energy balance for a wet-cooling tower as shown schematically in figure 7.2.1. yields

$$m_a \left(i_{a5} - i_{a1}\right) = m_w\, c_{pw} \left(T_{wi} - T_{wo}\right) \tag{7.2.1}$$

where m_a and m_w are the dry air and water mass flow rates through the tower respectively.

Energy is transferred in essentially three regions of the cooling tower shown in figure 7.2.1 i.e. rain zone, fill and spray zone.

In the rain zone the transfer coefficient is given by equation (4.6.17) or (4.6.18). The latter can be expressed as

$$\frac{h_{drz} a_{rz} H_3}{\rho_{av1} v_{av34}} = 3.15 \left(\frac{H_i}{d_d}\right)^{1.64} \left(\frac{\rho_{av1} v_{av34} H_3}{\mu_{av1}}\right)^{2.24} \left(\frac{D}{H_3 v_{av34}}\right)^{2.764} \left(\frac{p_{a1}}{\rho_{av1} v_{av34}^2}\right)^{1.483}$$

$$\left(\frac{v_{w3}}{v_{av34}}\right)\exp\left[\frac{\left\{\ell n\left(gH_3/v_{av34}^2\right) - 8.222\right\}^2}{26.626}\right]\left(\frac{v_{av34}^2}{R_v T_{w3}}\right)^{1.497}\left[0.205 + 0.00131\left(\frac{d_3}{H_3}\right)\right.$$

$$\left. + 0.0699\, w_{s3} - 0.191\, w_1 - 1.3 \times 10^{-5}\left(\frac{\rho_{w3}}{\rho_{av1}}\right) + 0.188\left(\frac{\sigma_{w3}}{H_3\, \rho_{av1} v_{av34}^2}\right)\right]$$

To simplify the analysis, the thermophysical properties of the water in this equation will all be evaluated at its inlet conditions to the tower i.e. at the spray nozzles corresponding to section 5. The properties of the air stream will be evaluated at 1 or 5 or at the mean of these values.

The above relation can thus be re-written as

$$\frac{h_{drz} a_{rz} H_3}{G_w} = 3.15\left(\frac{\rho_{av1} v_{av15}}{G_w}\right)\left(\frac{H_i}{d_d}\right)^{1.64}\left(\frac{\rho_{av1} v_{av15} H_3}{\mu_{av1}}\right)^{2.24}\left(\frac{D}{H_3 v_{av15}}\right)^{2.764}$$

$$\left(\frac{p_{a1}}{\rho_{av1} v_{av15}^2}\right)^{1.483}\left(\frac{v_{w5}}{v_{av15}}\right)\exp\left[\frac{\left\{\ell n\left(gH_3/v_{av15}^2\right) - 8.222\right\}^2}{26.626}\right]\left(\frac{v_{av15}}{R_v T_{w5}}\right)^{1.497}\left[0.205\right.$$

$$\left. + 0.00131\left(\frac{d_3}{H_3}\right) + 0.0699\, w_{s5} - 0.191\, w_1 - 1.3 \times 10^{-5}\left(\frac{\rho_{w5}}{\rho_{av1}}\right) + 0.188\left(\frac{\sigma_{w5}}{H_3\, \rho_{av1} v_{av15}^2}\right)\right]$$

Equations (4.3.1), (4.3.3) or (4.3.4) are applicable in the fill. Typically equation (4.3.3) for the entire fill height can be written as

$$\frac{h_d a_{fi} L_{fi}}{G_w} = a_d L_{fi} G_w^{\,b_d} G_a^{\,c_d}$$

In the spray zone above the fill the data of Lowe and Christie [61LO1] can be correlated to give

$$\frac{h_d a_{sp} L_{sp}}{G_w} = 0.2\ L_{sp}\left(\frac{G_a}{G_w}\right)^{0.5}$$

To deduce the corresponding draft equation, consider the variation of pressure with elevation in the atmosphere external to the cooling tower, i.e.

$$dp_a = -\rho_{av}\, g\, dz \tag{7.2.2}$$

As in the case of the dry-cooling tower the ambient temperature distribution for a DALR (- 0.00975 K/m) is assumed external to the tower.

$$T_a = T_{a1} - 0.00975\ z \tag{7.2.3}$$

where T_{a1} is found by extrapolating the DALR to ground level.

According to equation (A.3.1), the density of air containing water vapor is expressed as

$$\rho_{av} = (1 + w)\left[1 - w/(w + 0.62198)\right] p_a/(RT_a) \tag{7.2.4}$$

where R = 287.08 J/kg K

Substitute equations (7.2.3) and (7.2.4) into equation (7.2.2) and integrate to find, for an essentially constant humidity ratio, $w \approx w_1$, the difference in pressure between elevations 1 and 7 external to the tower.

$$p_{a1} - p_{a7} = p_{a1}\left[1 - (1 - 0.00975\ H_6/T_{a1})^{3.5(1+w_1)\{1 - w_1/(w_1+0.62198)\}}\right] \tag{7.2.5}$$

where $H_7 = H_6$.

By following a similar procedure, an expression can be obtained for the static pressure difference between ground level and the mean fill height at $(H_3 + L_{fi}/2)$.

Rising moist air inside the tower is adiabatically cooled, causing vapor to condense and precipitate out of the rising air. The energy removed by this condensation process is then available to heat the surrounding air. According to equation (10.1.16) the lapse rate for this pseudo-adiabatic process is given by

$$\xi_{Ta5} = \frac{-g(1 + w_5)}{c_{pma} + \frac{7.966\text{x}10^{14}}{(p_{a5}T_{a5}^2)}\left[i_{fgwo} - \left(c_{pw} - c_{pv}\right)\left(T_{a5} - 273.15\right)\right]\exp(-5406.1915/T_{a5})} \tag{7.2.6}$$

where $c_{pma} = c_{pa} + w_5 c_{pv}$ and T_{a5} is in K.

The difference in static pressure due to the column of moist air between the mean fill elevation and the outlet of the tower for this temperature lapse rate is approximately

$$p_{a34} - p_{a6}$$

$$= p_{a5}\left[1 - \left\{1 + \xi_{Ta5}\left(H_6 - H_3 - L_{fi}/2\right)/T_{a5}\right\}^{-\left(1 + w_5\right)\left\{1 - w_5/\left(w_5 + 0.62198\right)\right\}g/\left(R\xi_{Ta5}\right)}\right] \tag{7.2.7}$$

The net pressure differential between the ambient air and the air inside the tower may be determined from these expressions to give the draft equation for a natural draft counterflow wet-cooling tower, i.e.

$$(p_{a1} - p_{a7}) - (p_{a1} - p_{a34}) - (p_{a34} - p_{a6}) - (p_{a6} - p_{a7}) \approx$$

$$p_{a1}\left[1 - \left(1 - 0.00975\ H_6/T_{a1}\right)^{3.5\left(1 + w_1\right)\left\{1 - w_1/\left(w_1 + 0.62198\right)\right\}}\right]$$

$$-p_{a1}\left[1 - \left\{1 - 0.00975\left(H_3 + L_{fi}/2\right)/T_{a1}\right\}^{3.5\left(1 + w_1\right)\left\{1 - w_1/\left(w_1 + 0.62198\right)\right\}}\right]$$

$$-p_{a5}\left[1 - \left\{1 + \xi_{Ta5}\left(H_6 - H_3 - L_{fi}/2\right)/T_{a5}\right\}^{-\left(1 + w_5\right)\left\{1 - w_5/\left(w_5 + 0.62198\right)\right\}g/\left(R\xi_{Ta5}\right)}\right]$$

$$-(p_{a6} - p_{a7})$$

$$= (K_{ts}+K_{i\ell})(m_{av2}/A_2)^2/(2\rho_{av2})+K_{ct}(m_{av2}/A_3)^2/(2\rho_{av2})+(K_{rz}+K_{fs})(m_{av23}/A_{fr})^2$$

$$/(2\rho_{av23}) + K_{ctc}(m_{av3}/A_{fr})^2/(2\rho_{av3}) + K_{fi}(m_{av34}/A_{fr})^2/(2\rho_{av34})$$

$$+(K_{cte}+K_{sp}+K_{wd}+K_{de})(m_{av4}/A_{fr})^2/(2\rho_{av4})+\alpha_{e6}(m_{av6}/A_6)^2/(2\rho_{av6})$$

To simplify this equation assume $m_{av2} \approx m_{av23} \approx m_{av3} \approx m_{av4} \approx m_{av6} \approx m_{av34} \approx m_{av15}$ and $\rho_{av2} \approx \rho_{av3} \approx \rho_{av1}$ and $\rho_{av4} \approx \rho_{av5}$ such that

$$p_{a1}\left[1-\left(1-0.00975\ H_6/T_{a1}\right)^{3.5\ (1+w_1)\ \{1-w_1/(w_1+0.62198)\}}\right]$$

$$-p_{a1}\left[1-\left\{1-0.00975\ (H_3+L_{fi}/2)/T_{a1}\right\}^{3.5\ (1+w_1)\{1-w_1/(w_1+0.62198)\}}\right]$$

$$-p_{a5}\left[1-\left\{1+\xi_{Ta5}\ (H_6-H_3-L_{fi}/2)/T_{a5}\right\}^{-(1+w_5)\{1-w_5/(w_5+0.62198)\}g/(R\xi_{Ta5})}\right]$$

$$-(p_{a6} - p_{a7})$$

$$= (K_{ts} + K_{i\ell} + K_{ct} + K_{rz} + K_{fs} + K_{ctc} + K_{fi} + K_{cte} + K_{sp} + K_{wd} + K_{de})_{fi}$$

$$(m_{av15}/A_{fr})^2/(2\rho_{av15}) + \alpha_{e6}(m_{av15}/A_6)^2/(2\rho_{av6}) \tag{7.2.8}$$

The subscript fi implies that all loss coefficients are referred to the frontal area of the fill and the mean density through the fill.

With the previous simplifying assumptions and the assumption that the dynamic term at elevation 5 is negligible the approximate effective value for p_{a5} for substitution into equation (7.2.8) can be approximated by the following expression:

$$p_{a5} = p_{a1}\left[1 - 0.00975\left(H_3 + L_{fi}/2\right)/T_{a1}\right]^{3.5(1 + w_1)\{1 - w_1/(w_1 + 0.62198)\}}$$

$$- \left(K_{ts} + K_{i\ell} + K_{ct} + K_{rz} + K_{fs} + K_{ctc} + K_{fi} + K_{cte} + K_{sp} + K_{wd} + K_{de}\right)_{fi}$$

$$\times \left(m_{av15}/A_{fr}\right)^2/\left(2\rho_{av15}\right) \tag{7.2.9}$$

According to du Preez and Kröger [94DU1] the difference in the mean pressure at the tower outlet and the ambient pressure at the same elevation is given by

$$p_{a6} - p_{a7} = \left(0.02\ Fr_D^{-1.5} - 0.14/Fr_D\right)\left(m_{av15}/A_6\right)^2/\rho_{av6} \tag{7.2.10}$$

Substitute equations (7.2.9) and (7.2.10) into equation (7.2.8) and re-arrange to find the final simplified form of the draft equation.

$$p_{a1}\left[\left\{1 - 0.00975\left(H_3 + L_{fi}/2\right)/T_{a1}\right\}^{3.5(1 + w_1)\{1 - w_1/(w_1 + 0.62198)\}}\right.$$

$$\times \left\{1 + \xi_{Ta5}\left(H_6 - H_3 - L_{fi}/2\right)/T_{a5}\right\}^{-(1 + w_5)\left\{1 - w_5/(w_5 + 0.61298)\right\}g/(R\xi_{Ta5})}$$

$$\left. - \left\{1 - 0.00975\ H_6/T_{a1}\right\}^{3.5(1 + w_1)\left\{1 - w_1/(w_1 + 0.62198)\right\}}\right]$$

$$- \left(0.02\ Fr_D^{-1.5} - 0.14/Fr_D\right)\left(m_{av15}/A_6\right)^2/\rho_{av6}$$

$$= \left(K_{ts} + K_{i\ell} + K_{ct} + K_{rz} + K_{fs} + K_{ctc} + K_{fi} + K_{cte} + K_{sp} + K_{wd} + K_{de}\right)_{fi}$$

$$\times \left(m_{av15}/A_{fr}\right)^2/\left(2\rho_{av15}\right)$$

$$\times \left[1 + \xi_{Ta5}\left(H_6 - H_3 - L_{fi}/2\right)/T_{a5}\right]^{-(1 + w_5)\left\{1 - w_5/(w_5 + 0.61298)\right\}g/(R\xi_{Ta5})}$$

$$+ \alpha_{e6}\left(m_{av15}/A_6\right)^2/\left(2\rho_{av6}\right) \tag{7.2.11}$$

where the subscript fi implies that the loss coefficients are referred to the geometry and conditions through the fill.

The loss coefficient due to the tower supports, K_{ts}, may be determined according to equation (7.1.20).

In older counterflow natural draft cooling towers, louvers were installed at the tower inlet (not shown in figure 7.2.1) to reduce the effect of cross-winds. These louvers tend to distort the entering air flow pattern and offer a corresponding flow resistance. Kelly [76KE1] gives a value of $K_{i\ell} = 5$ for a crossflow tower while Jorgensen [61JO1] suggests that the value for this coefficient may vary between 2 and 5. The loss coefficient for inlet louvers based on experimental data may be given as an approximate constant value or expressed in terms of a flow Reynolds number through the louvers as

$$K_{i\ell} = a_{i\ell}\ Re_{i\ell}^{b_{i\ell}} \tag{7.2.12}$$

or

$$K_{i\ell fi} = a_{i\ell}\ Re_{i\ell}^{b_{i\ell}}\left(\rho_{av15}/\rho_{av1}\right)\left(A_{fr}/A_2\right)^2 \tag{7.2.13}$$

where the subscript fi implies that the coefficient is based on conditions through the fill.

Expressions for the tower inlet loss coefficient, K_{ct}, for a counterflow cooling tower as given in section 7.3 may be employed.

It follows from equation (4.6.10) that the loss coefficient through the rain zone can be expressed as

$$K_{rz} = \left[3.1724 - 0.1643(d_3/H_3) + 0.007004(d_3/H_3)^2\right](G_w/G_a)/d_r^{1.2}$$

or if referred to fill conditions

$$K_{rzfi} = K_{rz}(\rho_{av15}/\rho_{av2}) \approx K_{rz}(\rho_{av15}/\rho_{av1}) \tag{7.2.14}$$

This equation is valid for $10 \leq d_3 / H_3 \leq 15$ and $0\,°C \leq T_a \leq 40\,°C$ where $d_r = d_d/d_c$. The critical drop diameter d_c is defined by equation (4.3.9) and is found to be equal to 10.92 mm at 20 °C.

Losses due to the fill support structure including pillars and crossbeams, K_{fs}, may be expressed in terms of a drag coefficient or an approximate constant value. If the fill does not cover the entire cross-sectional area of the tower a contraction loss should be considered. Equation (7.1.23) can be employed for this purpose.

After the fill an expansion loss as given by equation (7.1.24) may be relevant if the fill does not cover the entire tower cross-section. The loss coefficient through the fill is given by either equation (4.3.2) or equation (4.3.5).

In the spray region above the fill, data presented by Cale [82CA1] suggests that the loss coefficient may be expressed approximately as

$$K_{sp} \approx L_{sp}\left[0.4\left(G_w/G_a\right) + 1\right] \tag{7.2.15}$$

or based on fill condition

$$K_{spfi} \approx L_{sp}\left[0.4\left(G_w/G_a\right) + 1\right]\left(\rho_{av15}/\rho_{av5}\right) \tag{7.2.16}$$

where L_{sp} is the height of the spray zone.

The spray should be uniformly distributed above the fill by a system of pipes fitted with spray nozzles. A typical value for the loss coefficient of such a system is $K_{wdfi} = 0.5(\rho_{a15}/\rho_{a5})$.

Losses through the drift or droplet eliminators located above the spray nozzles may be expressed as

$$K_{defi} = a_{de}\, Ry_{de}^{b_{de}} \left(\rho_{a15}/\rho_{a5}\right) \tag{7.2.17}$$

The values for a_{de} and b_{de} are obtained by fitting equation (4.2.26) to test data as shown for typical drift eliminators in figure 4.2.7.

It is important that the water flows uniformly through the fill since non-uniform flow tends to reduce tower performance [94LE1] and may cause freezing during cold periods [88VG1].

The approximate harmonic mean density in the fill is given by

$$\rho_{av34} \approx \rho_{av15} = 2/\left(1/\rho_{av1} + 1/\rho_{av5}\right) \tag{7.2.18}$$

Since the change in humidity and temperature in the rain zone is relatively small, assume

$$\rho_{av1} = (1 + w_1)\left[1 - w_1/(w_1 + 0.62198)\right] p_{a1}/\left(RT_{a1}\right)$$

and

$$\rho_{av5} = \left(1 + w_5\right)\left[1 - w_5/\left(w_5 + 0.62198\right)\right] p_{a5}/\left(RT_{a5}\right)$$

If dynamic effects are neglected the air temperature at the outlet of the tower is

$$T_{a6} \approx T_{a5} + \xi_{Ta5}\left(H_6 - H_3 - L_{fi} - L_{sp}\right)$$

The corresponding mean pressure p_{a6} follows from equation (7.2.10) where p_{a7} is given by equation (7.2.5). With these values find the density at 6.

$$\rho_{av6} = \left(1 + w_5\right)\left[1 - w_5/\left(w_5 + 0.62198\right)\right] p_{a6}/\left(RT_{a6}\right)$$

Distortions in velocity distribution at the tower outlet are taken into consideration by the factor α_{e6} which is for all practical purposes equal to unity for a hyperbolic counterflow tower [94DU1].

7.3 TOWER INLET LOSSES

As in the case of most duct inlets where flow losses occur due to separation or other disturbances, similar phenomena are observed at the inlets to natural draft cooling towers. If flow through such a tower could be maintained in the absence of any flow resistance due to heat exchangers or fills in the inlet to the tower, flow separation will occur at the lintel or lower edge of the shell, forming a vena contracta with a corresponding distorted inlet velocity distribution as shown schematically in figure 7.3.1 (a). A significant pressure difference will exist between a point inside the tower at the lower edge of the shell and the ambient stagnant conditions far from the tower.

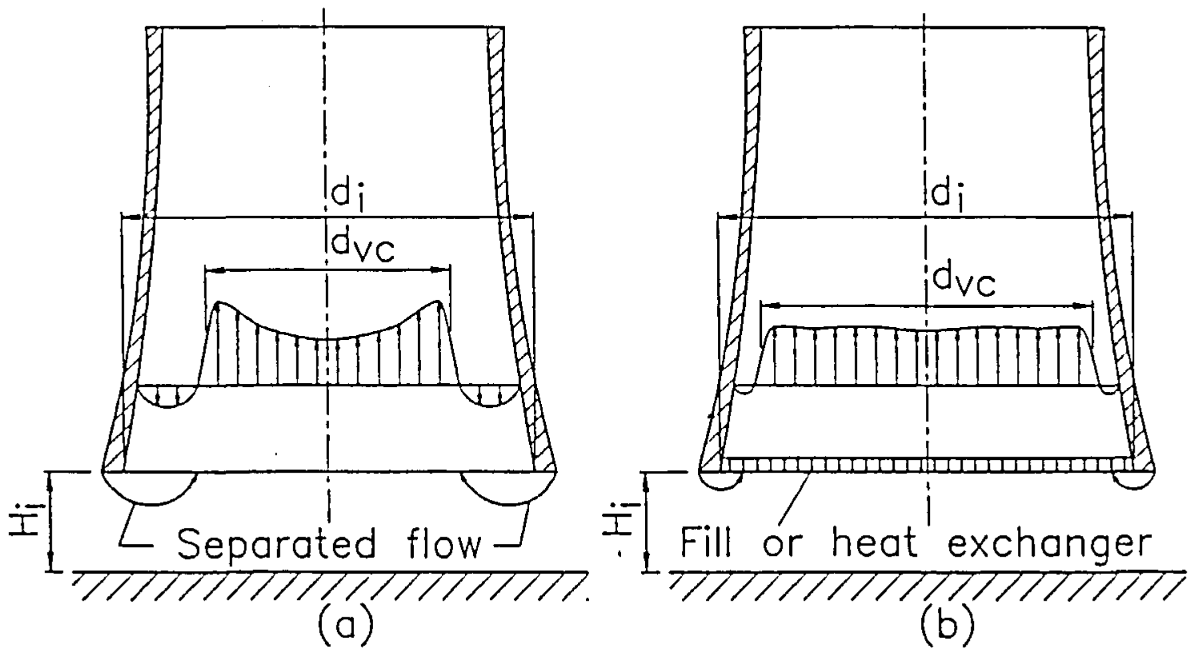

(a) Empty tower (b) Tower with horizontal heat exchanger or fill

Figure 7.3.1: Tower inlet flow patterns.

The tower static inlet loss coefficient may be defined as

$$K_{cts} = (p_a - p)/(\rho v^2/2) \qquad (7.3.1)$$

where p_a is the ambient stagnation pressure and p is the static pressure inside the tower at the lower edge of the shell. The mean velocity, v, is based on the horizontal cross-sectional flow area at the inlet.

A number of experimental and theoretical studies have been conducted to determine the tower inlet losses in the absence of heat exchangers or fills for different inlet diameters, d_i, to height, H_i, ratios and some of the results are shown in figure 7.3.2.

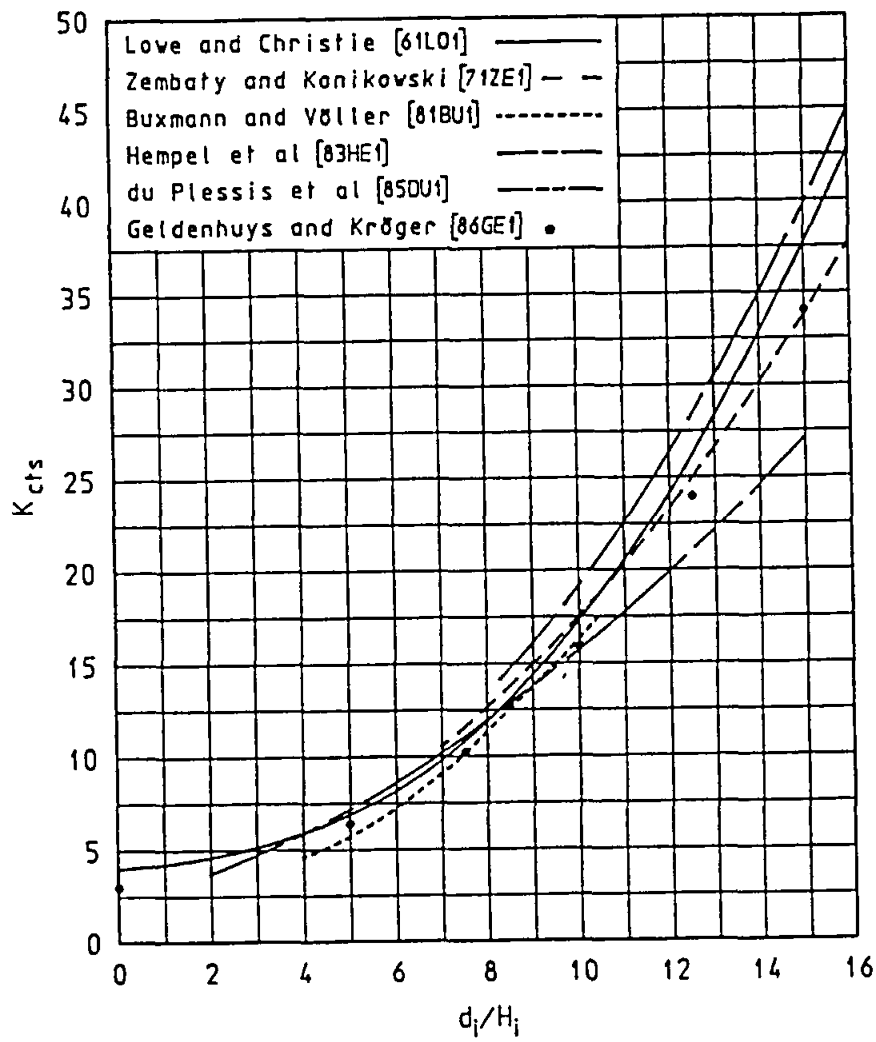

Figure 7.3.2: Empty tower static inlet loss coefficient.

When a fill or heat exchanger is installed horizontally in the tower, the velocity distribution tends to become more uniform as is shown in figure 7.3.1(b) and a corresponding reduction in tower inlet loss is observed.

Although most of the original studies on cooling tower losses were made with a view to the design of wet-cooling towers; [61LO1, 68VO1, 71ZE1, 81GA1, 81MO1, 81BU1, 83HE1, 83WI1, 86GE1, 88DU1, 94TE1] a few of the more recent papers make specific reference to dry-cooling towers.

Terblanche and Kröger [94TE1] performed model tests to determine the tower loss coefficient as a function of the fill or heat exchanger loss coefficient K_{he}. They express the loss coefficient in terms of the change in total pressure between the stagnant ambient air, p_a, far from the tower and that in the plane of the vena contracta after the fill or heat exchanger i.e.

$$K_{ct} = \frac{p_a/\rho - (p_{vc}/\rho_{vc} + \alpha_{evc} v_{vc}^2/2)}{v^2/2} - K_{he} \frac{\rho}{\rho_{he}} \left(\frac{A}{A_{fr}}\right)^2 \tag{7.3.2}$$

where A is the inlet cross-sectional area of the tower, A_{fr} is the total frontal area of the heat exchanger and ρ_{he} is the harmonic mean density of the air flowing through it. Furthermore, v_{vc} is the mean velocity in the plane of the vena contracta. The corresponding kinetic energy coefficient is α_{evc}. This equation is applicable to both the vertical and horizontal arrangements of heat exchanger bundles.

In the latter case where the velocity distribution may by relatively uniform over the tower cross-section equation (7.3.2) can be simplified to read:

$$K_{ct} = \frac{p_a/\rho - (p_o/\rho_o + v_o^2/2)}{v^2/2} - K_{he} \frac{\rho}{\rho_{he}} \left(\frac{A}{A_{fr}}\right)^2 \tag{7.3.3}$$

where v_o is the outlet air velocity based on the frontal area of the fill or the heat exchanger. If the heat exchanger is arranged in the form of A-frames or arrays of V-bundles, v_o is based on the projected frontal area thereof. Subscript o refers to conditions after the fill or heat exchanger.

A further simplification is possible for the case where the fill or heat exchangers are installed such that they essentially cover the entire inlet cross-section of the cooling tower i.e.

$$K_{ct} \approx \frac{(p_a/\rho - p_o/\rho_o)}{v^2/2} - 1 - K_{he}\left(\frac{\rho}{\rho_{he}}\right) \tag{7.3.4}$$

The recommended loss coefficient for this layout is given by

$$K_{ct} = 100 - 18\left(d_i/H_i\right) + 0.94\left(d_i/H_i\right)^2$$

$$\times K_{he}^{[-1.28 + 0.183(d_i/H_i) - 7.769\times 10^{-3}(d_i/H_i)^2]} \tag{7.3.5}$$

This equation is applicable in the ranges $10 \le (d_i/H_i) \le 15$ and $5 \le K_{he} \le 25$. Equation (7.3.5) can also be applied in conjunction with equation (7.3.2) where $\alpha_{evc} = 1.175$.

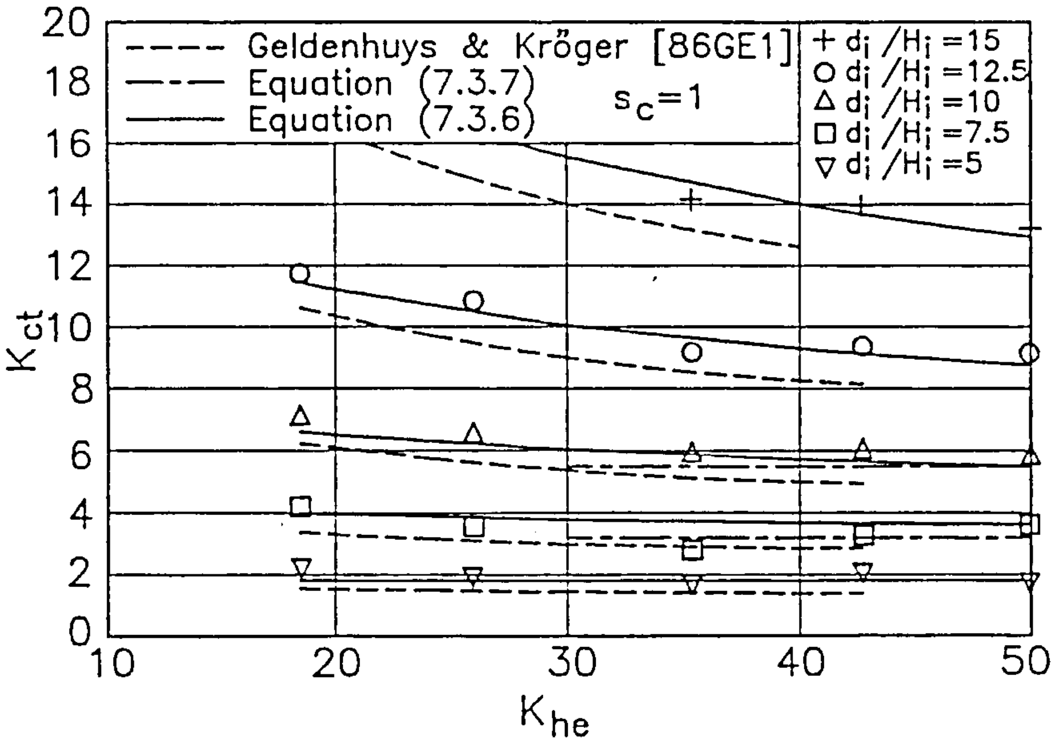

Figure 7.3.3: Cooling tower loss coefficient.

For higher values of K_{he} the following equation is preferred [88DU1]:

$$K_{ct} = \left[-18.7 + 8.095\ (d_i/H_i) - 1.084\ (d_i/H_i)^2 + 0.0575\ (d_i/H_i)^3\right]$$

$$\times\ K_{he}^{[0.165\ -\ 0.035\ (d_i/H_i)]} \qquad (7.3.6)$$

for $19 < K_{he}$ 50 and $5 < d_i/H_i < 15$

For dry-cooling towers where $K_{he} \geq 30$ and $5 \leq d_i/H_i < 10$, the following simplified expression is recommended [86GE1]:

$$K_{ct} = 0.072(d_i/H_i)^2 - 0.34(d_i/H_i) + 1.7 \qquad (7.3.7)$$

Equations (7.3.6) and (7.3.7) are shown graphically in figure 7.3.3.

Additional aerodynamic inlet losses occur in dry natural draft cooling towers, where the horizontally arranged rectangular heat exchangers do not cover the entire cross-sectional area or run continuously all along the circumference at the base of the tower.

Du Preez and Kröger [88DU1] define the following length ratio:

$$s_c = \frac{\text{Effective length of heat exchanger along tower circumference}}{\pi d_i} \qquad (7.3.8)$$

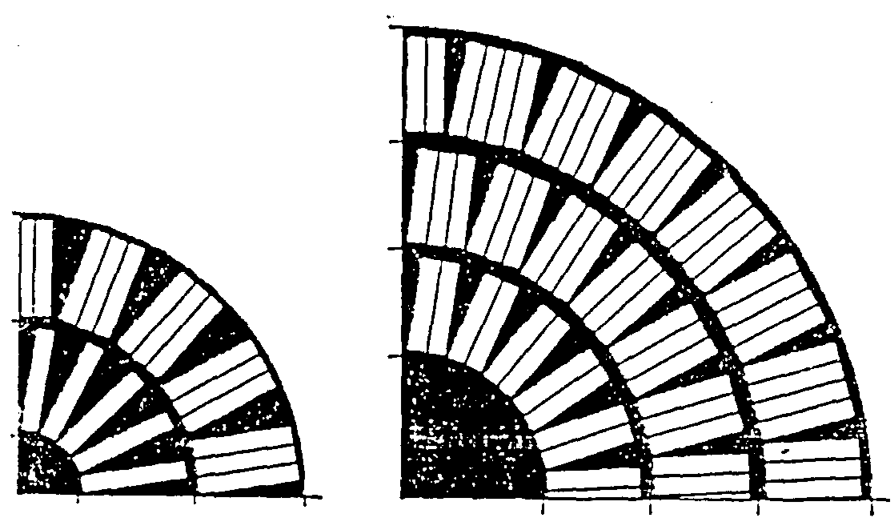

(a) Grootvlei 6 ($s_c = 0.62$) (b) Kendal ($s_c = 0.77$)

Figure 7.3.4: Arrangement of heat exchangers in tower cross-section.

The value of this ratio is generally less in a small tower than in a large tower, as is shown in figure 7.3.4, for respectively the Grootvlei 6 and the Kendal towers.

Based on measured values, the following equation for K_{ct} as defined by equation (7.3.3) is recommended for design purposes where the tower inlet cross-section is not necessarily entirely covered by heat exchanger bundles.

$$K_{ct} = \left[1.05 - 0.01\left(d_i/H_i\right)\right]\left[1.6 - 0.29\left(d_i/H_i\right) + \left(d_i/H_i\right)^2\right]/s_c$$

$$+ \left(0.271 - 0.0115\, K_{he} + 0.000124\, K_{he}^2\right)\left(d_i/H_i\right)\left(1.66 - 6.325\, s_c + 5.625\, s_c^2\right) \tag{7.3.9}$$

for $19 \le K_{he} \le 50$, $0.4 \le s_c \le 1$ and $5 \le d_i/H_i \le 10$.

This equation includes the contraction loss due to the reduction in flow area into the heat exchangers, but does not include the expansion loss thereafter.

For $s_c = 0.4$ and $d_i/H_i = 10$, the flow into the cooling tower becomes unstable and fluctuations in pressure are observed. Equation (7.3.9) can however be applied, since it gives results under these conditions that are conservative.

By rounding off the inlet to the tower, it is possible to reduce the inlet loss coefficient as is shown in figure 7.3.5 [94TE1].

Rounded inlets are potentially most beneficial in the case of counterflow wet-cooling towers where relatively large quantities of water have to be raised to the level of the spray nozzles located above the fill. This requires a significant amount of pumping power which can be reduced by lowering the fill and the corresponding tower inlet height. This leads to greater inlet losses which can however be reduced by rounding off of the inlet edge of the tower shell in which case

$$K_{ct} = 1.5\exp(0.2\, d_i/H_i)\, K_{he}^{\left[-0.4645 + 0.02303\, d_i/H_i - 0.00095\left(d_i/H_i\right)^2\right]} \tag{7.3.10}$$

in the ranges $10 \le (d_i/H_i) \le 15$, $5 \le K_{he} \le 25$ and $r_i/d_i \approx 0.01$. This expression is applied approximately in conjunction with equation (7.3.4) or with equation (7.3.2) for α_{evc} = 1.1.

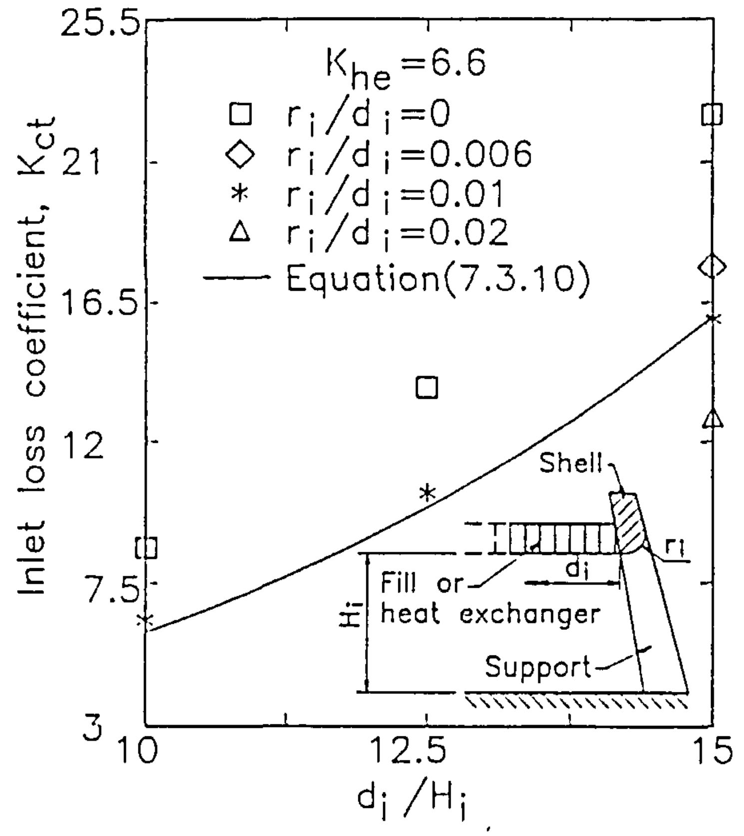

Figure 7.3.5: Loss coefficient with rounded tower inlet.

Vauzanges and Ribier [86VA1] investigated the influence of the shape of the lintel and tower supports on the inlet losses. They conclude that radial elongated support and a rounded lintel are advantageous in wet-cooling towers.

Terblanche and Kröger [94TE1] also studied the aerodynamic inlet losses obtained when the heat exchanger bundles are arranged vertically around the circumference of the tower. A prominent vena contracta, having an approximate kinetic energy coefficient of α_{evc} = 1.15, is formed.

7.4 COLD INFLOW

A natural draft cooling tower contains a mass of slowly moving air that is slightly buoyant relative to the surrounding air. If it were not for the air's upward motion an instability would exist, with cold outside air spilling into the tower at its upper edge. The inflow of cold air into the top of a natural draft cooling tower is not uncommon, especially in wet towers where the air velocity is low [75ER1, 77ER1, 78BA1]. Significant performance degradation is observed under these conditions. Premature flow separation in the tower results in an effective narrowing of the exit flow area of the tower [77RU1, 78MO1, 78MO2]. In a certain range of wind speeds, air inflow may be periodic. Typical flow patterns are shown in figure 7.4.1.

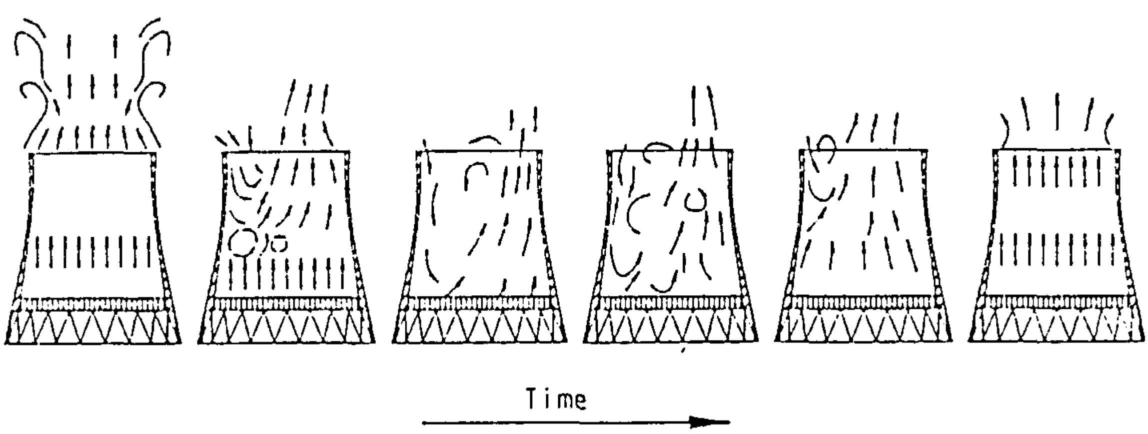

Figure 7.4.1: Periodic cold inflow into cooling tower.

Jörg and Scorer [67JO1] predict experimentally, the critical velocity needed for the onset of cold air inflow. Their test results are limited to relatively low Reynolds numbers and were obtained by using an inverted cylindrical vessel submerged in water. A salt water solution was injected at the top of the vessel and the solution descended to the bottom of the vessel due to a combination of buoyancy and inertia forces. They visualized the inflow of the exterior fluid near the rim using a dye injection technique. The following empirical formula, which relates the buoyancy force, $(\rho_a - \rho)\, g/\rho$, and the eddy stress force, v^2/L_{tb}, is based on their experimental observations.

$$\left(\rho_a - \rho\right) g L_{tb} / \left(\rho v^2\right) = 8\text{x}10^{-4} \tag{7.4.1}$$

L_{tb} is defined as ν/v, a turbulent boundary layer length scale. This length scale was chosen, since it was believed that the length scale of a turbulent shear flow is more important than the dimension of the tower outlet.

Other researchers express their findings in terms of the densimetric Froude number based on the tower outlet diameter i.e.

$$1/Fr_D = (\rho_a - \rho)gd/(\rho v^2) \tag{7.4.2}$$

where ρ_a is the density of the ambient air at the elevation of the tower outlet and ρ is the density of the air leaving the tower.

Lucas and Buchlin [86LU1] studied the problem of cold air inflow into a vertical heated tube. To test equation (7.4.2), measurements were made to determine the dependence of the bulk buoyancy and the velocity v on the inlet loss coefficient for different heat inputs and d/H ratios. As the loss coefficient through the tower increases, the flow tends to become more unstable. These observations are supported by Richter [69RI1] and Buchlin and Olivari [86BU1] who suspected that when $1/Fr_D$ is increased, the plume tends to become increasingly more unstable.

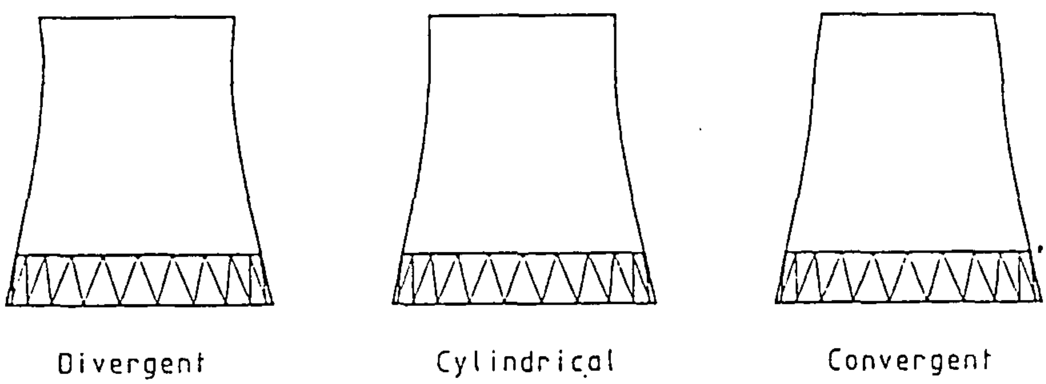

Figure. 7.4.2: Different cooling tower outlet shapes.

According to Richter [69RI1], small disturbances may cause flow instabilities in cooling towers, resulting in cold air inflow for $1/Fr_D$ as defined by equation (7.4.2) of greater than 3.05. This latter value is in fair agreement with a value of 2.8 subsequently proposed by

Moore [81MO1]. Cold inflow is entrained by the plume for $3.05 < 1/Fr_D < 6$ while penetration to the packing or heat exchanger elevation occurs at $1/Fr_D > 7$.

Grange [92GR1] analyzed the flow in a natural draft cooling tower and obtained an expression for the inside shape of the shell which will ensure that cold inflow does not occur in the upper part of the tower. Although it is not essential that the shell should have exactly this shape, it is important that the outlet diameter of the tower, d_o, does not exceed a prescribed value. For a turbulent mixing coefficient of 0.1 find

$$\frac{d_o}{d_i} = \left[1 + \frac{2}{F_{rD}}\left(\frac{d_i}{d_o}\right)^5\left(\frac{H_d}{d_i}\right)\right]^{-0.25} + 0.2\left(\frac{H_d}{d_i}\right) \tag{7.4.3}$$

where d_i is the tower inlet diameter and H_d is the effective draft height.

From this equation it follows that the maximum tower outlet diameter and thus the stability of the natural draft does not only depend on the densimetric Froude number at the outlet of the tower but also on the ratios H_d/d_i and d_i/d_o.

It should be noted that the assumption of a turbulent mixing coefficient of 0.1 in equation (7.4.3) tends to be conservative. Values of mixing coefficients of up to 0.17 are possible and this would increase the coefficient of the second term on the right hand side of equation (7.4.3) to 0.34.

Equation (7.4.3) can be re-written to give the densimetric Froude number in terms of the cooling tower dimensions.

$$Fr_D = 2\left(\frac{d_i}{d_o}\right)^5\left(\frac{H_d}{d_i}\right)\left[\left(\frac{d_o}{d_i} - 0.2\frac{H_d}{d_i}\right)^{-4} - 1\right]^{-1} \tag{7.4.4}$$

The critical densimetric Froude number for a given tower can thus be determined from this equation.

The value of $1/Fr_D$ may be reduced, and the outlet velocity in the boundary layer is accelerated by having a cylindrical or a convergent rather than a divergent tower outlet as shown in figure 7.4.2. Since dynamic losses increase with a reduction in outlet area, convergence should not be excessive.

Based on an approximate analysis, Moore [78MO1] suggests that a ratio of draft height to tower diameter of unity or even less, may be possible without cold inflow occurring, if the upper third of the tower converges slightly and vigorous flow mixing and turbulence is promoted near the wall at the outlet.

Although it has been demonstrated that the problem of cold inflow can be largely overcome in a cooling tower having a converging outlet, model tests suggest that the benefit of this geometry is limited to conditions at low wind speeds only, as shown in figure 7.4.3 [82RU1].

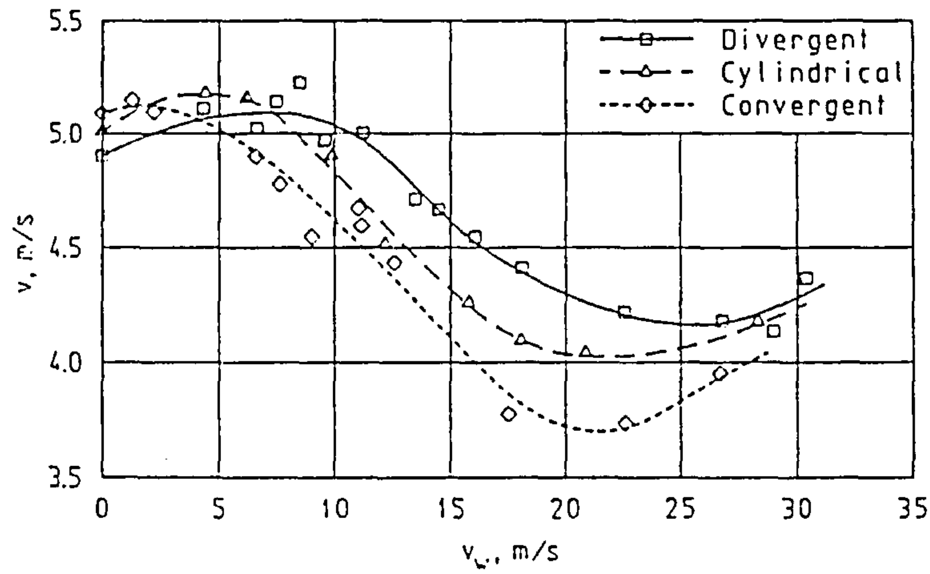

Figure 7.4.3: Air velocity at smallest cross-section in tower as function of wind velocity for different tower outlet shapes.

The flow at the outlet becomes more stable for the other shapes as the wind speed increases. Since the dynamic losses are less than for the converging shape under these conditions, their relative performance is better. The cylindrical shape appears to offer a good cost-effective compromise solution [84TE1].

In some cooling towers an inward projecting reinforcing ring at the outlet of the tower tends to trip the boundary layer and thereby reduces the tendency for cold inflow to occur.

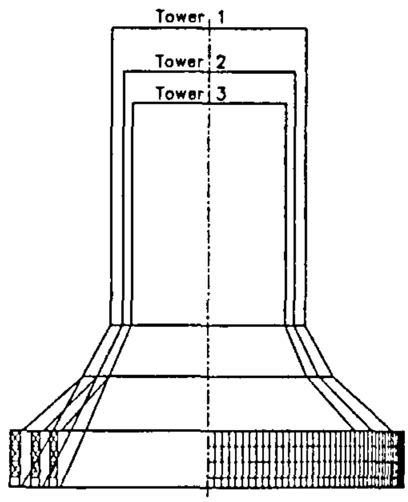

	Tower 1	Tower 2	Tower 3
Inlet temperature difference, $(T_{wi} - T_{ai})$	26°C	29°C	32°C
Tower height	146 m	132 m	122 m
Base diameter	127 m	114 m	103 m
Outlet diameter	62.5 m	59 m	57 m
Number of 15 m high deltas	156	140	126

Figure 7.4.4: Dry cooling tower geometries.

Where the heat exchangers or the fill are located vertically around the base of the tower, the flow pattern inside the tower can be very complex and a more conservative approach compared to the horizontal arrangement should be followed. Existing dry-cooling towers with horizontal fill or heat exchanger arrangements typically have ratios of tower outlet to base diameters of approximately 0.6 while those with vertical arrangements have ratios of 0.5 to 0.55 as shown in figure 7.4.4 [91SZ1] to avoid cold inflow and to minimize flow losses in the tower itself.

7.5 REFERENCES

26ME1 Merkel, F., Verdunstungskühlung, VDI - Zeitschrift, Vol. 70, pp. 123-128, 1926.

52CH1 Chilton, H., Performance of Natural-draught Water Cooling Towers, Proceedings of the Institution of Electrical Engineers, Vol. 99, No. 71, pp. 440-456, 1952.

61JO1 Jorgensen, R., Fan Engineering, Buffalo Forge Co., Buffalo, New York, 1961.

61LO1 Lowe, H.J., and Christie, D.G., Heat Transfer and Pressure Drop Data on Cooling Tower Packings, and Model Studies of the Resistance of Natural Draught Towers to Airflow, Intern. Development in Heat Transfer, Part V, ASME, New York, 1961.

61RI1 Rish, R.F., The Design of a Natural Draught Cooling Tower, Proceedings of the 2nd International Heat Transfer Conference, Colorado, 1961.

67JO1 Jörg, O. and Scorer, R.S., An Experimental Study of Cold Inflow into Chimneys, Atmos. Environment, Vol. 1, p. 645, 1967.

67SI1 Singham, J.R., The Thermal Performance of Natural Draught Cooling Towers: 1) Analysis of Test Data; 2) Design and Optimisation; 3) Prediction of Performance, Imperial College of Science and Technology Report ED/R/1, London, April 1967.

68VO1 Vogelsang, E. and Hackeschmidt, M., Experimentelle Untersuchungen über die Ungleichförmigkeit der Strömung in Verdunstungskühlern, Luft- und Kältetechnik, Vol. 7, pp. 306 - 318, 1968.

69RI1 Richter, E., Untersuchung der Stömungsvorgänge am Austritt von Naturzugkühltürmen und deren Einfluss auf die Kühlwirkung, Dr. Ing. - thesis, TU Dresden, 1969.

71ZE1 Zembaty, W. and Konikowski, T., Untersuchung über den aerodynamischen

Widerstand von Kühltürmen, Brennst. - Wärme-Kraft, No. 10, Vol. 23, pp. 441-445, 1971.

72PO1 Poppe, M., Wärme und Stoffübertragung bei der Verdunstungskühlung in Gegen-und Kreuzstrom, Doctoral thesis, Technische Universität, Hannover, 1972.

72ZI1 Zien, H.B., Problems of Airflow Through Large Natural Draft Cooling Towers, National Science Foundation Paper 72-75, April 1972.

73ME1 Mesarovic, M.M., Ararat - A Computer Code for Thermal Design of Cooling Towers, Nuclear Engineering and Design, Vol. 24, pp. 57-70, North Holland Publ. Co., 1973.

73RO1 Roma, C., An Advanced Dry Cooling System for Water from Large Power Station Condensers, Proc. Am. Power Conf., Vol. 35, p. 626, 1973.

74BU1 Buxmann, J., Berechnung der Kennfelder von Trockenkühlern, Brennstof-Wärme-Kraft, 26, No. 10, pp. 421-428, 1974.

74MO1 Moore, F.K. and Hsieh, T., Concurrent Reduction of Draft Height and Heat-Exchange Area for Large Dry Cooling Towers, Trans, ASME, Jnl. of Heat Transfer pp. 279-285, 1974.

74YA1 Yadigaroglu, G. and Pastor, E.J., An Investigation of the Accuracy of the Merkel Equation for Evaporative Cooling Tower Calculations, ASME Paper 74-HT-59, 1974.

75ER1 Ernst, G., Cooling Towers, Design and Plume Behaviour, Seminar of ICHMT, Dubrovnik, 1975.

75MO1 Moore, F.K., Analysis of Large Dry Cooling Towers with Spine-Fin Heat Exchange Performance, Trans. ASME, Jnl. of Heat Transfer, pp. 345-352, 1976.

75NA1 Nahavandi, N., Kershah, R.M. and Serico, B.J., The Effect of Evaporation Losses in the Analysis of Counterflow Cooling Towers, Nuclear Engineering and Design, Vol. 32, pp. 29-36, North Holland Publ. Co., 1975.

76KE1 Kelly, N.W., Kelly's Handbook of Crossflow Cooling Tower Performance, N.W. Kelly and Associates, Kansas City, MO, 1976.

76MO1 Moore, F.K., Analysis of Large Dry Cooling Towers with Power-law Heat Exchange Performance, Trans. ASME, Jnl. of Heat Transfer, pp. 345-352, 1976.

76MO2 Moore, F.K. Dry Cooling Towers, in Advances in Heat Transfer, Vol. 12, ed. Irvine, T.F. and Hartnett, J.P., Academic Press, 1976.

77ER1 Ernst, G. and Wurz D., Untersuchung zur Schwadenströmung in den Kronen von Naturzugkühltürmen, VDI Kühlturmseminar, Düsseldorf, 1977.

77MA1 Markóczy and Stämpfli, E., Experimentelle Untersuchung des Einflusses atmosphärischer Umgebungsbedingungen auf das Betriebsverhalten von Naturzug-Trockenkühltürmen, EIR-Bericht, No. 324, Würenlingen, Switzerland, 1977.

77NA1 Nahavandi, A.M. and Oellinger, J.J., An Improved Model for the Analysis of Evaporative Counterflow Cooling Towers, Nuclear Engineering and Design, Vol. 40, North Holland Publ. Co., 1977.

77NI1 Niemann, H.J., Ein Windlastkonzept für Naturzug Kühltürme, Techn. Mitteilungen 70, pp. 493-499, 1977.

77RU1 Rühl, H., Convergent Configuration of the Top of Larger Cooling Towers Together with an Upward Spray Water Distribution, VGB Congress, Copenhagen, 1977.

78BA1 Baer, E., Einfluss des Windes Auf die Strömung im Kamin eines Naturzugkühlturmes, D. Ing.-thesis, Universität Karlsruhe, 1978.

78BO1 Bouton, F., Design Studies for Natural Draught Dry Towers, SHF Conference, Paris, 1978.

78MO1 Moore, F.K., Cold Inflow and its Implications for Dry Tower Design, 2nd Conf. on Waste Heat Management and Utilization, Miami, 1978.

78MO2 Moore, F.K. Effects of Aerodynamic Losses on the Performance of Large Dry Cooling Towers, ASME Paper 78-WA/HT-18, WAM 1978.

78SH1 Shah, R.K., Afimiwala, K.A. and Mayne, R.W., Heat Exchanger Optimization, Heat Transfer 1978, Vol. 4, pp. 193-199, Hemisphere Publishing Corporation, Washington, 1978.

79HE1 Herberholz, P. and Schulz, S., The Influence of Atmospheric Precipitation on the Operation of a Natural Draught Indirect-contact Cooling Tower, Ger. Chem Eng., Vol. 2, No. 1, pp. 352-360, 1979.

80MO1 Montakhab, A., Waste Heat Disposal to Air with Mechanical and Natural Draft-Some Analytical Design Considerations, ASME Paper No. 78-WA/HT-17, 1978 and Jnl. of Eng. for Power, Vol. 102, No. 3, pp. 719-727, July 1980.

80MO2 Montakhab, A., Analysis of Heat Transfer Surface Geometries for Dry Cooling Tower Applications, Trans. of the ASME, Journal of Engineering for Power, Vol. 102, No. 4, pp. 807-812, October 1980.

81BU1 Buxmann, J. and Völler, G., Die Bedeutung des Eintrittsdruck-verlustes beim Naturzug-Trockenkühlturm, Brennst-Wärme-Kraft, No. 7/8, Vol. 33, pp. 313-316, 1981.

81GA1 Garde, M.A., Experimental Evaluations of Entrance Losses of Flared Natural Draft Cooling Towers, M.S. Thesis, Cornell University, 1981.

81MO1 Moore, F.K. and Garde, M.A., Aerodynamic Losses of Highly Flared Natural Draft Cooling Towers, 3rd Waste Heat Management and Utilization

Conference, Miami, 1981.

82RU1 Ruscheweyh, H., Modelluntersuchung zum Einfluss der Kühlturm-kronenform auf das Zugverhalten grosser Naturzugkühltürme unter Querwindeinfluss, Brennst - Wärme - Kraft, Vol. 34, No. 7, pp. 361-369, 1982.

83BO1 Bourillot, C., TEFERI, Numerical Model for Calculating the Performance of an Evaporative Cooling Tower, EPRI Report CS-3212-SR, August 1983.

83HE1 Hempel, D.C., Stephan, K. and Hesse, G., Strömungswiderstand, Geschwindigkeitsverteilung und Optimale Höhe für den Lufteintritt in Naturzug-Kühltürmen, Brennst.-Wärme-Kraft, No. 11, Vol. 35, pp.470-477, 1983.

83MA1 Majumdar, A.K., and Singhal, A.K., VERA2D: Program for 2-D Analysis of Flow, Heat, and Mass Transfer in Evaporative Cooling Towers, EPRI Report CS-2923, March 1983.

83MA2 Majumdar, A.K., Singhal, A.K. and Spalding, D.B., Numerical Modelling of Wet Cooling Towers, Trans. ASME Journal of Heat Transfer, Vol. 105, pp. 728-743, November 1983.

83SU1 Sutherland, J.W., Analysis of Mechanical-draught Counterflow Air/water Cooling Towers, Trans. of the ASME, J. Heat Transfer, Vol. 105, August 1983.

83WI1 Witte, R., Das Betriebsverhalten atmosphärisch beeinflusster Trockenkühltürme, Fortschr. -Ber VDI-Z, Reihe 6, No. 132, VDI-Verlag, Düsseldorf, 1983.

84AL1 Alomwooja, K.T., Gould, P.L. and Furzer, I., Optimization of Large Cooling Towers, Proc. 2nd Int Symp. on Natural Draught Cooling Towers, Ruhr-Universität, pp. 413 - 429, Bochum, Germany, September 1984.

84BE1 Becker, N., Druckverlust und Wärmeübertragung von Rippenrohrbündeln für Naturzug - trockenkühltürme, D.Ing. thesis, R-W Technische Hochschule Aachen, 1984.

84KR1 Krings, W., Economical Calculation for the Optimal Design of General Shells of Revolution for Natural Draft Cooling Towers by means of Membrane Theory, Proc. 2nd Int. Symp. on Natural Draught Cooling Towers, Ruhr-Universität, pp. 440 - 455, Bochum, Germany, September 1984.

84TE1 Tesche, W., Untersuchungen zur optimalen Schalenkontur grosser Naturzugkühltürme, VGB Kraftwerkstechnik, Vol. 9, No. 64, pp. 825-829, 1984.

85DU1 Du Plessis, J.P., Collins, M.R. and Kröger, D.G., Numerical Modelling of Air Flow in Confined Tapered Duct Inlets, Proc. 11th IMACS World Congress on System Simulation and Scientific Computation, Vol. 1, 1985.

85MA1 Majumdar, A.K., Singhal, A.K. and Mukerjee, T., VERA2D-84: A Computer Program for Two-dimensional Analysis of Flow, Heat and Mass Transfer in Evaporative Cooling Towers, EPRI Report CS-4073, Volume 1 and 2, 1985.

86BU1 Buxmann, J., Betriebsverhalten eines Naturzug - Trockenkühlturms bei windeinfluss, BWK, Vol. 38, No. 7/8, pp. 335-339, July/Aug. 1986.

86BU2 Buxmann, J., Dry Cooling Tower Characteristics Effected by the Cooling Circuit and the Top Shape of the Tower, Paper presented at the 5th IAHR Cooling Tower Workshop, Monterey, 1986.

86GE1 Geldenhuys, J.D. and Kröger, D.G., Aerodynamic Inlet Losses in Natural Draft Cooling Towers, Proc., 5th IAHR Cooling Tower Workshop, Monterey, 1986.

86LU1 Lucas, M.J. and Buchlin, J.M., A Study of Cold Air Inflow into a Vertical Heated Tube, Paper presented at the 5th IAHR Cooling Tower Workshop, Monteray 1986.

86VA1 Vauzanges, M. and Ribier, G., Variation of the Head Losses in the Air Inlets of Natural Draft Cooling Towers with the shape of the Lintel and Shell Supports, Proc. 5th IAHR Cooling Tower Workshop, Monterey, U.S.A., 1986.

87CA1 Caytan, Y., Numerical Simulation of the Operation of Natural Draft Cooling Towers, 5th International Conference on Numerical Methods in Thermal Problems, Montreal, June 1987.

88BR1 British Standards Institution, Water Cooling Towers : Part 2. Methods for Performance Testing, BS 4485, 1988.

88DU1 Du Preez, F. and Kröger, D.G., Experimental Evaluation of Aerodynamic Inlet Losses in Natural Draft Cooling Towers, Proc. 6th IAHR Cooling Tower Workshop, Pisa, Italy, 1988.

88RA1 Radosavljevic, D. and Spalding, D.B., Simultaneous Prediction of Internal and External Aerodynamic and Thermal Flow Fields of a Natural Draft Cooling Tower in a Cross-wind, 6th IAHR Cooling Tower Workshop, Pisa, Italy, 1988.

88VE1 Vereinigung der Grosskaftwerksbetreiber E.V., VGB - Empfehlung über den Winterbetrieb von Kraftwerks-Nasskühltürmen, VGB-R 129P, Essen, 1988.

89DE1 Deutsche Norm, DIN 1947, Wärmetechnische Abnahmemessungen an Nasskühltürmen (VDI - Kühlturmregeln), Berlin, Germany, 1989.

90GR1 Grange, J.L., A Computer Code for Particular Operating Conditions of Wet Cooling Towers, 7th IAHR Cooling Tower and Spraying Pond Symposium, Leningrad, 1990.

91PO1 Poppe, M. and Rögener, H., Berechnung von Rückkühlwerken, VDI - Wärmeatlas, pp. Mi1 - Mi15, VDI - Verlag Düsseldorf, 1991.

91SZ1 Szabó, Z., Why Use the "Heller System"? Circuitry Characteristics and Special Features, EGI - Contracting and Engineering, Hungary, March, 1991.

92GR1 Grange, J.L., The Shape of Natural Draft Cooling Towers, Paper presented at the 8th IAHR Cooling Tower and Spraying Pond Symposium, Karlsruhe, Germany, October 1992.

94DU1 Du Preez, A.F. and Kröger D.G., The Influence of a Buoyant Plume on the Performance of a Natural Draft Cooling Tower, 9th IAHR Cooling Tower and Spraying Pond Symposium, Brussels, 1994.

94GR1 Grange, J.L., Calculating the Evaporated Water Flow in a Wet Cooling Tower, Paper presented at the 9th IAHR Cooling Tower and Spraying Pond Symposium, von Karman Institute, Brussels, Belgium, September 1994.

94LE1 Lees, U.A. and Cooper, J.W., "Cost Effective" Thermal Performance Upgrade of the Callaway Plant Cooling Tower, Paper presented at the EPRI Cooling Towers and Advanced Cooling Systems Conference, St. Petersburg Beach, Florida, August 1994.

94LI1 Liu, B.M., Numerical Prediction for the Performance of a Natural-draft Cooling Tower with Comparison to the Field Test Data, Proc. of the 10th International Heat Transfer Conference, Vol. 7, pp. 309-314, Brighton, UK, 1994.

94TE1 Terblanche, J.E. and Kröger, D.G., Experimental Evaluation of the Aerodynamic Inlet Losses in Cooling Towers, South African Inst. of Mech. Engs. R & D Journal, Vol. 10, No. 2, pp.41-44, 1994.

CHAPTER 8

AIR-COOLED HEAT EXCHANGERS

8.0 INTRODUCTION

Many different types of mechanical draft air-cooled heat exchangers are found in a wide spectrum of industries. Some examples are shown in section 1.2.1. Air may either be blown, or drawn through the heat exchanger by means of a fan. The former configuration is referred to as a forced draft system while the latter is referred to as an induced draft system. Notwithstanding the poor cooling properties of air, it is available in unlimited quantities throughout the year. No costs are incurred for its procurement and there is no disposal problem or significant impact on the environment.

Operating temperatures, fan accessibility, process specifications, ambient conditions and other practical considerations will to a large extent influence the ultimate system design. To design small air-cooled heat exchangers or to evaluate the performance characteristics of a particular unit, relatively simple but approximate methods may be adequate [70RU1, 78BR1, 79ZA1, 83PA1, 83SH1, 92MC1]. The same applies to test methods usually employed [73RO1, 78AM1, 91AS1]. Such an approach is however less acceptable in the case of large specialized and expensive systems.

8.1.1 AIR-COOLED HEAT EXCHANGER

Air-cooled heat exchangers found in the refinery and petro-chemical plants may consist of bundles that are made up of headers (2 m to 3 m wide), finned tubes (8 m to 12 m long) and frames. The majority of finned tubes are composed of tubes ranging from 19 mm in diameter to 51 mm in diameter. The fins usually range from 300 to 450 fins/m. The fin heights range from 6 mm to 19 mm. Approximately 80 percent of the tubes have an outside diameter of 25.4 mm and have 350 - 450 fins/m of 16 mm fin height. More than 90 percent of the fins are made of aluminum and the remainder may be either copper, steel, stainless steel and galvanized steel. Type-L and type-G fins find most application. The number of rows of finned tubes usually ranges from 3 to 6 rows. One or more tube bundle served by two or more fans complete with structure plenum and other attendant equipment make up a typical bay [83SH2]. Fans normally range from 1.8 m to 4.1 m in diameter and may have from 3 to 6 blades. However, four to six blades are most common. A large heat exchanger may consist of a bank of many such bays. Other practical aspects of such heat exchangers that are required to provide purchase specifications to facilitate the procurement and manufacture of air-cooled heat exchangers for refinery service are presented in the American Petroleum Institute Standard 661 [78API] and complementary specifications [73RO1].

The Air-cooled Heat Exchanger Manufacturer Association (ACHEMA) recommends a standard to assist those who specify, design, purchase, install and maintain air-cooled heat exchangers in obtaining the necessary information for their proper and safe selection and application [86AC1].

Consider the example of a forced draft air-cooled heat exchanger unit as shown schematically in figure 8.1.1.

The heat exchanger consists of bundles of finned tubes located horizontally above the fans. A hot process fluid enters the tubes at a temperature T_{pi}, while cooler ambient air flows across the finned surfaces. A windwall of height, H_w, may be installed to reduce recirculation of hot plume air.

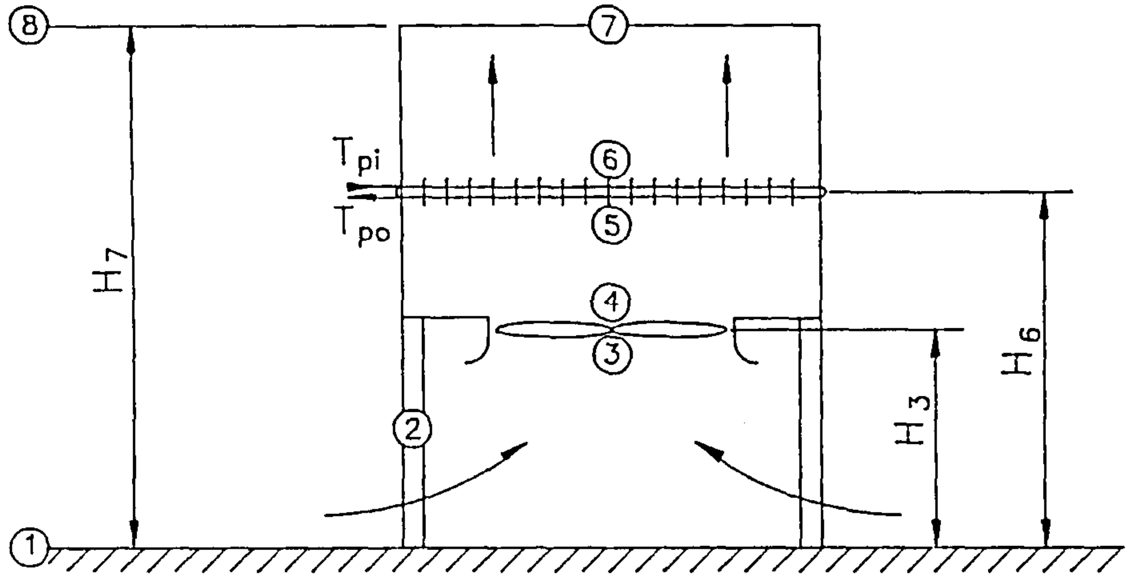

Figure 8.1.1: Forced draft air-cooled heat exchanger.

The amount of heat that is transferred to the air stream from the process fluid can be expressed as

$$Q = m_a c_{pa} (T_{a6} - T_{a5}) = m_p c_{pp} (T_{pi} - T_{po}) \tag{8.1.1}$$

where the subscript, p, refers to the process fluid.

The heat transfer rate is also given by equation (3.5.16) or it may be expressed in terms of the effectiveness of the heat exchanger i.e.

$$Q = e m_a c_{pa} (T_{pi} - T_{ai}) \tag{8.1.2}$$

where the effectiveness, e, depends on the geometry and flow pattern of the process fluid through the heat exchanger. For an air-cooled condenser, the effectiveness is given by equation 3.5.22, while the values for single pass cross-flow heat exchangers are listed in table 3.5.1. For an air-cooled heat exchanger having four or more tube passes in counterflow, the effectiveness for double pipe counterflow may be employed. If there are two tube passes in counterflow to the air stream then [83PA1]

$$e = \left[1 - \left\{1 + (1 - (1 - \exp N/2)/2)(\exp 2C(1 - \exp N/2) - 1)\right\}^{-1}\right]/C \tag{8.1.3}$$

where $N = UA/C_{min}$ and $C = C_{min}/C_{max}$.

Furthermore, the effectiveness will be influenced by the upstream turbulence of the air and the maldistribution of the fluids. In many practical systems enhancement of heat transfer due to upstream turbulence is approximately cancelled by maldistribution of the air flow through the heat exchanger.

Upon substitution of equation (1.4.7) into equation (1.4.2) and applying the latter between sections 1 and 5, find the approximate inlet air temperature to the heat exchanger.

$$\begin{aligned} T_{a5} &= T_{a1} + P_F/(m_a c_{pa1}) - gH_5/c_{pa1} \\ &= T_{a1} + P_F/(m_a c_{pa1}) - 0.00975H_5 \end{aligned} \tag{8.1.4}$$

where $H_5 \approx H_6$ is the mean heat exchanger height above ground level.

In practice the draft equation for an air-cooled heat exchanger is sometimes obtained by simply matching the fan performance curve and the flow characteristics through the heat exchanger bundles only, and evaluating the thermophysical properties of the air at ambient ground level conditions. Although this may give useful approximate values in some cases, serious errors have been incurred in other designs. Increasing competitiveness and high system costs generally justify the more detailed analysis which follows.

The choice of a suitable fan must be such that it will efficiently deliver a cooling air flow rate that will guarantee the desired heat transfer rate. In order to achieve this a series of flow resistances must be overcome.

Stagnant ambient air at 1 accelerates and flows across the heat exchanger supports at 2 before reaching the fan at section 3, where upstream obstacles such as structural supports or a screen may be located. After leaving the fan at 4 where further downstream obstacles may be located, the flow experiences losses in the plenum before entering the heat exchanger bundle at 5 and exiting at 6.

Apply the relevant isentropic relations given in equation (1.4.22) and equation (2.3.2) across the consecutive flow resistances as was done in the case of a cooling tower, to find upon addition, an expression for the pressure difference between sections 1 and 7.

$$\begin{aligned} p_{a1} - p_{a7} = {} & p_{a1}\left[1 - (1 - 0.00975\ H_6/T_{a1})^{3.5}\right] + K_{ts}(m_a/A_2)^2/(2\rho_{a2}) \\ & + K_{up}(m_a/A_3)^2/(2\rho_{a3}) - \rho_{a3}P_F/m_a + K_{pl}(m_a/A_c)^2/(2\rho_{a4}) \\ & + K_{do}(m_a/A_4)^2/(2\rho_{a4}) + K_{he}(m_a/A_{fr})^2/(2\rho_{a56}) \\ & + p_{a6}\left[1 - (1 - 0.00975(H_7 - H_6)/T_{a6})^{3.5}\right] + \alpha_{e7}(m_a/A_{fr})^2/(2\rho_{a7}) \end{aligned} \tag{8.1.5}$$

where the velocity has been replaced by the air mass flow rate and the corresponding flow area.

According to equation (7.1.13) the loss coefficient due to the heat exchanger supports can be expressed as

$$K_{ts} = C_{Dts}\ L_{ts}\ d_{ts}\ n_{ts}/A_2 \tag{8.1.6}$$

Details for evaluating the upstream and downstream loss coefficients, K_{up} and K_{do} respectively, are given in section 6.4. It should be noted that these loss coefficients are based on the area $A_3 = A_4 = A_e = A_c - A_h$ where A_c and A_h are the fan casing and hub cross-sectional areas respectively.

Fan performance characteristics incorporated in the $\rho_{a3} P_F/m_a$ term are obtained from standard installation tests. Not one of these installations is however truly representative of the air-cooled heat exchanger configuration shown in figure 8.1.1. Fan performance tests conducted on air-cooled heat exchanger systems, suggest that most of the kinetic energy at the outlet of the fan, when tested in an installation of type A, is lost in the plenum region. According to section 6.4, $K_{pl} \approx 0.75\ \alpha_{eF} \approx 0.75 \times 1.75 = 1.3125$ for a particular air-cooled system. It is thus convenient to combine the fan and the plenum characteristics as follows:

$$-\rho_{a3}P_F/m_a + K_{pl}(m_a/A_c)^2/(2\rho_{a4}) \approx -\left[K_{Fs} + (\alpha_{eF} - K_{pl})\right](m_a/A_c)^2/(2\rho_{a3})$$

(8.1.7)

where a fan static pressure rise coefficient is defined as

$$K_{Fs} = 2\Delta p_{Fs}\,\rho_{a3}/(m_a/A_c)^2 = 2P_F\rho_{a3}^2A_c^2/m_a^3 \tag{8.1.8}$$

A_c is the fan casing cross-sectional area and the fan static pressure, Δp_{Fs}, is obtained from tests conducted in an installation of type A.

The heat exchanger loss coefficient, K_{he}, as expressed in equations (5.4.22) and (5.4.23), is obtained experimentally or can be determined approximately with the aid of empirical equations as for instance given in section 5.5.2 for round tubes. The kinetic energy coefficient at the outlet of the heat exchanger, α_{e7}, must also be determined experimentally for a particular air-cooled system (according to section 6.4 a practical value is $\alpha_{e6} \approx \alpha_{e7} \approx 1.13$).

If the ambient air far from the heat exchanger is dry and the temperature distribution is according to the DALR, the difference in pressure between 1 and 8 follows from equation (10.1.9b)

$$\begin{aligned}(p_{a1} - p_{a8}) &= (p_{a1} - p_{a7}) = (p_{a1} - p_{a6}) + (p_{a6} - p_{a7})\\ &\approx p_{a1}\left[1 - (1 - 0.00975\ H_6/T_{a1})^{3.5}\right]\\ &+ p_{a6}\left[1 - \left\{1 - 0.00975\left(H_8 - H_6\right)/T_{a1}\right\}^{3.5}\right]\end{aligned} \tag{8.1.9}$$

where the ambient air temperature at elevation 6 is assumed to be approximately equal to T_{a1}. Although the air temperature distribution near ground level generally deviates considerably from the DALR, the error introduced by this assumption in equation (8.1.9) is small for large units.

Substitute equation (8.1.9) into equation (8.1.5) and find with equation (8.1.7) the draft equation for the forced draft air-cooled heat exchanger shown in figure 8.1.1.

$$
\begin{aligned}
p_{a6} & \left[\{1 - 0.00975(H_7 - H_6)/T_{a6}\}^{3.5} - \{1 - 0.00975(H_8 - H_6)T_{a1}\}^{3.5}\right] \\
& \approx p_{a1}\left[\{1 - 0.00975(H_7 - H_6)/T_{a6}\}^{3.5} - \{1 - 0.00975(H_7 - H_6)/T_{a1}\}^{3.5}\right] \\
& = K_{ts}(m_a/A_2)^2/(2\rho_{a1}) + K_{up}(m_a/A_e)^2/(2\rho_{a3}) \\
& + (K_{pl} - K_{Fs} - \alpha_{eF})(m_a/A_c)^2/(2\rho_{a3}) + K_{do}(m_a/A_e)^2/(2\rho_{a3}) \\
& + K_{he}(m_a/A_{fr})^2/(2\rho_{a56}) + \alpha_{e6}(m_a/A_{fr}^2/(2\rho_{a6})
\end{aligned}
\tag{8.1.10}
$$

where it is assumed that $p_{a6} \approx p_{a1}$ on the left hand side of equation (8.1.10) and $H_8 = H_7$ and $\rho_{a2} \approx \rho_{a1}$, $\rho_{a4} \approx \rho_{a3}$, $\rho_{a7} \approx \rho_{a6}$.

For a DALR the approximate air temperature at section 3 is according to equation (10.1.7b).

$$T_{a3} \approx T_{a1} - 0.00975H_3 \tag{8.1.11}$$

The corresponding approximate density of the air at this elevation is

$$\rho_{a3} \approx p_{a1}/(RT_{a3}) \tag{8.1.12}$$

The approximate density of the air immediately after the heat exchanger is

$$\rho_{a6} \approx p_{a1}/(RT_{a6}) \tag{8.1.13}$$

while the harmonic mean density through the heat exchanger is given by

$$\rho_{a56} \approx 2p_{a1}/\left[R(T_{a5} + T_{a6})\right] \tag{8.1.14}$$

In the above equations the thermophysical properties for dry air are usually employed since the influence of moisture is negligible.

Although the terms on the left hand side of equation (8.1.10) are often relatively small, they may become important where the system operates at low fan speeds or in a natural convection mode and with windwalls.

By following the above procedure the energy and draft equations can be deduced for an induced draft air-cooled heat exchanger fitted with a diffusor as shown in figure 8.1.2.

The heat transfer rate is

$$Q = m_a c_{pa}(T_{a4} - T_{a3}) = m_p c_{pp}(T_{pi} - T_{po}) \tag{8.1.15}$$

or

$$Q = e m_a c_{pa}(T_{pi} - T_{ai}) \tag{8.1.16}$$

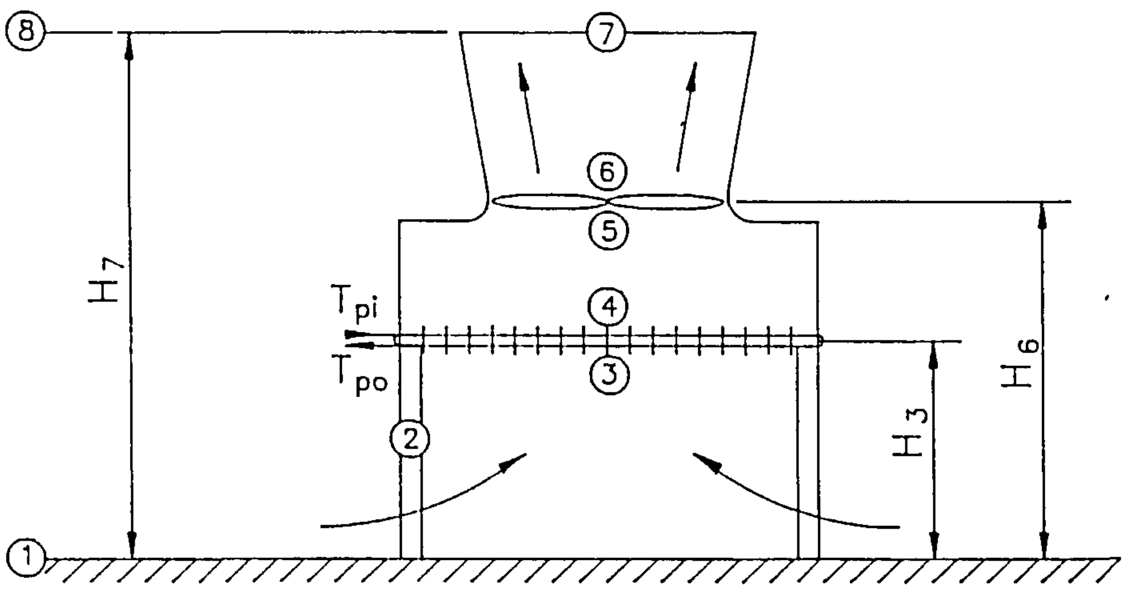

Figure 8.1.2: Induced draft air-cooled heat exchanger.

where

$$T_{a3} = T_{a1} - 0.00975 H_3 \tag{8.1.16}$$

In an induced draft heat exchanger the air flow through the heat exchanger is usually relatively uniform and upstream turbulence is low.

The draft equation is given by

$$\rho_{a1}\left[\left\{1 - 0.00975(H_7 - H_4)/T_{a4}\right\}^{3.5} - \left\{1 - 0.00975(H_7 - H_4)/T_{a1}\right\}^{3.5}\right]$$

$$= K_{ts}(m_a/A_2)^2/(2\rho_{a1}) + K_{he}(m_a/A_{fr})^2/(2\rho_{a34}) + K_{pl}(m_a/A_c)^2/(2\rho_{a4})$$

$$+ K_{up}(m_a/A_e)^2/(2\rho_{a4}) - (K_{Fs} + \alpha_{eF})(m_a/A_c)^2/(2\rho_{a4})$$

$$+ K_{do}(m_a/A_e)^2/(2\rho_{a4}) + K_{dif}(m_a/A_c)^2/(2\rho_{a4}) + \alpha_{e7}(m_a/A_7)^2/(2\rho_{a4})$$

$$= K_{ts}(m_a/A_2)^2/(2\rho_{a1}) + K_{he}(m_a/A_{fr})^2/(2\rho_{a34}) + K_{pl}(m_a/A_c)^2/(2\rho_{a4})$$

$$+ K_{up}(m_a/A_e)^2/2\rho_{a4}) - (K_{Fs})(m_a/A_c)^2/(2\rho_{a4}) + K_{do}(m_a/A_e)^2/(2\rho_{a4})$$

$$+ K_{dif}(m_a/A_c)^2/(2\rho_{a4}) + \alpha_{eF}(1/A_7^2 - 1/A_c^2)m_a^2/(2\rho_{a4}) \tag{8.1.18}$$

where K_{dif} is the diffusor loss coefficient and $H_8 = H_7$. It is furthermore assumed that $\rho_{a2} \approx \rho_{a1}$, $\rho_{a7} \approx \rho_{a6} \approx \rho_{a5} \approx \rho_{a4}$ and for a short diffusor $\alpha_{e7} \approx \alpha_{eF}$. Furthermore $H_4 \approx H_3$.

Also

$$\rho_{a3} \approx p_1/(RT_{a3}) \tag{8.1.19}$$

and

$$\rho_{a34} \approx 2p_{a1}/\left[R(T_{a3} + T_{a4})\right] \tag{8.1.20}$$

When the fans which move the air across the tube bank are shut off, the heat exchanger will operate in a natural convection heat transfer mode. The heat exchanger structure including the tube bundles plenum chamber and diffusor or stack will cause some draft, resulting in a corresponding amount of cooling. The weak draft is however very sensitive to even the lightest winds.

8.1.2 AIR-COOLED CONDENSER

Air-cooled steam condensers in power plants usually consist of arrays of A-frame heat exchanger units.

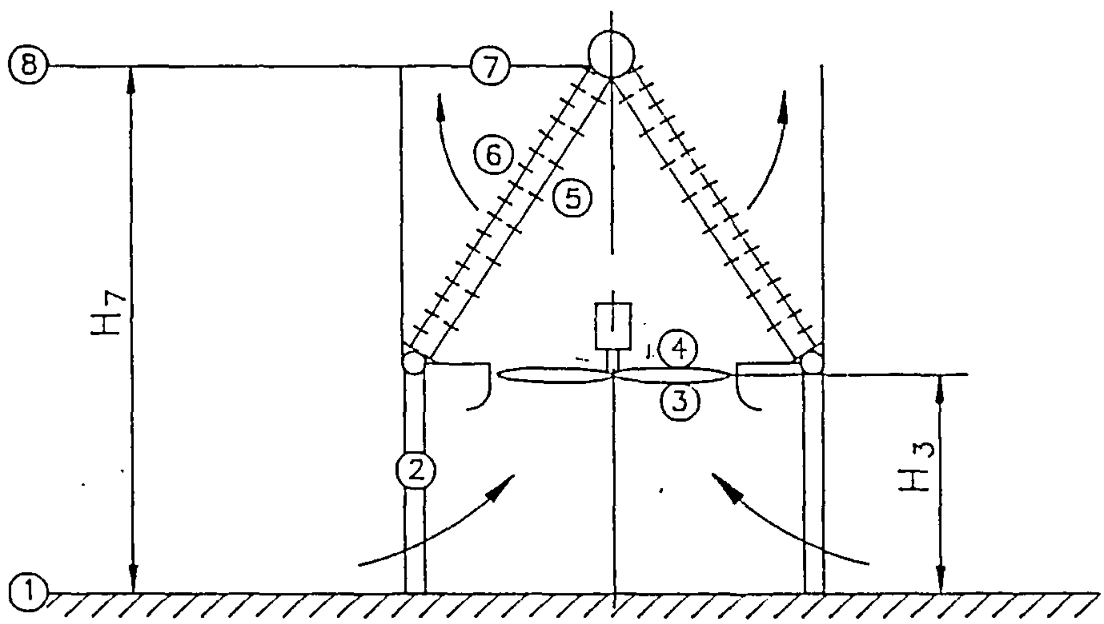

Figure 8.1.3: Air-cooled condenser unit.

Consider the example of a forced draft air-cooled steam condenser as shown schematically in figure 8.1.3. In this configuration the heat exchanger is arranged in the form of a delta or A-frame to drain condensate effectively, reduce distribution steam duct lengths and to minimize the required ground surface area. A windwall is provided to reduce recirculation of the hot plume air.

The heat transfer characteristics of the air-cooled condenser can be expressed as

$$Q = m_a c_{pa}(T_{a6} - T_{a5}) = m_c i_{fg} \tag{8.1.21}$$

where m_c is the condensate mass flow rate and i_{fg} is the latent heat. The temperature T_{a5} is given by equation (8.1.3). Subcooling of the condensate is neglected in the above relation.

In a practical air-cooled condenser the fin pitch may change in consecutive tube rows. If the performance data is available for individual finned tube rows, the energy equation is written as

$$Q = \sum_n m_a c_{pa}(T_{ao(n)} - T_{ai(n)}) = m_c i_{fg} \tag{8.1.22}$$

Furthermore the effectiveness of the condenser bundle or each tube row is according to equation (3.5.22)

$$e = 1 - \exp\left[-UA/(m_a c_{pa})\right] \tag{8.1.23}$$

With this expression the heat transfer rate becomes

$$Q = e m_a c_{pa} (T_s - T_{a1}) \tag{8.1.24}$$

The draft equation is deduced as for the air-cooled heat exchanger described in section 8.1.1, but taking into consideration additional losses as described by Kröger [94KR1]. Due to the inclined flow approaching and leaving the bundles, additional flow losses do however occur as described in section 4.6.

Taking into consideration all flow losses through the heat exchanger find the difference in pressure between 1 and 7.

$$\begin{aligned} p_{a1} - p_{a7} = {} & p_{a1}\left[1 - (1 - 0.00975\ H_6/T_{a1})^{3.5}\right] + K_{ts}(m_a/A_2)^2/(2\rho_{a2}) \\ & + K_{up}(m_a/A_e)^2/(2\rho_{a3}) - \rho_{a3} P_F/m_a + K_{do}(m_a/A_e)^2/(2\rho_{a4}) \\ & + K_{pl}(m_a/A_c)^2/(2\rho_{a4}) + K_{\theta t}(m_a/A_{fr})^2/(2\rho_{a56}) \\ & + p_{a6}\left[1 - \left\{1 - 0.00975(H_7 - H_6)/T_{a6}\right\}^{3.5}\right] \end{aligned} \tag{8.1.25}$$

where $K_{\theta t}$ as given by equation (5.6.19) includes losses across the heat exchanger and kinetic energy losses at the outlet elevation 7.

For this configuration $K_{pl} = \alpha_{eF}$, and it thus follows from equation (8.1.7) that

$$- \rho_{a3} P_F/m_a + K_{pl}(m_a/A_c)^2/(2\rho_{a4}) \approx - K_{Fs}(m_a/A_c)^2/(2\rho_{a3}) \tag{8.1.26}$$

For a DALR far from the heat exchanger the pressure difference between 1 and 8 is given by equation (8.1.8).

Substitute equation (8.1.9) into equation (8.1.24) and find with equation (8.1.25) the draft equation for the air-cooled condenser shown in figure 8.1.3

$$\begin{aligned} &\rho_{a1}\left[\left\{1 - 0.00975(H_7 - H_6)/T_{a6}\right\}^{3.5} - \left\{1 - 0.00975(H_7 - H_6)/T_{a1}\right\}^{3.5}\right] \\ &= K_{ts}(m_a/A_2)^2/(2\rho_{a1}) + K_{up}(m_a/A_e)^2/(2\rho_{a3}) - K_{Fs}(m_a/A_c)^2/(2\rho_{a3}) \\ &+ K_{do}(m_a/A_e)^2/(2\rho_{a3}) + K_{\theta t}(m_a/A_{fr})^2/(2\rho_{a56}) \end{aligned} \tag{8.1.27}$$

where $K_{\theta t}$ as given by equation (4.6.19) includes losses across the heat exchanger and kinetic energy losses at the outlet elevation 7 where $H_8 = H_7$. It is also assumed that $\rho_{a2} \approx \rho_{a1}$, $\rho_{a4} \approx \rho_{a3}$ and $\rho_{a7} \approx \rho_{a6}$.

The values of T_{a3}, ρ_{a3}, ρ_{a6} and ρ_{a56} are determined according to equations (8.1.11), (8.1.12), (8.1.13) and (8.1.14) respectively.

8.2 NONCONDENSABLES

The effectiveness of an air-cooled vapor condenser is reduced if noncondensable gases are present during the condensation process. In the case of steam condensers, atmospheric air leaking into the low pressure portion of the steam cycle equipment and gases resulting from chemicals used for boiler feedwater treatment will tend to accumulate in the condenser. Trapped noncondensables reduce performance, promote metal corrosion and cause freezing of the condensate in winter.

Figure 8.2.1 illustrates in more detail the trapping of noncondensables in a simple steam condenser, having just two rows of tubes and nondivided manifolds or headers.

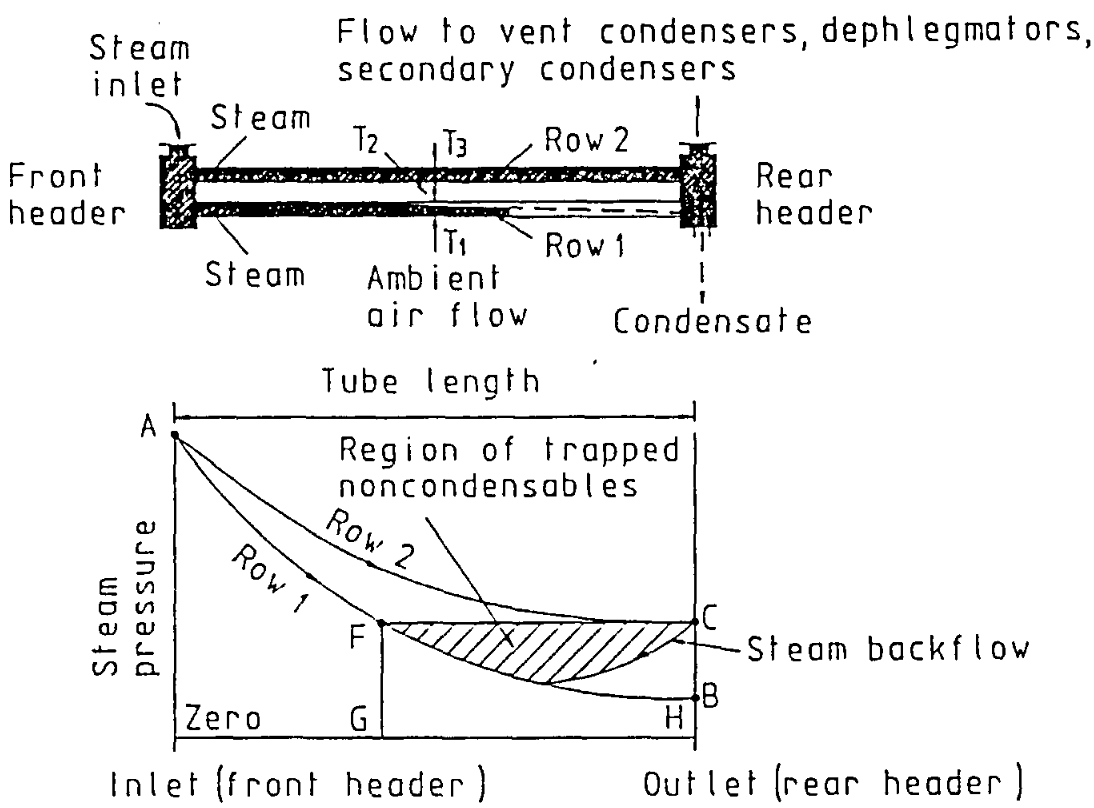

Figure 8.2.1: Trapping of noncondensable gases in an air-cooled condenser.

Since the first row of tubes is exposed to the lower ambient inlet air temperature, while the second row is contacted by preheated air, the second row condenses less steam than the first, and therefore has a lower steam pressure drop. The pressure in the outlet header equals the inlet header pressure minus the pressure drop in the second tube row. The pressure in the outlet header thus exceeds the pressure that would have existed at the outlet of the first tube row if the higher rate of condensation had occurred along its entire length. Instead, steam from the outlet header tends to flow into the outlet end of the first tube row, trapping noncondensables in these tubes as shown in figure 8.2.1.

A number of investigators have studied the process of condensation in a multi-tube-row air-cooled heat exchanger [67FO1, 74RO1, 80BE1, 82BR1, 84SC1].

To overcome this problem in multi-row air-cooled condensers, some designs add a dephlegmator or secondary condenser in series, thereby increasing the steam flow in the main condenser to such an extent that there is a net flow of steam out of every tube.

The effectiveness of this concept may be further improved by changing the fin height or fin pitch in consecutive tube rows in an attempt to achieve a more balanced drop in steam pressure.

According to Larinoff et al [78LA1], steam backflow and trapping of gases may occur in specific regions of the abovementioned arrangements under certain operating conditions. They describe a condenser in which the tube rows are connected to a common steam inlet header but individual outlet headers, vent tubes and ejectors. The vent tubes are installed in the heated portion of the air stream to avoid freezing. Other refinements to remove noncondensables have been proposed [90LA1].

The multi-row effect is eliminated in modern condensers consisting of bundles having only one row of finned tubes. Due to maldistribution of steam flow, de-aeration of the single-row condenser cannot be ignored [94SC1].

8.3 INLET LOSSES

Large air-cooled heat exchangers may typically consist of one or more fan units. Where many fan units are required these are usually arranged in long banks consisting of one or more rows of fans. Due to flow distortion and separation of the cooling air stream at the inlet to the banks, losses occur resulting in a reduction of the heat exchanger effectiveness.

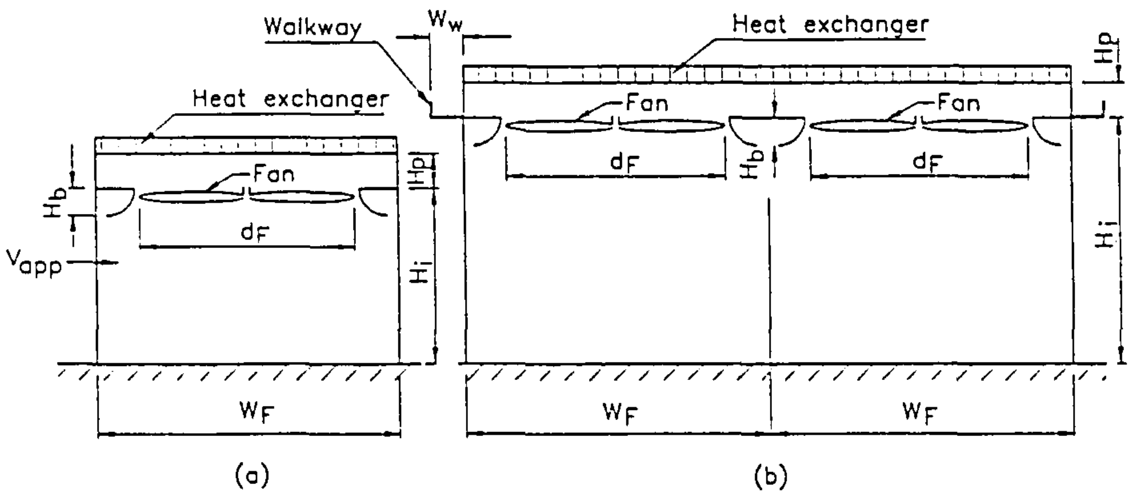

Figure 8.3.1: Forced draft heat exchangers

The flow through a forced convection system may be reduced considerably if the fan or fans are located too close to ground level. Generally it is considered good practice to ensure that the approach air velocity at the entrance to a fan as shown in figure 8.3.1 (a) is no more than approximately one half of the velocity through the fan throat i.e. $v_{app} < 0.5\ v_F$ or $H_i > 0.5\ d_F$ [79MO1].

The height of the fan inlets (for forced draft units as shown in figure 8.3.1 (b) or of the underside of the bundle (for induced draft units) for two rows of fans should preferably be at least one fan diameter i.e. $H_i \geq d_F$ above ground level. It is also important to consider the position of the air-cooled heat exchanger relative to buildings or other heat exchangers to avoid excessive flow distortions and losses [73RO1].

A few studies have been conducted to quantify the effect that flow disturbances at the inlet to the heat exchanger have on the performance of the fans in forced draft systems [82RU1, 81SP1, 95SA1].

Salta and Kröger [95SA1] report the results of tests conducted on models of two-dimensional single- and multi-row six-bladed fan units located at different heights above ground level. As shown in figure 8.3.2 they find that for units consisting of one or more fan rows, where the fans operate near maximum efficiency, there is a reduction in air volume flow rate through the heat exchanger as the fan platform height, H_i, is reduced. It should be noted that their findings are applicable to units where the ratio of the rounded inlet bell height to fan diameter $H_b/d_F = 0.19$, the ratio of the fan pitch to fan diameter $W_F/d_F = 1.27$ and there is no walkway along the edge of the fan platform.

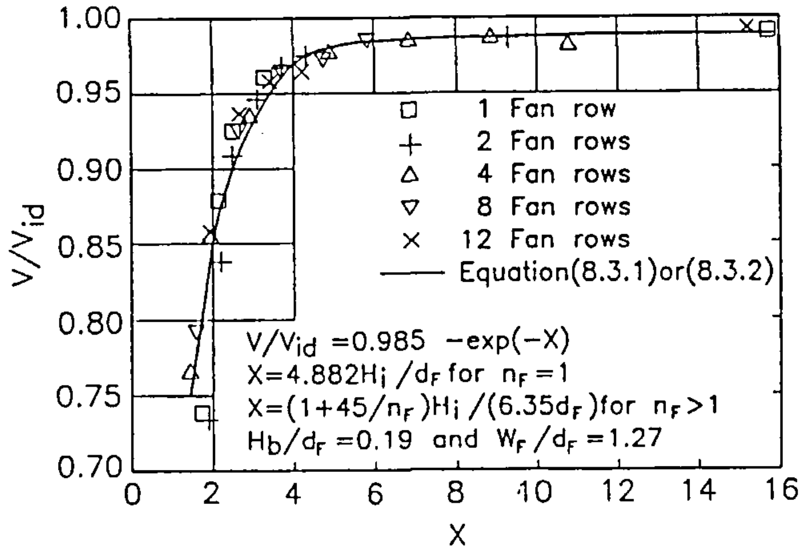

Figure 8.3.2: Reduction in air volume flow rate.

In the case of a long single row of fans the ratio of the actual air volume flow rate through the heat exchanger when compared to the ideal flow volume flow rate (sum of flows for individual free standing fan units with undisturbed inlet conditions) shown in figure 8.3.2 can be correlated by the following equation

$$V/V_{id} = 0.985 - \exp(-X) \tag{8.3.1}$$

where $X = 4.882\ H_i/d_F$

For essentially two-dimensional heat exchangers consisting of two or more long rows of fans, the following equation is applicable

$$V/V_{id} = 0.985 - \exp(-X) \qquad (8.3.2)$$

where $X = (1 + 45/n_F)H_i/(6.35\ d_F)$ and n_F is the number of fan rows.

Experiments show that the performance of the fans along the edge of the platform are most significantly affected. Upon reducing the platform height in a four-row heat exchanger (two fans on either side of the symmetry line) the flow through the individual rows is reduced as is shown in figure 8.3.3.

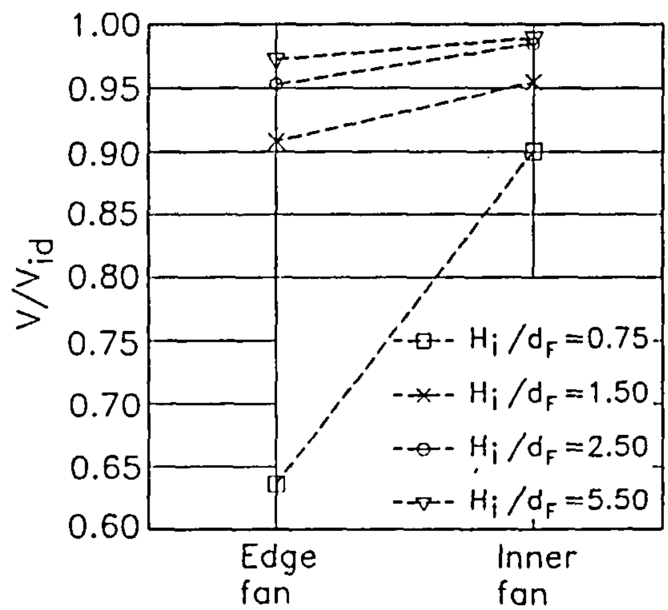

Figure 8.3.3: Reduction in air volume flow rate through individual fan rows in a four-fan-row heat exchanger.

If an unperforated walkway is affixed along the edge of the fan platform as shown in figure 8.3.1(b) for the particular heat exchanger geometry specified above, the air flow rate through the heat exchanger can actually be improved as shown in figure 8.3.4 for a four-fan row heat exchanger. The same trend can be achieved if the fan platform is extended along the edge.

The increased flow is primarily due to the improvement of flow through the fans along the edge of the four-fan-row heat exchanger as shown in figure 8.3.5.

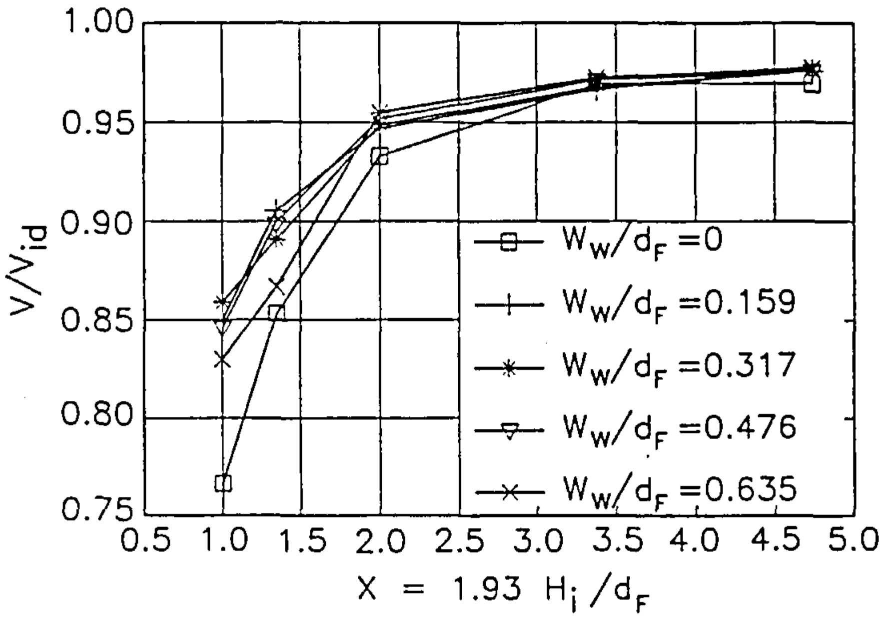

Figure 8.3.4: Influence of walkway on volume flow rate through a four-fan-row heat exchanger.

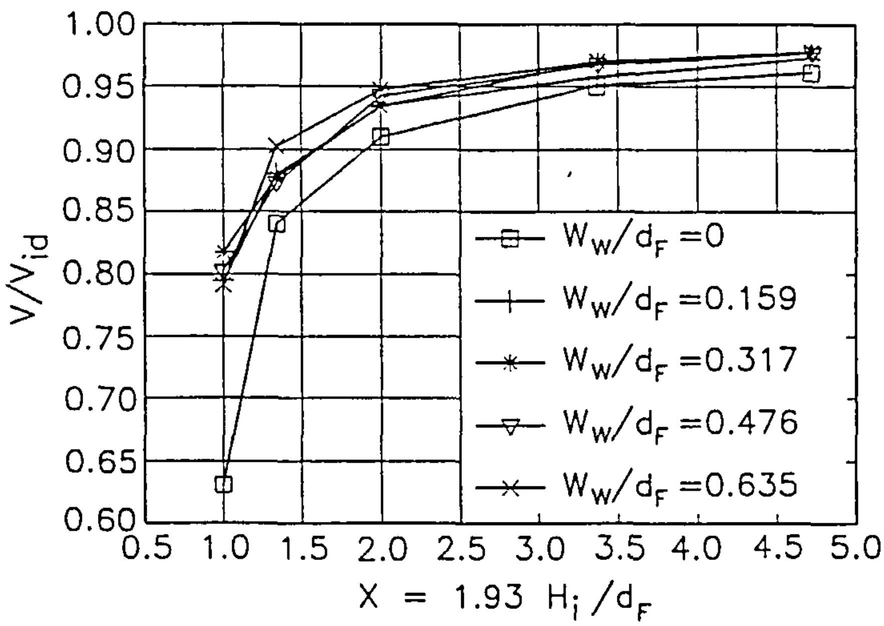

Figure 8.3.5: Effect of walkway width on the flow through edge fan in a four-fan-row heat exchanger.

In an induced draft air-cooled heat exchanger as shown schematically in figure 8.3.1, inlet losses due to separated flow must be considered when determining the system flow resistance. If the heat exchanger loss coefficient is small, inlet losses and the maldistribution of flow caused by the distorted inlet conditions may measurably reduce the effectiveness of the heat exchanger, as in the case of natural draft cooling towers.

Terblanche and Kröger [94TE1] performed isothermal model tests to determine the loss coefficient at the inlet to a two-dimensional induced draft unit. According to equation (7.3.4) the loss coefficient can be expressed approximately as

$$K_{ct} = \frac{\left(p_a/\rho - p_o/\rho_o\right)}{v^2/2} - 1 - K_{he}\left(\frac{\rho}{\rho_{he}}\right) \tag{8.3.3}$$

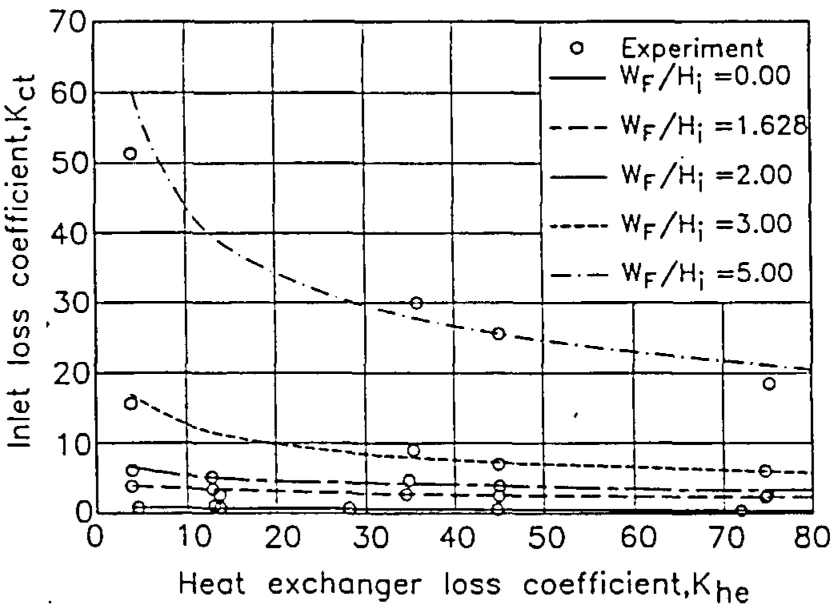

Figure 8.3.6: Inlet loss coefficients in a two-dimensional induced draft unit.

The results of the experiments performed by Terblanche and Kröger [94TE1] are shown in figure 8.3.6 and are compared to the following empirical correlation.

$$K_{ct} = \left[1.1 + 1.1\left(W_F/H_i\right)^3 - 0.05\left(W_F/H_i\right)\exp\left(W_F/H_i\right)\right]$$

$$\times\, K_{he}^{\left[-0.29 + 0.079\cos\left(W_F/H_i\right) + 0.102\sin\left(W_F/H_i\right)\right]} \tag{8.3.4}$$

8.4 RECIRCULATION

Heated plume air may recirculate in an air-cooled heat exchanger, thereby reducing the cooling effectiveness of the system. Figure 8.4.1 depicts, schematically, a cross-section of an air-cooled heat exchanger. In the absence of wind, the buoyant jet or plume rises vertically above the heat exchanger. A part of the warm plume air may however be drawn back into the inlet of the tower. This phenomenon is known as "recirculation".

Plume recirculation is usually a variable phenomenon influenced by many factors, including heat exchanger configuration and orientation, surrounding structures and prevailing weather conditions. Because of higher discharge velocities, recirculation is usually less in induced draft than in forced draft designs.

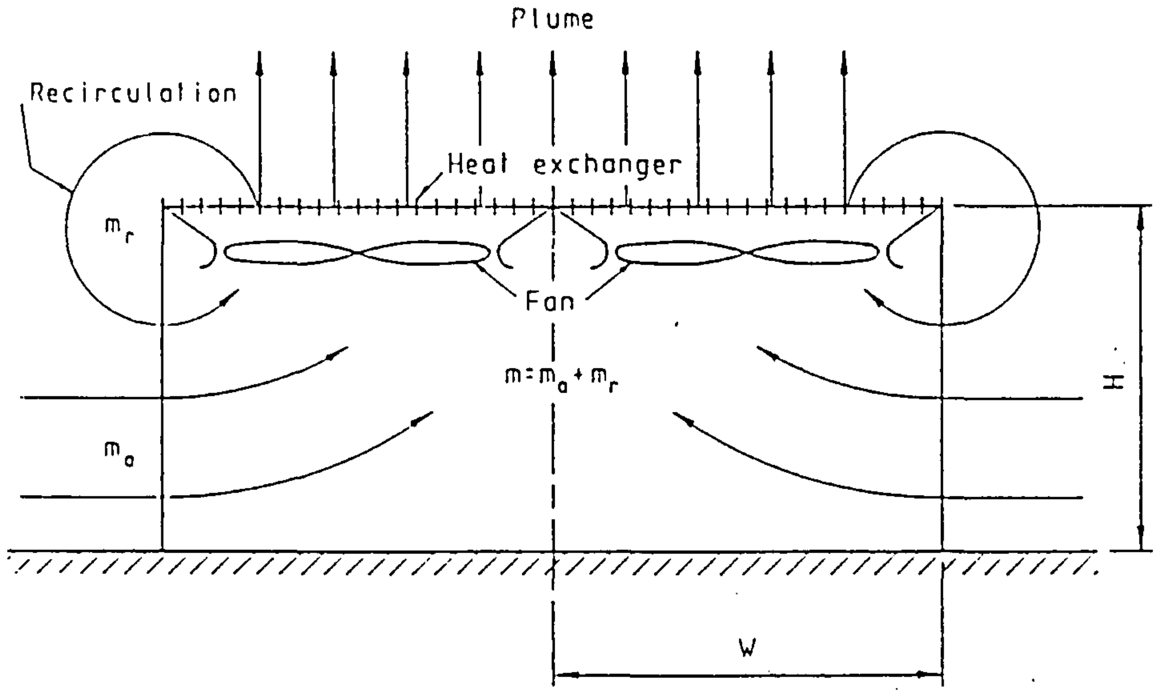

Figure 8.4.1: Air-flow pattern about forced draft air-cooled heat exchanger.

Lichtenstein [51LI1] defines a recirculation factor as

$$r = m_r/\left(m_a + m_r\right) = m_r/m \tag{8.4.1}$$

where m_r is the recirculating air mass flow rate, while m_a is the ambient air flow rate into the heat exchanger.

Although the results of numerous studies on recirculation do appear in the literature, most are experimental investigations performed on heat exchangers having specific geometries and operating under prescribed conditions e.g. [74KE1, 81SL1]. Gunter and Shipes [72GU1] define certain recirculation flow limits and present the results of field tests performed on air-cooled heat exchangers. Problems associated with solving recirculating flow patterns numerically have been reported [81EP1]. Kröger et al. investigated the problem analytically, experimentally and numerically and recommend a specific equation with which the performance effectiveness of essentially two-dimensional mechanical draft heat exchangers experiencing recirculation, can be predicted [88KR1, 89KR1, 91DU1, 93DU1, 95DU1].

8.4.1 RECIRCULATION ANALYSIS

Consider one half of a two-dimensional mechanical draft heat exchanger in which recirculation occurs. For purposes of analysis, the heat exchanger is represented by a straight line at an elevation H_i above ground level as shown in figure 8.4.2(a).

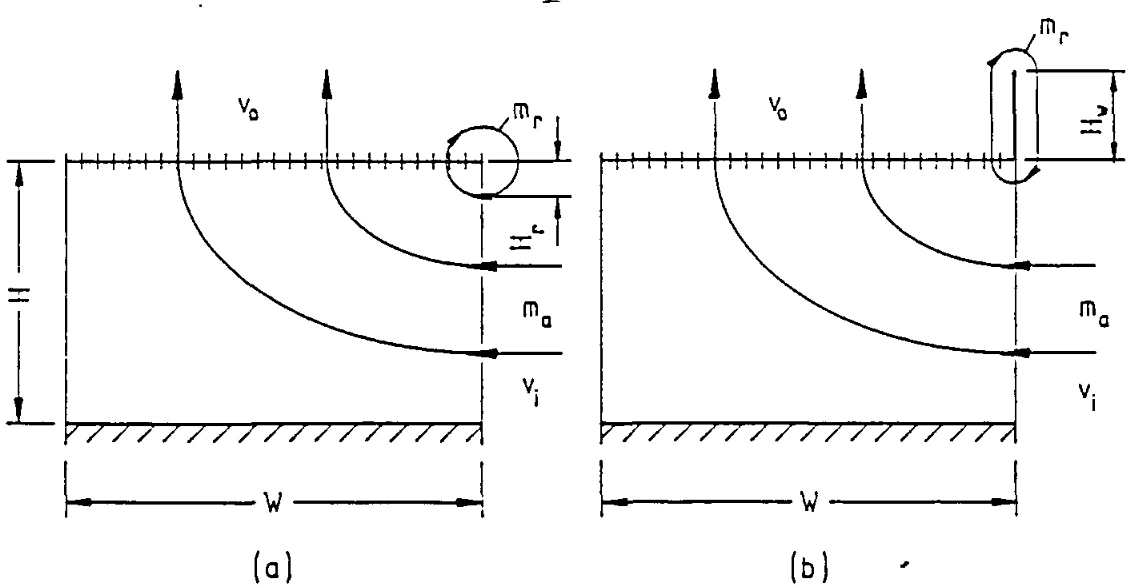

Figure 8.4.2: Flow pattern about heat exchanger.

It is assumed that the velocity of the air entering the heat exchanger along its periphery is in the horizontal direction and has a mean value, v_i (the actual inlet velocity is highest at the edge of the fan platform and decreases towards ground level). The outlet velocity, v_o, is assumed to be uniform and in the vertical direction.

Consider the particular streamline at the outlet of the heat exchanger that diverges from the plume at 1 and forms the outer "boundary" of the recirculating air stream. This streamline will enter the platform at 2, some distance H_r below the heat exchanger. For purposes of analysis it will be assumed that the elevation of 1 is approximately H_r above the heat exchanger. If viscous effects, mixing and heat transfer to the ambient air are neglected, Bernoulli's equation can be applied between 1 and 2 to give

$$p_1 + \rho_o v_1^2/2 + \rho_o g(H_i + H_r) = p_2 + \rho_o v_2^2/2 + \rho_o g(H_i - H_r) \tag{8.4.2}$$

It is reasonable to assume that the total pressure at 1 is equal to the stagnation pressure of the ambient air at that elevation i.e.

$$p_1 + \rho_o v_1^2/2 = p_{a1} \tag{8.4.3}$$

At 2 the static pressure can be expressed as

$$p_2 = p_{a2} - \rho_a v_2^2/2 \tag{8.4.4}$$

Furthermore for the ambient air far from the heat exchanger

$$p_{a1} + 2\,\rho_a\, g\, H_r = p_{a2} \tag{8.4.5}$$

Substitute equations (8.4.3), (8.4.4) and (8.4.5) into equation (8.4.2) and find

$$H_r = v_2^2/4g \tag{8.4.6}$$

Due to viscous effects the velocity at the inlet at elevation H_i is in practice equal to zero. The velocity gradient in this immediate region is however very steep and the velocity peaks at a value that is higher than the mean inlet velocity. Examples of numerically determined inlet velocity distributions for different outlet velocities and heat exchanger geometries are shown in figure 8.4.3 [95DU1]. Since most of the recirculation occurs in this region the velocity v_2 is of importance but difficult to quantify analytically. For $W/H_i \leq 1$ it will be assumed that v_2 can be replaced approximately by the mean inlet velocity, v_i, in equation (8.4.6). Thus

$$H_r \approx v_i^2/4\,g \tag{8.4.7}$$

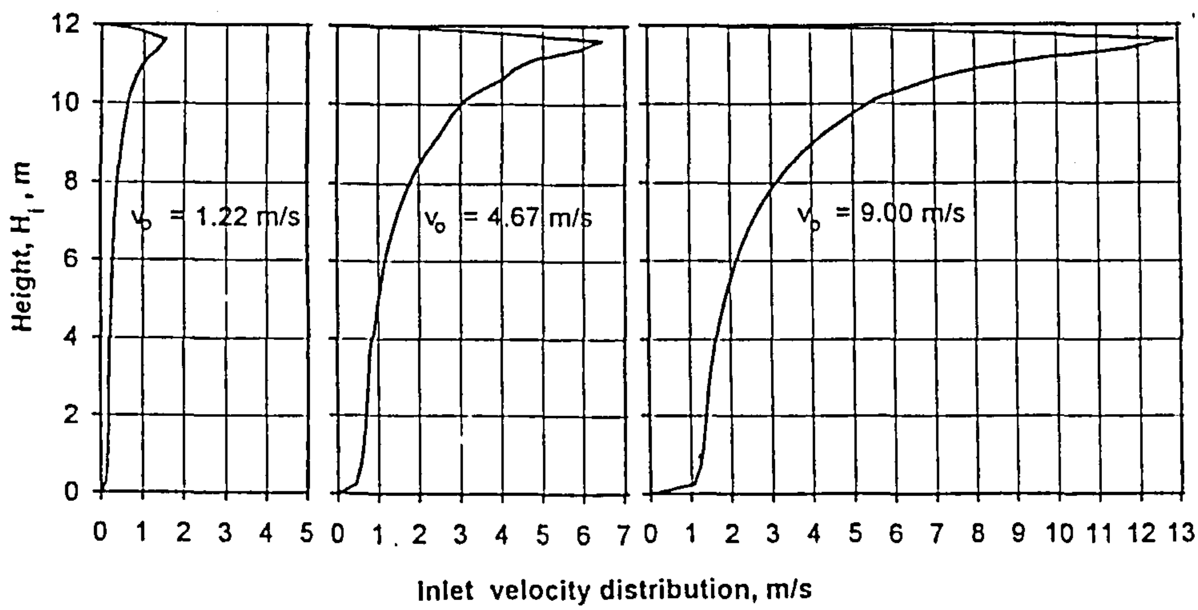

Figure 8.4.3: Two-dimensional inlet velocity distribution for W = 5.1 m.

According to the equation of mass conservation, the flow per unit depth of the tower can be expressed as

$$\rho_o\, H_r\, v_i + \rho_a \left(H_i - H_r\right) v_i = \rho_o\, v_o\, W$$

or

$$v_i \approx \rho_o\, v_o\, W/\left(\rho_a\, H_i\right) \tag{8.4.8}$$

if the amount of recirculation is small.

According to equation (8.4.1), the recirculation factor is

$$r = \frac{m_r}{m} = \frac{\rho_o v_i H_r}{\rho_o v_o W} = \frac{\rho_o H_r}{\rho_a H_i} \tag{8.4.9}$$

Substitute equations (8.4.7) and (8.4.8) into equation (8.4.9) and find

$$r = \frac{1}{4}\left(\frac{\rho_o W}{\rho_a H_i}\right)^3 \frac{v_o^2}{g W} = \frac{1}{4}\left(\frac{\rho_o W}{\rho_a H_i}\right)^3 Fr \tag{8.4.10}$$

where $Fr = v_o^2/g\, W$ is the Froude number based on the width of the heat exchanger.

The influence of a windwall or deep plenum can be determined approximately by considering flow conditions between the top of the windwall, $(H_i + H_w)$, as shown in figure 8.4.2(b) and elevation H_i. Consider the extreme case when H_w is so large ($H_w = H_{wo}$) that no recirculation takes place and the ambient air velocity near the top of the windwall is zero. In this particular case the static pressure at the tower exit is essentially equal to the ambient stagnation pressure. With these assumptions, apply Bernoulli's equation between the tower outlet at the top of the windwall and the elevation H_i.

$$p_{a1} + \rho_o v_o^2/2 + \rho_o g H_{wo} = p_{a2} \tag{8.4.11}$$

But

$$p_{a2} - p_{a1} = \rho_a g H_{wo} \tag{8.4.12}$$

Substitute equation (8.4.12) into equation (8.4.11) and find

$$H_{wo} = \rho_o v_o^2/\left[2(\rho_a - \rho_o)g\right] \tag{8.4.13}$$

If it is assumed that the recirculation decreases approximately linearly with increasing windwall height, equation (8.4.10) may be extended as follows:

$$r = \frac{1}{4}\left(\frac{\rho_o W}{\rho_a H_i}\right)^3 Fr\left(1 - a\frac{H_w}{H_{wo}}\right) \tag{8.4.14}$$

Since the recirculation is assumed to be essentially zero at $H_w = H_{wo}$, find a = 1. Substitute equation (8.4.13) into equation (8.4.14) and find

$$r = \frac{1}{4}\left(\frac{\rho_o W}{\rho_a H_i}\right)^3 \frac{v_o^2}{g\,W}\left[1 - 2\,\frac{(\rho_a - \rho_o)\,g\,H_w}{\rho_o\,v_o^2}\right]$$

$$= \frac{1}{4}\left(\frac{\rho_o W}{\rho_a H_i}\right)^3 Fr\left[1 - \frac{2}{Fr_D}\right] \tag{8.4.15}$$

where $Fr_D = \rho_o\,v_o^2/\left[(\rho_a - \rho_o)g\,H_w\right]$ is the densimetric Froude number based on the wind wall height.

It is important to determine the effectiveness of the system when recirculation occurs. Effectiveness in this case, is defined as

$$e_r = \frac{\text{heat transfer with recirculation}}{\text{heat transfer with no recirculation}} = \frac{Q_r}{Q} \tag{8.4.16}$$

The interrelation between the recirculation and the effectiveness is complex in a real heat exchanger. Two extremes can however be evaluated analytically i.e.

1. **No mixing**

The warm recirculating air does not mix at all with the cold ambient inflow, resulting in a temperature distribution as shown in figure 8.4.4(a). The recirculating stream assumes the temperature of the heat exchanger fluid T_{he}.

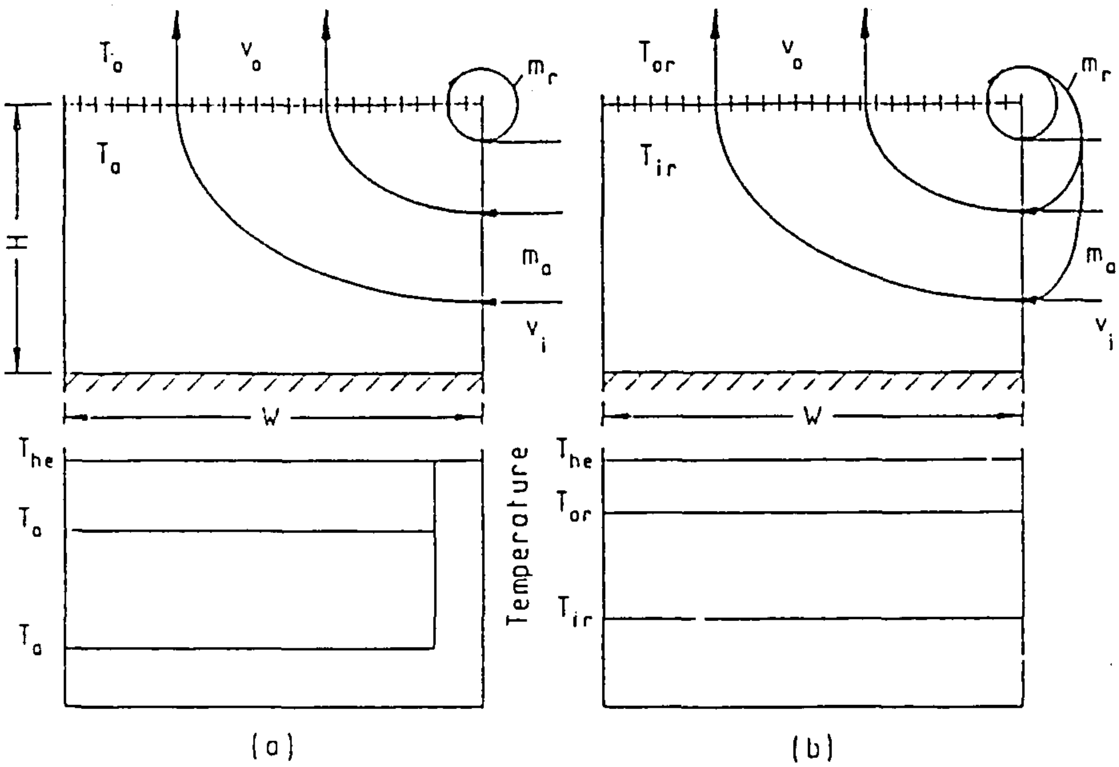

Figure 8.4.4: Recirculation flow patterns.

This in effect means that the part of the heat exchanger where recirculation occurs, transfers no heat. The actual heat transfer rate is thus given by

$$Q_r = m_a c_p \left(T_o - T_a\right) \tag{8.4.17}$$

resulting in an effectiveness due to recirculation of

$$e_r = \frac{m_a c_p \left(T_o - T_a\right)}{\left(m_a + m_r\right) c_p \left(T_o - T_a\right)} = \frac{\left(m - m_r\right)}{m} = 1 - r \tag{8.4.18}$$

Substitute equation (8.4.15) into equation (8.4.18) and find

$$e_r = 1 - \frac{1}{4}\left(\frac{\rho_o W}{\rho_a H_i}\right)^3 \frac{v_o^2}{g W}\left[1 - 2\,\frac{\left(\rho_a - \rho_o\right) g H_w}{\rho_o v_o^2}\right] \tag{8.4.19}$$

2. Perfect mixing

The recirculating air mixes perfectly with the inflowing ambient air, resulting in a uniform increase in both the effective inlet air temperature and the outlet air temperature as shown in figure 8.4.4(b).

If for purpose of illustration, it is assumed that the temperature of the heat exchanger, T_{he}, is constant, it follows from equation (3.5.22) that the effectiveness under cross-flow conditions is

$$e = \frac{mc_p\left(T_{or} - T_{ir}\right)}{mc_p\left(T_{he} - T_{ir}\right)} = \frac{\left(T_{or} - T_{ir}\right)}{\left(T_{he} - T_{ir}\right)} = 1 - \exp\left(-UA/mc_p\right) \tag{8.4.20}$$

or

$$T_{or} = T_{he} - \left(T_{he} - T_{ir}\right)\exp\left(-UA/mc_p\right) \tag{8.4.21}$$

Furthermore the enthalpy entering the heat exchanger is

$$mc_p\,T_{ir} = m_a c_p T_a + m_r c_p T_{or}$$

or

$$T_{ir} = \frac{\left(m - m_r\right)T_a}{m} + \frac{m_r T_{or}}{m} = \left(1 - r\right)T_a + r\,T_{or} \tag{8.4.22}$$

Substitute equation (8.4.22) into equation (8.4.21) and find

$$T_{or} = T_{he} - \left[T_{he} - (1 - r)\,T_a - r\,T_{or}\right]\exp\left(-UA/mc_p\right)$$

$$= \frac{T_{he} - \left[T_{he} - (1 - r)T_a\right]\exp\left(-UA/mc_p\right)}{1 - r\exp\left(-UA/mc_p\right)} \tag{8.4.23}$$

In this case the effectiveness due to recirculation is given by

$$e_r = \frac{mc_p\left(T_{or} - T_{ir}\right)}{mc_p\left(T_o - T_a\right)} = \frac{T_{or} - T_{ir}}{T_o - T_a}$$

From equations (8.4.22) and (8.4.23), substitute the values of T_{ir} and T_{or} into this equation, to find the effectiveness of the heat exchanger.

$$e_r = \frac{(1 - r)}{\left(T_{or} - T_{ar}\right)}\left[\frac{T_{he} - \left\{T_{he} - (1 - r)T_a\right\}\exp\left(-UA/mc_p\right)}{1 - r\exp\left(-UA/mc_p\right)} - T_a\right] \tag{8.4.24}$$

In practice the effectiveness will be some value between that given by equation (8.4.18) and equation (8.4.24). Actual measurements conducted on air-cooled heat exchangers appear to suggest that relatively little mixing occurs. This tendency is confirmed by numerical analysis of the problem [89KR1,95DU1].

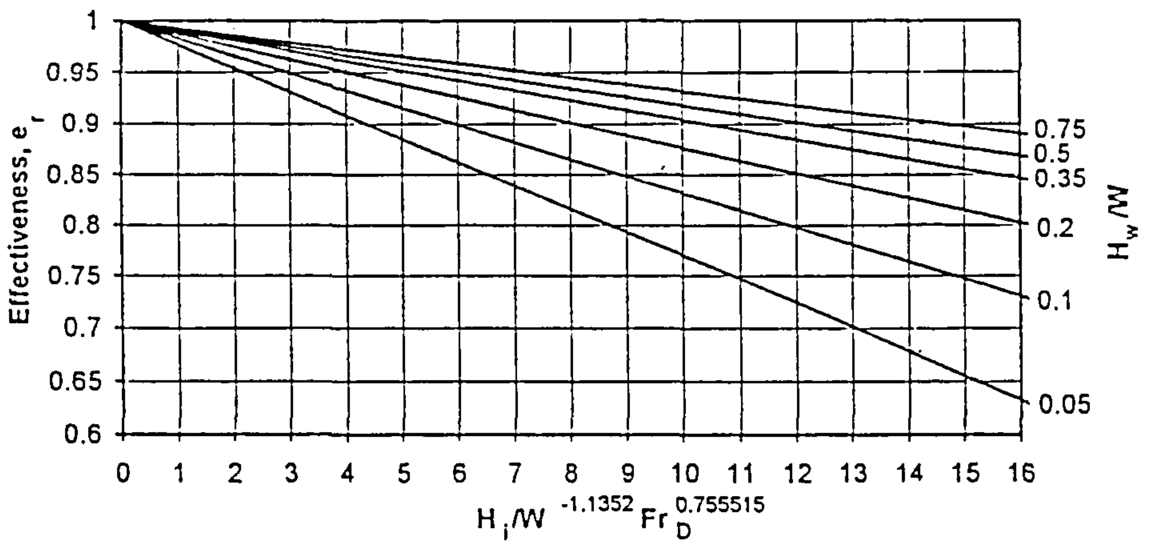

Figure 8.4.5: Heat exchanger effectiveness.

Duvenhage and Kröger [95DU1] solved the recirculation problem numerically and correlated their results over a wide range of operating conditions and heat exchanger geometries by means of the following empirical equation:

Model and full-scale tests have been conducted to determine the degree of recirculation in different types of air-cooled heat exchangers [71GU1, 72GU1, 88KR1, 89CO1].

In the absence of windwalls, recirculation can be significant resulting in a corresponding reduction in heat transfer effectiveness. As shown in figure 8.4.6, smoke generated at the outlet of an A-frame type forced draft air-cooled heat exchanger without windwalls, is drawn directly downwards into the low pressure region created by the fans.

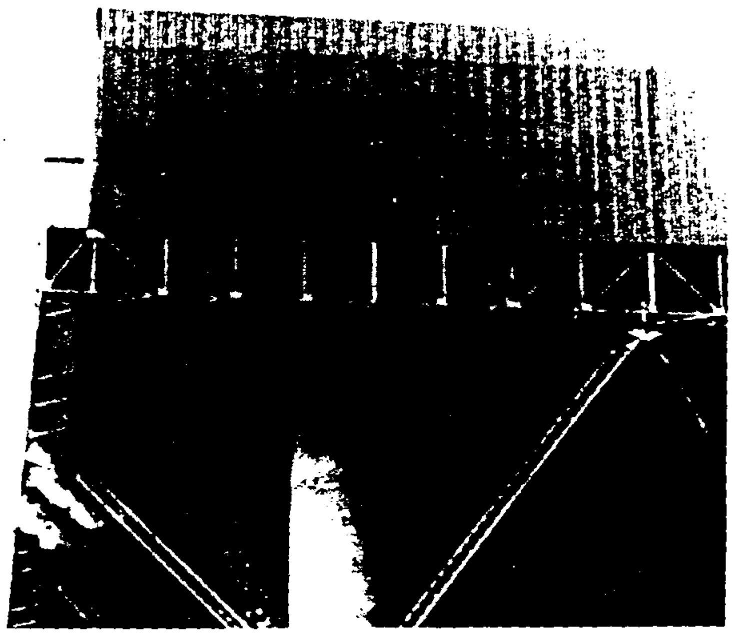

Figure 8.4.7: Visualization of recirculation with smoke at the Matimba power plant.

The results of recirculation tests conducted at the Matimba power plant are reported by Conradie and Kröger [89CO1]. They actually measured the vertical temperature distribution of the air entering the heat exchanger and observed a relatively higher value in the vicinity of the fan platform. As shown by the smoke trail in figure 8.4.7 recirculation of the plume air occurs in this region. Because of the approximately 10 m high windwall surrounding the array of A-frame heat exchanger bundles, a reduction in effectiveness of less that one percent is experienced under normal operating conditions in the absence of wind. The effectiveness can be determined according to equation (8.4.25).

Generally very little recirculation occurs in induced draft cooling systems due to the relatively high fan outlet velocity or diffusor height.

$$e_r = 1 - \left[0.006027\left(H_i/W\right)^{-1.1352}\left(H_w/W\right)^{-0.44641}Fr_D^{0.755515}\right] \qquad (8.4.25)$$

This equation is valid in the ranges $0.49 \leq H_i/W \leq 2.75$, $0.049 \leq H_w/W \leq 0.79$ and $0.175 \leq Fr_D \leq 14.3$ where $Fr_D = \rho_a v_o^2/\left[\left(\rho_a - \rho_o\right)gW\right]$.

Equation (8.4.25) is shown graphically in figure 8.4.5. For values of $H_i/W \geq Fr_D^{0.265}$, equation (8.4.19 is in good agreement with equation (8.4.25).

8.4.2 MEASURING RECIRCULATION

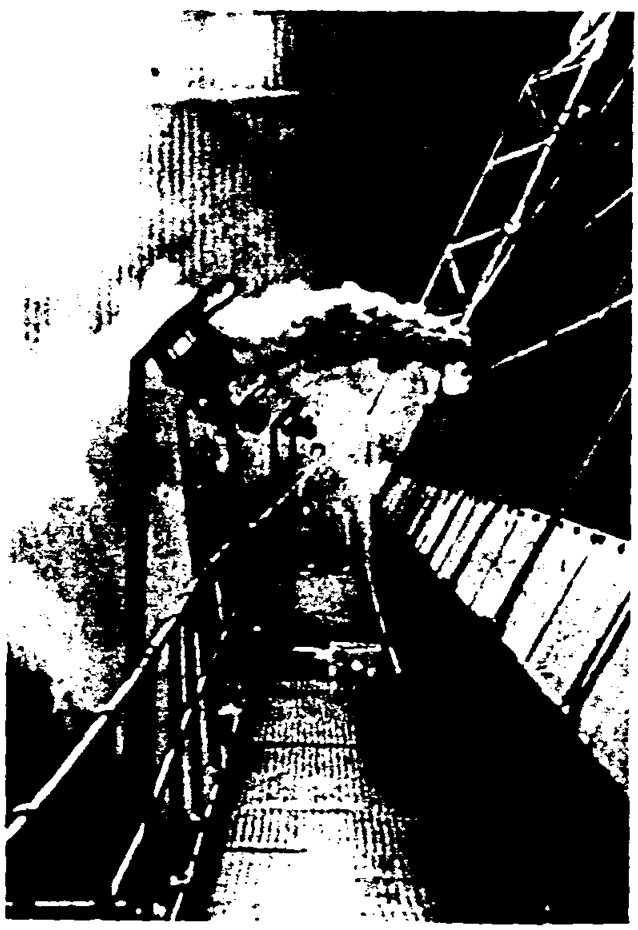

Figure 8.4.6: Plume air recirculating in air-cooled heat exchanger.

8.5 REFERENCES

51LI1 Lichtenstein, J., Recirculation in Cooling Towers, ASME Power Division Meeting, Atlanta, Ga., pp. 1037-1042, 1951.

65YI1 Yih, C.S., Dynamics of Nonhomogeneous Fluids, McMillan Co., New York, 1965.

67FO1 Forgó, L., Die Ursachen für schlechte Wärmeübertragung in Rohrbündel-Wärmeaustauschern bei kondensierendem Dampf, Brennst.-Wärme-Kraft, Vol. 19, No. 1, pp. 20-23, 1967.

70RU1 Russell, C.M.B. and Bos, W.H., The Economic Design of Air Coolers, Proc. Conf. on Air Coolers, I. Mech. E., pp. 14-40, London, 1970.

71GU1 Gunter, A.Y. and Shipes, K.V., Hot Air Recirculation by Air Coolers, Proc. 12th Nat. Heat Transfer Conference, AIChE - ASME, Tulsa, Aug. 1971.

72GU1 Gunter, A.Y. and Shipes, K.V., Hot Air Recirculation by Air Coolers, Chemical Engineering Progress, Vol. 68, No. 2, pp. 49-58, February 1972.

73RO1 Rose, J.C., Wilson, D.J. and Cowan, G.H., The Performance of Air-cooled Heat Exchangers, Part II. Air-cooled Heat Exchanger Performance Specification, AERE - R7450, Heat Transfer and Fluid Flow Service, Harwell, 1973.

74KE1 Kennedy, J.F. and Fordyce, H., Plume Recirculation and Interference in Mechanical-Draft Cooling Towers, Proc. of Cooling Tower Environment Symp., Univ. of Maryland, Baltimore, pp. 58-87, 1974.

74RO1 Rozenman, T. and Pundyk, J., Effect of Unequal Heat Loads on the Performance of Air Cooled Condensers, AIChE Symp. Ser., Vol. 70, No. 138, pp. 178-184, 1974.

78AM1 American Institute of Chemical Engineers, Air-cooled Heat Exchangers, A

Guide to Performance Evaluation, AIChE, New York, 1978.

78AP1 American Petroleum Institute (API) Standard 661, Air-Cooled Heat Exchangers for General Refinery Services, API, Washington, 1978.

78BR1 Brown, R., Ganapathy, V. and Glass, J., Design of Air-cooled Exchangers, Chemical Engineering, Vol. 85, No. 7, pp. 106-125, 1978.

78LA1 Larinoff, M.W., Moles, W.E. and Reichhelm, R., Design and Specification of Air-cooled Steam Condensers, Chemical Engineering, pp. 86-94, 1978.

79BE1 Berg, W.F. and Berg, J.L., Flow Patterns for Isothermal Condensation in One Pass Air Cooled Heat Exchangers, ASME Paper 79-WA/HT-5, 1979.

79MO1 Monroe, R.C., Improving Cooling Tower Fan System Efficiencies, Combustion Magazine, Vol. 50, No. 11, pp. 20-26, May 1979.

79ZA1 Zanker, A., Taking the Drudgery out of Designing Air-cooled Heat Exchangers, Machine Design, pp. 158-165, December 1979.

80SC1 Schrey, H.G. and Kern, J., Zum Rohrreiheneffekt bei Gasbeaufschlagten Kondensatoren, Int. J. Heat Mass Transfer, Vol. 24, pp. 335-342, 1981.

81EP1 EPRI Report CS-1665, Parts 1 and 2, Investigation of Numerical Modeling Techniques for Recirculation Flows, 1981.

81SL1 Slawson, P.R. and Sullivan, H.F., Model Studies on the Design and Arrangement of Forced Draft Cooling Towers to Minimize Recirculation and Interference, Proc. of Conf. on Waste Heat Management and Utilization, pp. 235-244, 1981.

81SP1 Speirs, R.R.M., Inlet Tests on Full Size Air-cooled Heat Exchanger, National Engineering Laboratory NEL/HTFS 12, HTFS RS 361, 1981.

82BR1 Breber, G., Palen, J.W. and Taborek, J., Study on Noncondensable Vapor Accumulation in Air-Cooled Condensers, Proc. 7th Int. Heat Transfer Conf., Vol. 6, pp. 263-268, 1982.

82RU1 Russell, C.M.B. and Peachey, J., Air Flow Effects on Fan Performance in Air Cooled Heat Exchangers, Proc. Int. Conf. on Fan Design and Applications, Paper B3, pp. 79-90, Guildford, England, 1982.

83PA1 Paikert, P., Air-cooled Heat Exchangers, Heat Exchanger Design Handbook, eds. Schlünder, E.U. et al., VDI-Verlag, Düsseldorf, 1983.

83SH1 Shaikh, N.M., Estimate Air-cooler Size, Chemical Engineering, Vol. 90, no. 25, pp. 65-68, 1983.

83SH2 Shipes, K.V., Mechanical Design of Air-cooled Heat Exchangers, Heat Exchanger Design Handbook, eds. Schlünder, E.U. et al., VDI-Verlag, Düsseldorf, 1983.

84SC1 Schrey, H.G., Zur Bestimmung des Leistungsverhaltens bei Mehrreihigen, luft- bzw. gasgekühlten Kondensatoren mit Inerten, Wärme und Stoffübertragung, Vol. 18, No. 3, pp. 185-191, 1984.

86AC1 Air-cooled Heat Exchanger Manufacturers Association (ACHEMA), Standard for Air-cooled Heat Exchangers, New York, 1986.

88KR1 Kröger, D.G., Recirculation in Air-cooled Mechanical Draught Heat Exchangers, South African Mining World, pp. 65-69, November 1988.

89CO1 Conradie, A.E. and Kröger, D.G., Plume Recirculation in Air-cooled Heat Exchangers, ASME Paper 89-HT-11 presented at the Jt. ASME/AIChE Nat. Heat Transfer Conf., Philadelphia, August 1989.

89KR1 Kröger, D.G., Reduction in Performance Due to Recirculation in Mechanical Draft Cooling Towers, Heat Transfer Engineering, Vol. 10, No. 4, pp. 37-43, 1989.

90LA1 Larinoff, M.W., Bundle-design Protects Air-cooled Condenser from Freezing, Power Engineering, pp. 33-35, Feb. 1990.

91AS1 ASME PTC 30-1991, Air-cooled Heat Exchangers Performance Test Codes, ASME, New York, 1991.

91DU1 Du Toit, C.G. and Kröger, D.G., Numerical Modelling of Recirculation in Mechanical-draught Heat Exchangers, Proc. 1st ICHMT Int. Num. Heat Transfer Conf. and Software Show, Guildford, England, 1991.

92MC1 McKetta, J.J., Heat Transfer Design Methods, Marcel Dekker, Inc., New York, 1992.

93DU1 Du Toit, C.G. and Kröger, D.G. Modelling of the Recirculation in Mechanical-draught Heat Exchangers, South African Inst. of Mech. Engrs. R and D Journal, Vol. 9, No. 1, pp. 2-8, 1993.

94KR1 Kröger, D.G., Fan Performance in Air-cooled Steam Condensers, Heat Recovery Systems CHP, Vol. 14, No. 4, pp. 391-399, 1994.

94SC1 Schrey, H.G., Operational Considerations for Air-cooled Steam Condensers with One or Higher Numbers of Tube Rows, Paper presented at the 9th IAHR Cooling Tower and Spraying Pond Symposium, von Karman Institute, Brussels, Belgium, September 1994.

95DU1 Duvenhage, K. and Kröger, D.G., Plume Recirculation in Mechanical Draught Air-cooled Heat Exchangers,

SYSTEM SELECTION AND OPTIMIZATION

9.1 POWER GENERATION

In the design of a base load power plant the selection and matching of various components is of the utmost importance in order to achieve effective operation and power output. Typically the net power output and the heat to be rejected by the cooling tower, for a given turbo-generator-surface-condenser system, may be presented in tabular form, or graphically as a function of the recooled condenser water temperature T_{wo} (temperature of water at outlet of cooling tower and condenser inlet), for a specified water mass flow rate m_w. The performance characteristics of an example of such a system, incorporating a surface condenser, are shown in figure 9.1.1. To obtain the net power output the auxiliary power required to drive the cooling water recirculating pump (1.2 MW) and the boiler pump etc. is subtracted from the gross generator output.

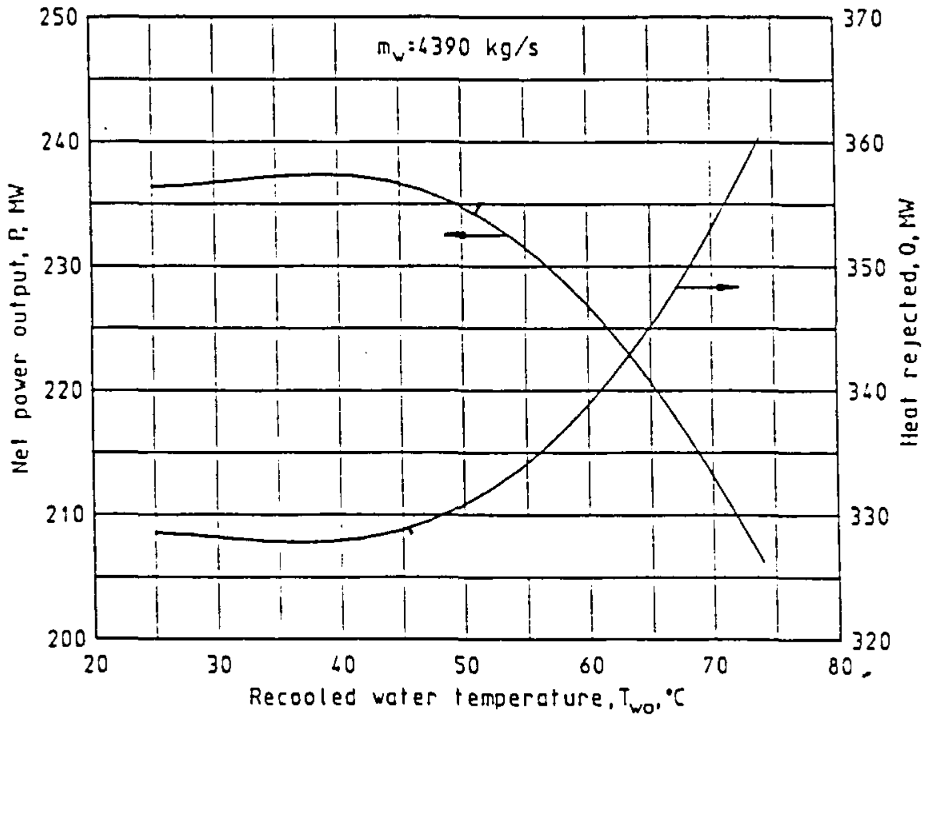

Figure 9.1.1: Performance characteristics of turbo-generator-condenser system.

Since prevailing atmospheric conditions influence the performance of cooling towers, the recooled water temperature may, especially in the case of dry-cooling towers, fluctuate over a relatively wide range. Changes in ambient temperature are the most important reason for this fluctuation, although other effects such as humidity, winds and inversions must also be considered.

The mean hourly frequency of different temperatures over a period of one year is normally supplied in tabulated or graphical form. An example of the frequency of dry- and wetbulb temperatures 2m above ground level at a particular location is shown in figure 9.1.2. It should be noted that significant temperature gradients exist near ground level, with the result that the measured temperatures may deviate considerably from the actual mean air temperature entering the cooling tower at a particular instant of time. More detailed information on the actual ambient temperature distribution would be preferred for a more sophisticated design.

To find the approximate net annual power output, the output is calculated at each specified ambient temperature, for the corresponding number of hours. These outputs are added to give the annual total value [87TR1].

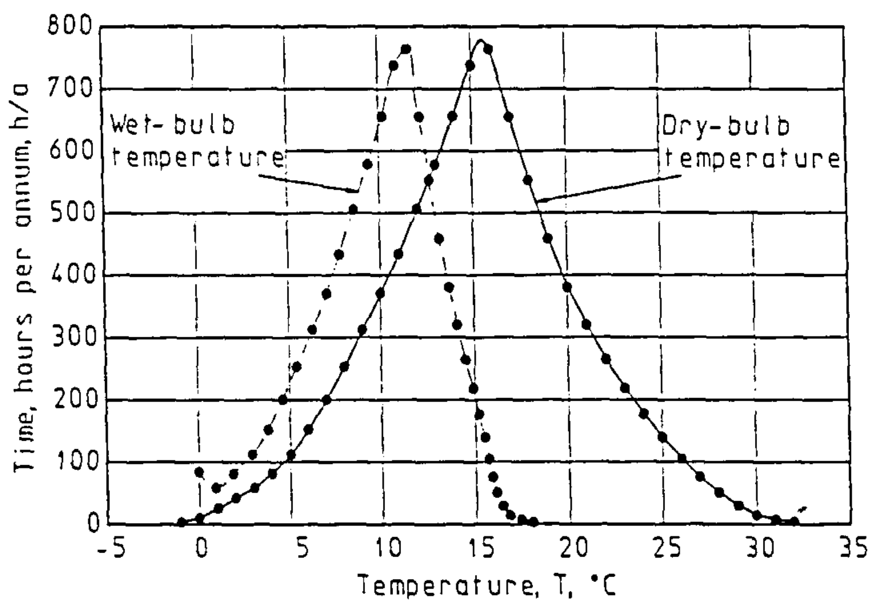

Figure 9.1.2: Frequency of ambient dry- and wetbulb temperatures.

9.2 COOLING TOWER OPTIMIZATION

Due to the high capital cost of air-cooled heat exchangers and dry-cooling towers, it is justified to optimize the design for a given cooling capacity taking into consideration practical limitations as far as possible. The degree of optimization that is ultimately achieved is usually a function of the sophistication of the design program, computational cost and quality of the available input data including various material, labor and energy cost structures.

In general, heat exchangers are designed for many varied applications, and hence may involve many different performance criteria. Some of these criteria may be minimum initial cost, minimum initial and operating costs, minimum weight or material, minimum volume or heat transfer surface area, minimum mean temperature difference, maximum heat transfer rate, minimum destruction of exergy [87BE1] and so on. When a single performance measure has been defined quantitatively and is to be minimized or maximized, it is called an "objective function" in a design optimization. A particular design may also be subjected to certain requirements such as required heat transfer, allowable pressure drop, limitations on height, width and/or length of the exchanger, etc. These requirements are called "constraints" in a design optimization. A number of different finned surfaces could be incorporated in a specific design problem and there are many geometrical parameters that could be varied for each surface geometry. In addition, operating flows and temperatures could also be changed. Thus a large number of "design variables" are associated with a heat exchanger design. The question arises as to how one can effectively adjust these design variables within imposed constraints and come up with a design having an optimum objective function.

Once the general configuration and surface are selected, an optimized heat exchanger design may be arrived at if the objective function and constraints can be expressed mathematically, and if all of the variables are automatically and systematically changed on some statistical or mathematical basis. Engineering judgments based on experience are involved in different stages of the thermal and mechanical design of a heat exchanger. Even during the thermal design, if many constraints are imposed, it may not be possible to satisfy all conditions. It is the designer's job to make judgments on these constraints that can be relaxed to obtain a good design.

Ideally the optimization exercise should in most cases not only be limited to the heat exchanger, but should be extended to include the entire system or process [87VE1]. Such a thermo economic analysis combines a second-law (exergy) analysis with an economic one [89TS1, 94MO1].

In a multi-dimensional design space, an intuitive approach to optimizing a system, becomes a futile exercise. For a limited number of variables, analytic approaches may indicate certain trends [72MO1, 73MO1, 80MO3], but these methods are inadequate in the case of more detailed system optimizations.

Heat exchanger optimization through a package of optimization computer programs has been suggested by Shah [78SH1, 81SH1]. A summary of optimization procedures applicable to air-cooled heat exchanger, is presented by Hedderich et al [82HE1].

Several papers have adressed the problem of economic optimization of dry-cooled power plants [70RO1, 70SM1, 71HA1, 74MI1, 76FR1, 79CH1, 85LI1, 87VE1, 90LO1]. More complex optimization studies are attempted by other investigators [78EC1, 89BU1, 89BU2].

9.3 REFERENCES

70RO1 Rossie, J.P. and Cecil, E.A., Research on Dry-type Cooling Towers for Thermal Electric Generation. Part I and II. EPA Report, Water Pollution Control Research Series 16130 EES.

70SM1 Smith, E.C. and Larinoff, M.W., Power Plant Siting, Performance and Economics with Dry Cooling Tower Systems, Proceedings of the American Power Conference, No. 32, pp. 544-572, 1970.

71HA1 Hauser, L.G., Oleson, K.A. and Budenholzer, R.J., An Advanced Optimization Technique for Turbine, Condenser, Cooling System Combinations, Proceedings of the American Power Conference, No. 33, pp. 427-445, 1971.

72MO1 Moore, F.K., On the Minimum Size of Natural-Draft Dry Cooling Towers for Large Power Plants, ASME Paper 72-WA/HT-60 presented at the 1972 Winter Annual Meeting, Nov., 1972.

73MO1 Moore, F.K., The Minimization of Air Heat-Exchange Surface Areas of Dry Cooling Towers for Large Power Plants, Heat Transfer Digest, Vol. 6, pp. 13-22, 1973.

74MI1 Miliaras, E.S., Power Plants with Air-cooled Condensing Systems, MIT Press, Cambridge, Massachusetts.

76FR1 Fryer, B.C., A Review and Assessment of Engineering Economic Studies of Dry Cooled Electrical Generating Plants, BNWL 1976.

77PO1 Powell, M.J.D., A Fast Algorithm for Nonlinearly Constrained Optimization Calculation, in Numerical Analysis, Proceedings Dundee, Springer Lecture Notes in Mathematics 630, ed G.A. Watson, pp. 114-157, 1977.

78EC1 Ecker, J.G. and Wiebking, R.D., Optimal Design of a Dry-type Natural-draft Cooling Tower by Geometric Programming, Journal of Optimization Theory and

Applications, Vol. 26, No. 2, pp. 305-323, 1978.

78LA1 Lasdon, L.S., Waren, A.D., Jain, A. and M. Ratner, Design and Testing of a Generalized Reduced Gradient Code for Nonlinear Programming, ACM Transactions on Mathematical Software 4, pp. 34-50, 1978.

78SH1 Shah, R.K., Afimiwala, K.A. and Mayne, R.W., Heat Exchanger Optimization, Heat Transfer 1978, Vol. 4, pp. 193-199, Hemisphere Publishing Corporation, Washington, 1987.

79CH1 Choi, M. and Glicksman, L.R., Computer Optimization of Dry and Wet/dry Cooling Tower Systems for Large Fossil and Nuclear Power Plants, MIT Energy Laboratory Report No. MIT-EL 79-034, Cambridge, Massachusetts, 1979.

81SH1 Shah, R.K., Compact Heat Exchanger Surface Selection, Optimization, and Computer-aided Thermal Design, Low Reynolds Number Flow Heat Exchangers, ed. Kakac, S., Shah, R.K. and Bergles, A.E., Hemisphere Publishing Corporation, Washington, 1983.

82HE1 Hedderich, C.P., Kelleher, M.D. and Van der Plaats, G.N., Design and Optimization of Air-Cooled Heat Exchangers, Trans. ASME, Jnl. of Heat Transfer, Vol. 104, pp. 683-690, 1982.

83PO1 Powell, M.J.D., VMCWD: A Fortran Subroutine for Constrained Optimization. SIGMAP Bulletin, No. 32, 1983.

85LI1 Li, K.W. and Sadiq, W., Computer-aided Optimization of Cooling Systems, ASME International Computers in Engineering Conference, No. 3, pp. 165-171, 1985.

87BE1 Bejan, A., The Thermodynamic Design of Heat and Mass Transfer Processes and Devices, Int, J. Heat and Fluid Flow, Vol. 8, No. 4, pp. 258-276, 1987.

87VE1 Veck, G.A., and Rubbers, P.J.E., Economic Evaluation of Dry Cooling: The

Options, Proc. VGB Conference, South Africa 1987, Vol. 1, pp. 80-89, Johannesburg, November 1987.

89BU1 Buys, J.D. and Kröger, D.G., Dimensioning Heat Exchangers for Existing Dry Cooling Towers, Energy Conversion Management, Vol. 29, No. 1, pp. 63 - 71, 1989.

89BU2 Buys, J.D. and Kröger D.G., Cost-optimal Design of Dry Cooling Towers through Mathematical Programming Techniques, ASME Jnl of Heat Transfer, Vol. 111, pp. 322 - 327, 1989.

89TS1 Tsatsaronis, G. and Valero, A., Thermodynamics Meets Economics, Mechanical Engineering, Vol. 111, No. 8, pp. 84-86, August 1989.

90LO1 Lovino, G., Hattoni, H., Hazzocchi, L., Senis, R. and Vanzan, R., Optimal Sizing of Natural Draft Dry Cooling Towers for ENEL Combined Cycle Power Plants, A Future for Energy, FLOWERS '90, Proceedings of the Florence World Energy Research Symposium, Firenze, Italy 1990, eds Stecco, S.S. and Moran, M.J., pp. 669-680, Pergamon Press, New York, 1990.

91CO1 Conradie, T.A. and Kröger, D.G., Enhanced Performance of a Dry-cooled Power Plant Through Air Precooling, ASME Paper 91-JPGC-Pwr-6 presented at the ASME International Joint Power Conference, San Diego, October 1991.

94MO1 Moran, M.J. and Sciubba, E., Exergy Analysis: Principles and Practice, Trans. of the ASME, Journal of Engineering for Gas Turbines and Power, Vol. 116, pp. 285-290, April 1994.

CHAPTER 10

ENVIRONMENTAL EFFECTS

10.0 INTRODUCTION

The performance of all air-cooled heat exchangers and cooling towers are affected by changes in ambient conditions. Changes in temperature generally exert the biggest influence while winds, inversions, rain, snow, hail and solar radiation have a lesser effect. The influences of winds and inversions are described in considerable detail in the following sections. Rain tends to reduce the drybulb temperature to nearly wetbulb values. Some wetting of finned surfaces may occur in dry systems. These effects generally have a beneficial influence on performance. In natural draft cooling towers, cooling of the air in the tower and a reduction of the draft due to the falling droplets will however have a detrimental effect on performance[79HE1]. Generally the effects on performance due to rain and snow are small. During periods of very low ambient temperatures, freezing of the cooling water can lead to serious structural and performance problems. Different devices and procedures are employed to avoid freezing [94FA1]. In certain areas where hail storms occur, protective screens are installed above finned surfaces. A maximum solar radiation of almost 1 kW/m^2 may strike the heat transfer surface for a short period during the day. This will reduce the rate of heat rejection in certain installations. In an aluminum clad natural draft dry-cooling tower, the draft and corresponding heat rejection rate will be slightly affected when the tower shell is exposed to solar radiation [94NO1].

Undoubtedly the most stringent heat exchanger specifications concerning the integrity and performance under different meteorological and seismic conditions are found in the nuclear industry [94BA1].

When designing a large industrial cooling system, ambient conditions must be considered. The orientation of the cooling system or even the entire plant may to some extent be determined by the direction of the prevailing winds.

10.1.1 THE ATMOSPHERE

The atmosphere is a mixture of gases of which oxygen and nitrogen are the main constituents, but it also contains small amounts of water vapor and other gases, including carbon dioxide, hydrogen and helium and the rare inert gases argon, krypton, neon etc. Over the range of altitudes involved in conventional aerodynamics the properties of the constituents varies little and the atmosphere may be regarded as a homogeneous gas of uniform composition.

Consider a small parcel of air that may be moved up or down in the atmospheric pressure field. If this process is adiabatic, i.e. no heat is transferred to the parcel by either conduction or radiation, it will experience a change in temperature as a result of the change in pressure.

The pressure gradient in a gravity field is given by

$$dp/dz = -\rho g \tag{10.1.1}$$

For an isentropic process

$$p/\rho^{\gamma} = \text{constant} \tag{10.1.2}$$

The air density may be expressed through the perfect gas law as

$$\rho = p/RT \tag{10.1.3}$$

Substitute equation (10.1.3) into equation (10.1.2) and differentiate with respect to altitude to find

$$\frac{(1-\gamma)}{\gamma p}\frac{dp}{dz} + \frac{1}{T}\frac{dT}{dz} = 0 \tag{10.1.4}$$

By combining the equations (10.1.1), (10.1.3) and (10.1.4) the temperature gradient may be expressed as

$$\frac{dT}{dz} = -\frac{g(\gamma - 1)}{\gamma R} = -\frac{g}{c_p} \tag{10.1.5}$$

The gravitational acceleration, g, is a function of both latitude and altitude. Changes in g are however so small that the influence thereof on the performance of an air-cooled heat exchanger or cooling tower is negligible.

For dry air with $\gamma = c_p/c_v = 1.4$ and $R = 287.08$ J/kg K, find for $g = 9.8$ m/s^2

$$\frac{dT}{dz} = -0.00975 \text{ K/m} \tag{10.1.6}$$

This temperature gradient is known as the dry adiabatic lapse rate (DALR).

Upon integration of equation (10.1.5), find

$$T = T_1 - g(\gamma - 1)z/(\gamma R) \tag{10.1.7a}$$

where T_1 is the temperature at ground level.

For dry air this equation reduces to

$$T = T_1 - 0.00975z \tag{10.1.7b}$$

From equations (10.1.1) and (10.1.3) it follows that:

$$\frac{dp}{p} = -\frac{g\,dz}{RT} \tag{10.1.8}$$

Substitute equation (10.1.7a) into equation (10.1.8) and integrate between ground level and an elevation z.

$$p = p_1\left[1 - g(\gamma - 1)z/(\gamma R T_1)\right]^{\gamma/(\gamma - 1)} \tag{10.1.9a}$$

For dry air with $g = 9.8$ m/s^2, equation (10.1.9a) becomes

$$p = p_1(1 - 0.00975\ z/T_1)^{3.5} \tag{10.1.9b}$$

Different results are obtained if the air contains a significant amount of water vapor [75SE1]. When a parcel of moist air is raised in a gravitational field, adiabatic cooling takes place until the air reaches the point of saturation. Upon a further rise in elevation, cooling will cause vapor to condense and precipitate out of the air parcel. The energy removed from the vapor during this condensation process is then available to heat the surrounding air. This heating that takes place during the precipitation is a pseudoadiabatic process. Consider a parcel of saturated air (m_a is the air constituent) rising through a height dz. The amount of condensate formed during this change in elevation is dm_w. According to the first law of thermodynamics, find

$$m_a (i_{ma} + di_{ma}) + (m_w + dm_w) c_{pw} (T + dT - 273.15) + m_a (1 + w + dw) g (z + dz)$$

$$+ (m_w + dm_w) g (z + dz) = m_a i_{ma} + m_w c_{pw}(T - 273.15) + m_a(1 + w)gz + m_w gz \tag{10.1.10a}$$

where according to equation (A.3.6b)

$$i_{ma} = c_{pa}(T - 273.15) + w [i_{fgwo} + c_{pv}(T - 273.15)]$$

and

$$di_{ma} = c_{pa}dT + dw[i_{fgwo} + c_{pv}(T - 273.15)] + wc_{pv}dT$$

with i_{fgwo} the latent heat of water at 273.15K.

When second order terms are neglected, equation (10.1.10a) reduces to

$$m_a(c_{pa} + wc_{pv}) dT + m_a dw [i_{fgwo} + c_{pv}(T - 273.15)] + m_w c_{pw} dT + dm_w c_{pw}$$

$$(T - 273.15) + m_a(1 + w)gdz + m_a dwgz + m_w gdz + dm_w gz = 0 \tag{10.1.10b}$$

According to the conservation of mass

$$dm_w = -m_a dw \tag{10.1.11}$$

Furthermore, for most practical cases $m_w << m_a$. Substitute equation (10.1.11) into equation (10.1.10b), to find with $m_w << m_a$

$$\frac{dT}{dz} = \xi_T = \frac{-(1 + w)g}{c_{pma} + \left[i_{fgwo} - (c_{pw} - c_{pv})(T - 273.15)\right]dw/dT} \tag{10.1.12}$$

where $c_{pma} = c_{pa} + w\, c_{pv}$.

According to equation (4.1.12) the humidity ratio can be expressed as

$$w = 0.622 p_v/(p - p_v) \tag{10.1.13}$$

where p is the measured atmospheric pressure.

The saturation pressure of water vapor is an exponential function of temperature, and can be determined according to equation (A.2.1), or more simply in the range 273.15 K to 313.15 K (0° to 40°C)

$$p_v = 2.368745 \times 10^{11} \exp(-5406.1915/T) \tag{10.1.14}$$

where T is in Kelvin.

Introducing the chain rule of differentiation, find

$$dw/dT = (dw/dp_v)\ (dp_v/dT) \tag{10.1.15}$$

Substitute equations (10.1.13) and (10.1.14) into equation (10.1.15) to find for $p_v << p$

$$\frac{dw}{dT} = \frac{7.966 \times 10^{14}}{pT^2}\exp\left(-\frac{5406.1915}{T}\right)$$

Substitute this expression for dw/dT into equation (10.1.12) and find

$$\xi_T = \frac{-(1+w)g}{c_{pma} + \dfrac{7.966 \times 10^{14}}{pT^2}\left[i_{fgwo} - \left(c_{pw}-c_{pv}\right)(T - 273.15)\right] \exp(-\ 5406.1915/T)} \tag{10.1.16a}$$

In general this temperature gradient is lower than the dry adiabatic lapse rate.

Since usually $w << 1$ and $(c_{pw} - c_{pv})(T - 273.15) << i_{fgwo}$, equation (10.1.16a) can be simplified to give [93AZ1]

$$\xi_T = -\ g/\left[c_{pa} + 7.966 \times 10^{14} i_{fgwo} \exp(-\ 5406.1915/T)/\left(pT^2\right)\right] \tag{10.1.16b}$$

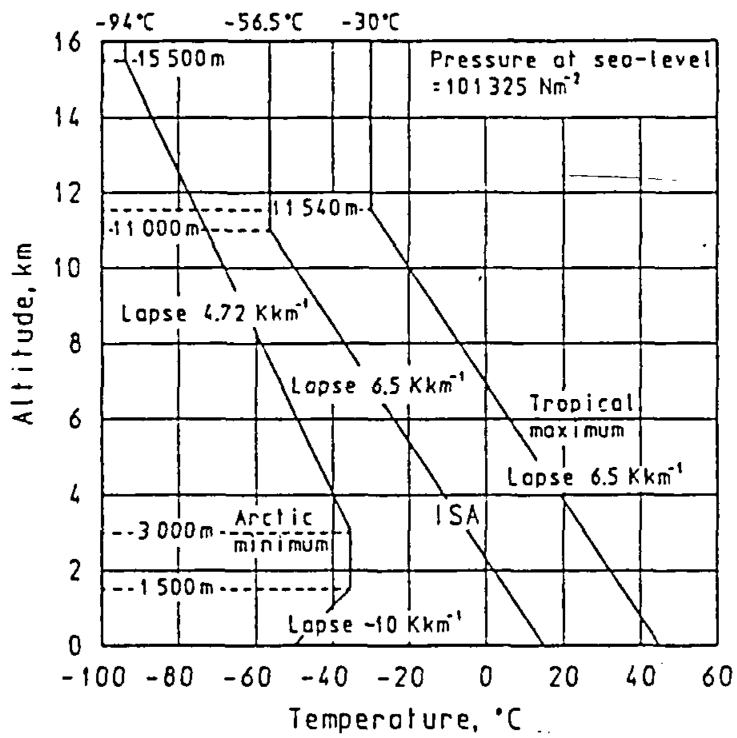

Figure 10.1.1 Variation of temperature with height in the International Standard, Tropical Maximum and Arctic Minimum Atmosphere.

Investigation has shown that the atmosphere actually consists of two distinct contiguous regions. The lower of these regions is called the troposphere, and it is found that the temperature within the troposphere decreases approximately linearly with height. The upper region is the stratosphere wherein the temperature remains almost constant with height. The supposed boundary between the two regions is termed the tropopause. The sharp distinction between the two, implied above, does not exist in reality, but one merges gradually into the other. Nevertheless, this distinction represents a useful convention for the purposes of calculation. An International Standard Atmosphere (ISA) intended to approximate the atmospheric conditions prevailing for most of the year in temperate latitudes is defined as having a mean sea level pressure of 101325 N/m^2, a corresponding temperature of 15°C with a mean lapse rate of 0.0065 K/m to a height of 11 km. These values are shown in figure 10.1.1 which also shows the characteristics of two other agreed upon "standard atmospheres" intended to represent the most extreme conditions likely to be encountered on earth. With this model of the atmosphere it is possible to find approximately the required physical characteristics at any altitude.

It is noted that the ISA lapse rate is lower than that given by equation (10.1.7) due to the absorption of solar radiation by the atmospheric gases, especially carbon dioxide and water vapor. According to the former the variation of temperature with altitude in the troposphere is

$$T = T_0 - z\, dT/dz = 288.15 - 0.0065\, z \tag{10.1.17}$$

According to this lapse, the ISA troposphere obeys a law of the form

$$p/\rho^{1.235} = \text{constant} \tag{10.1.18}$$

From equations (10.1.1) and (10.1.3) it follows that:

$$\frac{dp}{p} = \frac{g\, dz}{RT} = \frac{g\, dz}{R\,(288.15 - 0.0065\, z)} \tag{10.1.19}$$

Integrate equation (10.1.19) between sea level and some altitude z, to find with g = 9.8 m/s^2 and R = 287.08 J/kgK, the relation between atmospheric pressure and altitude up to 11000 m.

$$p = 101325 \left(1 - 2.2642 \times 10^{-5}\, z\right)^{5.2561} \tag{10.1.20}$$

10.1.2 THE PLANETARY BOUNDARY LAYER

The lower 1-2 km of the troposphere is usually called the planetary boundary layer (PBL) after Lettau [39LE1] and sometimes the friction layer. This boundary layer is characterized by large vertical gradients in the wind velocity, air temperature and humidity. Transport through the planetary boundary layer is by virtue of eddy diffusion, and the physical state of the boundary layer depends on the surface fluxes of momentum, heat and moisture.

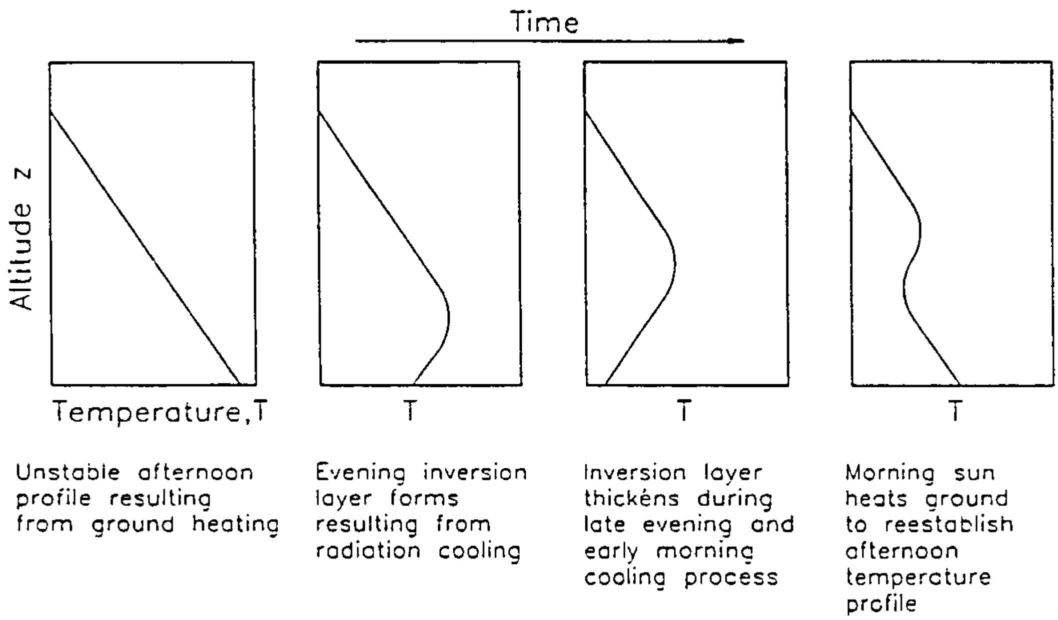

Figure 10.1.2: Typical diurnal variation of atmospheric temperature profile.

Significant diurnal variations in air temperature near the surface may be experienced due to radiative heating and cooling of the surface, as shown schematically in figure 10.1.2. In the afternoon the sun will have heated the ground to well above the mean air temperature, resulting in a net heat flux from the surface to the atmosphere. Convectively unstable conditions might be experienced where the temperature drops more sharply than predicted by the DALR. As the sun sets, the ground begins to cool by radiation (assuming a clear sky). The surface temperature may drop below the mean air temperature, whence the net heat flux is reversed, causing heat to flow from the lowest few meters of the atmosphere to the soil and a surface temperature inversion may be formed as shown. Cooling continues throughout the night so that the inversion layer thickens to its maximum value at about the time the sun rises. As morning arrives, and progressively greater amounts of solar radiation heats up the ground, a transition profile as shown, may be encountered. With sufficient heating the unstable afternoon profile is established once again.

An example of hourly temperature data actually measured at eight different heights on a 96m high weather mast over a period of 24 hours is listed in table 10.1.1 and shown graphically in figure 10.1.3.

The vertical temperature gradients obviously depend on local wind and weather conditions. Clouds reflect much of the earth's radiation loss back to the surface, thereby raising the surface temperature substantially, even to the extent where the forming of an inversion is suppressed. Furthermore, the turbulence associated with wind will enhance mixing in the atmospheric boundary layer, and a much subdued temperature profile will result. Golder [72GO1] stated that wind velocities above 8 m/s will invariably result in a neutral (adiabatic) atmosphere.

Table 10.1.2: Roughness lengths for various surfaces.

Surface configuration	Roughness length [m]
Urban areas:	
Central business district	8.000000
High density residential	4.500000
Low density residential	2.000000
Rolling relief:	
Coastal bush	1.000000
Open savanna	0.800000
Full grown root crops	0.250000
Shrubs	0.150000
Flat relief, vegetated:	
Uncut grass	0.070000
Crop stubble	0.020000
Snow and short grass	0.002000
Flat relief, unvegetated:	
Natural snow (temporary)	0.001000
Bare sand	0.000400
Open sea	0.000200
Water	0.000100
Snow (permanent)	0.000050
Mud flats and ice	0.000001

Table 10.1.1: Hourly temperatures in °C at different elevations.

Alt. m	12h00	13h00	14h00	15h00	16h00	17h00
96	28.15	29.61	29.79	30.35	30.91	30.31
65	28.43	29.90	30.20	30.72	31.41	30.73
40	28.65	30.36	30.53	31.23	31.89	30.93
20	29.04	30.52	30.81	31.42	31.88	31.04
10	29.55	31.07	31.27	31.95	32.01	31.20
5	30.21	31.59	31.92	32.46	32.45	31.53
2	30.88	32.21	32.57	33.01	32.75	31.69
1	31.45	32.90	33.10	33.63	33.32	31.94
	18h00	19h00	20h00	21h00	22h00	23h00
96	28.26	27.44	27.08	26.74	25.95	24.38
65	28.34	27.35	26.62	26.33	25.43	23.80
40	27.82	26.25	23.46	22.61	22.36	22.03
20	27.40	24.26	21.68	20.41	19.69	19.10
10	26.54	21.99	20.07	18.40	17.57	16.45
5	25.82	20.46	18.03	15.87	15.90	14.39
2	24.63	18.13	15.27	13.53	14.44	12.87
1	23.36	16.19	13.81	12.35	12.85	11.72
	00h00	01h00	02h00	03h00	04h00	05h00
96	24.90	23.36	22.41	21.55	22.12	23.11
65	24.74	22.57	20.99	18.80	20.62	20.85
40	22.71	20.50	18.90	16.11	18.07	17.19
20	18.97	16.63	15.96	15.58	15.51	14.43
10	14.80	11.48	13.78	10.81	10.83	11.16
5	11.81	10.50	11.38	9.30	8.70	9.12
2	10.65	9.85	9.81	8.40	7.94	8.24
1	9.86	9.17	8.95	7.66	7.44	7.62
	06h00	07h00	08h00	09h00	10h00	11h00
96	22.42	20.48	20.79	20.16	22.99	26.48
65	19.77	17.34	17.32	18.63	23.30	26.69
40	15.34	14.80	15.35	18.58	23.85	26.94
20	14.18	13.38	14.52	18.77	24.05	27.29
10	11.13	10.50	12.18	18.77	24.40	27.72
5	8.57	8.33	10.95	18.82	24.65	28.20
2	7.35	6.72	10.92	19.00	25.06	28.73
1	6.54	5.49	10.18	19.67	25.57	29.12

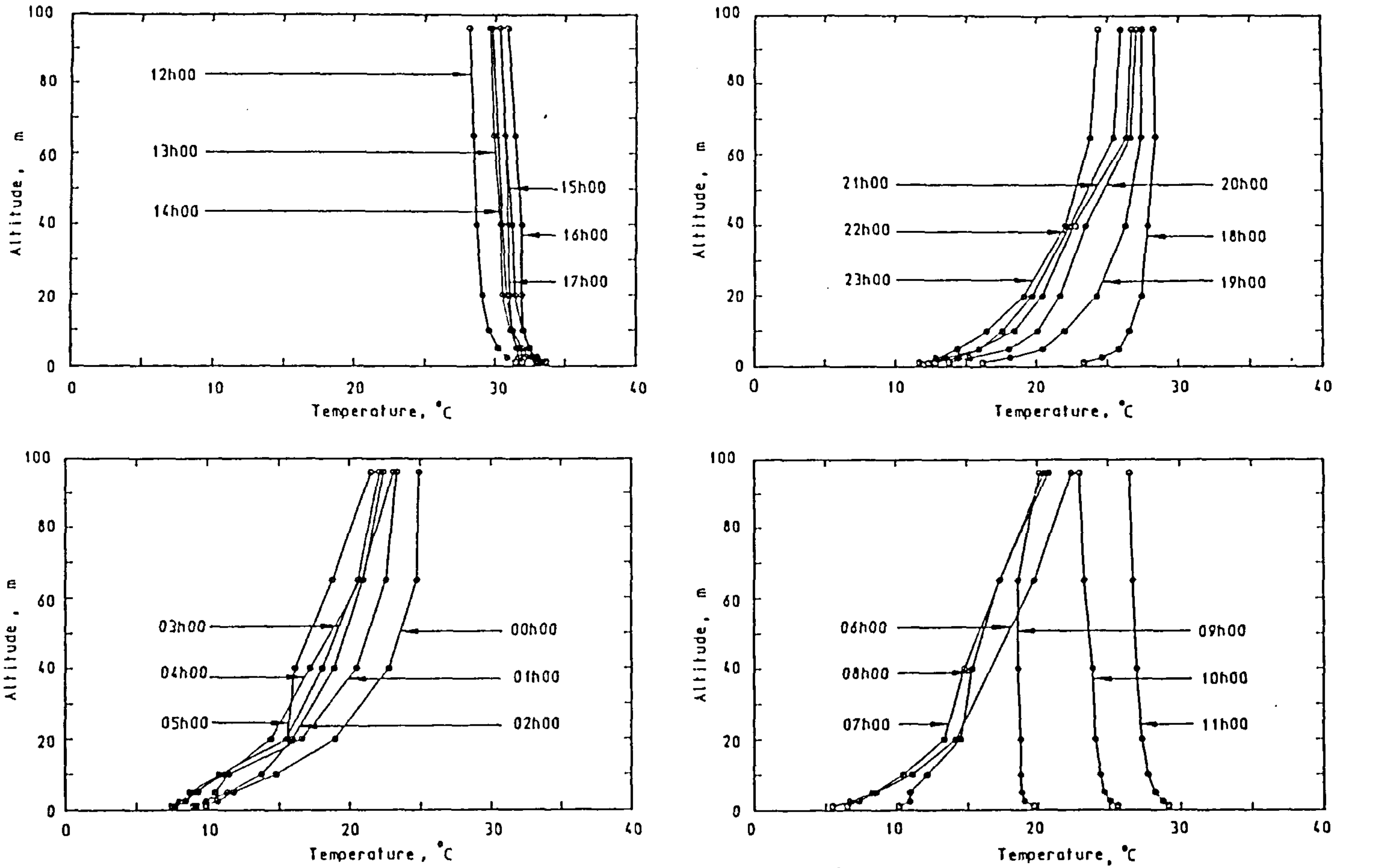

Figure 10.1.3: Hourly temperature distribution

The lowest ten per cent of the planetary boundary layer, often referred to as the constant flux layer or surface boundary layer (SBL), usually exhibits little, if any, change with height in the vertical fluxes of momentum, heat and water vapor. Dimensional analysis of the mean wind and temperature profiles in the constant flux layer, well above the aerodynamic roughness elements, is well treated in textbooks, for example Seinfeld [75SE1]. Values for the surface roughnesses corresponding to particular surface geometries, are listed in table 10.1.2. When the surface layer is non-neutral, the similarity theory of Monin and Obukhov [54MO1] suggests that the vertical fluxes of momentum and heat in the surface layer may be expressed by

$$\frac{dv}{dz} = \frac{v_s}{\kappa z}\phi_m\left(\frac{z}{L_{mo}}\right) \qquad (10.1.21)$$

and

$$\frac{d\theta}{dz} = \frac{\theta_s}{\kappa z}\phi_h\left(\frac{z}{L_{mo}}\right) \qquad (10.1.22)$$

respectively. κ is the von Karman constant ($\kappa = 0.4$) and θ the potential temperature, that is, the temperature a parcel of air will attain if it were brought adiabatically to a standard pressure at the earth's surface. ϕ_m and ϕ_h are universal functions for momentum and heat transfer in the constant flux layer, and depend on the thermal stability of the layer. Some values for ϕ_m and ϕ_h corresponding to various stability classes are listed in table 10.1.3. v_s is the shear velocity at the surface, defined as

$$v_s = \tau/\rho \qquad (10.1.23)$$

with τ the shear stress at the surface, and θ_s is the scaling temperature, defined as

$$\theta_s = -q/(\rho c_p \kappa\, v_s) \qquad (10.1.24)$$

where q is the sensible heat flux.

One way of establishing the stability class of the atmosphere, is by using Monin and Obukhov's scaling length, L_{mo}, which may be interpreted as that height at which the magnitudes of mechanical and thermal production of turbulence are equal. The Monin-

Obukhov length is defined in terms of the turbulent fluxes as follows :

$$L_{mo} = T_m v_s^2 / (g\kappa^2 \theta_s) \qquad (10.1.25)$$

and the atmospheric stability is divided into classes, based on the Monin-Obukhov length as follows :

$$L_{mo}^{-1} \begin{cases} \leq 0 \ ; & \text{unstable} \\ = 0 \ ; & \text{neutral} \\ > 0 \ ; & \text{stable} \end{cases}$$

T_m is the mean temperature of the layer under consideration.

Table 10.1.3: A summary of universal functions for the surface boundary layer.

Limits	Momentum, ϕ_m	Heat, ϕ_h
$-\infty \leq (z/L_{mo}) < -10$	$[1 - 16\,(z/L_{mo})]^{-0.25}$	$[1 - 16\,z/L_{mo})^{-0.5}$
$-10 \leq (z/L_{mo}) < 0$	$[1 - 16\,(z/L_{mo})]^{-0.333}$	$[1 - 16\,(z/L_{mo})^{-0.5}$
$0 \leq (z/L_{mo}) < 0.3$	$[1 + 6\,(z/L_{mo})]$	$[1 + 6\,(z/L_{mo})]$
$0.3 \leq (z/L_{mo}) \leq 10$	$[1 + 22.8\,(z/L_{mo})]^{0.5}$	$[1 + 22.8\,(z/L_{mo})]^{0.5}$

To close the solution of the above set of equations, one has to solve for the surface temperature. This task is easily performed by taking an energy balance for a thin slab at the surface, as shown in figure 10.1.4. All fluxes directed towards the surface are taken as negative. It is assumed that the earth's albedo, α, is known and constant, the soil is void of any moisture, and dew that forms during the night will not enter the soil, but evaporate again in the morning. Furthermore, evaporation from the soil and plants is ignored in the energy balance. If no information on the earth's albedo is available, Baer [78BA1] suggests that a value of $\alpha = 0.25$ is accepted by default.

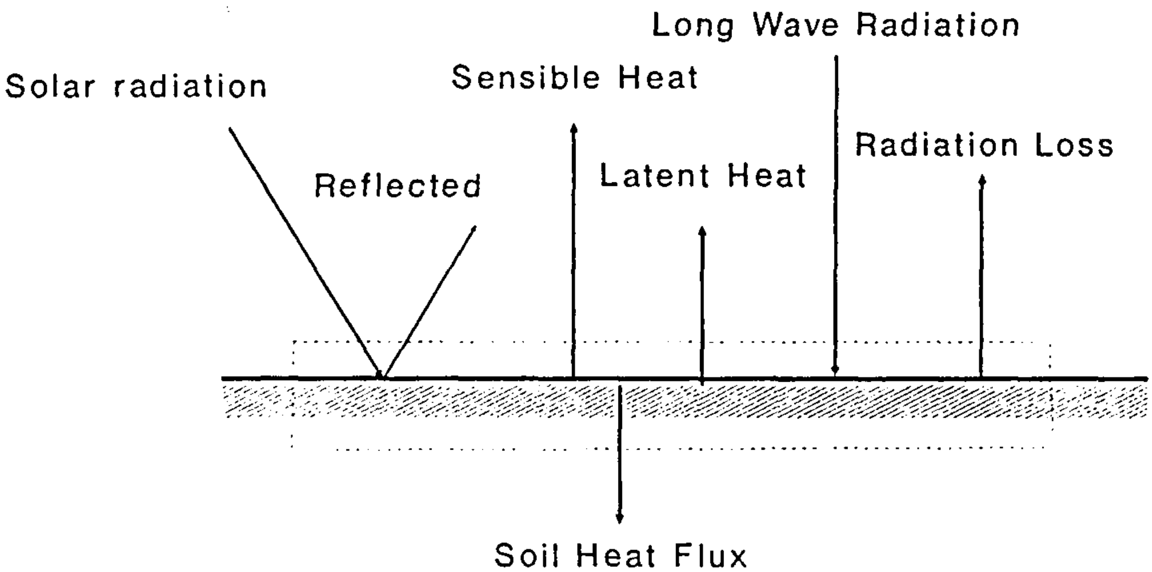

Figure 10.1.4: Control volume for energy balance at the earth's surface.

In the absence of evaporation or condensation at the surface, the energy balance yields

$$- q + \sigma T^4 + k_s dT_s/dz - (1 - \alpha)\, I_{solar} - I_{longwave} = 0 \tag{10.1.26}$$

De Bruin and Holtslag [82DE1] suggest that the value of the soil heat flux should be taken as ten per cent of the net radiation flux to the atmosphere. However, this simplification is no real substitute for the true value of the soil heat flux, since heat transfer in the soil is by virtue of conduction, which is easy to calculate. Details of the other fluxes are given by Hoffmann and Kröger [93HO1].

The outer part of the atmospheric boundary layer is called the Ekman layer, after the Swedish mathematician Ekman, who was the first to solve the simplified Navier-Stokes equations for wind and temperature in this layer, assuming a constant eddy diffusion coefficient. The behavior of the Ekman layer is complicated and difficult to predict, but numerous experimental studies have shown that empirical power law profiles to be applicable in quite a wide range of atmospheric conditions [82BU1]. The velocity profile is then given by

$$v = v_c + \{v_r - v_c\} \left[(z - z_c)/(z_r - z_c)\right]^b \tag{10.1.27}$$

where v_r and z_r are the reference velocity and height respectively, selected for the particular application, and z_c is the height of the constant flux layer. Quite often the planetary boundary layer thickness is selected as reference height, with the geostrophic wind the corresponding reference velocity. Although the 1/7 law is often quoted for neutral conditions, the value of the exponent b generally increases with increasing stability and surface roughness. Gee [65GE1] proposed:

$$b = 0.143 + 0.244\, L_{mo}^{-1} + 0.22\, L_{mo}^{-2} \tag{10.1.28}$$

The same procedure is also applicable in the evaluation of the temperature profile in this layer. The temperature in the upper atmosphere will not change significantly over the span of a few days, and it is assumed that the temperature gradient conforms to the International Standard Atmosphere. If no temperature readings in the upper atmosphere are available, one may proceed by assuming that the ISA holds for the remainder of the atmospheric boundary layer, from which it is possible to estimate the temperature at the top of the Ekman layer.

The most significant variations in temperature thus appear in the lower approximately 100m of the PBL, also known as the surface boundary layer (SBL). In general, the temperature distribution in the SBL can be expressed approximately by the following relation:

$$\frac{T - T_o}{T_r - T_o} = \left(\frac{z}{z_r}\right)^b \tag{10.1.29}$$

where T_o is the temperature at ground level, and T_r is some reference temperature measured at the reference height z_r. The latter may for example correspond to the elevation of the highest temperature measuring point, or in the case of a temperature inversion that point where the inversion ends, i.e. where $dT/dz = 0$.

On windy days or nights, particularly with thick clouds, the PBL, is completely turbulent and its depth is determined by wind speed and surface roughness. It is common engineering practice to describe the wind profile by means of a power law

$$v/v_r = \left(z/z_r\right)^b \tag{10.1.30}$$

where v_r is the wind speed at the reference height z_r. According to Panofsky and Dutton [84PA1] the exponent b can be approximated by the following relation

$$b = 1/\ln(z/z_o) \tag{10.1.31}$$

If the boundary layer dynamics are parameterized, the thickness of the atmospheric boundary layer under adiabatic conditions is given by O' Brien [70BR1]

$$z_{pbl} = \kappa v_s \;/\; (2\;\Omega \sin\psi) \tag{10.1.32}$$

with Ω the rotational velocity of the earth in radians per second, and ψ the latitude.

Zilitinkevic [72ZI1] derived the following expression for the boundary layer thickness under convectively stable stratification

$$z_{pbl} = \kappa\left[v_s\; L \;/\; (2\;\Omega \sin\psi)\right]^{0.5} \tag{10.1.33}$$

When convectively unstable conditions prevail in the atmosphere, the boundary layer thickness changes rapidly, and prognostic models should be used. Maul [80MA1] developed the following stepwise algorithm to estimate the boundary layer thickness at time $\tau + \Delta\tau$, provided that the boundary layer thickness was previously known at time τ.

$$z_{pbl} = \left[z_{pbl}^2\,(\tau) + \frac{2.3\;q\;\Delta\tau}{\xi_{sa}\;\rho\;c_p} + \frac{2\;\Delta T_{bl} z_{pbl}\;(\tau)}{\xi_{sa}}\right]^{0.5} + \frac{\Delta T_{bl}}{\xi_{sa}} \tag{10.1.34}$$

where ξ_{sa} is the temperature lapse rate in the upper troposphere i.e. ξ_{sa} = ISA temperature lapse rate = 0.0065 K/m, and ΔT_{bl} is the temperature discontinuity at the top of the atmospheric boundary layer, given by

$$\Delta T_{bl} = \left[0.3\ \xi_{sa}\ q\ \Delta\tau\ /\ (\rho\ c_p)\right]^{0.5} \qquad (10.1.35)$$

Equation (10.1.31) assumes horizontally homogeneous conditions; consequently, large errors might occur in situations near the coast or an escarpment.

10.2.1 EFFECT OF WIND ON COOLING TOWERS

Measurements performed on natural draft cooling towers subject to cross-winds indicate a rise in water temperature with increasing wind speed for a given heat rejection rate [67PR1, 69CH1, 76VA1, 77MA1, 78BA1, 79BA1, 79DI1, 79OL1, 80BO1, 87TR1, 89CA1, 92DU1]. Studies on dry-cooling towers show similar trends to those found in wet towers. In a dry tower the rise in outlet water temperature or change in the difference between this temperature and that of the ambient air entering the tower (change in approach temperature) may be expressed as follows:

$$\Delta T_{wo} = \Delta\left(T_{wo} - T_{ai}\right) = \left(T_{wo} - T_{ai}\right)_w - \left(T_{wo} - T_{ai}\right) \qquad (10.2.1)$$

where the first term on the right hand side of the equation represents the temperature difference during windy conditions while the second term is the difference in temperature in the absence of wind.

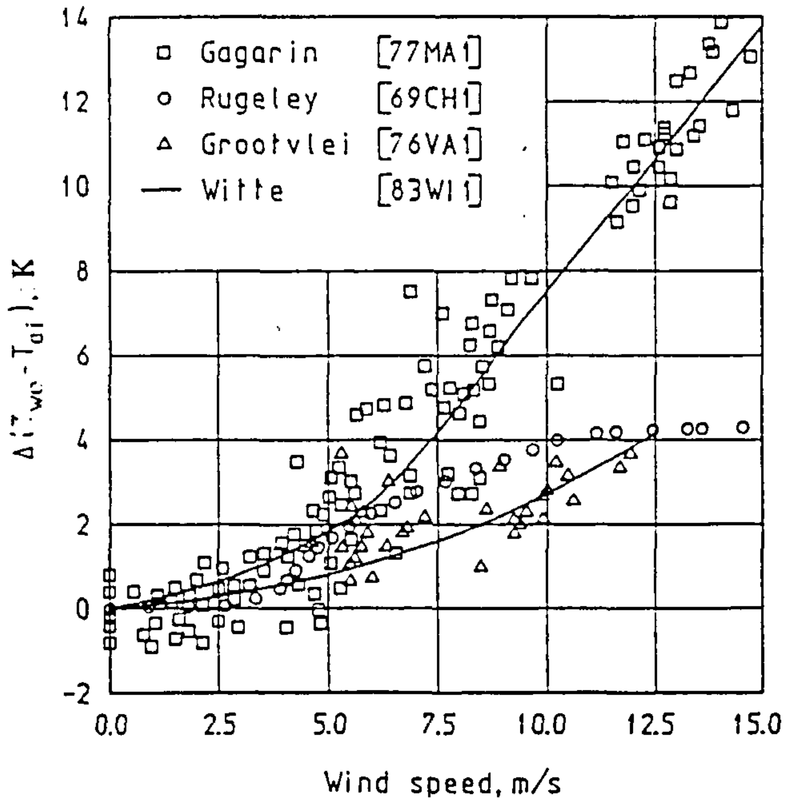

Figure 10.2.1: Rise in cooling water temperature due to wind measured approximately 10m above ground level.

Shortly after the dry-cooling towers at Rugeley and Ibbenbüren were commissioned, it was reported that their performance was measurably reduced during windy periods [67PR1, 69CH1]. Markòczy and Stämpfli [77MA1] report the results of measurements performed at the Gagarin (Visonta) power plant in Hungary. The trend of their data is similar to that observed at Rugeley up to wind speeds of 6 m/s. Above this value the two sets of data diverge as is shown in figure 10.2.1. Measurements conducted by Van der Walt et al [76VA1] on the Grootvlei 5 tower, in which the heat exchanger bundles are arranged horizontally in a rectangular pattern of A-frames, suggest that this layout is less sensitive to wind. Markòczy [77MA1] argues that the greater temperature difference in the Grootvlei towers ensures a better flow through the bundles and therefore the towers appear to be less affected by the wind. Approximate correlations of wind data for different dry-cooling towers are shown graphically in figure 10.2.2 [87TR1]. The curve for Grootvlei 6 appears to be unrealistically low and results are more likely to follow the dashed curve.

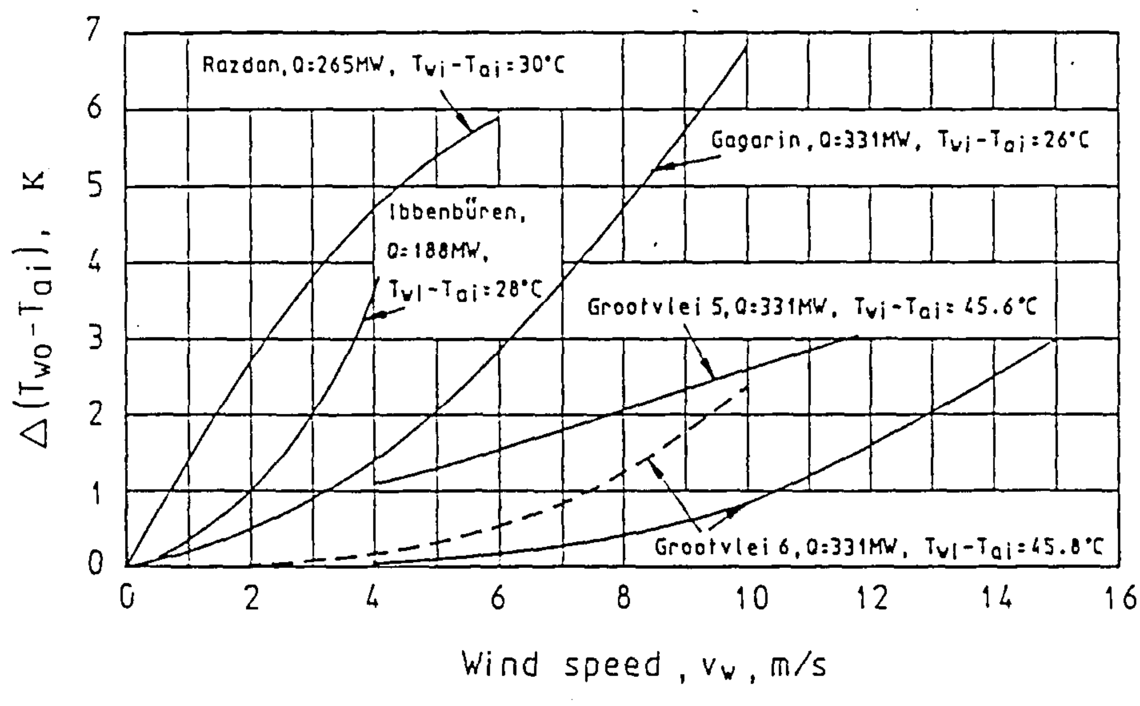

Figure 10.2.2: Rise in cooling water temperature due to wind (dry towers).

Wet towers with horizontal fills are also generally less sensitive to winds than cross-flow towers. The change in temperature difference between the water outlet temperature and the wetbulb temperature of the entering ambient air, T_{wb}, for different wet towers is shown in figure 10.2.3 [89CA1]. All are counterflow towers except for Saint Laurent and

Emile Huchet which are cross-flow towers. All wind speeds were measured at an elevation of 11m above ground level.

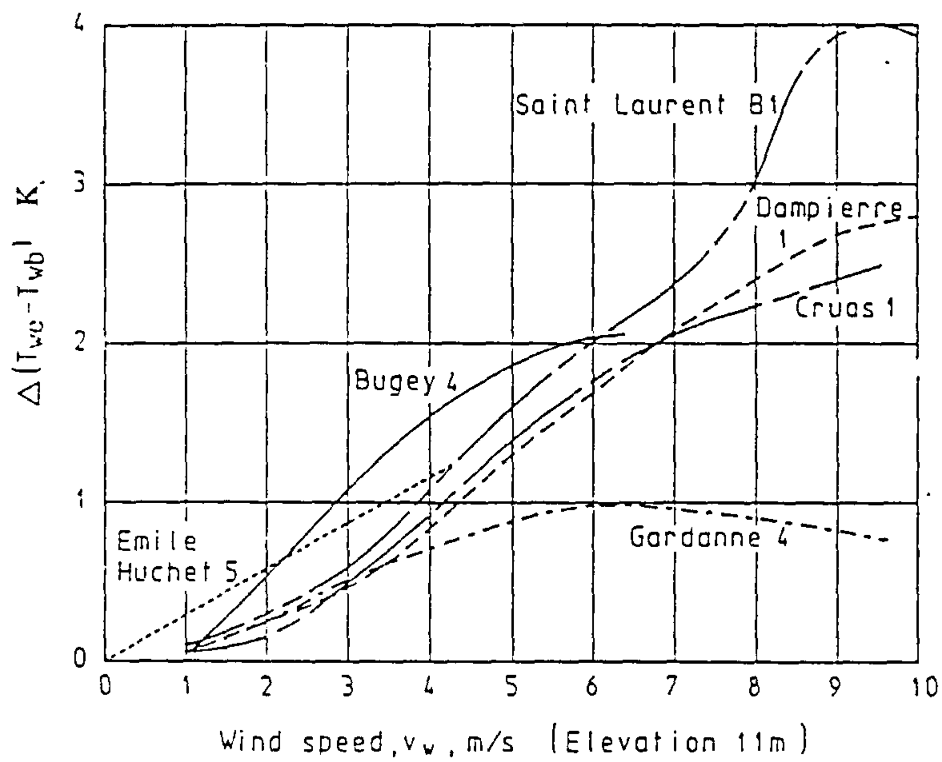

Figure 10.2.3: Rise in cooling-water temperature due to wind (wet towers).

Generally the scatter in the available test data may be due to a number of factors including cold air inflow at low wind speeds, variations in wind-speed, -direction and -profile [78MO1], inversions, changes in ambient temperature and in heat dissipated [77MA1].

Due to the variations in wind velocity it is important to know the wind velocity distribution, as well as the position and the height above ground level where the wind velocity was measured during any test. The closer to ground level the wind velocity is measured, the more sensitive the cooling tower will appear to be to a cross-wind. Van der Walt [76VA] measured the wind velocity with a cup-type anemometer at the inlet height of the tower, while for the Grootvlei 6 tower it was measured 7.5 m above ground level. Markòczy [77MA1] only states that the atmospheric conditions were obtained from a meteorologic station 500 m from the tower, but does not mention at which height the wind velocity was measured. He furthermore mentioned that the position of the cooling tower on which the measurements were performed was such that for the prevailing wind direction the approaching wind was not disturbed by structures or obstacles. Caytan [88CA1], who published results of measurements performed on wet towers, used the wind velocity as measured at an elevation of 11 meters as reference. Grange [82GR1], who performed measurements on the Saint-Laurent wet tower, based his observations on the wind velocity 140 meter above ground level as obtained from a weather mast erected 200m from the tower. Bourillot [80BO1] used the wind velocity as measured at the tower outlet elevation as reference. No reference heights are specified for the other results shown in figure 10.2.2. Furthermore no details are given concerning the wind profiles which will be different for the various tower sites.

The results of numerous model tests have been reported [78OL1, 78RU1, 80LE1, 82CH1, 82RU1, 83BU1, 85VO1] and a few attempts have been made to predict the influence of winds on the performance of cooling towers [83WI1, 85VO1, 86BU1, 92DU1]. For a small scale model it is usually impossible to satisfy both the densimetric Froude number and the Reynolds number, therefore model tests in the past were either based on Froude's similarity or on isothermal tests approximating Reynold's similarity. Each of the techniques offer some advantage, but because all the dimensional groups are not satisfied in either of the approximations, each technique also has its limitations. Bourillot [80BO1], Buchlin [82BU1], Grange [82GR1], Ruscheweyh [82RU1] and Sabaton [82SA1] performed tests based on Froude's similarity. This is achieved by doing non-isothermal tests. Buchlin [82BU1] mentioned that these models allow a realistic simulation of the possible interaction between the inlet and outlet thermal and aerodynamic phenomena. The fluid velocities obtained in these models are very low and special measuring techniques usually have to be used. Consequently the Reynolds numbers are approximately three orders of magnitude lower than those for a full scale tower, which may result in erroneous results. Bourillot [80BO1] furthermore observed large velocity fluctuations and tests were repeated several times to eliminate random errors. Although heating models can be of value for comparative surveys of different tower shapes [82RU1], it is still difficult to forecast the wind influence for a specific tower, due to uncertainties in the measurements.

If the densimetric Froude number is neglected, isothermal tests may be performed [78BO1, 78RU1, 80BO1, 80LE1, 82CH1, 83BU1, 85VO1, 86BL1, 86VA1]. The natural draft phenomenon is not represented in these tests and therefore the tower draft is achieved by sucking or blowing a fluid through the model. Although the Reynolds numbers obtained in these test are much higher than those which are found in non-isothermal models, they are still much lower than those found in full scale towers. The advantage of this test method is that the main fluid velocity inside the tower can however easily be determined because the fluid is forced through the model. Furthermore the measurements performed on these models are accurate and stable and both Bourillot [80BO1] and Buchlin [82BU1] mentioned that good reproducibility is obtianed.

Witte [83WI1] suggests that the wind effect on the performance of a dry-cooling tower may be predicted by employing the external pressure distribution near the base of the cooling tower shell.

When a fluid flows across a cylinder the static pressure varies circumferentially. A corresponding static pressure coefficient is defined as

$$C_p = \left(p_\theta - p_\infty\right) / \left(\rho_\infty v_\infty^2/2\right) \tag{10.2.2}$$

where p_θ is the local static pressure while the other variables refer to ambient conditions far from the cylinder. According to the potential flow theory, the distribution of this coefficient is as shown in figure 10.2.4.

Actual pressure measurements performed on model towers near or at the lower edge of the shell (lintel) are also shown in figure 10.2.4. Roshko [61RO1] measured the pressure distribution about a cylinder at a Reynolds number of 8.4×10^6. His results are compared to the potential flow theory shown in figure 10.2.4. Lowe [64LO1], Christopher [69CH1] and Ruscheweyh [82RU1] measured the pressure distribution near the inlet of a cooling tower model in a windtunnel. Heat exchanger bundles were arranged horizontally in the inlet cross-section of the tower in the tests conducted by Ruscheweyh, while vertical arrangements were tested in the other two cases. The pressure distribution about actual cooling towers were reported by Ruscheweyh [83RU1] and Blanquet [86BL1].

To analyze the problem, the tower is divided circumferentially into an arbitrary number of sectors. The cooling tower energy and draft equations are applied to each sector. The ambient pressure is however modified for each sector by introducing the corresponding local pressure coefficient. Finally the contribution of all sectors are added to give the heat rejected by the tower.

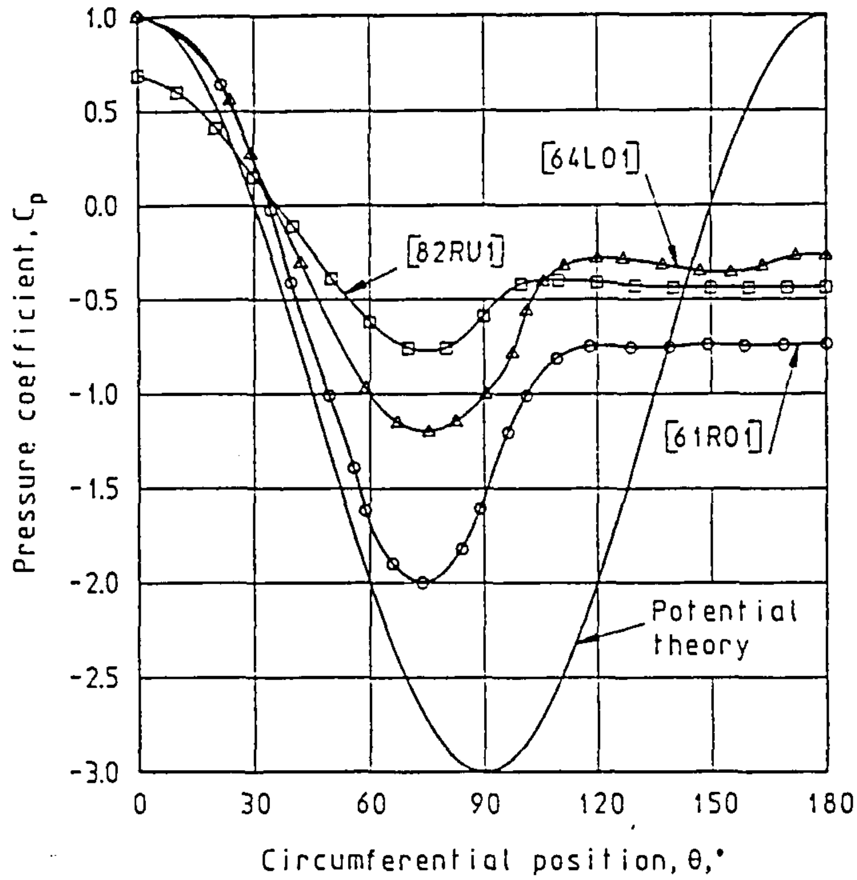

Figure 10.2.4: Pressure distribution about cooling tower.

It is noted that at the point where the wind strikes the tower normally (stagnation point), the pressure coefficient has a maximum value with the result that the total pressure at this point is greater than the ambient pressure. According to Witte, more cooling air will thus tend to flow through heat exchangers located at this point, than at other locations. Although this is true for towers with heat exchanger bundles arranged vertically around the base of the tower [77MA1], it does not apply to horizontally installed bundles where the tower inlet air flow pattern is such that less air flows through the bundles located near the upwind (stagnation point) side [85VO1, 92DU1]. Although Witte [83WI1] ignores any wind profile and the influence of wind induced air flow distortions through bundles arranged vertically in the form of deltas around the base of the tower as shown in figure 1.2.15(a), as well as effects at the outlet of the tower, his method satisfactorily predicts the reduction in performance due to wind in the Gagarin tower as is shown in figure 10.2.1. It is fortuitous that when his analysis is applied to the horizontally arranged bundles in the Grootvlei 5 tower, it predicts approximately the trend of the data as shown in figure 10.2.1.

Buxmann [83BU1] and Völler [85VO1] performed isothermal model tests to determine the effect of different tower outlet shapes and the arrangement of the heat exchanger bundles on the performance characteristics of the cooling tower in the presence of wind. To quantify the influence of wind on the air mass flow rate through the tower, Buxmann [83BU1] defined pressure coefficients for the inlet, C_{pi}, and outlet, C_{po}, in terms of the static pressure difference between the throat of the tower and the ambient i.e.

$$C_{pi},\ C_{po} = \left(\Delta p_w - \Delta p\right)/\left(\rho_w\, v_w^2/2\right) \tag{10.2.3}$$

where Δp_w is the static pressure difference with wind an Δp is the static pressure difference in the absence of any wind while the mean air mass flow rate through the tower is the same at both cases. Their tests were all conducted for the same d_i/H_i ratio and except for the vertical arrangement of the heat exchangers, a fixed value of heat exchanger loss coefficient. A uniform wind velocity distribution was maintained and it was assumed that this was representative of the mean value of a typical wind profile. The velocity distribution through the heat exchanger was measured in the presence of a cross-wind and a corresponding air-side heat transfer coefficient correction factor was defined to take into consideration the reduction in heat transfer due to the flow distortion.

By employing the results of these measurements, Völler [85VO1] evaluated the influence of winds on the performance of different cooling towers. Satisfactory agreement was found between the predicted and measured values for the Grootvlei 5 tower [76VA1], while the measured reduction in performance of the Rugeley tower [69CH1] was underpredicted.

Du Preez [92DU1] and Du Preez and Kröger [92DU2, 93DU1] performed tests similar to those of Völler but extended the investigation to include effects due to the conical inlet section of the tower, a range of heat exchanger flow resistances, and different inlet diameter to height ratios, d_i/H_i. Effects due to tower supports, wind velocity distribution and different flow rates through the tower were also studied. The influence of the distorted air flow distribution through the heat exchanger was also treated more rigorously. It should however be stressed that their tests were limited to cases where the heat exchanger bundles are arranged horizontally and cover the entire inlet cross-sectional area of the cooling tower. This arrangement is not typical of any practical cooling tower where bundles are usually installed in the form of A-frames or deltas covering only a part of the total available cross-section.

Due to the influence of the different parameters on the value of the inlet pressure coefficient, it is not possible to find a simple correlation for C_{pi}. If it is accepted that the influence of the tower supports, the form of the wind profile and the taper angle of the tower shell on the value of C_{pi} vary linearly between the values for which the tests were done, the following relation holds for cylindrical tower supports:

$$
\begin{aligned}
C_{pi} = & \left[-0.57 + 0.0503 \left(\frac{v_{wo}}{v_m}\right)^{0.8} \left(\frac{d_i}{H_i}\right)^{-0.64} - 1.2/\exp\left\{2.4 \left(\frac{v_{wo}}{v_m}\right)\left(\frac{d_i}{H_i}\right)^{-0.8}\right\}\right] \\
& \times \left[1 - \left\{\frac{0.0067}{\exp\left(0.2\, K_{he}\right)}\right\}\left\{40 - 6\left(\frac{v_{wo}}{v_m}\right)\left(\frac{d_i}{H_i}\right)^{-0.8}\right\}\right] \\
& + \left[\left[-0.6 + 0.01\left(\frac{d_i}{H_i}\right) + 0.054\left\{-0.65 + 0.06\left(\frac{d_i}{H_i}\right) + 0.1\, K_{he}\right.\right.\right. \\
& \left.\left. \times \left(0.23 - 0.039\left(\frac{d_i}{H_i}\right) + 0.001\left(\frac{d_i}{H_i}\right)^2\right)\right\}\left(24 - \frac{v_{wo}}{v_m}\right)\right] \\
& \left. + \sin\left\{\left(\frac{v_{wo}}{v_m}\right) / \left(1 + \frac{0.17\, v_{wo}}{v_m}\right)\right\} /\exp\left\{\frac{v_{wo}}{7\, v_m} + 0.2\left(15 - \frac{d_i}{H_i}\right) + \frac{K_{he}}{20}\right\}\right] \\
& \times \left(1 - 0.978\, K_{tse}\right)\left\{1 - \left(0.003 \times 2\theta_c + 2b + 0.027 \times 2\theta_c \times b\right)\right\} \qquad (10.2.4)
\end{aligned}
$$

for $5 \le d_i/H_i \le 15$; $0 \le K_{he} \le 30$; $0 \le v_{wo}/v \le 24$; $0 \le b \le 0.2$; $0 \le 2\theta_c \le 24°$; $0 \le K_{tse} \le 1.02$.

The wind velocity, v_{wo}, in equation (10.2.4) refers to the wind velocity at the top of the cooling tower while K_{he} is the value of the loss coefficient of the heat exchangers obtained at an arbitrary Ry value of 2 x 10^5. The mean free stream velocity through the heat exchanger is v_m. The effective loss coefficient of the tower supports, K_{tse}, is defined as the sum of the K_{ts} values of the different rings of supports based on the circumferential inlet area of the cooling tower (includes tower supports). Furthermore b is the value of the exponent in the power law used to approximate the wind profile as defined by equation (10.1.30).

As the loss coefficient for the tower supports, K_{tse}, approaches a value of 1.02, the second term in equation (10.2.4) becomes zero. This implies that under these conditions C_{pi} is independent of the wind profile and the contraction angle of the cooling tower shell. The range of the applicability of the equation can be extended to values of $K_{he} > 30$ if K_{tse} approaches its upper limit.

The wind effect at the outlet of a cooling tower has been studied by a number of investigators [72EC1, 79DI1, 80BO1, 82BU1, 82CH1, 82RU1, 83BU1, 85VO1].

A qualitative picture of the flow pattern at the outlet of the cooling tower in the presence of a cross-wind is shown in figure 10.2.7.

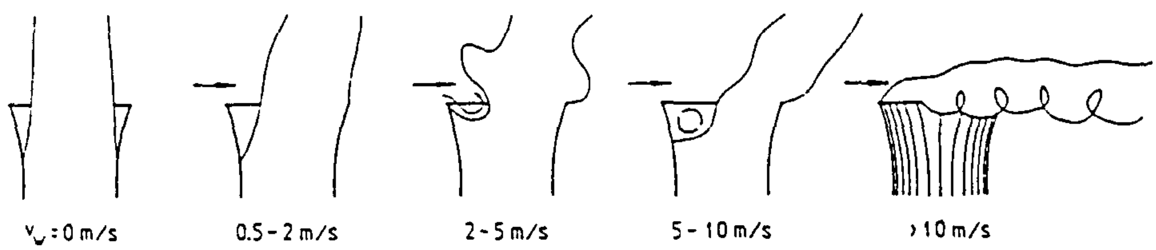

Figure 10.2.7: Flow patterns at outlet of cooling tower for different wind speeds.

According to du Preez and Kröger [92DU1] the pressure coefficient at the outlet of a cooling tower is given by the following empirical relation:

$$C_{po} = -0.405 + 1.07\left(\frac{v_{wo}}{v_m}\right)^{-1}\left(\frac{A_o}{A_t}\right)^{-1.65} + 1.8\log_{10}\left[\left(\frac{v_{wo}}{2.7v_m}\right)\left(\frac{A_o}{A_t}\right)^{1.65}\right]$$

$$\times\left[\left(\frac{v_{wo}}{v_m}\right)\left(\frac{A_o}{A_t}\right)^{1.65}\right]^{-2} + \left[-1.04+1.702\left(\frac{A_o}{A_t}\right) -0.662\left(\frac{A_o}{A_t}\right)^2\right]\left(\frac{v_{wo}}{v_m}\right)^{-0.7} \qquad (10.2.5)$$

for $1.8 \le v_{wo}/v_m \le 24$ if $A_o/A_t = 1$, $1.8 \le v_{wo}/v_o \le 12$ if $A_o/A_t \neq 1$ and $0.893 \le A_o/A_t \le 1.232$. A_o is the tower outlet cross-sectional area while A_t is the throat area.

This equation considers not only cylindrical outlets but also converging and diverging geometries. Experimental inlet and outlet pressure coefficients for particular operating and geometric conditions are compared graphically in figure 10.2.8 with equations (10.2.4) and (10.2.5) respectively

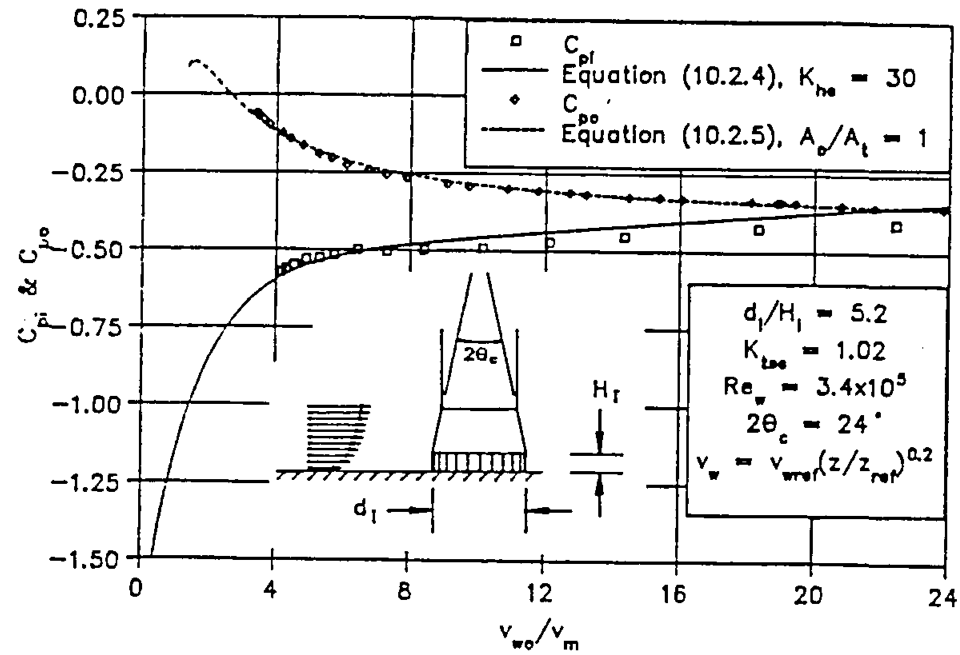

Figure 10.2.8: Inlet and outlet pressure coefficients [92DU1].

Taking into consideration the pressure coefficients at the inlet and the outlet of the cooling tower, the draft equation (7.1.7) is extended as follows [92DU1]:

$$p_{ao}\left[\left\{1 - 0.00975\left(H_3 + H_4\right)/\left(2T_{ao}\right)\right\}^{3.5}\left\{1 - 0.00975\left(H_5 - H_3/2 - H_4/2\right)/T_{a4}\right\}^{3.5}\right.$$

$$\left. - \left(1 - 0.00975\ H_5/T_{ao}\right)^{3.5}\right] - C_{po}\ \rho_{w6}v_{w6}^2/2$$

$$+ 0.5\ C_{pi}\ \rho_{w6}v_{w6}^2\left\{1 - 0.00975\left(H_5 - H_3/2 - H_4/2\right)/T_{a4}\right\}^{3.5}$$

$$= \left(K_{ts} + K_{ct} + K_{he}\right)_{he}\left(m_a/A_{fr}\right)^2/\left(2\ \rho_{a34}\right)\left[1 - 0.00975\left(H_5 - H_3/2 - H_4/2\right)/T_{a4}\right]^{3.5}$$

$$+ \left(m_a/A_5\right)^2/\left(2\ \rho_{a5}\right) \tag{10.2.6}$$

For a uniform air flow rate through a cross-flow finned tube heat exchanger with two or more tube passes (essentially counterflow) as commonly found in a dry-cooling tower, the approximate heat transfer rate can be expressed in terms of the relevant effectiveness, ϵ, as listed in table 3.5.1 i.e.

$$Q = \rho\ v_m\ A_{fr}\ c_p\left(T_{wi} - T_{ai}\right)\epsilon \tag{10.2.7}$$

where v_m is the mean upstream air velocity and the temperatures refer to inlet water and air values respectively.

A cross-wind distorts the velocity distribution through the heat exchangers [85VO1]. As the wind increases, the flow through the heat exchangers becomes increasingly more non-uniform with the maximum air speed at the lee side of the tower. On the upstream side the air flow through the heat exchanger decreases due to flow separation at the inlet edge of the shell (reverse flow may occur). An example of the velocity distribution observed in a model cooling tower is shown in figure 10.2.9.

The distorted or maldistributed air flow pattern through the heat exchangers reduces the effective heat transfer rate which can be expressed in terms of a correction factor i.e.

$$Q_e = \alpha_Q \; Q \tag{10.2.8}$$

where

$$\alpha_Q = \int_{A_{fr}} \rho \, v \, c_p \, \epsilon \, dA_{fr} \, / \, (\rho \, v_m \, A_{fr} \, c_p \, \epsilon) \tag{10.2.9}$$

In an air-cooled heat exchanger the effectiveness ϵ, is a function of UA, and UA $\alpha \; R_y^{b_{UA}}$ where $b_{UA} \approx 0.45$ for dry-cooling towers.

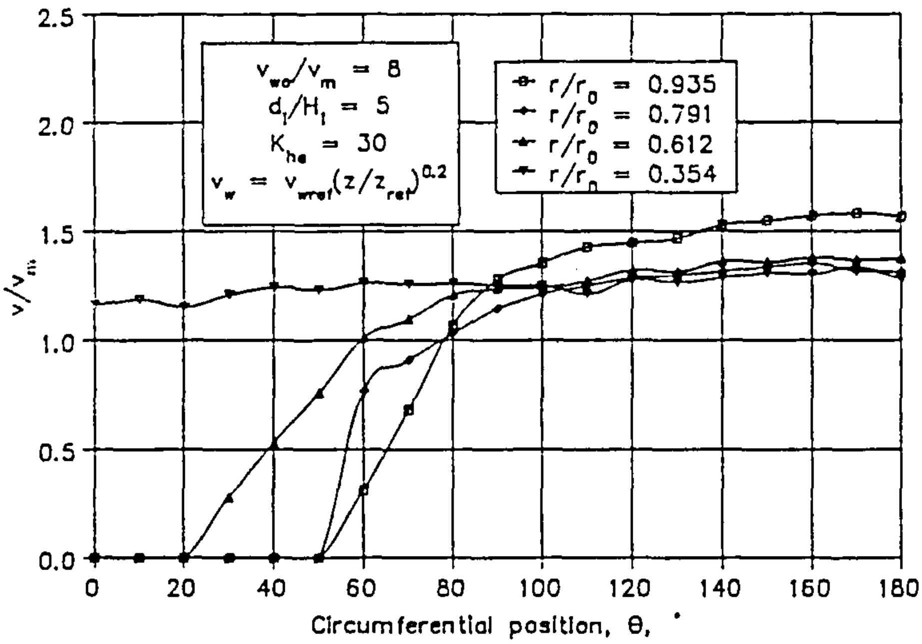

Figure 10.2.9: Velocity distribution through heat exchanger inside cooling tower [92DU1].

The following empirical relation for α_Q is based on experimentally obtained data:

$$\alpha_Q = \left[1 - \frac{\left(\frac{v_{wo}}{v_m}\right)^{3.6} \exp\left(-\frac{v_{wo}}{3.75 v_m}\right) v_m^{0.576}}{3561} \right]$$

$$\times \left[0.98 + 0.02 \left\{ \exp\left(5.2 - \frac{d_i}{H_i}\right) + \exp\left(-\frac{v_{wo}}{v_m}\right) \right\} \right]$$

$$- \left(1.5 - 0.05\, K_{he}\right) \left[\left\{ 0.013 - 0.0048 \left(\frac{d_i}{H_i}\right) + 0.000302 \left(\frac{d_i}{H_i}\right)^2 \right\} \right.$$

$$+ \left[\frac{v_{wo}}{v_m}\right] + \left\{ 0.0134 - 0.00129 \left[\frac{d_i}{H_i}\right] + 0.000038 \left[\frac{d_i}{H_i}\right]^2 \right\}$$

$$\left. + \left\{ 0.0035 + 0.00206 \left(\frac{d_i}{H_i}\right) - 0.000085 \left(\frac{d_i}{H_i}\right)^2 \right\} \sin\left(\frac{v_{wo}}{1.9 v_m}\right) \right]$$

$$- \left(0.0053 - \frac{K_{he}}{9182}\right) \left(11.26 - 25.64\, b_{UA}\right) \left[\frac{v_{wo}}{v_m}\right] \qquad (10.2.10)$$

for $5.2 \le d_i/H_i \le 15$; $10 \le K_{he} \le 30$; $0 \le v_{wo}/v_m \le 12$; $0 \le b \le 0.2$; $0 \le K_{tse} \le 1.02$; $0.4 \le b_{UA} \le 0.5$; $1 \le v_m \le 4$ m/s.

If $\alpha_Q > 1$ in the above equation a value of $\alpha_Q = 1$ is assumed.

To determine the operating point of a dry-cooling tower subject to cross-winds, the density of the air in the cooling tower has to be known. In view of the fact that the temperature distribution of the air leaving the heat exchanger is not uniform and the degree of mixing in the tower is unknown, the mean density cannot be evaluated accurately.

One extreme would be to assume that the air just above the heat exchangers is perfectly mixed. A mass mean air temperature would then be used to calculate the tower draft i.e.

$$T_{a4} = Q/\left(m_a c_{pa34}\right) + T_{a3} \qquad (10.2.11)$$

The other extreme would be to assume that no mixing occurs, in which case the lowest air temperature, associated with the maximum air velocity through the heat exchanger would be employed to determine the draft. Based on experimental results, the maximum velocity through the heat exchanger can be expressed as

$$\frac{v_{max}}{v_m} = 1.014 - 0.0095\left(\frac{d_i}{H_i}\right) + 0.0014\left(\frac{d_i}{H_i}\right)^2$$

$$+ \left\{- 0.1265 + 0.0509\left(\frac{d_i}{H_i}\right) - 0.00245\left(\frac{d_i}{H_i}\right)^2\right\}\left(\frac{v_{wo}}{v_m}\right) \times (1 - 0.26\ b)$$

$$+ \left[- 0.362 + 0.0865\left(\frac{d_i}{H_i}\right) - 0.00321\left(\frac{d_i}{H_i}\right)^2\right.$$

$$\left. + \left\{0.288 - 0.0572\left(\frac{d_i}{H_i}\right) + 0.00242\left(\frac{d_i}{H_i}\right)^2\right\}\left(\frac{v_{wo}}{v_m}\right)\right]\left(1.5 - 0.05\ K_{he}\right) \qquad (10.2.12)$$

for $5.2 \le d_i/H_i \le 15$; $10 \le K_{he} \le 30$; $0 \le v_{wo}/v_m \le 12$; $0 \le b \le 0.2$; and $0 \le K_{tse} \le 1.02$.

This latter approach would give the more pessimistic tower performance. The actual operating point of the particular cooling tower will be at some point between the two extreme values obtained by the abovementioned methods.

With these equations it can be shown that the wind effect on the performance of a particular cooling tower (see example 10.2.1) decreases as shown in figure 10.2.10, as the tower height is increased while the heat rejection rate and other geometric parameters remains unchanged [92DU1]. This is in agreement with similar findings published by Moore [78MO1].

The applicability of the above empirical equations which are based on experimental results are limited. More useful results can only be obtained by conducting tests in larger and more detailed models or by resorting to extensive numerical analysis of the problem [88RA1, 89RA1, 92DU1, 93DU3].

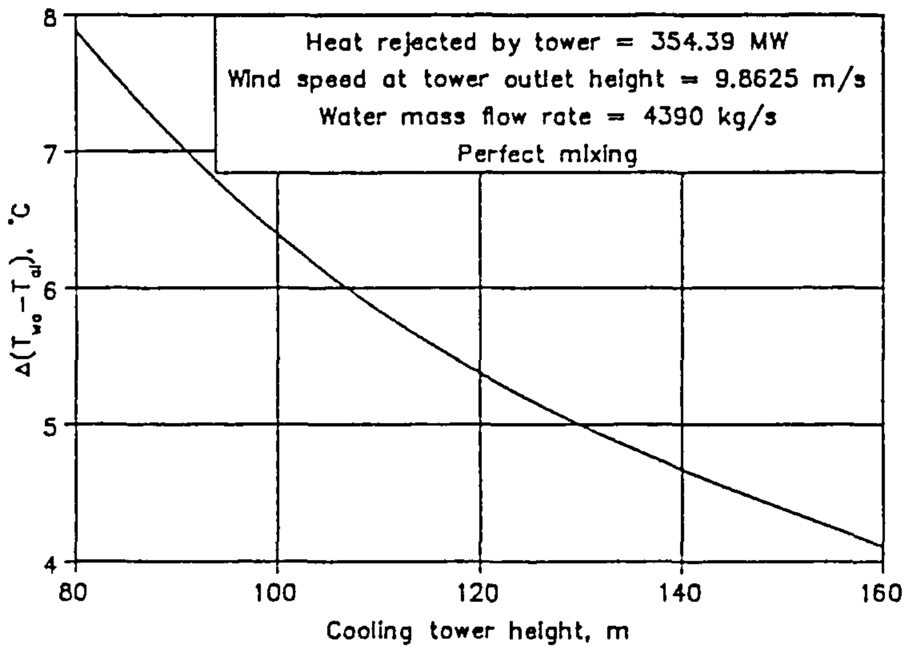

Figure 10.2.10: Change in approach temperature with cooling tower height.

Du Preez and Kröger [93DU2] studied the influence that different tower supports have on the performance during windy periods. They find that radially elongated supports have a beneficial effect under these conditions confirming the experimental findings of Vauzanges and Ribier [86VA1].

By employing a numerical procedure based on the PHOENICS code, the effect of the heat exchanger arrangement and wind break walls on the performance of natural draft dry-cooling towers is investigated [94DU1]. Body-fitted co-ordinates, which almost coincide with polar co-ordinates, are used to define the shape of a three-dimensional representative dry-cooling tower 165 m high, with an inlet height of 24.5 m and an inlet diameter of 144.5 m.

At the inlet of the computational domain a non-uniform wind velocity distribution has been specified with the value of the exponent in equation (10.1.30), b = 0.16. As a first approximation, finned tube heat exchanger bundles are simulated horizontally (no A-frame) over the entire inlet cross-section of the tower with the results of the calculations given by curve 1 in figure 10.2.11. The experimental results, obtained for a model cooling tower similar to that used in the numerical procedure, are shown by curve 2 in figure 10.2.11. Good agreement between the results predicted by the two methods is obtained for high wind velocities, while the numerical procedure becomes more optimistic at lower wind speeds. The flow field about the tower is shown in figure 10.2.12 for a wind speed of 12 m/s [92DU1].

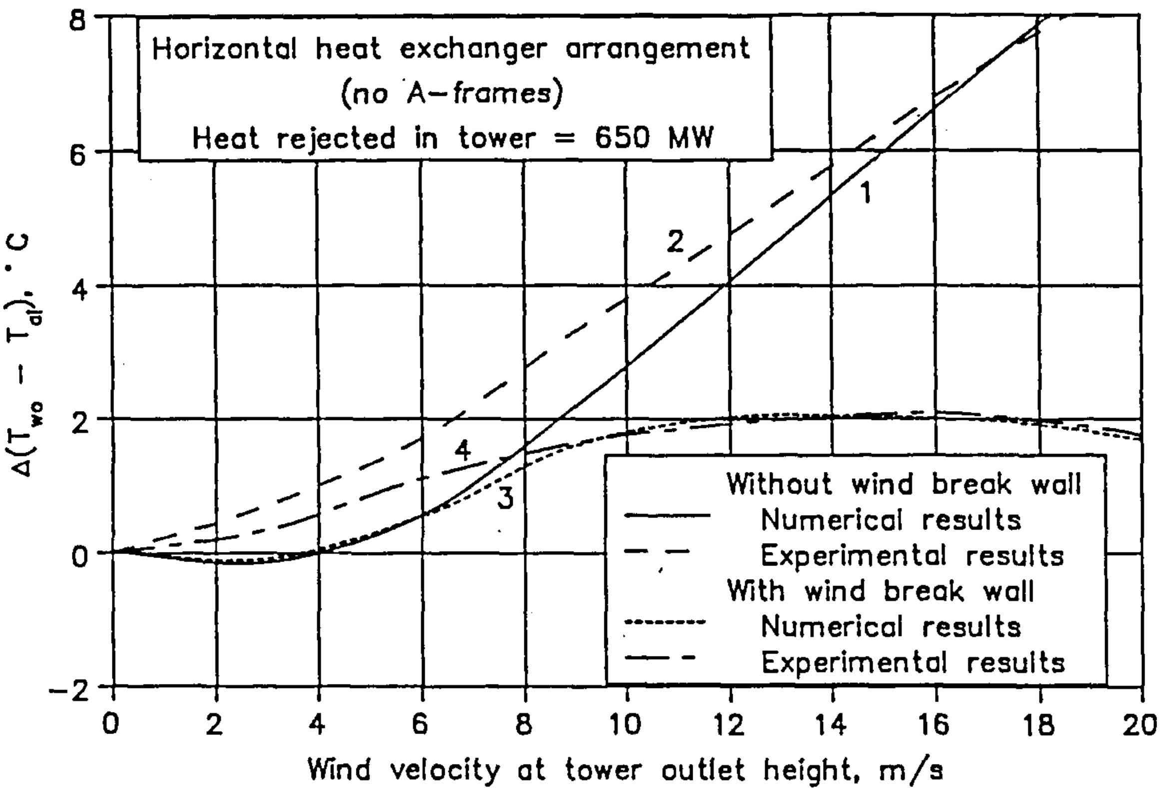

Figure 10.2.11: Effect of wind break wall on tower performance.

The reduction in cooling tower performance during windy periods is mainly due to inlet effects. By installing windbreaks in the form of two perpendicular porous walls (in the form of a cross) under the heat exchangers, this effect can be significantly reduced as shown in figure 10.2.11 for the particular example. The loss coefficient of the porous wall is correlated by

$$K_{wall} = 2\Delta p/\rho v^2 = 37.39\ v^{-0.5232} \tag{10.2.13}$$

where Δp is the difference in the total pressure across the wall and v the mean air velocity through it.

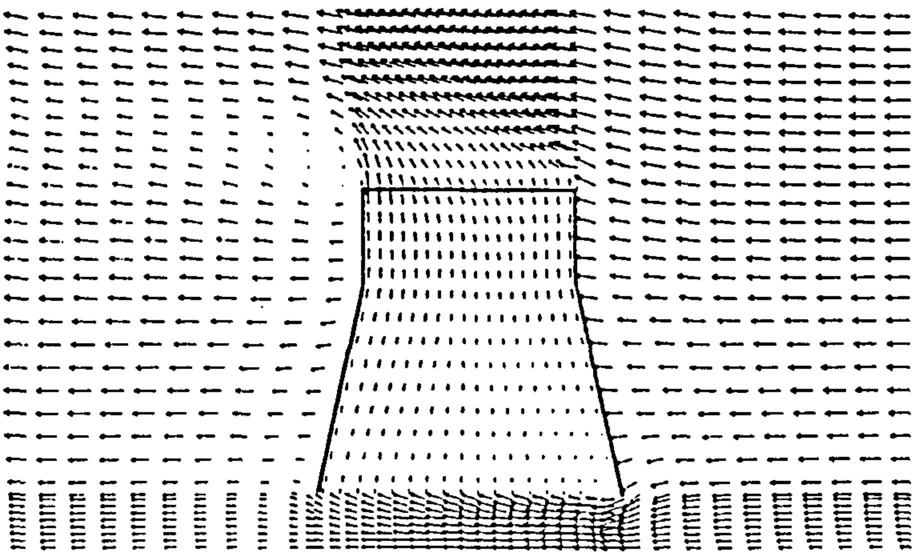

Figure 10.2.12: Flow field about cooling tower.

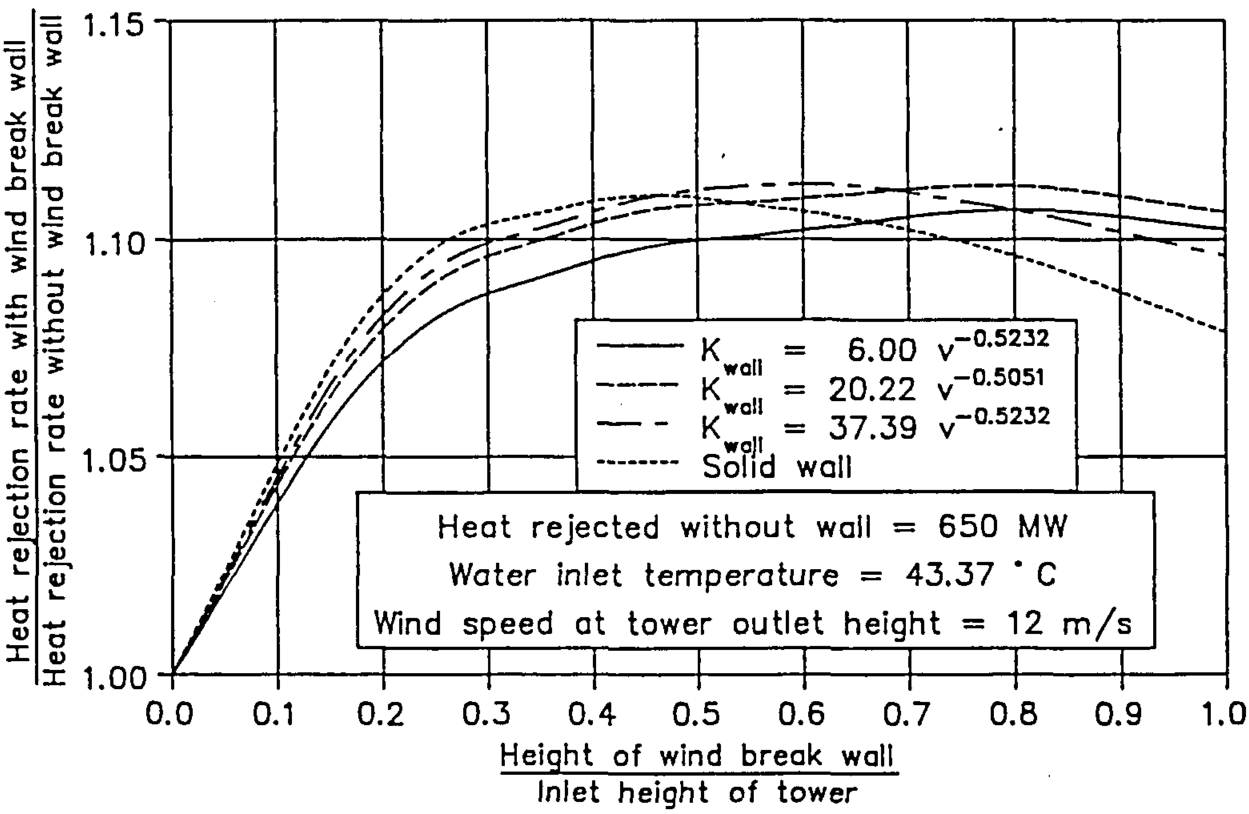

Figure 10.2.13: Relative change in the heat rejection rate of a tower as a function of the wall height.

The addition of wind break walls will of course increase the initial costs of a tower. Further calculations however show that the heights of these walls do not necessarily have to be equal to the inlet height of the tower to produce the best results [94DU1]. Figure 10.2.13 shows the relative increase in the heat rejection rate of the cooling tower as a function of the wind break wall height and different wall resistances (different porosities). The performance of the tower increases continuously as the height of the wall increases up to a wall height of approximately one third of the inlet height of the tower. Further increases in the wall height yield no significant improvements and a slight reduction in the heat rejection rate of the tower is observed when the height of the wall approaches the inlet height of the tower. The latter is due to a deterioration of the velocity distribution through the heat exchangers as shown by figure 10.2.14.

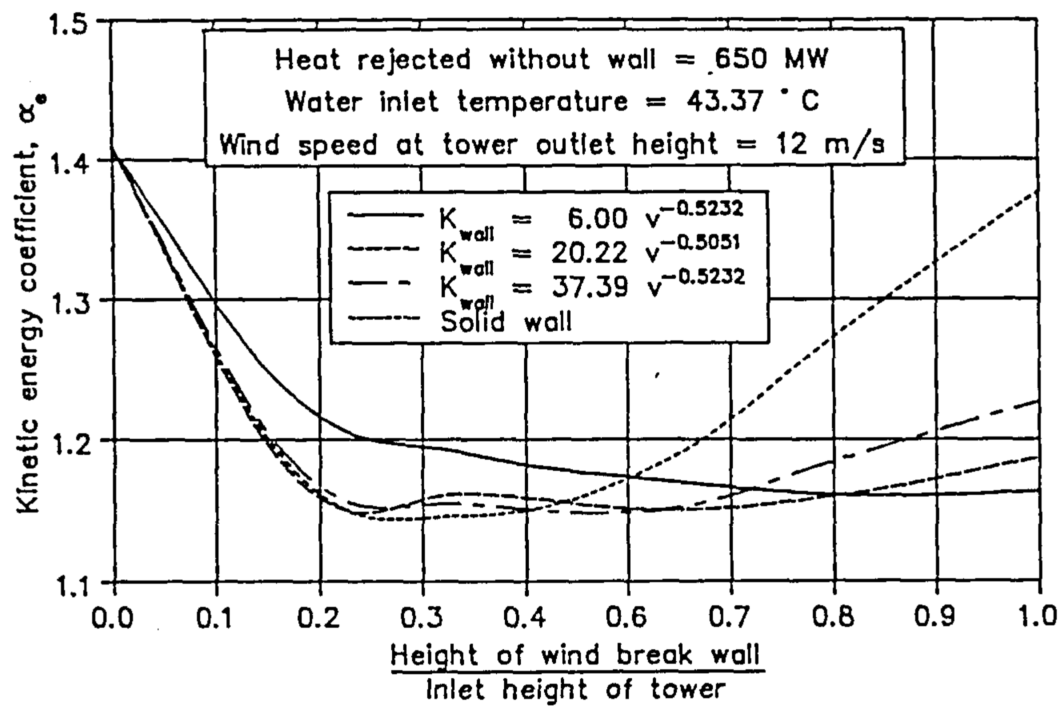

Figure 10.2.14: Kinetic energy coefficient as a function of the wall height.

The heat exchanger layout as shown in figure 1.2.15(c) incorporating a central cylinder is also found to be less sensitive to wind, when compared to the horizontal arrangement.

Du Preez and Kröger [93DU3] note that as the heat rejection rate in a tower in which the heat exchangers are arranged in the form of A-frames in a radial pattern increases, the tower becomes less sensitive to winds. This is due to a reduction in the effectiveness of the A-frame heat exchangers caused by distorted inlet air flow patterns. Curve 2 in figure 10.2.15 shows the wind effect on a tower with similar dimensions to that described in the previous figure, but in this case the heat exchangers are arranged radially in the horizontal inlet cross-section of the tower.

Since the tower dimensions, heat exchanger characteristics and heat exchanger arrangement used in the numerical analysis correspond to that of the Kendal tower, the wind effect indicated by curve 2 in figure 10.2.15 allow direct comparison with the full scale measurements [93DU3]. In the Kendal tower the finned tube heat exchangers are arranged essentially radially in the form of A-frames with an apex angle of 60° in the horizontal inlet cross-section. The wind velocity and temperature distribution was measured on a 96 m high weather mast 700 m from the tower. Air and water temperatures as well as the water flow rate through the tower were measured at the same time. The numerical prediction agrees favorably with the full scale measurements as shown by curve 1 in figure 10.2.16.

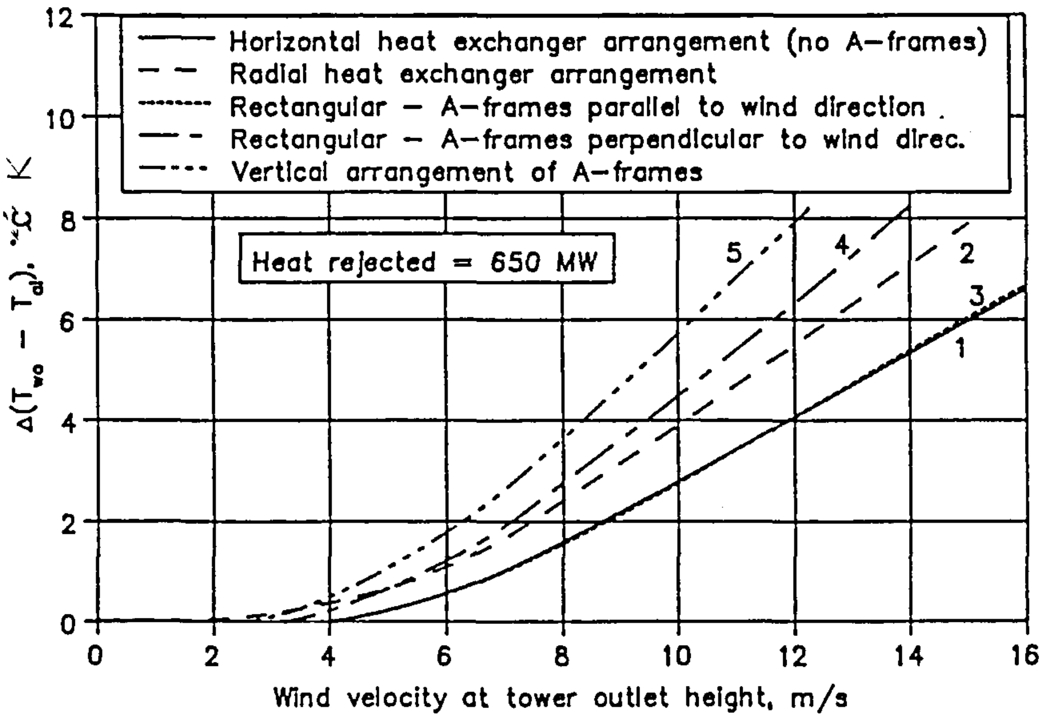

Figure 10.2.15: Wind effect on tower with different heat exchanger arrangements.

There are usually a number of water ducts and possibly one or two storage tanks at the base of most dry-cooling towers. These will act as wind breaks. For example the water ducts in the Kendal tower are approximately 3 m in diameter i.e. roughly one tenth of the inlet height of the tower. The effect of these ducts on the performance of the tower during windy periods is shown approximately by curve 2 in figure 10.2.16. This curve corresponds more closely with the full scale measurements especially at higher wind speeds. If a 5 m high wind break wall is installed on top of these ducts to increase the effective height to roughly one third of the inlet height of the tower, a significant reduction in the wind effect on this particular tower can be expected when the wind blows in a direction perpendicular to the wind break.

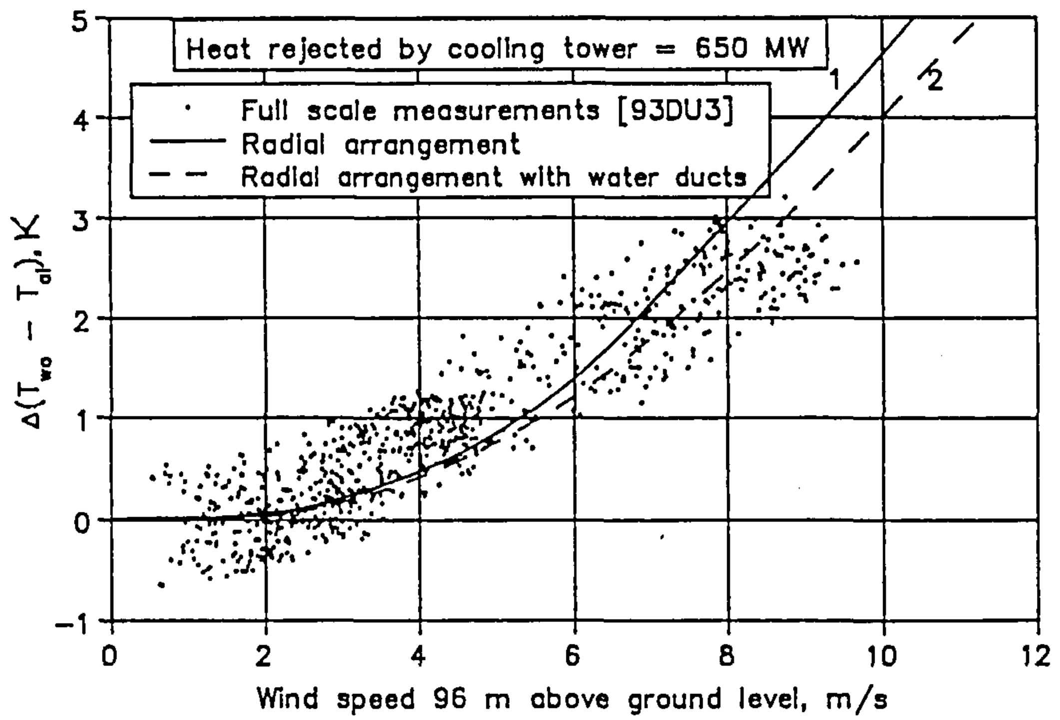

Figure 10.2.16: Wind effect on Kendal tower.

If A-frame heat exchangers are arranged in a horizontal rectangular pattern, the wind direction has a measurable effect on the tower performance. If the A-frames are positioned parallel to the wind direction, the effect of the A-frame is minimized with the wind influence on the tower correspondingly less as shown by curve 3 in figure 10.2.15. Conversely the tower performance deteriorates if the A-frames are positioned perpendicular to the wind direction as shown by curve 4.

Du Preez and Kröger [93DU3] found that the wind effect on a tower with a vertical heat exchanger arrangement is higher than the predicted influence on towers with a horizontal arrangement as shown by curve 5 in figure 10.2.15. The latter is in direct agreement with full scale observations. The adverse effect of wind on the mean mass flow rate through a tower with a vertical heat exchanger arrangement can be reduced by installing appropriate wind protecting devices around the tower inlet as suggested by Leene [80LE1].

Factors affecting the performance of cooling towers during windy periods may thus be summarized as follows:

1. Wind speed.
2. Velocity distribution of approaching wind.
3. Heat rejected by cooling tower.
4. Mean air velocity through heat exchanger or fill.
5. Degree of mixing of air after heat exchanger or fill.
6. Transfer characteristics of heat exchanger or fill.
7. Loss coefficient of heat exchanger or fill.
8. Location and arrangement of heat exchanger or fill.
9. Height of cooling tower.
10. Ratio of inlet diameter to tower height, d_i/H_i.
11. Inlet taper and shape of shell.
12. Loss coefficient of tower supports.
13. Shape of tower supports.
14. Obstacles and structures in or near tower inlet.

10.3 INVERSIONS

In the presence of an atmospheric temperature inversion the performance of an air-cooled heat exchanger and in particular that of a cooling tower is reduced. The reason for this reduction is the fact that the potential driving force or pressure differential is less, and the effective temperature of the air entering the cooling system is higher than during conditions where the adiabatic lapse rate prevails. In 1925 Merkel [25ME1] already mentions the fact that temperature inversions may be the cause of apparent inconsistencies in cooling tower performance predictions. Cooling tower acceptance tests should normally not be performed during periods of inversions [88LA1]. During a temperature inversion, the moist air in the plume of a wet-cooling tower may be trapped in the inversion and plume dispersion is greatly reduced. This may lead to fog formation and precipitation and in extreme cases to the formation of ice.

An indication of the nature and frequency of inversions is presented by Tesche [78TE1].

Exceptionally strong inversions have been observed, particularly in arid and desert areas where dry-cooling towers are most likely to be erected.

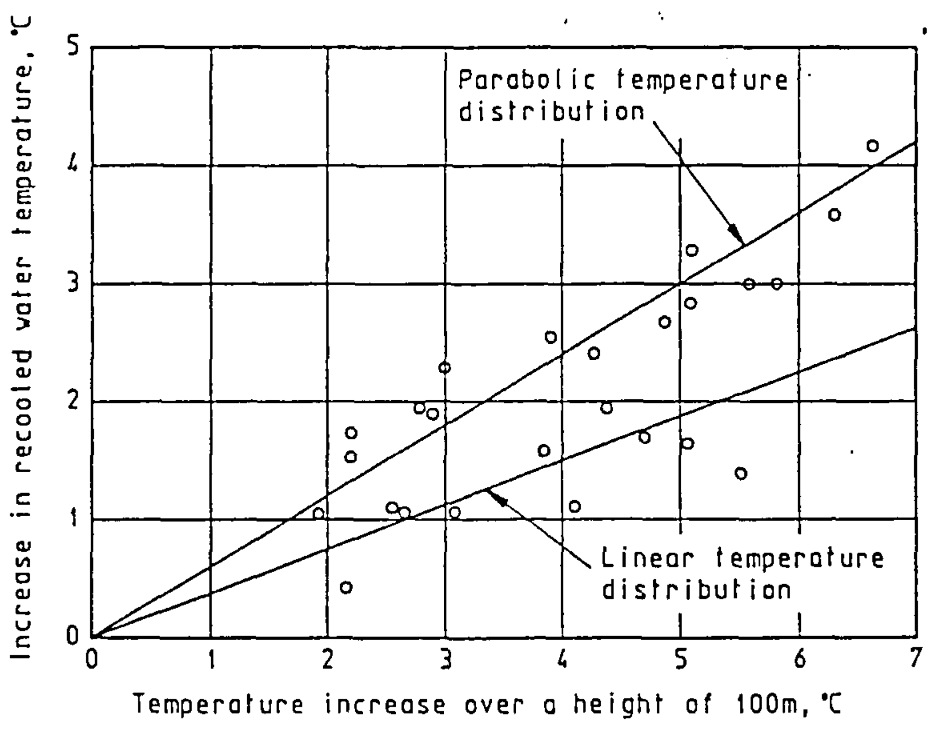

Figure 10.3.1: Reduction in performance due to inversion at Grootvlei 5.

Buxmann [77BU1, 82BU1] tries to quantify approximately the influence that an inversion has on the performance of a natural draft dry-cooling tower. Employing the temperatures measured 1.2m above ground level and at the tower top, he assumes a linear profile between the two. According to his model, the effective air inlet temperature is the average of the two values. This approach enables him to obtain an improved estimate of the air inlet temperature, as well as quantifying the effect of the inversion on the effective density difference between the ambient air and the heated air inside the tower. His model is at best approximate since it implies that the air entering the tower is effectively drawn from an elevation between ground level and the top of the tower and adiabatic compression is ignored. As shown in figure 10.3.1 his analytical method (assuming respectively a linear and a parabolic temperature distribution) does predict the trend of data obtained at the dry-cooling tower Grootvlei 5 [76VA1].

10.4 REFERENCES

26ME1 Merkel, F., Verdunstungskühlung, VDI Zeitschrift, Vol. 70, pp. 123 - 128, 1926.

39LE1 Lettau, H., Atmosphärische Turbulenz, Akademische Verlagsgesellschaft, Leibzig, 1939.

54MO1 Monin, A.S. and Obukhov, A.M., Basic Regularity in Turbulent Mixing in the Surface Layer of the Atmosphere, Frud. Geofig. Inst. Akkad. Nauk. SSSR, Vol. 24, pp. 151-163, 1954.

61RO1 Roshko, A., Experiments on the Flow Past a Circular Cylinder at very High Reynolds Number, J. Fluid. Mech., Vol. 10, (Pt 3) No. 17, 1961.

64LO1 Lowe, H.J. et al, Aerodynamic Implications of the Ferrybridge Research Investigation, Proc. Symp. ICE on Natural Draught Cooling Towers, Paper 9, 1964.

65GE1 Gee, J.H., An Approximate Treatment of the Effect of Thermal Stability on Turbulant Diffusion, Quarterly Journal of the Royal Meteorological Society, Vol. 91, pp. 301 - 305, 1965.

67PR1 Preussag, A.G., Steinkohlenbergwerke Ibbenbüren, Kraftwerke Ibbenbüren 150 MW Block. Bericht über die am 22 und 23.8.1967 durchgeführten Messungen am Kühlturm der luftgekühlten Kondensationsanlage, 6 Nov, 1967.

69CH1 Christopher, P.J. and Forster, V.T., Rugeley Dry Cooling Tower System, Proc. Instn. Mech. Engrs. (London), Vol. 184, Pt. 1, No. 11, pp.197-211, 1969-1970.

70BR1 O'Brien, J.J., A Note on the Vertical Structure of the Eddy Exchange Coefficient in the Planetary Boundary Layer, Journal of the Atmospheric Sciences, Vol. 27, pp. 1213-1215, November 1970.

72EC1 Eck, B., Ventilatoren, Entwurf und Betrieb der Radial-, Axial- und

Querstromventilatoren, Springer-Verlag, Berlin, 1972.

72GO1 Golder, D., Relations Among Stability Parameters in the Surface Layer, Boundary-Layer Meteorology, Vol. 3, pp. 47-57, 1972.

72ZI1 Zilitinkević, S.S., On the Determination of the Height of the Ekman Boundary Layer, Boundary Layer Meteorology, Vol. 3, pp. 141-145, 1972.

75SE1 Seinfeld, J.H., Air Pollution: Physical and Chemical Fundamentals, McGraw Hill Book Co., New York, 1975.

76VA1 Van der Walt, N.T., West, L.A., Sheer, T.J. and Kuball, D., The Design and Operation of a Dry Cooling System for a 200 MW Turbo-generator at Grootvlei, Power Station, South Africa, The South African Mechanical Engineering, Vol. 26, No. 12, pp. 498-511, 1976.

77BU1 Buxmann, J., The Effect of Temperature Layers on the Heat Capacity of a Natural Draft Dry Cooling Tower, Brennst.-Wärme-Kraft, Vol. 29, No. 3, pp. 90-94, 1977.

77MA1 Markoczy and Stämpfli, E., Experimentelle Untersuchung des Einflusses atmosphärischer Umgebungsbedingungen auf das Betriebsverhalten von Naturzug-Trockenkühltürmen, EIR-Bericht, No. 324, Würenlingen, Switzerland, 1977.

78BA1 Baer, E., Einfluss des Windes Auf die Strömung im Kamin eines Naturzug-kühlturmes, D. Ing.-thesis, Universität Karlsruhe, 1978.

78BO1 Bouton, F., Design Studies for Natural Draught Dry Towers, SHF Conference, Paris, 1978.

78MO1 Moore, F.K., Effects of Aerodynamic Losses on the Performance of Large Dry Cooling Towers, ASME Paper 78-WA/HT-18, WAM, 1978.

78OL1 Olivari, D. and Thiry, F., Von Karman Institute for Fluid Dynamics, Report VKI TR 148, Brussels, 1978.

78RU1 Russell, C.M.B., McChesney, H.R., Holder, D.W. Jones, T.V. and Verlinden, M., Cross Wind and Internal Flow Characteristics of Dry Cooling Towers, Combustion, pp. 20-24, May 1978.

78TE1 Tesche, W., Inversionen Häufigkeit und Einflüsse auf natürlich belüftete Kühltürme, VGB Kraftwerkstechnik 61 Jahrgang, Heft 7, pp.611-618, 1978.

78VD1 VDI-Guide Lines, VDI 2049, Thermal Acceptance and Performance Tests on Dry Cooling Towers, 1978.

79BA1 Baer, E., et al, Thermodynamische Untersuchungen am Naturzug- Nasskühlturm C des Kraftwerkes Neurath und Modelle für das Betriebsverhalten und die Schwadenausbreitung, Fortschritt-Berichte der VDI-Zeitschriften, Reihe 15, No. 7, VDI-Verlag, Düsseldorf, 1979.

79DI1 Dibelius, G. and Eberhof, A., Der Windeinfluss auf den Volumenstrom von Naturzugkühltürmen, BWK, Vol. 31, No. 8, pp. 319-326, August 1979.

79HE1 Heberholz, P. and Schulz, S., The Influence of Atmospheric Precipitation on the Operation of a Natural Draught Indirect - contact Cooling Tower, Ger. Chem. Eng., Vol. 2, No. 1, pp. 352-360, 1979.

79OL1 Olivari, D. and Thiry, F., Von Karman Institute for Fluid Dynamics, Report VKI TR165, Brussels, 1979.

80BO1 Bourillot, C., Grange, J.L. and Lecoeuvre, J.M., Effect of Wind on the Performance of a Natural Wet Cooling Tower, Proc. 2nd, IAHR Cooling Tower Workshop, San Fransisco, 1980.

80LE1 Leene, J.A., Draught Reduction of Hyperbolic Natural-draught Cooling Towers as a Result of Wind, Proc. 4th Colleq. on Ind. Aerod. Part 2, Fachhochschule

Aachen, pp. 71-82, 1980.

80MA1 Maul, P.R., Atmospheric Transport of Sulphur Compound Pollutants, Central Electricity Generating Bureau MID/SSD/80/0026/R, Nottingham, England.

81KO1 Kosten, G.J., Morgan, J.I., Burns, J.M. and Curlett, P.L., Operating Experience and Performance Testing of the World's Largest Air-cooled Condenser, American Power Conference, Chicago, April 1981.

81TE1 Tesche, W., Inversions - frequency and Influence on Natural Draught Cooling Towers, VGB - Kraftwerkstechnik, Vol. 7, pp. 535-542, 1981.

82BU1 Buchlin, J.M. and Olivari, D., Experimental Investigation of Flow in Natural Draft Cooling Towers by use of Heated Models, Proc. 3rd IAHR Cooling Tower Workshop, Budapest, 1982.

82BU2 Buxmann, J., Operating Characteristics Influenced by Inversion and Inlet Pressure Losses at Dry Cooling Towers, IAHR Cooling Tower Workshop, Budapest, 1982.

82CH1 Chaboseau, J., Calculation of the Characteristics of an Air Cooling Tower Exposed to Wind, Proc. 3rd IAHR Cooling Tower Workshop, Budapest, 1982.

82DE1 De Bruin, H.A.R. and Holtslag, A.A.M., A Simple Parameterization of the Surface Fluxes of Sensible and Latent Heat During Daytime Compared with the Penman-Monteith Concept, Journal of Applied Meteorology, Vol. 21, pp. 1610-1621, 1982.

82GR1 Grange, J.L. and Simon, J.Y., Behaviour of Crossflow and Natural Draft Cooling Towers in the Presence of Wind, Proc. 3rd IAHR Cooling Tower Workshop, Budapest, 1982.

82RU1 Ruscheweyh, H., Modelluntersuchung zum Einfluss der Kühlturmkronenform auf das Zugverhalten grosser Naturzugkühltürme unter Querwindeinfluss, Brennst-

Wärme-Kraft, Vol. 34, No. 7, pp. 361-369, 1982.

82SA1 Sabaton, M., Cayton, Y. and Goussebaile, J., Numerical and Experimental Studies for the Cooling Tower Optimization, Proc. 3rd IAHR Cooling Tower Workshop, Budapest, 1982.

83BU1 Buxmann, J., Strömungsverteilung und Wärmeübertragung bei unterschiedlichen Elementanordnugen im Trockenkühlturm, Sonderforschungsbereich 61, Teilproject E10, Bericht Nr. 54, Universität Hannover, 1983.

83PA1 Panofsky, H.A. and J.A. Dutton, Atmospheric Turbulence, John Wiley & Sons, New York, 1983.

83RV1 Ruscheweyh, H., Full-scale Measurements on a Large Natural Draught Cooling Tower, Proc. 6th Int. Conf. on Wind Engineering, Australia 1983.

83WI1 Witte, R., Das Betriebsverhalten atmosphärisch beeinflusster Trockenkühltürme, Fortschr. -Ber VDI-Z, Reihe 6, No. 132, VDI-Verlag, Düsseldorf, 1983.

85VO1 Völler, G., Untersuchungen zum Windeinfluss auf die Strömung im Naturzug-Trockenkühlturm, Dr. Ing.-thesis, Universität Hannover, 1985.

86BL1 Blanquet, J.C., Goldwirt, F. and Manas, B., Wind Effects on the Aerodynamic Optimization of a Natural Draft Cooling Tower, Proc. 5th IAHR Cooling Tower Workshop, Monterey, 1986.

86BU1 Buxmann, J., Dry Cooling Tower Characteristics Effected by Cooling Circuit and the Top Shape of the Tower, Proc. 5th IAHR Cooling Tower Workshop, Monterey, 1986.

86SU1 Surridge, A.D., Extrapolation of the Noctural Temperature Inversion form Ground-based Measurements, Atmospheric Environment, Vol. 20, 1986.

86VA1 Vauzanges, M. and Ribier, G., Variation of the Head Losses in the Air Inlets of

Natural Draft Cooling Towers with the Shape of the Lintel and Shell Supports, Proc. 5th IAHR Cooling Tower Workshop, Monterey, 1986.

87SU1 Surridge, A.D. and Hayton, D., The Operation of a Natural-Draught Dry Cooling System under Stable Atmospheric Conditions, Physico, Chemical Hydrodynamics, Vol. 8, No. 2, pp. 95-104, 1987.

87TR1 Trage, B. and Hintzen F.J., Design and Construction of Indirect Dry Cooling Units, Proc. VGB Conference, South Africa 1987, Vol. 1, pp. 70-79, Johannesburg, 1987.

88LA1 Lauraine, H., Lemmens, P. and Monjoie, M., Experimental Data Coupling Atmospheric Temperature Inversions and Cooling Tower Performances, Proc. of the 6th IAHR Cooling Tower Workshop, Pisa, 1988.

88RA1 Radosavljevic, D. and Spalding, D.B., Simultaneous Prediction of Internal and External Aerodynamic and Thermal Flow Fields of a Natural-draft Cooling Tower in a Cross-Wind, Proc. 6th IAHR Cooling Tower Workshop, Pisa, 1988.

89CA1 Caytan, Y. and Fabre, L., Wind Effects on the Performance of Natural Draft Wet Cooling Towers Comparison of Constructors Proposals and Realization of Performance Control Tests, Proc. Int. Cooling-Tower Conf., EPRI GS-6317, 1989.

89RA1 Radosavljevic, D. and Spalding, D., The Use of PHOENIX to Simulate Three-dimensional Effects in Natural-draught Cooling Towers, The PHOENIX Journal of Computational Mechanics, CHAM Ltd, London, 1989.

92DU1 Du Preez, A.F., The Influence of Cross-winds on the Performance of Natural Draft Dry-cooling Towers, Ph.D thesis, University of Stellenbosch, South Africa, November 1992.

92DU2 Du Preez, A.F. and Kröger D.G., Investigation into the Influence of Cross-winds on the Performance of Dry-cooling towers, Paper presented at the 8th IAHR Cooling Tower and Spraying Pond Symposium, Karlsruhe, 1992.

93AZ1 Azad, R.S., The Atmospheric Boundary Layer for Engineers, Kluwer Academic Publishers, Dordrecht, Netherlands, 1993.

93DU1 Du Preez, A.F. and Kröger, D.G., Experimental Investigation into the Influence of Cross-winds on the Performance of Dry-cooling Towers, Research and Development Journal, South African Institution of Mechanical Engineers, Vol. 9, No. 2, pp. 1-11, 1993.

93DU2 Du Preez, A.F. and Kröger, D.G., Effect of Wind on Performance of a Dry-cooling Tower, Heat Recovery Systems and CHP, Vol. 13, No. 2, pp. 139-146, 1993.

93GO1 Goldschagg, H.B., Lessons Learned from the World's Largest Forced Draft Direct Air Cooled Condenser, Paper presented at the EPRI Int. Symp. on Improved Technology for Fossil Power Plants - New and Retrofit Applications, Washington, March 1993.

94BA1 Barbaud, J., Cooling Tower of the NPP Civaux Auxiliary Systems. Features of the Function and Requirements Related to Nuclear Safety, Paper presented at the 9th IAHR Cooling Tower and Spraying Pond Symposium, von Karman Institute, Brussels, Belgium, September 1994.

94DU1 Du Preez Tower supports, Heat Transfer Engineering

94FA1 Fabre, L., Wet Cooling Towers. The Different Antifreeze Systems. Experience Feed-back, Paper presented at the 9th IAHR Cooling Tower and Spraying Pond Symposium, von Karman Institute, Brussels, Belgium, September 1994.

94NO1 Nouri-Borujerdi, A., Effects of Shell Materials and Atmospheric Conditions on Natural Draft Cooling Tower Performance, Paper presented at the 9th IAHR Cooling Tower and Spraying Pond Symposium, von Karman Institute, Brussels, Belgium, September 1994.

APPENDIX A

PROPERTIES OF FLUIDS

A.1 The thermophysical properties of dry air from 220K to 380K at standard atmospheric pressure (101325 N/m^2).

Density:

$$\rho_a = p_a/(287.08\ T),\ kg/m^3 \tag{A.1.1}$$

Specific heat [82AN1]:

$$c_{pa} = 1.045356 \times 10^3 - 3.161783 \times 10^{-1}\ T + 7.083814 \times 10^{-4}\ T^2 - 2.705209 \times 10^{-7}\ T^3,\ J/kgK \tag{A.1.2}$$

Dynamic viscosity [82AN1]:

$$\mu_a = 2.287973 \times 10^{-6} + 6.259793 \times 10^{-8}\ T - 3.131956 \times 10^{-11}\ T^2 + 8.15038 \times 10^{-15}\ T^3,\ kg/sm \tag{A.1.3}$$

Thermal conductivity:

$$k_a = -4.937787 \times 10^{-4} + 1.018087 \times 10^{-4}\ T - 4.627937 \times 10^{-8}\ T^2 + 1.250603 \times 10^{-11}\ T^3,\ W/mK \tag{A.1.4}$$

Table A.1: The thermophysical properties of dry air at standard atmospheric pressure.

T K	ρ_a kg/m^3	c_{pa} J/kgK	$\mu_a \times 10^5$ kg/ms	k_a W/mK	$\alpha_a \times 10^5$ m^2/s	Pr_a
220	1.60432	1007.20	1.46304	0.0197973	1.22518	0.744330
225	1.56866	1006.99	1.48797	0.0202127	1.27957	0.741309
230	1.53456	1006.81	1.51278	0.0206262	1.33500	0.738428
235	1.50191	1006.66	1.53746	0.0210378	1.39145	0.735680
240	1.47062	1006.53	1.56201	0.0214475	1.44892	0.733056
245	1.44061	1006.43	1.58643	0.0218553	1.50738	0.730550
250	1.41180	1006.35	1.61073	0.0222613	1.56684	0.728156
255	1.38411	1006.30	1.63490	0.0226655	1.62727	0.725867
260	1.35750	1006.28	1.65894	0.0230678	1.68867	0.723678
265	1.33188	1006.28	1.68286	0.0234683	1.75103	0.721585
270	1.30722	1006.30	1.70666	0.0238669	1.81433	0.719581
275	1.28345	1006.35	1.73033	0.0242638	1.87857	0.717663
280	1.26053	1006.42	1.75388	0.0246589	1.94373	0.715828
285	1.23842	1006.52	1.77731	0.0250521	2.00980	0.714070
290	1.21707	1006.64	1.80061	0.0254436	2.07677	0.712387
295	1.19644	1006.78	1.82380	0.0258334	2.14463	0.710776
300	1.17650	1006.95	1.84686	0.0262213	2.21336	0.709233
305	1.15721	1007.14	1.86980	0.0266075	2.28297	0.707755
310	1.13854	1007.35	1.89263	0.0269920	2.35342	0.706340
315	1.12047	1007.59	1.91533	0.0273747	2.42472	0.704985
320	1.10297	1007.85	1.93792	0.0277558	2.49685	0.703688
325	1.08600	1008.13	1.96039	0.0281351	2.56980	0.702446
330	1.06954	1008.43	1.98274	0.0285127	2.64356	0.701258
335	1.05358	1008.76	2.00498	0.0288886	2.71811	0.700122
340	1.03808	1009.11	2.02710	0.0292628	2.79345	0.699035
345	1.02304	1009.48	2.04911	0.0296353	2.86957	0.697997
350	1.00842	1009.87	2.07100	0.0300062	2.94645	0.697004
355	0.99422	1010.28	2.09278	0.0303754	3.02408	0.696056
360	0.98041	1010.71	2.11444	0.0307430	3.10246	0.695151
365	0.96698	1011.17	2.13599	0.0311098	3.18156	0.694288
370	0.95392	1011.64	2.15743	0.0314732	3.26138	0.693465
375	0.94120	1012.13	2.17876	0.0318359	3.34191	0.692681
380	0.92881	1012.65	2.19998	0.0321970	3.42313	0.691935

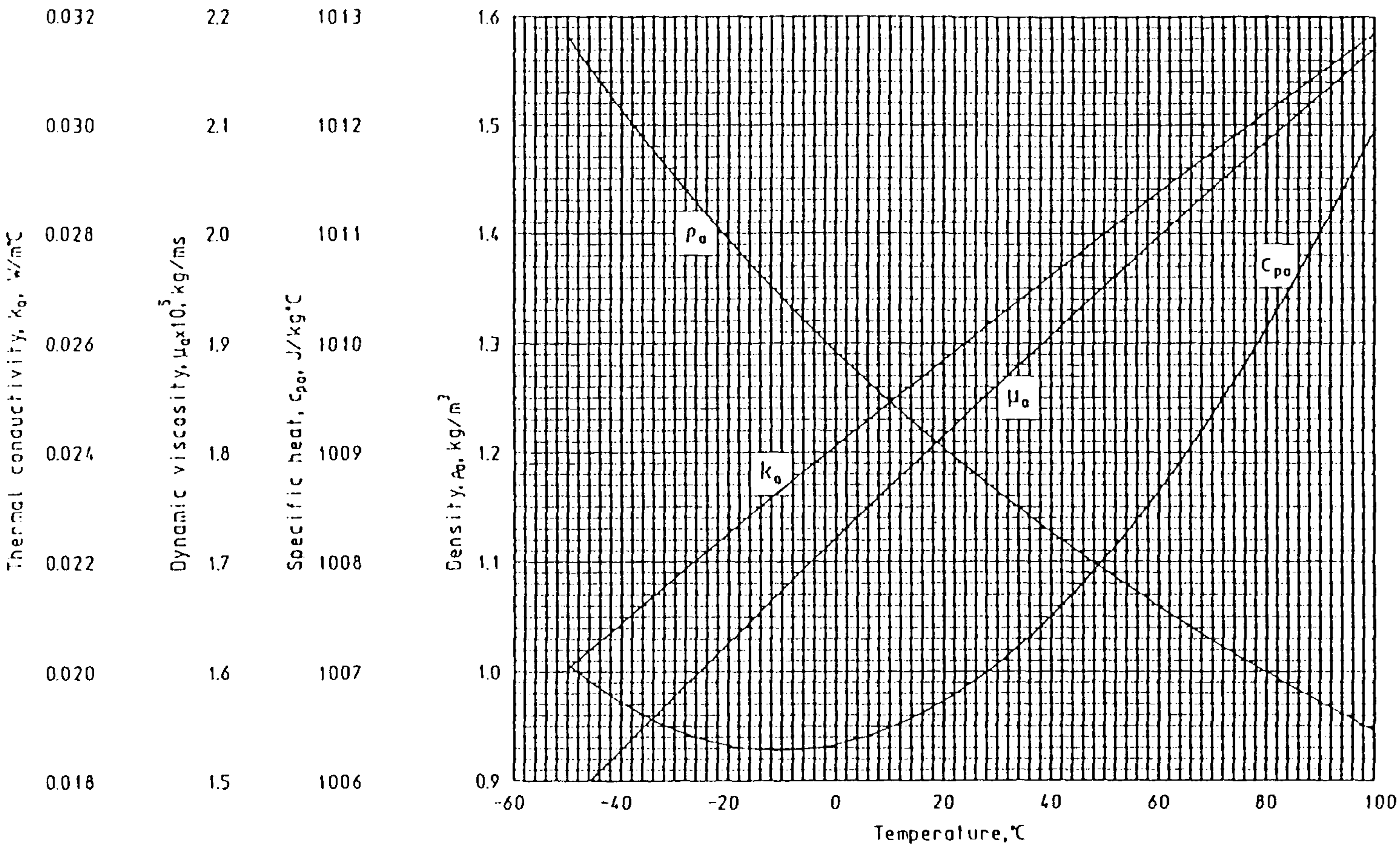

Figure A.1: The thermophysical properties of dry air at standard atmospheric pressure (101325 N/m^2).

A.2 The themophysical properties of saturated water vapor from 273.15K to 380K.

Vapor pressure [65GO1]:

$$p_v = 10^z, \text{ N/m}^2 \tag{A.2.1}$$

$$z = 10.79586(1 - 273.16/T) + 5.02808 \log_{10}(273.16/T)$$

$$+ 1.50474 \times 10^{-4} [1 - 10^{-8.29692\{(T/273.16) - 1\}}]$$

$$+ 4.2873 \times 10^{-4}[10^{4.76955(1 - 273.16/T)} - 1] + 2.786118312$$

Specific heat:

$$c_{pv} = 1.3605 \times 10^3 + 2.31334T - 2.46784 \times 10^{-10}T^5$$

$$+ 5.91332 \times 10^{-13}T^6, \text{ J/kgK} \tag{A.2.2}$$

Dynamic viscosity:

$$\mu_v = 2.562435 \times 10^{-6} + 1.816683 \times 10^{-8}T + 2.579066 \times 10^{-11}T^2$$

$$- 1.067299 \times 10^{-14}T^3, \text{ kg/ms} \tag{A.2.3}$$

Thermal conductivity [82AN1]:

$$k_v = 1.3046 \times 10^{-2} - 3.756191 \times 10^{-5}T + 2.217964 \times 10^{-7}T^2$$

$$- 1.111562 \times 10^{-10}T^3, \text{ W/mK} \tag{A.2.4}$$

Vapor density [70UK1]:

$$\rho_v = -4.062329056 + 0.10277044T - 9.76300388 \times 10^{-4}T^2 + 4.475240795 \times 10^{-6}T^3$$

$$- 1.004596894 \times 10^{-8}T^4 + 8.9154895 \times 10^{-12}T^5, \text{ kg/m}^3 \tag{A.2.5}$$

Temperature:

$$T = 164.630366 + 1.832295 \times 10^{-3}\, p_v + 4.27215 \times 10^{-10}\, p_v^2 + 3.738954 \times 10^{3}\, p_v^{-1}$$

$$- 7.01204 \times 10^{5}\, p_v^{-2} + 16.161488 \ln p_v - 1.437169 \times 10^{-4}\, p_v \ln p_v \text{ , K}$$

Table A.2: The thermophysical properties of saturated water vapor.

T K	p_v N/m^2	ρ_v kg/m^3	c_{pv} J/kgK	$\mu_v \times 10^6$ kg/ms	k_v W/mK	$\alpha_v \times 10^5$ m^2/s	Pr_v
275	697.820	0.00550	1864.29	9.28676	0.0171781	167.602	1.00786
280	990.897	0.00767	1868.46	9.4368	0.0174774	121.992	1.00887
285	1387.70	0.01056	1872.66	9.58775	0.0177831	90.0091	1.00964
290	1918.11	0.01436	1876.92	9.73950	0.0180951	67.2777	1.01023
295	2618.61	0.01928	1881.31	9.89208	0.0184134	50.8805	1.01068
300	3533.19	0.02557	1885.89	10.0454	0.0187378	38.9260	1.01103
305	4714.45	0.03355	1890.74	10.1996	0.0190684	30.1011	1.01135
310	6224.58	0.04360	1985.92	10.3546	0.0194049	23.5132	1.01168
315	8136.44	0.05611	1901.52	10.5104	0.0197474	18.5427	1.01207
320	10534.7	0.07155	1907.63	10.6670	0.0200957	14.7547	1.01259
325	13516.9	0.09045	1914.35	10.8244	0.0204498	11.8400	1.01329
330	17194.7	0.11341	1921.79	10.9825	0.0208095	9.57698	1.01425
335	21694.5	0.14108	1930.04	11.1414	0.0211749	7.80452	1.01551
340	27158.9	0.17418	1939.25	11.3010	0.0215457	6.40488	1.01716
345	33747.7	0.21352	1949.63	11.4614	0.0219219	5.29095	1.01927
350	41638.4	0.26000	1961.03	11.6225	0.0223035	4.39779	1.02191
355	51027.6	0.31455	1973.90	11.7844	0.0226904	3.67653	1.02516
360	62131.3	0.37821	1988.29	11.9470	0.0230824	3.09016	1.02910
365	75186.3	0.45213	2004.37	12.1102	0.0234795	2.61037	1.03382
370	90450.0	0.53750	2022.33	12.2742	0.0238816	2.21538	1.03940
375	108201	0.63568	2042.35	12.4389	0.0242886	1.888304	1.04595
380	128743	0.74799	2064.63	12.6043	0.0247005	1.615964	1.05355

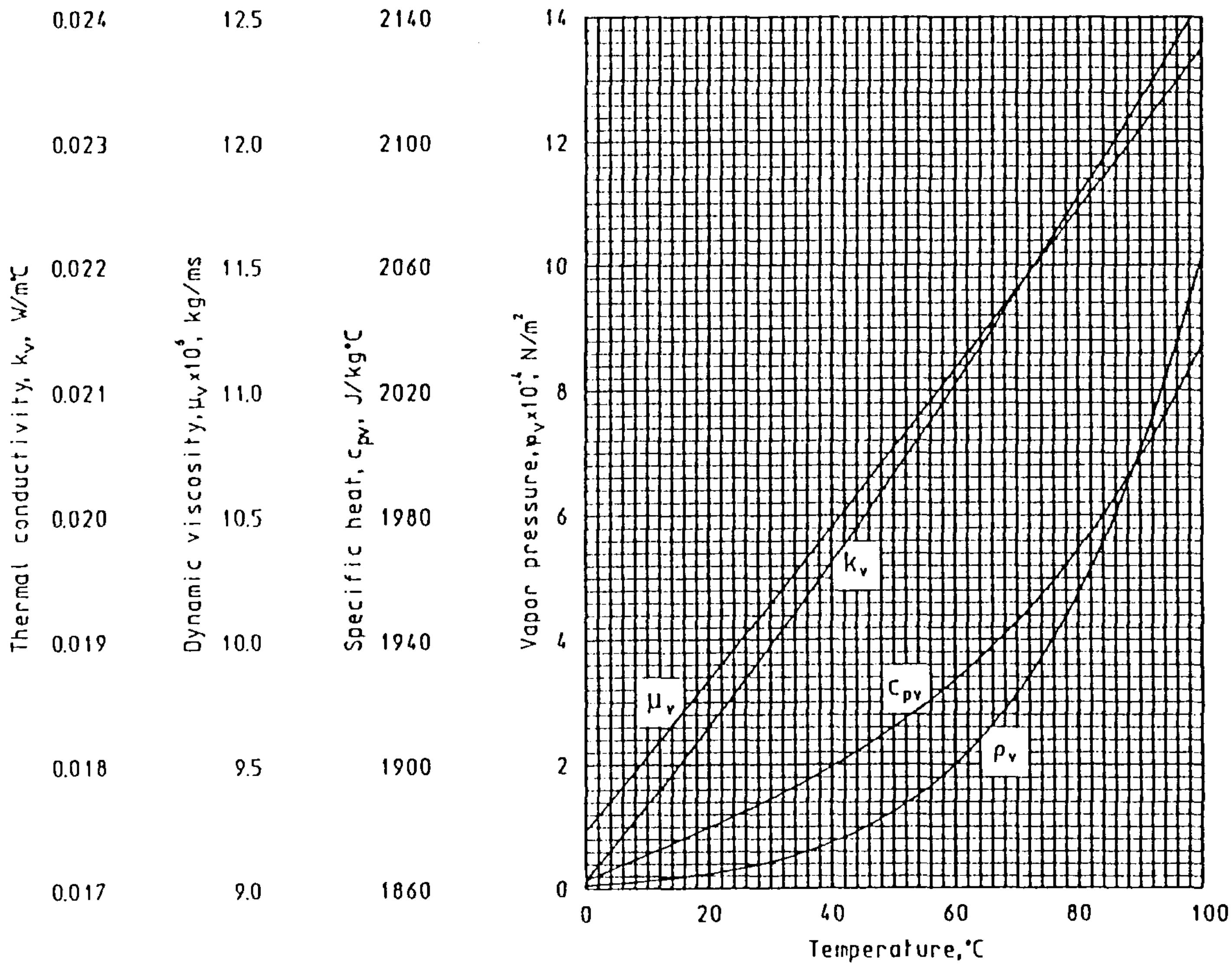

Figure A.2: The thermophysical properties of saturated water vapor.

A.3 The thermophysical properties of mixtures of air and water vapor.

Density [72AS1]:

$$\rho_{av} = (1 + w)\,[1 - w/(w + 0.62198)]\,p_{abs}/(287.08T),\ \text{kg air-vapor/m}^3 \qquad (A.3.1)$$

Specific heat [78FA1]:

$$c_{pav} = (c_{pa} + wc_{pv})/(1 + w),\ \text{J/kg air-vapor K} \qquad (A.3.2a)$$

or the specific heat of the air-vapor mixture per unit mass of dry air

$$c_{pma} = (c_{pa} + w_{cpv}),\ \text{J/K kg dry air} \qquad (A.3.2b)$$

Dynamic viscosity [54GO1]:

$$\mu_{av} = (X_a\mu_a M_a^{0.5} + X_v\mu_v M_v^{0.5})/(X_a M_a^{0.5} + X_v M_v^{0.5}),\ \text{kg/ms} \qquad (A.3.3)$$

where M_a = 28.97 kg/mole, M_v = 18.016 kg/mole, $X_a = 1/(1 + 1.608\ w)$ and $X_v = w/(w + 0.622)$

Thermal conductivity [57LE1]:

$$k_{av} = (X_a k_a M_a^{0.33} + X_v k_v M_v^{0.33})/(X_a M_a^{0.33} + X_v M_v^{0.33}),\ \text{W/mK} \qquad (A.3.4)$$

Humidity ratio [82JO1]:

$$w = \left(\frac{2501.6 - 2.3263(T_{wb} - 273.15)}{2501.6 + 1.8577(T - 273.15) - 4.184(T_{wb} - 273.15)}\right)\left(\frac{0.62509p_{vwb}}{p_{abs} - 1.005p_{vwb}}\right)$$

$$- \left(\frac{1.00416\ (T - T_{wb})}{2501.6 + 1.8577(T - 273.15) - 4.184(T_{wb} - 273.15)}\right),\ \text{kg/kg dry air} \qquad (A.3.5)$$

Enthalpy:

$$i_{av} = [c_{pa}(T - 273.15) + w\{i_{fgwo} + c_{pv}(T - 273.15)\}]/(1+w), \text{ J/kg air-vapor} \tag{A.3.6a}$$

or the enthalpy of the air-vapor mixture per unit mass of dry air

$$i_{ma} = c_{pa}(T-273.15) + w\left[i_{fgwo} + c_{pv}(T-273.15)\right], \text{ J/kg dry air} \tag{A.3.6b}$$

where the specific heats are evaluated at (T + 273.15)/2 and the latent heat i_{fgwo}, is evaluated at 273.15 K according to equation (A.4.5) i.e. $i_{fgwo} = 2.5016 \times 10^6$ J/kg.

A.4 The thermophysical properties of saturated water liquid from 273.15K to 380K.

Density:

$$\rho_w = (1.49343 \times 10^{-3} - 3.7164 \times 10^{-6}T + 7.09782 \times 10^{-9}T^2$$

$$- 1.90321 \times 10^{-20}T^6)^{-1}, \text{ kg/m}^3 \qquad \text{(A.4.1)}$$

Specific heat:

$$c_{pw} = 8.15599 \times 10^3 - 2.80627 \times 10T + 5.11283 \times 10^{-2}T^2$$

$$- 2.17582 \times 10^{-13}T^6, \text{ J/kgK} \qquad \text{(A.4.2)}$$

Dynamic viscosity [82AN1]:

$$\mu_w = 2.414 \times 10^{-5} \times 10^{247.8/(T - 140)}, \text{ kg/ms} \qquad \text{(A.4.3)}$$

Thermal conductivity:

$$k_w = -6.14255 \times 10^{-1} + 6.9962 \times 10^{-3}T - 1.01075 \times 10^{-5}T^2$$

$$+ 4.74737 \times 10^{-12}T^4, \text{ W/mK} \qquad \text{(A.4.4)}$$

Latent heat of vaporization:

$$i_{fgw} = 3.4831814 \times 10^6 - 5.8627703 \times 10^3T + 12.139568T^2$$

$$- 1.40290431 \times 10^{-2}T^3, \text{ J/kg} \qquad \text{(A.4.5)}$$

Critical pressure:

$$p_{wc} = 22.09 \times 10^6, \text{ N/m}^2 \qquad \text{(A.4.6)}$$

Surface tension [70UK1]:

$$\sigma_w = 5.148103 \times 10^{-2} + 3.998714 \times 10^{-4}T - 1.4721869 \times 10^{-6}T^2$$

$$+ 1.21405335 \times 10^{-9}T^3, \text{ N/m} \quad \text{(A.4.7)}$$

Table A.3: The thermophysical properties of saturated water liquid.

T K	ρ_w kg/m^3	c_{pw} J/kgK	$\mu_w \times 10^4$ kg/ms	k_w W/mK	$\beta_w \times 10^5$ 1/K	Pr_w
275	1000.03	4211.21	16.5307	0.572471	0.780333	12.1603
280	999.864	4202.04	14.2146	0.581432	6.184114	10.2730
285	999.422	4194.41	12.3510	0.590001	11.45765	8.78055
290	998.721	4188.27	10.8327	0.598179	16.59011	7.58474
295	997.768	4183.53	9.58179	0.605972	21.57093	6.61511
300	996.572	4180.10	8.54057	0.613383	26.38963	5.82026
305	995.141	4177.92	7.66576	0.620417	31.03593	5.16215
310	993.487	4176.87	6.92443	0.627079	35.49975	4.61225
315	991.618	4176.88	6.29125	0.633372	39.77122	4.14887
320	989.547	4177.83	5.74650	0.639300	43.84070	3.75534
325	987.284	4179.63	5.27468	0.644870	47.69877	3.41871
330	984.842	4182.17	4.86348	0.650084	51.33626	3.12881
335	982.232	4185.32	4.50304	0.654948	54.74422	2.87758
340	979.469	4188.98	4.18540	0.659466	57.91392	2.65859
345	976.564	4193.01	3.90407	0.663644	60.83688	2.46665
350	973.532	4197.28	3.65373	0.667486	63.50480	2.29754
355	970.386	4201.67	3.43001	0.670997	65.90961	2.14781
360	976.141	4206.01	3.22924	0.674182	68.04338	2.01462
365	963.811	4210.17	3.04839	0.677046	69.89838	1.89562
370	960.409	4213.99	2.88488	0.679595	71.46697	1.78884
375	956.952	4217.31	2.73656	0.681833	72.74164	1.69263
380	953.453	4219.96	2.60158	0.683767	73.71494	1.60560

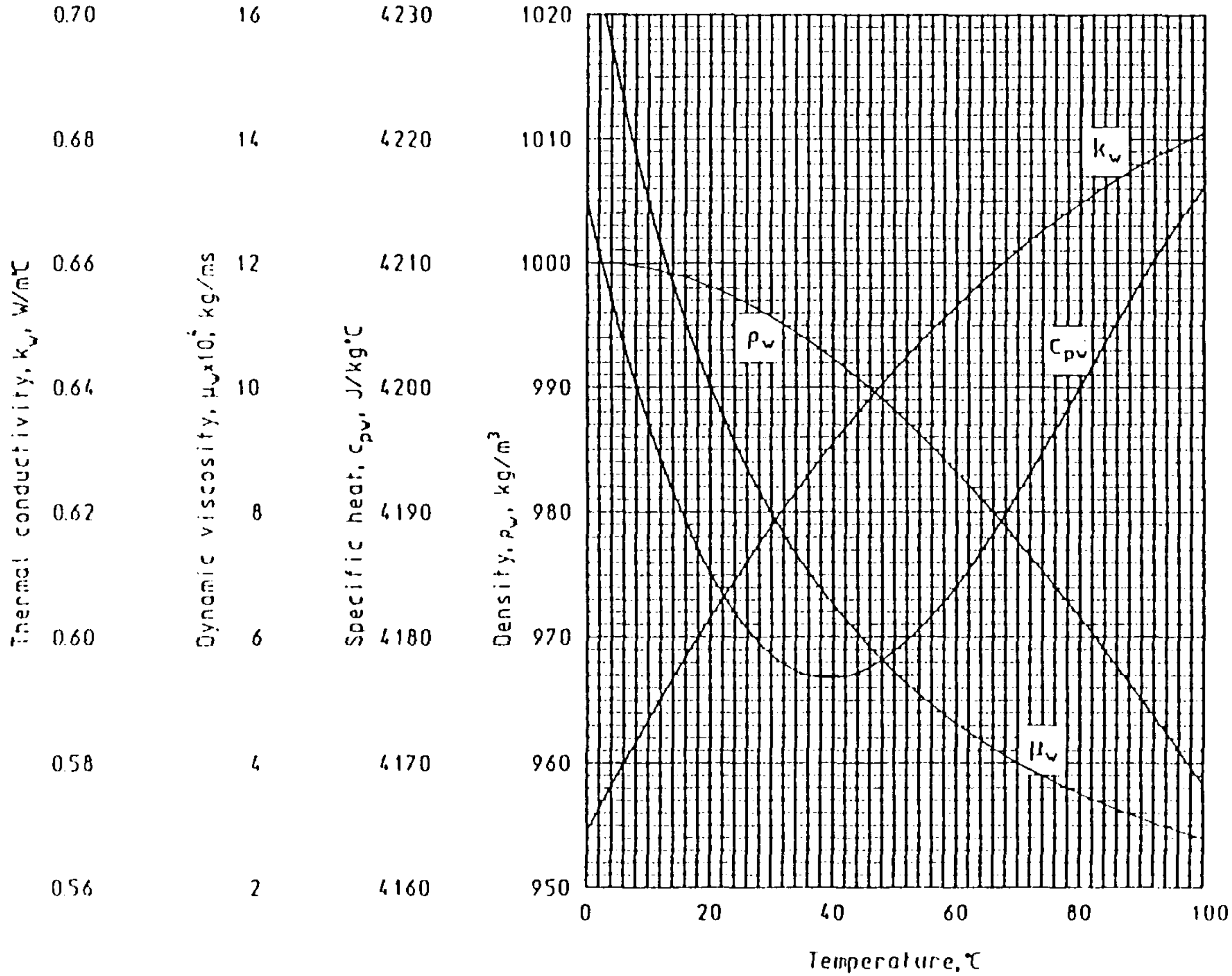

Figure A.3: The thermophysical properties of saturated water liquid.

A.5 The thermophysical properties of saturated ammonia vapor.

Vapor pressure [76RA1], (230K to 395K):

$$p_{ammv} = 1.992448 \times 10^6 - 57.56814 \times 10^3 T + 0.5640265 \times 10^3 T^2 - 2.337352 T^3$$

$$+ 3.54143 \times 10^{-3} T^4,\ N/m^2 \qquad (A.5.1)$$

Density [76RA1], (260K to 390K):

$$\rho_{ammv} = -6.018936 \times 10^2 + 5.361048 T - 1.187296 \times 10^{-2} T^2 - 1.161479 \times 10^{-5} T^3$$

$$+ 4.739058 \times 10^{-8} T^4,\ kg/m^3 \qquad (A.5.2)$$

Specific heat [72AS1], (230K to 325K):

$$c_{pammv} = -2.7761190256 \times 10^4 + 3.39116449 \times 10^2 T - 1.3055687 T^2$$

$$- 1.728649 \times 10^{-3} T^3;\ J/kgK \qquad (A.5.3)$$

Dynamic viscosity [72AS1], (240K to 370K):

$$\mu_{ammv} = -2.748011 \times 10^{-5} + 2.82526 \times 10^{-7} T - 5.201831 \times 10^{-10} T^2$$

$$- 6.061761 \times 10^{-13} T^3 + 2.12607 \times 10^{-15} T^4,\ kg/sm \qquad (A.5.4)$$

Thermal conductivity [72AS1], (245K to 395K):

$$k_{ammv} = -0.1390216 + 1.35238 \times 10^{-3} T - 2.532035 \times 10^{-6} T^2 - 4.884341 \times 10^{-9} T^3$$

$$+ 1.418657 \times 10^{-11} T^4,\ W/mK \qquad (A.5.6)$$

Table A.4: The thermophysical properties of saturated ammonia vapor.

T K	$p_{ammv} \times 10^{-3}$ N/m^2	ρ_{ammv} kg/m^3	c_{pammv} J/kgK	$\mu_{ammv} \times 10^6$ kg/sm	k_{ammv} W/mK	Pr_{ammv}
230	60.58		2230.48			
235	79.09		2265.33			
240	102.08		2322.84	9.0376		
245	130.32		2377.30	9.2605	0.019611	1.12261
250	164.65		2430.01	9.4734	0.019920	1.15567
255	205.93		2482.27	9.6774	0.020185	1.19009
260	255.10	1.78881	2535.37	9.8737	0.020414	1.22632
265	313.14	2.56766	2590.61	10.0635	0.020613	1.26477
270	381.09	3.28963	2649.29	10.2480	0.020790	1.30588
275	460.03	3.98405	2712.69	10.4284	0.020954	1.35007
280	551.10	4.68094	2782.13	10.6060	0.021111	1.39774
285	655.51	5.41106	2858.89	10.7822	0.021270	1.44924
290	774.50	6.20583	2944.27	10.9583	0.021439	1.50491
295	909.36	7.09745	3039.57	11.1356	0.021627	1.56503
300	1061.74	8.11876	3146.08	11.3156	0.021843	1.62979
305	1232.21	9.30337	3265.10	11.4997	0.022096	1.69932
310	1423.06	10.68557	3397.93	11.6894	0.022394	1.77368
315	1635.53	12.30036	3545.87	11.8862	0.022748	1.85280
320	1871.19	14.18346	3710.20	12.0917	0.023166	1.93654
325	2131.65	16.37130	3892.24	12.3074	0.023660	2.02466
330	2418.59	18.90102		12.5349	0.024238	
335	2733.73	21.81047		12.7758	0.024911	
340	3078.86	25.13821		13.0318	0.025690	
345	3455.81	28.92352		13.3047	0.026586	
350	3866.46	33.20637		13.5961	0.027608	
355	4312.75	38.02745		13.9078	0.028769	
360	4796.68	43.42818		14.24159	0.030080	
365	5320.28	49.45067		14.5993	0.031551	
370	5885.67	56.13774		14.9827	0.033196	
375	6494.98	63.53294			0.035026	
385	7854.27	80.62539			0.039289	
395	9416.42				0.044441	

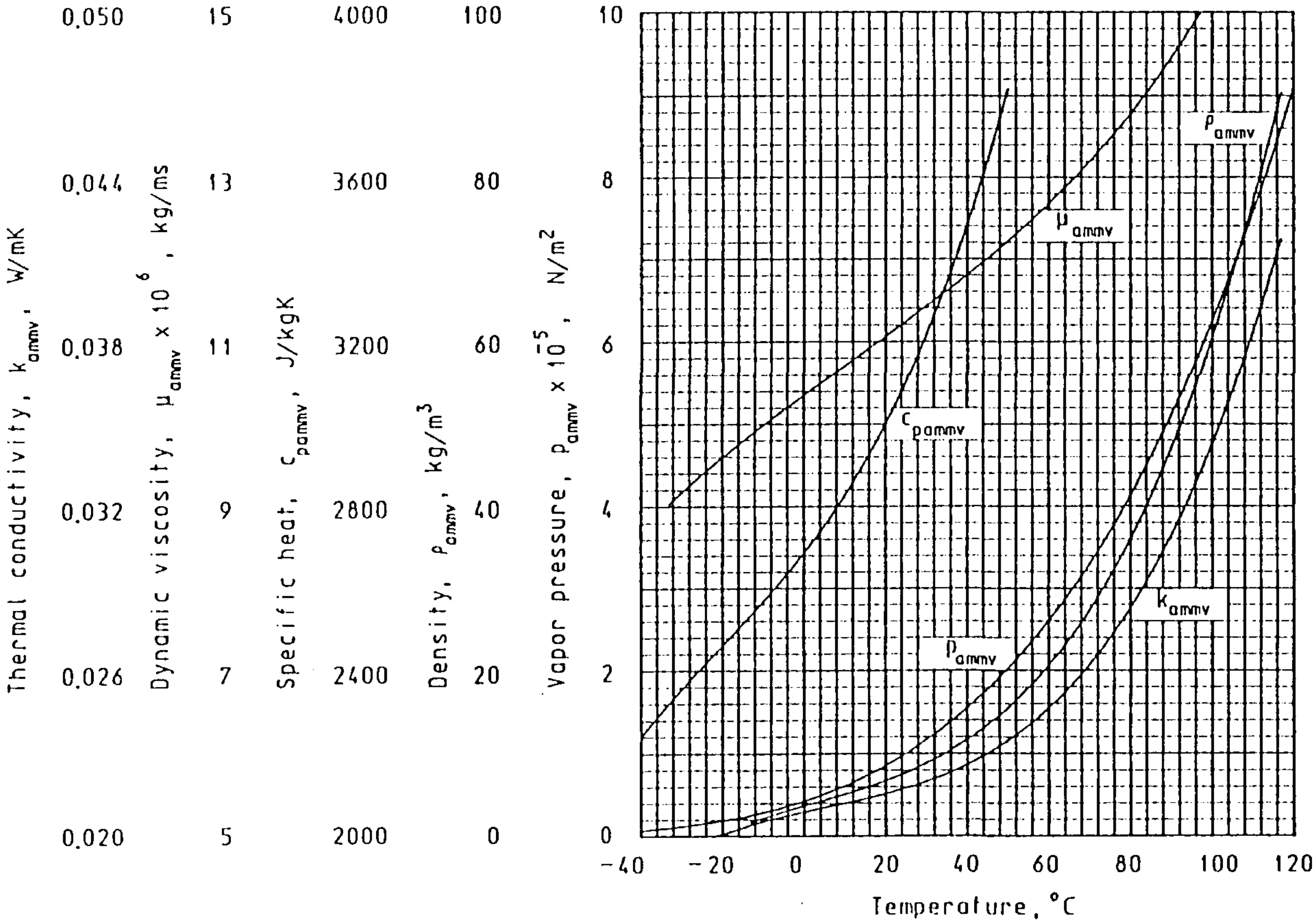

Figure A.4: Thermophysical properties of saturated ammonia vapor.

A.6. The thermophysical properties of saturated ammonia liquid from 200 K to 405 K.

Density [77YA1]:

$$\rho_{amm} = 2.312 \times 10^2 \times 0.2471^{\left[-(1 - T/405.5)^{0.285714}\right]},\ \mathrm{kg/m^3} \tag{A.6.1}$$

Specific heat [77YA1], (200K to 375K):

$$c_{pamm} = -2.497276939 \times 10^3 + 7.7813907 \times 10T - 3.006252 \times 10^{-1}T^2$$

$$+ 4.06714 \times 10^{-4}T^3,\ \mathrm{J/kgK} \tag{A.6.2}$$

Dynamic viscosity [77YA1]:

$$\mu_{amm} = 0.001 \times 10^{(-8.591 + 876.4/T + 0.02681T - 3.612 \times 10^{-5}T^2)},\ \mathrm{kg/sm}$$

Thermal conductivity [77YA1], (200K to 375K):

$$k_{amm} = 1.068229 - 1.576908 \times 10^{-3}T - 1.228884 \times 10^{-6}T^2,\ \mathrm{W/mK} \tag{A.6.4}$$

Latent heat of vaporization [77YA1]:

$$i_{fgamm} = 1.370758 \times 10^6[(405.55 - T)/(165.83)]^{0.38},\ \mathrm{J/kg} \tag{A.6.5}$$

Critical pressure:

$$p_{ammc} = 11.28 \times 10^6,\ \mathrm{N/m^2} \tag{A.6.6}$$

Surface tension [77YA1]:

$$\sigma = 0.0366[(405.55 - T)/177.4]^{1.1548},\ \mathrm{N/m} \tag{A.6.7}$$

Table A.5: The thermophysical properties of saturated ammonia liquid.

T	ρ_{pamm}	c_{pamm}	$\mu_{amm} \times 10^5$	k_{amm}	Pr_{amm}	$i_{fgamm} \times 10^{-3}$
K	kg/m^3	J/kgK	kg/sm	W/mk		J/kg
200	731.094	4294.20	51.0740	0.703692	3.11673	1487.29
205	725.217	4324.69	45.9440	0.693319	2.86583	1473.44
210	719.282	4352.65	41.6429	0.682885	2.65428	1459.37
215	713.288	4378.38	37.9998	0.672389	2.47443	1445.08
220	707.232	4402.21	34.8841	0.661832	2.32034	1430.55
225	701.111	4424.42	32.1948	0.651213	2.18736	1415.78
230	694.923	4445.33	29.8529	0.640532	2.07181	1400.75
235	688.663	4465.24	27.7961	0.629791	1.97076	1385.45
240	682.329	4484.46	25.9749	0.618988	1.88184	1369.87
245	675.918	4503.28	24.3494	0.608123	1.80313	1354.00
250	669.424	4522.03	22.8875	0.597197	1.73306	1337.82
255	662.844	4540.99	21.5630	0.586210	1.67035	1321.31
260	656.173	4550.48	20.3543	0.575161	1.61390	1304.46
265	649.406	4580.79	19.2438	0.564050	1.56284	1287.25
270	642.537	4602.25	18.2170	0.552878	1.51641	1269.65
275	635.560	4625.14	17.2617	0.541645	1.47399	1251.65
280	628.469	4649.78	16.3678	0.530351	1.43503	1233.21
285	621.255	4676.47	15.5271	0.518994	1.39909	1214.31
290	613.912	4705.52	14.7325	0.507577	1.36578	1194.92
295	606.428	4737.23	13.9783	0.496098	1.33478	1175.01
300	598.794	4771.90	13.2596	0.484557	1.30581	1154.52
305	590.999	4809.85	12.5727	0.472955	1.27861	1133.42
310	583.029	4851.37	11.9141	0.461292	1.25300	1111.67
315	574.868	4896.77	11.2814	0.449567	1.22879	1089.19
320	566.500	4946.35	10.6723	0.437781	1.20584	1065.93
325	557.905	5000.43	10.0853	0.425933	1.18401	1041.82
330	549.060	5059.31	9.5189	0.414024	1.16320	1016.75
335	539.936	5123.28	8.9722	0.402054	1.14331	990.644
340	530.501	51.92.66	8.4445	0.390022	1.12428	963.355
345	520.717	5267.75	7.9351	0.377928	1.10604	934.743
350	510.534	5348.86	7.4438	0.365773	1.08855	904.625
355	499.893	5436.29	6.9704	0.353557	1.07177	872.776
360	488.718	5530.35	6.5146	0.341279	1.05568	838.908
365	476.910	5631.34	6.0765	0.328940	1.04028	802.648
370	464.337	5739.56	5.6561	0.316539	1.02558	763.498
375	450.814	5855.32	5.2534	0.304077	1.01160	720.764
380	436.074		4.8684			673.437
385	419.697		4.5011			619.951
395	378.461		3.8199			481.199
405	285.772		3.2093			156.612

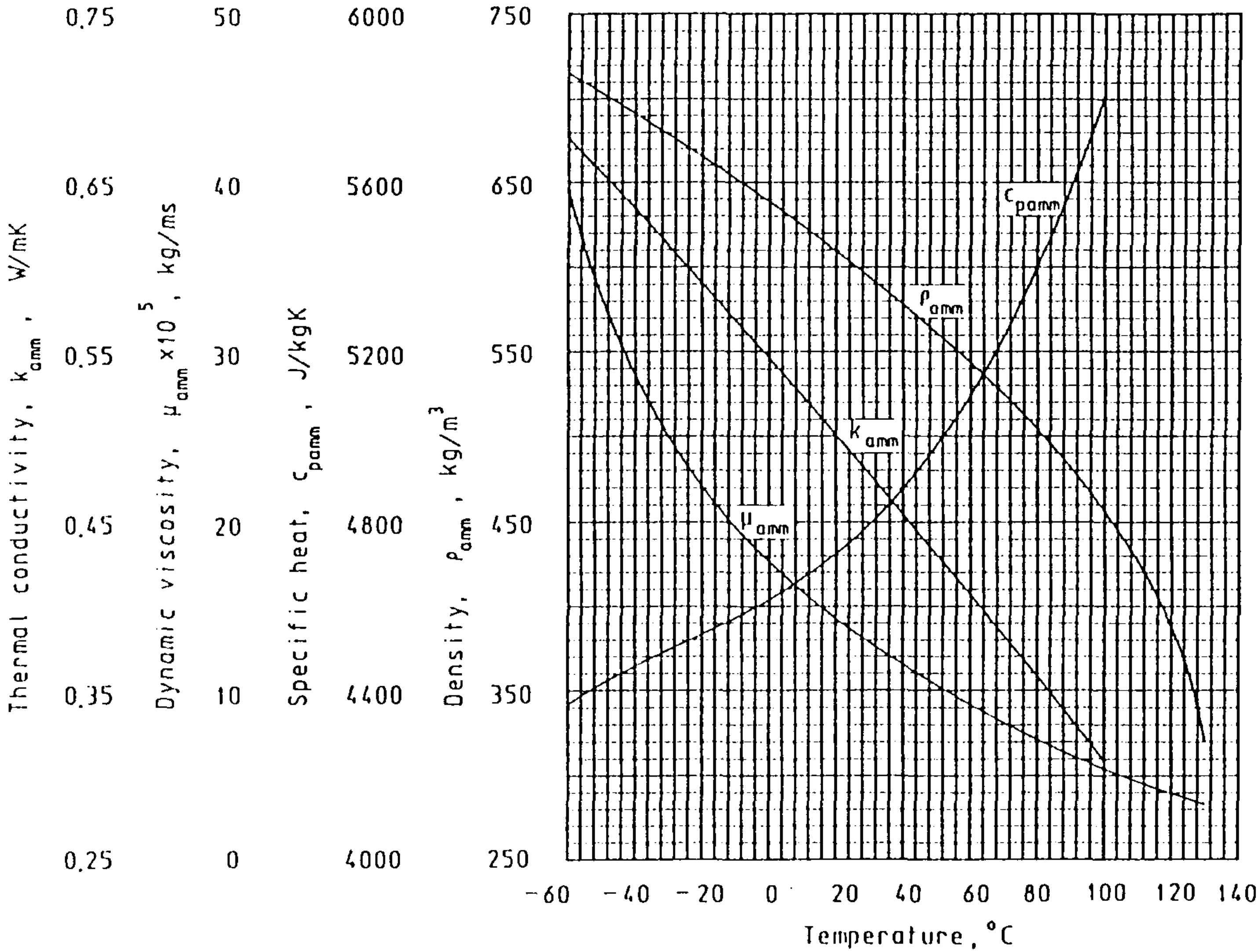

Figure A.5: Thermophysical properties of saturated ammonia liquid.

A.7 REFERENCES

54GO1 Godridge, A.M., British Coal Utilisation Research Association Monthly, Vol. 18 No. 1, 1954.

57LE1 Lehmann, H., Chemical Technology, Vol. 9, pp. 530, 1957.

65GO1 Goff, J.A., Saturation Pressure of Water on the New Kelvin Scale, Humidity and Moisture Measurement and Control in Science and Industry, eds., Wexler, A. and Wildhack, W.H., Reinhold Publishing Co., New York, 1965.

70UK1 United Kingdom Committee on the Properties of Steam , U.K. Steam Tables in SI Units 1970, Edward Arnold Ltd., London 1970.

72AS1 ASHRAE Handbook of Fundamentals, Published by the American Society of Heating, Refrigeration and Air Conditioning Engineers, Inc., 1972.

76RA1 Raznjevic, K., Handbook of Thermodynamic Tables and Charts, McGraw-Hill Book Co., New York, 1976.

77YA1 Yaws, C.L., Physical Properties, Chemical Engineering Publ., McGraw-Hill Book Co., New York, 1977.

78FA1 Faires, V.M., and Simmang, C.M., Thermodynamics, 6th ed., Macmillan Publishing Co. Inc., 1978.

82AN1 Anon., Heat Transfer and Fluid Flow Data Book, General Electric Co., Corporate Research Division, New York, 1982.

82JO1 Johannsen, A., Plotting Psychrometric Charts by Computer, The South African Mechanical Engineer, Vol. 32, July 1982.

APPENDIX B

TEMPERATURE CORRECTION FACTOR

To determine the performance characteristics of heat exchangers it is essential that the mean temperature difference between fluids be accurately determined. Since this difference depends on the geometry and the flow pattern through the heat exchanger, relatively simple analytic solutions are not always possible. For computational purposes the method proposed by Roetzel [79RO1, 80RO1, 84RO1] is of value.

Consider the heat exchanger shown schematically in figure B.1.

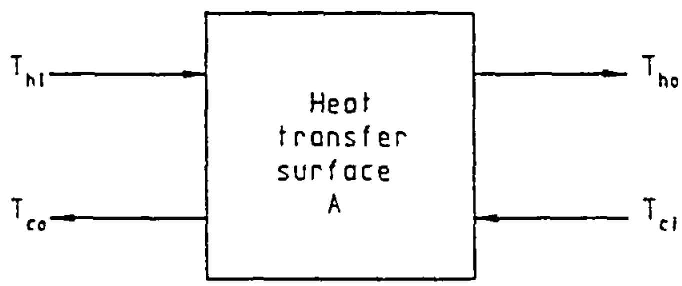

Figure B.1: Schematic of heat exchanger.

In such an exchanger the heat transfer rate is given by

$$Q = UA\Delta T_m \tag{B.1}$$

where UA is the conductance of the exchanger. The overall heat transfer coefficient U, is assumed to be constant. The heat Q flows from the hot fluid (subscript h) to the cold fluid (subscript c).

According to equation (B.1) the mean temperature difference between the two streams,

ΔT_m, may be expressed as

$$\Delta T_m = Q/UA$$

or if made dimensionless with respect to the largest temperature difference

$$\phi = \frac{\Delta T_m}{T_{hi} - T_{ci}} = \frac{Q}{UA(T_{hi} - T_{ci})} \tag{B.2}$$

Dimensionless temperature changes of the two streams may respectively be defined as

$$\phi_h = \frac{T_{hi} - T_{ho}}{T_{hi} - T_{ci}} = \frac{Q}{m_h\, c_{ph}\, (T_{hi} - T_{ci})} \tag{B.3}$$

and

$$\phi_c = \frac{T_{co} - T_{ci}}{T_{hi} - T_{ci}} = \frac{Q}{m_c\, c_{pc}(T_{hi} - T_{ci})} \tag{B.4}$$

where m is the mass flow rate and c_p is the specific heat of the fluid.

In the case of counterflow, a dimensionless mean temperature difference can be expressed in terms of the logarithmic mean temperature difference i.e.

$$\phi_{cf} = \frac{\Delta T_{lm}}{(T_{hi} - T_{ci})} = \frac{\phi_h - \phi_c}{\ln[(1 - \phi_c)/(1 - \phi_h)]} \tag{B.5}$$

According to Roetzel [84RO1], a temperature correction factor can in general be expressed as

$$F_T = \frac{\phi}{\phi_{cf}} = 1 - \sum_{i=1}^{4} \sum_{k=1}^{4} a_{i,k}\left(1 - \phi_{cf}\right)^k \sin\left(2i \arctan \frac{\phi_h}{\phi_c}\right) \tag{B.6}$$

Tables B.1 to B.10 present the sixteen values of the empirical constant $a_{i,k}$ for ten different heat exchanger geometries.

Table B.1: Crossflow with one tube row.

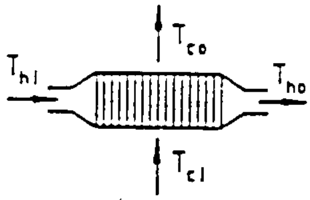

$a_{i,k}$	$i = 1$	2	3	4
$k = 1$	-4.62×10^{-1}	-3.13×10^{-2}	-1.74×10^{-1}	-4.20×10^{-2}
2	5.08×10^{0}	5.29×10^{-1}	1.32×10^{0}	3.47×10^{-1}
3	-1.57×10^{1}	-2.37×10^{0}	-2.39×10^{0}	-8.53×10^{-1}
4	1.72×10^{1}	3.18×10^{0}	1.99×10^{0}	6.49×10^{-1}

Table B.2: Crossflow with two tube rows and one pass.

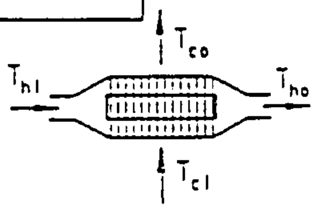

$a_{i,k}$	$i = 1$	2	3	4
$k = 1$	-3.34×10^{-1}	-1.54×10^{-1}	-8.65×10^{-2}	5.53×10^{-2}
2	3.30×10^{0}	1.28×10^{0}	5.46×10^{-1}	4.05×10^{-1}
3	8.70×10^{0}	-3.35×10^{0}	-9.29×10^{-1}	9.53×10^{-1}
4	8.70×10^{0}	2.83×10^{0}	4.71×10^{-1}	-7.17×10^{-1}

Table B.3: Crossflow with three tube rows and one pass.

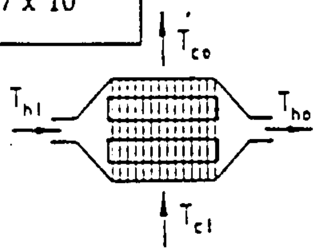

$a_{i,k}$	$i = 1$	2	3	4
$k = 1$	-8.74×10^{-2}	-3.18×10^{-2}	-1.83×10^{-2}	7.10×10^{-3}
2	1.05×10^{0}	2.74×10^{-1}	1.23×10^{-1}	-4.99×10^{-2}
3	-2.45×10^{0}	-7.46×10^{-1}	-1.56×10^{-1}	1.09×10^{-1}
4	3.21×10^{0}	6.68×10^{-1}	6.17×10^{-2}	-7.46×10^{-2}

Table B.4: Crossflow with four tube rows and one pass.

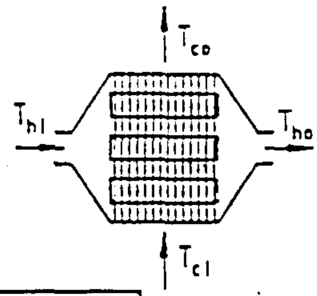

$a_{i,k}$	i = 1	2	3	4
k = 1	4.14×10^{-2}	-1.39×10^{-2}	-7.23×10^{-3}	6.10×10^{-3}
2	6.15×10^{-1}	1.23×10^{-1}	5.66×10^{-2}	-4.68×10^{-2}
3	-1.20×10^{0}	-3.45×10^{-1}	-4.37×10^{-2}	1.07×10^{-1}
4	2.06×10^{0}	3.18×10^{-1}	1.11×10^{-2}	7.57×10^{-2}

Table B.5: Crossflow with two tube rows and two tube passes.

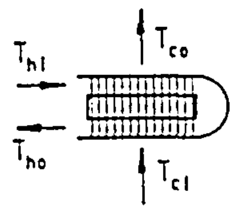

$a_{i,k}$	i = 1	2	3	4
k = 1	-2.35×10^{-1}	-7.73×10^{-2}	-5.98×10^{-2}	5.25×10^{-3}
2	2.28×10^{0}	6.32×10^{-1}	3.64×10^{-1}	-1.27×10^{-2}
3	-6.44×10^{0}	-1.63×10^{0}	-6.13×10^{-1}	-1.14×10^{-2}
4	6.24×10^{0}	1.35×10^{0}	2.76×10^{-1}	2.72×10^{-2}

Table B.6: Crossflow with three tube rows and three tube passes.

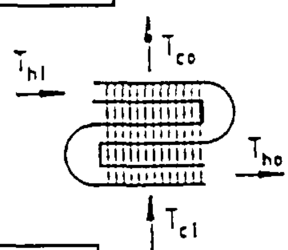

$a_{i,k}$	i = 1	2	3	4
k = 1	-8.43×10^{-1}	3.02×10^{-2}	4.80×10^{-1}	8.12×10^{-2}
2	5.85×10^{0}	-9.64×10^{-3}	-3.28×10^{0}	-8.34×10^{-1}
3	-1.28×10^{1}	-2.28×10^{-1}	7.11×10^{0}	2.19×10^{0}
4	9.24×10^{0}	2.66×10^{-1}	-4.90×10^{0}	-1.69×10^{0}

Table B.7: Crossflow with four tube rows and four tube passes.

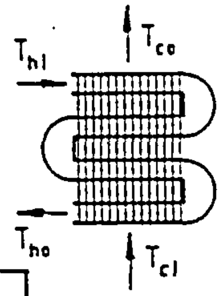

$a_{i,k}$	i = 1	2	3	4
k = 1	-3.39×10^{-1}	2.77×10^{-2}	1.79×10^{-1}	-1.99×10^{-2}
2	2.38×10^{0}	-9.99×10^{-2}	-1.21×10^{0}	4.00×10^{-2}
3	-5.26×10^{0}	9.04×10^{-2}	2.62×10^{0}	4.94×10^{-2}
4	3.90×10^{0}	-8.45×10^{-4}	-1.81×10^{0}	-9.81×10^{-2}

Table B.8: Crossflow with four tubes and two passes through two tubes.

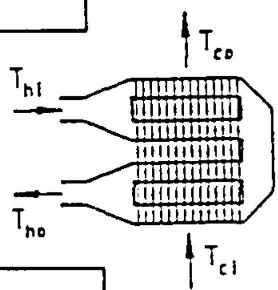

$a_{i,k}$	i = 1	2	3	4
k = 1	-6.05×10^{-1}	2.31×10^{-1}	2.94×10^{-1}	1.98×10^{-2}
2	4.34×10^{0}	5.90×10^{-3}	-1.99×10^{0}	-3.05×10^{-1}
3	-9.72×10^{0}	-2.48×10^{-1}	4.32×10^{0}	8.97×10^{-1}
4	7.54×10^{0}	2.87×10^{-1}	-3.00×10^{0}	-7.31×10^{-1}

Table B.9: Crossflow with both streams unmixed.

$a_{i,k}$	i = 1	2	3	4
k = 1	6.69×10^{-2}	0.0	3.95×10^{-2}	0.0
2	-2.78×10^{-1}	0.0	-2.20×10^{-1}	0.0
3	1.11×10^{0}	0.0	4.54×10^{-1}	0.0
4	1.36×10^{-1}	0.0	-2.58×10^{-1}	0.0

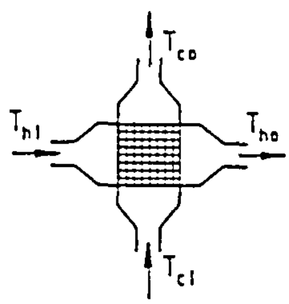

Table B.10: Crossflow with both streams mixed.

$a_{i,k}$	$i = 1$	2	3	4
$k = 1$	-4.775×10^{-1}	0.0	-1.292×10^{-1}	0.0
2	6.097×10^{0}	0.0	1.349×10^{0}	0.0
3	-2.153×10^{1}	0.0	-3.986×10^{0}	0.0
4	2.596×10^{1}	0.0	3.593×10^{0}	0.0

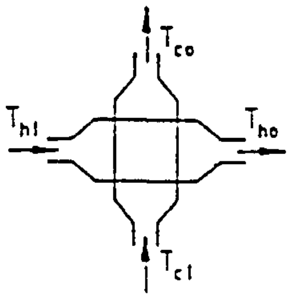

B.2 REFERENCES

79RO1 Roetzel, W. and Neubert, J., Calculation of Mean Temperature Difference in Air-cooled Cross-flow Heat Exchangers, Jnl. Heat Trans., Trans. ASME, Vol. 101, pp. 511 - 513, Aug., 1979.

80RO1 Roetzel, W. and Fürst, J., Schnelle Berechnung der mittleren Temperaturedifferenz in luftgekühlten Kreuzstrom Wärmeaustauschern, Wärme und Stoffübertragung 14, pp. 131 - 136, 190.

84RO1 Roetzel, W., Berechnung von Wärmeübertragern, VDI - Wärmeatlas, pp. Ca1 - Ca31, VDI - Verlag GmbH, Düsseldorf, 1984.

APPENDIX C

CONVERSION FACTORS

1.	Acceleration	1 cm/s^2	= 1.000×10^{-2} m/s^2
		1 m/h^2	= 7.716×10^{-8} m/s^2
		1 ft/s^2	= 0.3048 m/s^2
		1 ft/h^2	= 2.352×10^{-8} m/s^2
2.	Area	1 ha	= 10^4 m^2
		1 acre	= 4.047×10^3 m^2
		1 cm^2	= 1.000×10^{-4} m^2
		1 ft^2	= 9.290×10^{-2} m^2
		1 in^2	= 6.452×10^{-4} m^2
		1 $yard^2$	= 0.8361 m^2
		1 square mile	= 2.59×10^6 m^2
3.	Density	1 g/cm^3	= 1000 kg/m^3
		1 lb/ft^3	= 16.02 kg/m^3
		1 kg/ft^3	= 35.31 kg/m^3
4.	Energy, work, heat	1 cal	= 4.187 J
		1 kcal	= 4187 J
		1 Btu	= 1055 J
		1 erg	= 1.000×10^{-7} J
		1 kWh	= 3.600×10^6 J
		1 ft pdl	= 4.214×10^{-2} J
		1 ft lbf	= 1.356 J
		1 Chu	= 1899 J
		1 therm	= 1.055×10^8 J
5.	Force	1 dyne	= 1.000×10^{-5} N
		1 kgf	= 9.807 N
		1 pdl	= 0.1383 N

		1 lbf	= 4.448 N
6.	**Heat flux**	1 cal/s cm^2	= 4.187×10^4 W/m^2
		1 kcal/h m^2	= 1.163 W/m^2
		1 Btu/h ft^2	= 3.155 W/m^2
		1 Chu/h ft^2	= 5.678 W/m^2
		1 kcal/h ft^2	= 12.52 W/m^2
7.	**Heat transfer coefficient**	1 cal/s cm^2 °C	= 4.187×10^4 W/m^2 K
		1 kcal/h m^2 °C	= 1.163 W/m^2 K
		1 Btu/h ft^2 °F	= 5.678 W/m^2 K
		1 Chu/h ft^2 °C	= 5.678 W/m^2 K
		1 kcal/h ft^2 °C	= 12.52 W/m^2 K
8.	**Latent Heat**	See specific enthalpy	
9.	**Length**	1 cm	= 1.000×10^{-2} m
		1 ft	= 0.3048 m
		1 micron	= 1.000×10^{-6} m
		1 in	= 2.540×10^{-2} m
		1 yard	= 0.9144 m
		1 mile	= 1609 m
10.	**Mass**	1 g	= 1.000×10^{-3} kg
		1 lb	= 0.4536 kg
		1 tonne	= 1000 kg
		1 grain	= 6.480×10^{-5} kg
		1 oz	= 2.835×10^{-2} kg
		1 ton (long)	= 1016 kg
		1 ton (short)	= 907 kg
11.	**Mass flow rate**	1 g/s	= 1.000×10^{-3} kg/s
		1 kg/h	= 2.778×10^{-4} kg/s
		1 lb/s	= 0.4536 kg/s

	1 tonne/h	= 0.2778 kg/s
	1 lb/h	= 1.260×10^{-4} kg/s
	1 ton/h	= 0.2822 kg/s
Mass flux	1 g/s cm^2	= 10.00 kg/s m^2
	1 kg/h m^2	= 2.778×10^{-4} kg/s m^2
	1 lb/s ft^2	= 4.882 kg/s m^2
	1 lb/h ft^2	= 1.356×10^{-3} kg/s m^2
	1 kg/h ft^2	= 2.990×10^{-3} kg/s m^2
Mass transfer coefficient	1 lb/h ft^2	= 1.3385×10^{8} kg/sm^2
	1 g/s cm^2	= 9.869×10^{-5} kg/sm^2
	1 kg/h m^2	= 2.7415×10^{-9} kg/sm^2
Power	1 cal/s	= 4.187 W
	1 kcal/h	= 1.163 W
	1 Btu/s	= 1055 W
	1 erg/s	= 1.000×10^{-7} W
	1 hp (metric)	= 735.5 W
	1 hp (British)	= 745.7 W
	1 ft pdl/s	= 4.214×10^{-2} W
	1 ft 1bf/s	= 1.356 W
	1 Btu/h	= 0.2931 W
	1 Chu/h	= 0.5275 W
	1 ton refrigeration	= 3517 W
Pressure	1 $dyne/cm^2$	= 0.100 N/m^2
	1 kgf/m^2	= 9.807 N/m^2
	1 pdl/ft^2	= 1.488 N/m^2
	1 standard atm.	= 1.0133×10^{5} N/m^2
	1 bar	= 1.000×10^{5} N/m^2
	1 kgf/cm^2 (1 at)	= 9.807×10^{4} N/m^2
	1 $1bf/ft^2$	= 47.88 N/m^2
	1 lbf/in^2	= 6895 N/m^2